INTERNATIONAL JOURNAL OF COMPUTATIONAL ENGINEERING RESEARCH (IJCER)

EDITORIAL BOARD

Lugen M.Zake Sheet
Qualification: Phd, Department of Mathematics
Affiliation: University of Mosul, Iraq

Mohamed Abdellatif
Qualification: PhD Intelligence Technology
Affiliation: Graduate School of Natural Science and Technology

Meisam Mahdavi
Qualification: Phd Electrical and Computer Engineering
Affiliation: University of Tehran, North Kargar st. (across the ninth lane), Tehran, Iran

Dr. Ahmed Nabih Zaki Rashed
Qualification: Ph. D Electronic Engineering
Affiliation: Menoufia University, Egypt

Dr. José M. Merigó Lindahl
Qualification: Phd Business Administration
Affiliation: Department of Business Administration, University of Barcelona, Spain

Dr. Mohamed Shokry Nayle
Qualification: Phd, Engineering
Affiliation: faculty of engineering Tanta University Eygpt

CONTENTS :

Single Slot Rectangular Microstrip Antenna for Wireless Applications

P.A. Ambresh*, P. M. Hadalgi[#] and P.V.Hunagund[$]

[*, #, $] Microwave Research Laboratory,
Department Of P.G. Studies & Research in Applied Electronics,
Gulbarga University, Gulbarga-585106.Karnataka. (INDIA).

Abstract:
This article presents the design of rectangular microstrip antenna. The prototype antenna is designed and fabricated on FR4 substrate of dielectric constant $\mathcal{C}_r = 4.4$ and thickness $h = 1.66$ mm. The proposed antenna is excited using co-axial probe feed. The experimental result of rectangular-shaped microstrip antenna exhibits the excellent radiation characteristic corresponding to impedance bandwidth of 320 MHz from 3.23 to 3.69 GHz, exceeding Federal Communication Commission (FCC) frequency range with a return-loss performance $S_{11} = -10$ dB. The experimental radiation patterns of this antenna are omni-directional. This proposed antenna can be useful for WiMax, WLAN, UK fixed satellite services, UWB system, microwave imaging and vehicular radar.

Keywords: microstrip antenna, FR4, radiation, Omni-directional, spacer.

I Introduction

Microstrip antennas are popular and are getting increased attention due to their advantages. Depending upon the application, microstrip antennas having different geometrical shapes are used [1]. Nowadays, researchers are interested in the design and development of compact microstrip radiating elements [2]-[6]. In literature, the authors have experimentally demonstrated the development of compact microstrip antenna. Many techniques have also been studied in order to overcome the narrow impedance bandwidth of microstrip patch antenna. Among the various techniques, there have been the popular ones such as use of increased substrate thickness, the use of a low dielectric constant substrate, the use of air filled dielectric medium, use of various impedance matching and feeding techniques, the use of multiple resonators, and the use of slot antenna geometry and so on [7] - [14]. In particular, the slot technique shows excellent improvement characteristics suitable for microstrip antennas with air as dielectric substrate medium. Since coaxial probe feeding technique is adopted and it introduces capacitance between the feed and the radiating patch and this capacitance cancels out the inductance due to a probe itself, this effect makes it possible to improve the impedance bandwidth of the microstrip patch antenna and the improvement in gain is also achieved. In general, this type of feed can be easily implemented by directly connecting the probe to the E-shape patch acting as a radiating element. Therefore, in this article, a new microstrip antenna structure is proposed to be suitable for easy fabrication with its good features preserved.

II Antenna Layout Configuration

The design and drafting of the proposed antenna is prepared using AutoCAD 2006 – computer application software. The rectangular patch with length $L = 17.76$ mm and a width $W = 23.28$ mm is designed and fabricated. A single slot is embedded on the patch because it is more effective in enhancing impedance bandwidth [15] of the antenna compared to the conventional antenna. A standard SMA connector with probe having 1.3 mm diameter is being soldered to the proposed patch antenna as a feeding element. For the superstrate where the patch and the slot printed on it, a FR4 dielectric material with dielectric constant $\mathcal{C}_r = 4.4$, thickness $h = 1.66$ mm is used. The slot dimensions are $L_{S3} = 16.14$ mm and $W_{S3} = 2.68$ mm with the spacing of the slots $S_1 = 18.57$ mm, $S_2 = 1.68$ mm and $S_3 = 5.17$ mm as shown in Figure 1. In order to support the superstrate and suspend it in air, silicon spacers are used with air filled dielectric substrate of $\mathcal{C}_o \approx 1$ having air thickness of $\varDelta = 8.5$ mm between the patch and ground plane. Alternatively, other kind of spacers can be used to suspend the superstrate and ground plane. However, the results show no difference between two methods. The feed point location is selected on the radiating patch element on the center line of Y- axis from the edge of the patch as in Figure 1. In order to avoid drilling a hole through superstrate an inverted patch configuration is adopted, wherein a vertical probe is soldered to a horizontal slotted patch printed on the lower side of the suspended superstrate. On the other hand, the use of superstrate also provides the necessary protection for the patch from the environmental effects. These techniques offer easy patch fabrication especially for antenna array structures. The slot dimensions are taken in terms of λ_o where, λ_o is operating free space wavelength. A copper plate of dimension $L_g = W_g = 40$ mm with thickness $h_1 = 1$ mm is used as a ground plane.
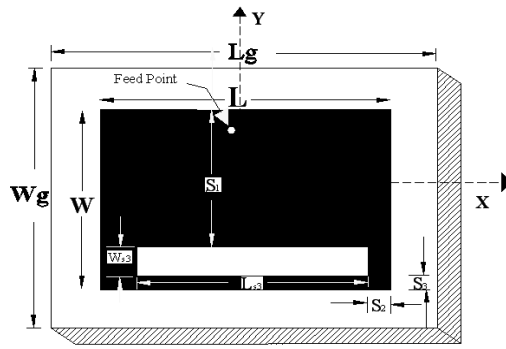
Figure1. Geometry of fabricated patch

III   Results and Discussion

The designed frequency of the proposed antenna is 3.85 GHz and the antenna resonates at lower frequency of 3.55 GHz. The impedance bandwidth with return loss (RL) less than -10 dB is measured for the frequency range of $2 - 6$ GHz as shown in Figure 2. The measurements are taken on Vector Network Analyzer (Rohde and Schwarz, Germany make ZVK model 1127.8651). Defining the impedance bandwidth as the frequency range where $S_{11} \leq - 10$ dB, the proposed patch antenna provides 9.41 % (320 MHz) impedance bandwidth with a return loss of -19 dB with a gain of 3.47 dB at resonant frequency 3.55 GHz when compared to conventional antenna providing 1 - 2 % (45 MHz) impedance bandwidth. Since the proposed antenna resonates at a lower frequency 3.55 GHz compared to the designed frequency, a compactness of 21 % is obtained suitable for portable wireless applications.
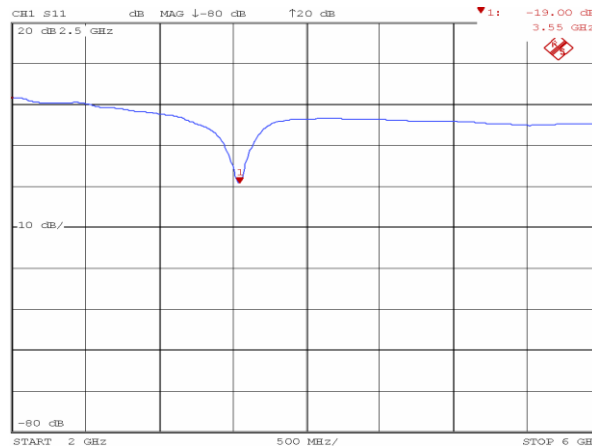
Fig. 2 Return loss (RL) versus Frequency (f) of proposed antenna

Figure 3 shows co-polar and cross-polar omni-directional radiation pattern measured at 3.55 GHz. Figure 4 (a) shows measured VSWR of 1.249 which is less than 1.5 at frequency 3.55 GHz signifying less reflected power and Figure 4 (b) shows the input impedance of $52.06 + j9.798\ \Omega$ on Smith chart validating better matching characteristics between input and load.
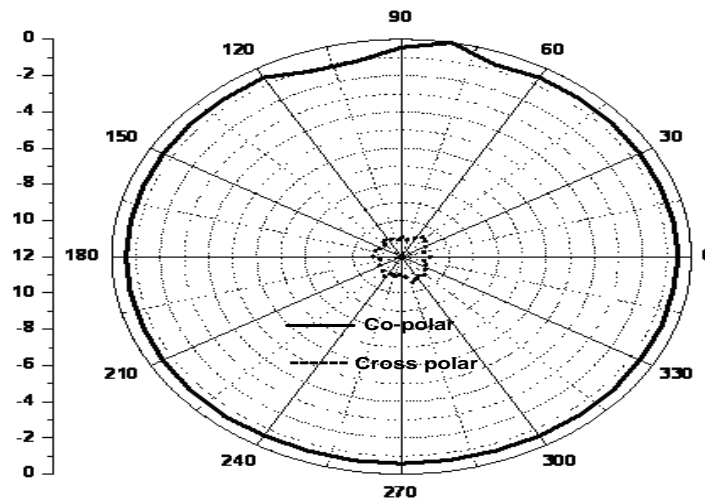
Fig. 3 Radiation pattern of the proposed antenna

(a)   (b)
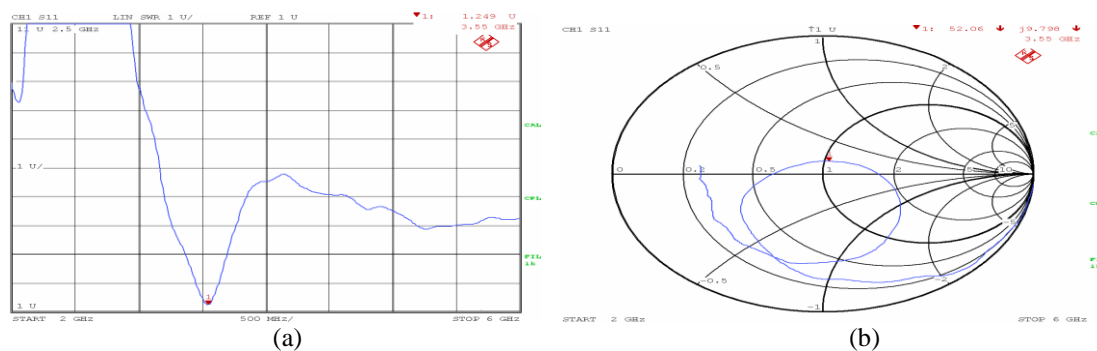
Fig. 4 (a) Variation of measured VSWR with frequency (f) in GHz,
(b) S mith chart diagram

IV. Conclusion

A single slot rectangular microstrip antenna element has been studied experimentally and presented. It consists of a superstrate patch with slot embedded on patch and placed above the ground plane, developed for various wireless applications. Compared with a conventional patch antenna, it has a better omni directional radiation pattern and provides an increase in bandwidth upto 9.41 % (320 MHz) with a compactness of 21 %. Hence, the proposed antenna is quite easy in design, fabrication and implementation and uses low-cost dielectric material as cost effective method. Designed antenna finds application in European fixed satellite services and in WiMax applications.

References

1. J. R. James and P. S. Hall, Handbook of Microstrip Antennas. Stevenage, U.K: Peter Peregrinus, London, 1989.
2. K. L. Woiig, C. L. Tang, and H. T. Chen. 1997, "A compact meandered circular microstrip antenna with a shorting pin." Microwave Opt. Technol. Lett., Vol. 15, No. 3, pp. 147-149.
3. C. L. Tang, H. T. Chen, and K. L. Wong. 1997, "Small circular microstrip antenna with dual frequency operation." Electron. Letters, Vol. 33, No. 13,pp. 1112-1113.
4. K. L. Wong and S. C. Pan.1997, "Compact triangular microstrip antenna." Electron. Letters, Vol. 33, No. 6, pp. 433-434.
5. K. L. Wong and W. S. Chen. 1997, "Compact microstrip antenna with dual frequency operation." Electron. Letters, Vol. 33, No. 8, pp. 646-647.
6. R. Waterhouse.1997, "Small microstrip patch antenna." Electron. Letters, Vol. 31, No. 8, pp. 604-605.
7. J. George, M. Deepukumar, C. K. Aanandan, P. Mohanan and K. G. Nair. 1996, "New compact microstrip antenna." Electron. Letters, Vol. 32, No. 6, pp. 508-509.
8. K.F.Lee, K.M.Luk, K.F.Tong, S.M.Shum, T.Huynh, & R.Q. Lee.1997, "Experimental and simulation studies of coaxially fed U-slot rectangular patch antenna." Inst. Elect. Eng. Microwave Antennas Propagation, Vol.144, No.5, pp. 354-358.
9. D.M.Pozar & D.H.Schaubert. 1995, Microstrip Antennas: The Analysis and design of microstrip antenna and arrays. Newyork: IEEE Press.
10. F.Yang, X.Zhang, & Y. Rahmat-Samii. 2001, "Wideband E-shaped patch antennas for wireless communications." IEEE Transactions on Antennas and Propagation, Vol. 49, No.7, pp.1094-1100.
11. C.L.Mak, & K.M Luk. 2000, "Experimental study of a microstrip patch antenna with an L-shaped probe." IEEE Transactions on Antennas and Propagation, Vol. 48, No.5, pp.77-78.
12. M.T.Islam, N.Misran, & K.G. Ng. 2007, "A 4x1 L-Probe fed inverted hybrid E-H microstrip patch antenna array for 3G Application." American Journal of Applied Science, Vol. 4, pp. 897-901.
13. M.M.Matin, B.S.Sharif, & C.C.Tsimenidis. 2007. "Probe fed Stacked Patch Antenna for Wideband applications." IEEE Transactions on Antennas and Propagation, Vol. 48, No.5, pp.2385-2388.
14. S.H.Wi, J.M.Kim, T.H.Yoo, H.J.Lee, J.Y.Park, J.G.Yook, & H.K. Park. 2002, "Bow- tie Shaped Meander Slot antenna for 5-GHz application." Proc. IEEE. Int. Symp. Antenna Propag., Vol. 2, pp.456 -459.
15. I. J.Bhal, & P. Bhartia, 1981. Microstrip antennas, Dedhame, New Delhi. Artech House.

AN ORDEAL RANDOMIZED SECURE DATA ENCRYPTION SCHEME (ORSDES)

Ramveer Singh[1]
Head & Associate Professor
Deptt. of I. T.,
R. K. G. I. T., Ghaziabad, U.P., 201003, INDIA

Deo Brat Ojha[2]
Professor, Deptt. of Mathematics,
Mewar University, Rajasthan, INDIA

Abstract :
In this paper, we present a new Data encryption scheme named as Ordeal Randomized Secure Data Encryption Scheme (ORSDES). The theoretical security measures are also discussed and ORSDES advocates its competency. Through this paper, we encourage and motivate the user to use DES as ORSDES with more efficiency and security. Mainly we emphasis on secrecy of key because all knows, In cryptography key always have important role. Using a variable pseudo random number and operational function, the new generated key for each block of message make ORSDES more attractive and usable. ORSDES motivates itself the user to use it with new destiny of confidence, integrity and authentication.

Keywords: Cryptography, Data Encryption Standard, Pseudo Random Number Generator, Secret key.

Introduction

Data Encryption Standard (DES) symmetric key cryptosystem, which was the natural choice, given that this cryptosystem had been around since 1976 and adopted by the US government in 1977, is the US government's secret-key data encryption standard and is widely used around the world in a variety applications

The input message is also known as "plaintext" and the resulting output message as "ciphertext". The idea is that only recipients who know the secret key can decrypt the ciphertext to obtain the original message. DES uses a 56-bit key, so there are 256 possible keys [1].

Due to its importance, DES has received a great deal of cryptanalytic attention. However, besides using the complementation property, there were no short-cut attacks against the cipher until differential cryptanalysis was applied to the full DES in 1991 [2–4].

In [5], Chaum and Evertse presented several meet-in-the-middle attacks on reduced variants of DES.

In 1987 Davies described a known plaintext attack on DES [6]. In [7] these results were slightly improved but still could not attack the full DES faster than exhaustive key search.

In 1994 Biham and Biryukov [8] improved the attack to be applicable to the full DES. A chosen ciphertext variant of the attack is presented in [9]; it has a data complexity of 245 chosen plaintexts. The first attack on DES that is faster than exhaustive key search was presented in [10]. In [11] another attack on DES is presented, linear cryptanalysis. This attack was later improved in [12] by exploiting nonlinear relations as well. The improved attack has a data complexity of 242.6 known plaintexts. Using chosen plaintexts, Knudsen and Mathiassen reduced the data complexity in by a factor of 2.

Even after DES was theoretically broken, RSA published a plaintext and its ciphertext encrypted using DES under some unknown key, and offered a prize of several thousand US dollars for whoever finds the secret key [13]. The first exhaustive key search took about 75 days and the key was found using 14,000–80,000 computers over the Internet [14]. In 1997 the Electronic Frontier Foundation (EFF) built a special purpose machine that costs 250,000 US dollars which retrieved the key in 56 hours by means of exhaustive key search [15]. The approach of treating reduced-round DES as an algebraic equation was also suggested in [16].

Motivation behind our work: Despite the weaknesses of DES, the cipher is still widely deployed and used. In addition, DES-like ciphers are being suggested as a solution for encryption in RFID systems [17]. The results of this paper shed more light on the security of DES, leading to a better understanding on the way DES can be used [18]. The entire discussed articles describe the attack on DES, because DES has a single key to encrypt and decrypt to all blocks of message. After, study the entire journey of data encryption standard, now we are going to improve the vigour of key.

Contribution of this paper: This current article represent a new dimension in the field of cryptography with amplify the security of data encryption standard. In practical, data encryption standard is almost impossible to break. Due to the lack of security level possibility to break it, becomes easier. So, we went in search of suitable procedure to reduce the possibility of breaking security level, which certainly provides improvedness in DES. In our Ordeal Randomized Secure Data Encryption Scheme (ORSDES) suggestion, we keen about the security of symmetric key which can provide us to further secure data.

1. Preliminaries

The three most important objectives of cryptography with respect to the information security include-

1. Confidentiality.
2. Data integrity.
3. Authentication [19].

Confidentiality refers to the protection of information from unauthorized access.

Data integrity ensures that information has not been manipulated in an unauthorized way.

Authentication methods are studied in two groups: Entity authentication and message authentication.

Modern cryptographic techniques provide solutions for these three objectives.

In general, there are two types of cryptosystems:

1. Symmetric (private) key cryptosystems.
2. Asymmetric (public) key cryptosystems [21].

1.1. Symmetric key cryptosystems

All classical cryptosystems (that is cryptosystems that were developed before 1970s) are examples of symmetric key cryptosystems. In addition, most modern cryptosystems are symmetric as well. Some of the most popular examples of modern symmetric key cryptosystems include AES (Advanced Encryption Standard), DES (Data Encryption Standard), IDEA, FEAL, RC5, and many others. All symmetric key cryptosystems have a common property: they rely on a shared secret between communicating parties. This secret is used both as an encryption key and as a decryption key (thus the keyword "symmetric" in the name). This type of cryptography ensures only confidentiality and fails to provide the other objectives of cryptography. On the other hand, an advantage over public key cryptosystems is that symmetric cryptosystems require much smaller key sizes for the same level of security. Hence, the computations are much faster and the memory requirements are smaller [20].

1.2. Data Encryption Standard (DES)

DES relies upon the encryption techniques of confusion and diffusion. Confusion is accomplished through substitution. Specially chosen sections of data are substituted for corresponding sections from the original data. Diffusion is accomplished through permutation. The data is permuted by rearranging the order of the various sections. These permutations, like the substitutions, are based upon the key and the original plaintext.

There are initial and final permutations which occur before and after the sixteen rounds. These initial and final permutations exist for historical reasons dealing with implementation on hardware and do not improve the security of the algorithm. For this reason they are sometimes left out of implementations of DES. They are, however, included in this analysis as they are part of the technical definition of DES [22].

1.3. Cryptanalysis

Cryptanalysis is an art of deciphering an encrypted message in whole or in part, when the decryption key is not known. Depending on the amount of known information and the amount of control over the system by the adversary (cryptanalyst), there are several basic types of cryptanalytic attacks [23, 24, 25, 26, 27, 28, 29]. There are several known attacks on DES like:

Ciphertext-only attack, Brute force attack, Known-plaintext attack, Chosen-plaintext attack and Chosen-ciphertext attack.

1.4. Pseudo Random Number Generator

The two major requirements for a PRNG are

efficiency, as one may wish to produce a large bulk of numbers in a small amount of time, and security. Particularly, one will wish to provide a particular level of cryptographic security, where information leakage is minimized. Such a PRNG will leak a mere one bit of information after producing 2n/2 blocks of output, where n is the block size of the cipher in bits (and assuming the key length is at least as long as the block length).

One should prefer block ciphers in CTR mode to generators based on a dedicated stream cipher. CTR mode requires only that the block cipher be a pseudorandom permutation, which is widely believed to be a reasonable assumption. Dedicated stream ciphers, on the other hand, need to be strong ciphers and also need to resist related key attacks. For example, due to a related key attack, the naïve use of RC4 as a PRNG is fundamentally flawed, even disregarding biases in the cipher. Cryptographic hash functions can also be a good foundation for a PRNG. Many constructs have used MD5 or SHA1 in this capacity, but the constructions are often ad hoc. When using a hash function, we would recommend HMAC in CTR mode (i.e., one MACs counters for each successive output block). Ultimately, we prefer the use of block ciphers, as they are generally better-studied constructs. Depending on the threat model, one may wish to consider protected memory, which is difficult to ensure [30, 31, 32, 33].

2. Our Approach

In this approach, we encourage the user to use data encryption standard with more efficiency and security. Mainly we emphasis on secrecy of key because all knows key always play vital role in cryptography.

In Traditional DES:
The key block size is 56 bit.
Data block size 64 bit,
DES follows the block cipher mode encryption and decryption.
Message (M) = $\{m_1, m_2, m_3,................, m_n\}$
Key (K) = {K}
For Encryption/Decryption:
$C_i = E_K\{m_i\}$
Cipher Text C = $\{C_1, C_2, ..., Cn\}$
And
$m_i = D_K\{C_i\}$
Plain Text M = $\{m_1, m_2, ..., m_n\}$
As per traditional DES, Encryption process follows the feistel structure (16- round) and make a new key for each round by the permutation on bits of key k. Same key k applies on each block of message m using shifting property for encryption and decryption through DES.

Orsdes Approach:

We also using the same feistel structure and same process for encryption and decryption but we add a new process for key generation. In this process, key itself generate n different keys using a function and random number generated by Pseudo Random Number Generator (PRNG) then new generated key block applies on the each block of message for all round of DES. For each block of message, the process generates a separate key. This new generated key used in encryption phase as well as the decryption phase.
The key block size is 56 bit.
Data block size 64 bit,
DES follows the block cipher mode encryption and decryption.
Message (M) = $\{m_1, m_2, m_3,................, m_n\}$
Key (K) = $\{K_{new\ i}\}$

Key Generation
$F\{K \text{ and } R_j\} = K_{new\ i}$
$R_j = \{K_j \| Id_{encryptor}\}$
Where K_j generated by Pseudo Random Number Generator (PRNG)
and $[1 \leq K_j \leq (256 = 2,057,594,037,927,936)]$

Function F
Step 1:
Input the bit value of initial key K (56-bit).
Step 2:
Input generated R_j with random number K_j and Id of encryptor, generated by PRNG[*].
([*]PRNG Property- 256 no., random number generator)
Step 3:
Convert K_j into 56- bit binary number.
Step 4:
Now, we have
Key K = {KB1, KB2, KB3, ..., KB56}
And K_j ={Rb1, Rb2, Rb3, ..., Rb56}
Where KBr is the bit of Key and Rbr is the bit of Random no. Here r =1, 2, 3...............56.
Step 5:
 Apply condition on K and Rj.
IF Rbr = 1 then, Complement (convert 1 to 1 or 0 to 0) of corresponding KBr.
ANDIF Rbr = 0 then, Retain the same (1 to 1 or 0 to 0) of corresponding KBr.
Step 6:
 $K_{new\ i}$ = Result of step 5.
Using this function F every time we get the result $K_{new\ i}$ for each block of message. For each block of M we generate a new no. R_j and implement function F. Finally get a new key for each block of message.

For Encryption/Decryption

In encryption phase, ORSDES take a message block m_n and a new generated key $K_{new\ i}$ implement encryption process as per traditional DES. One special thing make aur process is different- PLAUSIBLE KEYING.

PLAUSIBLE KEYING have the property to make various key for various block of message.

Now, we have a new key for every block of message. This new key $K_{new\ i}$ is apply on each block of message M.

In this process, New key is also make 16 different key for every round of DES using shifting property as per traditional DES. For every block of message M, new $K_{new\ i}$ makes a new key block for every round of DES to implement in the encryption process.

Decryption Process is the inverse step of encryption process. In decryption, we also use the same key which is used in encryption.

$C_i = E_{K_{new\ i}} \{mi\}$

and

$m_i = D_{K_{new\ i}} \{Ci\}$,

where $1 \leq i \leq n$.

Cipher Text C = {C_1, C_2, ..., C_n} and

Plain Text M = {m_1, m_2, ..., m_n}.

3. Security Analysis of ORDES

In modern cryptography, Encryption / Decryption process based on the key. The strength of key shows that the strongness of scheme. In various cryptosystem (symmetric & asymmetric) have tedious way to find out the key.

The basic concern related to security of key are:

1. No sharing.

2. No transfer.

Benjamin Franklin says "Three people can keep a secret if two of them are dead". This statement describes itself the major security of key is no sharing.

Cryptographic scheme strength is often described by the bit length of encryption key. The more bits in the key, the harder it is to decrypt data simply by all possible key. DES uses 56 bit, Cracking 56- bit algorithm with a single key search might take around a week on a very powerful computer.

Now,

At time t, the generated key is $K_{new\ x}$,

At time t + 1, the generated key is $K_{new\ y}$

And At time t + n, the generated key is $K_{new\ z}$

Here,

$K_{new\ x} \neq K_{new\ y} \neq K_{new\ z}$

It might be possible that, $K_{new\ x} \neq K_{new\ y} \neq K_{new\ z}$, are equal if and only if the generated no. R_j at time t, t + 1, t + n are same, But the probability of generate the same no. at different time is very much low because of we are using PRNG.

Now, Compare with traditional DES, we simply analyze the security level of ORSDES. If message have n blocks then the security of ORSDES is increase n times more than traditional DES. We also accept that the process might be face one problem – Increase the overhead. But due to aspect of security level, we can compromise with that problem.

Meet-in-the-Middle Attacks:

Meet-in-the-middle can minimise the number of brute force permutations required to decrypt message that has been encrypted by more than one key. This attack targets block cipher cryptographic schemes. The attackers apply brute force technique to both the plaintext and ciphertext of a block cipher. He then attempts to encrypt the plaintext according to various possible combinations of keys to achieve an intermediate ciphertext (a text that has only been encrypted by one key). Simultaneously, he attempts to decrypt the ciphertext according to various possible combinations of keys, seeking a block of intermediate ciphertext that is the same as the one achieved by encrypting the plaintext. If there is a match of intermediate ciphertext, it is highly probable that the key used to encrypt the plaintext and the key used to decrypt the ciphertext are the two encryption keys used for the block cipher.

Remark: ORSDES successfully meet with this requirement.

Linear Factors:

DES consist a plaintext, a key size, a ciphertext and a family of invertible maps indexed by the key space. We say that cryptosystem X is a factor of cryptosystem Y if there are maps (called factor maps) between the plaintext, key and ciphertext such that the enciphering and deciphering action of cryptosystem A can be recovered from those of cryptosystem B using factor of B. If the key space of A is smaller than that of B one can profitably break B by first breaking A.

Remark: ORSDES successfully meet with this requirement.

Weak Keys:
A weak key 'K' is a key for which encryption is the same function as decryption. A pair of semi-weak keys, K and K, are keys for which encryption with K is the same as decryption with K' and vice versa. DES has weak keys, if the number of weak keys is relatively small, they may not compromise the cipher when used to assure confidentiality.

Remark: ORSDES successfully meet with this requirement.

Detectable Key Classes:
One way to reduce the effective keyspace is to divide the keyspace into classes, and then find an attack that reveals to which class the key belongs. In some instances, the workload of identifying a key with a specific class is very small; these too are sometimes referred to as weak keys. IDEA has several classes of keys detectable with just two chosen-plaintext encryptions. The key schedule allows two different keys to have several round keys in common; this reduces the affective keyspace by almost a factor of four using 233chosen plaintexts. Due to the weak mixing in its key schedule, RC4 has a class of detectable keys. One out of 256 keys is detectable, and a detectable key has about a 13.8% chance of revealing 16 bits of the key in the first output byte.

Remark: ORSDES successfully meet with this requirement.

Simple Relations and Equivalent Keys:
A simple relation occurs between two different keys, manifesting itself as a relationship between the resulting plaintexts and ciphertexts. This also allows the keyspace to be reduced in a search. DES has a simple relation known as the complementation property: if K encrypts P to C, then the bitwise complement of K encrypts the bitwise complement of P to the bitwise complement of C. This reduces the effective keyspace by one bit. DES has pairs of keys for which a simple relation exists, for at least a fraction of all plaintexts.
Two keys are equivalent if they transform all plaintexts identically. This can be considered a special kind of simple relation.

Remark: ORSDES successfully meet with this requirement.

Attacks on One-Wayness:
A key schedule is one-way if, given several round subkeys, it is infeasible for an attacker to gain any new information about the master key or about other unknown round subkeys. For instance, recovering a few round subkeys allows one to recover most of the master key in the DES key schedule. Furthermore, it may be easier to find weak keys and related keys for key schedules which are not one-way.

Remark: ORDES successfully meet with this requirement.

Related Key Attack:
A related-key attack is one where the attacker learns the encryption of certain plaintext not only under the original (unknown) key K, but also under some derived keys K'= f (K). In a chosen-related-key attack, the attacker specifies how the key is to be changed; known-related-key attacks are those where the key difference is known but cannot be chosen by the attacker. We emphasize that the attacker knows or chooses the relationship between keys, but not the actual key values.
Three-key triple-DES is a well-known method for strengthening DES with a 168-bit key; it is also vulnerable to related-key attacks. This mode can be considered a 3-round cipher with independent 56-bit round subkeys, realizing that each round is very strong. Quixotically, one might use rotational related-key cryptanalysis; however, such an approach would require many known plaintexts.

Remark: ORSDES successfully meet with this requirement.

4. Conclusion:
Our section 4 completely advocates the plausibility of ORSDES. This plausibility of key gives an authenticated encryption due to concatenation of identity of encryptor. It is successful and needful for current communication scenario.

Case I
If we take one and only one Key on the place of n keys then $K_{new\ I}$ is K, at this condition our approach works like DES.

Case II
If $K_{new\ 1} = K_{new\ 1} = K_{new\ 1}$, than our approach also works like DES.

References

[1]   Data Encryption Standard, Federal Information Processing Standards Publication (FIPS PUB) 46, National Bureau of   Standards, Washington, DC (1977).

[2]   Eli Biham, Adi Shamir, Differential Cryptanalysis of DES-like Cryptosystems, Journal of Cryptology, Vol. 4 No. 1, Springer, pp. 3–72, 1991.

[3]   Eli Biham, Adi Shamir, Differential Cryptanalysis of the Full 16-Round DES, Advances in Cryptology, proceedings of CRYPTO '92, Lecture Notes in Computer Science 740, Springer, 1993.

[4]   Eli Biham, Adi Shamir, Differential Cryptanalysis of the Data Encryption Standard, Springer, 1993.

[5]   David Chaum, Jan-Hendrik Evertse, Cryptanalysis of DES with a Reduced Number of Rounds: Sequences of Linear Factors in Block Ciphers, Advances in Cryptology, proceedings of CRYPTO '85, Lecture Notes in Computer Science 218, pp. 192–211, Springer, 1986.

[6]   Donald W. Davies, Investigation of a Potential Weakness in the DES Algorithm, private communications, 1987.

[7]   Donald W. Davies, Sean Murphy, Pairs and Triplets of DES S-Boxes, Journal of Cryptology, Vol. 8, No. 1, pp. 1–25, Springer, 1995.

[8]   Eli Biham, Alex Biryukov, An Improvement of Davies' Attack on DES, Journal of Cryptology, Vol. 10, No. 3, pp. 195–206, Springer, 1997.

[9]   Sebastien Kunz-Jacques, Frederic Muller, New Improvements of Davies-Murphy Cryptanalysis, Advances in Cryptology, proceedings of ASIACRYPT 2005, Lecture Notes in Computer Science 3788, pp. 425–442, Springer, 2005.

[10]   Kunz-Jacques, S., Muller, F.: New Improvements of Davies-Murphy Cryptanalysis.In: Roy, B. (ed.) ASIACRYPT 2005. LNCS, vol. 3788, pp. 425–442. Springer, Heidelberg (2005)

[11]   Mitsuru Matsui, Linear Cryptanalysis Method for DES Cipher, Advances in Cryptology, proceedings of EUROCRYPT '93, Lecture Notes in Computer Science 765, pp. 386–397, Springer, 1994.

[12]   Takeshi Shimoyama, Toshinobu Kaneko, Quadratic Relation of S-box and Its Application to the Linear Attack of Full Round DES, Advances in Cryptology, proceedings of CRYPTO '98, Lecture Notes in Computer Science 1462, pp. 200–211, Springer, 1998.

[13]   CNET News.com, Users take crack at 56-bit crypto. Available on-line at http://news.com.com/2100-1023-278658.html?legacy=cnet, 1997.

[14]   RSA Data Security, Team of Universities, Companies and Individual Computer Users Linked over the Internet Crack RSA's 56-Bit DES Challenge. Available on-line at: http://www.rsasecurity.com/news/pr/970619-1.html, 1997.

[15]   Electronic Frontier Foundation, Cracking DES, Secrets of Encryption Research, Wiretap Politics & Chip Design, O'reilly, 1998.

[16]   Nicolas T. Courtois, Gregory V. Bard, Algebraic Cryptanalysis of the Data Encryption Standard. Available on-line at: http://eprint.iacr.org/2006/402.pdf, 2006.

[17]   Axel Poschmann, Gregor Leander, Kai Schramm, Christof Paar, New Light-Weight DES Variants Suited for RFID Applications, proceedings of Fast Software Encryption 14, Lecture Notes in Computer Science, Springer (to appear), 2007.

[18]   Orr Dunkelman, Gautham Sekar, and Bart Preneel: "Improved Meet-in-the-Middle   Attacks on Reduced-Round DES", to appear in Indocrypt 2007.

[19]   A.M. Eskicioglu, "Protecting Intellectual Property in Digital Multimedia Networks," IEEE Computer, July 2003, pp. 39-45.

[20]   Whitfield Diffie and Martin E. Hellman, "New Directions in Cryptography" IEEE   transactions on Information Theory, 22, 644-654

[21]   P.C. van Oorschot, A.J. Menezes, and S.A. Vanstone, "Handbook of Applied Cryptography," CRC Press, Inc., 1997.

[22]   D.B. Ojha, Ramveer Singh, Ajay Sharma, Awakash Mishra and Swati garg "An Innovative Approach to Enhance the Security of Data Encryption Scheme" International Journal of Computer Theory and Engineering, Vol. 2,No. 3, June, 2010,1793-8201

[23]   M.Matsui: "The First Experimental Cryptanalysis of the Data Encryption   Standard", Crypto'94, LNCS 839, Springer, pp. 1-11, 1994.

[24]   Eli Biham and Adi Shamir: "Differential Cryptanalysis of DES-like   Cryptosystems". Journal of Cryptology, vol. 4, pp. 3-72, IACR, 1991.

[25]   M. Matsui: "Linear Cryptanalysis Method for DES Cipher",Eurocrypt'93",   LNCS 765,Springer, pp. 386-397, 1993.

[26]   Orr Dunkelman, Gautham Sekar, and Bart Preneel: "Improved Meet-in-the-   Middle Attacks on Reduced-Round DES", To appear in Indocrypt 2007.

[27]   Alejandro Hevia, Marcos Kiwi, "Strength of two data encryption standard   implementation under timing attacks", ACM Transactions on Information and   System Security (TISSEC), Volume 2, Issue 4 (November 1999) Pages: 416 –   437.

[28]   M.Matsui: "The First Experimental Cryptanalysis of the Data Encryption Standard",   Crypto'94, LNCS 839, Springer, pp. 1-11, 1994.

[29]   Lars R. Knudsen, John E. Mathiassen, A Chosen-Plaintext Linear Attack on DES, proceedings of Fast Software Encryption 7, Lecture Notes in Computer Science 1978, pp. 262–272, Springer, 2001.

[30]   M. Bellare, A. Desai, E. Jokipii and P. Rogaway, "A concrete security treatment of symmetric encryption: analysis of the DES modes of operation", In Proc. 38th Annual Symposium on Foundations of Computer Science, 1997.

[31]   S. Fluhrer, I. Mantin and A. Shamir, "Weaknesses in the key scheduling algorithm of RC4", in Proc. Eighth Annual Workshop on Selected Areas in Cryptography, Aug. 2001.

[32]   S. Fluhrer and D. McGrew, "Statistical analysis of the alleged RC4 stream cipher", in Proc. Fast Software Encryption Seventh International Workshop, Springer-Verlag, Mar. 2000.

[33]   P. Gutmann, "The design and verification of a cryptographic security architecture," Ph.D. dissertation, Dept. Comp. Sci., Univ. of Auckland, Aug. 2000.

Development of Virtual Experiment on Amplitude Modulation

Bhaskar Y. Kathane, *Pradeep B. Dahikar

PCD ICSR, VMV College Campus, Wardhaman Nagar, Nagpur (MS), India
*Kamla Nehru Mahavidyalaya Sakkardara, Nagpur (MS), India

Abstract:-
The scope of this paper includes development and implementation of virtual lab for amplitude Modulation. The study of amplitude modulation is important in data communications and network. The amplitude modulation experiment can be performed by using the concept of virtual Intelligent SoftLab (VIS). The virtual experiment described here will help students to perform it any time anywhere. The screen shows virtual carrier, modulating and modulated waves and the necessary circuit for studying Amplitude modulation. There is a facility for change of amplitude and frequency of modulating signal. The effect of mixing of carrier and modulating signal is also visible on the screen.

Keywords: - Modulation, SoftLab, Virtual, VIS Model

1. Introduction

Science subjects always have a component of practical. In subject like Physics and Electronics students have to perform a large number of experiments in an academic year. Many times students do not get time to repeat experiments which they have performed during the session. Also many of the laboratories lack in resources to perform experiments in which sophisticated instruments are required. Therefore to provide access to laboratory experiments, anytime anywhere, concept of virtual laboratory is being developed. This virtual laboratory can cater to students at under graduate (UG) and post graduate (PG) levels. Some software's like Mat Lab and Lab View are available for simulation of experiments and for other purposes. However, these software's are generally available only in Institutes/Laboratories and student can use them only during college hours. It is therefore decided to develop software for performing individual experiments virtually on computer screen. In this laboratory an attempt has been made to develop software for electronics experiments from basic to advance level. Basic experiments such as study of characteristics of devices, have been describe else ware [1-2]. Software based on Visual Basic for constructing and virtually performing an experiment on amplitude modulation is virtual environment described in this paper.

2. Modulation

Modulation is defined as a process by which some characteristic usually amplitude, frequency or phase of the voltage of carrier wave is varied in accordance with the instantaneous voltage of some other wave called the modulating signal. The modulating signal is a low frequency signal where as the carrier is of high frequency. In modulation the low frequency (modulating signal) is supper imposed on the high frequency (carrier) thereby shifting the low frequency (message) to higher frequency. It is possible to radiate the message through space and therefore known as wireless communication. Fig-1 shows the modulating and carrier waves where as Fig-2 shows the amplitude, frequency and phase modulated waves [3]. In the next section complete amplitude modulation experiment in virtual environment is described so that students can perform and understand the concept of modulation.

Sign wave Signal   Carrier Signal

Fig – 1

Amplitude modulation   Frequency modulation

Phase Modulation
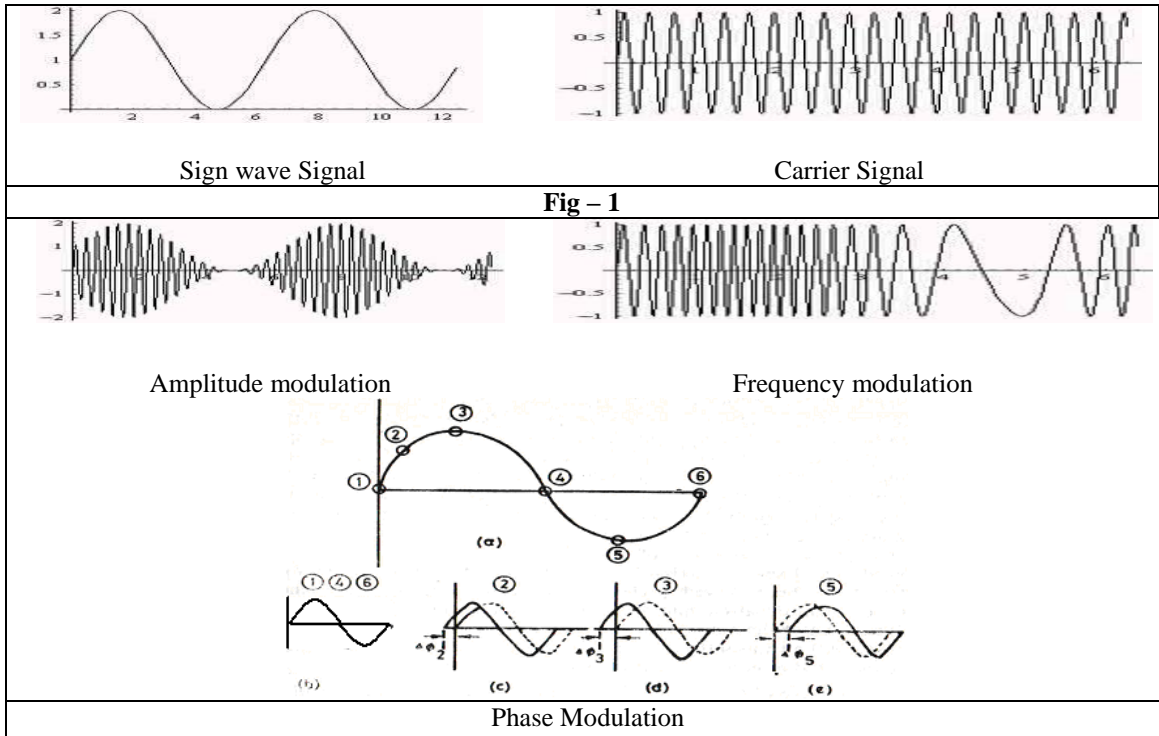
Fig – 2

3. Methodology

Visual Basic is a third generation event-driven programming language and integrated development environment from Microsoft for its COM programming model. VB is also considered as relatively easy to learn and use programming language, because of its graphical features. Visual Basic was derived from BASIC and enables use of graphics user interface, access to database and creation of ActiveX controls and objects. A programmer can put together the component provided with Visual Basic itself to develop an application. The language not only allows programmers to create simple GUI applications, but can also develop complex applications. Programming in VB is a combination of visually arranging component or control on a form, specifying attributes and actions of those components. Visual Basic can create executables (EXE files), ActiveX control or DLL files, but is primarily used to develop Windows applications. The beauty of this model is that it does not require the Database to manage data [5].

4. VIS MODEL

A program is constructed for conduct of Amplitude modulation experiment in VIS in 'VB' such that all the blocks in the model can be fully visualized on the screen. This model also can demonstrate the activities of Amplitude Modulation including circuit connection visually. Inputs accepted through virtual carrier signal generator and modulating signal generator generates Modulated virtual output which is observable on screen. In an experiment, one can provide different amplitude and frequency values for modulating signal and observe modulated signal. This model provides circuit connection facility to user so that the user can practice circuit connection also.

4.1 DESIGN SPECIFICATIONS

An amplitude modulation VIS Model requires virtual sine wave generators, virtual CRO and virtual connection wires. Virtual sine wave generator allowed different setting of amplitude and frequency in both carrier wave signal and modulating wave signal. The virtual instruments required for complete experimental setup like virtual AC supply, carrier wave generator, modulating wave generator, CRO and DC power supply are visible on the screen. With this arrangement modulation from 0% to 100% or more can be very easily studied.

Important screen shots of the experiment which appear on the monitor screen are shown in Fig-3, Fig-4, Fig-5 and Fig-6.
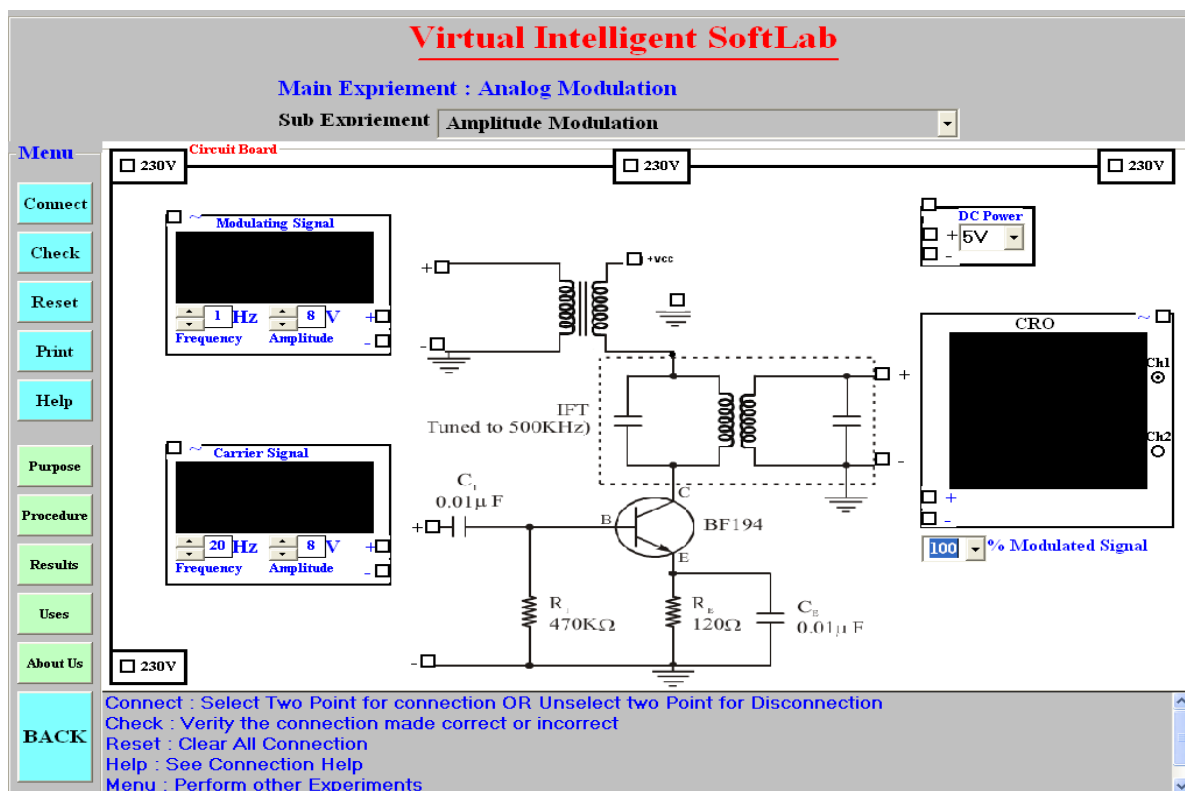
Fig-3: VIS Model before Connection
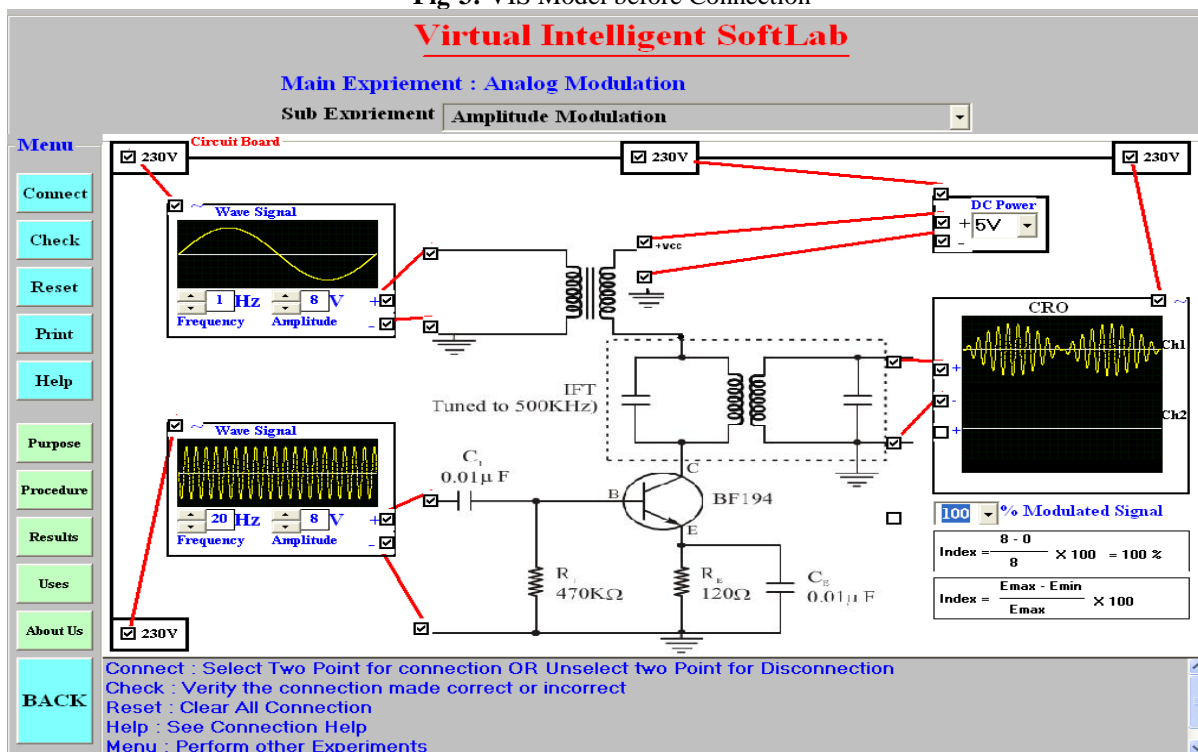
Fig-4: VIS Model 100% Amplitude Modulation
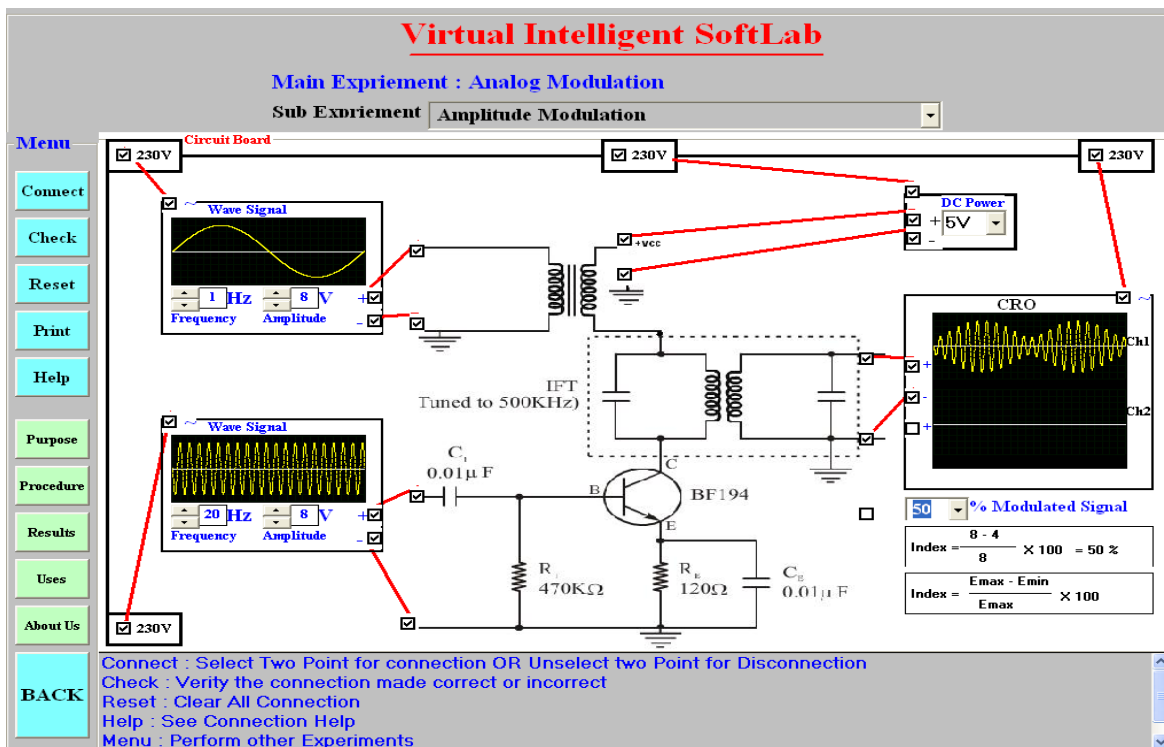
Fig-5: VIS Model 50% Amplitude Modulation
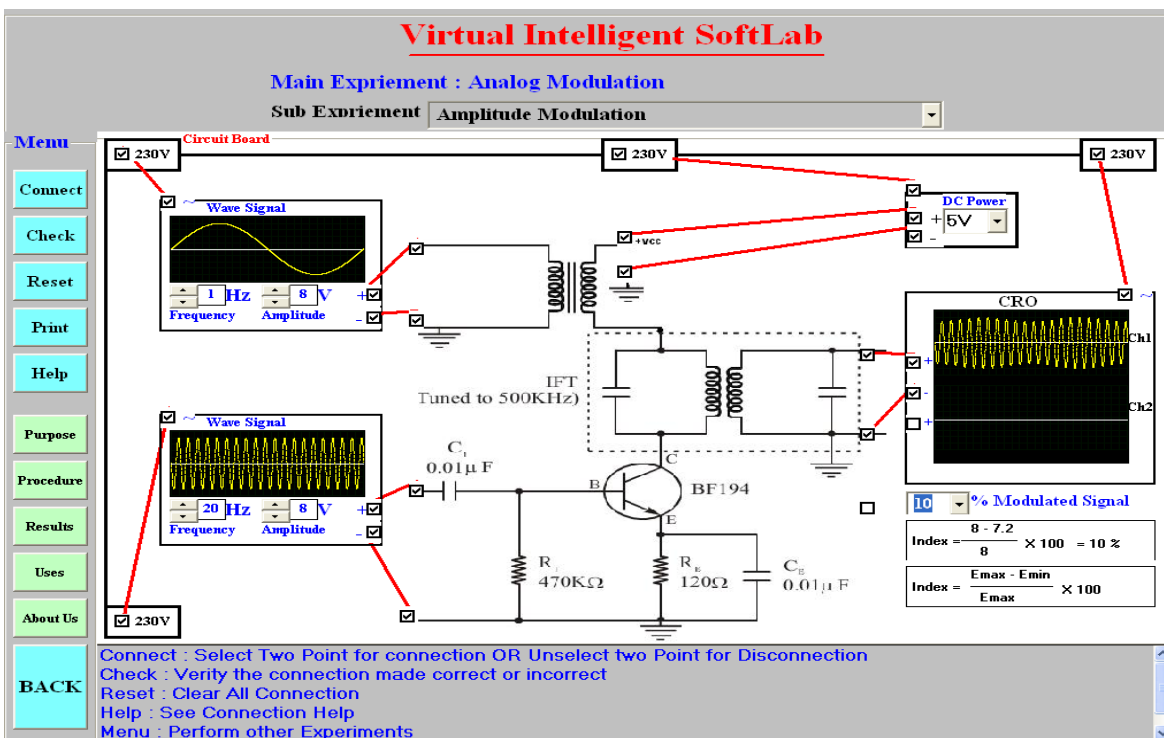
Fig-6: VIS Model 10% Amplitude Modulation

4.2   IMPLEMENTATIONS

To perform the experiment with VIS Model one has to go through the following steps.

Step: 1. Connect AC socket to DC Converter device.

Step: 2. Connect DC power supply to V_{cc} pin.

Step: 3. Connect Ground Socket to Ground Pin.

Step: 4. Connect AC power supply to virtual sine wave generators and CRO.

Step: 5. Change Amplitude and/or frequency and observe modulated waves on CRO.

This model is user friendly. Here, the instructor/student can access the detail procedure to connect the circuit. This procedure includes following steps –

- Select two switches for connection.
- Click the "Check Button" to verify the connection.
- Click the "Reset Button" if the connections are WRONG.
- Click the "Help Button" if you need Connection HELP
- Click the "Menu Button" if you want to perform other Experiments

4.3 RESULTS

Effect of change in amplitude or frequency of modulating signal on modulated signal is observable from no modulation to 100% or above. Actual calculations of % modulation also can be performed from on screen measurements.

5 CONCLUSIONS

SoftLab will help Electronics, Computer Science and Engineering students to perform and practice experiments to improve their understanding of the subject. The design of the VIS model is more effective and realistic as necessary variable inputs and outputs are visible on the monitor screen. This virtual experiment provides practice to students for the 'touch & feel' part they have already performed in the laboratory.

Acknowledgement

References

[1]   "Virtual Labs:" Nov 2010, http://www.vlab.co.in/
[2]   "A Virtual Laboratory:", March 2011; http://www.virtlab.com/main.aspx
[3]   N. D. Deshpande, D. A. Deshpande and P.K. Rangole, Communication Electronics, Tata McGraw-Hill, 2000.
[4]   SoftLab- A Virtual Laboratory for Computational Science 1 (1980), By CM Hoffman
[5]   B.Y. Kathane, P.B. Dahikar (Sept 2011), "Virtual Intelligent SoftLab for p-n junction Experiment", "Journal of the Instrument Society of India", ISSN 0970-9983, Vol.41 No.3, pp161-162.
[6].   Magazine: Electronics for you, Jan-Dec 2009

Authors Profile

Mr. Bhaskar Y. Kathane completed M.Sc. (Computer Science) and pursuing Ph.D. from R.T.M. Nagpur University, Nagpur. He is Assistant Professor in the Department of Master in Computer Application, VMV College, Nagpur (MS), India. Presently he is working as a research scholar in University Campus, RTM Nagpur University, Nagpur. His research interests include Virtual Intelligent SoftLab (VIS); A Software Solution for Laboratories. He is associate member of IETE (India).

Dr. P.B. Dahikar is a Reader in the Department of Electronics, Kamla Nehru Mahavidyalaya, Nagpur (India). He has more than 20 years of experience in teaching and research. His current area of research includes Electronics Instrumentation and Simulation. He has published more than twenty papers in referred national and international journals. He has also presented more than twenty research articles in national and international conferences. He has written few books related to his research work. He is currently dealing with few projects sponsored by UGC.

NON LINEAR MODEL CITY TRANSPORTATION SYSTEM AND CONTROL OF FUEL CONSUMPTION

Ir. Mudjiastuti Handajani,

MT (Doctor Candidate)

Lecturer of the Engineering Faculty, Department of Civil Engineering, Semarang University,

Abstract

The national economy development affects the vehicle ownership which ultimately increases fuel consumption. The rise of the vehicle ownership is dominated by the increasing number of motorcycles. This research aims to analyze and identify the characteristics of fuel consumption, the city transportation system, and to analyze the relationship and the effect of the city transportation system on the fuel consumption. A multivariable analysis is used in this study. The data analysis techniques include: a Corelational Analysis, a Multivariate Regression Analysis by using the R software. More than 70% of fuel is consumed in metropolitan cities, 14.2% in large cities and 15.67% in moderate cities. The city transportation system variables that strongly affect the fuel consumption are population, public vehicles, and private vehicles. The effect of the net population density is not too big. The higher the population density is, the larger the fuel consumption will be. This not same the Kenworthy theory (1999) that the higher the population density is, the lower the fuel/per capita consumption will be.

The model for the effect of the city transportation system on the fuel consumption = $0.1441*MPU^{0.1590} * MPP^{0.2148} * JP^{0.7659}$. This method can be developed to control the fuel consumption by improving qualified and reliable public transportation services, efficient routes, improving the city potentials, reducing the number of private vehicles and land use arrangement, transforming transportation to information technology.

Key words: consumption, fuel, city typology, transportation system, relationship.

1.   Introduction

The development of the national economy affects the vehicle ownership which will increase the fuel consumption (Marcotullio, 2007). In 1983, Indonesia has a total of 5 million units of vehicles; in 2003 the number grew quickly and reached over 20 million units or 7.2% each year (Department of Mineral Energy Resources, 2004). The growth of vehicle ownership is dominated by motorcycles. The Department of Mineral Energy Resources (2004) states that fuel consumption for transportation in Indonesia has risen sharply. If in 1993 fuel consumption was around 200 million oil-equivalent barrels (sbm), in 2003 it doubled to 400 million oil-equivalent barrels. Fuel consumption of the industrial sector is relatively constant when compared to the fuel consumption by the transportation sector (Department of Mineral Energy Resources, 2004). This means that the transportation sector is the largest fuel consumer (Official Nebraska Government Website, 2003), which is around 50% of the world fuel consumption, road transportation in developed countries consumes around 80% of the entire fuel consumption in the transportation sector. In developing countries, energy consumption in the transportation sector is 70 % (Robert Q. Riley Enterprise, 2006). The transportation sector is the largest fuel consumer and in the status quo, the need for fuel is bigger than the government's capability in providing subsidies (Observing and Evaluating Team on the National Transportation Performance/TPEKTN, 2008). Therefore, the fuel consumption for road transportation should be a concern, for example energy saving through more beneficial policies (Breheny, 1992) or by raising awareness on the issue of sustainable energy consumption (Regional Office for Europe, 2002).

Pearece dan Warford (1996) point out that the concept of sustainable transportation is the foundation as well as the challenge in developing and implementing it effectively. One of the challenges in sustainable transportation is the urban resource conserving mobility (Carrol, 1977; Cheng-Min and Cheng-Hsien , 2007) or by developing a transportation mobility strategy in developing countries (World Bank, 2006). Improving the city transportation system, specifically those triggered by growing ownership and consumption of private vehicles, has a negative effect on the city, such as traffic jams and traffic accidents, space usage, environment conservation (gas emission, air pollution, energy resource exploitation, etc.). This occurs in large cities in developed countries and large cities in developing countries, like Rio de Jenairo, Mexico City, Jakarta, New Dehli, Bangkok.

In implementing the city transportation system, vehicles are direct consumers of the fuel (except for pedestrians and engineless vehicles). To repress the fuel consumption, there needs to be an attempt to find out the effect of the city transportation system on the fuel consumption. Stopher And Meyburg (1987), state that there is a significant relationship between the city transportation system and fuel consumption with uncovered influencing factors.

The city typology and the city transportation system affect each other. The parameter of the city typology in this regard is a demand, including: population density, population, land usage and regional gross domestic product (RGDP). Whereas the parameter of the city transportation system is divided into 2 (two) parts, which are: supply: road length, road network pattern, road condition, public transportation vehicles, cargo vehicles and public transportation route length. There is also demand: private vehicles.

One thing rarely found in developing cities, especially in Indonesia is research on the fuel consumption using the city transportation system variable presented in the model. The research that creates the model of the effect of the city

transportation system on the fuel consumption in developing countries, can hopefully be made into a macro model, which is a useful basis in making decisions and national policies, based on a strongly justified research. This research aims to create a tool to help the planner and designer of the city transportation system in examining the effect of the city transportation system on the fuel consumption.

2. Literature review

The literature review in this research contains in detail varies theories and has three objectives. First, it presents theories and experience that clarify and strengthen what has been previously mentioned in the introduction (especially reaffirming the various backgrounds and reasons for choosing the research topic). Second, it presents the result of searching through various theoretical and conceptual knowledge considered relevant to the research, like the concepts of the city transportation system, city typology, fuel consumption, factors that influence the city transportation system on fuel consumption. The review is used as knowledge enrichment and background knowledge relevant with the research, explaining the theoretical and pragmatic knowledge from searching the city transportation system, city typology and fuel consumption both in the world (globally), in certain cities abroad and cities in Indonesia.

The literature review is used to gain information on: (a) the source and elements of the city transportation system; (b) city typology; (c) fuel consumption; (d) the effect of the city transportation system on the fuel consumption. The cross-reference review is to gain information on the parameter, factors, and variables, also to gain information and support (justification of researh) of research opportunities from parameters that have barely been touched and have not been done in developing countries, like the model for the effect of the city transportation system on the fuel consumption which is considered the key in the sustainable and environmental transportation system.

The Concept of City Transportation System

Transportation is the attempt of transferring, moving, carrying, or transmitting an object from one place to another so the object will be more beneficial or can be useful for certain purposes. The above definition can mean that transportation is the proses of transferring, the process of moving, the process of carrying, and transmitting that can not be separated from supporting tools to ensure the process runs smoothly according to the desired time (Miro, 2005).

The Concept of City Typology

City is a very complex human-lead environment. A city seen as a container has very complex humans inside, have experienced interrelation processes between humans and the environment. The product of interrelation produces an orderly pattern in land usage which caused the city structure theory to rise (Rodrigue, 2004). City can be discussed through various perspectives. City morphology is the city public space, like downtown areas, city space, main roads. City forms basically occur due to interactions between inhabitants. Individuals in city societies are not isolated in individual activities, but interact in the form of city space.

The Concept of Fuel Consumption

Fossil energy is a form of unrenewable energy. This energy type has long been known as fossil fuel. Meanwhile, fossil fuel supplies are limited, because it is unrenewable energy, in time it will not meet the people's needs or run out altogether (Department of Land Transportation, 2008). Therefore, there should be a national fuel consumption conservation especially in the land transportation sector. Fossil fuel is an organic substance needed in combustion to create energy or force which is the result of crude oil distillation into the desired fractions. The types of fossil fuel include: avgas, petrol, karosene, avtur, diesel oil as well as burning oil. The fuel consumption observed in this research includes petrol and diesel oil, because motor vehicles in the Java island (2007 and 2008 data) use more petrol and diesel oil.

3. RESEARCH METHODS

As stated in the theoretical study, this research includes many variables and data, so the focus is on multivariate analysis which is an application method related to the large number of variables made in each object in one or more data simultaneously, whereas the development analysis for the nonlinear model is done with the help of software R (nonlinear least square). To determine which independent variable should be put into the nonlinear least square (nls) model, the Cobb-Douglas production function is used, which is a production function involving the influence of the input used with the output desired. The diagram of the research process can be seen in Picture 1 below.
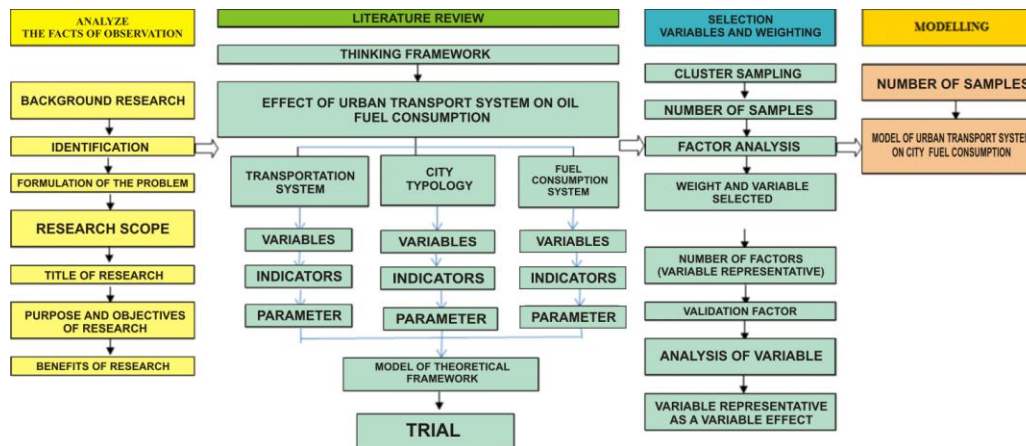
Picture 1. *Research Process Diagram*

Picture 2. *Research Location*

4. Analysis

Data on Fuel Consumption

The data on the fuel consumption was collected in 2007 and 2008 based on petrol station purchases from Pertamina (Indonesian Oil Company) in each city each year. The average fuel consumption (petrol+diesel) of cities in Java is 3.411.421 kilo litres /year, where the petrol is 2,432,872 kl/year, diesel fuel is 978,549 kl/year. The comparison between petrol and diesel fuel consumption is 71%: 29%. Petrol is used more by motor vehicles in Java island because the number of private vehicles is very high (6,384,406 units or 99.37% of the total number of passenger vehicles), the number of public transportation vehicles is low (40,726 units or 0.63% of the total number of passenger vehicles), the percentage of motorcycles is more than 82% of private vehicles.

The highest fuel consumption/year in 2008 was Surabaya (650,085 kilo litres/year), the lowest fuel consumption/year was in Mojokerto in 2007 (13,568 kilo litres/year). Meanwhile, Sukabumi had the highest fuel consumption/population/day (0.6 litres). The city of Sukabumi has a developed area width of 19.63 km2, 12 units of petrol stations. The population of the Sukabumi District partly live around the city of Sukabumi, buying fuel in petrol stations in the city of Sukabumi. Sukabumi District has a population of 2,391,736 people with an administrative area of 4,199.7 km2, the largest throughout Java and Bali, 4.48 % of developed area (18.814 ha). The population of Sukabumi District is almost the same as the city of Bandung's population (2,329,928 people). Bandung has 96 petrol station units. The number of petrol stations in Sukabumi District is 20 units. So there is a big possibility that the people of Sukabumi District buy fuel in the city of Sukabumi.

The total total fuel consumption of moderate cities in Java ranges between 13.568 kl/year- 87.898 kl/year. The total fuel consumption of large cities ranges between 99.968 kl/year- 152.155 kl/year. The fuel consumption of metropolitan cities is 292.923 kl/year – 650.260 kl/year. The average, maximum, minimum fuel consumption and number of gas stations can be seen in Table 1.

Table 1. Fuel Consumption all Cities in Java

No.	Description	Maximum	Minimum	Average
1.	Number of gas stations	96	3	22.32
2.	Total Fuel Consumption (kl)	650,260	13,568	155,064.56
	Petrol Consumption (kl)	456,962	9,776	110,585.09
	Diesel Fuel Consumption (kl)	193,123	3,792	44,479.47
3.	Petrol fuel consumption/population/day(l)	0.65	0.12	0.36
4.	Diesel Fuel consumption/population/day(l)	0.29	0.07	0.15

Source: Total Results, Mudjiastuti Hadajani, 2011.

Model Development

The Total City Fuel Consumption Model for total fuel consumption in all cities in Java is:

Lntot= A0 + A1lnpj + A2lnbu + A3lnmpu + A4lnmpp +A5lnbp + A6lnab + A7lnsm + A8lnkpdt + A9lnjp + A10lnpdrb + A11lnptr + A12lnldt

The above equation is analyzed using the R program (Fox, 2002). Table 1 shows the VIF value for independent variables in the model 1 equation. Some VIF value of independent variables are more than 10 and some are less than 10, variables with a VIF value above 10 is the Lnptr variable of 11.0181. The next process is to remove the Lnptr variable, and produce a new model that does not include that variable.

Table 2 VIF (model 1) All Cities Total Fuel Consumption

vif(model 1) –Total Fuel of All Cities					
lnpj	lnbu	lnmpu	lnmpp	lnbp	lnab
5.4793	1.9281	6.5396	25.9299	2.0185	21.4938
lnsm	lnkpdt	lnjp	lnpdrb	lnptr	lnldt
24.2485	238.7008	1,963.4482	6.7604	11.0181	1,404.2180

Once the Lnptr variable is removed, a new model is obtained like in Table 3. Although the Lnptr variable has been removed, it is evident that the VIF value of independent variables is still big though not as big as it was previously (the non multicolinierity assumption has not been fulfilled). In the second model, the VIF value above 10 is in the Lnsm variable of 18.8100. The next process is to remove the Lnsm variable, and produce a new model that does not include that variable.

Table 3 VIF (model 2) Total Fuel Consumption of All Cities

Vif (model 2) –Total Fuel of All Cities					
lnpj	Lnbu	lnmpu	lnmpp	lnbp	lnab
3.4898	1.6866	6.5382	25.7073	1.9401	19.3867
lnsm	Lnkpdt	lnjp	lnpdrb	lnldt	
18.8100	236.2672	1963.0924	6.5579	1399.1252	

Table 4 shows that the Lnsm variable has been removed. Although the Lnsm variable has been removed, the VIF value for independent variables is still big though not as big as it was previously (the non multicolinierity assumption has not been fulfilled). In the third model, the VIF value above 10 in the Lnab variable is 10,6945. The next process is to remove the Lnab variable, and produce a new model that does not include that variable.

Table 4 VIF (model 3) Total Fuel Consumption of All Cities

Vif (model 3) – Total fuel consumption of all cities					
lnpj	lnbu	lnmpu	lnmpp	lnbp	lnab
2.9457	1.6268	4.7517	21.5801	1.9112	10.6944
lnkpdt	lnjp	lnpdrb	lnldt		
196.1071	1623.0934	6.5568	1170.7635		

Table 5 shows that the Lnab variable has been removed. Although the Lnab variable has been removed, the VIF value of independent variables is still big though not as big as it was previously (the non multicolinierity assumption has not been fulfilled). In the fourth model, the VIF value above 10 is the Lnkpdt variable of 189,9373. The next process is to remove the Lnkpdt variable, and produce a new model that does not include that variable.

Table 5 VIF (model 4) Total Fuel Consumption of All Cities

Vif (model 4) – Total fuel consumption of all cities					
lnpj	lnbu	lnmpu	Lnmpp	lnbp	lnkpdt
2.8547	1.3956	4.5583	9.5120	1.9070	189.9373
lnjp	lnpdrb	lnldt			
1578.5464	6.4243	1125.1742			

Table 6 shows the Lnkpdt variable has been removed. Although the Lnkpdt variable has been removed, the VIF value for independent variables is still big though not as big as it was previously (the non multicolinierity assumption has not been fulfilled). In the fifth model, the VIF value above 10 is the Lnldt variable of 11,2038. The next process is to remove the Lnldt variable, and produce a new model that does not include that variable.

Table 6 VIF (model 5) Total Fuel Consumption of All Cities

Vif (model 5) – Total fuel consumption of all cities					
Lnpj	lnbu	lnmpu	lnmpp	lnbp	lnjp
2.8185	1.3807	4.5464	9. 0588	1. 8982	19.2361
Lnpdrb	lnldt				
6.2855	11.2038				

According to Table 7 (model 6), the VIF value of each variable is now lower than 10. This means the non multicolinierity assumption has been fulfilled, next the variable with the significant value is chosen. From Table 8 (model 7), the Public Passenger Vehicles, Private Passenger Vehicles and JP variables have significant values and will be used in the Total Fuel Consumption of All Cities model.

Table 7 VIF (model 6) Total Fuel Consumption of All Cities

vif(model 6) – Total fuel consumption of all cities					
lnpj	lnbu	lnmpu	lnmpp	lnbp	lnjp
2.3793	1.3803	4.4183	8.9208	1.8683	9.6168
lnpdrb					
6.1371					

Table 8 VIF (model 7) Total Fuel Consumption of All Cities

Vif (model 6) – Total fuel consumption of all cities					
lnpj	lnbu	lnmpu	lnmpp	lnbp	lnjp
2.3793	1.3803	4.4183	8.9208	1.8683	9.6168
lnpdrb					
6.1371					

Model on the Effect of The City Transportation System – Fuel Consumption of All Cities
By using the R program the following output is produced:

lm(formula = lntot ~ lnmpu + lnmpp + lnjp)
Residuals:
    Min   1Q   Median   3Q   Max
-0.47247 -0.14277 0.02748 0.14329 0.35725
Coefficients:
        Estimate Std. Error t value Pr(>|t|)
(Intercept) -1.93692   0.55982 -3.460 0.00141 **
lnmpu   0.15898   0.05539   2.870 0.00683 **
lnmpp   0.21475   0.06668   3.221 0.00271 **
lnjp   0.76590   0.08850   8.654 2.55e-10 ***

Signif. Codes: 0 '***' 0.001 '**' 0.01 '*' 0.05 '.' 0.1 ' ' 1
Residual standard error: 0.2102 on 36 degrees of freedom
Multiple R-squared: 0.9723,   Adjusted R-squared: 0.97
F-statistic: 421.1 on 3 and 36 DF, p-value: < 2.2e-16

Based on the above output, the total fuel consumption model is:

Lntotal = -1.9369 + 0.1590 Lnmpu + 0.2148 Lnmpp + 0.7659 Lnjp

This equation can also be written as:

Total fuel consumption = $e^{-1.9369}$. $MPU^{0.1590}$. $MPP^{0.2148}$. $JP^{0.7659}$

The total fuel consumption model of all cities in Java has a model accuracy of 0.9723, meaning 97.23% consumption. Total fuel consumption of all cities in Java is influenced by variables of public passenger cars, private passenger cars, and population. The remaining 2.77% total fuel consumption of all cities in Java is influence by other variables. The resulting model of the influence of the city transportation system, cities in Java toward fuel consumption:

Total fuel $= 0,1441 * MPU^{0.1590} * MPP^{0,2148} * JP^{0,7659}$ (1)

Note:

MPU= public passenger vehicles; MPP= private passenger vehicles; JP= population

From the model (1) above, the city typology variable which is the number of city people has a strong effect on the total fuel consumption. This strong effect is shown through the power value that approaches 1. This means that the cities with a bigger population will have higher total fuel consumption. Public passenger vehicles has an effect on the total fuel consumption, though not too strongly. Public transportation is actually very helpful in controlling fuel consumption because people who use private passenger vehicles can be accommodated by public passenger vehicles. The existing condition shows that the number of public passenger vehicles in each city is generally higher than the number of buses. The bigger the number of public passenger vehicles is, the bigger the total fuel consumption will be. To manage fuel consumption there needs to be a transition from motorcyle/private vehicle usage to public transportation.

Elasticity is measuring the sensitivity of one variable to another variable. In detail, elasticity can be explained as a number which shows the percentage of change happening to one variable as a reaction to each 1 percent rise of another variable (Robert S.P. dan Daniel L.R., 2009). From the above definition, it can be interpreted that one percent change in public passenger vehicles by assuming that the values of private passenger vehicles and population remain constant will cause a change to the total fuel consumption of all cities in Java up to 0.1590 percent. One percent change of private passenger vehicles by assuming that the values of public passenger vehicles and JP remain constant, will change the total fuel consumption of all cities in Java up to 0.2148 percent. One percent of population by assuming that the values of private passenger vehicles and public passenger vehicles remain constant, will change the total fuel consumption of all cities in Java up to 0.7659 percent.

The Effect of public passenger vehicles on Total Fuel Consumption in All Cities

The effect of public passenger vehicles on fuel consumption is measured by using elasticity. An increase of public passenger vehicles of 1 percent causes an increase in the fuel consumption prediction of up to 0.1590 percent. Figure 3 shows the simulation of the effect of the number of public passenger vehicles in the prediction of the Total Fuel Consumption of All Cities in Java.
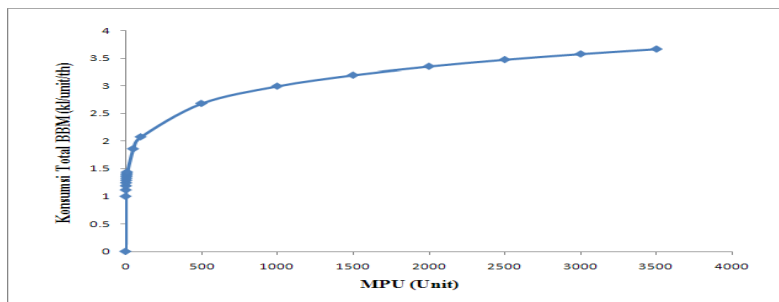
Figure 3. Simulation on the Effect of Public Passenger Vehicles in the Prediction of the Total Fuel Consumption of all Cities in Java

The Effect of Private Passenger Vehicles on Total Fuel Consumption in All Cities

The effect of private passenger vehicles on the total fuel consumption can be measured using elasticity. An increase of private passenger vehicles of 1 percent causes an increase in the fuel consumption prediction of up to 0.2148. Figure 4 shows the simulation of the inflluence of the number of private passenger vehicles in the prediction of the Total Fuel Consumption of all Cities in Java.
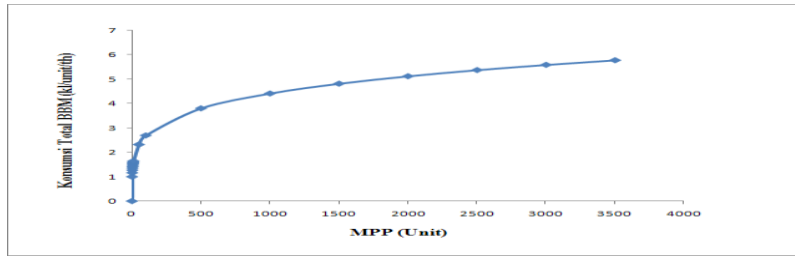
Figure 4. Simulation on the Influence of private passenger vehicles in the Prediction of the Total Fuel Consumption of All Cities in Java

The Effect of Population on the Total Fuel Consumption in All Cities

The effect of population on total fuel consumption can be measured using elasticity. An increase of population of 1 percent causes an increase in the fuel consumption prediction of up to 0.7659. Figure 5 shows the simulation of the inflluence of the number of population in the prediction of the Total Fuel Consumption of all Cities in Java.
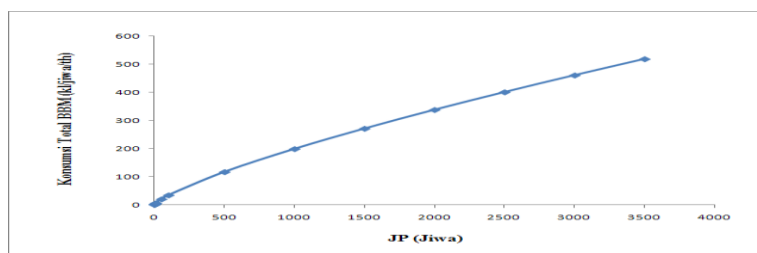
Figure 5. Simulation on the Influence of population in the Prediction of the Total Fuel Consumption of All Cities in Java

Controlling Fuel Consumption

From the results of the above model, the transportation system variables that influence fuel consumption include public passenger vehicles, private passenger vehicles, population. To control fuel consumption due to the public passenger vehicles variable is by changing public passenger vehicles with a larger capacity vehicle/buses/Bus Rapid Transit (BRT), if possible, use *Light Rapid Transit* (LRT) or *Mass Rapid Transit* (MRT). For the private passenger vehicles variable, it is by suppressing the growth of private vehicles (private passenger vehicles and motorcycles), using them as little as possible, providing reliable, qualified and cheap public transportation, setting an age limit on operating vehicles (private passenger vehicles + motorcycles), schools or work provide pick-up services, car-pooling.

The concept of moving people from one place to another from passenger vehicles is based on the people's need to move or the people's presence for certain purposes, not movement of vehicles. Nowadays the people's presence can be exchanged with voices, writing, pictures and activities can still be done. Therefore, to control the fuel consumption due to the population variable is by transforming transportation to information technology, especially passenger transportation. By transforming transportation to information technology, fuel consumers will reduce and activities can still be done in an even shorter time than the transporting process.

Some examples of transforming transportation to information technology are as below:
1) Invitation to various meetings: at the beginning paper invitations were used and sent to each place personally through transportation, later they have been shifted to inviting through short message service (SMS).
2) Booking traveling tickets: it was previously done by visiting personally to travel agents, now people can get tickets on-line without having to travel.
3) Using e-banking: to know the account or savings balance and do transactions can be done without having to go to the bank, but just by using the *e-banking* facility, so the purpose of checking the balance and doing transactions can be completed. The same goes for ATM, people do not have to go to the bank to withdraw money and do transactions, as well as pay monthly water, electricity and telephone bills.
4) Talking through SKYPE, communicating through Facebook and email, people do not need to travel or use transportation.
5) School or work registration, shopping can be done *on-line*.

5. Conclusion

The effect of the city transportation system on the fuel consumption :
1.   Population has a very strong effect on the fuel consumption.
2.   Personal and public vehicles affect the fuel consumption.
3.   The model of the effect of the city transportation system on the total fuel consumption = $0.1441 * MPU^{0.1590} * MPP^{0.2148} * JP^{0.7659}$
5.   Controlling fuel consumption: controlling the fuel consumption by improving qualified and reliable public transportation services, efficient routes, improving city potential, reducing the number of personal vehicles and *land use* arranging, transforming transportation to information technology.

References

1. Aman, Djauhari, *Pedekatan Fungsi Cobb-Douglas dengan Elastisitas Variabel dalam Studi Ekonomi Produksi, Informatika Pertanian*, 1999, Vol 8.
2. Breheny, M., *Sustainable Development and Form Europiean, Research in Regional Science*, 1992, vol 2.
3. Carrol, T.A., *Calculating Community Energy Demand. In Energt and the Community*, edited by R.J. Burby and A. Flemming Bell. Cambridge, MA: Ballinger, 1977.
4. Cheng-Min F., and Cheng-Hsien H., The Implicaion of Transort Diversity for Sustainable Urban Transportation, *Journal of The Eastern Asia Society for Transportation Studies*, 2007, Vol. 7, 1236-1249.
5. Departement ESDM, *Konsumsi Energi di Indonesia*, 2004
6. Departement Perhubungan Darat, *Perencanaan Umum Pengembangan Transportasi Massal di Pulau Jawa*, Jakarta, 2008.
7. Fox John, *Appendix to An R and S-Plus Companion to Applied Regresion, Strutural Equation Models*. 2002.
8. Marcotullio Peter J., Limited Provision of Roads as Botleneck on Vihecle, *Journal Environment and Pollutan vol.30*, no 1, Hunter college CUNY, NY, USA 2007.
9. Miro Fidel, *Perencanaan Transportasi*, Erlangga, Jakarta, 2005.
10. Mudjiastuti Handajani, Model of the Urban Transport System in Java on City Fuel Consumption, *World Academy of Science, Engineering and Technology, an International Journal of Science, Engineering and Technology*, WASET, Cemal Ardil, Paris, issue November 2011.
11. Newman, P.W.G dan Kenworthy J., Gasoline Consumption and Cities : a comparison of us cities with global survey, *Journal of The American Planning Association*, 55: 24-37, 1989.
12. Official Nebraska Goverment Website, *Energy Consumption Transportation Sector*, 2003, Nebraska.
13. Pearece dan Warford, *World Without End,* World Bank, Oxford University Press pp 43-44, 1996.
14. Regional Office for Europe, *Sustainable Consumption and Transport*, United Nations Environment Programme, 2002
15. Robert Q. Riley Enterprise, LLC, *Energy Consumption and The Environment, Impact and Option for Personal Transportation*, Phonix, 2006.
16. Robert, S.P. and Daniel L.R., *Mikroekonomi*, Edisi 6, Jilid 1, P.T. Indeks, Jakarta, 2009
17. Rodrigue Jean-Paul, Transportation and The Environment, Dept. of Economics & Geography Hofstra University, Hempstead, NY, 11549 USA, 2004.
18. Stopher Peter R. dan Meyburg Armin H., Urban Transportation Modelling and Planning, Lexington books, London, 1987.
19. Tim Pemantau dan Evaluasi Kinerja Transportasi nasional (TPEKTN), Urgensi Kebijakan dan Program Komprehensif Dalam Penghematan BBM Transportasi, 2008.
20. World Bank, A Panorama of Urban Mobility Strategies in Developing Countries, Hubert Metge, Aurelie Jehanno, Systra 2006.

FINGERPRINT BASED IGNITION SYSTEM

Karthikeyan.a
(k.c.g college of technology,chennai)
Sowndharya.j
(k.c.g college of technology,chennai)

Abstract
Human identification is field very significant and which has undergone rapid changes with time. An important and very reliable human identification method is fingerprint identification. Fingerprint of every person is unique. So this helps in identifying a person or in improving security of a system.

Finger print of a person is 'read' by a special type of sensor. Finger print sensor can be interfaced with a microcontroller. Through keypad we can add new user and delete the existing user, also identify the user by selecting corresponding option through keypad. In this paper we use a fingerprint module to read once identity to start the equipment. For this we use a microcontroller to enable the ignition system if the matching between scanned data and the already existing data is correct. Comparison is done inside the fingerprint module itself and its output is given to microcontroller. Result is displayed in a LCD display whether the user is authorised or not.

The sensor used is FIM 3030 by NITGEN. Microcontroller used is AT89c52. AT89c52 is a low power, high power CMOS 8 bit microcontroller. It consists of 32 I/O lines. The other main components are the decoder and the latch. The decoder used is DM74LS138 where as the latch used is 74HC373.

Keywords: Sensor, relay, FIM, latch, decoder, LCD.

BLOCK DIAGRAM
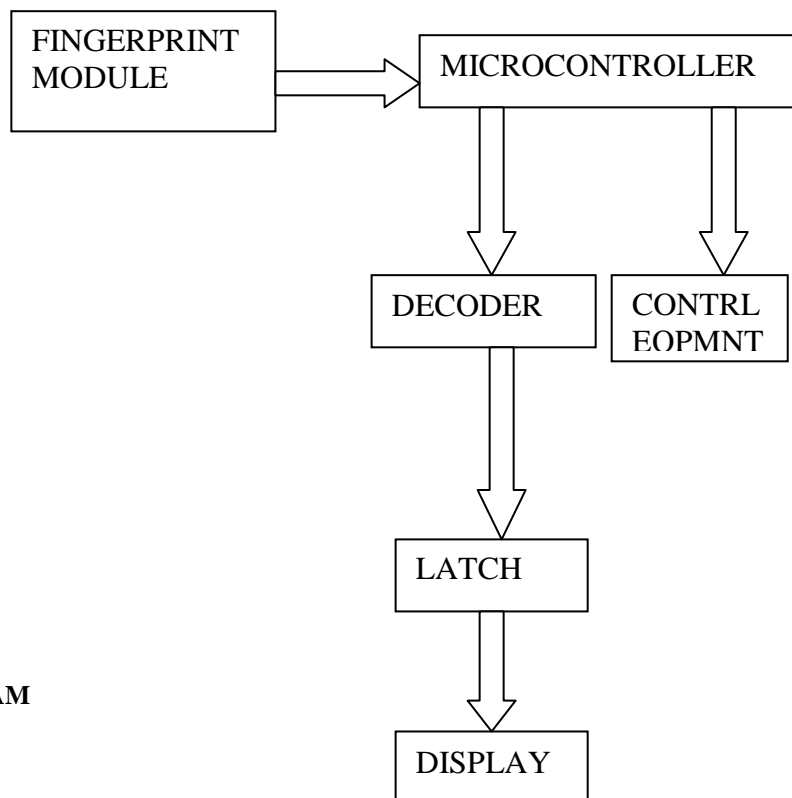
CIRCUIT DIAGRAM
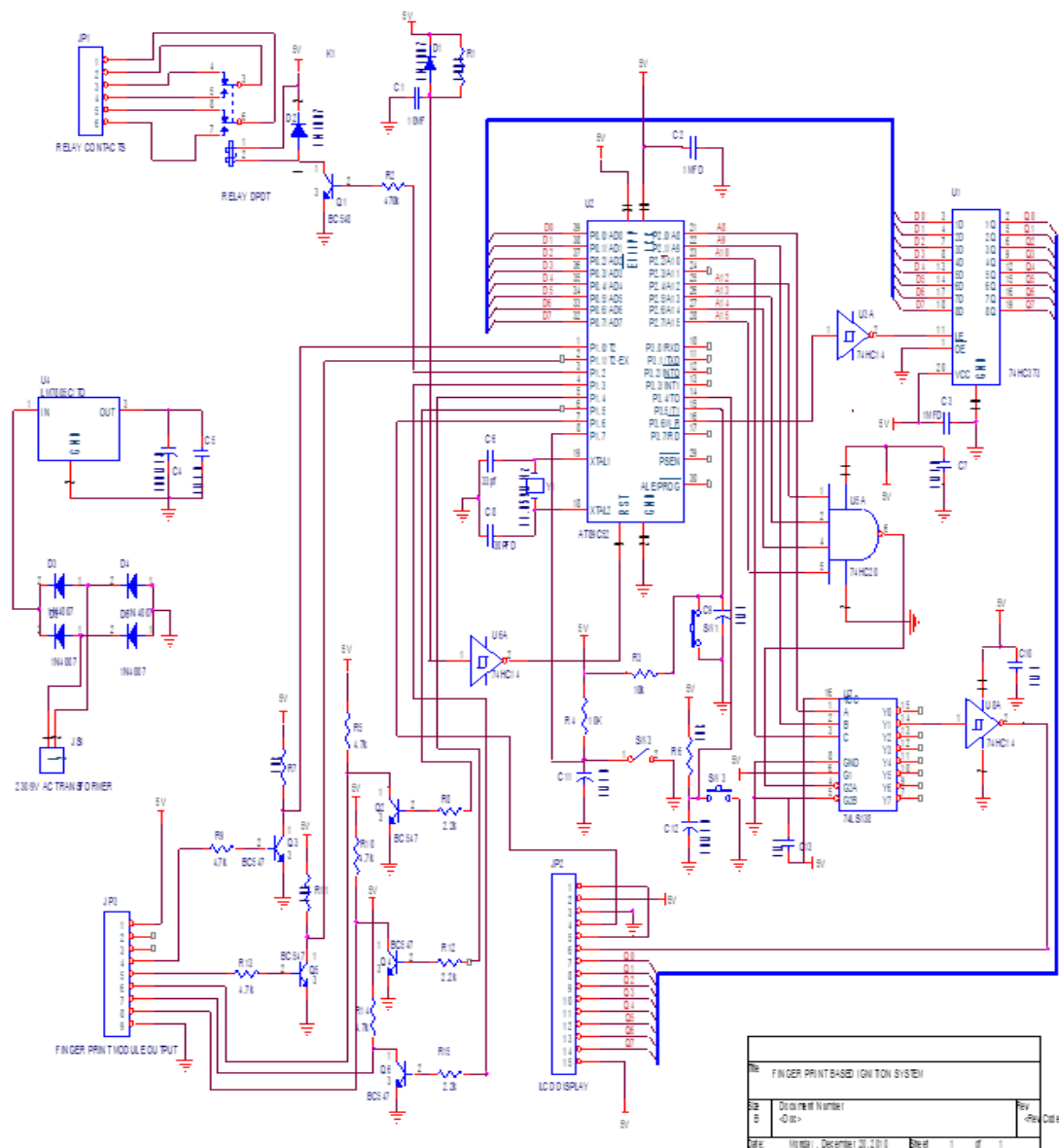
Working

The fingerprint module used here is FIM 3030HV. When a person places his finger on the module, it scans his fingerprint and if he is the first user the module assigns him as master. If another user wants to use this module then he will be regarded as slave.

If a person wants to start the vehicle he has to scan his fingerprint and if the scanned image matches with the one stored in fingerprint module memory then the module give a high signal on its fourth pin, ie the module indicates a success. Otherwise a high signal will be present on the fifth pin of fingerprint module, ie it indicates a failure (user does not exist).

When a high on fourth pin is observed, it will cause microcontroller to activate the ignition circuit.

When a high on fifth pin is observed, that is a failure so microcontroller will not activate the ignition circuit.

When a success is observed, a LCD display will show that the matching is correct and if it is failure then incorrect matching will be observed on the LCD display.

MAIN COMPONENTS OF THE CIRCUIT
MICROCONTROLLER

AT89C52

```
         (T2)  P1.0 ▭ 1        40 ▭ VCC
      (T2 EX)  P1.1 ▭ 2        39 ▭ P0.0  (AD0)
               P1.2 ▭ 3        38 ▭ P0.1  (AD1)
               P1.3 ▭ 4        37 ▭ P0.2  (AD2)
               P1.4 ▭ 5        36 ▭ P0.3  (AD3)
               P1.5 ▭ 6        35 ▭ P0.4  (AD4)
               P1.6 ▭ 7        34 ▭ P0.5  (AD5)
               P1.7 ▭ 8        33 ▭ P0.6  (AD6)
                RST ▭ 9        32 ▭ P0.7  (AD7)
        (RXD)  P3.0 ▭ 10       31 ▭ EA/VPP
        (TXD)  P3.1 ▭ 11       30 ▭ ALE/PROG
       (INT0)  P3.2 ▭ 12       29 ▭ PSEN
       (INT1)  P3.3 ▭ 13       28 ▭ P2.7  (A15)
         (T0)  P3.4 ▭ 14       27 ▭ P2.6  (A14)
         (T1)  P3.5 ▭ 15       26 ▭ P2.5  (A13)
         (WR)  P3.6 ▭ 16       25 ▭ P2.4  (A12)
         (RD)  P3.7 ▭ 17       24 ▭ P2.3  (A11)
              XTAL2 ▭ 18       23 ▭ P2.2  (A10)
              XTAL1 ▭ 19       22 ▭ P2.1  (A9)
                GND ▭ 20       21 ▭ P2.0  (A8)
```
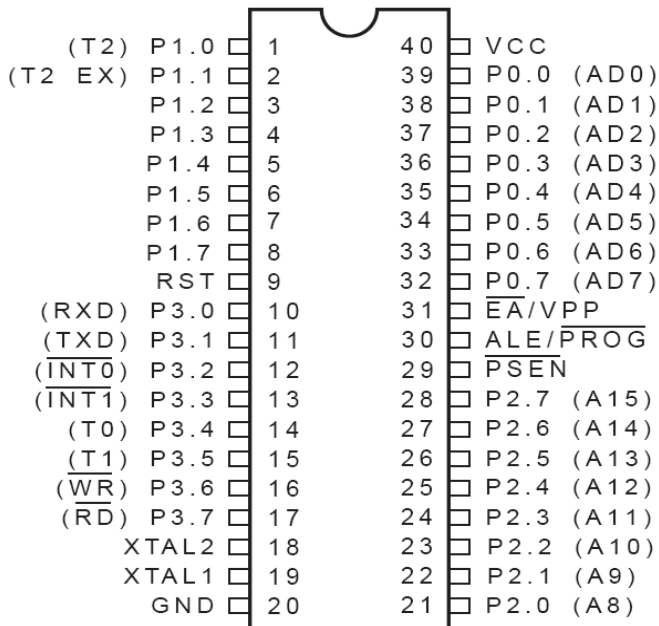
Description

A microcontroller is a complete microprocessor system built on a single IC. Microcontrollers were developed to meet a need for microprocessors to be put into low cost products. Building a complete microprocessor system on a single chip substantially reduces the cost of building simple products, which use the microprocessor's power to implement their function, because the microprocessor is a natural way to implement many products. This means the idea of using a microprocessor for low cost products comes up often.

The microcontroller contains full implementation of a standard MICROPROCESSOR, ROM, RAM, I/0, CLOCK, TIMERS, and also SERIAL PORTS. Microcontroller also called "system on a chip" or "single chip microprocessor system" or "computer on a chip".

A microcontroller is a Computer-On-A-Chip, or, if you prefer, a single-chip computer. Micro suggests that the device is small, and controller tells you that the device' might be used to control objects, processes, or events. Another term to describe a microcontroller is embedded controller, because the microcontroller and its support circuits are often built into, or embedded in, the devices they control.

The AT89C52 is a low power, high performance CMOS 8 bit microcomputer with 8kB of flash programmable and erasable read only memory (PEROM). The device is manufactured using Atmel's high density non-volatile memory technology and is compatible with the industry standard 80C51 and 80C52 instruction set and pin out. The on-chip Flash allows the program memory to be reprogrammed in-system or by a conventional non-volatile memory programmer. By combining a versatile a 8 bit CPU with flash on a monolithic chip, the Atmel AT89C52 is a powerful microcomputer which provides a highly flexible and cost effective solution to many embedded control applications.

Port 0

Port 0 is an 8-bit open drain bidirectional I/O port. As an output port, each pin can sink eight TTL inputs.

Port 1

Port 1 is an 8-bit bidirectional I/O port with internal pullups. The Port 1 output buffers can sink/source four TTL inputs.

Port 2

Port 2 is an 8-bit bidirectional I/O port with internal pullups. The Port 2 output buffers can sink/source four TTL inputs.

Port 3

Port 3 is an 8-bit bidirectional I/O port with internal pullups. The Port 3 output buffers can sink/source four TTL input

FINGERPRINT MODULE
FIM 3030HV
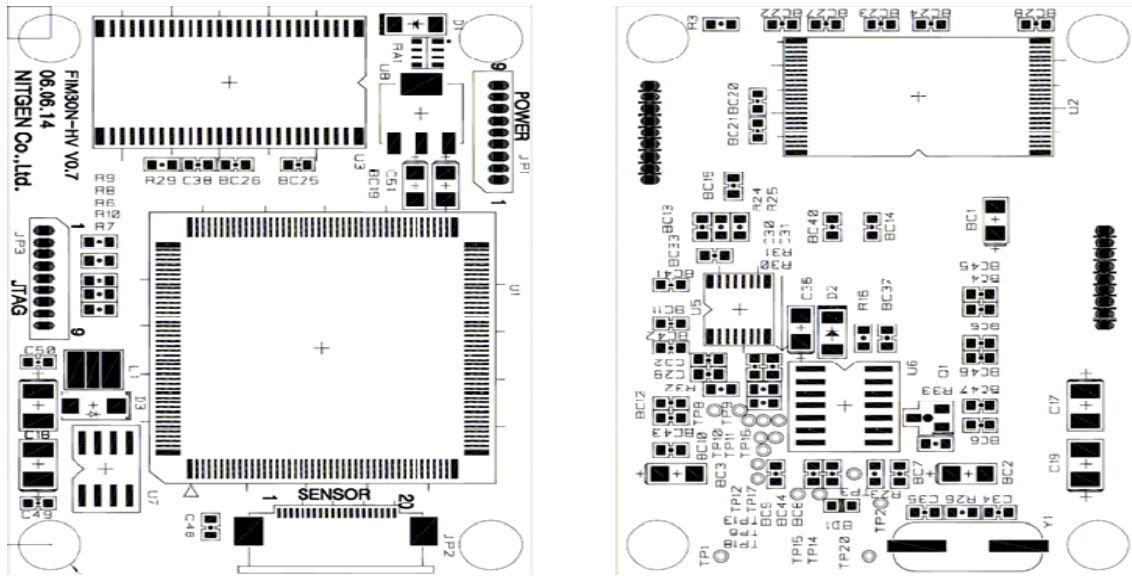
When a user places their finger on NITGEN's Fingerprint Recognition Device (FRD) for the first time, the fingerprint is scanned and a 3-D fingerprint image is captured. All fingerprints contain a number of unique physical characteristics called minutiae, which includes certain visible aspects of fingerprints such as ridges, ridge endings, and bifurcation (forking) of ridges. Most of the minutiae are found in the core points of fingerprints, and the core points themselves are found near the centre of the fingerprint on the fleshy pad. Figure shows the positions of core points within fingerprints.

The user is enrolled, or registered, in the database after a special minutiae-based algorithm extracts key minutiae points from the live image at the time of acquisition and converts the data into a unique mathematical template comparable to a 60-digit password. This unique template is then encrypted and stored – it is important to note that no actual image of the fingerprint is stored, only the minutiae-based template. The next time a new fingerprint image for an individual is scanned by the FRD, another template is created and the two templates are compared to verify the user's identity.

Operations performed by fim 3030hv

VERIFICATION- This command is used to verify user with the ID number. If the host request user verification with the number, the device checks if the ID number exists in user DB. If the ID number exists in user DB, the device scans fingerprint image through the sensor module. After internal processing, matching results is returned to the host.

IDENTIFICATION- the command is used to verify user with the ID number, the device scans the fingerprint image through the sensor module. The device searches DB for user matched with input fingerprint. If there exists the matched user, the device returns that user ID number to the host. Otherwise the device returns failed result.

INSTANT MATCHING- This command is used to match template data with input fingerprint. If the host requests instant matching with template data, the device matches those with fingerprint scanned through sensor module, and return result to the host.

GET TEMPLATE- The device returns template data get from the image scanned through sensor.

CANCEL- The device cancels current processing task such as verification, Identification and so on and returns result caused by cancel to a host.

INSTANT VERIFICATION -This command is used to verify user with the ID   and the fingerprint data. It is similar to Verification except that Instant verification gets fingerprint data from host instead of the sensor module.

ENROLL FP1 -This command is used to add new user. The host requests enrolment of user with the ID number. The device checks if the ID number exists in DB. If the same ID number does not exist, the device gets the first fingerprint image through sensor module and returns the success of the first step. Then, the host requests another image capture. A device gets the second fingerprint image, save the new user to DB, and returns the success of the second step. This command is available only in 'Master Mode'. This command will be obsolete, Instead, use 'Register FP' command.

DELETE FP -This command is used to delete user. The host requests the deletion of user with the ID number. The device checks if the ID number exists in DB. And if the same ID number exists, the device deletes the user from DB, and returns results to the host. This command is available only in 'Master Mode'.

Power supply

The ac voltage, typically 220V rms, is connected to a transformer, which steps that ac voltage down to the level of the desired dc output. A diode rectifier then provides a full-wave rectified voltage that is initially filtered by a simple capacitor filter to produce a dc voltage. This resulting dc voltage usually has some ripple or ac voltage variation.

A regulator circuit removes the ripples and also remains the same dc value even if the input dc voltage varies, or the load connected to the output dc voltage changes. This voltage regulation is usually obtained using one of the popular voltage regulator IC units.

Block diagram
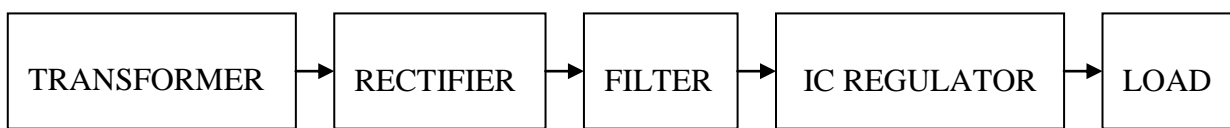
When four diodes are connected as shown in figure, the circuit is called as bridge rectifier. The input to the circuit is applied to the diagonally opposite corners of the network, and the output is taken from the remaining two corners. Let us assume that the transformer is working properly and there is a positive potential, at point A and a negative potential at point B. the positive potential at point A will forward bias D3 and reverse bias D4. The negative potential at point B will forward bias D1 and reverse D2. At this time D3 and D1 are forward biased and will allow current flow to pass through them; D4 and D2 are reverse biased and will block current flow. The path for current flow is from point B through D1, up through RL, through D3, through the secondary of the transformer back to point B. this path is indicated by the solid arrows. Waveforms (1) and (2) can be observed across D1 and D3.One-half cycle later the polarity across the secondary of the transformer reverse, forward biasing D2 and D4 and reverse biasing D1 and D3. Current flow will now be from point A through D4, up through RL, through D2, through the secondary of T1, and back to point A. This path is indicated by the broken arrows. Waveforms (3) and (4) can be observed across D2 and D4. The current flow through RL is always in the same direction. In flowing through RL this current develops a voltage corresponding to that shown waveform (5). Since current flows through the load (RL) during both half cycles of the applied voltage, this bridge rectifier is a full-wave rectifier.

IC voltage regulators

Voltage regulators comprise a class of widely used ICs. Regulator IC units contain the circuitry for reference source, comparator amplifier, control device, and overload protection all in a single IC. IC units provide regulation of either a fixed positive voltage, a fixed negative voltage, or an adjustable set voltage. The regulators can be selected for operation with load currents from hundreds of milli amperes to tens of amperes, corresponding to power ratings from milli watts to tens of watts.
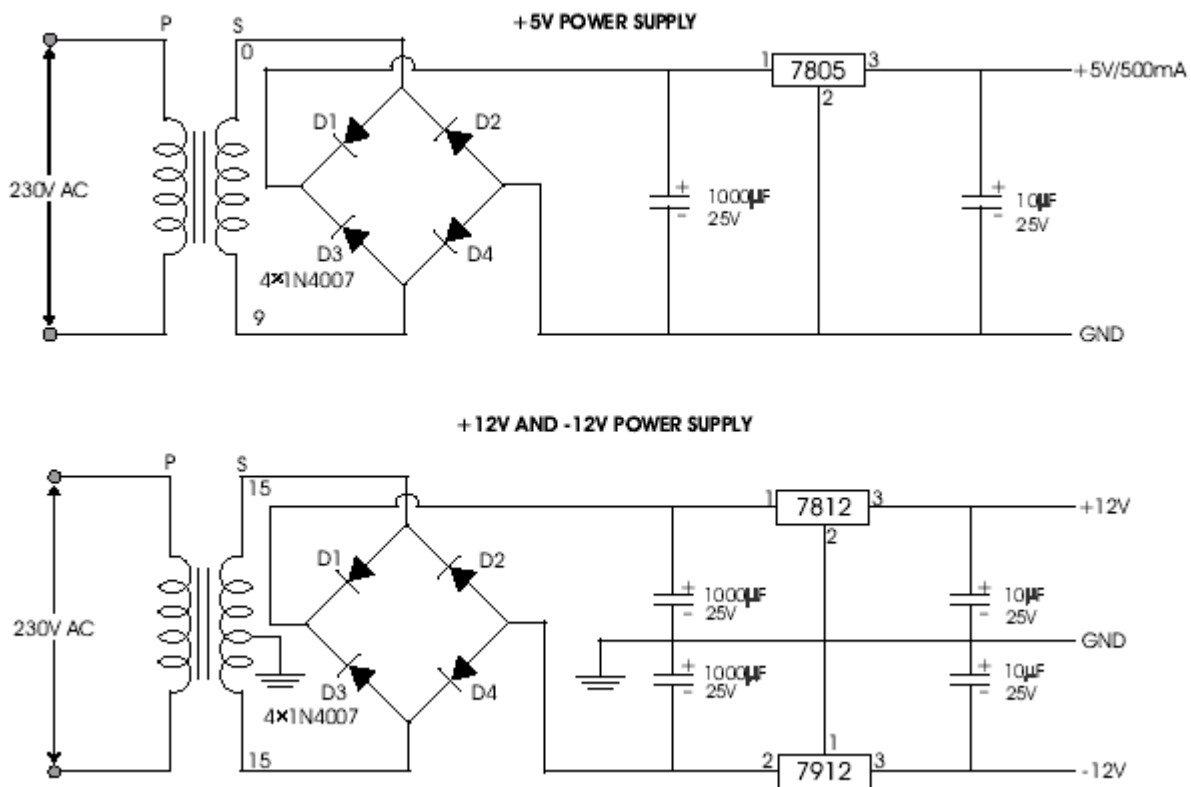
Circuit diagram (Power supply)

A fixed three-terminal voltage regulator has an unregulated dc input voltage, Vi, applied to one input terminal, a regulated dc output voltage, Vo, from a second terminal, with the third terminal connected to ground. The series 78 regulators provide fixed positive regulated voltages from 5 to 24 volts. Similarly, the series 79 regulators provide fixed negative regulated voltages from 5 to 24 volts.

DECODER
DM74LS138
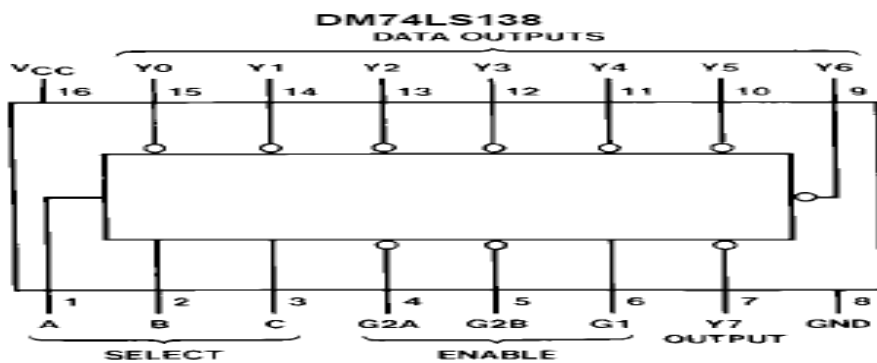
Description:
These schottky – clamped circuits are designed to be used in high – performance, memory – decoding or data routing applications, requiring very short propagation delay times. In high – performance memory systems these decoders can be used to minimize the effects of system decoding. When used with high speed memories, the delay times of these decoders are usually less than the typical access time of the memory. This means the effective system delay introduced by the decoder is negligible.
The DM74LS138 decodes one-of-eight lines, based upon the conditions at the three binary select inputs and the three enable inputs. Two active-low and one active-high enable inputs reduce the need for external gates or inverters when expanding. A 24-line decoder can be implemented with no external inverters, and a 32-line decoder requires only one inverter. An enable input can be used as a data input for demultiplexing applications.

LATCH
74HC373
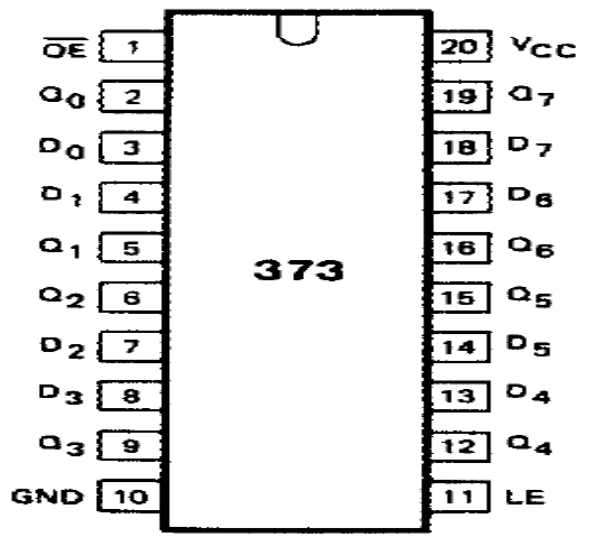
Description:

The 74HC/HCT373 are high-speed Si-gate CMOS devices and are pin compatible with low power Schottky TTL (LSTTL). The 74HC/HCT373 are octal D-type transparent latches featuring separate D-type inputs for each latch and 3-state outputs for bus oriented applications. A latch enable (LE) input and an output enable (OE) input are common to all latches.

The "373" consists of eight D-type transparent latches with 3-state true outputs. When LE is HIGH, data at the D inputs enters the latches. In this condition the latches are transparent, i.e. a latch output will change state each time its corresponding D-input changes. When LE is LOW the latches store the information that was present at the D-inputs a set-up time preceding the HIGH-to-LOW transition of LE. When OE is LOW, the contents of the 8 latches are available at the outputs. When OE is HIGH, the outputs go to the high impedance OFF-state. Operation of the OE input does not affect the state of the latches.

RELAY
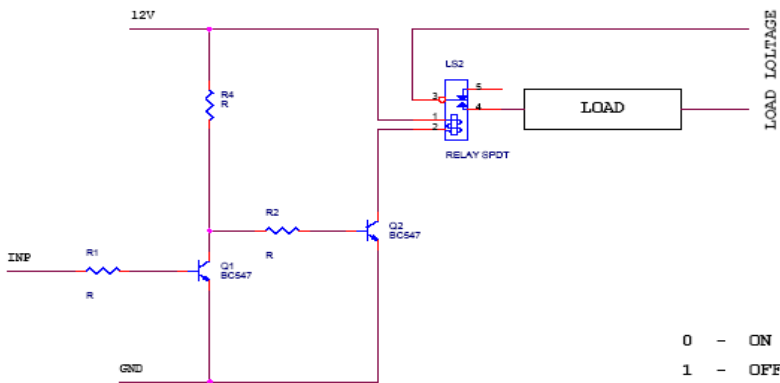
Relay:

A relay is an electrically operated switch. Current flowing through the coil of the relay creates a magnetic field which attracts a lever and changes the switch contacts. The coil current can be on or off so relays have two switch positions and they are doublethrow (changeover) switches. Relays allow one circuit to switch a second circuit which can be completely separate from the first. For example a low voltage battery circuit can use a relay to switch a 230V AC mains circuit. There is no electrical connection inside the relay between the two circuits; the link is magnetic and mechanical.

The coil of a relay passes a relatively large current, typically 30mA for a 12V relay, but it can be as much as 100mA for relays designed to operate from lower voltages. Most ICs (chips) cannot provide this current and a transistor is usually used to amplify

the small IC current to the larger value required for the relay coil. The maximum output current for the popular 555 timer IC is 200mA so these devices can supply relay coils directly without amplification.

Relays are usually SPDT or DPDT but they can have many more sets of switch contacts, for example relays with 4 sets of changeover contacts are readily available. Most relays are designed for PCB mounting but you can solder wires directly to the pins providing you take care to avoid melting the plastic case of the relay. The animated picture shows a working relay with its coil and switch contacts. You can see a lever on the left being attracted by magnetism when the coil is switched on. This lever moves the switch contacts. There is one set of contacts (SPDT) in the foreground and another behind them, making the relay DPDT.
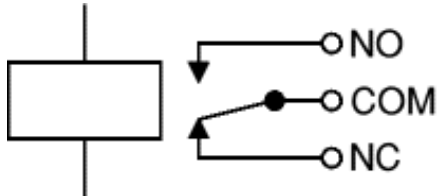
The relay's switch connections are usually labelled COM, NC and NO:
COM = Common, always connect to this, it is the moving part of the switch.
NC = Normally Closed, COM is connected to this when the relay coil is **off**.
NO = Normally Open, COM is connected to this when the relay coil is **on**.

Lcd :
Liquid crystal displays (LCDs) have materials, which combine the properties of both liquids and crystals. Rather than having a melting point, they have a temperature range within which the molecules are almost as mobile as they would be in a liquid, but are grouped together in an ordered form similar to a crystal.

An LCD consists of two glass panels, with the liquid crystal material sand witched in between them. The inner surface of the glass plates are coated with transparent electrodes which define the character, symbols or patterns to be displayed polymeric layers are present in between the electrodes and the liquid crystal, which makes the liquid crystal molecules to maintain a defined orientation angle.

One each polarizes are pasted outside the two glass panels. These polarizes would rotate the light rays passing through them to a definite angle, in a particular direction. When the LCD is in the off state, light rays are rotated by the two polarizes and the liquid crystal, such that the light rays come out of the LCD without any orientation, and hence the LCD appears transparent.

Conclusion:
Thus fingerprint identification enhances the security of a vehicle and makes it possible only for some selected people to start the car. Thus by implementing this relatively cheap and easily available system on a car one can ensure much greater security and exclusivity than that offered by a conventional lock and key.
In actual case a success would initiate a trigger in the spark plug. But due to limitation in initiating a spark plug and due to safety reason a prototype has been developed here. The output can be seen using an LED.

Bibliography:
[1] Lin Hong. "Automatic Personal Identification Using Fingerprints", Ph.D. Thesis, 1998.
[2] D.Maio and D. Maltoni. "Direct gray-scale minutiae detection in fingerprints" IEEE Trans. Pattern Anal. And Machine Intel., 19(1):27-40, 1997.
[3] Jain, A.K., Hong, L., and Bolle, R.(1997), "On-Line Fingerprint Verification," IEEE Trans. On Pattern Anal and Machine Intell, 19(4), pp. 302-314.
[4] N. Ratha, S. Chen and A.K. Jain, "Adaptive Flow Orientation Based Feature Extraction in Fingerprint Images", Pattern Recognition, Vol. 28, pp. 1657-1672, November 1995.
[5] Alessandro Farina, Zsolt M.Kovacs-Vajna, Alberto leone, "Fingerprint minutiae extraction from skeletonized binary images, Pattern Recognition", Vol.32, No.4, pp877-889, 1999.

An Appraisal of Mobile Technology

EktaAgrawal*[1], Anupam Yadav[2], Pragati Gupta[3]

(Assistant Professor, E & C Engineering Department)
MIT, Moradabad

Introduction

From ancient to modern times, mankind has been looking for means of long distance communications. For centuries, letter proved to be the most reliable means to transmit information. Fire, flags, horns etc. were used to transmit information faster. Technical improvement in 19th century simplified long distance communications with use if telegraphy and telephony. Both techniques were used for wired communication. In 1873, J.C. Maxwell laid the foundation of electromagnetic theory by summarizing empirical results in four equations, which are still valid today.[1] It however took several decades before Marconi made economic use of this theory by developing devices for wireless transmission of Morse signal took place. Voice was transmitted for the first time in 1906 and one of the first radio broadcast transmission was done in 1909 in New York.

Keywords: Mobile generations, 1G, 2G, 3G, Advantages, Limitations

History of Mobile Communication-

The history and status of mobile communications are shortly listed in the following, together with the respective evaluations on the chief contributions.

1) Traditionally, wireless systems were considered as anauxiliary approach that was used in regions where it wasdifficult to build a connection by wireline.

2) 1G was based on analogy technique and deployed in the1980s. It built the basic structure of mobile communicationsand solved many fundamental problems, e.g. cellulararchitecture adopting, multiplexing frequency band, roamingacross domain, non-interrupted communication in mobilecircumstances, etc. Speech chat was the only service of 1G.

3) 2G was based on digital signal processing techniquesand regarded as a revolution from analog to digitaltechnology, which has gained tremendous success during1990s with GSM as the representative. The utilization of SIM(Subscriber Identity Module) cards and support capabilitiesfor a large number of users were 2G's main contributions

4) 2.5G extended the 2G with data service and packetswitching methods, and it was regarded as 3G services for 2Gnetworks. Under the same networks with 2G, 2.5G broughtthe Internet into mobile personal communications.

5) 3G is deploying a new system with new services instead of only providing higher data rate and broader bandwidth. Based on intelligent DSP techniques, various multimedia data communications services are transmitted by convergent 3G networks.

Table 1 summarizes the entire development of mobile communications with the properties of each generation including starting time, driven technique, representative standard, radio frequency, bandwidth, multi-address technique, cellular coverage, core networks, and service type.

Property	1G	2G	2.5G	3G
Starting Time	1985	1992	1995	2002
Driven Technique	Analogue signal Processing	Digital signal Processing	Packet switching	Intelligent signal processing
Representative Standard	AMPS, TACS, NMT	GSM, TDMA	GPRS, I-Mode, HSCSD, EDGE	IMT-2000 (UMTS, WCDMA, CDMA2000)
Radio Frequency (HZ)	400M-800M	800M-900M	1800M-1900M	2G
Bandwidth (bps)	2.4K-30K	9.6K-14.4K	171K-384K	2M-5M
Multi-address Technique	FDMA		TDMA , CDMA	CDMA
Cellular Coverage	Large area		Medium area	Small area
Core Networks	Telecom networks	Telecom networks		Telecom networks, Some IPnetworks
Service Type	Voice Mono-servicePerson-to-person	Voice, SMS Mono-media Person-to-person	Data service	Voice, Data Some Multimedia Person-to-machine

Table1: Generation and development of mobile communication

Limitations of 3G

3G still leaves some unsolved problems that it does not concern or concerns only partly. The limitations and difficulties of 3G include:

- Difficulty in continuously increasing bandwidth and high data rate to meet multimedia services requirements, together with the coexistence of different services needing different QoS and bandwidth.
- Limitation of spectrum and its allocation.
- Difficult to roam across distinct service environment in different frequency bands.
- Lack of end-to-end seamless transport mechanism spanning a mobile sub-network and a fixed one.

The development trends of mobile communications can The development trends of mobile communications can besummarized by the improvement of three aspects, includingnetwork area, e.g. data rate, bandwidth, and networkcapacity; mobility field, e.g. mobile spatial range, speed,coverage ability; and service property, e.g. services quantity,quality, cost, and category.

Limitation of 3G in India

- With WCDMA based 3G, as the data speed increases the coverage area of the cell become smaller and smaller. For data rates of 2 Mbps and above, a WCDMA cell can cover only an area of 10 meter radius i.e. about 300 sq. meters. Therefore, to provide 2Mbps data connectivity to an Airport terminal of say, 600-meter square (360,000 Sq.Mtr.), there should be 1200 W-CDMA cells.

- There has been some improvement with HSPDA, but still it is impossible to connect these by wireless links in cellular technology and therefore, will have to use Optical Fiber cable connectivity / PON up to the Cell terminal. In this situation the wireless portion of the network is only at the end link of 10 meter that can be better managed with alternate technology terminals and higher reach by WiMax / WiFi wireless system.

- As far as mobility is concerned; using W-CDMA cells, with increase in data rate the speed of movement of user terminal also become lesser and lesser. For 2Mbps, the speed of movement will be limited to 10 meters /second, i.e. A vehicle moving at 36 K.M per hour. Intricacy of 'hand over' at every 20 to 25 meters is also innumerable. Its products can generate. Volume can be built only when the product is available, accessible and affordable to community who are interested in such products.

- The success of any business comes from the volume its products can generate. Volume can be built only when the product is available, accessible and affordable to community who are interested in such products.

4G Review-

Different 4G feature frameworks have been defined from the standpoints of service subscriber, service provider, researcher and engineer. In the following we give some representatives of 4G perspectives.

1) It is easy to say, based on the developing trends of mobile communication, that 4G will have broader bandwidth, higher data rate, smoother and quicker handoff, wider mobile area, more various service, lower cost, etc. Obviously these ideas do not make too much sense as such.

2) Other than the words "more", "any" and/or "all" are preferred over expressions used by some others, e.g. anyone can communicate with anyone else, anywhere and anytime, or enjoy any service of any network operator, through any network of any network service provider. These sentences are truly attractive from a subscriber's viewpoint, and they sound quite like advertisements or word games.

3) DoCoMo introduced the concept of MAGIC for the vision of 4G [2]: Mobile multimedia; anytime, anywhere, anyone; Global mobility support; integrated wireless solution; and Customized personal service, which mostly focused on public systems and treat 4G as the extension of 3G cellular service.

4) European Commission (EC) presented a perspective focusing on ensuring seamless service provisioning across a multitude of wireless systems and networks, and providing for optimum delivery via the most efficient network available. Further discussion did continuous promotion around 4G concepts [3-5], e.g. private systems and ad-hoc networks, optimal resource utilization, multiple radio interfaces, WLAN use, standards for interoperability, etc.

5) A broader, all-encompassing perspective of 4G was proposed in [6], according to which 4G will encompass all systems from public to private, operator-driven to ad-hoc, broadband to personal area and ad hoc networks, 2G systems to 3G systems. It focused mainly on personalized services.

It is amusing to see that it is quite easy for anyone to give a prediction on some 4G characteristics, whereas it is more difficult to provide an exhaustive description and sufficient investigations, especially on the support of advanced techniques.

Features in 4G
1) User Diversity:
The external diversity of users, i.e. people in different situations, includes e.g. culture, educational background, economic capability, physical property, personal preference, etc. The internal diversity of users, i.e. people with different interfaces, include e.g. vision, hearing, speech, touch sense, hands and fingers, body, etc. Note that as for users, both their external and internal diversity are to be adapted by the other two targets: terminal and application. Moreover, for adapting the two kinds of user diversity, both the external and internal diversity of terminals and applications are the solution.

2) Terminal Diversity and Adaptability:
The terminals' external diversities are the differences of terminals in both static and mobile attributes. Static attributes include e.g. functionality, weight, size, battery life, human interface, antenna, processing capability, security, style, and cost. Mobile attributes include dynamic attributes of both temporal and spatial features. The former category contains e.g. moving speed and acceleration, along with stationary, pedestrian or vehicular qualities, while the latter is connected to spatial range, e.g. indoors, on-campus, in urban and rural environments, and also direction. The internal diversity of terminals means that one terminal may integrate multiple functions, modes, interfaces, flexibilities etc. There are three targets for terminal adaptability. For users, it includes the provision of different terminals to satisfy different users and an individual user's various requirements. As for applications, we hope that miscellaneous services can be delivered to one single terminal. When networks are concerned, a single terminal can reach a wide range of networks despite of location and mobile rate.

3) Network Diversity and Adaptability:
The external diversity of networks is obvious. Internet is assorted by nature, while wireless networks keep the same property. For instance air interfaces can integrate all kinds of standards and work on different frequencies. Moreover, multiple operators deploy networks with multiple standards and protocols. The internal diversity of networks means that one network can interconnect with other different networks and transfer various kinds of loads, e.g. cellular systems with coverage. Three targets are related to network adaptability. In reference to terminals, network adaptability aims to make multiform mobile devices with a wide range of moving speeds and mobile areas connectable to wireless networks. For applications, there is a requirement that any type and/or quality of service can be delivered through diverse fixed and mobile networks in the most suitable and efficient way. Thetarget for networks themselves is to make it easy to build a new network or remove an old one, and to make interoperability with one's neighbors seamless despite its heterogeneous nature.

4)Application Diversity and Adaptability:
The external diversity of applications will be a reasonable property, and this need not mean that 4G services and applications must be multifarious, in all the aspects of quantity, quality, and type. With internal diversity we mean that one application can be tailored into e.g. multiple levels of quality, various styles, and different kinds of release shape, etc. Application adaptability is a main feature of 4G services. To users, this means that services can be delivered automatically according to personal preferences of different users. In view of terminals, we hope that various terminals are able to run one application with different formats, such as e-mail in text message, voice, image, or even video. In connection with networks, applications can be transformed into various forms and levels in order to be transmitted correctly and efficiently.

Advantages of 4G (Next Generation Mobile Technology)-
• 3G/4G visions take into account installed base and past investments.
• Strong position of telecommunications vendors expected in the marketplace.
• Faster data transmission and higher bit rate and bandwidth, allow more business applications and commercialization.
• Has advantage for personalized multimedia communication tools.

Conclusion
This paper presents 4G visions from a technical perspective. 4G is esteemed to possess benefits such as high usability providing accessibility anytime and anywhere through a range of technologies, increased data transfer speed, improved quality of service, and wide variety of interactive services. The success of Second-generation (2G) mobile systems in the previous decade prompted the development of third-generation (3G) mobile systems. While 2G systems such as GSM, IS-95, and cdmaOne were designed to carry speech and low-bit-rate data, 3G systems are designed to provide higher data-rate services. A range of wireless systems including GPRS, IMT-2000, Bluetooth, WLAN and HiperLAN have been developed with their own merits and demerits targeting different service types, data rates, and users. However, no single efficient system exists for integration of all these technologies. 4G system that integrates existing and newly developed wireless systems is in incipient stage and international standards do not exist.
Future wireless networks will need to support diverse IP multimedia applications to allow sharing of resources among multiple users. There must be a low complexity of implementation and an efficient means of negotiation between the end users and the

wireless infrastructure. The fourth generation promises to fulfill the goal of PCC (personal computing and communication)—a vision that affordably provides high data rates everywhere over a wireless network.

References

[1]. B.G. Evans and K. Baughan, "Visions of 4G," *Electronics & Communication Engineering Journal*, Vol. 12, No. 6, pp. 293–303, Dec. 2000.

[2]. K. Murota, NTT DoCoMo, "Mobile communications trends in Japan and NTT DoCoMo's activities towards 21st century," in ACTS Mobile Summit99, Sorrento, Italy, June 1999.

[3]. J. Silva, European Commission, "Beyond IMT-2000," in *ITU-R WP8F workshop*, Geneva, Mar. 2000.

[4]. F. Williams, Ericsson, "Fourth generation mobile," in *ACTS Mobile Summit99*, Sorrento, Italy, June 1999.

[5]. H. Huomo, Nokia, "Fourth generation mobile," in ACTS Mobile Summit99, Sorrento, Italy, June 1999.

[6]. J. M. Pereira, "Fourth generation: now, it is personal," in *Proc.11th IEEE Int.Symp.Personal, Indoor and Mobile Radio communications,* London, UK, Sep. 2000, Vol. 2, pp. 1009–1016.

A User Friendly Guide for Spleen Ultrasound Image Enhancement

Nasrul Humaimi Mahmood, Wan Fairuz Jamilah Wan Mohd Ridzwan, Norshazwana Mat Taib and Ismail Ariffin

Bio-Medical Instrumentation and Electronic Research Group
Faculty of Electrical Engineering, Universiti Teknologi Malaysia
81310 UTM Johor Bahru, Johor, MALAYSIA.

Abstract: -
 Spleen ultrasound screening was rarely used because usually people will scan their body thoroughly using CT scan or x-ray to observe any abnormalities. However, it is a fact that ultrasound machine is far safer than any other imaging modalities, and it can be used to scan any parts of the body except for hard tissue such as bone. In this paper, we proposed an approach to obtain spleen ultrasound image and perform image quality enhancement so that the image of spleen is clearer and easier to analyze. The used method is Region of Interest based image filtering using a MATLAB. The Graphical User Interface (GUI) of the work is also created to have user friendly analysis. This approach is really suitable for new learners to learn one of the biomedical image processing techniques. From the results, it shows that this method can enhance the image quality especially at the region of interest specified.

Keywords: - Spleen Ultrasound, Image Enhancement, MATLAB, Region of Interest, GUI

1 Introduction

Ultrasound is one of the diagnostic equipments to diagnose human internal organs, tendons, to capture their size and structure. Ultrasound is usually used for pregnancy, as the images for others' internal organs that are not very clear. Typically, the image of ultrasound is depending on the operator view. Hence, the purpose of this work is to help operator view to get a clear image of ultrasound and could be use not only for viewing the fetus in mother's womb but to view other soft organs or abnormalities in the human body. Since ultrasound is the safest imaging modalities compared to other image modalities, so it would be very safe to diagnose patient. This work will focus on spleen as a subject or soft tissue that taken from human via ultrasound. One of the problems of spleen ultrasound image is how to get a clear view of spleen since a normal size spleen is hard to be seen in the ultrasound image. It is good to examine with the patient rolled onto the right side at a 45-90° angle and in the left-side-up decubitus position. Region of Interest (ROI) mask, ROI Filter, Histogram Equalization and Active contour techniques from MATLAB is used to get a clearer spleen image.

2 Literature Review

The spleen is a soft, blood-rich organ that filters blood and the largest lymphoid organ in the body and interposed within the circulatory system. The spleen lies in left hypochondrium behind the stomach, above the left colic flexure and to the side (laterally) of the left kidney. It lies underneath the diaphragm, in front and to the side of the left 9th to 11th, sometimes 12th ribs. The size of spleen is about the size of a cupped hand. The length is approximately 10 cm, the width is approximately 5 cm and the spleen is about 3-4 cm thick. The weight of the spleen may vary between 150 to 200 grams (5 to 7 ounces) [1].

Enlarged Spleen (splenomegaly) is one of the spleen diseases. An enlarged spleen can be caused by infections, cirrhosis and other liver diseases, blood diseases characterized by abnormal blood cells, problems with the lymph system, or other conditions. It may be caused by Viral infections, such as mononucleosis, parasitic infections, such as toxoplasmosis, bacterial infections, such as endocarditis (an infection of heart's valves), Leukemia, Lymphoma (a cancer of lymph tissue, such as Hodgkin's disease), sickle-cell anemia, sarcoidosis, malaria, bacterial andocarditis, pernicious anemia, leishmaniasis, Banti's disease, hereditary spherocytosis, glandular fever and tumors. Figure 1(a) and (b) are the comparison between mild splenomegal with normal spleen [1].

(a)   (b)

Figure 1: (a) Normal Spleen. (b) Longitudinal view of the spleen shows mild splenomegal (length 13cm) due to infectious mononucleosis and a typical splenunculus at the hilum.

Usually, a normal sized spleen is hard to be seen in ultrasound image however it is best examined with the patient rolled onto the right side at a 45-90° angle, in the left-side-up decubitus position [2-3].

3   Material and Methods
There were several processes involved in this work. Generally, Figure 2 describes the flow of methodology, from obtaining the image until the image being processed. First, few spleen images were taken from human body using ultrasound. The most suitable image was then selected as an image subject. After the image was obtained, the image is processed and enhanced using a MATLAB software. A few processes involved, which were loading the image, creating the mask in a spleen shape to be used for filtering, a few techniques of filtering, histogram equalization, and also an enhancement technique using active contour. One of the functions which is the localized segmentation is modified from [8].

Scanning spleen image → Load the spleen image → Apply ROI Mask → Apply ROI Filter → Histogram Equalization → Active contour
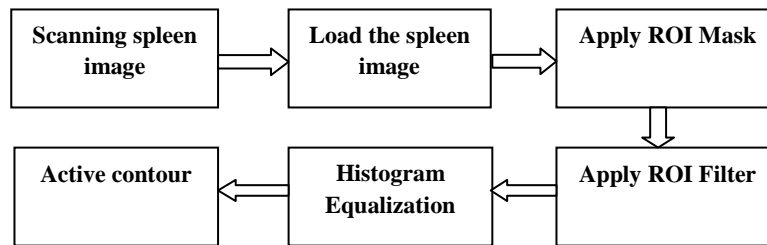
Figure 2: Flow chart of the methodology.

There are a lot of standard operation procedures for using ultrasound machine. Firstly, operator must decide the most suitable probe to use and to plug into the ultrasound machine. Normally, 3.5MHz or 5MHz probes frequency can be used to scan the spleen image. Current probes such as 7.5MHz probes provide adequate penetration of spleen. The most appropriate probe is sector or curvilinear probe as shown in Figure 3. Wide probe footprint allows accurate measurement thus useful in obtaining maximum length of spleen on the image. As a routine part of splenic assessment, color Doppler or amplitude imaging can be used to assess vascularity (appearance of veins through skin). The operator must sit or stand to sit comfortably in front of the machine so that you can reach the patient without bending sideways unnecessarily. After switching on the machine, operator must register for new patient data. Then, operator can start scanning for patient's spleen. Sufficient acoustic coupling gel must be used, especially on hairy patient to reduce the resistance between the probe and skin. The transducer must be held with the tips of right thumb and fingers. This is important as it allows the operator to roll the probe around its long axis. The transducer wire also must be arranged so that its weight does not drag on the hand holding the probe.

Figure 3: Curvilinear probe.

General approach to scan spleen is intercostals approach as the spleen is situated posteriorly and subcostally in the left upper quadrant. If the spleen was scanned via anterior approach, where the patient in a supine position, it will result in no visualization of spleen. This is because gas in the intervening stomach and splenic flexure will prevent sound transmission.

After the image has successfully obtained, a graphical user interface (GUI) was developed using MATLAB software. The purpose of this GUI is to provide user friendly environment for enhance the image quality so that the image can be analyzed easier. Next, selected image is load into Matlab for enhancement processes. Region of Interest (ROI) mask is applied to the image so that only the selected region is filtered using ROI filter. To enhance the contrast of the grayscale image, histrogram equalization is applied to image using contrast-limited adaptive histogram equalization. Finally, an active contour technique is applied to outline the object or region of interest in the image. The example of MATLAB coding [9] for ROI mask, ROI filter, histogram equalization and active contour is shown in Table 1.

Table 1: Examples of MATLAB coding used in the program.

Process	Matlab Coding	Process	Matlab Coding
ROI mask	A=imread('mask2.jpg'); I = imresize(A,.5); figure, imshow (I), title('Fixed Mask Kidney');	Active Contour	image = getappdata(0,'MyImagePass'); image2 = rgb2gray(image); I = adapthisteq(image2); c = [140 325 160]; r = [70 75 300]; m = roipoly(image,c,r); I = imresize(I,.5); m = imresize(m,.5); (I, m, 80); axes(handles.axes2); imshow(imagepushbutton4);
ROI filter	BW = roipoly; I = imresize(BW,.5); figure, imshow (I); B = rgb2gray(image); h = fspecial('unsharp'); filteredimage = roifilt2(h,B,BW);		
Histogram Equalization	imagepushbutton2 = adapthisteq(filteredimage); imagepushbutton4 = adapthisteq(image2);		

The key point in this work is *'roipoly'* and *'adapthisteq'* because this function is not only enhance the contrast of the grayscale image which makes image clearer but it act as preparation of active contour so that the region of interest is easy to be selected. The function *'roipoly'* also enable user to select region of interest themselves thus enhance the selected part of the image.

Figure 4: Spleen mask

Figure 4 shows the result of ROI Mask where the spleen mask is created. This process is necessary to select the region so that a portion in the shape could perform some other operations later. This mask is prepared beforehand, thus, when used for filtering this image is called using *'imread'* function. The complete GUI system is shown in Figure 5.
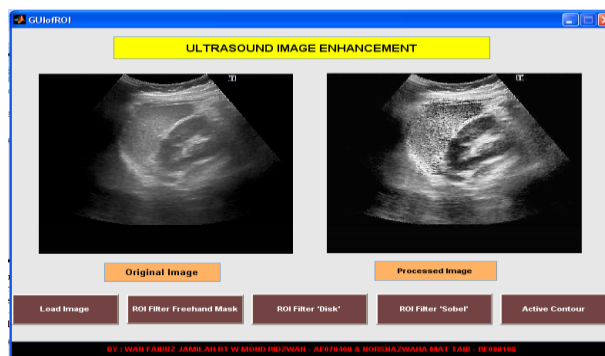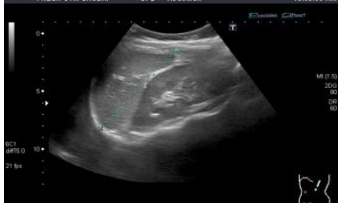
Figure 5: GUI for the project using MATLAB.

After the desired region is masked, it is then being filtered using ROI Filter. Here, only the masked region (where the picture of spleen is covered by spleen mask) is filtered, and the rest is still in its original condition. Then the contrast of the image is adjusted using Histogram Equalization so that it becomes clearer and easier for active contour to select the region of interest. Finally, an active contour is applied to outline the object or region of interest in the image [4-8].

4 Result and Analysis

For both machines, images of spleen were obtained from different views and angles to find the best angle and position of the probe so that image obtained can fully and clearly show the spleen. Since all the subjects chosen have a normal spleen, thus, all spleen images that have been collected only consist of normal spleen image. After a GUI is developed, the program was tested on five different samples of spleen ultrasound image, which were obtained earlier using Kontron™ and Toshiba™ ultrasound machines. Table 2 shows the result obtained after using the filtering of ROI function.

Table 2: Results of GUI for 5 different images of spleen

Original Scanned Image	Results of Processed Image

This result obtained after loading the sample image and clicking the *'ROI Filter Freehand Mask'* button. User must locate the ROI themselves after clicking the button by moving the pointer around the image of spleen so that the mask calculated will fit the spleen. After that, MATLAB function will enhance the selected ROI with *'unsharp'* filter and perform histogram equalization to the image. The output image shows a clearer image than the original image scanned with the machine.

In GUI, there are also buttons for fixed mask. The advantage of this fixed mask function is that the image can be enhanced more than once, and the ROI of the image can be enhanced using various other functions such as Sobel filter and active contour function. However, using this function, only one image can be enhanced because the fixed mask created can only fit that particular image which is for single spleen image.
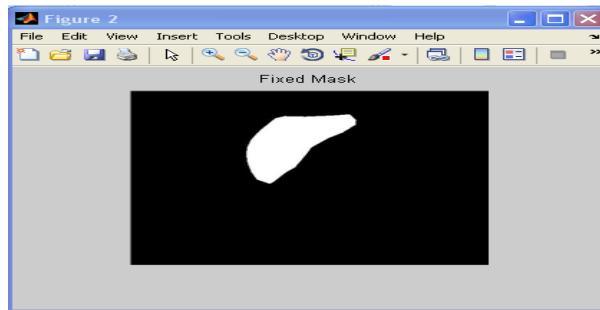
Figure 6: Fixed mask for the spleen

The fixed mask created as shown in the Figure 6 can only fit the image of spleen as in the Figure 7, thus, if this function is used for other images, the mask cannot overlap to the real position of spleen in that particular image. The ROI is enhanced at the fixed location. There is also a limitation to this function where the image and the mask must be in the same size. Otherwise, an error will occur and image processing cannot be continued.

Figure 7: Filtered image using Sobel filter.

There is also a function in the GUI which used a fixed mask as shown in Figure 8 for kidney so that the image of kidney will be blurred, thus, making the image of spleen look clearer. This function can be obtained by clicking *'ROI Filter Disk'* button.
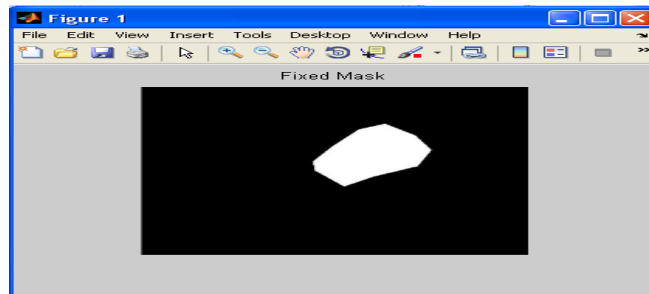
Figure 8: Fixed mask for Kidney.

Figure 9: Blurred image of Kidney.

The blurred image of kidney (Figure 9) is also used fixed mask of kidney, which also gives the same disadvantage. Only single spleen image can be used for this function. However, the filtered image shows a clear image of spleen when the image of kidney is blurred.

Figure 10: Final output of Active Contour function

Lastly, the other function of GUI created is an active contour function. For this function, the mask is also a fixed mask which is a predefined triangle. From the triangle mask, this function will find the region of interest automatically. The output of this function is in black and white form where black is the background while white is the region of interest as shown in Figure 10. Although the output cannot precisely locate the boundary of the spleen, we can see the output image obtained have similarities in the shape of a real spleen. This problem may be caused due to limited mask, and the number of iteration performed in the image. Further research is required to achieve a better mask that can automatically find the region of interest regardless the position of spleen in the image.

5 Conclusion

The ultrasound image of spleen has been successfully obtained using the allocated machine. The image was processed using MATLAB software to obtain a higher-quality image of spleen. GUI that has been created using MATLAB makes the image enhancement more users friendly and easier to analyze. Although the study is only focused on developing the user friendly interface, it is hope that new learners in biomedical image processing will learn and appreciate a simple tool to enhance the medical ultrasound image effectively.

References

[1] Andrews, M.W., (M.D., M. Med.), *"Ultrasound of the Spleen"*, World Journal of Surgery 2000, 24(2):183-187.
[2] Ng, H.P.,Ong, S.H.,Foong, K.W.C.,Goh, P.S.,Nowinski, W.L. , *"Medical Image Segmentation Using K-Means Clustering and Improved Watershed Algorithm,"* IEEE Southwest Symposium on Image Analysis and Interpretation, 2006, pp.61-65.
[3] Zhengmao Ye, Mohamadian, H.,Yongmao Ye, *"Analyzing contrast enhancement and watershed segmentation using quantitative information measuring,"* 7th World Congress on Intelligent Control and Automation, 2008. *WCICA 2008,* pp.248-253.
[4] Yim, P.J, Foran D.J, *"Volumetry of Hepatic Metastases in Computed Tomography using the Watershed and Active Contour Algorithms"*, 16th IEEE Symposium Procedings on Computer-Based Medical Systems, 2003, pp. 329-336.
[5] Niethammer M, Tannenbaum A, Angenent S, "*Dynamic Active Contour for Visual Tracking"*, IEEE Transactions on Active Control. April 2006. pp. 562-580.
[6] Sundaramoorthi G., Yezzi A., Mennucci A.C, *"Coarse-to-Fine Segmentation and Tracking Usingsobolev Active Contours"*, IEEE Transaction on Pattern Analysis and Machine Intelligence, 2008.pp.851-858.
[7] Chen Sagiv, Sochen N.A, Zeevi Y.Y, *"Intergrated Active Contours for Texture Segmentation",* IEEE Transaction on Image Processing, 2006, pp.1633-1640.
[8] Lankton, S., Tannenbaum, A., *"Localizing Region-Based Active Contours"* , IEEE Transactions on Image Processing, 2008, vol.17, no.11, pp.2029-2039.
[9] Rafael C. Gonzalez**,** Richard E. Woods**,** Steven L. Eddins**, "***Digital Image Processing Using MATLAB",* Prentice Hall, 2004.

COMPUTER ASSISTED MEDICAL HEALTH SYSTEM FOR THE BENEFIT OF HARD TO REACH RURAL AREA

Priti Kalode, Onkar Kemkar and D.A.Deshpande
PCD ICSR, VMV College Campus, Wardhaman Nagar, Nagpur (MS), India

Abstract
It is a known fact that medical practitioners seldom prefer to work in rural areas. For providing medical help to rural population more particularly to people from hard to reach areas computer assisted medical health system is developed. This paper discusses the method for fast clinical assistance in hard to reach places & its applicability.

Keywords: CAMH, Gynecology, emr

1. Introduction
Decision making by the clinician in the management of his patients is a highly intellectual activity which involves:
1.   His skill in gathering and evaluating new information about the patient,
2.   His ability to readily recapitulate the information he has already logged in the patients record and,
3.   His ability to effectively utilize the large body of medical knowledge which expresses the relationship between the data describing each individual patient and the diagnostic, prognostic and therapeutic options available for managing the patients problems optimally. (1)
To carry out this intellectual activity medical professionals are not available in rural areas. Unavailability of health care in rural areas is the outcome of paucity of medical professionals. Even the Government is unable to retain Doctors for rural areas.
A national level workshop was held in July 2011 to identify implementation research priorities. Following important questions emerged as highest priorities (2).
1. How can doctors, nurses and technicians be attracted in rural and hard to reach areas?
2. How can mothers, newborns and children needing health care be reached in hard to reach places?
3. How can quality of health care received by mothers, newborns and children in health facilities be improved?
Using Information Communication Technology all the three questions can be solved. In this paper a Computer Assisted Medical Health System (CAMH) for fast clinical assistance in Gynecology and Obstetrics in the hard to reach places is described which may be extended across most of the disciplines of medical sciences. Not only government but private medical practitioners and hospitals may get involved in this activity and therefore success on implementation of the method is guaranteed.

2. Methodology
The model of medical health system described here is hoped to provide a solution to much of the health problems faced by rural populous. Properly designed Information Communication Technology based programmes have been generated to enable the semi-trained personnel to collect data using pre defined questions and derive conclusion. A pre meditated computer programme in the discipline, Gynecology; has been developed with proper medical data base at the back end. Also a provision for collecting and recording some primary data on temperature, blood pressure, blood glucose, pulse rate etc of the patient has been made. These measurements are possible with some hardware attachments such as devices for recording temperature, blood pressure, blood glucose, pulse rate, etc. The paramedics trained to operate this computer system will collect the data from the patients with the help of the computer based health care system which itself will provide decision about the ailment and possible treatment. The paramedics will forward this data via wireless connectivity to the Registered Medical Practitioner under whom the paramedics is working. The RMP after making some further enquiry, if necessary, will convey/forward the required treatment. A pharmacy diploma holder accompanying the paramedics will be carrying necessary medicines and shall deliver the medicine to the patient. The patient will be asked to report the next day for further assessment. If the condition of the patient remains unaltered may be within two days, he/she will be referred to the concerned RMP for further treatment.   This tool will be superior to the ability of the semiskilled personnel/paramedics in retrieving and processing information provided by the patient.

3. Content Of The ICT Based Computer Assisted Medical Health Care System:
The front end shows a questionnaire of yes/no type for each of the complaints related to Gynecology and Obstetrics. Screen shots 1 to 6 show the patients data, symptomatic questionnaire, diagnosis and report of the patient.   The back end will have medical knowledge data related to the complaint
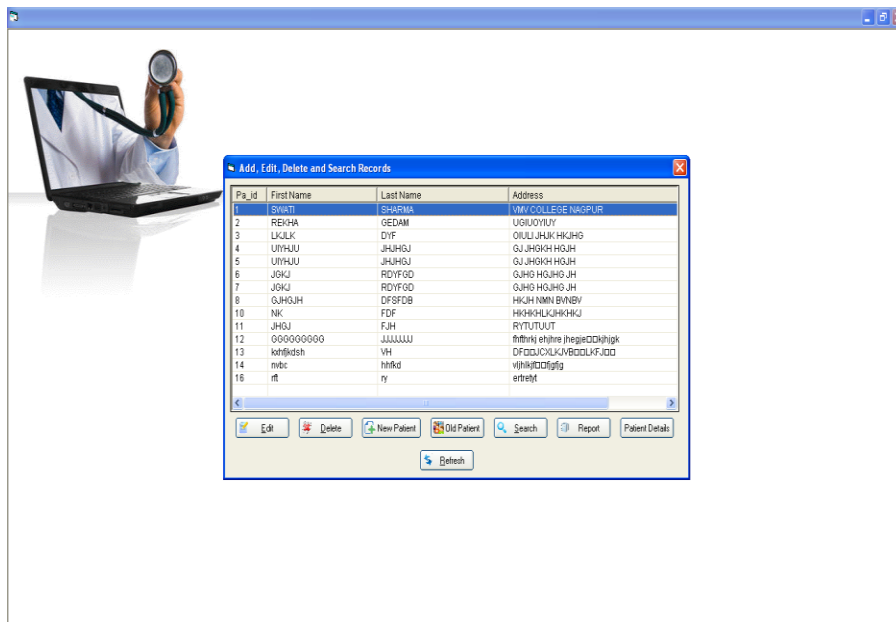
Screen Shot 1 - Patient Information
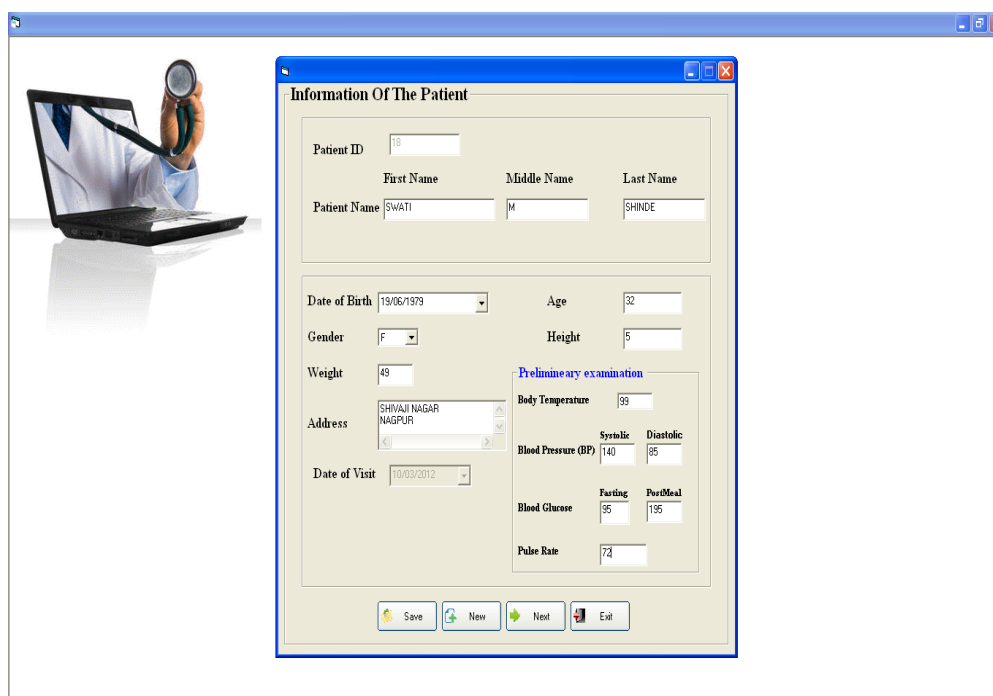
Screen Shot 2 - Input Patient Information
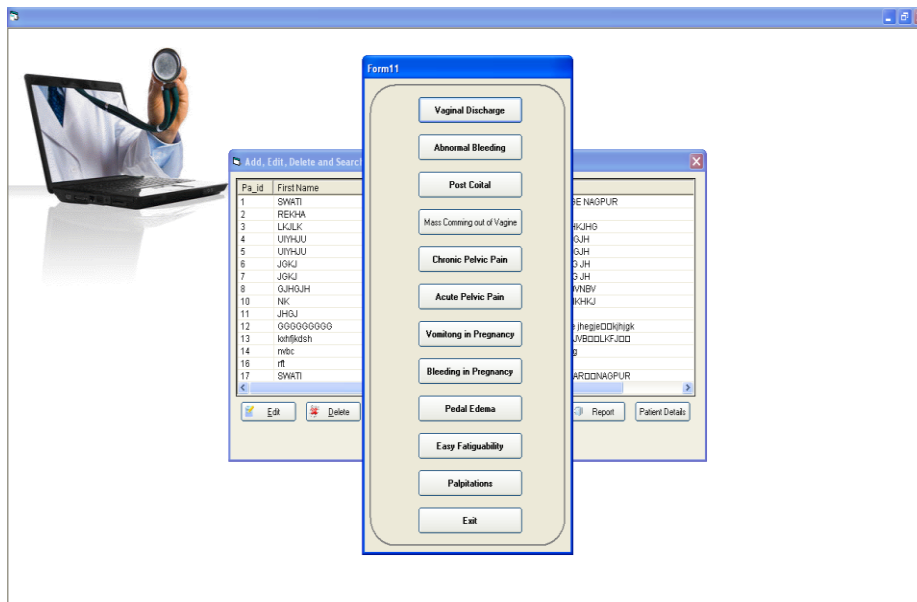
Screen Shot 3 - Gynecology Symptoms
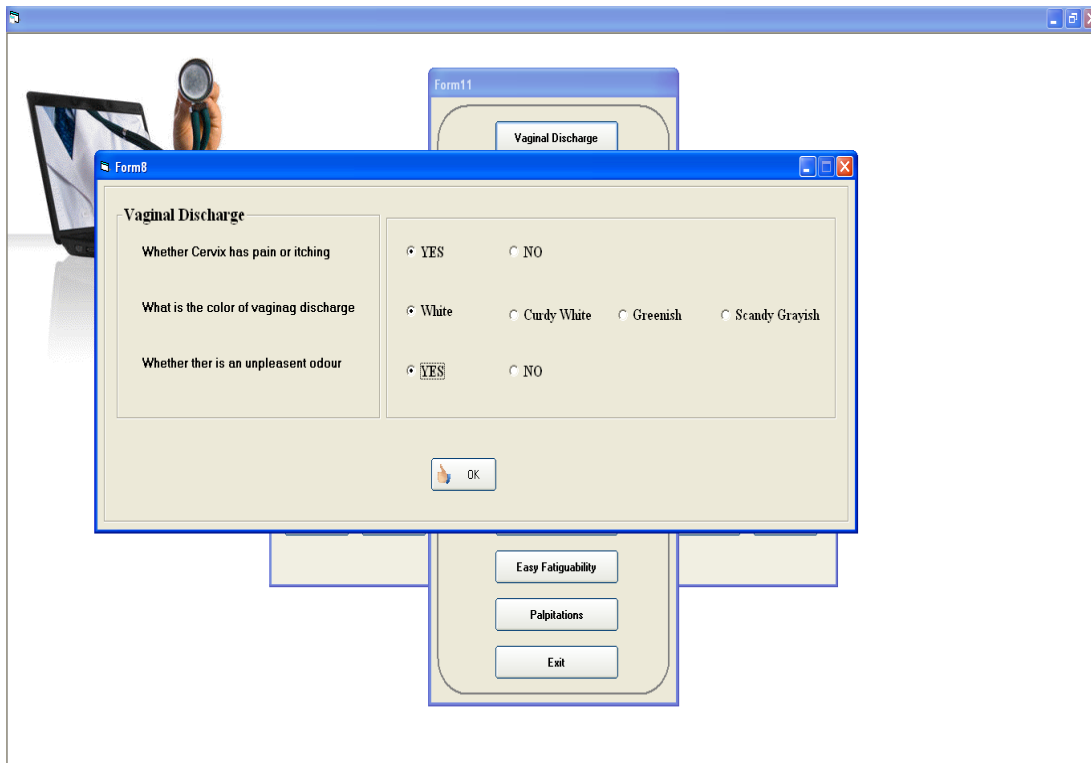
Screen Shot 4 - Gynecological Problem's Symptoms
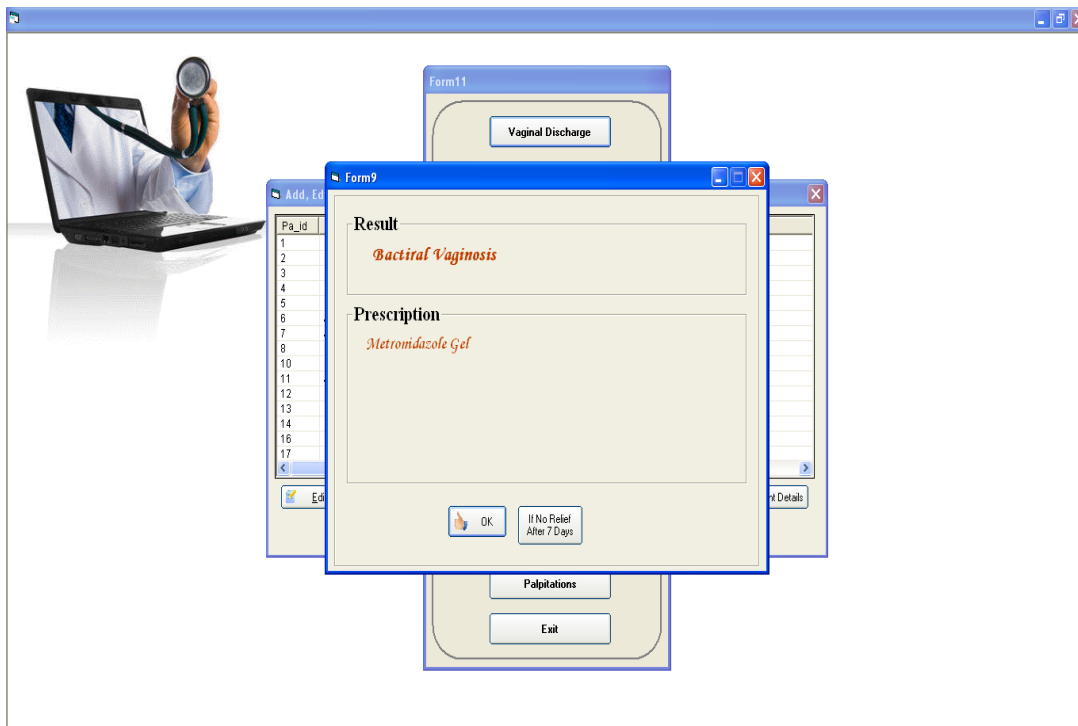
Screen Shot 5 - Gynecological Problem's Result

Diagnosis	Prescription1	Prescription2	Prescription3	Prescription4	Prescription5
Vaginal Discharge	Metronidazole Gel				
Excessive abnormal bleeding. Reproductiv age grp.	Iv Estrogen (CEE) 2.5 mg every 4 hrs till bleeding stop.	Then tapered to Tb Conjugated Equine Estrogens 1.25 mg 1 x 7 days	Tb Nor-Ethisterone Acetate 10 mg tds for 24 - 48 hrs	Then Tb Nor-Ethisterone Acetate 5 mg 1 x 20 days	Continue for 2 - 3 cycles from Day 16 to 25

Date : 09/03/2012

PATIENT REPORT

Screen Shot 6 - Patient Report

4. Different Approaches Adhered By The CMD:

The Computer Assisted Medical Decision Making System (CMD) adheres to the following approaches:

1.   Categorical Approaches: Deterministic, algorithmic, flow-chart or protocol-based. They provide clear cut guides to action based on clear cut criteria. Indeed the concept of a protocol as a clinical algorithm arose out of the experience of research workers with computers and information science.

2.   Probabilistic Approaches: Statistical decision approaches and statistical inference, Bayesian approaches, discriminate analysis, Multivariate analysis; Clinical analysis-case based reasoning and exploratory analysis etc. The entire above are derived from the same perspective-to develop predictive power through the analysis of past data to support future decisions.

3.   Artificial Intelligence Approaches: Production rule systems based on first order predicate calculus-conditional rules, IF/THEN; Cognitive models based on generalized set covering (GSC) theory; Frame descriptions; Semantic networks; Hypothesis and test (abduction); and Artificial Neural Networks (ANNs).

Out of the above approaches, two simple and easily useable by the computer scientists for preparing software tools are described below.

5. General model of CMD

Dr. James Reggia (3) has described a general model of CMD system as depicted in Fig.1.

Individual Patient Description → Inference Mechanism → Useful Information about Patient

Inference Mechanism ↕ Knowledge Base
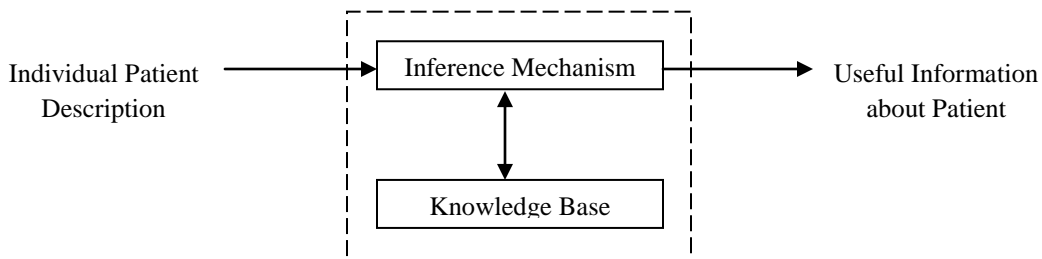
The input is typically a description of some specific patient (age, symptoms and signs, past medical history etc.) and the output is useful information about that patient (e.g. appropriate screening tests, diagnosis, therapy plan etc). The CMD system itself contains two basic components:

1.   A knowledge base and
2.   An inference mechanism.

6. Production rule systems

Artificial Intelligence seeks to capture the expertise of humans largely through the use of non-numeric symbol processing. The CMD mimics human decision making, its reasoning is transparent and it has an explanatory capacity. The AI approach most widely used in CMD research is that of rule-based deductions. Medical knowledge is represented as a set of conditional rules or productions. Each rule/production has the basic form, IF/THEN.

7. Camh Model

Fig.2. depicts CAMH model used in the development of computer programme to record patient – Para-medico dialogue and diagnosis.
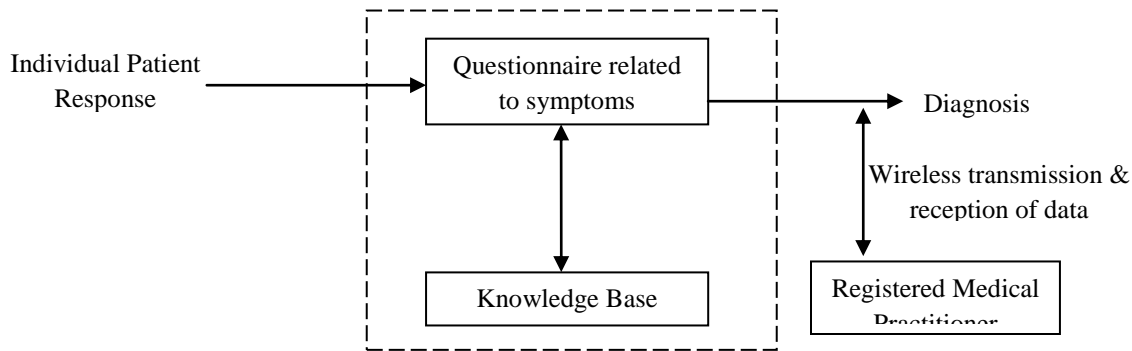
For our system the knowledge base is a collection of encoded knowledge that is needed to solve problems in some particular medical area (Gynecology). The inference mechanism is a program that, given a case description, uses the information in the knowledge base to generate decision. Medical experts have provided the knowledge for design and development of the supporting software for the CAMH system for being used by the health care service personnel.

7. Conclusion

It is concluded that the CAMH model used in developing computer programme can be extremely useful in providing medical help to people of hard to reach area. The system can be handled by the semiskilled/paramedics so that the patients get immediate medical assistance. Doctor based in the city area will offer diagnosis and treatment to the patient. Such a system can be extended across all specialties of medical sciences.

Acknowledgement

References:

1. R.D.Lele, Computers in Medicine, TMH Publishing Company Limited, New Delhi, 2005, Page 261-319.

2. http://www.icmr.nic.in/icmrnews/call/rhn_anirp.pdf

3. Reggia J., A production rule system for Neurological localization, Proc. Second Ann. Symp. Comp. Appllic. Med. Care, IEEE, 1978, pp 254-260

Numerical and Experimental Investigations for Effect of Gravity to the Heat Transfer and Fluid Flow Phenomena of Microchannel Heat Exchangers

Thanhtrung Dang[1,*], Ngoctan Tran[2], and Jyh-tong Teng[2]

[1] Department of Heat and Refrigeration Technology, Ho Chi Minh City University of Technical Education, Ho Chi Minh City, Vietnam
[2] Department of Mechanical Engineering, Chung Yuan Christian University, Taiwan

Abstract

For both numerically and experimentally, effect of gravity on the heat transfer and fluid flow phenomenon of microchannel heat exchangers was presented. The influence was determined by two cases: one with horizontal channels, the other with vertical channels. For vertical channels, the hot water is flowing upward which is against the gravitational field, while the cold water is flowing downward which is in the same direction as the gravitational field. In this study, the difference between the results obtained from horizontal channels and those from vertical ones is negligibly small; the impact of gravity on the fluid through the microchannel heat exchangers was found to be small, with the maximum difference between the two cases being less than 8%. The results obtained from numerical simulation and experimental data are in good agreement. In addition, good agreements were also achieved between the results obtained in the present study and the results obtained in literatures.

Keywords: <u>micro heat exchanger, gravity,</u> heat transfer rate, pressure drop, performance index.

I. INTRODUCTION

The development of effective cooling devices has promoted attractive area of study in microchannel heat transfer in recent years. A review on micro heat exchangers was done by Dang et al. [1] with five sections. The first section dealt with the single-phase micro heat exchangers which consist of the micro channel heat exchangers as well as the micro porous/foam heat exchangers. The second section reviewed the two-phase micro heat exchangers which consist of micro evaporators and micro condensers. The third section dealt with micro heat exchangers for carbon dioxide air conditioning system. The fourth section reviewed optimization of micro heat exchanger. The last section dealt with other types of micro heat exchangers. David et al. [2] studied hydraulic and thermal characteristics of a vapor venting two-phase microchannel heat exchanger. They found 60% improvement in the normalized pressure drop and up to 4.4 °C reduction in the average substrate temperature between the control and vapor venting device under similar operating conditions.

Brandner et al. [3] described microstructure heat exchangers and their applications in laboratory and industry. Several micro heat exchangers were introduced: polymer microchannel heat exchanger with aluminum separation foil, electrically powered lab-scale microchannel evaporator, ceramic counter-flow microstructure heat exchanger, etc. Ameel et al. [4] presented an overview of the miniaturization technologies and their applications to energy systems. Based on the MEMS technologies (silicon-based micromachining, deep X-ray lithography, and the micro mechanical machining), processes were discussed in the context of applications to fluid flow, heat transfer, and energy systems. Review on experimental results concerning single-phase convective heat transfer in microchannels was presented by Morini [5], with additional review results obtained for the friction factor, the laminar-to-turbulent transition, and the Nusselt number in channels having a hydraulic diameter less than 1 mm.

Mathew and Hegab [6] studied on the application of effectiveness-NTU relationship to parallel-flow microchannel heat exchangers. Besides, development of nondimensional parameters (such as axial distance, temperature, and heat transfer rate) was carrier out. However, the results were analyzed theoretically only. Studies of effectiveness and pressure drop for micro cross-flow heat exchanger were presented by Kang and Tseng [7]. At the same effectiveness, heat transfer rate and pressure drop were expressed as a function of average temperature. However, in their study, they did not study for the cases with varying mass flow rates at each side.

Chein and Chen [8] presented a numerical study of the effect of inlet/outlet arrangement on the performance of microchannel heat sink. Six types of heat sink were studied with the best performance being the V-type. Because that if the microchanels have the same cross-section area and width of microchannel, the depth of microchannel obtained from V-shaped microchannel is deeper than that obtained from rectangular-shaped one. So it is not easy to design a heat exchanger with the subtrate thickness from 1.2 to 2 mm using V-type microchannels. Foli et al. [9] studied numerically on the heat flux, heat transfer rate, and pressure drop in channels with numerous aspect ratios. However, the results in Ref. [9] were presented without experiments.

A study on the simulations of a trapezoidal shaped micro heat exchanger was presented by Dang et al. [10]. For the microchannel heat exchanger, behaviors of the temperature, heat flux, and velocity profiles were determined. Effect of flow arrangement on the heat transfer related behaviors of a microchannel heat exchanger was presented by Dang et al. [11, 12]. For all cases done in the study, the heat flux and performance index obtained from the counter-flow arrangement are always higher

than those obtained from the parallel-flow one: the values obtained from the counter-flow are 1.1 to 1.2 times of those obtained from the parallel-flow. Dang and Teng [13] studied effect of the substrate thickness of counter-flow microchannel heat exchangers on the heat transfer behaviors. It was found that the actual heat transfer rate varies insignificantly with the substrate thicknesses varying from 1.2 to 2 mm. However, the results obtained in [13] only mentioned the heat transfer behaviors of the heat exchangers, while the fluid flow behaviors of the heat exchangers were not discussed. Dang et al. [14] presented an experimental study of the effects of gravity on heat transfer and pressure drop behaviors of a microchannel heat exchanger. However, the results in [14] were presented only for a microchannel heat exchanger evaluated under the condition of rising the inlet temperature for the hot side. Dang and Teng [15, 16] studied the effects of configurations on performance of the microchannel and minichannel heat exchangers. However, their study ignored the effects of gravity on the performance index of microchannel heat exchangers.

To summarize, it is goal of this paper to study the effects of gravity on the heat transfer and fluid flow characteristics of microchannel heat exchangers, for both numerically and experimentally. In the following section, two microchannel heat exchangers will be discussed under the condition of rising mass flow rate for the cold side.

II. METHODOLOGY

A. Mathematical model

The governing equations in this system consist of the continuity equation, momentum equations, and energy equation [17,18]. The equations can be expressed by

Continuity equation

$$\frac{\partial \rho}{\partial t} + u\frac{\partial \rho}{\partial x} + v\frac{\partial \rho}{\partial y} + w\frac{\partial \rho}{\partial z} + \rho\left[\frac{\partial u}{\partial x} + \frac{\partial v}{\partial y} + \frac{\partial w}{\partial z}\right] = 0 \tag{1}$$

Momentum equations

$$\frac{\partial u}{\partial t} + u\frac{\partial u}{\partial x} + v\frac{\partial u}{\partial y} + w\frac{\partial u}{\partial z} = \rho g_x - \frac{1}{\rho}\frac{\partial p}{\partial x} + \frac{\mu}{\rho}\left(\frac{\partial^2 u}{\partial x^2} + \frac{\partial^2 u}{\partial y^2} + \frac{\partial^2 u}{\partial z^2}\right) \tag{2a}$$

$$\frac{\partial v}{\partial t} + u\frac{\partial v}{\partial x} + v\frac{\partial v}{\partial y} + w\frac{\partial v}{\partial z} = \rho g_y - \frac{1}{\rho}\frac{\partial p}{\partial y} + \frac{\mu}{\rho}\left(\frac{\partial^2 v}{\partial x^2} + \frac{\partial^2 v}{\partial y^2} + \frac{\partial^2 v}{\partial z^2}\right) \tag{2b}$$

$$\frac{\partial w}{\partial t} + u\frac{\partial w}{\partial x} + v\frac{\partial w}{\partial y} + w\frac{\partial w}{\partial z} = \rho g_z - \frac{1}{\rho}\frac{\partial p}{\partial z} + \frac{\mu}{\rho}\left(\frac{\partial^2 w}{\partial x^2} + \frac{\partial^2 w}{\partial y^2} + \frac{\partial^2 w}{\partial z^2}\right) \tag{2c}$$

For steady-state conditions, $\partial u/\partial t = 0$; the boundary conditions of inlet flow are $u = 0$, $v = 0$, and $w = w_0$; the boundary conditions of outlet flow are $\mu(\nabla u + (\nabla u)^T)n = 0$ and $p = p_0$, where μ is dynamic viscosity, ρ is density, g is gravity force, u is velocity field, u is velocity in the x-direction, v is velocity in the y-direction, w is velocity in the z-direction, p is pressure, and p_0 is pressure at the outlet.

For the energy transport, the walls have no-slip conditions for velocity and temperature at the walls; these conditions are expressed by $u_{wall} = 0$ and $T_{wall} = T_{fluid\ at\ wall}$, respectively, where T_{wall} is wall temperature.

The heat transfer equation for the energy transport within the fluid is:

$$\frac{\partial T}{\partial t} + u\frac{\partial T}{\partial x} + v\frac{\partial T}{\partial y} + w\frac{\partial T}{\partial z} = \frac{\lambda}{\rho c_p}\left(\frac{\partial^2 T}{\partial x^2} + \frac{\partial^2 T}{\partial y^2} + \frac{\partial^2 T}{\partial z^2}\right) + Q_i \tag{3}$$

For steady-state conditions, $\partial T/\partial t = 0$; the boundary condition of inlet flow is $T = T_0$; the boundary condition of outlet flow is convective flux, expressed by $n \cdot (-\lambda\nabla T) = 0$; the thermal boundary condition of the bottom and top walls of the microchannel heat exchanger are assumed to be constant heat flux, expressed by $-n \cdot (-\lambda\nabla T) = q_0$; and the four side-walls are insulated thermally, expressed by $n \cdot q = 0$, where heat flux $q = -\lambda\nabla T + \rho C_p Tu$, T is temperature, c_p is specific heat at constant pressure, Q_i is internal heat generation, and λ is thermal conductivity.

B. Experimental set-up

Three major parts are used in the experimental system: the test section (the microchannel heat exchanger), syringe system, and overall testing loop, as shown in Fig. 1. In this study, two microchannel heat exchangers were tested. The heat transfer process of these devices is carried out between two liquids which are hot water and cold water; the hot and cold fluids are flowing in the opposite directions. Fig. 2 shows the dimensions of the test sections. The substrate material used for the heat exchangers is aluminum, with the thermal conductivity of 237 W/(mK), density of 2,700 kg/m³, and specific heat at constant pressure of 904 J/(kgK).

For each microchannel heat exchanger, the top side for the hot water has 10 microchannels and the bottom side for the cold water also has 10 microchannels. The length of each microchannel is 32 mm. Microchannels have rectangular cross-section with the width and the depth being W_c and D_c, respectively. In a microchannel heat exchanger, all channels are connected by

manifolds for the inlet and outlet of hot water and for those of cold water, respectively. The manifolds of the heat exchangers are of the same cross-sections: having a rectangular shape with a width of 3 mm and a depth of 300 μm.
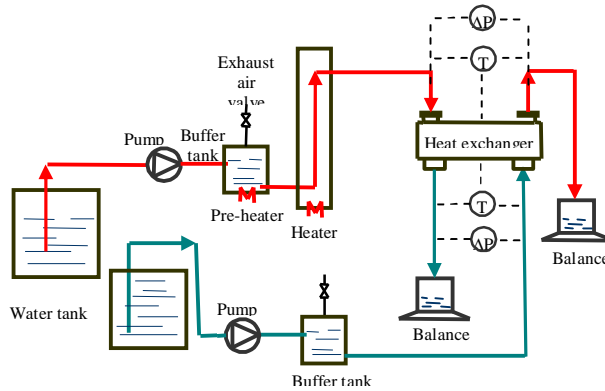
Fig. 1. Schematic of the test loop for microchannel heat exchangers

Table 1. Geometrical parameters of microchannel heat exchangers

No.	Dimensions of the substrate (mm)			Dimensions of the channel (μm)	
	L	W	T	W_c	D_c
T1	46	26.5	1.2	500	300
T2	46	26.5	1.2	500	180

Fig. 2 shows the dimensions of the test section. In this study, two microchannel heat exchangers were designed and manufactured, with their dimensions listed in Table 1. Fig. 3 shows a photo of the microchannel heat exchanger. These test sections were manufactured by precision micromachining [4]. Each inlet hole or outlet hole of the heat exchangers has a cross-sectional area of 9 mm^2. The four sides of the heat exchanger were thermally insulated by the glass wool with a thickness of 5 mm. To seal the microchannels, two layers of PMMA (polymethyl methacrylate) are bonded on the top and bottom sides of the substrate by UV (ultraviolet) light process, as indicated in Fig. 3. The physical properties of the PMMA and the glass wool are listed in Table 2 [17].
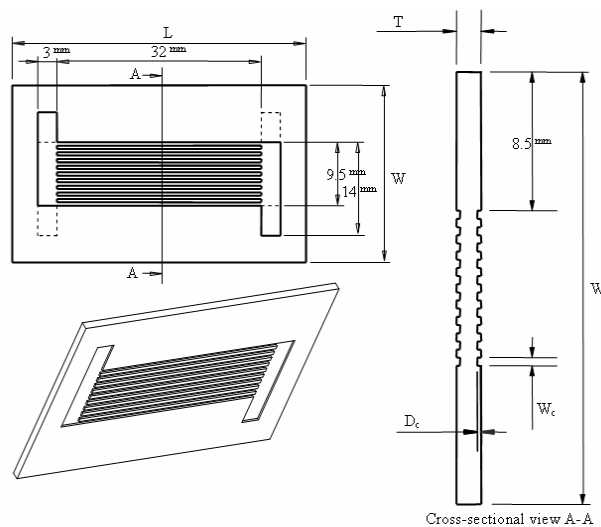
Fig. 2. Dimensions of the test section

PMMA

Test sample
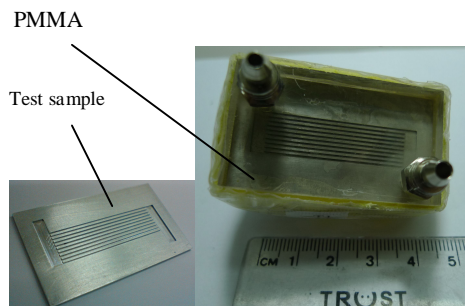
Fig. 3. A photo of the microchannel heat exchanger

Table 2. The physical properties of the PMMA and the glass wool

Material	Density kg/m³	Thermal conductivity W/(mK)
PMMA	1420	0.19
Glass wool	154	0.051

Experimental data for the microchannel heat exchanger were obtained under the constant room temperature of 25 ºC. For this study, DI water (deionized water) was used as the working fluid. Each inlet or outlet of the heat exchanger has a set of two thermocouples to record temperature values. So, there are eight thermocouples in total. At each side, a differential pressure transducer was used to measure the pressure drop. To assess the accuracy of measurements presented in this work, the uncertainty values for measured parameters are listed in Table 3. In addition, the uncertainties on the dimensions of microchannel evaluated by using a scanning laser made by Mitaka/Ryokosha model NH-3. The uncertainties of the scanning laser were estimated to be ± 0.03 μm. Equipments used for the experiments are listed as follows [13-16]:

   1. Thermocouples, T-type
   2. Pump, Model PU-2087, made by Jasco
   3. Pump, VSP-1200, made by Tokyo Rikakikai
   4. Heater, Model AXW-8, made by Medilab
   5. Differential pressure transducer, Model PMP4110, made by Duck
   6. Micro electronic balance, Model TE-214S, made by Sartorious.

Table 3. Uncertainty data for measured parameters

Parameter	Uncertainties
Temperature	± 0.1 °C
Pressure	± 0.025% FS
Mass flow rate	± 0.0015 g
Channel height	± 7 μm
Channel width	± 10 μm
Channel length	± 70 μm

In order to study the effects of gravity on heat transfer and fluid flow behaviors of the heat exchangers, all experimental conditions for the two microchannel heat exchangers were kept the same. Throughout the paper, the experimental conditions of testing were discussed: the case is studied under condition of increasing the mass flow rate of the cold side. Further details of the case are as follows:

The inlet temperature and the mass flow rate of the hot side were fixed at 70 ºC and 0.2308 g/s, respectively; at the cold side, the inlet temperature was fixed at 22.5 ºC and the mass flow rates were varying from 0.2135 to 0.401 g/s.

C. Data of analysis

In the following analyses, the major assumptions were made:

   - The fluid is a laminar flow

   - The fluid flow is incompressible and continuum

- Heat transfer is steady

- Negligible radiation heat transfer.

For the experiments carried out in this study, the effects on the heat transfer and fluid flow – such as heat flux, effectiveness, pressure drop, and performance index – of the heat exchangers will be discussed as follows.

The energy balance equation for the counter-flow microchannel heat exchanger is expressed by:

$$Q_h - Q_{loss} = Q_c = Q \tag{4}$$

$$\text{Or} \quad m_h c_h (T_{h,i} - T_{h,o}) \eta = m_c c_c (T_{c,o} - T_{c,i}) \tag{5}$$

where Q_h is heat transfer rate of the hot side, Q_c is heat transfer rate of the cold side, Q is actual heat transfer rate, Q_{loss} is heat loss rate from the heat exchanger to the ambient, m is mass flow rate (subscripts h and c stand for the hot side and cold side, respectively), c is specific heat, $T_{h,i}$, $T_{h,o}$, $T_{c,i}$ and $T_{c,o}$ are inlet and outlet temperatures of the hot and cold side, respectively, and η is actual effectiveness.

The maximum heat transfer rate, Q_{max} is evaluated by
$$Q_{max} = (mc)_{min}(T_{h,i} - T_{c,i}) \tag{6}$$
The effectiveness (NTU method) is determined by

$$\varepsilon = \frac{Q_c}{Q_{max}} \tag{7}$$

Heat flux is calculated by $q = \dfrac{Q_c}{A} = \dfrac{m_c c_c (T_{c,o} - T_{c,i})}{n L_c W_c} \tag{8}$

$$\text{Or} \quad q = k \Delta T_{lm} = \frac{\Delta T_{lm}}{\Sigma R} \tag{9}$$

The overall thermal resistance ΣR is determined by

$$\Sigma R = R_{cond} + R_{conv} \tag{10}$$

The log mean temperature difference is calculated by

$$\Delta T_{lm} = \frac{\Delta T_{max} - \Delta T_{min}}{\ln \dfrac{\Delta T_{max}}{\Delta T_{min}}} \tag{11}$$

where m is mass flow rate (subscripts h and c stand for the hot side and cold side, respectively), n is number of microchannels, c is specific heat, $T_{h,i}$, $T_{h,o}$, $T_{c,i}$ and $T_{c,o}$ are inlet and outlet temperatures of the hot and cold sides, respectively, q is heat flux, A is heat transfer area, k is overall heat transfer coefficient, $R_{cond} = \dfrac{\delta}{\lambda}$ is conductive thermal resistance, $R_{conv} = \dfrac{1}{h_h} + \dfrac{1}{h_c}$ is convective thermal resistance, h_h and h_c are the convective heat transfer coefficients of the hot side and the cold sides, respectively, δ is thickness of heat transfer, λ is thermal conductivity, and ΔT_{lm} is the log mean temperature difference.

The Reynolds number is calculated by:

$$\text{Re} = \frac{\rho w D_h}{\mu} = \frac{2m}{\mu (W_c + D_c)} \tag{12}$$

where $D_h = \dfrac{4A_c}{P}$ is the hydraulic diameter, w is velocity in the z-direction, μ is dynamic viscosity, ρ is density, A_c is cross-sectional area, and P is wetted perimeter.

The total pressure drop of the heat exchanger is given by
$$\Delta p_t = \Delta p_h + \Delta p_c \tag{13}$$
where Δp_h and Δp_c are pressure drops of hot and cold sides, respectively.

The performance index, ξ, is determined by

$$\xi = \frac{Q_c}{\Delta p_t} = \frac{m_c c_c (T_{c,o} - T_{c,i})}{\Delta p_h + \Delta p_c} \tag{14}$$

The experimental uncertainties were estimated, following the method described by Holman [19]; the final expressions for uncertainties were given as follows:

$$\frac{U_{Q_c}}{Q_c} = \left[\left(\frac{\partial m_c}{m_c}\right)^2 + \left(\frac{\partial c_c}{c_c}\right)^2 + \left(\frac{\partial T_{c,o} + \partial T_{c,i}}{T_{c,o} + T_{c,i}}\right)^2\right]^{1/2} \tag{15}$$

$$\frac{U_{Re}}{Re} = \left[\left(\frac{\partial m}{m}\right)^2 + \left(\frac{\partial \rho}{\rho}\right)^2 + \left(\frac{\partial \mu}{\mu}\right)^2 + \left(\frac{\partial W_c}{W_c}\right)^2 + \left(\frac{\partial D_c}{D_c}\right)^2\right]^{1/2} \tag{16}$$

$$\frac{U_\xi}{\xi} = \left[\left(\frac{\partial m_c}{m_c}\right)^2 + \left(\frac{\partial c_c}{c_c}\right)^2 + \left(\frac{\partial T_{c,o} + \partial T_{c,i}}{T_{c,o} + T_{c,i}}\right)^2 + \left(\frac{\partial \Delta p_h}{\Delta p_h}\right)^2 + \left(\frac{\partial \Delta p_c}{\Delta p_c}\right)^2\right]^{1/2} \tag{17}$$

By using the estimated errors of parameters listed in Table 3, the maximum experimental uncertainties in determining Q_c, Re, and ξ were 2,1%, 3.1%, and 3.3%, respectively, for all cases being studied.

D. Numerical simulation

Numerical study of the 3D behaviors of heat transfer by the microchannel heat exchangers with single-phase fluid flowing through was done by using the CFD ACE$^+$ software, version 2008.2. The algorithm of this software is based on the finite volume method. For this study, water was used as the working fluid. No internal heat generation is occurred, resulting in $Q_i = 0$. Nodalization of this model was done by using 172,224 cells and a relative tolerance was 10^{-14}. Fig. 4 shows the convergence of the numerical solver for components of velocity, pressure, and enthalpy.

Number of iteration
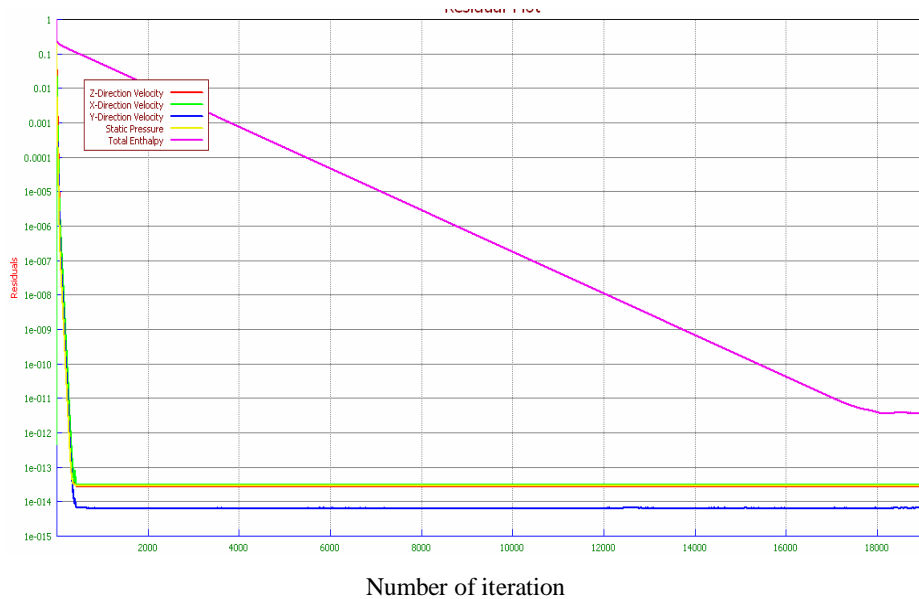
Fig. 4. Convergence of the numerical solver

III. RESULTS AND DISCUSSION

A. Numerical results

For the experiments carried out in the study, the inlet temperature and the mass flow rate of the hot side were fixed at 70 ℃ and 0.2308 g/s, respectively; at the cold side, the inlet temperature was fixed at 22.5 ℃ and the mass flow rates were varying from 0.2135 to 0.401 g/s [20].
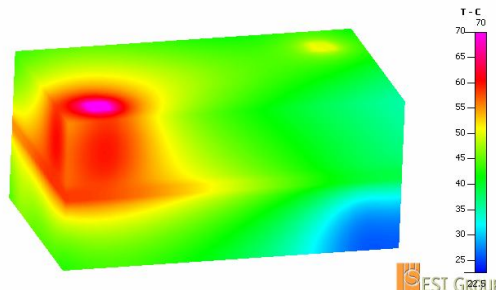
Fig. 5. The temperature profile of the microchannel heat exchanger
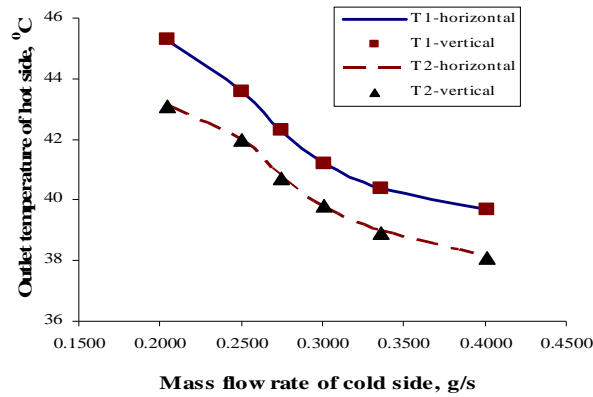
Fig. 6. Numerical comparison of the outlet temperatures of hot side

The thermal boundary conditions of the top and bottom walls of the heat exchanger are assumed to be constant heat flux. The convective heat transfer coefficient between the wall and the ambient used for this solver was 10 W/(m^{2}K) [18]. The temperature profile of the microchannel heat exchanger T1 is shown in Fig. 5 for the mass flow rate of 0.2135 g/s at the cold side.

Fig. 6 shows a numerical comparison of the outlet temperature of hot side of two microchannel heat exchangers under the effect of gravity. It is observed that the outlet temperatures of hot side obtained from horizontal channels and those from the vertical ones are negligibly small. A numerical comparison of the outlet temperatures of cold side of two microchannel heat exchangers is also shown in Fig. 7. The outlet temperatures (for both the hot and the cold sides) are functions of the mass flow rate of cold side; the outlet temperatures decrease as the mass flow rate of the cold side increases. It is shown from Figs. 6 and 7 that the difference of outlet temperatures obtained from horizontal channels and those from the vertical ones, respectively with T1 and T2, are negligibly small with the maximum percentage error of 0.1%.
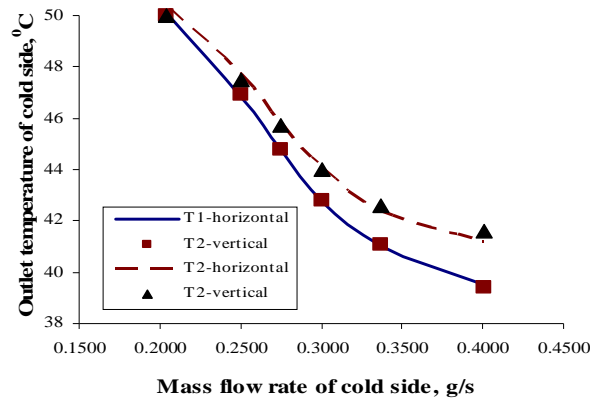
Fig. 7. Numerical comparison of the outlet temperatures of cold side

B. Experimental results

For the experimental system, the inlet temperature and the mass flow rate of the hot side were fixed at 70 ºC and 0.2308 g/s, respectively; at the cold side, the inlet temperature was fixed at 22.5 ºC and the mass flow rates were varying from 0.2135 to 0.401 g/s [20].
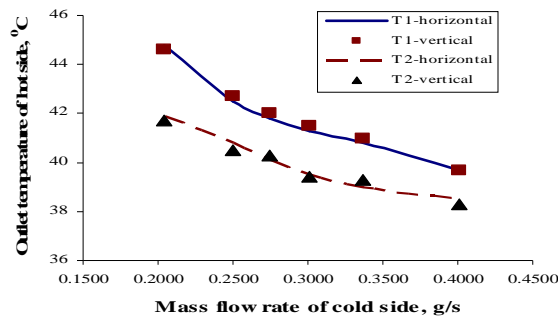
Fig. 8. Experimental comparison of the outlet temperatures of hot side

In this study, influence of gravity was determined by two cases: one with horizontal channels, the other with vertical channels. For vertical channels, the hot water is flowing upward which is against the gravitational field, while the cold water is flowing downward which is in the same direction as the gravitational field. Two microchannel heat exchangers T1 and T2 were tested: these two microchannel heat exchangers have the same physical configurations for their substrates, manifolds, and lengths of channels; only the cross-sectional areas of microchannels are different. The microchannels of T1 have a rectangular cross-section with width of 500 μm and depth of 300 μm; the microchannel of T3, width of 500 μm and depth of 180 μm. Parameters of the heat exchangers (T1 and T2) are listed in more detail in Table 1.
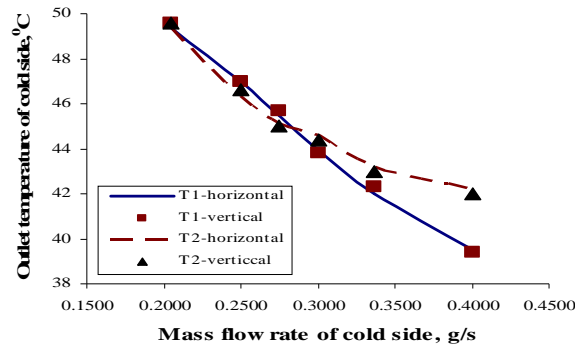
Fig. 9. Experimental comparison of the outlet temperatures of cold side

Experimental comparisons for the outlet temperatures of two microchannel heat exchangers are shown in Figs. 8 and 9 under the effect of gravity. From Figs. 6-9, it is indicated that the numerical results obtaned from Fig. 6 are in good agreement with the experimental results obtained from Fig. 8 and the numerical results obtaned from Fig. 7 are in good agreement with those obtained from Fig. 9. The maximum difference of outlet temperatures for the comparisons in of hot side obtained from horizontal channels and those from the vertical ones are negligibly small, with the maximum percentage of 2.9%.
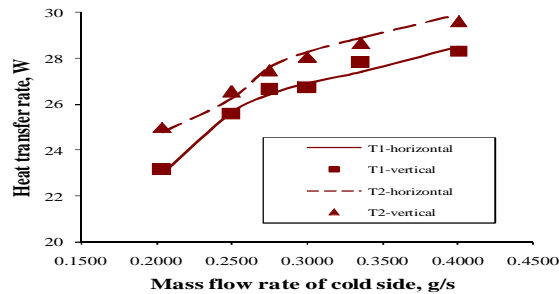
Fig. 10. Experimental comparison of the heat transfer rates

The outlet temperatures of hot side obtained from T1 is higher than those obtained from T2; however, the outlet temperatures of cold side obtained from T1 is lower than those obtained from T2. As a result, the heat transfer rate obtained from T2 is higher than that obtained from T1, as shown in Fig. 10. The results obtained from the present study are in good agreement with those obtained from [9]. Foli et al. [9] indicated that under the constant mass flow rate condition, the higher the heat flux, the lower the aspect ratio (defined as the ratio of the microchannel height to its width).

It is also shown from Fig. 10 that the heat transfer rates obtained from horizontal channels and those from the vertical ones are negligibly small. The heat transfer rate of the heat exchangers is a function of the mass flow rate of cold side: it increases from 24.8 to 29.92 W with the mass flow rate of cold side rising from 0.2043 to 0.401 g/s (for the heat exchanger T2).
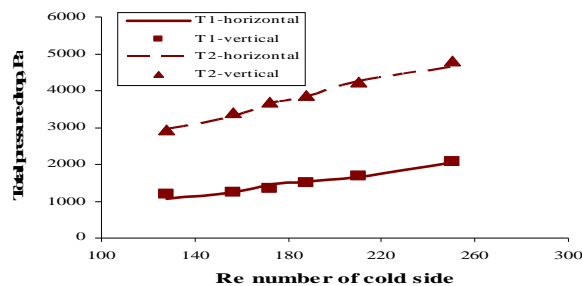
Fig. 11. Experimental comparison of the total pressure drops
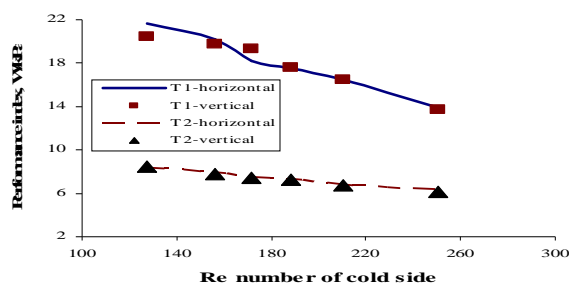
Fig. 12. Experimental comparison of the performance indices

Because that the hydraulic diameter of channel in T2 is smaller than that of channel in T1, this results in the velocity in the channel of T2 to be higher than that of T1, leading to a higher total pressure drop in T2 than that in T1, as shown in Fig. 11. Besides, the Figure shows that the total pressure drop is a function of Reynolds number of cold side; the total pressure drop increases as rising the Re number of cold side.

Experimental results for effects of gravity on the behavior of pressure drop for the microchannel heat exchanger are also shown in Fig. 11. It is observed that the change of pressure drop between the two cases (horizontal channels and vertical channels) is negligibly small; the maximum change in pressure is 7.2% for a pressure drop from 1060 to 2044 Pa.

It was found that the pressure drop of T2 is 2 times higher than that of T1, while the heat transfer rate of T2 is 1.06 times higher than that of T1. As a result, the performance index (defined as the ratio of the heat transfer rate to the pressure drop in the heat exchanger) obtained from T1 is higher than that obtained from T2, as shown in Fig. 12. For heat exchanger T1, a performance index of 21.68 W/kPa was achieved for water from the hot side having an inlet temperature of 70 °C and a mass flow rate of 0.2308 g/s and for water from the cold side having an inlet temperature of 22.5 °C and mass flow rate of 0.2135 g/s. It is also observed that the change of performance between the two cases (horizontal channels and vertical channels) is negligibly small; the maximum change in performance is 5.5%, out of a performance index from 13.69 to 21.68 W/kPa.

A comparison between numerical and experimental results for heat transfer rate with horizontal channels is shown in Fig. 13. It is observed that the numerical results are in good agreement with those obtained from the experimental ones, with the maximum percentage error of 2.94%.
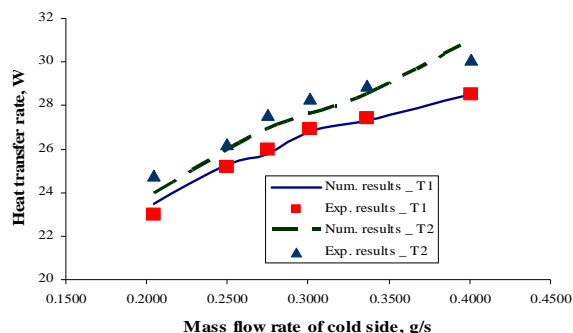
Fig. 13. Comparison of the heat transfer rates between numerical and experimental results with horizontal channels

In summary, it is concluded that the impact of gravity on the fluid flowing through the microchannel heat exchanger can be ignored as indicated in [10-15,17,18,20].

IV. CONCLUSION

Numerical and experimental works were done on two microchannel heat exchangers to carry out the evaluation of their performance for the varying the mass flow rates of the cold side. These two microchannel heat exchangers have the same physical configurations for their substrates, manifolds, and lengths of channels; only the cross-sectional areas of microchannels are different.

For heat exchanger T1, a performance index of 21.68 W/kPa was achieved for water from the hot side having an inlet temperature of 70 °C and a mass flow rate of 0.2308 g/s and for water from the cold side having an inlet temperature of 22.5 °C and mass flow rate of 0.2135 g/s.

The impact of gravity on the fluid through the microchannel heat exchanger was found to be small, with the maximum difference between the results of horizontal and vertical channels being less than 8%. The results obtained from numerical simulations and experimental data are in good agreement. In addition, in this study, good agreements were achieved between the results obtained from the present study and the results obtained from the literatures.

REFERENCES

[1]   T.T. Dang, J.T. Teng, and J.C. Chu, Pressure drop and heat transfer characteristics of microchannel heat exchangers: a review of numerical simulation and experimental data, International Journal of Microscale and Nanoscale Thermal and Fluid Transport Phenomena, Vol. 2, Issue 3, 2011

[2]   M.P. David, J. Miler, J.E. Steinbrenner, Y.Z. Yang, M. Touzelbaev, K.E. Goodson, Hydraulic and thermal characteristics of a vapor venting two-phase microchannel heat exchanger, International Journal of Heat and Mass Transfer, Volume 54, Issues 25-26, 2011, pp. 5504-5516

[3]   J.J. Brandner, L. Bohn, T. Henning, U. Schygulla, and K. Schubert, Microstructure heat exchanger applications in laboratory and industry, Proceedings of ICNMM2006, ICNMM2006-96017, Limerick, Ireland, 2006, pp. 1233-1243

[4]   T.A. Ameel, R.O. Warrington, R.S. Wegeng, and M.K. Drost, Miniaturization technologies applied to energy systems, Energy Conversion and Management, Volume 38, 1997, pp. 969–982

[5]   G.L. Morini, Single-phase convective heat transfer in microchannels: a review of experimental results, International Journal of Thermal Sciences, Volume 43, Issue 7, 2004, pp. 631-651

[6]   B. Mathew and H. Hegab, Application of effectiveness-NTU relationship to parallel flow microchannel heat exchangers subjected to external heat transfer, International Journal of Thermal Sciences, Volume 49, Issue 1, 2010, pp. 76-85

[7]   S.W. Kang and S.C. Tseng, Analysis of effectiveness and pressure drop in micro cross-flow heat exchanger, Applied Thermal Engineering, Volume 27, Isuue 5-6, 2007, pp. 877-885

[8]   R. Chein and J. Chen, Numerical study of the inlet/outlet arrangement effect on microchannel heat sink performance, International Journal of Thermal Sciences, Volume 48, Issue 8, 2009, pp. 1627-1638

[9]   K. Foli, T. Okabe, M. Olhofer, Y. Jin, and B. Sendhoff, Optimization of micro heat exchanger: CFD, analytical approach and multi-objective evolutionary algorithms, International Journal of Heat and Mass Transfer, Volume 49, Issue 5-6, 2006, pp. 1090-1099

[10]   T.T. Dang, Y.J. Chang, and J.T. Teng, A study on the simulations of a trapezoidal shaped micro heat exchanger, Journal of Advanced Engineering, Volume 4, Issue 4, 2009, pp. 397-402

[11]   T.T. Dang, J.T. Teng, and J.C. Chu, Effect of flow arrangement on the heat transfer behaviors of a microchannel heat exchanger, Proceedings of the International MultiConference of Engineers and Computer Scientists 2010, Hongkong, 2010, pp. 2209-2214

[12]   T.T. Dang and J.T Teng, Influence of flow arrangement on the performance index for an aluminium microchannel heat exchanger, IAENG Transactions on Engineering Technologies Volume 5, the American Institute of Physics (AIP), Vol. 1285, 2010, pp. 576-590

[13]   T.T. Dang and J.T. Teng, Effect of the substrate thickness of counter-flow microchannel heat exchanger on the heat transfer behaviors, Proceedings of the international symposium on computer, communication, control and automation 2010, Taiwan, 2010, pp. 17-20

[14]   T.T. Dang, J.T. Teng, and J.C. Chu, A study on the simulation and experiment of a microchannel counter-flow heat exchanger. Applied Thermal Engineering, Volume 30, Issue 14-15, 2010, pp. 2163-2172

[15]   T.T. Dang and J.T. Teng, Comparison on the heat transfer and pressure drop of the microchannel and minichannel heat exchangers, Heat and Mass Transfer, Vol, 47, 2011, pp. 1311-1322

[16]   T.T. Dang and J.T. Teng, The effects of configurations on the performance of microchannel counter-flow heat exchangers – An experimental study, Applied Thermal Engineering, Vol. 31, Issue 17-18, 2011, pp. 3946-3955

[17]   COMSOL Multiphysics version 3.5 – Documentation, Sept 2008

[18]   S.G. Kandlikar, S. Garimella, D.Q. Li, S. Colin, and M.R. King, Heat transfer and fluid flow in minichannels and microchannels. Elsevier, 2006.

[19]   J.P. Holman, Experimental methods for engineers, McGraw-Hill, New York, 1984

[20]   T.T. Dang, J.T. Teng, and J.C. Chu, Influence of gravity on the performance index of microchannel heat exchangers - Experimental investigations, Lecture Notes in Engineering and Computer Science: Proceedings of The World Congress on Engineering 2011, WCE 2011, 6-8 July, 2011, London, pp. 2094-2099.

Jyh-tong Teng, PhD, PE, is a professor in the Department of Mechanical Engineering and the Senior consultant of the Office of International Affairs at Chung Yuan Christian University (CYCU), Taiwan. He is also the principal investigator of an international education enhancement program sponsored by the Ministry of Education, Republic of China. He received his BS in Mechanical Engineering from Montana State University, MS and PhD in Mechanical Engineering from UC Berkeley. His research areas include thermo-fluidic analyses of compartment fires and smokes, nuclear safety, thermo-fluidics of microchannels, and thermal management of electronic devices.

Thanhtrung Dang, PhD, is a lecturer in the Department of Heat and Refrigeration Technology and the Vice Dean of the Faculty of Automotive Engineering, Hochiminh City University of Technical Education (HCMUTE), Vietnam. He received his BS and MS in the Department of Thermal Technology at Vietnam National University Hochiminh city – Hochiminh city University of Technology (HCMUT), PhD in the Department of Mechanical Engineering, Chung Yuan Christian University (CYCU), Taiwan. His main research interests are nano/microscale heat transfer, energy and sustainable development, industrial refrigeration and air conditioning, and energy economics.

Ngoctan Tran received his BS in the Department of Heat and Refrigeration Technology, Ho Chi Minh City University of Technical Education (HCMUTE), Hochiminh City, Vietnam in 2009. He employed part –time for P.Dussmann Vietnam Co., Ltd as a Supervisor of Engineering from 2008 to 2009, employed full –time for P.Dussmann Vietnam Co., Ltd as a Manager of Laundry Factory from 2009 to 2010, and employed for Darling Electronic – refrigerator Co., Ltd as a technical director in 2010. Presently, he is a master student at Department of Mechanical Engineering, Chung Yuan Christian University, Taiwan. He interested in studying on nano/microscale heat transfer, energy and sustainable development, industrial refrigeration and air conditioning, electronic and control system engineering, and energy economics.

OPERATION ON IDEALS

Adagba O Henry,

Dept. of Industrial Mathematics & Applied Statistics,
Ebonyi State University,
Abakaliki.

Abstract

We provide basic operations on ideals such as addition, intersection, multiplication, the formation of ideal quotients, radicals, and the extensions and contractions of ideals.

Keywords: Ideals, Commutative Algebra, Integral Domain, Field, Commutative Rings, Extensions of Ideals, Contraction of Ideals.

Mathematics Subject Classification: 46H10, 52B20, 13Gxx, 16S70

1.0 Introduction

Throughout this work we shall carry out certain exercises set by Professor $M.A$. Atiyah in his Notes on Commutative Algebra. This monograph was first published in mimeograph by Mathematical Institute at Oxford University in 1965. The whole of our presentation relies heavily on Atiyah's prototype which was later published as our reference [1] by Addison Wesley in 1969.

We discuss general method by which one can determine the operation on ideals that is, behavior of the ideals in a commutative unital ring. By operations, we mean basic operations on ideals such as addition, multiplication, intersection, the formation of ideal quotients, radicals, the extensions and contraction of ideals. If $A \neq \{0\}$ be a ring, then A has a maximal ideal and a minimal prime ideals is the major objective of this work. In specific cases which have been extensively studied this questions are extremely hard to answer.

The literatures covered by this study are fairly extensive, see for example [3], [4], or [6]. We consider the formation of radicals of ideals which is a natural consideration in the context of solution of equations and the factorization of elements in commutative rings. Let a be an ideal of A. The radical of a, $r(a)$ is the set of all $x \in A$, such that $x^n \in a$ for some integer $n \geq 1$ (or equivalently, it is the set of elements x in A whose image $\overline{x}$ in the factor ring A/a is nilpotent). Recently Lipman [5], Eakin et-al [8] and Sally et-al [9] have removed the assumption on characteristic. We can recover this result. Indeed, we find considerably more. Johnson [7] has conjectured that maximal ideals reduces the centralizers and operators and Eagon et-al [2] has conjectured that ideals defined by matrices and certain complex associated to them have a unique properties. We are able to show:

1.1 Definition

When we say that A is a ring, we shall mean that multiplication is commutative in A and that the multiplicative identity, denoted by 1, also belongs to A. Moreover, $1 \neq 0$, where 0 is additive identity. Also; if A, B are rings, a ring homomorphism

$$f : A \rightarrow B$$

Is a mapping such that whenever $x, \ y \in A$, we have

$$f(x+y) = f(x) + f(y)$$
$$f(xy) \quad = f(x)f(y)$$
$$f(1) \qquad = 1$$

We shall denote the ideal of multiples of an element x by (x). That is $(x) = \{ax : a \in A\}$. In general, we donate an ideal of A by notation a, b, p, m e.t.c. In this work, we discuss the basic operation on ideals, such as addition, intersection, multiplication, the formation of ideal quotients, radicals, and the extensions and contractions of ideals. We start with the class of ideals which are by far the most important in Commutative Algebra.

By definition, an ideal p is to be the prime ideal of A if:

    (i) $p \neq (1), \ (= A)$, and

    (ii) $xy \in p \Rightarrow x \in p \ \ or \ \ y \in p$.

Part of the reason for the importance of prime ideals lies in the following proposition which we state without proof:

1.2   Proposition

An ideal of A is a prime ideal if and only if its associated quotient ring A/a is an integral domain.

An ideal m in A is said to be maximal if:

    (i) $m \neq (1) \ (= A)$ and

    (ii) a is an ideal in A such that $m \subseteq a \subseteq A$; then either $a = m \ \ or \ \ a = A$.

We prove that every maximal ideal is a prime ideal by obtaining the following results:

1.3   Proposition

An ideal a of A is maximal if and only if its associated quotient A/a is a field.

Proof

Suppose a is a maximal ideal of A, then $a \neq A$ and so $A/a \neq \{0\}$, the zero ring. For any $x \in A$, we write $\overline{x} = x + a = \{x + y : y \in a\}$ and suppose that $\overline{x} \neq \overline{0}$ in A/a. To find its inverse, we note that $a + (x)$ is an ideal such that $a \neq a + (x)$. Moreover, we have $a \subseteq a + (x) \subseteq A$; hence $a + x = (1)$. And so there exists y such that $1 \equiv xy \ (\mathrm{mod} \ a)$. Hence $\overline{x}\,\overline{y} = \overline{1} \in A/a$. This proves that A/a is a field.

Conversely, suppose that A/a is a field and $a \subseteq b \subseteq A$ for any ideal b of A, the first inclusion being strict. Let $x \in A, \ y \in b, \ y \notin a$. Then $\overline{y} \neq \overline{0}$ in A/a. Since A/a is a field, one can find Σ such that $\overline{x} = \overline{y}\,\overline{z} \Rightarrow x - yz \in a \subseteq b \Rightarrow x \in b$, since $y \in b$, by hypothesis. This proves that $A \subseteq b \subseteq A \Rightarrow b = A$. Hence a is maximal. *Q. E. D.*.

Combining (1.2) and (1.3), it is clear that every maximal ideal is prime. The converse is obviously false, since $\{0\}$ is prime in $\square$, the ring of integers, without being maximal.

Next, to demonstrate the abundance of prime ideal, we prove the following:

1.4   Proposition

Let $A \neq \{0\}$ be a ring, then A has a maximal ideal.

Proof

Let S be the set of ideal $a \neq A$ of the ring A. By hypothesis, $(0) = A$ and so S is non-empty. We can therefore order S by inclusion. Consider any ascending chain $\{b_i : i \in I\}$ in S, so that for any $i, j \in I$ either $b_i \subseteq b_j \ or \ b_j \subseteq b_i$. Consider the set $b = \underset{i=I}{\cup} b_i$, we claim that b is an ideal.

Indeed, if $x \in b$, then $x \in b_i$ for some $i \in I$. Hence, $a = A \Rightarrow ax \in b_i \Rightarrow Ab \subseteq b$. Furthermore, if $x, \ y \in b$, then $y \in b_j$ for some $j \in I$ and without loss of generality, we may assume $b_i \subseteq b_j \Rightarrow x, y \in b_j \Rightarrow x \pm y \in b_j \subseteq b$.

Thus, our claim has been established. Moreover, since $i \in I \Rightarrow i \notin b_i$ by hypothesis, we deduce that $i \notin b$. Hence $b \in S$. Thus, any ascending chain in S has upper bound in S and so by zorn's lemma S has a maximal element, m say. This proves our proposition.

1.5   Proposition

If $A \neq \{0\}$ is a ring, then A has a minimal prime ideal.

Proof

Let Σ be the set of prime ideals in A. Σ is non-empty by (1.4). Let $\{p_i\}$ be a chain of prime ideals in Σ. Their intersection is an ideal $a = \underset{i=I}{\cap} \ p_i = \underset{p_i \subseteq p_j}{\cap} p_i$ for some $j \in I$.

To prove that a is indeed a prime ideal, suppose that $xy \in a,\ y \notin a$, then $y \notin p_j$ for some $j \in I$. Since $xy \in p_i$, $i \in I$, by the supposition that $xy \in a$ and by hypothesis p_j is prime, it follows that $x \in p_j$.

Moreover, if $p_i \subseteq p_j$, then $y \notin p_j \Rightarrow y \in p_i$, and by the argument, we have just used, we deduce that $x \in p_i$. Thus $x \in a = \underset{p_i \subseteq p_j}{\cap} p_i$.

Clearly $a \neq (1)$, since $i \in I \Rightarrow 1 \notin p_i$. Thus, a is a prime ideal. Moreover, since $p = \underset{i \in I}{\cap} p_i \subseteq p_i$ for all i, it follows that any chain in Σ has a lower bound in Σ and by zorn's lemma, Σ has a minimal element. This proves our proposition.

Next we turn to some results related to the formulation of ideals quotients.

Let a, b be ideals in a commutative ring A, the ideal quotient of a by b written $(a:b)$ is defined by $(a:b) = \{x \in A : xb \subseteq a\}$.

1.6   Proposition

Let a, b and c be ideals of ring A, then

    (i) $a \subseteq (a:b)$

    (ii) $(a:b)b \subseteq a$

    (iii) $((a:b):c) = (a:b\ c) = ((a:c):b)$

    (iv) $\left(\underset{i}{\cap}\ a_i : b \right) = \underset{i}{\cap}(a_i : b)$

    (v) $\left(a : \underset{i}{\Sigma}\ b_i \right) = \underset{i}{\cap}(a:b_i)$

Proof

(i) $a \subseteq (a:b)$. By definition of ideal, $x \in a \Rightarrow xb \subseteq a$ (because a is an ideal) $\Rightarrow x \in (a:b)$ by definition of $(a:b) \Rightarrow a \subseteq (a:b)$.

(ii)   By definition $(a:b)b$ is generated by products of the form xy where $x \in (a:b)$ and $y \in b$. But then $x \in (a:b),\ y \in b \Rightarrow xy \in a$. Hence, each generator of $(a:b)b$ lies in a and so $(a:b)b \subseteq a$ as required.

(iii)   Let $x \in ((a:b)c)$ and consider any generator yz of bc.

Then $z \in c \Rightarrow zx \in (a:b) \Rightarrow yzx \in a$, since $y \in b$. Hence multiplication by x transforms every generator of bc into an element of a.

Hence $xbc \subseteq a \Rightarrow x \in (a:bc) \Rightarrow ((a:b):c) \subseteq (a:bc)$

Next, let $u \in (a:bc)$. For any element $v \in c,\ w \in b$, we have

$vw \subseteq b = bc \Rightarrow uvw \in a \Rightarrow uw \in (a:c) \Rightarrow u \in ((a:c)b) \Rightarrow (a:bc) \subseteq ((a:c)b)$.

Let $s \in ((a:c)b),\ t \in b, r \in c$.

Then $st \in (a:c) \Rightarrow str \in a \Rightarrow srb \subseteq a \Rightarrow sc \subseteq (a:b) \Rightarrow s \in ((a:b)c)$

           $\Rightarrow ((a:c)b) \Rightarrow ((a:b)c)$ proving equality of the giving ideals.

(iv)   Let $x \in \left(\bigcap_i a_i : b \right)$; then $xb \subseteq a_i$ for each $i \Rightarrow x \in (a_i : b)$ for each $i \Rightarrow x \in \bigcap_i (a_i : b)$

$$\Rightarrow \left(\bigcap_i a_i : b \right) \subseteq \bigcap_i (a_i : b).$$

Conversely, $y \in \bigcap_i (a_i : b) \Rightarrow y \in (a_i : b)$ for each

$i \Rightarrow yb \subseteq \left(\bigcap_i a_i : b \right) \Rightarrow y \in \left(\bigcap_i (a_i : b) \right) \Rightarrow \bigcap_i (a_i : b) \subseteq \left(\bigcap_i a_i : b \right).$

This proves equality

(v)   Let $x \in (a_i : \Sigma b_i) \Rightarrow (\Sigma b_i) \subseteq a$. In particular, $b_i \subseteq \Sigma b_i \Rightarrow xb_i \subseteq a \Rightarrow x \in (a : b_i)$ for each

$i \Rightarrow x \in \bigcap_i (a : b_i)$. Hence $(a : \Sigma b_i) \subseteq \bigcap_i (a_i : b)$. Since an element of Σb_i is of the form

$u = y_1 + y_2 + \dots + y_n$, where $y_i \in b_{ij}$, then

$z \in \bigcap_i (a : b_i) \Rightarrow zy \subseteq a \Rightarrow z \in (a : \Sigma b_i) \Rightarrow \bigcap_i (a : b_i) \subseteq (a : \Sigma b_i)$. By Axiom of Extension

$(a : \Sigma b_i) = \bigcap_i (a : b_i)$.

Next, we consider the formation of radicals of ideals, which is a natural consideration in the context of solution of equations and the factorization of elements in commutative rings.

Let a be an ideal of A. The radical of a, $r(a)$ is the set of all $x \in A$, such that $x^n \in a$ for some integer $n \geq 1$ (or equivalently, it is the set of elements x in A whose image $\bar{x}$ in the factor ring A/a is nilpotent).

1.7   Proposition

Let a, b be ideals of a ring A and p be a prime ideal of A. Then

(i) $r(a) \supseteq a$

(ii) $r(r(a)) = r(a)$

(iii) $r(ab) = r(a \cap b) = r(a) \cap r(b)$

(iv) $r(a) = (1) \Leftrightarrow a = 1$

(v) $r(a + b) = r(r(a) + r(b))$

(vi)   if p is a prime, $r(p^n) = p$ for some $n > 0$

Proof

(i)   if $x \in a$, then taking $n = 1$, we have $x = x' \in r(a)$. Hence $a \subseteq r(a)$.

(ii)   By (i), $r(a) \subseteq r(r(a))$.

Conversely, $x \in r(r(a)) \Rightarrow x^n \in r(a)$ for some $n > 0 \Rightarrow (x^n)^m \in a$

for some $m > 0 \Rightarrow x^{nm} \in a$ for $nm > 0$. That is, $r(r(a)) = r(a)$.

(iii) $ab \subseteq a \cap b \Rightarrow r(ab) \subseteq r(a \cap b)$. Also, let $x \in (a \cap b)$, then $x^n \in a \cap b$ for some

$n > 0 \Rightarrow x^n \in a, x^n \in b \Rightarrow x \in r(a), x \in r(b) \Rightarrow x \in r(a) \cap r(b) \Rightarrow r(a \cap b) \subseteq r(a) \cap r(b)$.

Finally, let $y \in r(a) \cap r(b)$, then $y^n \in a, n > 0$ and $y^{m+n} = y^m y^n \in ab \Rightarrow y \in r(ab)$. Hence,

$r(a) \cap r(b) \subseteq r(ab)$ and we have the chain of inclusion

$r(ab) \subseteq r(a \cap b) \subseteq r(a) \cap r(b) \subseteq r(a \cap b)$.

By axiom of extension, we deduce that

$$r(ab) = r(a \cap b) = r(a) \cap r(b)$$

(iv) $\quad r(a) = (1) \Rightarrow 1 = 1^n \in a$ for some $n > 0 \Rightarrow a \supseteq (1) \supseteq a \Rightarrow a = (1).$

$\quad a = (1) \Rightarrow (1) = a \subseteq r(a)$ by $(i) \Rightarrow 1 = a \subseteq r(a) \subseteq (1) \Rightarrow r(a) = 1.$

(v) $\quad a + b \subseteq r(a) + r(b)$ by $r(a+b) \subseteq r(r(a) + r(b)).$

Conversely, let $y \in r(r(a) + r(b))$, then $y^n \in (r(a) + r(b))$ for some $n > 0$.

Suppose $y^n = u + v$, where $u \in r(a)$, $v \in r(b)$ with indices t, s; that is, $u^t \in a$, $v^s \in b$ for $t > 0$, $s > 0$. Hence $y^{n(t+s-1)} = (u+v)^{t+s-1} = \Sigma u^1 v^k$ where it is impossible for $1 < s$ and $k < t$ simultaneously. Hence $\Sigma u^1 v^k \in a + b$. Thus $y \in r(a+b)$.

(vi) $\quad$ Let $x \in r(p)$, then $x^n \in p^n$ for $n > 0 \Rightarrow x \in p$, since p is prime. Hence $p \subseteq r(p) \subseteq p$. Thus $r(p) = p$ by

(ii) $r(p^n) = \cap r(p) = \cap p = p$. *Q.E.D.*

Next, we consider extensions and contractions of ideals. Indeed, let A, B be commutative unital rings and let $f : A \to B$ be a ring homomorphism. The extension of an ideal a of A relative to f denoted by a^e, is the ideal b of B generated by $f(a)$ the image of a under f.

That is, $a^e = Bf(a) = \{y = \Sigma y_i f(x_i) : x_i \in a, y_i \in B\}.$

Conversely, if b is an ideal in B, then the inverse image, $f^{-1}(b)$ is easily verified to be an ideal in A. This ideal is denoted by b^c and is called the contraction of b in A induced by f. That is, $b^c = f^{-1}(b)$.

1.8 Proposition

Let a_1, a_2 be ideals of A, b_1, b_2 ideals of B and $f : A \to B$ be any ring homomorphism.

(i) $\quad (a_1 + a_2)^e = a_1^e + a_2^e, \ (b_1 + b_2)^c \supseteq b_1^c + b_2^c$

(ii) $\quad (a_1 \cap a_2)^e \subseteq a_1^e \cap a_2^e, \ (b_1 \cap b_2)^c = b_1^c \cap b_2^c$

(iii) $\quad (a_1 a_2)^e \subseteq a_1^e a_2^e, \ (b_1 b_2)^c \supseteq b_1^c b_2^c$

(iv) $\quad (a_1 a_2)^e \subseteq (a_1^e : a_2^e), \ (b_1 : b_2)^c \supseteq (b_1^c : b_2^c)$

(v) $\quad r(a)^e \subseteq r(a^e), \ r(b)^c \supseteq r(b^c)$

(vi) $\quad$ The set E of extensions in A is closed under the operation of sum and product while the set C of contractions in B is closed under the remaining three.

Proof

(i) (a) $\quad$ Let $x \in (a_1 + a_2)^e$, then $x = \Sigma u_i f(x_i)$ where $x_i \in a_1 + a_2$. Let $x_i = x_{1i} + x_{2i}$ for some i,

so that $f(x_i) = f(x_{1i}) + f(x_{2i})$, where $x_{1i} \in a_1$, $x_{2i} \in a_2$. But then, we have

$x = \Sigma u_i f(x_i) = \Sigma u_i f(x_{1i}) + \Sigma u_i f(x_{2i}) \in (a_1 + a_2).$

Hence $(a_1 + a_2)^e \subseteq a_1^e + a_2^e$. Then $w = \Sigma u_i f(x_i) + \Sigma v_j f(y_j)$, where

$x_i \in a_1 \subseteq a_1 + a_2$, $y_j \in a_2 \subseteq a_1 + a_2$.

Hence $w \in (a_1 + a_2)^e$. That is, $a_1^e + a_2^e = (a_1 + a_2)^e$

(b) Let $x \in b_1^c + b_2^c$, then $x = x_1 + x_2$, where $f(x_1) \in b_1$ and $f(x_2) \in b_2$.

Thus, $f(x) = f(x_1 + x_2) = f(x_1) + f(x_2) \in b_1 + b_2$.

Whence $x \in (b_1 + b_2)^c$. That is, $b_1^c + b_2^c \subseteq (b_1 + b_2)^c$.

(ii)(a) Let $x \in (a_1 \cap a_2)^e$, then $x \in \Sigma u_i f(x_i) \Rightarrow x_i \in a_1 \cap a_2$. But then

$x_i \in a_1$, $x_i \in a_2 \Rightarrow x = \Sigma u_i f(x_i) \in a_1^e$ and $x = \Sigma u_i f(x_i) \in a_2^e$

That is, $x = \Sigma u_i f(x_i) \in a_1^e \cap a_2^e$. Hence $(a_1 \cap a_2)^e \subseteq a_1^e \cap a_2^e$

(b) If $x \in (b_1 \cap b_2)^e \Rightarrow f(x) \in (b_1 \cap b_2) \Rightarrow f(x) \in b_1$,

$f(x) \in b_2 \Rightarrow x \in b_1^c$, $x \in b_2^c \Rightarrow x \in b_1^c \cap b_2^c \Rightarrow (b_1 \cap b_2)^c \subseteq b_1^c \cap b_2^c$

Conversely, let $y \in b_1^c \cap b_2^c$, then $f(y) \in b_1$, $f(y) \in b_2$.

Hence $f(y) \in b_1 \cap b_2 \Rightarrow y \in (b_1 \cap b_2)^c \Rightarrow b_1^c \cap b_2^c \subseteq (b_1 \cap b_2)^c$.

It follows that $b_1^c \cap b_2^c = (b_1 \cap b_2)^c$.

(iii)(a) Let $x \in (a_1 a_2)^e$. Then $x \in \Sigma u_i f(x_i)$, where, $x_i \in a_1 a_2$ for each i.

Since $x_i = \Sigma v_{j_i} w_{j_i}$, $v_{j_i} \in a_1$, $w_{j_i} \in a_2$ and

$\Sigma u_i f(x_i) = u_i f(\Sigma v_{j_i} w_{j_i}) = \Sigma u_i f(v_{j_i}) f(w_{j_i}) \in a_1^e a_2^e$ for each i.

It follows that $x \in a_1^e a_2^e$. Hence $(a_1 a_2)^e \subseteq a_1^e a_2^e$.

Conversely, let $y \in a_1^e a_2^e$, then $y = \Sigma u_1 v_1$ where $u_i \in a_1$ and $v_i \in a_2$. For any i,

we have $u_i = \Sigma z_j f(x_j)$, $x_j \in a_1$, $z_j \in B$, $v_i = \Sigma w_k f(s_k)$, $s_k \in a_2$, $w_k \in B$ and

$u_i v_i = (\Sigma z_j f(x_j))(\Sigma w_k f(s_k)) = \Sigma z_j w_k f(x_j) f(s_k) = \Sigma z_j w_k f(x_j s_k)$, $x_j \in a_1$, $s_k \in a_2$. Hence

$u_i v_i = \Sigma z_j w_k f(x_j s_k) \in (a_1 a_2)^e$ for each i. That is, $y \in (a_1 a_2)^e$. Thus $a_1^e a_2^e \subseteq (a_1^e a_2^e)^e$.

Finally, $(a_1^e a_2^e)^e \subseteq a_1^e a_2^e$.

(b) Let $x \in b_1^c b_2^c$, then $x \in \Sigma x_i y_i$, where $f(x_i) \in b_1$ and $f(y_i) \in b_2$. That is,

$f(x) = f(\Sigma x_i y_i) = \Sigma f(x_i) f(y_i) \in b_1 b_2 \Rightarrow x \in (b_1 b_2) \Rightarrow b_1^c b_2^c \subseteq (b_1 b_2)^c$.

(iv)(a) Let $x \in (a_1 : a_2)^e$, then $x = \Sigma u_i f(x_i)$ where $u_i \in B$ and $x_i \in (a_1 : a_2)$. Thus $x_i \in a_2 \subseteq a_1$, for

all i. Let $y \in a_2^e$, then $y = \Sigma v_j f(y_j)$ where $v_j \in B$, $y_j \in a_2$.

Thus $xy = \{\Sigma u_i f(x_i)\}\{\Sigma v_j f(y_j)\}$. Since $x_i y_j \in a_1$, for all i and it follows that

$xy = \Sigma u_i v_j f(x_i y_j) \in a_1^e \Rightarrow a_2^e \subseteq a_1^e \Rightarrow x \in (a_1^e : a_2^e) \Rightarrow (a_1 : a_2)^e \subseteq (a_1^e \subseteq a_2^e)$.

(b) Let $y \in (b_1 : b_2)^c \Rightarrow f(y) \in (b_1 : b_2)$. Let $x \in b_2^c$, then

$f(x) \in b_2 \Rightarrow f(y) f(x) \in b_1 \Rightarrow f(xy) \in b_1 \Rightarrow yx \in b_1^c \Rightarrow b_2^c y \subseteq b_1$

$\Rightarrow y \in (b_1^c : b_2^c) \Rightarrow (b_1 : b_2)^c \subseteq (b_1^c : b_2^c)$

(v)(a) Let $y \in r(a)^e$, then $y = \Sigma u_i f(y_i)$ where $y_i \in r(a)$ for each i.

$y^{ni} \in a$ for some $ni > 0 \Rightarrow f\left(y^{ni}\right) = \left\{f\left(y_i\right)\right\}^{ni} \in a^e \Rightarrow f\left(y\right) \in r\left(a^e\right)$ for each i.

Hence $y = \Sigma u_i f\left(y_i\right) \in r\left(a^e\right)$. Thus $r\left(a\right)^e \subseteq r\left(a^e\right)$.

(b) $y \in r\left(b\right)^c \Rightarrow f\left(y\right) \in r\left(b\right) \Rightarrow f\left(y\right)^n \in b$ for some $n > 0$

   $\Rightarrow y^n \in b^c \Rightarrow y \in r\left(b^c\right) \Rightarrow r\left(b^c\right) \subseteq r\left(b\right)^c$

Conversely, if $x \in r\left(b^c\right)$, then $x^m \in b^c$ for some $m > 0$.

Thus $f\left(x^m\right) \in b \Rightarrow f\left(x\right)^m \in b \Rightarrow f\left(x\right) \in r\left(b\right) \Rightarrow x \in r\left(b^c\right) \Rightarrow r\left(b^c\right) \subseteq r\left(b^c\right)$.

Hence $r\left(b\right)^c = r\left(b^c\right)$.

(vi)(a)   The set E of extensions is closed under the operations of sum and product. Indeed,

(i)(a) $a_1^e + a_2^e = \left(a_1 + a_2\right)^e$ and this ensures that the sum of two extensions is itself an   extension. Moreover

(ii)(a) $a_1^e a_2^e = \left(a_1 a_2\right)^e$ shows the product of two extensions is itself an extension.

The set C of contractions is closed under intersection by virtue of

(ii)(b) $b_1^c \cap b_2^c = \left(b_1 \cap b_2\right)^c$ and is closed under the formation of radicals by virtue of

$\left(v\right)\left(b\right),\ r\left(b^c\right) = r\left(b\right)^c$.

To prove that C is closed under the formation of ideal quotient, we first note that for any ideal a in A, we have $a \subseteq a^{ec}$ and also for $b \in B$, we have $b^{cec} = b^c$. Hence, we have the equality, $\left(b_1^c : b_2^c\right) = \left(b_1^{ce} : b_2^{ce}\right)^e$.

Conclusion

Our discussion of operation on ideals (and ideals of commutative rings as a special case), helps to explain the supreme importance of prime ideals in commutative Algebra. Intuitively we consider the formation of radicals of ideals, which is a natural consideration in the context of solution of equations and the factorization of elements in commutative rings. The extension of an ideal a of A relative to f denoted by a^e, is the ideal b of B generated by $f\left(a\right)$ the image of a under f.

That is, $a^e = Bf\left(a\right) = \left\{y = \Sigma y_i f\left(x_i\right) : x_i \in a,\ y_i \in B\right\}$.

Conversely, if b is an ideal in B, then the inverse image, $f^{-1}\left(b\right)$ is easily verified to be an ideal in A. This ideal is denoted by b^c and is called the contraction of b in A induced by f. That is, $b^c = f^{-1}\left(b\right)$.

Our results (1.4) and (1.5) shows that the ideals of non-trivial unital ring form a complete lattice. This is a property which A-module does not share.

References
1.   Atiyah, M. F.(1969), Introduction to Commutative Algebra. Addison-Wesley.
2.   Eagon J. and Northcoth D. (1962), Ideal defined by matrices and a certain complex associated to them, proc, Royal soc. A269, 188-204
3.   Eisenbud D. and Evans E.G.(1976), A generalized principal ideal theorem, Nagoya Math. J. 62, 41-53
4.   Henriksen, M.(1953), On the prime ideals of the ring of entire function. Pacific J.Math. 3, 711-720
5.   Lipman J. (1971), Stable ideals and Arf rings, Amer. J. Math. 93, 649-685.
6.   Recs J. (1961), Transforms of local rings and a theorem on multiplicities of ideals, proc. Combridges philos.soc.57, 8-17
7.   Johnson B.E. (1968), centralizers and operators reduced by maximal ideals, J. London Math. Soc. 43, 231-233
8.   Eakin P. and Sathaye A. (1976), prestable ideals, J. of Alg. 41, 439-454
9.   Sally J. D. and Vasconcelos W. V. (1975), Flat ideal 1, comm. in Alg. 3, 531-543

COMMUNICATION BY 31 BIT HAMMING CODE TRANSCEIVER WITH EVEN PARITY AND ODD PARITY CHECK METHOD BY USING VHDL

[1] **Mr.Brajesh Kumar Gupta** [2] **Prof. Rajeshwar Lal Dua**

M.Tech scholar   HOD

Department of Electronics & Communication engineering JNU, Jaipur

Abstract

In communication system communication is possible in three modes. They are simplex, half duplex and full duplex mode. Here, we are working on full duplex mode by using the property of transceiver. Transceiver can transmits and receives data simultaneously.

Here we generate 31 bit code to transmit 25 bit information data. And also find 25 bit actual information data from 31 bit received code.

To generate 31 bit data string form 25 bit actual information data for transmission at transmitting end we use Hamming code method. Here we also use Hamming code methodology for finding 25 bit actual information data from received 31 bit data string at receiving end.

To transmit 25 bit actual information data by using Hamming code even parity and odd parity check method we have to add 5 redundancy bits and 1 bit for deciding the type of parity used (even parity and odd parity) in actual data string . After adding these 6 bits in 25 bit information data we get 31 bit data string for transmission at transmitting end.

At receiver section, we find 25 bit actual information data string from 31 bit received data string. To find 25 bit information data from 31 bit received data sting we need 5 bit for finding error bit location (if any single bit or double bit error is occurred) and 1 bit is needed for selecting the same parity check method, which we have used at transmitting end.

Here we have written VHDL code for generating 31 bit data string code form 25 bit information data by Hamming code even parity and odd parity check methodology for transmission at transmitting end. Here we also written VHDL code at receiving end for finding 25 bit actual information data from received 31 bit data string code by Hamming code even parity and odd parity check method.

Here we have used Xilinx ISE 10.1 simulator to simulate this VHDL code. Xilinx simulator is a tool which is used for simulation of VHDL, Verilog HDL and schematic circuits.

In this paper we have described, what is communication and their respective mode in detail, in communication section.

In this paper we have also described, what is Hamming code and how it can generate 31 bit data for transmission by 25 bit information data at transmitting end, and how it can find 25 bit actual information from 31 bit received data string at receiving end.

In this paper, we have also described what transceiver is and how it works for communication at transmitting and receiving end.

Till now, from transmitting end we can only transmit data, not receive. And at receiving end we can only receive data but can't transmit.

Now, we can transmit as well as receive data at both ends (transmitting and receiving end) by using transceiver at both ends.

Key words- Hamming code , even parity check method , odd parity check method , redundancy bit , transceiver, transmitter , receiver , VHDL, Xilinx ISE 10.1 simulator

I. Introduction

Communication through 31 bit Hamming code transceiver with even and odd parity method is possible in full duplex mode. Here we design transceiver with even and odd parity check method for source and destination using VHDL code. [1][2][15][20].

In this paper we want to communication in full duplex mode with even and odd parity check method with 25 bit information data string. [1][2][15][20].

To transmit 25 bit information data string need minimum 5 redundancy bit and one extra bit for decide parity used for generate redundancy bit .

Here we generate 31 bit data string for transmit 25 bit information data at both section with even and odd parity check method.

Suppose at source section we want to transmit '25`h1B7777D' 25 bit information data, to transmit this 25 bit information data we generate 31 bit data string for secure communication with even and odd parity check method. To transmit '25`h1B7777D' 25 bit information data we get '31`h6DDCEFC9 or 31`h6DDDEEDE' 31 bit data string by even parity and odd parity check method respectively. To know how we get this 31 bit data string from 25 bit information data string we must be go through working of transceiver at source section.

Suppose, destination section transmit '31`h7DDDF6CF or 31`h7DDCF7D8' 31 bit data string for '25`h1F777BD' 25 bit information data string with even and odd parity check method . During transmission due to noise, source section`s transceiver receives '31`h79DDF6CF or 31`h7D9CF7D8'. Now source section transceiver finds actual information 25 bit data from corrupted data string. How source section transceiver find actual information data from corrupted data string describe in working of transceiver at source section.

At destination section suppose we want o transmit '25`h1F777BD' 25 bit information data string. To transmit this 25 bit information data string we transmit 31 bit data string to make communication secure. Here we transmit '31`h7DDDF6CF or 31`h7DDCF7D8' 31 bit data string for '25`h1F777BD' 25 bit information with even parity and odd parity check method. To know how we get this 31 bit data string for transmission of 25 bit information data describe in working of transceiver at destination section. [1][2][3][4][14][17][18].

Suppose , source section transceiver transmit '31`h6DDCEFC9 or 31`h6DDDEEDE' 31 bit data string by even parity check and odd parity check method respectively for communication between source and destination. During the transmission this data may be corrupt due to noisy and destination transceiver receives noisy '31`h6FDCEFC9 or 31`h6DDAEDE' 31 bit corrupted data string. Now destination transceiver finds actual 25 bit information data from received corrupted 31 bit data string by even parity or odd parity check method. To know how destination transceiver find 25 bit actual information data string from 31 bit corrupted data string describe in working of transceiver at destination section. . [1][2][3][4][14][17][18].

Here we use evenparity and oddparity out put pin to indicate received data is in even parity or in odd parity .

In this paper we write VHDL code for both source section transceiver and destination transceiver for find actual 25 bit information data string from received 31 bit corrupted data string.

In this paper we also write VHDL code for both section (source section and destination section) to generate 31 bit data string for transmission of 25 bit information data. [1][2][3][9][10][11][12][13]

Here we used Xilinx ISE 10.1 simulator to simulate this VHDL code for both section (source section and destination section). Xilinx ISE 10.1 simulator simulates VHDL code and gives their output in time cycle waveform.[7][8]

II. Communication

For communication we require minimum two sections, one of them is for transmitting data called source section and another for receiving data called destination section. According to the property of source and destination section, communication is possible in three different modes . They are Simplex mode communication , Half Duplex mode communication and Full Duplex mode communication [1][2][4][15][20].

Ii.i   simplex mode communication

In this mode communication is possible only in one way. In this mode source section is capable only for transmitting data string (cannot receive data string) and receiver section is capable only for receiving data string (cannot transmit data string) [1][2][15][20].
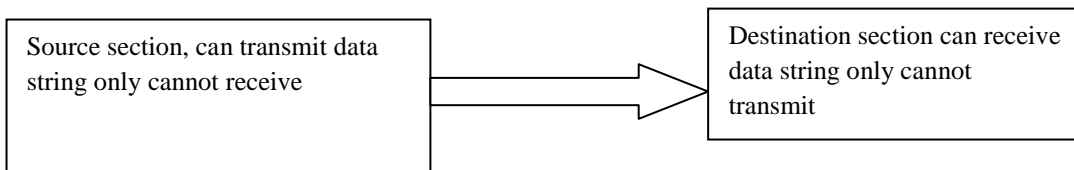
Fig.1 -   Communication in simplex mode

Ii.ii   half duplex mode communication

In this mode of communication is possible in two ways. In this mode both section can receives data string as well as transmit data string but cannot receives data string when transmitting and vice-versa[1][2][4][15][20]..
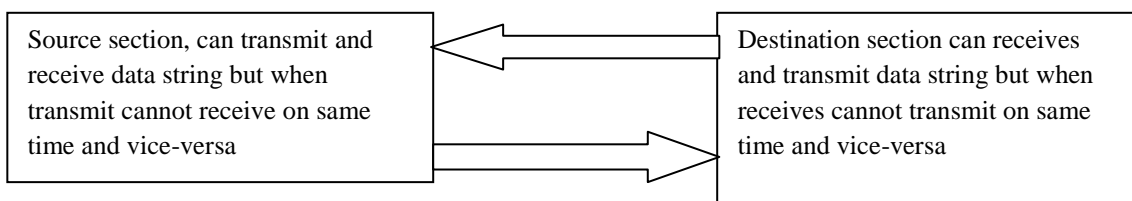
Fig. 2- Communication in Half duplex mode

Ii.iii   full duplex mode communication

In this mode of communication is possible in two ways. In this mode both source and destination section can receive data string as well as transmit data string simultaneously [1][2][4][15][20].

Source section, can receives as well as transmit data string	⟷	Destination section, can receives as well as transmit data string simultaneously
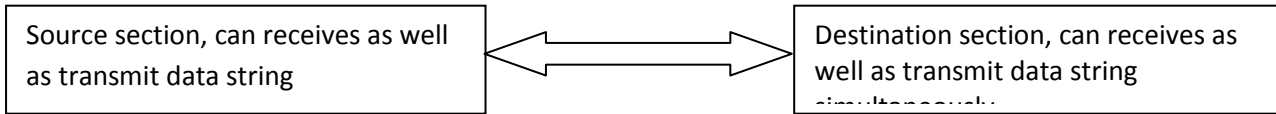
Fig. 3 -   Communication in Full duplex mode

III. Transceiver

Transceiver is a combination of transmitter section and receiver section. It can transmit data string as well as receive data string simultaneously. By using the transceiver we can communicate in full duplex mode.

Receiver section of transceiver works for finding 25 bit actual data string from received 31 bit data string and then check LSB bit whether it is zero or one. If LSB bit is zero then use odd parity check method else use even parity check method[4][15][19][20].

Receiving antenna

31 bit received data string

LSB is 'one'   LSB is 'zero'

EVEN parity method used to find actual data

ODD parity method used to find actual

Actual 25 bit information data
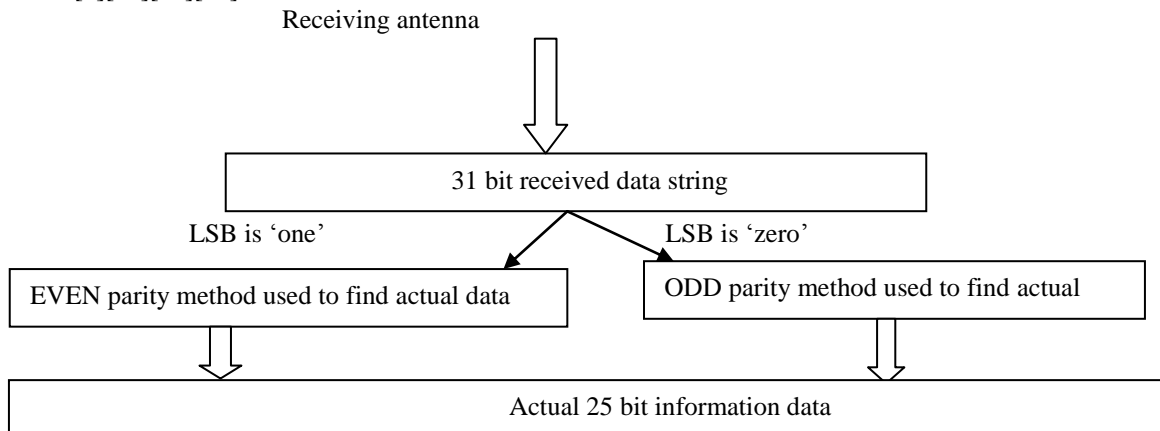
Fig .4 - Working Of Receiver Section of Transceiver

Transmitter section of transceiver generate 31 bit information data string for transmit 25 bit information data string with 5 redundancy bits and 'one' bit for parity decide.

Transmitting antenna

31 bit data string for transmission

Even parity method used for generating transmitting data string from given 25 bit actual information data

Odd parity method used for generating transmitting data string from given 25 bit actual information data

25 bit information data
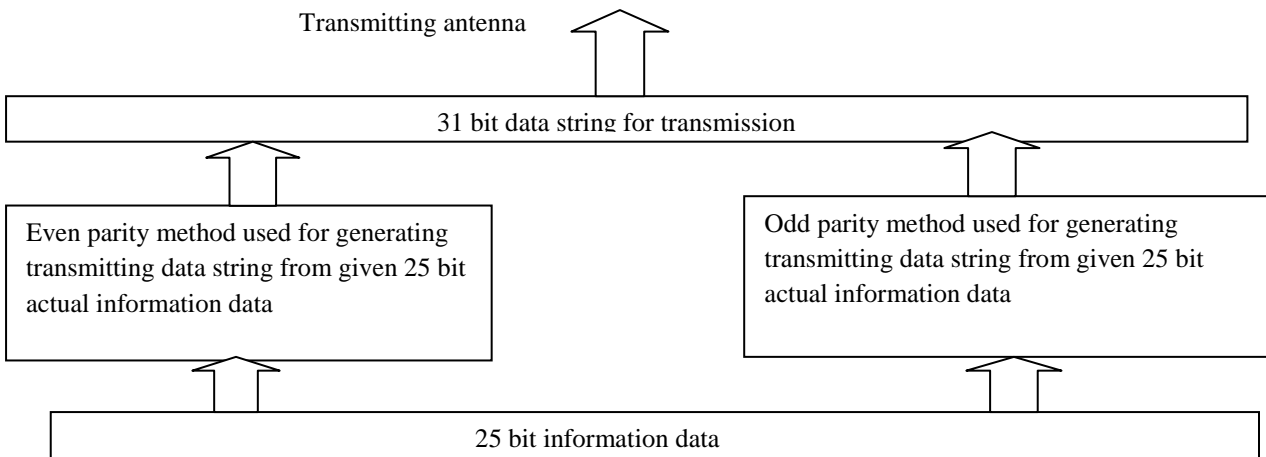
Fig.5 - Transmission section for Transceiver
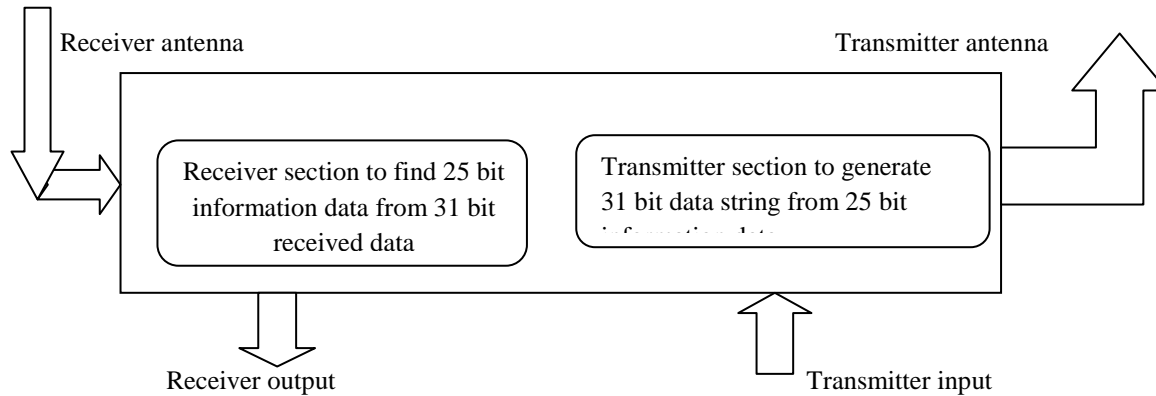
Fig.6 – Transceiver

IV. Hamming code

Hamming code is a linear error-correcting code named after its inventor, Richard Hamming. Hamming code can detect maximum two bit error, and correct only single-bit error. Thus, reliable communication is possible when the Hamming distance between the transmitted and received bit pattern is less than or equal to one. While the simple parity code cannot correct errors, it can only detect an odd number of errors.

In 1950 Hamming introduced the (7, 4) code. It encodes 4 data bits into 7 bits by adding three parity bits. Hamming (7, 4) can detect and correct single – bit errors. With the addition of overall parity bit, it can also detect (but not correct) double bit errors. Hamming code is an improvement on parity check method. It can correct 1 bit error [1][2][3][4][14][17][18].

Hamming code method works on only two methods (even parity, odd parity) for generating redundancy bit. In Hamming code method for generating the number of redundancy bit use formula .The number of redundancy depends on the number of information data bits [1][2][3][4][14][17][18]..

Formula for generating redundancy bit ----

$$2^r \;\; >= \;\; D + r \; + 1 \;\text{--- (1)}$$

Here   r = number of redundancy bit

D = number of information data bit Calculate the number of number of redundancy bit for 25 bit of input data string by above formula We get 5 redundancy bit required.

Iv.I   Redundancy

The central concept in detecting or correcting errors is redundancy. To be able to detect or correct errors, we need to send some extra bits with our data. These redundant bits are added by the sender and removed by the receiver. Their presence allows the receiver to detect or correct corrupted bits. The concept of including extra information in the transmission for error detection is a good one. But instead of repeating the entire data stream, a shorter group of bits may be appended to the end of each unit. This technique is called redundancy because the extra bits are redundant to the information [1][2][3][4][14][17][18]..

Iv.Ii   Even Check Parity Method

In even check parity method, count the number of one`s at transmitter and receiver section. if number of one`s are odd, add 'one' else add 'zero.' [1][2][3][4][14][17][18].

Iv.Iii   Odd Parity Check Method

In odd parity check method, count the number of one`s, if number of ones are odd add 'zero' and if number of one`s are even add 'one'. [1][2][3][4][14][17][18].

V. Working Of Transceiver At Source Section

At source section of transceiver, transceiver wants to transmit 31 bit encrypted data string to transmit 25 bit information data with 5 redundancy bit and 1 bit for parity check. And it receives 31 bit encrypted data string for finding 25 bit information data which was transmitted by destination section of the transceiver.

Suppose, Source section wants to transmit '25`h1B7777D' information data. To transmit '25`h1B7777D' information data transceiver needs to add 5 redundancy bit and one bit for deciding parity with 25 bit information data to make 31 bit encrypted data string for transmission. [1][2][3][4][14][17][18].

Suppose we want to transmit '25`h1B7777D' information data with even parity and odd parity check method. For even parity and odd parity check method transceiver generates 5 redundancy bits are '01000 = 5`h08 or 10111 = 5`h17' respectively. [1][2][3][4][14][17][18].

Now transceiver transmits '31`h6DDCEFC9 = 1101101110111001110111111001001 or 31`h6DDDEEDE = 1101101110111011110110011011110' 31 bit data string for 25`h1B7777D = 1101101110111011101111101, 25 bit information data for even parity and odd parity check method respectively.

To know how we can get this 31 bit data string and 5 redundancy bit for 25 bit information data we must go through the section of working of transmitter of transceiver at source section. [1][2][3][4][14][17][18].

Suppose, Destination section transmits '31`h7DDDF6CF = 1111101110111011111011011001111 and 31`h7DDCF7D8 = 1111101110111001110111110111000' 31 data string for '25`h1F777BD = 1111101110111011110111101' bit information data with even parity check and odd parity check method respectively. Now transmitter of destination section transmits 31 bit data string travel through channel from destination to source section. [1][2][3][4][14][17][18].

Suppose, this channel is noisy due to this noisy channel source section transceiver receives corrupted 31 bit data string. After receiving this corrupted 31 bit data string , source section transceiver find the corrupted data bit location and correct that error bit and find correct 31 bit data string whose transmit by destination section. After finding correct 31 bit data string transceiver pass actual 25 bit information data. To know how transceiver find actual 25 bit information data string from 31 bit corrupted data string go through working of receiver of transceiver at source section transceiver.

V.I   Working Of Transmitter Of Transceiver At Source Section

Transmitter of transceiver at source section generates 31 bit data string for 25 bit information data.

In this paper we want to transmit 25 bit information data with even and odd parity check method. To transmit 25 bit information data we need minimum 5 redundancy bit according to equation 1.

Suppose these redundancy bits are $r(1),r(2),r(4),r(8),r(16)$. To calculate the redundancy bit, we count the number of ones in appropriate address of information data bit according to given below...

$r(1)$ = 1,2,4,5,7,9,11,12,14,16,18,20,22,24.
$r(2)$ = 1,3,4,6,7,10,11,13,14,17,18,21,22,25
$r(4)$ = 2,3,4,8,9,10,11,15,16,17,18,23,24,25
$r(8)$ = 5,6,7,8,9,10,11,19,20,21,22,23,24,25
$r(16)$ = 12,13,14,15,16,17,18,19,20,21,22,23,24,25

Suppose, we want to transmit '25`h1B7777D = 1101101110111011101111101' 25 bit information data with even and odd parity check method. To transmit this 25 bit information data we must need to add 5 redundancy bit. Calculation of redundancy bit depends on the parity check method (which one we use). For even parity method the value of these 5 redundancy bits are '5`h08 = 01000' and for odd parity method the value of redundancy bits are '5`h17 = 10111'.Now we add these redundancy bit with 25 bit information data and get 30 bit data string according to parity check method. [1][2][3][4][14][17][18].

Before transmission of this data string we must add decided parity bit "stransmitterevenodd" bit to this 30 bit data string to make 31 bit data string for transmission. If stransmitterevenodd bit is one it indicates that we have used even parity check method else we have used odd parity check method to generate 31 bit data string for transmission. Now we have 31 bit data string for transmit of 25 bit information data with even and odd parity check method. [1][2][3][4][14][17][18].

Here "stransmitterinput" indicates 25 bit information data string, which we want to transmit by transceiver at Source section.

The block diagram of transmitter of transceiver shown below..

25 bit stransmitterinput

One bit Stransmitterevenodd
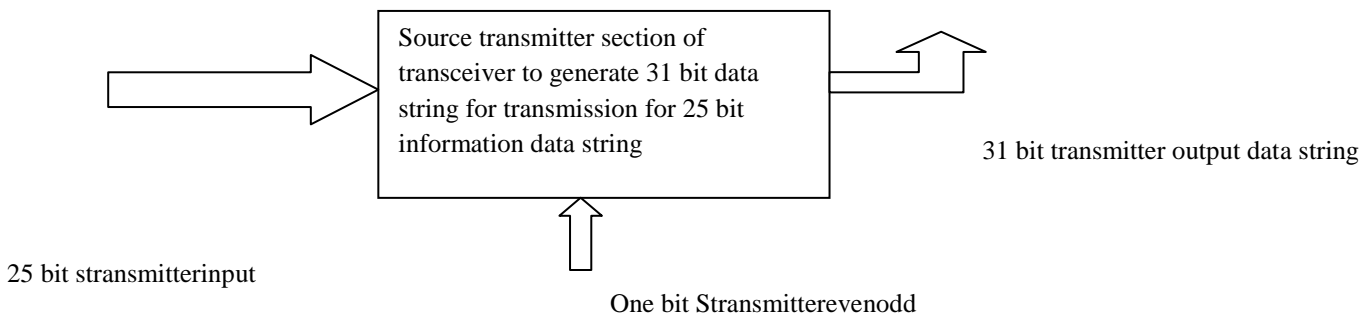
Fig. 7 Block diagram of transmitter of transceiver at source section

V.II Working Of Receiver Of Transceiver At Source Section

At receiver section of transceiver, transceiver receives 31 bit data string which was transmitted by source section. After receiving this 31 bit data string receiver checks that is there any error in data string? If any error is occurred receiver finds the error bit location and corrects that error bit. [1][2][3][4][14][17][18].

Suppose, at source section receiver receives '31`h79DDF6CF = 1111001110111011111011011001111 or 31`h7D9CF7D8 = 1111101100111001111011111011000' 31 bit data string in place of '31`h7DDDF6CF = 1111101110111011111011011001111 or 31`h7DDCF7D8 = 1111101110111001111011111011000' 31 bit data string due to noisy channel. Now to find the error bit location we need minimum 5 error address bit. [1][2][3][4][14][17][18].

Suppose the name of error address bit is "serroraddress" . To find the value of "serrorradderss" bit we use formula given below. [1][2][3][4][14][17][18].

serroraddress (1) = 1,3,5,7,11,13,15,17,19,21,23,27,29
serroraddress (2)=2,3,6,7,10,11,14,15,18,19,22,23,26,27,30
serroraddress (3)=4,5,6,7,12,13,14,15,20,21,22,23,28,29,30
serroraddress (4)=8,9,10,11,12,13,14,15,24,25,26,27,28,29,30
serroraddress (5)=16,17,18,19,20,21,22,23,24,25,26,27,28,29,30

Before calculation of 'serroraddress' bits, we must know about the received data is generated in even parity method or odd parity check method at destination section. To know about 31 bit received data is in even parity method or odd parity check method, first check the LSB bit of received data. If LSB bit is 'one' means it generated in even parity check method else is generated in odd parity method. [1][2][3][4][14][17][18].

Suppose, the name of 31 bit input pins are "sreceiverinput". At receiver for '31`h79DDF6CF or 31`h7D9CF7D8' 31 bit data string the value of sreceiverinput(0) is 'one' and 'zero' respectively. Sreceiverinput(0) bit indicate that '31`h79DDF6CF' 31 bit data string is designed by even parity check method and '31`h7D9CF7D8' 31 bit data string is designed by odd parity check method at destination section.

After finding the parity, we find the value of "serroraddress" bits are '5`h1A = 11010 or 5`h16 = 10110' for '31`h79DDF6CF or 31`h7D9CF7D8' received 31 bit data string by even and odd parity check method. Now receiver find correct 31 bit data string is '31`h7DDDF6CF or 31`h7DDCF7D8' whose transmitted by destination section. After correcting the corrupted received 31 bit data string, receiver of source section regenerates the 25`h1F777BD' actual 25 bit information data string which was transmitted by the destination section. [1][2][3][4][14][17][18].

The block diagram of receiver section shown below...

31 bit sreceiverinput → Receiver section of transceiver, find 25 bit actual information data from 31 bit received data string → ``25 bit sreceiveroutput / one bit evenparity / One bit Oddparity
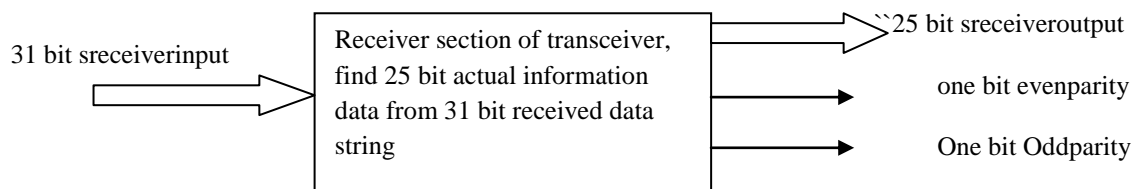
Fig. 8 –Bblock diagram of receiver of transceiver at source section

In this paper we have written VHDL code for transmitter and receiver for transceiver of source section. At transmitter section we have written VHDL code for generate 5 redundancy bit for 25 bit information data string to make 31 bit data string for transmission. [1][2][3][9][10][11][12][13]

At receiver section we also written VHDL code for finding error bit location and correcting that error bit by replacing 'zero' by 'one' and 'one' by 'zero'. We have written VHDL code for regenerate 25 bit information data string from 31 bit correct data string. [1][2][3][9][10][11][12][13]

In this paper, we use Xilinx ISE 10.1 simulator to simulate this VHDL code for transmitter and receiver section of transceiver. The VHDL code for transceiver shown in Xilinx ISE 10.1 project navigator window and input output wave form for transceiver at source section shown in Xilinx ISE 10.1 simulation window. [7][8]

Xilinx ISE 10.1 project navigator and Xilinx ISE 10.1 simulation window shown below.

Fig . 9 - Xilinx ISE 10.1 project navigator window shows VHDL code for source section
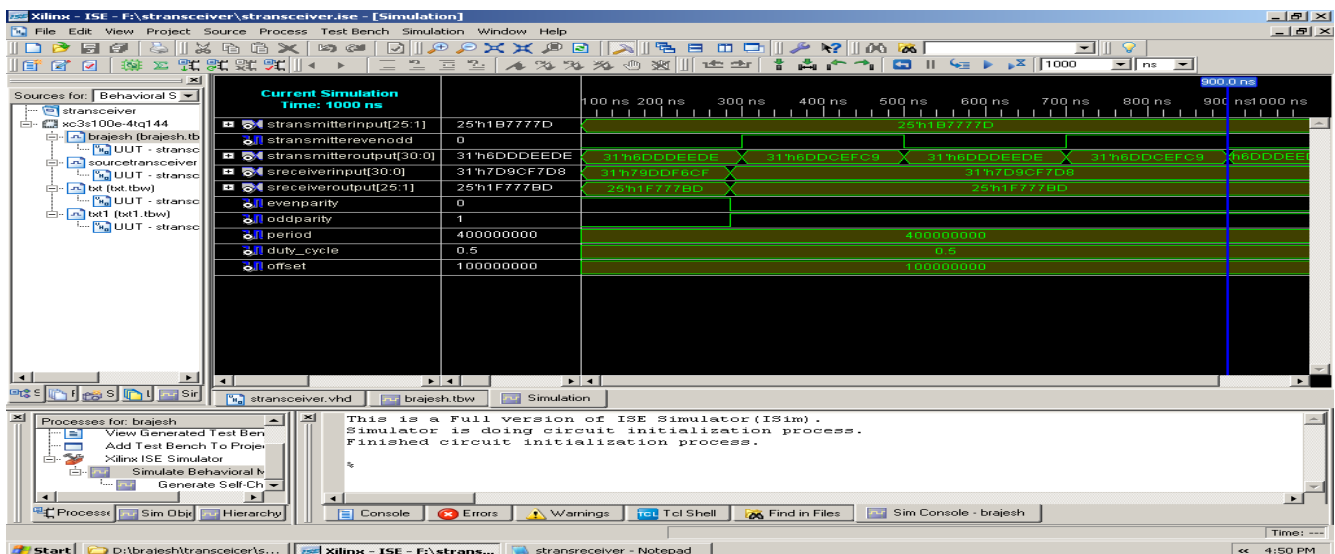
Fig .10 - Xilinx ISE 10.1 simulation window display input output waveform for source section

VI. Working Of Transceiver At Destination Section

At destination section transceiver want to transmit '25`h1F777BD = 1111101110110111110111101' 25 bit information data string. To transmit this 25 bit information data need minimum 5 redundancy bits and 'one' parity decide bit to make 31 bit data string for transmission by transceiver. [1][2][3]

In this paper, If parity decide bit is 'one' means we use even parity method to generate 5 redundancy bit else we use odd parity check method to generate 5 redundancy bit. . [1][2][3][4][14][17][18].

Suppose the name of 25 bit information data is 'dtransmitterinput', one bit parity decides bit is 'dtransmitterevenodd' and 31 bit transmitted data is 'dtransmitteroutput'. [1][2][3][4][14][17][18].

In this paper at destination section we want to transmit "25`h1F777BD" 25 bit information data; to transmit 25`h1F777BD information data first we check the value of "dtransmitterevenodd" bit. If "dtransmitterevenodd" bit is 'one' use even parity method to calculate the value of redundancy bits else we use odd parity method to calculate the value of redundancy bits. . [1][2][3][4][14][17][18].

The value of redundancy bits are '5`h13 = 10011 or 5`h0C = 01100' for 25`h1F777BD information data string by even parity check method or odd parity check method respectively.

Now to generate 31 bit encrypted data string for transmission, we use 25 bit information data , 5 redundancy bits and 'one' parity decide bit. By using these bits we get '31`h7DDDF6CF or 31`h7DDCF7D8' 31 bit encrypted data string for transmission by even parity check method or odd parity check method respectively.

The generation method of 31 bit data transmission for 25 bit information data at destination is same as transmitter of transceiver at source section. . [1][2][3][4][14][17][18].

At destination section, transceiver receives 31 bit data string, and find is there any error or not? If any error is occurred transceiver find this error bit location and correct that error bit by replacing 'zero' by 'one' and one by zero. After correcting error bit transceiver regenerate actual 31 bit data string who's transmitted by source section transceiver. Now transceiver find actual 25 bit information data string from corrected 31 bit data string.

Suppose , source section want transmit '25`h1B7777D = 1110101110111011101111101 ' 25 bit information data by encrypted '31`h6DDCEFC9 = 1101101110111001110111111001001 or 31`h6DDDEEDE = 1101101110111011110111011011110' 31 bit data string is generated by even parity check or odd parity check method. Now transceiver of destination section receives '31`h6FDCEFC9 = 1101111110111001110111111001001 or 31`h6DDAEDE = 1101101110110101110111011011110' 31 bit corrupted data string due to noise. . [1][2][3][4][14][17][18].

After receiving of '31`h6FDCEFC9 or 31`h6DDAEDE' 31 bit corrupted data string , receiver section of transceiver at destination check is there any error is occurred or not ? If any error is occurred receiver find that error bit location. . [1][2][3][4][14][17][18].

To find the error bit location we have written VHDL code for generate "derroraddress" bits(name of error bit address) by even parity check or odd parity check method. [1][2][3][4][14][17][18].

The calculation of finding "derroraddress" bits is same as the "serroraddress" bits at source section. By using this method we find the value of "derroraddress" is '5`h19 = 11001 or 5`h0E = 01110' by even parity check or odd parity check method respectively.

Now transceiver of destination section knows that the location of error bit for '31`h6FDCEFC9 or 31`h6DDAEDE' 31 bit received corrupted data string. After finding the address of error bit location transceiver correct this error bit by replacing one by zero or zero by one and get actual 31 bit data string is '31`h6DDCEFC9 or 31`h6DDDEEDE' whose transmitted by transceiver of source section.

After correcting error bit, we capable to generate actual 25 bit information data string from corrected 31 bit data string. we get 25`h1B7777D actual 25 bit information data string Form '31`h6DDCEFC9 or 31`h6DDDEEDE' 31 bit data string. . [1][2][3][4][14][17][18].

The generation method of 25 bit information data string from received 31 bit corrupted data string is same as generation method 25 bit information data string from received corrupted 31 bit data string at source section.

Here we already described the method for generating actual 25 bit actual information data string from received 31 bit corrupted data string above in working of receiver of transceiver at source section. [1][2][3][4][14][17][18].

Here we use the term dtransmitterinput , dtransmitteroutput , dtransmitterevenodd , dreceiverinput , dreceiverout ,evenparity ,oddparity for representing destination 25 bit information data input , destination 31 bit encrypted data string for transmission , destination 1 bit parity decide bit for generation 31 bit encrypted data string , destination 31 bit received corrupted data string , destination 25 bit actual information data string output , received data string is generated in even parity , received data is generated in odd parity method.

At destination section, we have written VHDL code for generating 31 bit encrypted data string form 25 bit information string for transmission. We written VHDL code for finding 25 bit information data string from received 31 bit corrupted data string. [1][2][3][4][14][17][18].

Here we use Xilinx ISE 10.1 simulator for simulate VHDL code of transceiver at destination section. The VHDL code for transceiver at destination section shown in Xilinx ISE 10.1 project navigator window and Input output time wave form for transceiver at destination shown in Xilinx ISE 10.1 simulation window below.[7][8]
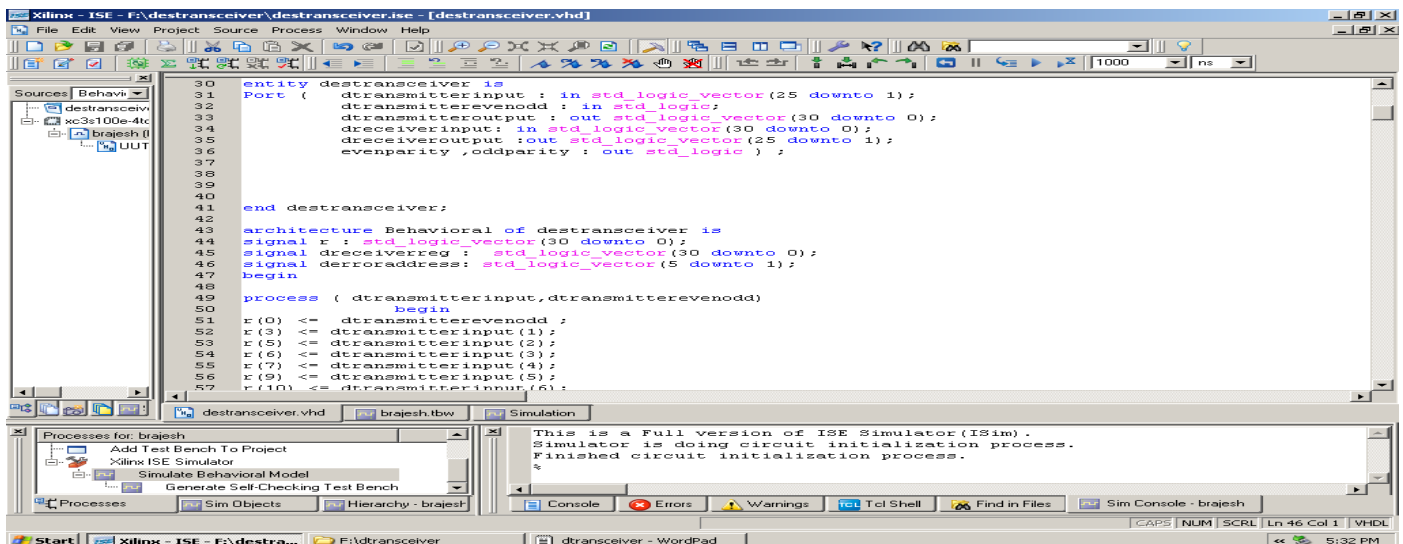
Fig. 11 - Xilinx ISE 10.1 project navigator window display VHDL code for destination section

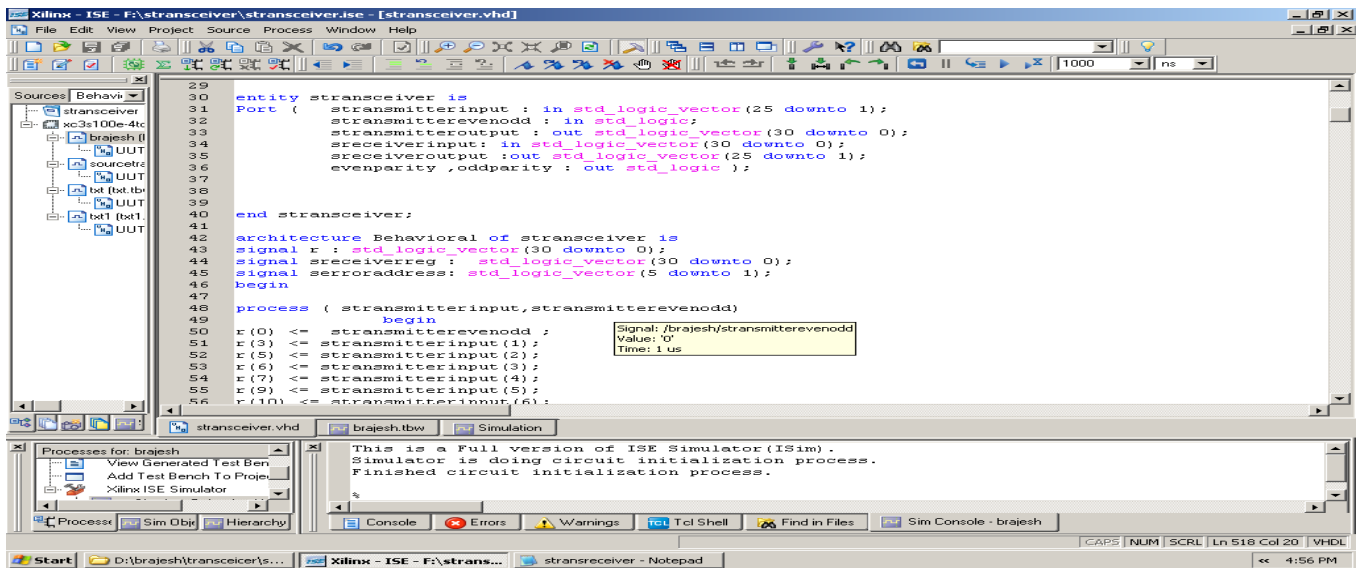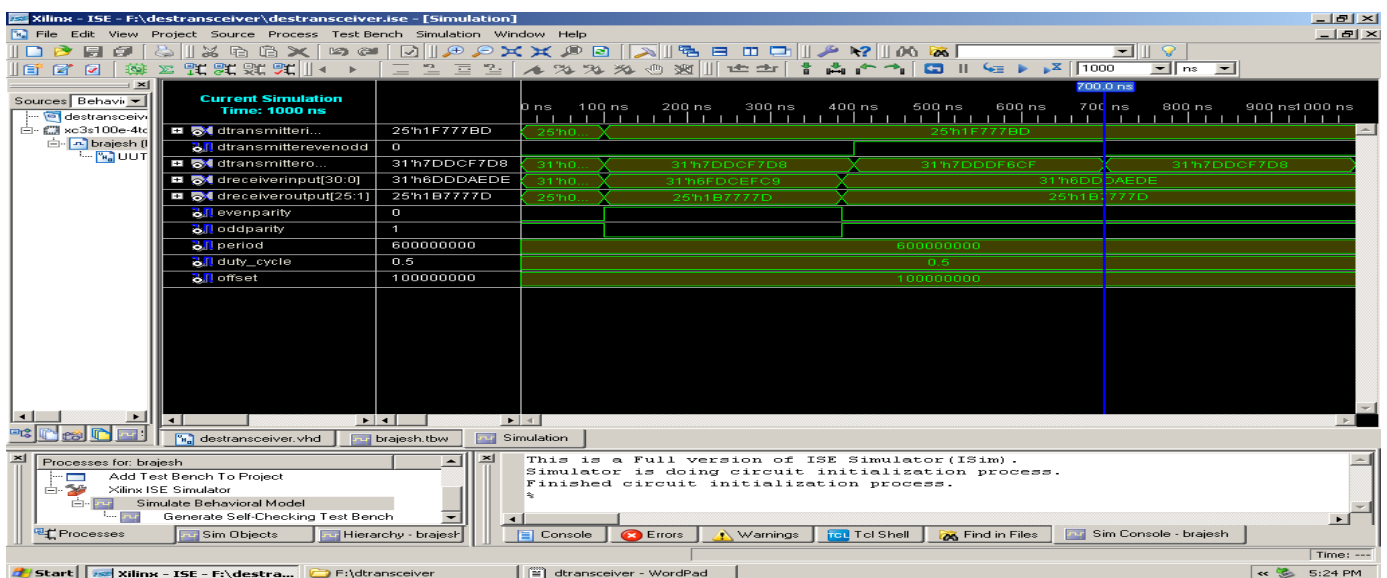Fig. 12 - Xilinx ISE 10.1 simulation window display simulated results for destination section

VII. Application

Hamming code methodologies is capable for detecting 2 bit error and correcting single bit error. When we use Hamming code methodology for communication, if single bit error is occurred due to noisy channel no need to retransmit data string again for proper communication because it is able to correct single bit error.

In this paper we design system, to be able to communicate in full duplex mode with 25 bit information data string by even parity and odd parity check method.

The application of this system is that now we can communicate with 25 bit information data string in full duplex mode.

Error detection and correction codes are used in many common systems including: storage devices (CD, DVD, and DRAM), mobile communication (cellular telephones, wireless, and microwave links), digital television, and high-speed modems (ADSL, xDSL).

VIII. Advantage

Before publication of my research paper, communication is possible by 7 bit information data string only. After publication of my some research papers communication is possible by 25 bit information data string. But till now, communication is possible in simplex mode only by transmitting 30 bit data string with even parity and odd parity check method for 25 bit information data.

Till now, source section is capable only for generating 30 bit data string for transmission and destination is capable for regenerate actual 25 bit information data string from received 30 bit corrupted data string.

In this paper, we use transceiver at source section and destination to make both sections capable for receiving and transmitting data string.

Here we transmit 31 bit data string for transmit 25 bit information data with 5 redundancy bits and '1' extra bit for parity decide.

The advantage of this paper is that now communication is possible in full duplex mode (means both section source and destination can transmit as well as receives data string simultaneously).

Speed of communication system also depends on the number of frame (combination of number of bit is called frame) that can be transmitted in a second. To increase the speed of communication system increases the number of frame per second or increase the number of bits in a frame.

Here we have increased the frame size to increase the number of bits in a single frame. Up to today we can transmit only 11 bit (7 bit data and 4 redundancy bit) in a frame but now we can transmit 31 bits (25 bit information data with 5 redundancy bit and 'one' extra bit for parity decide) in a single frame.

IX.   Conclusion

The overall conclusion is that, now communication is possible in full duplex mode with 25 bit information data string without retransmit data string if any single bit error is occurred.

By using this paper both sections are capable to generate31 bit data string for transmit 25 bit information data with even parity and odd parity check method. Both sections are also capable to receive 31 bit corrupted data string and finding actual 25 bit information data string from received 31 bit corrupted data string.

Speed of communication depends on the number of frame (combination of number of bit is called frame) can be transmitted in a second. To increase the speed of communication system increases the number of frame per second or increase the number of bits in a frame. Here we have increased the frame size to increase the number of bits in a single frame. Up to today we can transmit only 11 bit (7 bit data and 4 redundancy bit) in a frame but now we can transmit 31 bit (25 bit information data with 5 redundancy bit and one parity decide bit) in a single frame.

X. Reference –

[1].   Brajesh Kumar Gupta, Rajeshwar Lal Dua, "30 bit Hamming code for Error Detection and correction using VHDL" National Journal of Engineering Science And Management (ISSN : 2249-0264) volume number I issue II .

[2].   Brajesh Kumar Gupta, Rajeshwar Lal Dua, B.Surya Narayana Raju "30 bit Hamming code for Error Detection and correction with Odd parity Method using VHDL" International Journal of Computer Science And Communication (ISSN : 0973-7931) volume III Number I .

[3].   Brajesh Kumar Gupta, Rajeshwar Lal Dua, "30 bit Hamming code for Error Detection and correction with Even parity and Odd parity Check Method By Using VHDL" International Journal Of computer Applications (ISBN : 978-93-80865-96-2) Volume 35 Number 13.

[4].   Data communication and networking , Behrouz A. Forouzan , 2nd edition Tata McGrawHill publication.

[5].   .http://www.pragsoft.com/books/CommNetwork.pdf

[6].   http://www.eng.uwaterloo.ca/~tnaqvi/downloads/DOC/sd192/ISE8_1i_manuals.pdf

[7].   http://www.xilinx.com/training/xilinx-training-courses.pdf

[8].   http://www.xilinx.com/itp/xilinx10/books/docs/qst/qst.pdf

[9].   http://en.wikipedia.org/wiki/VHDL

[10]. http://www.vhdl-online.de/tutorial/

[11]. http://www.doulos.com/knowhow/vhdl_designers_guide/

[12]. A VHDL Primer , J. Bhasker , 3 rd edition PHI   publication.

[13]. Digital Logic Design with VHDL , Stephen Brown & Zvonko Vranesic , 2 nd edition TMH publication

[14]. Hamming r.w error detection and correction code, bell sys. Tech. J.29:147-60 1950 bell telefone laboratories ,murray hill

[15]. Http://www.britannica.com/ebchecked/topic/585799/telecommunication/76275/repetition-codes#ref608200-

[16]. Http://www.britannica.com/ebchecked/topic/253662/richard-wesley-hamming#ref1073410

[17]. Http://www.cs.princeton.edu/courses/archive/spring12/cos126/assignments/hamming.html

[18]. logic and computer design fundamental 4th edition error detection and correction

[19]. computer architecture and interfacing by dr. T itagaki -- http://people.brunel.ac.uk/~eesttti

[20]. data and computer communication , chapter 6 digital data communication technique

Professor Rajeshwar Lal Dua a Fellow Life Member of IETE and also a Life member of: I.V.S & I.P.A, former "Scientist F" of the Central Electronics Engineering Research Institute (CEERI), Pilani has been one of the most well known scientists in India in the field of Vacuum Electronic Devices for over three and half decades. His professional achievements span a wide area of vacuum microwave devices ranging from crossed-field and linear-beam devices to present-day gyrotrons.

He was awarded a degree of M.Sc (Physics) and M.Sc Tech (Electronics) from BITS Pilani. He started his professional carrier in1966 at Central Electronics Engineering Research Institute (CEERI), Pilani. During this period he designed and developed a specific high power Magnetron for defence and batch produced about 100 tubes for their use. Trained the Engineers of Industries with know how transfer for further production of the same.

In 1979 he visited department of Electrical and Electronics Engineering at the University of Sheffield (UK) in the capacity of independent research worker, and Engineering Department of Cambridge University Cambridge (UK) as a visiting scientist. After having an experience of about 38 years in area of research and development in Microwave field with several papers and a patent to his credit. In 2003 retired as scientist from CEERI, PILANI & shifted to aipur and joined the profession of teaching. From last eight years he is working as professor and head of electronics department in various engineering colleges. At present he is working as head and Professor in the department of Electronics and communication engineering at JNU, Jaipur. He has guided several thesis of M.tech .of many Universities.

Mr. Brajesh Kumar Gupta , student of Mtech IV sem of Jaipur National University, Jaipur , I have completed my B.E from "R.K.D.F institute of science & Technology ",Bhopal in 2007 in Electronics & Communication Engineering under the university of R.G.P.V Bhopal . I also done VLSI design Advanced post Graduation Diploma in DEC- 2007 from VEDANT , SCL (semiconductor of laboratory) Mohali , Chandighar,it comes under Department of Space government of India (ISRO).

SYNTHESIS, CHARACTERIZATION, ANTIMICROBIAL STUDIES OF CERTAIN TRIAZOLE CONTAINING S-TRIAZINE DERIVED COMPOUND.

Dr.K.N.Sarmah*,Dr.N.K.Sarmah[1],Talha V.Patel[2],K.B.Kurmi[3].

Department of Chemistry, Shree Jayendrapuri Arts & Science College, Bharuch.
Gujarat, India-392002.

Abstract

Some new substituted 1,3,5 triazine with 1,2,4 triazole and substituted urea/thiourea were synthesized and evaluated for their *in vitro* antimicrobial activity against Gram positive and Gram negative strains using a microdilution procedure. Synthesized compounds **1a to 1i** prove to be effective with MIC (mg/ ml), among them **1c**, **1e**, **1g** showed excellent activity against a panel of microorganisms. The newly synthesized compounds were characterized using **IR**, **^{1}H-NMR**.

Keywords: - 1, 2, 4 Triazole, Substituted urea/thiourea, Cyanuric chloride and Antimicrobial activity.

Introduction:-

S-Triazine derivatives represent an important class of compounds due to their potential to be biologically active. They are known to be anti-protozoals[1], anticancer agents[2], estrogen receptor modulators[3], antimalarials[4], cyclin-dependent kinase modulators[5], and antimicrobials[6]. These are valuable bases for estrogen receptor modulators [7] and also used as bridging agents to synthesize herbicides and in the production of drugs or polymers[8].

1,2,4 – Triazole have wide range of biological activities such as anti bacterial[9] , anti caner[10] , anti tubercular[11], anti HIV[12] and anti depressant activity, anti tumor [13] and anti viral[13] activity, anti hypertensive[14] activity , analgesic and anti inflammatory[15] activity.

Thiourea derivatives possess antibacterial [16], hypnotic antitubercular and possible anticonvulsant activities. It also represent a new class of human immuno deficiency virus type (HIV-1), non-nucleoside reverse transcriptase (NNRT) inhibitors [17], found as antagonist [18], and high density lipoprotein (HDL) elevating agents [19].

Urea derivatives are reported to possess antibacterial[20], antimicrobial antifungal, anticancer[21] and anticonvulsant[22] activities. Urea derivatives possess wide therapeutic activities such as antithyroidal, hypnotic and anesthetic, antibacterial, diuretic[23] and anthelmintics.

we wish to describe a simple and efficient protocol for the rapid preparation of ***1-(4-(3-(4-METHOXYPHENYL)THIOUREIDO)-6-(1H-1,2,4-TRIAZOL-1-YL)-1,3,5-TRIAZINE-2-YL)-3-PHENYLUREA*** at different temperature conditions. To the best of our knowledge, there are no reports on three-component coupling of triazole, substituted urea and thiourea to produce a title compound.We planned to undertake the synthesis and characterization of some triazine derivatives carrying the above biodynamic heterocyclic systems with the hope to achieve enhanced biological activity.

Experimental:-

General

All the melting points were taken in open capillaries tube and are uncorrected. The purity of compounds was checked routinely by TLC (0.5 mm thickness)Using silica gel – G coated Al – plates (Merck) and spots were visualized by exposing the dry plates in iodine vapours. IR spectra were recorded on FTIR spectrophotometer using KBr or Nujol technique. ^{1}H NMR spectra on a Varian 400 FT MHz NMR instrument at using CDCl$_3$ or DMSO-d$_6$ as solvent and TMS as internal reference.

Scheme:-

Step-1

Preparation Of 1-(4,6-Dichloro-1,3,5-Triazin-2-Yl)-3-(4-Methoxy Phenyl)Thiourea: (A)

To a stirred solution of cyanuric chloride (0.1 mole, 18.4 g.) in acetone (100 ml) at 0-5^{0}C, the solution of 1–(4-methoxyphenyl)thiourea (0.1 mole,17.3g) in acetone (45 ml) was added and pH being maintained neutral by the addition of 10% sodium bi-carbonate solution from time to time as per requirement of reaction condition. The stirring was continued at   0-5$^°$C for 2 hours. After the completion of reaction the stirring was stopped and the solution was treated with crushed ice. The solid product obtained was filtered and dried. The crude product was purified by crystallization from absolute alcohol to get title compound.

Step-2

Preparation   Of 1-(4-Chloro-6-(1 H-1,2,4-Triazol-1-Yl)-1,3,5-Triazine-2-Yl)-3-(4-Methoxyphenyl) Thiourea : (B)

To a stirred solution of (A) (0.1 mole, 33.0 g) in acetone (100 ml) was added, the solution of 1,2,4 triazole (0.1 mole, 6.9 g) in acetone (25 ml) was added drop wise maintaining the temperature at 40°C, the pH being maintained neutral by the addition of 10% sodium bi-carbonate solution from time to time as per requirement of reaction condition. The temperature was gradually raised to 45°C during three hours. After the completion of reaction, the resultant content was poured into ice-cold water. The solid product obtained was filtered and dried. The crude product was purified by crystallization from absolute alcohol to get the title compound.

Step-3

Preparation Of Final Compound:-

A mixture of (B) (0.01 mole, 3.62 g) and aryl urea (0.01 mole) in DMF (20ml) was refluxed in oil bath. The temperature was gradually raised to 80-100^{0}C during four hours, the pH being maintained neutral by the addition of 10% sodium bi-carbonate solution from time to time as per requirement of reaction condition. After the completion of reaction, add little charcoal in R.B.F. and then filter it into cold water. The solid product obtained was filtered and dried. The crude product was purified by recrystallization from absolute alcohol. Prepare all derivatives by this method. Analytical data are given below.

ROUTE OF SYNTHESIS :-

STEP-1

2,4,6-trichloro-1,3,5-triazine   1-(4-methoxyphenyl)thiourea   1-(4,6-dichloro-1,3,5-triazin-2-yl)-3-(4-methoxyphenyl)thiourea

[A]

STEP-2

A + 1*H*-1,2,4-triazole

1-(4-chloro-6-(1*H*-1,2,4-triazol-1-yl)-1,3,5-triazin-2-yl)-3-(4-methoxyphenyl)thiourea

[B]

STEP-3

1-(4-(3-(4-methoxyphenyl)thioureido)-6-(1*H*-1,2,4-triazol-1-yl)-1,3,5-triazin-2-yl)-3-phenylurea
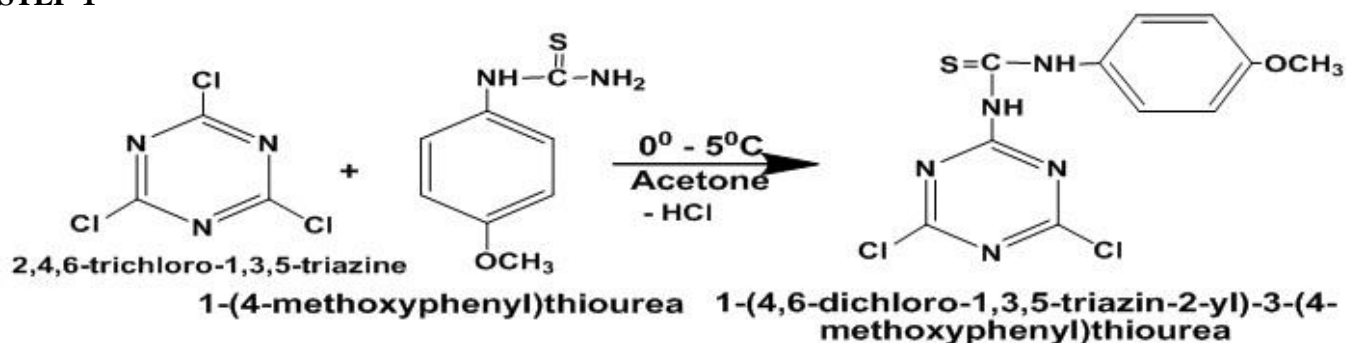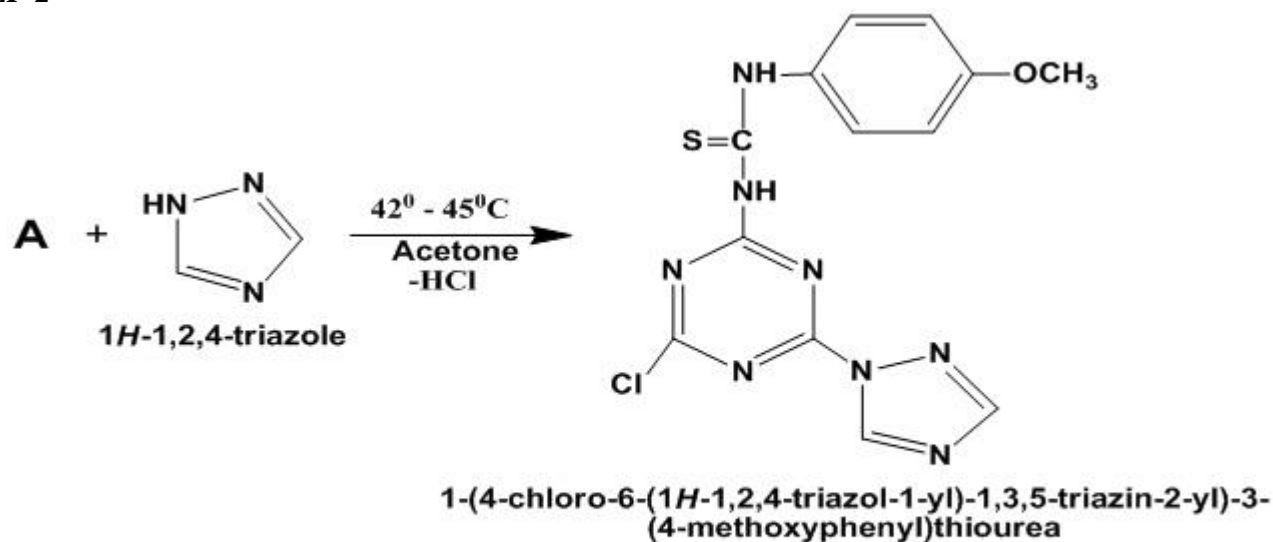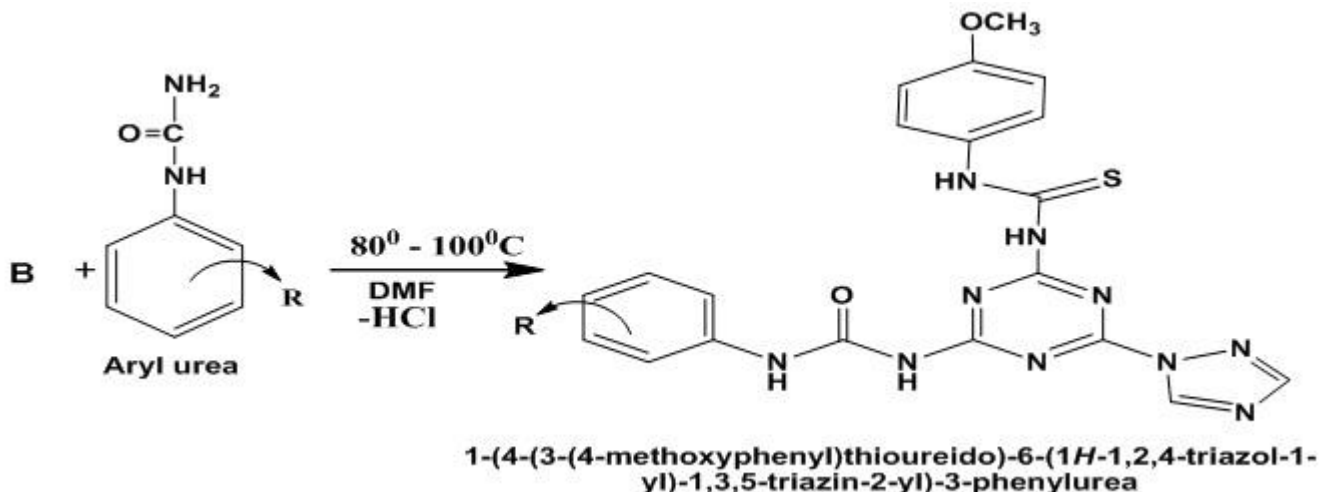
Where **R** = given in below table.

Table 1 Physical data of synthesized compounds:-

Sr. No.	R	Mol. Formula	Mol. Weight	M.P. ^{O}C	Yield %
1a	H	$C_{20}H_{18}N_{10}O_2S$	462.49	120	60
1b	2-OCH$_3$	$C_{21}H_{20}N_{10}O_3S$	492.51	122	61
1c	4-CH$_3$	$C_{21}H_{20}N_{10}O_2S$	476.51	190	59
1d	4-Cl	$C_{20}H_{17}ClN_{10}O_2S$	496.93	220	74
1e	4-OCH$_3$	$C_{21}H_{20}N_{10}O_3S$	492.51	140	59
1f	2-CH$_3$	$C_{21}H_{20}N_{10}O_2S$	476.51	140	58
1g	2-Cl	$C_{20}H_{17}ClN_{10}O_2S$	496.93	135	62
1h	4-Br	$C_{20}H_{17}BrN_{10}O_2S$	541.38	180	60
1i	4-F	$C_{20}H_{17}FN_{10}O_2S$	480.48	175	65

Compound (1a): Yield: 60%; m.p. 120^{0}C (dec.); **IR (KBr,cm^{-1}) :** 798 cm^{-1}
(-C=N- s-triazine) 818.47 cm^{-1}(1,4 Di sub. in benzene) 1416.15 cm^{-1}(>N-,3^0 amine) 1548.50 cm^{-1}(-NH-def)1656.15 cm^{-1} (-C=O-) 3290.15 cm^{-1}(-NH-str) 2800.50 cm^{-1}(–OCH$_3$ str) 1170.64 cm^{-1}(-C=S-)1023.14 cm^{-1} (-N-N-str) **^{1}H-NMR:δ** 8.90(s,2H,-CONH), 10.30(s,2H,-CSNH),3.64(s,3H, -OCH$_3$), 7.20-7.98 (m,11H, Ar-H).
Compound (1b): Yield: 61%; m.p. 122^{0}C (dec.); **IR (KBr,cm^{-1}) :** 801 cm^{-1} (-C=N- s-triazine) 819.25 cm^{-1}(1,4 Di sub. in benzene) 1410.98 cm^{-1}(>N-,3^0 amine)1562.70cm^{-1} (-NH-def)1643.16 cm^{-1} (-C=O-) 3311.16 cm^{-1}(-NH-str)2916.48 cm^{-1} (–OCH$_3$ str)1177.34cm^{-1}(-C=S-)1033.34 cm^{-1} (-N-N-str) **^{1}H-NMR:δ** 8.64(s,2H,-CONH) 10.22(s,2H,-CSNH),3.69(s,6H, -OCH$_3$)7.40-7.78 (m,10H, Ar-H).
Compound (1c): Yield: 59%; m.p. 190^{0}C (dec.); **IR (KBr,cm^{-1}) :** 783.0**7** cm^{-1}
(-C=N- s-triazine) 821.07 cm^{-1}(1,4 Di sub. in benzene)1410.98 cm^{-1}(>N-,3^0 amine) 1596.6 cm^{-1}(-NH-def) 1643.16cm^{-1} (-C=O-) 3311.16 cm^{-1}(-NH-str) 2916.48 cm^{-1} (–OCH$_3$ str) 1177.34 cm^{-1}(-C=S-)1308.20 cm^{-1} (-C-CH$_3$ str) 1033.34 cm^{-1} (-N-N-str) **^{1}H-NMR:δ** 8.55(s,2H,-CONH) 10.10(s,2H,-CSNH),3.71(s,3H, -OCH$_3$)3.74(s,3H,C-CH$_3$) 7.32-7.66 (m,10H, Ar-H).
Compound (1d): Yield: 74%; m.p. 220^{0}C (dec.); **IR (KBr,cm^{-1}) :** 795 cm^{-1}

Sr. No & Comp no.		R	Minimum Inhibitory Concentration (µg/ml)				
			Gram positive bacteria		Gram negative bacteria		Fungus
			S. aureus	B. subtilis	E. coli	P. aeruginosa	C. albicans
1.	1a	H	125	250	125	125	125
2.	1b	2-OCH$_3$	125	125	125	250	125
3.	1c	4-CH$_3$	125	**31.25**	125	**31.25**	**31.25**
4.	1d	4-Cl	125	250	125	125	125
5.	1e	4-OCH$_3$	**62.5**	125	125	125	125
6.	1f	2-CH$_3$	125	125	125	125	125
7.	1g	2-Cl	**62.5**	125	125	125	250
8.	1h	4-Br	125	125	125	125	250
9.	1i	4-F	125	125	125	125	125
Ampicillin		------	250	100	100	100	------
Nystatin		------	---	---	---	---	100

(-C=N- s-triazine) 816.34 cm^{-1}(1,4 Di sub. in benzene) 1418.09 cm^{-1}(>N-,3^0 amine)1559.90 cm^{-1}(-NH-def)1638.80 cm^{-1} (-C=O-) 3330.30 cm^{-1}(-NH-str)2890.50 cm^{-1} (–OCH$_3$ str)1180.80cm^{-1}(-C=S-)707 cm^{-1}(-C-Cl-str)1029.34 cm^{-1} (-N-N-str) **^{1}H-NMR:δ** 8.64(s,2H,-CONH) 10.22(s,2H,-CSNH),3.69(s,3H, -OCH$_3$)7.40-7.78 (m,10H, Ar-H).

Compound (1e): Yield: 59%; m.p. 140^{0}C (dec.); **IR (KBr,cm^{-1}) :** 804 cm^{-1}

(-C=N- s-triazine) 812.40 cm^{-1}(1,4 Di sub. in benzene) 1416.30 cm^{-1}(>N-,3^0 amine)1569.70 cm^{-1}(-NH-def)1651.60 cm^{-1} (-C=O-) 3334.11 cm^{-1}(-NH-str)2930.30 cm^{-1} (–OCH$_3$ str)1169.64cm^{-1}(-C=S-)1028.71 cm^{-1} (-N-N-str) **^{1}H-NMR:δ** 8.90(s,2H,-CONH) 10.90(s,2H,-CSNH),3.80(s,6H, -OCH$_3$)7.50-8.18 (m,10H, Ar-H).

Compound (1f): Yield: 58%; m.p. 140^{0}C (dec.); **IR (KBr,cm^{-1}) :** 795.65 cm^{-1}

(-C=N- s-triazine) 819.40 cm^{-1}(1,4 Di sub. in benzene)1418.30 cm^{-1}(>N-,3^0 amine) 1584.20 cm^{-1}(-NH-def) 1637.60cm^{-1} (-C=O-) 3320.65 cm^{-1}(-NH-str) 2898.28 cm^{-1} (–OCH$_3$ str) 1169.70 cm^{-1}(-C=S-)1316.60 cm^{-1} (-C-CH$_3$ str) 1040.85 cm^{-1} (-N-N-str) **^{1}H-NMR:δ** 8.60(s,2H,-CONH) 9.95(s,2H,-CSNH),3.66(s,3H, -OCH$_3$)3.60(s,3H,C-CH$_3$) 7.22-7.90 (m,10H, Ar-H).

Compound (1g): Yield: 62%; m.p. 135^{0}C (dec.); **IR (KBr,cm^{-1}) :** 789.30 cm^{-1}

(-C=N- s-triazine) 825.30 cm^{-1}(1,4 Di sub. in benzene) 1430.10 cm^{-1}(>N-,3^0 amine)1565.60 cm^{-1}(-NH-def)1650.70 cm^{-1} (-C=O-) 3310.80 cm^{-1}(-NH-str)2900.50 cm^{-1} (–OCH$_3$ str)1170.60cm^{-1}(-C=S-)717 cm^{-1}(-C-Cl-str)1036.74 cm^{-1} (-N-N-str) **^{1}H-NMR:δ** 8.70(s,2H,-CONH) 10.29(s,2H,-CSNH),3.75(s,3H, -OCH$_3$)7.50-7.84 (m,10H, Ar-H).

Compound (1h): Yield: 60%; m.p. 180^{0}C (dec.); **IR (KBr,cm^{-1}) :** 797.40 cm^{-1} (-C=N- s-triazine) 829.90 cm^{-1}(1,4 Di sub. in benzene) 1420.10 cm^{-1}(>N-,3^0 amine)1560.50cm^{-1} (-NH-def)1654.90 cm^{-1} (-C=O-) 33170.55 cm^{-1}(-NH-str)2920.45 cm^{-1} (–OCH$_3$ str) 1162.70cm^{-1}(-C=S-)692 cm^{-1}(-C-Br-str) 1028.47 cm^{-1} (-N-N-str) **^{1}H-NMR:δ** 8.67(s,2H,-CONH) 10.75(s,2H,-CSNH),3.66(s,3H,-OCH$_3$)7.42-7.74(m,10H, Ar-H).

Compound (1i): Yield: 65%; m.p. 175^{0}C (dec.); **IR (KBr,cm^{-1}) :** 790.30 cm^{-1}

(-C=N- s-triazine) 820.40 cm^{-1}(1,4 Di sub. in benzene) 1435.10 cm^{-1}(>N-,3^0 amine)1561.50 cm^{-1}(-NH-def)1642.60 cm^{-1} (-C=O-) 3300.75 cm^{-1}(-NH-str)2914.50 cm^{-1}

(–OCH$_3$ str)1160.60cm^{-1}(-C=S-)1055 cm^{-1}(-C-F-str) 1040.10 cm^{-1} (-N-N-str) **^{1}H-NMR:δ** 8.75(s,2H,-CONH) 10.40(s,2H,-CSNH),3.85(s,3H, -OCH$_3$)7.70-7.94 (m,10H, Ar-H).

Antimicrobial Activity

For the testing antimicrobial activity various microorganism were used for the study. The **broth dilution** method was used for this study. Following general procedure is adopted[24].The antimicrobial activity of all the compounds was studies at 1000 ppm concentration *in vitro*. The

different types of microorganism used were some gram negative bacteria [*Escherichia coli, Pseudomonas aeruginosa*], gram positive bacteria [*Bacillus subtilis*, *Staphylococcus aureus*] and fungus [*Candida albicans*].

80% DMSO are used as solvent to dissolve compound 1a to 1i to 10**(μg/ml).**

Conclusions:-
A series of cyanuric chloride derivatives were prepared and tested for their *in vitro* antibacterial activity against the four strains of bacteria (gram +ve, gram –ve).Three compounds of the obtained series showed high *in vitro* antimicrobial activity. Compound (**1c, 1e, 1g**) showed excellent activity against *Staphylococcus aureus.* Whereas compound 1c has excellent activity against *B. subtilis*, *P. aeruginosa, C. albicans.*

Reference:-
1. Balini, A., Bueno, G.J., Stewart, M.L., Yardley, V., Brun, R., Barrett,P.M.**,**J. Med. Chem. 48, **(2005)**, 5570–5579.
2. Menicagli, R., Samaritani, S., Signore, G., Vaglini, F., Via, L.D.,. J. Med. Chem. 47,**(2004),** 4649–4652.
3. Henke, B.R., Consler, T.G., Go, N., Hale, R.L., Hohman,. J. Med. Chem. 45, **(2002)**, 5492–5505.
4. Agarwal, A., Srivastava, K., Puri, S.K., Chauhan, P.M.S.,. Bioorg. Med. Chem. Lett. 15,**(2005)**, 531–533.
5. Kuo, G.H., DeAngelis, A., Emanuel, S., Wang, A., Zhang, Y., Connolly,. J.Med. Chem. 48,**(2005)**, 4535–4546.
6. Koc, Z.E., Bingol, H., Saf, A.O., Torlak, E., Coskum, A.,. J. Hazard. Mater. 183,**(2010)**, 251–255.
7. Sirivinas K.,Sirivinas U.,Jayathirtha R.,Bioorg. Med. Chem. Lett. 15,**(2005)**,1121–1123.
8. Hoog D.P., Gamez P., Dressen W.L., Reedijk J., 43, **(2002)**, 6783–6786.
9. Nisha Aggarwal a,b, Rajesh Kumar a,., Euro. J. Med. Chem.,46, **(2011)**, 4089**.**
10. Kamal Ahmed ,, Prabhakar S., Euro. J. Med. Chem.,46, **(2011),** 3820.
11. Alessandro K. Jordão a, Plínio C. Sathler., Bioorganic & Medicinal Chemistry 19, **(2011)**, 5605.
12. Fernando de C. da Silva , Maria Cecilia., Euro. J. Med. Chem., 44, **(2009),** 373**.**
13. Al-Soud Yaseen A., Mohammad N., IL FARMACO 59, **(2004)**, 775**.**
14. Siddiqui Anees A., Mishra Ravinesh., Bioorganic & Medicinal Chemistry Letters 21, **(2011),** 1023**.**
15. Manikraoa Anil M., Fursuleb Ravindra A., Ind. J. chem.,49B, **(2010),** 1642**.**
16. Chikhalia K. H. and Desai K. R.,Acta. Cienecia. Indica., XXIV C, **(1998)**.
17. Campiani G., Fabbrini M. and Caccia S.,J. Med. Chem., 44, **(2001)**, 305.
18. Lee J. and Blamberg P. M.,*J. Med. Chem.*, 46, **(2001)**, 3116.
19. Cappola C. M., Damon R. E,*Biorg.* and Med. Chem. Lett., 15, **(2005)**, 809.
20. Nagaprasada R. L. and Reddy Shankar B.,Ind. J. Chem.,40(B)*,* **(2001)**, 817.
21. Hamby J. M., Grohar P. J. and Dohetry A. M.,J. Med. Chem., 44, **(2001)**, 1915.
22. Paria M. R., Miskell L. and Tylor C. P.,J. Med. Chem., 33, **(1990),** 854.
23. Christer S., Noréen R., Engelhardt P., Vrang L., Sahlberg C., Bioorg. Med. Chem. Lett*.,* 8, **(1998**), 1511.
24. Dr. Hancock, www.cmdr.ubc.ca/bobh

A NOVEL APPROACH ON SIMULATION OF VOLTAGE SAGS/SWELLS MITIGATION USING DYNAMIC VOLTAGE RESTORER (DVR)

S.Radha Krishna Reddy[1]   G. Rameshwar Rreddy[2]
V. Hari Padma Priyanka[3]   K. Ramakrishna Reddy[4]
I.V.Koteswara Rao[5]

Abstract
This paper describes the problem of voltage sags and swells and its severe impact on non linear loads or sensitive loads. The dynamic voltage restorer (DVR) has become popular as a cost effective solution for the protection of sensitive loads from voltage sags and swells. The control of the voltages in DVR based on dqo algorithm is discussed. It first analyzes the power circuit of a DVR system in order to come up with appropriate control limitations and control targets for the compensation voltage control. The proposed control scheme is simple to design. Simulation results carried out by Matlab/Simulink verify the performance of the proposed method.

Keywords- Dynamic Voltage Restorer (DVR), voltage sags, voltage swells, sensitive load.

1. Introduction
Power Quality problems encompass a wide range of disturbances such as voltage sags/swells, flicker, harmonics distortion, impulse transient, and interruptions [1]. Voltage sags can occur at any instant of time, with amplitudes ranging from 10 – 90% and a duration lasting for half a cycle to one minute [3]**.** Voltage swell, on the other hand, is defined as a swell is defined as an increase in rms voltage or current at the power frequency for durations from 0.5 cycles to 1 min. typical magnitudes are between 1.1 and 1.8 up. Swell magnitude is also is also described by its remaining voltage, in this case, always greater than 1.0. [2,3,4]. Voltage swells are not as important as voltage sags because they are less common in distribution systems. Voltage sag and swell can cause sensitive equipment (such as found in semiconductor or chemical plants) to fail, or shutdown, as well as create a large current unbalance that could blow fuses or trip breakers. These effects can be very expensive for the customer, ranging from minor quality variations to production downtime and equipment damage [5-7]. There are many different methods to mitigate voltage sags and swells, but the use of a custom Power device is considered to be the most efficient method. Switching off a large inductive load or Energizing a large capacitor bank is a typical system event that causes swells [1]. This paper introduces Dynamic Voltage Restorer and its operating principle. Then, a simple control based on dqo method is used to compensate voltage sags/swell. At the end, MATLAB/SIMULINK model based simulated results were presented to validate the effectiveness of the proposed control method of DVR.

2. Conventional system configuration of DVR
Dynamic Voltage Restorer is a series connected device designed to maintain a constant RMS voltage value across a sensitive load. The DVR considered consists of:

a. an injection ⁄ series transformer
    b. a harmonic filter,
    c. a Voltage Source Converter (VSC),
    d. an energy storage and
    e. a control system , as shown in Figure1
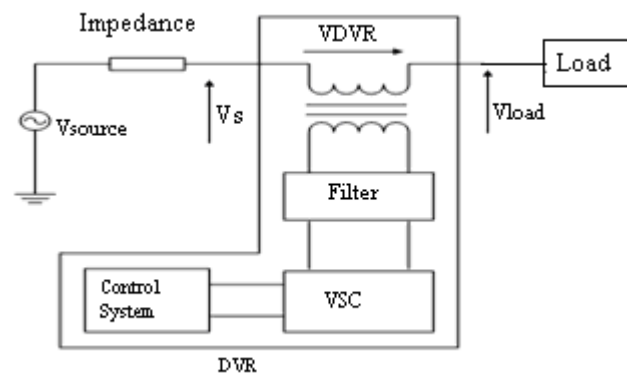
Figure 1: *Schematic diagram of DVR*
The main function of a DVR is the protection of sensitive loads from voltage sags/swells coming from the network. Therefore as shown in Figure 1, the DVR is located on approach of sensitive loads. If a fault occurs on other lines, DVR inserts series voltage VDVR and compensates load voltage to pre fault value. The momentary amplitudes of the three injected phase voltages are controlled such as to eliminate any detrimental effects of a bus fault to the load voltage *VL*. This means that any differential voltages caused by transient disturbances in the ac feeder will be compensated by an equivalent voltage generated by the converter and injected on the medium voltage level through the booster transformer.

The DVR works independently of the type of fault or any event that happens in the system, provided that the whole system remains connected to the supply grid, i.e. the line breaker does not trip. For most practical cases, a more economical design can be achieved by only compensating the positive and negative sequence components of the voltage disturbance seen at the input of the DVR. This option is Reasonable because for a typical

distribution bus configuration, the zero sequence part of a disturbance will not pass through the step down transformer because of infinite impedance for this component.

The DVR has two modes of operation which are: standby mode and boost mode. In standby mode (*VDVR*=0), the booster transformer's low voltage winding is shorted through the converter. No switching of semiconductors occurs in this mode of operation, because the individual converter legs are triggered such as to establish a short-circuit path for the transformer connection. Therefore, only the comparatively low conduction losses of the semiconductors in this current loop contribute to the losses. The DVR will be most of the time in this mode. In boost mode (*VDVR*>0),
the DVR is injecting a compensation voltage through the booster transformer due to a detection of a supply voltage disturbance [4].
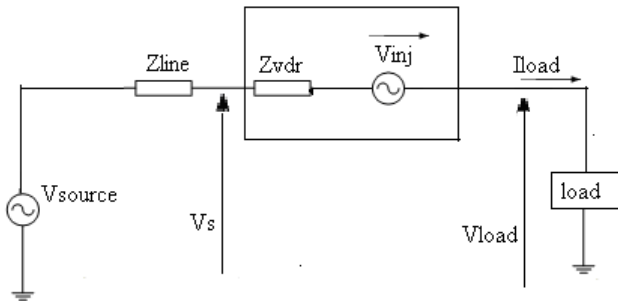
Figure 2: Equivalent Circuit of DVR

Figure 2 shows the equivalent circuit of the DVR, when the source voltage is drop or increase, the DVR injects a series voltage Vinj through the injection transformer so that the desired load voltage magnitude VL can be maintained. The series injected voltage of the DVR can be written as

$$V_{inj} = V_{load} + V_s \qquad (1)$$

Where;

VLoad is the desired load voltage magnitude

Vs is the source voltage during sags/swells condition

The load current ILoad is given by,

$$\left(\frac{(P_{load} \pm J * Q_{load})}{V_{load}} \right) \qquad (2)$$

3. Proposed Method

A. Main Circuit

Figure 3 shows the configuration of the proposed DVR design using MATLAB/SIMULINK, where the outputs of a three-phase half-bridge inverter are connected to the utility supply via wye-open connected series transformer. Once a voltage disturbance occurs, with the aid of dqo transformation based control scheme, the inverter output can be steered in phase with the incoming ac source while the load is maintained constant. As for the filtering scheme of the proposed method, output of inverter is installed with capacitors and inductors.

B. Control Algorithm

The basic functions of a controller in a DVR are the detection of voltage sag/swell events in the system; computation of the correcting voltage, generation of trigger pulses to the sinusoidal PWM based DC-AC inverter, correction of any anomalies in the series voltage injection and termination of the trigger pulses when the event has passed. The controller may also be used to shift the DC-AC inverter into rectifier mode to charge the capacitors in the DC energy link in the absence of voltage sags/swells. The dqo transformation or Park's transformation [8-10] is used to control of DVR.

The dqo method gives the sag depth and phase shift information with start and end times. The quantities are expressed as the instantaneous space vectors. Firstly convert the voltage from abc reference frame to d-q-o reference. For simplicity zero phase sequence components is ignored. Figure 4 illustrates a flow chart of the feed forward dqo transformation for voltage sags/swells detection. The detection is carried out in each of the three phases.

The control scheme for the proposed system is based on the comparison of a voltage reference and the measured terminal voltage (Va,Vb,Vc).The voltage sags is detected when the supply drops below 90% of the reference value whereas voltage swells is detected when supply voltage increases up to 25% of the reference value. The error signal is used as a modulation signal that allows to generate a commutation pattern for the power switches (IGBT's) constituting the voltage source converter. The commutation pattern is generated by means of the sinusoidal pulse width modulation technique (SPWM); voltages are controlled through the modulation.

The block diagram of the phase locked loop (PLL) is illustrated in Figure 4. The PLL circuit generate a unit sinusoidal wave in phase with mains voltage.
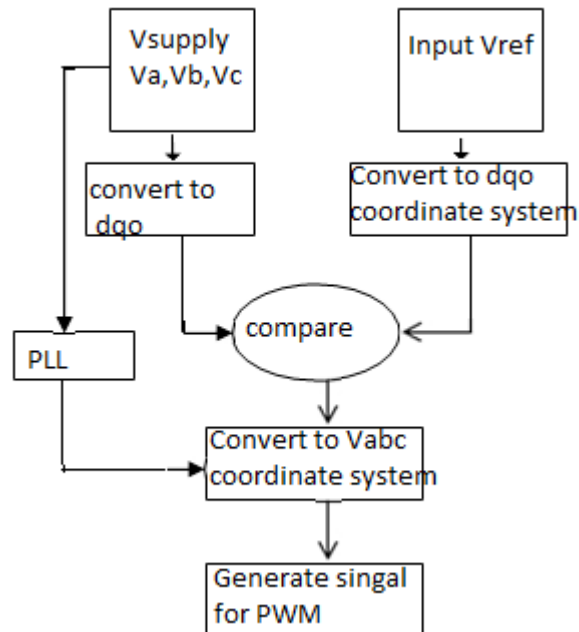
Figure 4 : *Flow chart of feed forward control technique for DVR based on dqo transformation*

Equation (3) defines the transformation from three phase system a, b, c to dqo stationary frame. In this transformation, phase A is aligned to the d axis that is in quadrature with the q-axis. The theta (θ) is defined by the angle between phase A to the d-axis.

$$\begin{pmatrix} V_d \\ V_q \\ V_o \end{pmatrix} = \begin{pmatrix} \cos(\theta) & \cos\left(\theta - \dfrac{2\pi}{3}\right) & 1 \\ -\sin(\theta) & -\sin\left(\theta - \dfrac{2\pi}{3}\right) & 1 \\ \dfrac{1}{2} & \dfrac{1}{2} & \dfrac{1}{2} \end{pmatrix} \begin{pmatrix} V_a \\ V_b \\ V_c \end{pmatrix} \quad (3)$$

4. Simulation Results And Discussion

A detailed system as shown in Figure 3 has been modelled by **MATLAB/SIMULINK** to study the efficiency of suggested control strategy. The system parameters and constant value are listed in Table I. It is assumed that the voltage magnitude of the load bus is maintained at 1 pu during the voltage sags/swells condition. The results of the most important simulations are represented in Figures 5-8. The load has been assumed linear with power factor pf =0.85 lagging and its capacity of 5 KVA.

TABLE I: SYSTEM PARAMETERS AND CONSTANT VALUES

Main Supply Voltage per phase	200v
Line Impedance	Ls =0.5mH Rs = 0.1 Ω
Series transformer turns ratio	1:1
DC Bus Voltage	100v
Filter Inductance	1mH
Filter capacitance	1uF
Load resistance	40 Ω
Load inductance	60mH
Line Frequency	50Hz

4.1 Voltage Sags

The first simulation show of three phase voltage sag is simulated. The simulation started with the supply voltage 50% sagging as shown in Figure 5 (a).In Figure 5 (a) also shows a 50% voltage sag initiated at 0.15s and it is kept until 0.35s, with total voltage sag duration of 0.2s. Figures 5 (b) and (c) show the voltage injected by the DVR and the corresponding load voltage with compensation. As a result of DVR, the load voltage is kept at 1 pu. The effectiveness of the DVR under unbalanced conditions is shown in figure 6, in figure 6 also shows the occurrence of 50% single phase voltage sag on a utility grid. Through simulation the supply voltage with one phase voltage dropped down to 50% as shown in Figure 6 (a). The DVR injected voltage and the load voltage are shown in Figures 6 (b)

and (c) respectively. Its corresponding load voltages are shown in Figure 6(c) where it is possible to see that the compensation method is keeping the load voltages constant at 1 p.u.
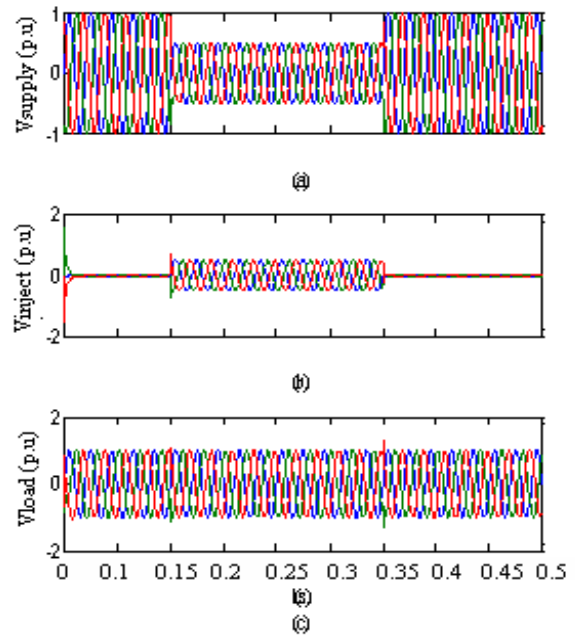
Figure 5 Three-phase voltages sag: (a)-Source voltage, (b)-Injected voltage, (c)-Load voltage
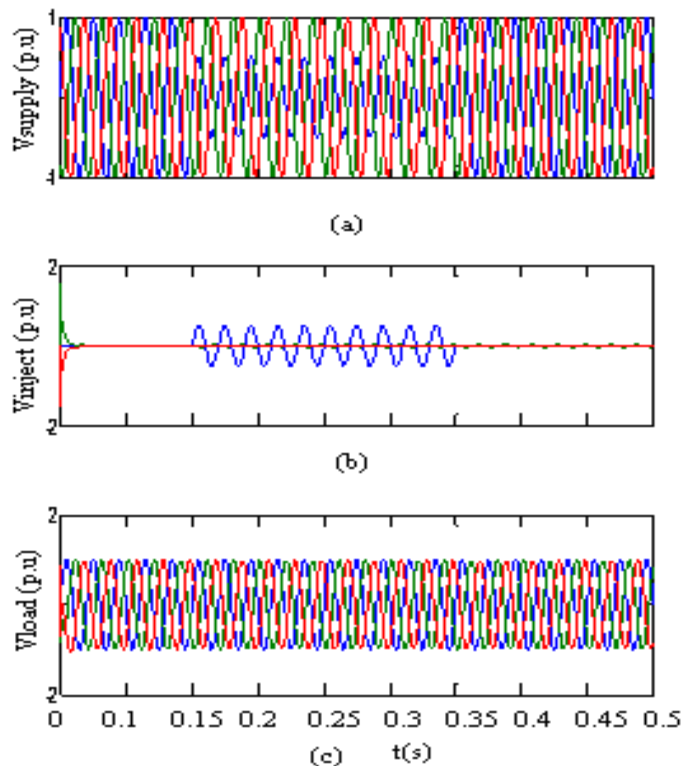
Figure 6 Single-phase voltage sag: (a)-Source voltage, (b)-Injected voltage, (c)-Load voltage
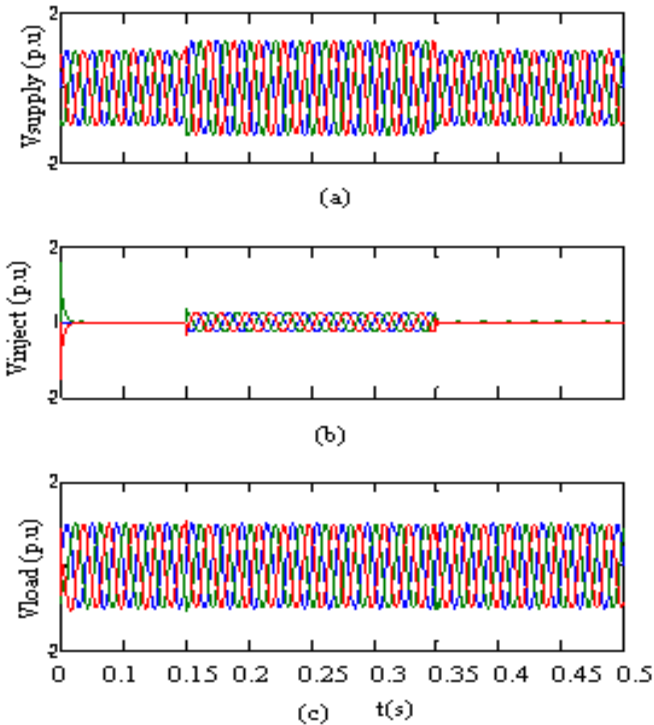
Figure 7 Three-phase voltages swell: (a)-Source voltage, (b)-Injected voltage, (c)-Load voltage
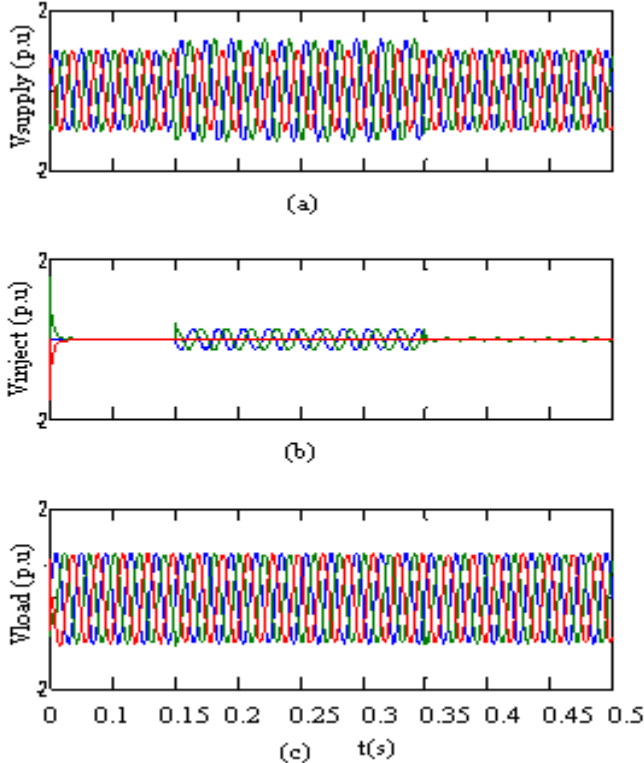
Figure. 8 *Two-phase voltages swell: (a)-Source voltage, (b)-Injected voltage, (c)-Load voltage*

4.2 Voltage Swells

The second simulation shows the DVR performance during a voltage swell condition. The simulation started with the supply voltage swell is generated as shown in Figure 7 (a). As observed from this figure the amplitude of supply voltage is increased about 25% from its nominal voltage. Figures 7(b) and (c) show the injected and the load voltage respectively.

As can be seen from the results, the load voltage is kept at the nominal value with the help of the DVR. Similar to the case of voltage sag, the DVR reacts quickly to inject the appropriate voltage component (negative voltage magnitude) to correct the supply voltage. Figure 8 shows that the performances of the DVR with an unbalanced voltage swell. In this case, two of the three phases are higher by 25% than the third phase as shown in Figure 8(a). The injected voltage that is produced by DVR in order to correct the load voltages and the load voltages maintain at the constant are shown in Figures 8 (b) and (c), respectively.

5. Conclusion

The modelling and simulation of a DVR using MATLAB/SIMULINK has been presented. A control system based on dqo technique which is a scaled error of the between source side of the DVR and its reference for sags/swell correction has been presented. The simulation shows that the DVR performance is satisfactory in mitigating voltage sags/swells. The main advantage of this DVR is low cost and its control is simple. It can mitigate long duration voltage sags/swells efficiently. Future work will include a comparison with a laboratory experiments in order to compare simulation and experimental results.
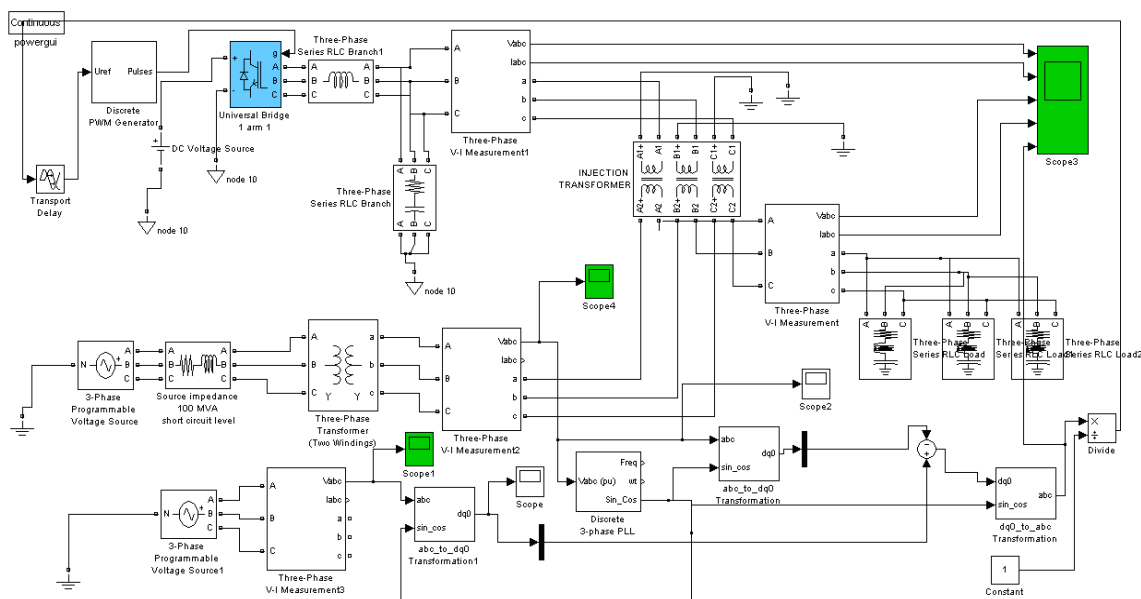
Fig:9 *Proposed System Configuration*

References

[1] N.G. Hingorani, "Introducing Custom Power in IEEE Spectrum," 32p, pp. 4l-48, 1995.

[2] IEEE Std. 1159 − 1995, "Recommended Practice for Monitoring Electric Power Quality".

[3] P. Boonchiam and N. Mithulananthan, "Understanding of Dynamic Voltage Restorers through MATLAB Simulation," Thammasat Int. J. Sc. Tech., Vol. 11, No. 3, July-Sept 2006.

[4] J. G. Nielsen, M. Newman, H. Nielsen, and F. Blaabjerg, "Control and testing of a dynamic voltage restorer (DVR)
at medium voltage level," *IEEE Trans. Power Electron.*
vol. 19, no. 3, p.806, May 2004.

[5] A. Ghosh and G. Ledwich, "Power Quality Enhancement Using Custom Power Devices," Kluwer Academic Publishers, 2002.

[6] S. Chen, G. Joos, L. Lopes, and W. Guo, "A nonlinear control method of dynamic voltage restorers," in 2002 IEEE 33rd Annual Power Electronics Specialists Conference, 2002, pp. 88- 93.

[7] R. Buxton, "Protection from voltage dips with the dynamic voltage restorer," in IEE Half Day Colloquium on Dynamic Voltage Restorers Replacing Those Missing Cycles, 1998, pp. 3/1- 3/6.

[8] H. Awad, J.Svensson, M. Bollen, "Mitigation of Unbalanced Voltage Dips Using Static Series Compensator", IEEE Trans. On Power Elec., Vol. 19, No. 13, May 2004

[9] B. Singh, A. Adya, J. Gupta, "Power Quality Enhancement with DSTATCOM for small Isolated Alternator feeding Distribution System" Power Electronics,
And Drive System 2005, (PEDS 2005), Vol1., 16-18 Jan Pages: 274-279

[10] C. Hochgraf, R. Lasseter, "Statcom controls for Operation with Unbalanced Voltages " IEEE Trans. On Power delivery, Vol. 13, No. 2, April 1998.

Authors Biography

[1]**S.RADHA KRISHNA REDDY** received the **B.Tech**. degree in **EEE** from MITS ENGG College, Madanapalle, Chittor(Dt), Andhra Pradesh, India, from JNTU University and **M.Tech**. in **Power Electronics** from S.K. University in the year 2007. He has teaching experience of 06 years & Currently working as Associate Professor in Holy Mary Institute of Technology & Science, Bogaram, R.R. Dist, Hyderabad, Andhra Pradesh, India in the Dept. of Electrical & Electronics Engg. He published **08** research papers in reputed International Journals and **04** papers in International and National conferences. His Interest areas are Neural Networks, Power electronics & Drives FACTS, etc.

[2]**G. Rameshwar Reddy** was born in Sanjamala,Kurnool Dist,INDIA in 1990.Presently he is pursuing **IV B.Tech** Degree in **Electrical & Electronics Engineering** from Holy Mary Institute of Technology & Science,Bogaram, R.R. Dist, Hyderabad, Andhra Pradesh, India.His Interest areas are Power electronics & Drives, etc.

[3]**V. Hari Padma Priyanka** was born in Safilguda,R.R.Dist,INDIA in 1991.Presently She is pursuing **IV B.Tech** Degree in **Electrical & Electronics Engineering** from Holy Mary Institute of Technology & Science,Bogaram, R.R. Dist, Hyderabad, Andhra Pradesh, India. Her Interest areas are Power electronics & Drives, etc

[4]**K.Ramakrishna Reddy** was born in Podil,Prakasham Dist,INDIA in 1990.Presently he is pursuing **IV B.Tech** Degree in **Electrical & Electronics Engineering** from Holy Mary Institute of Technology & Science,Bogaram, R.R. Dist, Hyderabad, Andhra Pradesh, India. His Interest areas are Power electronics & Drives, etc.

[5]**I.V. KoteswaraRao** was born in Markapur, India, in 1987. He received the B.Tech. degree in Electrical &Electronics Eengineering from Khader Memorial College of Engg & Tech, Devarakonda, J.N.T.U.Hyd in 2008. Presently he is pursuing the M.Tech.Degree Electrical Power Systems from Holy Mary Tnstitute of Tech &Science(coe), Bogaram,Rangareddy (dist), Hyd.J.N.T.U. Hyderabad. He is interested in Power Systems,FACTS.

NEURAL NETWORK ARCHITECTURE DESIGN FOR FEATURE EXTRACTION OF ECG BY WAVELET

Priyanka Agrawal
student, electrical, mits, rgpv,
gwalior, mp 474005, india†
Dr. A. K. Wadhwani
professor, electrical ,mits, rgpv
gwalior, mp 474005, india

Abstract :

This paper deals with the designing of feed forward neural network (FFNN) with the effect of ANN parameters for feature extraction of ECG signal by employing wavelet decomposition. Extraction of ECG features has a significance role in disease diagnosis of heart.ECG signal is decomposed in to it's higher and lower frequency components by using Daubechies wavelet then statistical features of all components are given as input of neural network. A Multi-layer Feed forward Neural Network (MFNN) employing back propagation algorithm is used for learning and to train the ANN. The ANN is designed and trained by MATLAB software. Effect of ANN parameters on error is also found out. Two different type of ECG signals has been taken from MIT-BIH: Normal rhythm(128 Hz) and Atrial fibrillation(250 Hz).

Keywords: ECG; Wavelet decomposition; Features ; Neural Network.

1. Introduction

The ECG is nothing but the recording of the heart's electrical activity. It is graphical tracing of the electrical activity that is generated by depolarization and re-polarization of the atria and ventricles. ECG is one of the important signals among bioelectrical ones that represent heart electrical activity. The signal is constructed by measuring electrical potentials between various points of the body using a galvanometer. A typical ECG of a normal heartbeat (or cardiac cycle) consists of a P wave, a QRS complex and a T wave. A small U wave is normally visible in 50 to 75% of ECGs. Typical ECG waveform is shown in Fig .1. Analysis of ECG is the gold standard for the evaluation of cardiac arrhythmias.
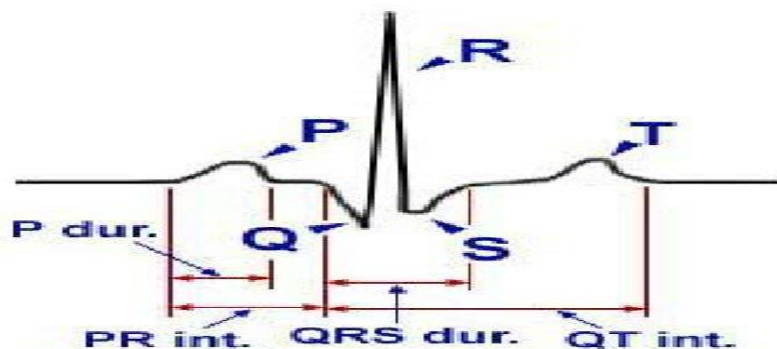
Fig .1. EGG Waveform

Its analysis has been widely used for diagnosing many cardiac diseases. Most of the clinically useful information in the ECG is found in the intervals and amplitudes defined by its features (Statistical and morphological features). Change in shape in any main section of ECG represent arrhythmia [1].The development of accurate and quick methods for automatic ECG feature extraction is of very important, especially for the analysis of long term ECG. Features can also be analyzed by operators but it is time taken and error may also be introduced. The objective of computer aided digital signal processing of ECG signal is to reduce the time taken by the cardiologists in interpreting the results.ECG feature extraction system provides fundamental features which are used in automatic detection. Various ECG feature extraction techniques have been developed so far which have their own merits and demerits [2]. The main differences among them are the way of characteristics extraction of features. The common problems in all earlier proposed method is that ECG signal itself was utilized to extract the features but in this paper, Wavelet Transform (WT) is used to extract the features and neural network is used to minimize the error.

2. Materials Required

2.1. *Discrete Wavelet Transform*
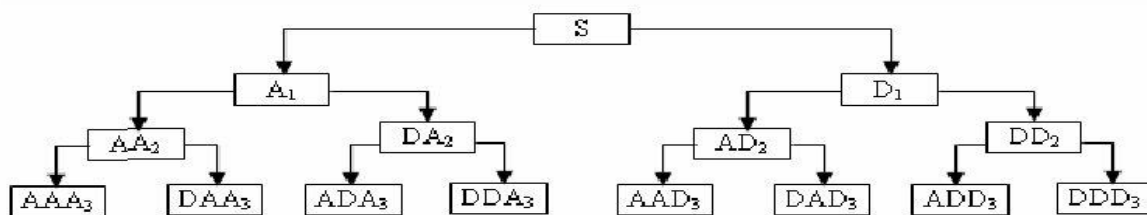
Fig .2. Process of decomposition of signal by DWT

As a result of the infinite extent of the Fourier integral, analysis of signal is time averaged as it contains only globally averaged information. A number of time–frequency methods are now available for signal analysis out of which Wavelet Transform has been proved as a powerful and favored tool in the field of science and engineering for analyzing non-stationary signals. Wavelet method of signal processing is found to be superior to the conventional FFT method in detecting the small changes in ECG signals. Recently wavelets have been used in a large number of biomedical applications and the time and frequency localization of wavelets makes it into a powerful tool for feature extraction [3].It is popular because it satisfies energy conservation law and original signal can be reconstructed [4] .In wavelet transform, a linear operation transforms the signal to decompose it at different scales .It is based on a set of analyzing wavelets allowing the decomposition of ECG signal in a set of coefficients [5]. The wavelet coefficient resulting from the wavelet transformation corresponds to a measurement of the ECG components in this time segment and frequency band. In case of discrete wavelet transform (DWT), filters of different cut-off frequencies are used for analyzing the signal at different scales. For this purpose, the signal is passed through a series of high pass and low pass filters in order to analyze low as well as high frequencies in the signal as shown in Fig .2. It allows signal S to be represented as A1 + AAD3 +DAD3 + DD2.Different types of wavelet are Bi-orthogonal , Coiflet , Harr , Symmlet ,Daubechies wavelets.

2.2. *Neural Network*

An Artificial Neural Network (ANN) is an information processing model that is inspired by the way biological nervous systems, such as the brain, process information. The key element of this model is the novel structure of the information processing system. ANN is usually formed from many hundreds or thousands of simple processing units called neurons, connected in parallel and feeding forward in several layers. ANN's, similar to people, learn by examples. An ANN is configured for a specific application, such as pattern recognition, control and feature classification, through a learning process. Learning in biological systems involves adjustments to the synaptic connections that exist between the neurons. Using neural network terminology, the strength of an interconnection is known as its weight. The perceptron is the neural computational model.ANN has a function f(x) which shows the relation between the inputs, weights, bias and the activation function. The activation function relates the output of a neuron to its input based on the neuron's input activity level.
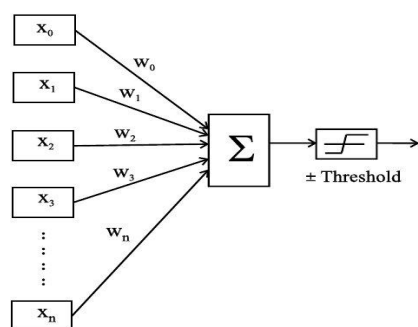
Fig .3.Perceptron
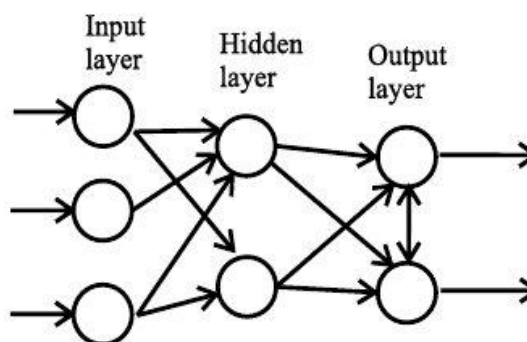
Fig .4.Structure of Feed Forward Neural Network

Some of the commonly used functions include: the threshold, piece-wise linear, sigmoid, tangent hyperbolic, and the Gaussian. It is a single layer neuron that contains the adjustable weight & some threshold values. The inputs are more than one & their weight should be more. The inputs are (x1, x2 ,..., xn) corresponding weights are (w0 , w1,..., wn) as shown in Fig .3.Neural networks are trained and adjusted until network output matches a specific target. Typically many such input/target pairs are needed to train a network. There are varieties of kinds of network structures. In a feed forward network, links are unidirectional and there are no cycles. The importance of the lack of cycles is that computation can take place uniformly from input to output units [6].In this paper feed forward neural network has been used shown in Fig .4.

2.3. *MATLAB Environment*

MATLAB is a powerful, comprehensive, and easy to use environment for technical computations. It provides engineers, scientist, and other technical professionals with a single interactive system that integrates numeric computation, visualization and programming .It includes a family of application specific solutions called toolboxes. In this paper, Wavelet and ANN analysis of ECG signal is performed using MATLAB R2009a Software. It is provided with Wavelet and ANN tool box [7]. It is a collection of functions built on the MATLAB technical computing environment. It provides tools for the analysis and reconstruction of signals and images using wavelets within the MATLAB domain. Customized special functions and programs can be easily created in MATLAB code.

2.4. *Data Acquisition*

For analysis of ECG signal, it is necessary that a standard database must be chosen. ECG signals required for analysis in this paper are downloaded from Physionet MIT-BIH arrhythmia database available online [8] where annotated ECG signals are described by- a text header file (.hea), a mat file (.mat) and a binary annotation file (.atr).Header file consists of detailed information such as number of samples, sampling frequency, format of ECG signal, type of ECG leads and number of ECG leads, patients history and the detailed clinical information. Two types of ECG signal has been taken: MIT BIH Normal (16265) and Atrial fibrillation (05091) Data Base having sampling frequency 128 Hz and 250 Hz respectively of time duration of 1 min then data has been divided in to group of 512 samples.

3. Description Of Algorithm

Preprocessing of ECG signal, decomposition of ECG, feature extraction and then training of features by variation of different parameters takes place in following given steps:

3.1. *Selection of Wavelet*

The selection of relevant wavelet is an important task before starting the detection procedure. It's depends upon the type of signal to be analyzed [9].Wavelet having similar look to the signal being analyzed is usually or One of the key criteria of selection of wavelet is its ability to fully reconstruct the signal from the wavelet decompositions. In this paper, **db6** has been chosen because it has highest correlation coefficient with ECG waveform and its energy spectrum is also concentrated around low frequencies.

3.2. *De-noising of ECG and R peak detection*

- De- noising of ECG signal before extracting its feature can be resulted in better extracted features which in turn can be resulted in an increase in efficiency of system. By using DWT, frequency domain filtering is implicitly performed, making the system robust and allowing the direct application over raw ECG signals. DWT may also be also considered as decomposition by wavelet filter banks.
- After the noise elimination from ECG signal, R peaks are identified by writing a suitable MATLAB code. Specific details of the signal are selected. R peaks are the largest amplitude points which are greater than threshold points are located in the wave. Those maxima points are stored which denotes R peak locations. De-noised ECG signal (Normal and Atrial Fibrillation) and their R wave positions are shown in Fig. 5. and Fig .6 by star.
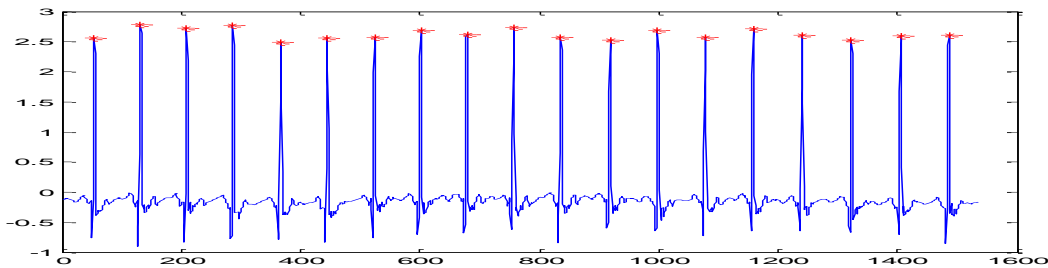
Fig .5. De-noised normal ECG and R wave positionn
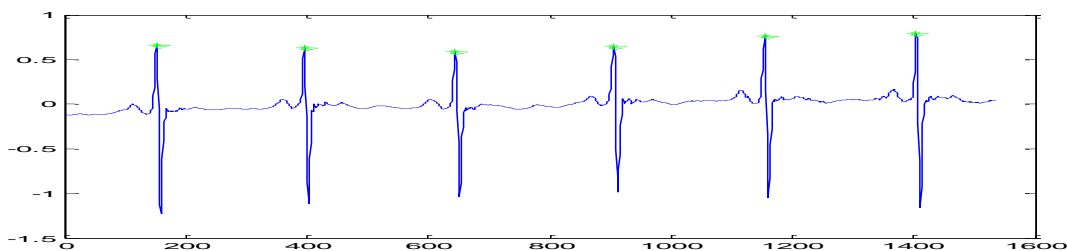
Fig .6. De-noised Atrial Fibrillation ECG and R wave positions

3.3. *Decomposition of ECG Waveform*
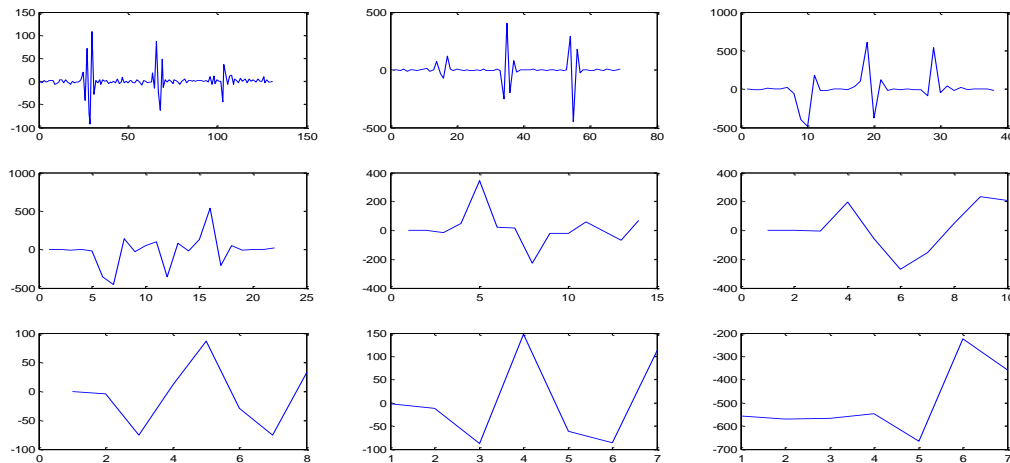
Fig .7 Decomposition of ECG waveform in to wavelet coefficients: Lower Frequency coefficients (d1-d8) and higher frequency Coefficient (a8)

3.4. *Feature Extraction and Normalization*
As ECG waveform has been decomposed in to 8 levels so statistical features like variance, maximum, minimum and standard deviation is found out of each high and low frequency component and also ECG signal. Thus total 68 features are obtained [10]. Feature vector is a matrix of 68x1.This total vector is normalized as shown by "Eq. (1) to obtain the optimal results and given as input of MFFNN (multi layer feed forward network). This is done to prevent the simulated neurons from being driven too far into saturation.

$$\text{Nor.} = 0.1 + \{(\text{Act.-Min.})*0.8\} / \{\text{Max.-Min.}\} \tag{1}$$

Where   Act. = actual value of the parameter and Min. = minimum value of the parameter.
    Max. =maximum value of the parameter and Nor. = normalized value of the parameter.

3.5. *Selection of Algorithm*
Back propagation algorithm (BPA) is supervised learning algorithm. It permits experiential acquisition of input/output mapping knowledge within multi-layer networks. It reduces mean square error between input and output by adjustment of weights. It is highly accurate for most classification problems because of the property of the generalized delta rule. The Multi-Layer Feed-forward Neural Network (MFFNN) falls into this category. It is found that the best architecture of the ANN consists of three layers (an input layer, one hidden layer and output layer) using feed-forward BPA.

4. Results And Discussions
Total feature vectors of some signals are used to teach the neural network and some others are accidentally chosen to test it. In order to simplify the architecture of ANN, data is divided in two groups (normal and atrial fibrillation ECG).Each group consists of a matrix of 68x3.The mean squared error (MSE) is employed as the error function. The ANN is trained under three conditions:
- Keeping the error goal, learning rate and no. of iterations constant and varying the momentum factor.
- Keeping the learning rate, no. of iterations, momentum factor constant and varying the no. of iterations
- Keeping the error goal, no. of iterations and momentum factor constant and varying learning rate.
- Keeping the momentum factor, learning rate, no. of iterations constant and varying the error goal.

The Mean Square Error (MSE) is a good performance measure for judging the accuracy of the ANN System. Effect of different ANN parameters on MSE has been evaluated. Results for training and testing data set are shown from Table .1. to Table .4

Table .1. Variations in MSE by varying momentum factor in normal and atrial fibrillation ECG ANN system

Momentum factor	Learning Rate	Error Goal	Iterations	MSE
0.5	0.5	10^{-5}	1000	2.9×10^{-5}
0.6	0.5	10^{-5}	1000	8.6×10^{-5}
0.7	0.5	10^{-5}	1000	4.98×10^{-6}

Momentum factor	Learning Rate	Error Goal	Iterations	MSE
0.5	0.5	10^{-5}	1000	4.7×10^{-5}
0.6	0.5	10^{-5}	1000	6.1×10^{-5}
0.7	0.5	10^{-5}	1000	7.8×10^{-5}

Table .2. Variations in MSE by varying no. of iterations in normal and atrial fibrillation ECG ANN system

Momentum Factor	Learning Rate	Error Goal	Iterations	MSE
0.5	0.5	10^{-5}	500	2.47×10^{-5}
0.5	0.5	10^{-5}	800	4.9×10^{-6}
0.5	0.5	10^{-5}	1000	7.95×10^{-6}

Momentum Factor	Learning Rate	Error Goal	Iterations	MSE
0.5	0.5	10^{-5}	500	4.9×10^{-5}
0.5	0.5	10^{-5}	800	6.93×10^{-5}
0.5	0.5	10^{-5}	1000	4.95×10^{-5}

Table .3. Variations in MSE by varying learning rate in normal and atrial fibrillation ECG ANN system

Momentum Factor	Learning Rate	Error Goal	Iterations	MSE
0.5	0.4	10^{-5}	1000	2.5×10^{-4}
0.5	0.55	10^{-5}	1000	4×10^{-5}
0.5	0.7	10^{-5}	1000	9.19×10^{-5}

Momentum Factor	Learning Rate	Error Goal	Iterations	MSE
0.5	0.4	10^{-5}	1000	4.4×10^{-5}
0.5	0.55	10^{-5}	1000	6.65×10^{-5}
0.5	0.7	10^{-5}	1000	6.9×10^{-5}

Table .4. Variations in MSE by varying error goal in normal and atrial fibrillation ECG ANN system

Momentum Factor	Learning Rate	Error Goal	Iterations	MSE
0.5	0.5	10^{-4}	1000	6.6×10^{-5}
0.5	0.5	10^{-2}	1000	2.3×10^{-3}
0.5	0.5	10^{-1}	1000	1.2×10^{-2}

Momentum Factor	Learning Rate	Error Goal	Iterations	MSE
0.5	0.5	10^{-4}	1000	4.8×10^{-5}
0.5	0.5	10^{-2}	1000	2.5×10^{-3}
0.5	0.5	10^{-1}	1000	2.2×10^{-2}

Above results show that mean square error varies from 10^{-4} to 10^{-6} indicating that overall MSE consideringall cases is low so proposed ANN model is effective. In this paper, it has been shown that by combining features of ECG and its coefficients leads to higher network efficiency as MSE is low. Based on experiments results, it has been shown that determining feature vector, learning rate, momentum factor, no. of iterations and error goal are the main influential factors in learning and testing of the network.

Acknowledgement

References

[1]   Porterfield, Linda M. "ECG Interpretation Made Incredibly Easy" Ones Edition, Spring House Co, Pennsylvania, 1997.

[2]   Juan Pablo Martínez, Rute Almeida, Salvador Olmos, Ana Paula Rocha, and Pablo Laguna, ―A Wavelet-Based ECG Delineator: Evaluation on Standard Databases, IEEE Transactions on Biomedical Engineering Vol. 51, No. 4, pp. 570-581, 2004.

[3]   Cuiwei Li, Chongxun Zheng, and Changfeng Tai.1995. Detection of ECG characteristic points using wavelet transforms. IEEE Trans.Biomed. Eng. 42(1):21-28, January.

[4]   S.C. Saxena, V. Kumar and S.T. Hande, "QRS Detection using New Wavelets", Journal of Medical Engineering & Technology,   Volume 26, November1, pages 7-15, (2002).

[5]   C.S. Burrus, R.A. Gopinath, H. Guo, (1997) Introduction to Wavelets and Wavelet Transforms, a Primer, Prentice Hall Inc.

[6]   Simpson P.K., "Fuzzy min-max neural networks - Part I :Classification", IEEE Trans. Neural Networks, Vol. 3, pp. 776-   786,Sep.1992

[7]   Available: http://www.mathworks.com.

[8]   MIT-BIH Arrhythmia Database,www.physionet.org.

[9]   S. Z. Mahmoodabadi, A .Ahmadian , M. D.Abolhasani, M. Eslami, J. H. Bidgoli, "ECG Feature Extraction Based on Multiresolution Wavelet Transform," Proceedings of the 2005 IEEE, Engineering in Medicine and Biology 27th Annual Conference Shanghai, China,September 1-4, 2005.

[10] Liro Hartimo. "A Heart Sound Extraction Algorithm Based On Wavelet Decomposition And Reconstruction" Proceedings of the 20th Annual International Conference of The IEEE Engineering in Medicine and Biological Society, Vol. 20 No3, pp.1539-1542, 1998.

SELECTION OF MIXED SAMPLING PLANS WITH CONDITIONAL DOUBLE SAMPLING PLAN AS ATTRIBUTE PLAN INDEXED THROUGH MAPD AND LQL USING IRPD

R. Sampath Kumar[1], R. Vijaya Kumar[2] and R. Radhakrishnan[3]

1. Assistant Professor, Department of Statistics, Government Arts College, Coimbatore - 18.
2. Assistant Professor, Department of Statistics, SSM College of Arts and Science,
3. Associate Professor, Department of Statistics, PSG College of Arts and Science, Coimbatore – 14.

Abstract

This paper presents the procedure for the construction and selection of mixed sampling plan (MSP) using Intervened Random effect Poisson Distribution (IRPD) as a baseline distribution. Having the conditional double sampling plan as attribute plan, the plans are constructed through limiting quality level (LQL) and maximum allowable percent defective (MAPD). Tables are constructed for easy selection of the plan.

Key Words And Phrases: intervened random effect poisson distribution, limiting quality level, mixed sampling plan, maximum allowable percent defective, operating characteristic, poisson, intervened random effect poisson distribution.

AMS (2000) Subject Classification Number: Primary: 62P30   Secondary: 62D05

1. Introduction

Mixed sampling plans consist of two stages of rather different nature. During the first stage the given lot is considered as a sample from the respective production process and a criterion by variables is used to check process quality. If process quality is judged to be sufficiently good, the lot is accepted. Otherwise the second stage of the sampling plan is entered and lot quality is checked directly by means of an attribute sampling plan. The mixed sampling plans have been designed under two cases of significant interest. In the first case, the sample size n_1 is fixed and a point on the OC curve is given. In the second case, plans are designed when two points on the OC curve are given.

There are two types of mixed sampling plans called independent and dependent plans. If the first stage sample results are not utilized in the second stage, then the plan is said to be independent otherwise dependent. The principal advantage of mixed sampling plan over pure attribute sampling plan is a reduction in sample size for a similar amount of protection.

Schilling (1967) proposed a method for determining the operating characteristics of mixed variables – attributes sampling plans, single sided specification and standard deviation known using the normal approximation. Baker and Brobst (1978) have introduced the Conditional Double Sampling Plan procedures. It has Operating Characteristic Curves identical to those of comparable Double Sampling procedures when the second sample is required to make a decision, it can be obtained from a related lot and not from the current lot. Conditional Double Sampling Plan by using sample information from related lot results in more attractive Operating Characteristic Curves and smaller sample sizes. This reduction in sample size is the Principal advantage of these procedures over traditional sampling procedures.

Devaarul (2003) has studied the mixed sampling plans and reliability based sampling plans. Radhakrishnan and Sampath Kumar (2006, 2007 and 2009) have constructed the mixed sampling plans using Poisson distribution as a baseline distribution. Sampath Kumar (2007) has constructed mixed variables – attributes sampling plans indexed through various parameters.

In the product control, the defective units are either rebuilt or replaced by new units during the sampling period. Quality engineers are always interested in improving the quality level of product to enhance the satisfaction of the customers and hence, they keep making changes in the production process. These actions trigger a change in the expected incidence of defective items in the remaining observational period. Any action for reducing the number of defectives during the sampling period is called an intervention and such intervention parameter ranges from 0 to 1.

In Intervened Random effect Poisson Distribution (IRPD), Poisson parameter   is modified in two ways: one method is multiplying an intervention parameter ρ (a constant) and secondly, multiplying an unobserved random effect   which follows Gamma probability distribution. The IRPD can be very useful to the quality and reliability engineers, who always make changes in the production system in the observational period of quality checking to ensure reliability of the system, because, the failure rate of the components may vary in different time intervals. The other areas of application of IRPD are queuing, demographic studies and process control and so on.

Shanmugam (1985) has used Intervened Poisson Distribution (IPD) in the place of Zero Truncated Poisson Distribution (ZTPD) for the study on cholera cases. Radhakrishnan and Sekkizhar (2007a, b, c) introduced Intervened Random effect Poisson Distribution in the place of Poisson distribution for the construction of attribute sampling plans.

In this paper, using the operating procedure of mixed sampling plan (independent case) with conditional double sampling plan as attribute plan, tables are constructed using IRPD as a baseline distribution. The tables are constructed for mixed sampling plan (MSP) indexed through i) LQL ii) MAPD. The plan indexed through MAPD is compared with the plan indexed through LQL.

2. Conditions For Applications Of IRPD - Mixed Sampling Plan

- Production process is modified during the sampling inspection by an intervention.
- Lots are submitted substantially in the order of their production.
- Inspection is by variable in the first stage and attribute in the second stage with quality defined as the fraction defective.
- Lot quality variation exists.

3. Glossary of symbols:

The symbols used in this paper are as follows:

p : submitted quality of lot or process

$P_a(p)$: probability of acceptance for given quality ' p '

p_2 : submitted quality such that $P_a(p_2) = 0.10$ (also called LQL)

p_* : maximum allowable percent defective (MAPD)

n : sample size for each lot

$n_{1,1}$: first sample size for variable sampling plan

$n_{1,2}$: first sample size for attribute sampling plan

$n_{2,2}$: second sample size for attribute sampling plan

c_1 : first attributes acceptance number

c_2 : second attributes acceptance number

c_3 : third attributes acceptance number

d_i : number of defectives in the ith sample (j=1,2,3,.....)

β_j : probability of acceptance for the lot quality ' p_j '

β_j' : probability of acceptance under variables plan for percent defective ' p_j '(with sample size n_1)

β_j'' : probability of acceptance under attributes plan for percent defective ' p_j '(with sample size n_2)

z (j) : 'z' value for the jth ordered observation

k : variable factor such that a lot is accepted if $\bar{X} \geq A = L + k\sigma$

4. Operating Procedure Of Mixed Sampling Plan Having Conditional Double Sampling Plan As Attribute Plan

Schilling (1967) has given the following procedure for the independent mixed sampling plan with lower specification limit (L) and standard deviation (σ).

Determine the parameters of the mixed sampling plan $n_{1,1}$, $n_{1,2}$, $n_{2,2}$, k, c_1, c_2 and c_3

- Take a random sample of size $n_{1,1}$ from the lot
- If a sample average $\bar{X} \geq A = L + k\sigma$, accept the lot
- If a sample average $\bar{X} < A = L + k\sigma$ take a second sample of size $n_{1,2}$ (ie., $n_{1,2} = n_{1,1}$)
- Inspect all the articles included in the sample. Led 'd_i' be the number of defectives in the sample
- If $d_i \leq c_1$, accept the lot
- If $d_i > c_2$, reject the lot
- If $c_1 + 1 \leq d_i \leq c_2$, then take a second sample of size $n_{2,2}$ from the preceding (i-1) lot or the next (i+1) lot
- Find the number of defectives d_{i-1} or d_{i+1}. Then find d= $d_i + d_{i-1}$ or d=$d_i + d_{i+1}$
- If $d \leq c_3$, accept the lot otherwise reject the lot.

5. Construction of mixed sampling plan having conditional double sampling plan as attribute plan using irpd.

Schilling (1967) has given the OC function of mixed sampling plan as

$$L(p) = \text{Pn}_1(\overline{X} \le A) + \text{Pn}_1(\overline{X} > A) \sum_{j=0}^{c} p(j; n_2) \tag{1}$$

The above expression is given as

$$\beta_j = \beta_j' + (1 - \beta_j')\beta_j'' \tag{2}$$

The operation of mixed sampling plans can be properly assessed by the OC curve for given values of the fraction defective. The development of mixed sampling plans and the subsequent discussions are limited only to the upper specification limit 'U'. By symmetry, a parallel discussion can be made for lower specification limits.

The procedure for the construction of mixed variables – attributes sampling plans is provided by Schilling (1967) for a given '$n_{1,1}$', 'k' and a point 'p_j' on the OC curve is given below.

- Assume that the mixed sampling plans are independent
- Split the probability of acceptance (β_j) determining the probability of acceptance that will be assigned to the first stage.

  Let it be β_j'

- Decide the sample size $n_{1,1}$ (for variable sampling plan) to be used

- Calculate the acceptance limit for the variable sampling plan as

  $A = L + k\sigma = L + [z(p_j) + \{z(\beta_j')/\sqrt{n_{1,1}}\}]\sigma$, where L is the lower specification limit and

  z (t) is the standard normal variate corresponding to 't' such that $t = \int_{z(t)}^{\infty}\left(\frac{1}{\sqrt{2\pi}}\right)e^{-u^2/2}\,du$

- Determine the sample average $\overline{X}$. If a sample average $\overline{X} < A = L + k\sigma$, take a second stage sample size '$n_{1,2}$' using attribute sampling plan.

- Split the probability of acceptance β_j as β_j' and β_j'', such that $\beta_j = \beta_j' + (1 - \beta_j')\beta_j''$ and fix the value of β_j'.

- Now determine β_j'', the probability of acceptance assigned to the attributes plan associated with the second stage sample

  as $\beta_j'' = (\beta_j - \beta_j')/(1 - \beta_j')$

- Determine the appropriate second stage sample size '$n_{1,2}$' from

  $P_a(p) = \beta_j''$ for $p = p_j$

Using the above procedure, tables can be constructed to facilitate easy selection of mixed sampling plan with conditional double sampling plan as attribute plan using IRPD as a baseline distribution indexed through MAPD and LQL.

Radhakrishnan and Sekkizhar (2007a, b and c) suggested the probability mass function of the CDSP using IRPD as a baseline distribution for $n = n_{1,2} = 2n_{2,2}$ is

$$P_a(p) = \sum_{i=0}^{c_1} p_i + p_{c_1+1} \sum_{i=0}^{c_3-c_1-1} q_i + p_{c_1+2} \sum_{i=0}^{c_3-c_1-2} q_i + \ldots\ldots\ldots + p_{c_2} \sum_{i=0}^{c_3-c_2} q_i \tag{3}$$

where $p_i = \left[\frac{e^{-m\theta}(m\theta)^i}{(1+\rho m\theta)^\alpha}\sum_{l=0}^{i}\left(\frac{\rho}{1+\rho m\theta}\right)^l \frac{(\alpha+l-1)!}{l!(i-l)!(\alpha-1)!}\right]$

$q_i = \left[\frac{e^{-\theta}\theta^i}{(1+\rho\theta)^\alpha}\sum_{l=0}^{i}\left(\frac{\rho}{1+\rho\theta}\right)^l \frac{(\alpha+l-1)!}{l!(i-l)!(\alpha-1)!}\right]$ and $\theta = \left(\frac{np}{1+\rho}\right)$

The tables furnished in this paper are for the case when $\alpha=1$, $m=2$ and $n = n_{1,2} = 2n_{2,2}$.

6. Construction Of Mixed Sampling Plans Indexed Through MAPD And MAAOQ

MAPD, introduced by Mayer (1967) and studied by Soundararajan (1975) is the quality level corresponding to the inflection point of the OC curve. The degree of sharpness of inspection about this quality level ' p_* ' is measured by ' p_t ', the point at which the tangent to the OC curve at the inflection point cuts the proportion defective axis for designing, Soundararajan (1975) proposed a selection procedure for single sampling plan indexed with MAPD and K= $\frac{p_t}{p_*}$.

Using the probability mass function of the IRPD, given in expression (3), the inflection point (p_*) is obtained by using $\frac{d^2 P_a(p)}{dp^2} = 0$ and $\frac{d^3 P_a(p)}{dp^3} \neq 0$. The $n_{1,2}$MAPD values are calculated for different values of c_1, c_2, c_3 and ρ=0.7 for $\beta_*' = 0.04$ using c++ program and presented in Table 1.

The MAAOQ (Maximum Allowable Average Outgoing Quality) of a sampling plan is defined as the Average Outgoing Quality (AOQ) at the MAPD.

By definition AOQ = $p\ P_a(p)$ and

$$MAAOQ = p_*\ P_a(p_*)$$

The values of MAPD and MAAOQ are calculated for different values of c_1, c_2, c_3 and ρ for $\beta_*' = 0.30$ and the ratio

$R = \frac{MAAOQ}{MAPD}$ is presented in Table 1.

Table 1: $n_{1,2}$MAPD and $n_{1,2}$MAAOQ values for a specified values of c_1, c_2, c_3 and different values of ρ for mixed sampling plan when $\beta_*' = 0.04$

ρ	c_1	c_2	c_3	β_*	β_*''	$n_{1,2}$MAPD	$n_{1,2}$MAAOQ	$R = \frac{MAAOQ}{MAPD}$
0.8	3	6	10	0.5970	0.5802	3.0373	1.7622	0.5802
			11	0.5916	0.5745	3.1474	1.8081	0.5745
			12	0.5879	0.5707	3.2213	1.8383	0.5707
			13	0.5853	0.5680	3.2704	1.8575	0.5680
	3	7	10	0.5944	0.5775	3.2913	1.9006	0.5775
			11	0.5879	0.5707	3.4784	1.9851	0.5707
			12	0.5833	0.5659	3.6171	2.0469	0.5659
			13	0.5799	0.5623	3.7172	2.0901	0.5623
	6	7	10	0.6075	0.5911	3.5044	2.1162	0.5911
			11	0.6066	0.5902	3.5802	2.1130	0.5902
			12	0.6045	0.5880	3.6438	2.1425	0.5880
			13	0.6015	0.5848	3.6964	2.1616	0.5848
			14	0.5981	0.5813	3.7387	2.1733	0.5813
			15	0.5947	0.5778	3.7729	2.1510	0.5778
			16	0.5916	0.5745	3.8005	2.1833	0.5745
	6	8	10	0.6075	0.5911	3.6546	2.1602	0.5911
			11	0.6065	0.5901	3.8083	2.2472	0.5901
			12	0.6036	0.5870	3.9475	2.3171	0.5870
			13	0.5995	0.5828	4.0650	2.3690	0.5828
			14	0.5996	0.5829	4.0482	2.3596	0.5829
			15	0.5946	0.5777	4.2141	2.4344	0.5777
			16	0.5890	0.5718	4.2820	2.4484	0.5718
0.7	3	6	10	0.5577	0.5392	3.1080	1.6758	0.5392
			11	0.5520	0.5333	3.2963	1.7579	0.5333
			12	0.5481	0.5292	3.3761	1.7866	0.5292

			13	0.5452	0.5262	3.4292	1.8044	0.5262
	3	7	10	0.5560	0.5375	3.4287	1.8429	0.5375
			11	0.5489	0.5489	3.5514	1.9493	0.5489
			12	0.5440	0.5250	3.7765	1.9826	0.5250
			13	0.5405	0.5213	3.8828	2.0241	0.5213
	6	7	15	0.4799	0.4582	4.3490	1.9927	0.4582
			16	0.4744	0.4525	4.3954	1.9889	0.4525
	6	8	10	0.5680	0.4875	4.0860	1.9919	0.4875
			11	0.5644	0.5465	3.9768	2.1733	0.5465
			12	0.5622	0.5439	4.1224	2.2421	0.5439
0.5	3	6	10	0.4813	0.4596	3.4175	1.5706	0.4596
			11	0.4759	0.4540	3.5452	1.6095	0.4540
			12	0.4717	0.4496	3.6332	1.6334	0.4496
			13	0.4688	0.4466	3.6897	1.6478	0.4466*
	3	7	10	0.4801	0.4584	3.6635	1.6793	0.4584
			11	0.4737	0.4517	3.8760	1.7507	0.4517
			12	0.4688	0.4466	4.0378	1.8032	0.4466

Selection of the plan

For the given values of ρ, β_*', MAPD and MAAOQ, the ratio $R = \dfrac{MAAOQ}{MAPD}$ is found and the nearest value of R is located in Table 1. The corresponding value of c_1, c_2, c_3 and $n_{1,2}$MAPD values are noted and the value of $n_{2,2}$ is obtained using $n_{1,2} = \dfrac{n_{1,2}MAPD}{MAPD}$.

Example 1: Given ρ=0.8, $\beta_*' = 0.04$, MAPD=0.092 and MAAOQ=0.041, the ratio $R = \dfrac{MAAOQ}{MAPD} = \dfrac{0.041}{0.092} = 0.4456$ is computed. In Table 1 the nearest R value is 0.4466 which is corresponding to c_1=3, c_2=6, c_3=13. The value of $n_{1,2}$MAPD=3.6897 is found and hence the value of $n_{1,2}$ is determined as $n_{1,2} = \dfrac{n_{1,2}MAPD}{MAPD} = \dfrac{3.6897}{0.092} = 40$. Thus $n_{1,2}$=40, $n_{2,2}$=20, c_1=3 , c_2=6 and c_3=13 are the parameters of mixed sampling plan having CDSP as attribute plan using IRPD as a baseline distribution for the given values of ρ=0.8, MAPD=0.092 and MAAOQ=0.041.

Practical problem: Suppose the plan $n_{1,1}$=17, k=2g is the lot by lot acceptance inspection of a health drink product with carbohydrate specification 62g (500g pack) with known S.D(σ)=1.25g. In this example L=62g, σ =1.25g and k=2g, $A = L + k\sigma$ = 62 + 2(1.75)=64.5g

Now by applying the variables inspecting first, take random sample of size $n_{1,1}$=17 from the lot. Record the sample results and find $\bar{X}$. If $\bar{X} \geq A = L + k\sigma$ =64.5g, then accept the lot. If $\bar{X} < A$, take a random sample of size $n_{1,2}$ and apply the attribute inspection.

Under attributes inspection, by using Conditional double sampling plan as attribute plan using intervened Random effect Poisson Distribution (IRPD) as a baseline distribution, if the manufacturer fixes the values MAPD= 0.092(9.2 non conformities out of 100), MAAOQ=0.041(41 non conformities out of 100) and $\beta_*' = 0.04$, take a sample of size $n_{1,2}$ =40 and observe the number of defectives d_i . If $d_i \leq 3$, accept the lot and if $d_i > 6$, reject the lot. If $4 \leq d_i \leq 6$, take a second sample of size $n_{2,2}$ =20 from the remaining lot and find the number of defectives (d). If $d \leq 13$ accept the lot otherwise reject the lot and inform the management for further action.

7. Construction Of Mixed Sampling Plans Indexed Through LQL

The procedure given in section 5 is used for constructing the mixed sampling plan indexed through LQL (p_2). By assuming the probability of acceptance of the lot be β_2 =0.10 and β_2' =0.14, the $n_{1,2} p_2$ values are calculated for different values of c_1, c_2, c_3 and 'ρ' using c++ program and is presented in Table 2.

Table 2: $n_{1,2}$ LQL values for a specified values of c_1, c_2, c_3 and ρ of mixed sampling plan when β_2 =0.10 and β_2' =0.04

c_1	c_2	c_3	ρvalues								
			0.1	0.2	0.3	0.4	0.5	0.6	0.7	0.8	0.9
3	6	10	5.2156	5.3555	5.5233	5.7037	5.8894	6.0771	6.2646	6.4508	6.6350
		11	5.4061	5.5541	5.7304	5.9190	6.1127	6.3079	6.5026	6.6957	6.8865
		12	5.5506	5.7069	5.8918	6.0886	6.2902	6.4928	6.6947	6.8945	7.0918
		13	5.6541	5.8189	6.0124	6.2174	6.4268	6.6368	6.8457	7.0522	7.2558
3	7	10	5.4281	5.5720	5.7452	5.9316	6.1237	6.3178	6.5116	6.7041	6.8944
		11	5.7003	5.8537	6.0374	6.2344	6.4368	6.6408	6.8442	7.0458	7.2449
		12	5.9235	6.0866	6.2805	6.4876	6.6998	6.9133	7.1259	7.3362	7.5437
		13	6.0990	6.2717	6.4756	6.6923	6.9140	7.1364	7.3576*	7.5763	7.7918
6	7	10	5.9484	6.1517	6.3931	6.6517	6.9183	7.1883	7.4591	7.7293	7.9980
		11	6.0411	6.2441	6.4854	6.7442	7.0111	7.2815	7.5529	7.8237	8.0929
		12	6.4105	6.3437	6.5854	6.8445	7.1120	7.3829	7.6549	7.9262	8.1960
		13	6.2334	6.4378	6.6806	6.9407	7.2091	7.4809	7.7536	8.0257	8.2963
		14	6.3116	6.5183	6.6806	7.0251	7.2349	7.5681	7.8421	8.1153	8.3869
		15	6.3717	6.5818	6.8297	7.0942	7.3662	7.6414	7.9171	8.1919	8.4649
		16	6.4143	6.6285	6.8801	7.1479	7.4228	7.7005	7.9785	8.2553	8.5301
6	8	10	6.0153	6.2187	6.4607	6.7202	6.9878	7.2589	7.5310	7.8024	8.0723
		11	6.1758	6.3791	6.6215	6.8818	7.1505	7.4229	7.6964	7.9693	8.2407
		12	6.3564	6.5604	6.8040	7.0657	7.4662	7.6100	7.8851	8.1596	8.4326
		13	6.5334	6.7396	6.9855	7.2495	7.5220	7.7982	8.0753	8.3518	8.6266
		14	6.6915	6.9013	7.1507	7.4179	7.6934	7.9723	8.2521	8.5309	8.8080
		15	6.8229	7.0377	7.2916	7.5630	7.8423	8.1246	8.4075	8.6892	8.9689
		16	6.9253	7.1462	7.4058	7.6822	7.9659	8.2524	8.5389	8.8240	9.1069

Selection of the plan

Table 2 is used to construct the plans when p_2, ρ, c_1, c_2 and c_3 are given. For any given values of p_2, ρ, c_1, c_2 and c_3 one can determine $n_{1,2}$ value using $n_{1,2} = \dfrac{n_{1,2}\, p_2}{p_2}$.

Example 2: Given ρ=0.7, p_2 =0.10194, c_1=3, c_2=7, c_3=13 and β_2' =0.04. Using Table 2, find $n_{1,2} = \dfrac{n_{1,2}\, p_2}{p_2} = \dfrac{7.3576}{0.10194} = 72$.

For a fixed $\beta_*' = 0.04$, the mixed sampling plan with CDSP as attribute plan is $n_{1,2}$=72, $n_{2,2}$=36, ρ=0.7, c_1=3, c_2=7 and c_3=13.

8. Comparison Of Mixed Sampling Plan Indexed Through MAPD And LQL

In this section MSP indexed through MAPD is compared with MSP indexed through IQL by fixing the parameters c_1, c_2, c_3 and β_j'.

For the specified values of ρ, MAPD and MAAOQ with the assumption for $\beta_*' = 0.04$ one can find the values of c_1, c_2 and c_3 indexed through MAPD. By fixing the values of c_1, c_2 and c_3 find the value of p_2 by equating $P_a(p) = \beta_2$ =0.10. For β_2' =0.04, c_1, c_2 and c_3 one can find the values of $n_{2,2}$ using $n_{1,2} = \dfrac{n_{1,2}\, p_2}{p_2}$ from Table 2. For different combinations of ρ, MAPD and MAAOQ the values of c_1, c_2, c_3 and $n_{1,2}$ (indexed through MAPD) and c_1, c_2, c_3 and $n_{1,2}$ (indexed through LQL) are calculated and presented in Table 3.

Construction of OC curve

The OC curves for the plan ρ=0.8, $n_{1,2}$=40, $n_{2,2}$=20, c_1=3, c_2=6, c_3=13 (indexed through MAPD) and $n_{1,2}$=44, $n_{2,2}$=22, c_1=3, c_2=6, c_3=13 (indexed through LQL) based on the different values of ' $n_{1,2} p_2$ ' and $P_a(p)$ are presented in Figure 1.

Table 3: Comparison of the Plans

Given Values			Indexed Through MAPD					Indexed Through LQL				
MAPD	MAAOQ	ρ	c_1	c_2	c_3	$n_{1,2}$	$n_{2,2}$	c_1	c_2	c_3	$n_{1,2}$	$n_{2,2}$
0.092	0.041*	0.8	3	6	13	40	20	3	6	13	44	22
0.112	0.063	0.7	3	7	13	66	33	3	7	13	72	36
0.069	0.039	0.5	3	7	12	52	26	3	7	12	57	29
0.156	0.092	0.8	6	7	12	23	12	6	7	12	25	13

*OC curves are drawn
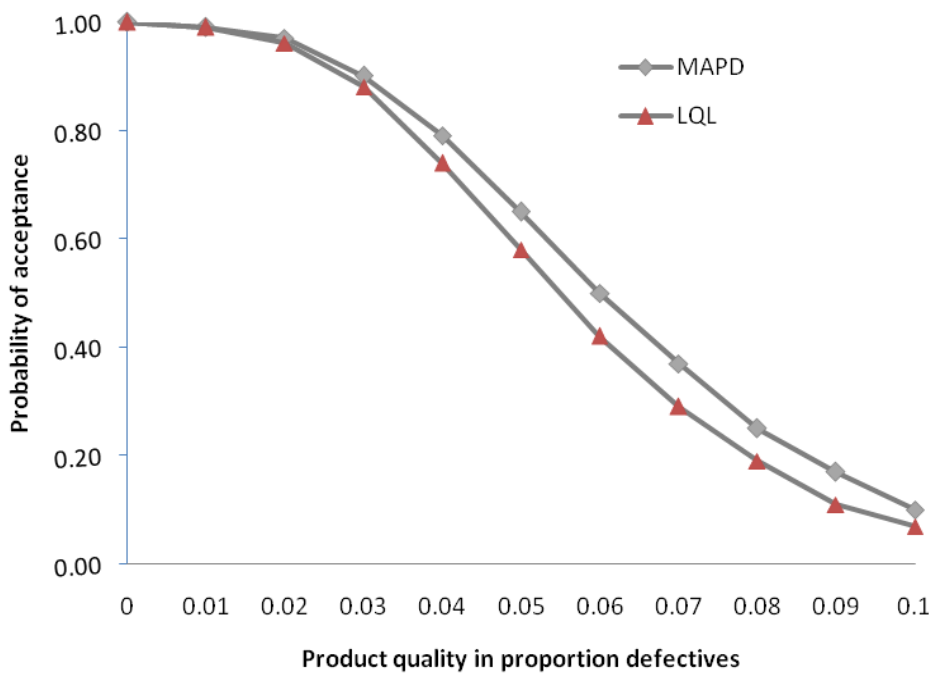
Fig1: OC curves for the plans (ρ=0.8, c_1=3, c_2=6, c_3=13, $n_{1,2}$=40, $n_{2,2}$=20) and (ρ=0.8, c_1=3, c_2=6, c_3=13, $n_{1,2}$=44, $n_{2,2}$=22)

9. Conclusion

In this paper the construction of mixed sampling plan with conditional double sampling plan as attribute plan indexed through the parameters MAPD and LQL are presented by taking IRPD as a baseline distribution. Further the plan indexed through MAPD is compared with the plan indexed through LQL. It is concluded from the study that the second stage sample size required for conditional double sampling plan indexed through MAPD is less than that of second stage sample size of the conditional double sampling plan indexed through LQL. If the floor engineers know the levels of MAPD or LQL, they can have their sampling plans on the floor itself by referring to the tables.   This provides the flexibility to the floor engineers in deciding their sampling plans.

Various plans can also be constructed to make the system user friendly by changing the first stage probabilities (β_*' , β_2') and can also be compared for their efficiency.

References
1. R.C. Baker, and R.W. Brobst, 1978, Conditional Double Sampling Plan, *Journal of Quality Technology*, Vol. 10, No. 4, pp.150-154.
2. Devaarul, S., 2003, Certain Studies Relating to Mixed Sampling Plans and Reliability Based Sampling Plans, Ph.D., Dissertation, Bharathiar University, Coimbatore, Tamil Nadu, India.
3. P.L. Mayer, 1967, A note on sum of Poisson probabilities and an application, *Annals of Institute of Statistical Mathematics*, Vol.19, pp.537-542.
4. R. Radhakrishnan, and R. Sampath Kumar, 2006, Construction of mixed sampling plan indexed through MAPD and AQL with chain sampling plan as attribute plan, STARS, Vol.7, No.1, June 2006, pp.14-22. .
5. R. Radhakrishnan, and R. Sampath Kumar, 2007, Construction and comparison of mixed sampling plans having repetitive group sampling plan as attribute plan, *National Journal of Technology,* Vol. 4, No. 3. pp. 1-6.

6. R. Radhakrishnan, and R. Sampath Kumar, 2009, Construction and comparison of mixed sampling plans having ChSP-(0,1) plan as attribute plan, *The International Journal of Statistics and Management System,* Vol.4, No.1-2, pp. 134-149.

7. R. Radhakrishnan, and J. Sekkizhar, 2007a, Construction of sampling plans using intervened random effect Poisson distribution. *The International Journal of Statistics and Management Systems*, Vol.2, 1-2, pp 88-97.
8. R. Radhakrishnan, and J. Sekkizhar, 2007b, Construction of conditional double sampling plans using intervened random effect Poisson distribution, Proceedings volume of *SJYSDNS-2005, Acharya Nagarjuna University, Guntur.* Pp.57-61.
9. R. Radhakrishnan, and J. Sekkizhar, 2007c, Application of intervened random effect Poisson distribution in process control plans, *International Journal of Statistics and Systems.* Vol. 2. No.1. pp.29-39.
10. Sampath Kumar, R., 2007, Construction and Selection of Mixed Variables – Attributes Sampling Plans, Ph.D., Dissertation, Bharathiar University, Coimbatore, Tamil Nadu, India.
11. Schilling, E.G., 1967, A General Method for Determining the Operating Charateristics of Mixed Variables – Attribute Sampling Plans Single Side Specifications, S.D. known, Ph.D Dissertation – Rutgers – The State University, New Brunswick, New Jersy.
12. R. Shanmugam, 1985, An intervened Poisson distribution and its medical applications, *Biometrics*, 41, 1025-1029.

13. V. Soundararajan, 1975, Maximum allowable percent defective (MAPD) single sampling inspection by attributes plan, *Journal of Quality Technology*, Vol.7, No.4, pp.173-182.

REDUCTION OF POWER LINE INTERFERENCE IN ECG SIGNAL USING FIR FILTER

Ms. Geeta Kadam[1]
[1]Master of Technology, Electronics Department,
Department of Technology,
Shivaji University, Kolhapur
India (MS)

Prof.P.C.Bhaskar[2]
[2]Electronics Department,
Department of Technology,
Shivaji University, Kolhapur
India (MS)

Abstract-
Filtering of power line interference is very meaningful in the measurement of biomedical events recording, particularly in the case of recording signals as weak as the ECG. The available filters for power line interference either need a reference channel or regard the frequency as fixed 50/60Hz. Methods of noise reduction have decisive influence on performance of all electro-cardio-graphic (ECG) signal processing systems. This work deals with problems of power line interference reduction. Some analogue and digital approaches to this problem are presented and its properties, advantages and disadvantages are shown. Present paper deals with design and development of digital FIR equiripple filter. The basic ECG has the frequency range from .5Hz to 100Hz.

Keywords- Electrocardiogram, Simulation, Equiripple Filter, Real Time Filtering, Noise reduction.

I. Introduction

Signal processing, in general, has a rich history, and its importance is evident in such a diverse fields as biomedical engineering, acoustics, Sonar, radar, Seismology, speech communication, data communication, nuclear science, and many others. In many applications, for example, in EEG and ECG analysis or speech processing it can be used to extract some characteristic parameters. Alternatively, to remove interference, such as noise, from the signal or to modify the signal to present it in a form this is more easily interpreted by an expert. The field of biomedical signal analysis or processing has advanced to the stage of practical application of signal processing and pattern analysis techniques foe efficient and improved noninvasive diagnosis, online monitoring of critical patients, and rehabilitation and sensory aids for the handicapped. Techniques developed by engineers are gaining wider acceptance by practicing clinicians, and the role of engineering in diagnosis and treatment is gaining much–observed respect. The major strength in the application of computers in biomedical signal analysis lies in the potential use of signal processing and modeling technique for the quantitative or the objective analysis. Analysis of signals by human observers is almost always accompanied by perceptual limitations, inter-personal variations, errors caused by fatigue, errors caused by the very low rate of incidence of certain sign of abnormality, environmental distortions, and so on.

Electrocardiogram (ECG) is an important clinical tool for investigating the activities of heart, which is one of the signals of vitality. Interpretation of these details allows diagnosis of a wide range of heart conditions. These conditions can vary from minor to life threatening. A typical ECG tracing of a normal heartbeat (or cardiac cycle) consists of a P wave, a QRS complex and a T wave. Figure 1 shows the typical ECG trace.

Figure 1: Typical ECG trace.
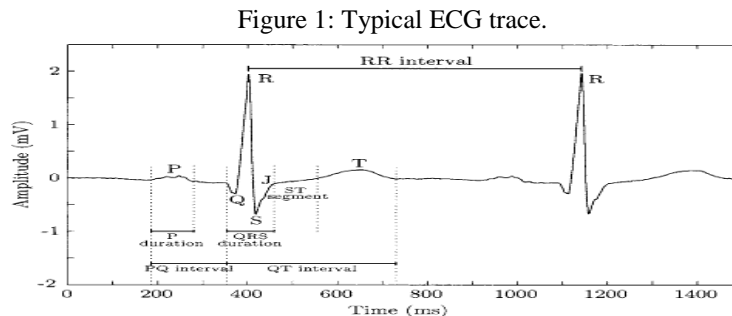
The electrical activity of the heart is generally sensed by monitoring electrodes placed on the skin surface. The electrical signal is very small (normally 0.0001 to 0.003 volt). These signals are within the frequency range of 0.05 to 100 Hertz (Hz.) or cycles per second. Unfortunately, other artifactual signals of similar frequency and often larger amplitude reach the skin surface and

mix with the ECG signals. Artifactual signals arise from several internal and external sources. Means Electro-cardio-graphic signals (ECG) may be corrupted by various kinds of noise. Typical examples are:

1. Power line interference
2. Electrode contact noise.
3. Motion artifacts.
4. Muscle contraction.
5. Base line drift.
6. Instrumentation noise generated by electronic devices.
7. Electrosurgical noise.

From various artifacts contaminate electrocardiogram (ECG) recording, the most common are power line interference and baseline drift. Power line interference is easily recognizable since the interfering voltage in the ECG may have frequency 50 Hz. The interference may be due to stray effect of the alternating current fields due to loops in the patient's cables. Other causes are loose contacts on the patient's cable as well as dirty electrodes. When the machine or the patient is not properly grounded, power line interference may even completely obscure the ECG waveform. The most common cause of 50 Hz interference is the disconnected electrode resulting in a very strong disturbing signal, and therefore needs quick action. Electromagnetic interference from the power lines also results in poor quality tracings. Electrical equipments such as air conditioner, elevators and X-ray units draw heavy power line current, which induce 50 Hz signals in the input circuits of the ECG machine. Electrical power systems also induce extremely rapid pulse or the spike on the trace, as a result of switching action. Care should be taken to suppress these transients. Figure 2 shows the ECG signal with power line interference.

For the meaningful and accurate detection, steps have to be taken to filter out or discard all these noise sources. Analog filters help in dealing with these problems; however, they may introduce nonlinear phase shifts, skewing the signal. Also, the instrumentation depends on resistance, temperature, and design, which also may introduce more error. With more recent technology, Digital filters are now capable of being implemented offering more advantages over the analog one. Digital filters are more precise due to a lack of instrumentation. The work on design and implementation of Digital filter on the ECG signal is in progress in the different part of the world.
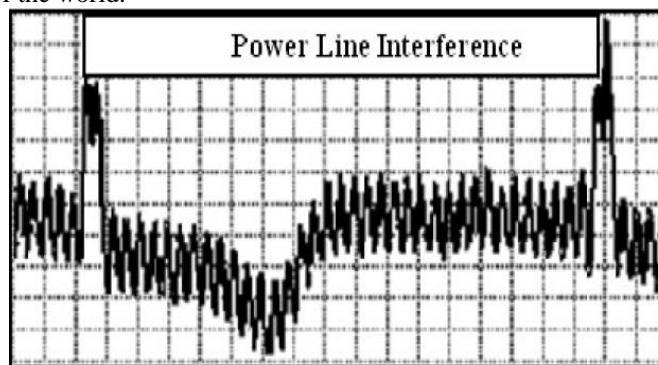
Figure 2: ECG corrupted Due to Power line Interference.

Many researchers have worked on development of method for reduction of noise in ECG signal. Choy TT, Leung P M. have used 50 Hz notch filters for the real time application on the ECG signal it is found that filter was capable of filtering noise by 40dB.with bandwidth of4Hz and causes the attenuation in the QRS complex[3].McManus CD, Neubert KD and Cramer E have surveyed different digital filter method like notch filters, adaptive filters and globally derived filters their performances are compared on artificial signals as well as actual ECGs and found that AC interference in these ECGs is shown to exhibit two qualities especially relevant to filter design: considerable deviations from a nominal 50 Hz frequency and substantial noise at higher harmonics. For this they suggested presented different digital filter methods to eliminate it [1].Cramer E, McManus CD, and Neubert D have introduced Global filtering of AC interference in the digitized ECG as a new concept. Two different filters embodying a global approach are developed. One is based on a least-squares error fit, the other uses a special summation method. Both methods are compared with a local predictive filter by applying each filter to artificial signals and to real ECGs [4].Some researchers have used analog filters for removal of the power line interference. Hejjel L, used the analog digital notch filter for the reduction of the power line interference in the ECG signal for the heart rate variability analysis. The investigation addressed the analysis of the effects of AC interference and its filtering on the precision and accuracy of heart rate detection. Artificial ECG recordings with predefined parameters were simulated by a computer and a data acquisition card, consecutively filtered by an analog notch filter. It is found that the filtering of uncorrupted ECG signals does not result in heart rate period deviations. Power-line interference contamination proportionally alters the accuracy of representative point detection. Literature encouraged using the digital notch filter for the power line contamination removal [5].

Mihov G, Dotsinsky IV and Georgieva TS described the subtraction procedure for the power line interference removal in the ECG signal. In contrast to the well-known hardware and software filters, the procedure does not affect the signal

frequency components around the rated power line frequency. Originally, the procedure was developed for multiplicity between the sampling rate and the interference frequency. The implementation of the subtraction procedure can be extended to almost all possible cases of sampling rate and interference frequency variation. The work was initially carried out in a MATLAB environment and latter on programs have been written in C + + language for DSPs [6]. Hamilton PS had worked on the application of the adaptive and non-adaptive digital filter on the ECG signal. He worked for the performance evaluation based on two implementations of the notch filters based on transient response time, signal distortion, and implementation complexity. Before filtration and after filtration results are given in the literature [7]. Sander A. et. al. designed and implemented a digital notch filter. A 50/60 Hz notch filter system was designed to eliminate power line interferences from the high-resolution ECG. This special filter causes only minimal distortions of the power spectra and thus permits us to filter high-resolution ECG's without any appreciable changes in the frequency distribution of the original signal. Since the filter is based on an integer coefficient filter technique, the calculation time is relatively short and the programming effort comparatively low [8]. Kumaravel N et.al. suggested the power line interference removal technique to enhance the signal characteristics for diagnosis. They suggested the performances of the linear FIR filter, Wave digital filter (WDF) and adaptive filter for the power-line frequency variations from 48.5 to 51.5 Hz in steps of 0.5 Hz. The performances of Rule-based FIR filter and Rule-based Wave digital filter are compared with the LMS adaptive filter. They found the adaptive filter more effective than the rule base filtering technique [9]. Wu Y, Yang Y, discussed the advantages and disadvantages of several conventional digital filter methods. Then, based on Levkov method, they proposed a new filter method. By using these methods to remove 50 Hz interference from more than 50 persons' ECG signals, results show that this new method is the best, and it can satisfy the real time requirement of digital ECG machine [10]. Van Alste JA et.al. suggested the application of an efficient FIR filter with reduced number of taps for the removal of the base line wonder and power line interference in the ECG [11]. Mitov IP described a method for reduction of power line interference (PLI) in electrocardiograms with sampling rate integer multiple of the nominal power line frequency and tested using simulated signals and records from the databases of the American Heart Association and the Massachusetts Institute of Technology. The method involves parabolic detrending of the ECG, estimation of the signal components with frequencies corresponding to PLI by discrete Fourier transform, and minimum-squared-error approximation of decimated series of averaged instantaneous values of PLI using appropriately defined weights. The main advantage of the developed method in comparison with other simpler and faster approaches is the accurate interference reduction in cases when the power line frequency deviates from the nominal 50 or 60 Hz. That means the track on the variation on the frequency has been kept. Due to computational burden, the method is more suitable for off-line application instead of the on line method [12]. Ziarani AK and Konrad A. suggested the adaptive digital filtering method for the power line interference reduction. This method employs, as its main building block, a recently developed signal processing algorithm capable of extracting a specified component of a signal and tracking its variations over time. Design considerations and performance of the method are with the aid of computer simulations. Superior performance is observed in terms of effective elimination of noise under conditions of varying power line interference frequency. This method is a simple and robust structure which complies with practical constraints involved in the problem such as low computational resource availability and low sampling frequency [13]. Dotsinsky I, Stoyanov T have assessed the efficiency of notch filters and a subtraction procedure for power-line interference cancellation in electrocardiogram (ECG) signals. In contrast with the subtraction procedure, widely used digital notch filters unacceptably affect QRS complexes [14]. Ider YZ, Saki MC, Gcer HA described a method for line interference reduction to be used in signal-averaged electrocardiography (SAECG) systems and its performance is analyzed. This new method is an adaptation of a different technique for removal of line interference from conventional electrocardiograms. It involves the recording of a line interference signal simultaneous with the lead signals, so that a shifted and scaled version of it can be used to subtract line interference from the leads. It is seen that this line interference subtraction method can reduce line interference effectively and without introducing any additional noise into the ECG signal [15]. Ider YZ, Koymen H. Suggested a theory that power line frequency must be accurately known if line interference is to be accurately subtracted from the output of a bi-potential amplifier[16].

There are different methods like window method and equiripple method also available [17]. The simplest technique is known as "Windowed" filters. This technique is based on designing a filter using well-known frequency domain transition functions called "windows". The use of windows often involves a choice of the lesser of two evils. Some windows, such as the Rectangular, yield fast roll-off in the frequency domain, but have limited attenuation in the stop-band along with poor group delay characteristics. Other windows like the Blackman, have better stop-band attenuation and group delay, but have a wide transition-band (the band-width between the corner frequency and the frequency attenuation floor). Windowed filters are easy to use, are scalable.

Ii. Design Of Fir Notch Filter

FIR filters are widely used due to the powerful design algorithms that exist for them, their inherent stability when implement in non-recursive form, the ease with which one can attain linear phase, their simple extensibility to multirate cases, and the ample hardware support that exists for them among other reasons.

A.   Design of Equiripple notch filter:

Linear-phase equiripple filters are desirable because they have the smallest maximum deviation from the ideal filter when compared to all other linear-phase FIR filters of the same order.

An Equiripple or Remez Exchange (Parks-McClellan) design technique provides an alternative to windowing by allowing the designer to achieve the desired frequency response with the fewest number of coefficients. This is achieved by an iterative process of comparing a selected coefficient set to the actual frequency response specified until the solution is obtained that requires the fewest number of coefficients. Though the efficiency of this technique is obviously very desirable, there are some concerns. For equiripple algorithms some values may converge to a false result or not converge at all. Therefore, all coefficient sets must be pre-tested off-line for every corner frequency value.

Equiripple designs are based on optimization theory and require an enormous amount of computation effort. With the availability of today's desktop computers, the computational intensity requirement is not a problem, but combined with the possibility of convergence failure.

B.   Design of Least Square notch filter:

Equiripple designs may not be desirable if we want to minimize the energy of the error (between ideal and actual filter) in the pass/stop band. Consequently, if we want to reduce the energy of a signal as much as possible in a certain frequency band, least-squares designs are preferable.

III.   Performance Measures

The efficiency of FIR filter based de-noising is measured by evaluating SNR of enhanced ECG signal. SNR of denoised ECG signal is given by

$$SNR = 10\log_{10}\frac{\sum(x_{denoised})^2}{\sum(x_{org}-x_{denoised})^2} \tag{1}$$

In which x_{org} is raw ECG signal and $x_{denoised}$ is filtered ECG signal.

IV. Results

On implementation of above designed filters on ECG signals with powerline interference, the following results are obtained.Fig 3 shows the results for Equiripple notch filter. Fig 4 shows the results for Least square filter.Table1. shows the results of comparison for different FIR filter design.
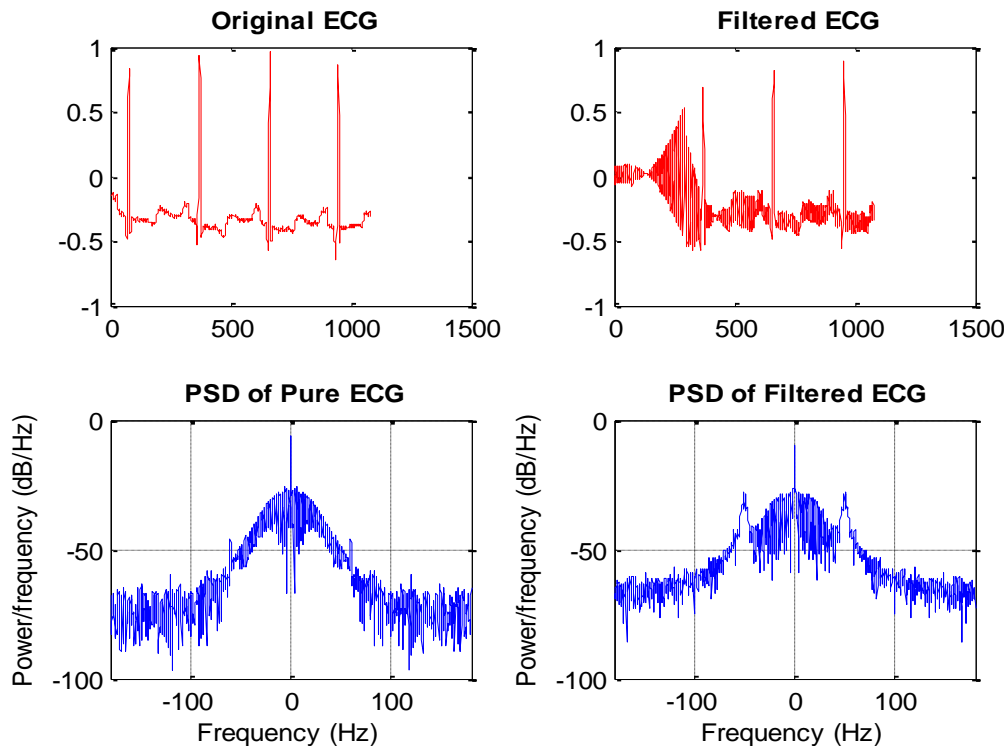
Figure 3: Results for Equiripple notch filter.
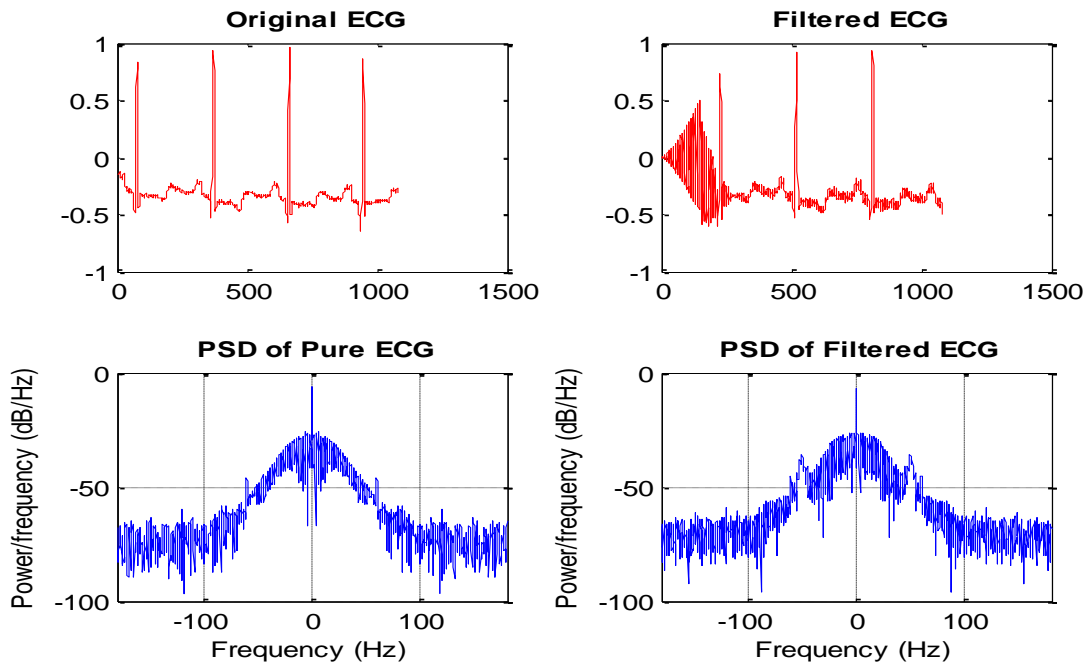
Figure 4: Results for Least square filter.

V. Conclusion

The Finite Impulse Response [FIR], filter produces the impulse response which has a limited number of terms. These types of filters are generally realized non recursively, which means that there is no feedback involved in computation of the output data. The output of the filter depends only on the present inputs. FIR filters based on equiripple design have been designed and implemented. Table 1 shows the comparison of the present work with other known methods .In comparison with the window method reduction in signal power of 50 Hz is more in the Equiripple and Least squares methods. In the window method the numbers of elements required are less while in equiripple method more computational elements are required therefore computational time is the major difficulty of the equiripple type digital filter implemented on the noisy ECG signal. Method is cost effective and flexible.

TABLE I. Comparison for Different Fir Filter Design Techniques

Type of FIR Filter	Filter order	Output SNR	Adder	Delay units
Equiripple	582	7.1544	581	581
Least Square	298	5.069	298	297
Bartlett	298	-4.873	298	298
Blackman	298	-5.9249	298	298
Hamming	298	-4.217	298	298
Hann	298	-10.3437	298	298
Rectangular	298	3.8913	298	298
Kaiser	298	1.9241	298	298

References

[1] McManus CD, Neubert KD, Cramer E, "Characterization and elimination of AC noise in electrocardiograms: a comparison of digital filtering methods", Comput Biomed Res. 1993 Feb;26(1):48-67.

[2] Ch. Yu, G. Li, L. Lin, Stephen C-Y. Lu, "The Realization of Tracking Power-line Interference Adaptive Coherent Model Based on Part FFT", *Journal of Physics: Conference Series 13* (2005) 274–279.

[3] Choy TT, Leung PM., "Real time microprocessor-based 50 Hz notch filter for ECG",*JBiomedEng*.1988May;10(3):285-8.

[4] Cramer E, McManus CD, Neubert D, "Estimation and removal of power line interference in the electrocardiogram: a comparison of digital approaches", *Comput Biomed Res.* 1987 Feb;20(1):12-28.

[5] Hejjel L, "Suppression of power-line interference by analog notch filtering in the ECG signal for heart rate variability analysis: to do or not to do?", *Med Science Monit.*2004Jan; 10(1):MT6-13.

[6] Mihov G, Dotsinsky IV, Georgieva TS, "Subtraction procedure for powerline interference removing from ECG: improvement for non-multiple sampling", *J Med Eng Technol.* 2005 Sep-Oct;29(5):238-43.

[7] Hamilton PS, "A comparison of adaptive and nonadaptive filters for reduction of power line interference in the ECG", *IEEE Trans Biomed Eng. 1996* Jan; 43(1):105-9.

[8] Sander A, Voss A, Griessbach G, "An optimized filter system for eliminating 50 Hz interference from high resolution ECG", *Biomed Tech (Berl). 1995* Apr; 40(4):82-7.

[9] Kumaravel N, Senthil A, Sridhar KS, Nithiyanandam N, "Integrating the ECG power-line interference removal methods with rule-based system", *Biomed Sci Instrum. 1995*; 31:115-20.

[10] Wu Y, Yang Y "A new digital filter method for eliminating 50Hz interference from the ECG", *Zhongguo Yi Liao Qi Xie Za Zhi.* 1999 May; 23(3):145-8.

[11] Van Alste JA, Schilder TS, "Removal of base-line wander and power-line interference from the ECG by an efficient FIR filter with a reduced number of taps", *IEEE Trans Biomed Eng. 1985* Dec; 32(12):1052-60.

[12] Mitov IP., "A method for reduction of power line interference in the ECG", *Med Eng Phys. 2004* Dec;26(10):879-87.

[13] Ziarani AK, Konrad A, "A nonlinear adaptive method of elimination of power line interference in ECG signals", *IEEE Trans Biomed Eng. 2002* Jun;49(6):540-7.

[14] Dotsinsky I, Stoyanov T, "Power-line interference cancellation in ECG signals", *Biomed Instrum Technol. 2005* Mar-Apr;39(2):155-62.

[15] Ider YZ, Saki MC, Gcer HA, "Removal of power line interference in signal-averaged electrocardiography systems", *IEEE Trans Biomed Eng.* 1995 Jul;42(7):731-5.

[16] Ider YZ, Koymen H, "A new technique for line interference monitoring and reduction in biopotential amplifiers", *IEEE Trans Biomed Eng.* 1990 Jun; 37(6):624-31.

[17] Mahesh S. Chavan, RA. Agarwala, M.D.Uplane, "Design and implementation of Digital FIR Equiripple Notch Filter on ECG Signal for removal of Power line Interference", WSEAS TRANSACTIONS on SIGNAL PROCESSING, Volume 4, April 2008

PERFORMANCE OF WAVELET PACKET TRANSFORM BASED ENERGY DETECTOR FOR SPECTRUM SENSING

Ms. Shrutika S. Sawant[1]
[1]Master of Engg. Department of Electronics
Rajarambapu Institute of Technology, Sakharale, M.S., India
Prof. M. S. Kumbhar[2]
[2]Asso. Prof. Department of Electronics
Rajarambapu Institute of Technology, Sakharale, M.S., India

Abstract-
Today wireless field is rapidly evolving. Due to the large number of standards, spectrum availability has become an important issue. In this context, an emerging technology, cognitive radio (CR) has been come out to solve this spectrum scarcity problem. The most important function of cognitive radio is spectrum sensing which requires more accuracy & low complexity. In this paper we analyze the performance of energy detector spectrum sensing algorithm based on wavelet packet transform (WPT) in cognitive radio.

Keywords- Cognitive radio (CR), Energy detection (ED), Primary user (PU), Wavelet Packet Transform (WPT).

I. Introduction

The Cognitive Radio is an emerging technology, for the efficient use of the limited spectrum available [1]. The concept was first originated by Defense Advance Research Products Agency (DARPA) scientist, Dr. Joseph Mitola and the result of that concept is IEEE 802.22, which is a standard aimed at using cognitive radio for Wireless Regional Area Network (WRAN) using white spaces in the TV frequency spectrum while assuring that no harmful interference is caused to the incumbent operation, i.e., digital TV and analog TV broadcasting, and low power licensed devices [2]. As an intelligent spectrum sharing technology, CR has ability to opportunistically adapt behavior of secondary user (SU) to reuse or share the same spectrum allocated to primary user (PU), according to sensing environment, and learning about application requirements [3]. IEEE 802.22 is going on establishing the standard of CR technology. This standard is based on the scenario that unlicensed (or CR) users communicate using idle or unused licensed frequency bands without interfering with licensed users.

The most important function of CR is spectrum sensing i.e. obtaining awareness about the spectrum usage and existence of PUs in a geographical area. Many methods have been proposed to detect whether PU is on, such as energy detection (ED), matched filtering detection (MFD) and cyclostationary feature detection (CFD). Energy detection is the most common method of spectrum sensing due to its low computational and implementation complexity [4]. Matched filtering is known as the optimum method in additive white Gaussian noise (AWGN) channel, it needs to know the exact information of PU [5]. Cyclo-stationary detection (CSD) can detect the PU signal which has cyclostationary period feature. Cyclostationary period feature is embedded in the physical properties of a digital communications signal, which may be generated by modulation, and it is used in communication pattern identification [5] [6]. Spectrum sensing techniques based on the fast Fourier transform (FFT) are easy to implement to find energy level. This is applicable only for low frequency. It may be disadvantage of this technique. In this paper, we address the energy detection technique using wavelet packet transform under the background of uncertain AWGN. We analyze performance of an energy detection algorithm on the basis of wavelet packet transform and estimated noise power and signal power for spectrum sensing.

The remainder of this paper is organized as follows. Section II briefly describes the wavelet analysis and power measurement. Section III, the wavelet packet transform based energy detection algorithm is presented. It explains how to realize efficient energy detection under noise unknown. Section IV discusses the results of the simulations and, finally the conclusions are given in Section V.

Ii. Wavelet Analysis And Power Measurements

A. Discrete Wavelet Transform (DWT)

DWT is designed from the multi-resolution analysis that decomposes the given signal space into a approximate space, *V,* and detail spaces, *W*, as shown in (1),

$$V_{j+1} = W_j \oplus V_j = W_j \oplus W_{j-1} \oplus V_{j-1} \qquad (1)$$

Where *Wj* is the orthogonal complement of *Vj* in *Vj*+1 and $\oplus$ represents the orthogonal sum of two subspaces. Two space, *Vj* and *Wj* are constructed by orthonormal scaling functions, *φj,k*, and orthonormal wavelet functions, *ψj,k*, respectively. Scaling function, *φj,k*, and wavelet, *ψj,k*, are obtained as,

$$\phi_{j,k}(t) = 2^{j/2}\phi(2^j t - k) = \sum_i h_{i-2k}\phi_{j+1}k(t) \tag{2}$$

$$\psi_{j,k}(t) = 2^{j/2}\psi(2^j t - k) = \sum_i g_{i-2k}\phi_{j+1}k(t)$$

With high-pass filter, $g_{i-2k} = \langle \psi_{j,k}, \phi_{j+1,l} \rangle$ and low-pass filter, $h_{i-2k} = \langle \phi_{j,k}, \phi_{j+1,l} \rangle$ () means inner product. Using these functions, DWT of a given signal, f, provides scaling coefficients and wavelet coefficients. The scaling coefficient at the jth level kth time is computed by,

$$C_{j,k} = \langle f, \phi_{j,k} \rangle = \sum_i h^*_{i-2k}\langle f, \phi_{j+1,l} \rangle = \sum_i h^*_{i-2k}C_{j+1,l} \tag{3}$$

The wavelet coefficient at the jth level and kth time is,

$$d_{j,k} = \langle f, \psi_{j,k} \rangle = \sum_i g^*_{i-2k}\langle f, \phi_{j+1,l} \rangle = \sum_l g^*_{l-2k}C_{j+1,l} \tag{4}$$

Fig. 1 and 2 show 2-level analysis part of the DWT and its frequency separation property.
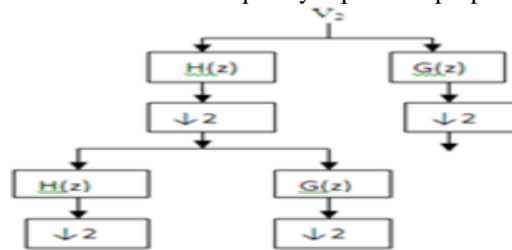
Fig.1. 2-level analysis part of DWT
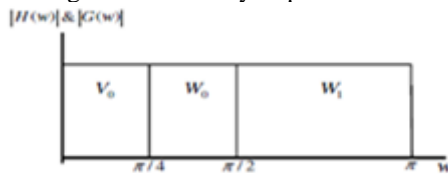
Fig.2. Frequency separation of 2-level analysis part of DWT

B. Wavelet Packet Transform (WPT)

The difference between DWT and WPT just lies in the decomposition of detail space. WPT decomposes not only the approximation space but also the detail space. This means that it can separate frequency band uniformly. Fig. 3 and 4 represent 2-level analysis part of the WPT and its frequency separation property.

Fig.3. 2-level analysis part of WPT

Fig.4. Frequency separation of 2-level analysis part of WPT
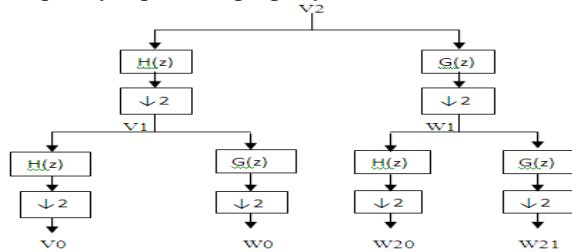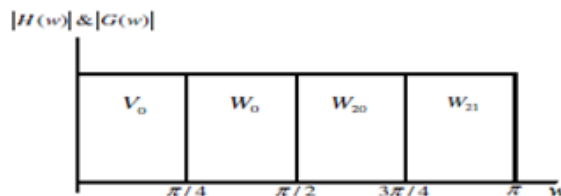
C. Power Measurements Using Wavelets

Power measurements using wavelets are explained in [7]. If a received signal, $r(t)$ is periodic signal with period T, then, the power of this signal is computed by,

$$P = \frac{1}{T} \int_0^T r^2(t)dt \cdot \tag{5}$$

and $r(t)$ can be represented as

$$r(t) = \sum_k C_{j0,k} \phi_{j0,k}(t) + \sum_{j \geq j0} \sum_k d_{j,k} \psi_{j,k}(t) \tag{6}$$

Where $C_{j0,k}$ and $d_{j,k}$ are scaling coefficients and wavelet coefficients respectively. Therefore, we can easily compute the power of the signal using orthonormal wavelet and scaling function properties.

$$P = \frac{1}{T} \int_0^T r^2(t)dt$$
$$= \frac{1}{T} \left[\int_0^T \left\{ \sum_k C_{j0,k} \phi_{j0,k}(t) + \sum_{j \geq j0} \sum_k d_{j,k} \psi_{j,k}(t) \right\} dt \right]$$
$$= \frac{1}{T} \left[\sum_k c_{j0,k}^2 + \sum_{j \geq j0} \sum_k d^2_{j,k} \right] \tag{7}$$

It means that the power of each sub band can be calculated using the scaling and wavelet coefficients.

III. Energy Detection Algorithm

The model for energy detection based on wavelet packet transform is described in Fig.5
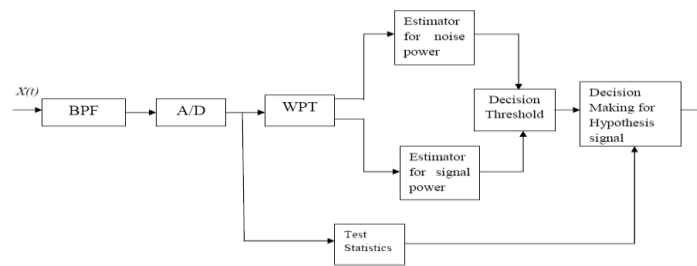
Fig.5 Block diagram of Energy Detection Model based on WPT

From the center frequency fc of band pass filter (BPF) removes the out of band signals & selects the bandwidth of interest W. After this signal is converted into digital & we get digital signal $x(n)$ which is given by,

$x(n) = s(n) + w(n)$ $n = 0,1,\ldots, N-1.$ (8)

Where, $s(n)$ is the Primary User (PU) signal with zero mean and variance of σ_s^2 & $w(n)$ is Additive White Gaussian Noise (AWGN) with zero mean and variance of σ_w^2.

If there is no transmission by PU, $s(n) = 0$. Then hypothesis can be tested as,

H_0: $x(n) = w(n,)$ $n=0,1,\ldots\ldots.N-1;$ (9)

If there is transmission by PU, $s(n) \neq 0$. Then hypothesis can be tested as,

H_1: $x(n) = s(n) + w(n,)$ $n=0,1,\ldots..N-1;$ (10)

Digital signal $x(n)$ will be processed separately by four step which described as follows.

Step 1: $x(n)$ is sent to WPT to estimate current noise power (σ_w^{*2}) and signal power (σ_s^{*2}).

Step 2: By calculating the energy of $x(n)$ we get the test statistic (X),

$$X = \sum_{n=0}^{N-1} |x(n)|^2 \tag{11}$$

The test statistic X is a random variable whose probability density function (PDF) is chi-square distributed. When N is sufficiently large, we can approximate the PDF using Gaussian distribution according to the central limitation theorem [8]

$$H_0 \square \ N(N\sigma_w^2, 2N\sigma_w^4) \tag{12}$$

$$H_0 \square \ N(N(\sigma_s^2 + \sigma_w^2), 2(N\sigma_s^2 + \sigma_w^2)^2) \tag{13}$$

Referred to constant false alarm rate (CFAR) principle [9], we have probability of false alarm PF as follows,

$$P_f = P(X > \gamma H_0)$$

$$= Q\left[\frac{\gamma - N\sigma_w^2}{\sigma_w^2 \sqrt{2N}}\right] \tag{14}$$

$$P_D = P(X > \gamma H_1)$$

$$= Q\left[\frac{\gamma - N(\sigma_s^2 + \sigma_w^2)}{(\sigma_s^2 + \sigma_w^2)\sqrt{2N}}\right] \tag{15}$$

Where $Q(a) = \frac{1}{2}erfc(\frac{a}{\sqrt{2}})$, $erfc(.)$ is the complementary error function, γ is the decision threshold,

$$\gamma = N\sigma_w^2 + \sqrt{2N}\sigma_w^2 Q^{-1}(P_F) \tag{16}$$

Replace the exact noise variance in (16) with the estimated noise σ_w^{*2} in step 1, we can get,

$$\gamma^* = N\sigma_w^{*2} + \sqrt{2N}\sigma_w^{*2} Q^{-1}(P_F) \tag{17}$$

Put $\sigma_w^{*2}, \sigma_s^{*2}$ & γ^* into (15), we get

$$P_D = \frac{1}{2}erfc\left(\frac{\gamma^* - N(\sigma_s^2 + \sigma_w^2)}{2(\sigma_s^{*2} + \sigma_w^{*2})\sqrt{N}}\right) \tag{18}$$

If $X > \gamma^*$, we can make a decision that the channel is occupied by one PU or more. Otherwise, the channel is vacant, and SUs could make use of the channel at this moment.

iv. Simulations and analysis

In this section, we give some simulations of WPED algorithm proposed in this paper. Simulation uses the two stage wavelet packet decomposition with db5 as wavelet filter and chooses BPSK as PU signal. Experiments are performed under AWGN channel and SNR is changed from -10 dB to 0 dB. The results of two groups are given below.

i) The sampling frequency is 1000Hz and the sample number N is 500. The probability of false alarm *Pf* is set to 0.01. Due to using the WPT to estimate noise power, the performance of proposed WPED with uncertain noise is almost as perfect as the ED with noise certain known, as shown in Fig.6. It means that the proposed WPED is robust to uncertain noise. Hence WPT is quite a robust method for CR applications when the noise is unknown.

ii) The sampling frequency is 1000Hz and the sample number N is 500. The probability of false alarm *Pf* is set to 0.1, 0.01, and 0.001 respectively. Higher the *Pf* is the performance of WPED method raises evidently with the increase of probability of false alarm.

iii) Set the probability of false alarm *Pf* to be 0.01 and the sample number N to be 500,750, 1000 respectively. It is described in Fig.8. The simulation results show that the performance of WPED method rises evidently with the increase of sample number N. the larger the N is, the more information about the signal and noise we can get.
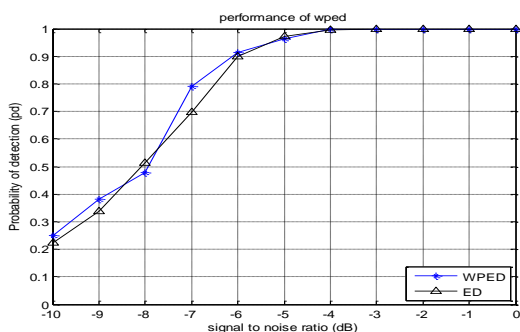
Fig.6. Comparison of performance of proposed WPED and ED
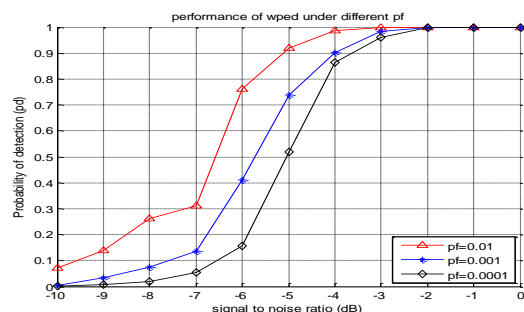
Fig.7. Performance of proposed WPED under different probabilities of false alarm.
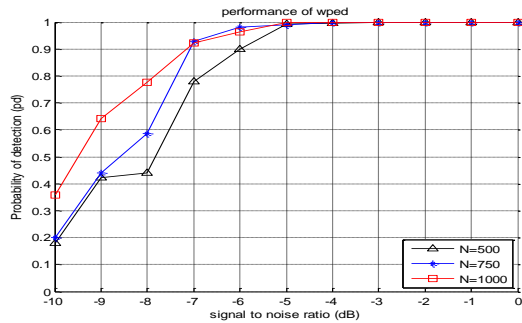
Fig. 8 Performance of proposed WPED under different sample numbers

V. Conclusion

The main purpose of the paper was to study the performance of energy detection algorithm for spectrum sensing in cognitive radio by drawing the curves between SNR vs. probability of detection. Energy Detection spectrum sensing using Wavelet Packet Transform (WPED) method outperforms the traditional energy detection method when the noise was unknown which is the real scenario. The estimated noise power, signal power and decision threshold by Wavelet Packet Transform (WPT) method were in match with the values.

Hence it is quite a robust method for spectrum sensing in Cognitive Radio when the noise is unknown.

References

[1]   Federal Communications Commission, "Spectrum Policy Task Force Report," ET Docket No. 02-135, November. 2002.

[2]   IEEE 802 LAN/MAN Standards Committee 802.22 WG on WRANs (Wireless Regional Area Networks).

[3]   Q. Zhang, A. B. J. Kokkeler and G. J. M. Smit, "A Reconfigurable Radio Architecture for Cognitive Radio in Emergency Networks," The 9th European Conference on Wireless Technology, vol.1, 2006, p p.35-38.

[4]   S. Ciftci and M. Torlak, "A Comparison of Energy Detectability Models for Spectrum Sensing", in Proceedings of IEEE "GLOBECOM" 2008, pp. 1-5.

[5]   P. D. Sutton, K. E. Nolan and Linda E. Doyle, "Cyclostationary Signatures in Practical Cognitive Radio Applications," IEEE Journal on selected areas in communications, vol. 26, no. 1, January 2008, pp.13-24.

[6]   W. A. Gardner, "Exploitation of spectral redundancy in cyclostationary signals," *IEEE Signal Process. Mag.*, vol. 8, no. 2, pp. 14–36, Apr. 1991.

[7]   Weon-Ki Yoon and Michael J. Devaney,"Power Measurement Using the Wavelet Transform" *IEEE Transactions on Instrumentation and Measurement,* vol. 47, no. 5, October 1998

[8]   J. G.Proakis, "Digital Communications", 4th Edition, McGraw-Hill, 2001.

[9]   E. Peh and Y. Liang, "Optimization of Cooperative Sensing in Cognitive Radio Networks", in Proceedings of WCNC2007, pp.27-32.

WEB MINING: A COMPARATIVE STUDY

Aishwarya Rastogi
Assistant Professor
Dept. of CS & IT
MIT Moradabad

Smita Gupta
Assistant Professor
Dept. of CS & IT
MIT Moradabad

Srishti Agarwal
Assistant Professor
Dept. of CS & IT
MIT Moradabad

Nimisha Agarwal
Assistant Professor
Dept. of CS & IT
MIT Moradabad

Abstract:
Currently, World-Wide Web has developed to a distributed information space with nearly 100 million workstations and several billion pages, which brings the people great trouble in finding needed information although huge amount of information available on webs. The search engine is a very important tool for people to obtain information on Internet, but the low-precision and low-recall exist widely in current search engines. With the rapid development of Internet, the effective and accurate intelligent search engine based on the Web mining technology has become the most important research issue.

Web Data Mining is an important area of Data Mining which deals with the extraction of interesting knowledge from the World Wide Web. It can be classified into three different types. Web content mining, web structure mining and web usages mining. Through this paper we presents a view about how to extract the useful and relevant information on the web using web mining and also give the superficial knowledge and brief comparison about data mining. This paper discusses the current, past and future of web mining. Here we introduce online resources for retrieval Information on the web i.e. web content mining, and the discovery of user access patterns from web servers, i.e. web usage mining that improve the data mining drawback. Furthermore, we also described web mining through cloud computing i.e. cloud mining. That can be seen as future of Web Mining.

Keywords- Data mining: Web Mining; Web Content Mining; Web Structure Mining; Web Usage Mining; Semantic Web; Cloud Mining.

1.   Introduction
Because of the rapid development and wide application of the Internet, World Wide Web has become a pool, exchange, sharing of information and effective tool for collaborative work. People's attention and frequent use of the Web not only promotes the development of various technologies, but also make the Web information resources on the rapid growth. The wide adoption of the Internet has fundamentally changed the ways in which we communicate, gather information, conduct businesses and make purchases. Therefore, resulting in flood of information resources distributed on the Web that provides various facilities to satisfy the user's need. Earlier people used to communicate through postal services, purchase the products from nearby markets, and gather information from news papers and magazines. Even people do business and banking transactions manually through paper work. But in today era we have a vast ocean of data which we called as internet or web. This huge library of data originates as a result of modernization and globalization of data over internet. All the activities discussed above, which we used to do manually earlier, now becomes the part of internet and hence the result of increasing data over web.

The expansion of the World Wide Web (Web for short) has resulted in a large amount of data that is now in general freely available for user access. The different types of data have to be managed and organized in such a way that they can be accessed by different users efficiently. For example a science student is concerned about the text or videos related to physics, chemistry or any other subject of his concern while a commerce student is in need of a statistical or economical knowledge. Similarly engineers, doctors, scientist, homemakers, search the web according to their own requirements. If a person is only concerned about a small information of Web, and not interested in the rest of the information contained in Web, because of the two reasons he may become unsatisfactory: first, the desired search results will be submerged by the traditional search engines which are based on the keywords; second, since the majority of Web data is unstructured, which lead to the traditional data mining results

will be unsatisfactory. Therefore, to avoid all these problems, the application of data mining techniques on the Web is now the focus of an increasing number of researchers. Various data mining methods are used to discover the hidden and useful information in the Web. However, Web mining does not only mean applying data mining techniques to the data stored in the Web. The algorithms have to be modified such that they better suit the demands of the Web. New approaches should be used which better fit the properties of Web data. Furthermore, not only data mining algorithms, but also artificial intelligence, information retrieval and natural language processing techniques can be used efficiently. Thus, Web mining has been developed into an autonomous research area. This paper is organized as follows: Section 2 describes background and origin of web mining. Section 3 describes about the web mining and all its categories Section 4 describes the comparative study between the web mining and data mining. Section 5 contains some prominent applications that can be used as future directions of web mining. Section 6 finally concluded with all the necessary aspects of web mining.

2. Origin Of Web Mining

Web mining techniques are the result of long process of research and product development. This evolution began when the amount of data kept in computer files and databases is growing at a phenomenal rate. At the same time users of these data are expecting more sophisticated information from them .A marketing manager is no longer satisfied with the simple listing of marketing contacts but wants detailed information about customers' past purchases as well as prediction of future purchases. Simple structured / query language queries are not adequate to support increased demands for information. Data mining steps is to solve these needs. Data mining is defined as finding hidden information in a database alternatively it has been called exploratory data analysis, data driven discovery, and deductive learning [1].

In the data mining communities, there are three types of mining: data mining, web mining, and text mining [2]. There are many challenging problems [3] in data/web/text mining research. This is sometimes related to the problem of mining for "deep knowledge," which is the hidden cause for many observations. For example: can we discover Newton's laws from observing the movements of objects [3]. The mining data may vary from structured to unstructured. Data mining mainly deals with structured data organized in a database while text mining mainly handles unstructured data/text. Web mining lies in between and copes with semi structured data and/or unstructured data. Web mining calls for creative use of data mining and/or text mining techniques and its distinctive approaches. Data mining can be best applied by using a data warehouse as well as flexible interactive business analysis tools. Many data mining tools currently operate outside of the warehouse, requiring extra steps for extracting, importing, and analyzing the data. The resulting analytic data warehouse can be applied to improve business processes throughout the organization, in areas such as promotional campaign management, fraud detection, new product rollout, and so on. Figure 1 illustrates architecture for advanced analysis in a large data warehouse.
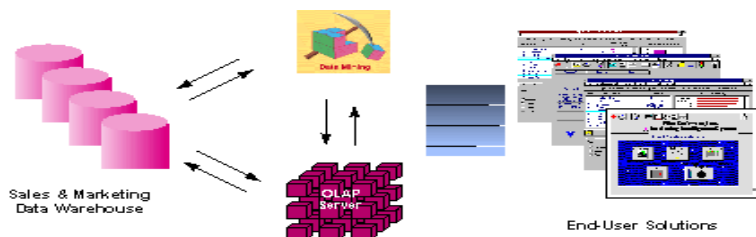
Figure 1 - Integrated Data Mining Architecture

In the evolution from business data to business information each new step has built upon the previous one. For example, the ability to store large databases is critical to web mining. From the user point of view, the five step listed in Table 1 were revolutionary because they allowed new business question to be answered accurately and quickly.

Mining the web data is one of the most challenging tasks for the data mining and data management scholars because there are huge heterogeneous, less structured data available on the web and we can easily get overwhelmed with data [2]. There is no agreed definition of Web Data Mining but we present one simple definition:

"Web Data Mining is the application of data mining techniques to find interesting and potentially useful knowledge from web data. It is normally expected that either the hyperlink structure of the web or the web log data or both have been used in the mining process." Word Wide web is the interactive and popular medium to distribute information today. Data on the web is rapidly increasing day by day and Web data is huge, diverse and dynamic so information users could encounter the following problems while interacting with the web [4].

1. *Finding Relevant Information*- People either browse or use the search service when they want to find specific information on the web. However today's search tools have problems like low precision which is due to irrelevance of many of the search results. This results in a difficulty in finding the relevant information. Another problem is low recall which is due to inability to index all the information available on the web.

Evolutionary Step	Business Question	Enabling Technologies	Product Providers	Characteristics
Data Collection (1960s)	"What was my total revenue in the last five years?"	Computers, tapes, disks	IBM, CDC	Retrospective, static data delivery
Data Access (1980s)	"What were unit sales in Mumbai last March?"	Relational databases (RDBMS), Structured Query Language (SQL), ODBC	Oracle, Sybase, Informix, IBM, Microsoft	Retrospective, dynamic data delivery at record level
Data Warehousing & Decision Support (1990s)	"What were unit sales in Mumbai last March? Drill down to Delhi."	On-line analytic processing (OLAP), multidimensional databases, data warehouses	Pilot, Comshare, Arbor, Cognos, Microstrategy	Retrospective, dynamic data delivery at multiple levels
Data Mining (2000s)	"What's likely to happen to Delhi unit sales next month? Why?"	Advanced algorithms, multiprocessor computers, massive databases	Pilot, Lockheed, IBM, SGI, numerous startups (nascent industry)	Prospective, proactive information delivery
Web Mining (Emerging Today)	"What's likely to happen to Delhi unit sales next/previous millions months? "	WWW, Internet, monumental scale Database	RockWare, Apteco Ltd., Simon Fraser University, IBM, Web Trends, SPSS, Flowerfire, Angoss, Net Genesis	Powerful, Affordable tool to mine large data warehouse and Relational databases fast and efficiently using multiple mining functions

2. *Creating new knowledge out of the information available on the web*-This problem is basically sub problem of the above problem. Above problem is query triggered process (retrieval oriented) but this problem is data triggered process that presumes that we already have collection of web data and we want to extract potentially use full knowledge out of it.
3. *Personalization of information*- When people interact with the web they differ in the contents and presentations they prefer.

4**.** *Learning about Consumers or individual users*-This problem is about what the customer do and want. Inside this problem there are sub problem such as customizing the information to the intended consumers or even to personalize it to individual user, problem related to web site design and management and marketing etc.

There are many tools like Database (DB), Information Retrieval (IR), and Natural Language Processing (NLP) etc. available to solve the above stated problem. Web mining techniques could be more efficiently used to solve the information overload problem directly or indirectly.

Drawbacks in the existing approaches

1. The explosive growth of the Web has imposed a heavy demand on networking
2. Resources and Web servers.
3. Hence, an obvious solution in order to improve the quality of Web services would be the increase of bandwidth, but such a choice involves increasing economic cost.
4. Web caching scheme has three significant drawbacks: If the proxy is not properly updated, a user might receive stale data, and, as the number of users grows, origin servers typically become bottleneck.
5. Main drawback of systems which have enhanced prefetching policies is that some prefetched objects   may not be eventually requested by the users.

The purpose of the paper is to provide past, current evaluation and future direction in each of the three different types of web mining i.e. web content mining, web structure mining and web usages mining.

3. Web Mining
OVERVIEW: Web mining means employing the technique of data mining into the documents on the net. Web mining can be used for studying varied aspects of a site can recognize the patterns and relationships in the user behavior so as to get the insight in crucial information**.**
Web mining is an extension of data mining. Web Mining is based on knowledge discovery from web. It is the extraction of the knowledge framework represents in a proper way. Web mining is useful to extract the information, image, text, audio, video, documents and multimedia. By using web mining easily extract all features and information about multimedia before this web mining difficult to extract information in proper way from web. We search the any topic from web difficult to get accurate topic information but Now's day it is easy to get the proper and relevant information. Web mining is based on data mining technique by using data mining technique discover the hidden data in web log.

The main component of Web Mining Technology has been under development for decades, in research area such as internet, artificial intelligence, and machine learning. Today, the maturity of these techniques, coupled with high performance relational database engines and broad data integration efforts, make these technologies practical for current data warehouse environments. [10].

Web Mining Categories:
Web mining can be categorized in to three area of interest based on which part of the web to mine:
a) Web Content Mining
b) Web Structure Mining
c) Web Usage Mining

i. Web Content Mining-Web Mining is basically extracts the information on the web. Which process is happen to access the information on the web. It is web content mining. Many pages are open to access the information on the web. These pages are content of web. Searching the information and open search pages is also content of web. Last accurate result is defined the result pages content mining.

*ii. Web Structure Mining-*We can define web structure mining in terms of graph. The web pages are representing as nodes and Hyperlinks represent as edges. Basically it's shown the relationship between user & web. The motive of web structure mining is generating structured summaries about information on web pages/webs. It is shown the link one web page to another web page.

iii. Web Usage Mining- It is discovery of meaningful pattern from data generated by client server transaction on one or more web localities. A web is a collection of inter related files on one or more web servers. It is automatically generated the data stored in server access logs, refers logs, agent logs, client sides cookies, user profile, meta data, page attribute, page content & site

structure. Web mining usage aims at utilize data mining techniques to discover the usage patterns from web based application. It is technique to predict user behavior when it is interact with the web.

	Web Mining			
	Web Content Mining		Web Structure Mining	Web Usage Mining
	IR View	DB View		
View Of Data	- Unstructured -Semi Structured	-Semi Structured - Web Site as DB	-Links Structure	- Interactivity
Main Data	-Text Documents -Hypertext Documents	-Hypertext Documents	-Links Structure	- Server Logs - Browser Logs
Representation	- Bag of Words, n-grams - Terms, phrases - Concepts or Ontology - Relational	- Edge-Labeled Graph - Relational	- Graph	- Relational Table - Graph
Method	- TFIDF and Variants -Machine Learning -Statistical (including NLP)	-Proprietary algorithms - ILP -(Modified) association rules	- Proprietary algorithms	- Machine Learning - Statistical -(Modified) association rules
Application Categories	- Categorization - Clustering -Finding Extraction Rules - Finding Pattern in text - User Modeling	-Finding Frequent Sub-Structures -Web site schema discovery	- Categorization - Clustering	- Site Construction, Adaptation and Management -Marketing -User Modeling

4. Comparison Between Data Mining And Web Mining

Comparison	Web Mining	Data Mining
Scale	In this the search processing is not a big, 10 million job in web server database	In this the search processing is large, a 1 million jobs in data base
Access	Web Mining is access data publicly. In this not hide the data which is access in web database. But take permission to web log master and access the Data	Data Mining is access data privately and only authorize user access data in the database**.**
Structure	In Web mining get the information from structured, unstructured and semi structured fromweb pages. web mining fetch the information from wide database	In Data mining get the information from explicit structure. Data mining is not fetch the information from wide database compares to web mining database.
Data	Data mining is work upon Off-Line data	Web mining is work upon On-Line Data
Data Storage	In data mining data stored in (database) data warehouse	In web mining data stored in server database & web log.

5.   Future Directions

This area of research is so huge today partly due to the interests of various research communities, the tremendous growth of information sources available on the Web and the recent interest in e-commerce. This phenomenon partly creates confusion when we ask what constitutes Web mining and when comparing research in this area. This trend is likely to continue as Web services continue to flourish. As the Web and its usage grow, it will continue to generate evermore content, structure, and usage data, and the value of Web mining will keep increasing. Outlined here are some research directions that must be pursued to ensure that we continue to develop Web mining technologies that will enable this value to be realized.

i) Web mining using cloud computing: Cloud Computing is clearly one of today's most seductive technology areas due at least in part to its cost efficiency and flexibility. However, despite increased activity and interest, there are significant, persistent concerns about cloud computing that are impeding momentum and will eventually compromise the vision of cloud computing as a new IT procurement model. The term 'cloud' is a symbol for the Internet, an abstraction of the Internet's underlying infrastructure, used to mark the point at which responsibility moves from the user to an external provider. Basically Cloud Mining is new approach to faced search interface for data. SaS (Software-as-a-Service) is used for reducing the cost of web mining and try to provide security that become with cloud mining technique. Now a day we are ready to modify the framework of web mining for demand cloud computing. With the significant advances in Information and Communications Technology over the last half century, there is an increasingly perceived vision that computing will one day be the 5th utility (after water, electricity, gas, and telephony). This computing utility, like all other four existing utilities, will provide the basic level of computing service that is considered essential to meet the everyday needs of the general community. To deliver this vision, a number of computing paradigms have been proposed, of which the latest one is known as Cloud computing.

ii) Web metrics and measurements

 From an experimental human behaviorist's viewpoint, the Web is the perfect experimental apparatus. Not only does it provide the ability of measuring human behavior at a micro level, it (i) eliminates the bias of the subjects knowing that they are participating in an experiment, and (ii) allows the number of participants to be many orders of magnitude larger. Research needs to be done in developing the right set of Web metrics, and their measurement procedures, so that various Web phenomena can be studied.

iii) Process mining

Mining of 'market basket' data, collected at the point-of-sale in any store, has been one of the visible successes of data mining. However, this data provides only the end result of the process, and that too decisions that ended up in product purchase. Research needs to be carried out in (i) extracting process models from usage data, (ii) understanding how different parts of the process model impact various Web metrics of interest, and (iii) how the process models change in response to various changes that are made - changing stimuli to the user.

iv) Temporal evolution of the Web

Society's interaction with the Web is changing the Web as well as the way the society interacts. While storing the history of all of this interaction in one place is clearly too staggering a task, at least the changes to the Web are being recorded by the pioneering Internet Archive project. Research needs to be carried out in extracting temporal models of how Web content, Web structures, Web communities, authorities, hubs, etc. are evolving.

v) Web services optimization

As services over the Web continue to grow, there will be a need to make them robust, scalable, efficient, etc. Web mining can be applied to better understand the behavior of these services, and the knowledge extracted can be useful for various kinds of optimizations.

vi) Fraud and threat analysis

The anonymity provided by the Web has led to a significant increase in attempted fraud, from unauthorized use of individual credit cards to hacking into credit card databases for blackmail purposes.

6. Conclusions

As the Web and its usage continues to grow, so grows the opportunity to analyze Web data and extract all manner of useful knowledge from it. The past five years have seen the emergence of Web mining as a rapidly growing area, due to the efforts of the research community as well as various organizations that are practicing it. In this paper we have briefly described the key computer science contributions made by the field, the prominent successful applications, and outlined some promising areas of future research. Our hope is that this overview provides a starting point for fruitful discussion.

7. References

[1]   Margaret H. Dunham, "Data Mining Introductory & Advanced Topics", Pearson Education.

[2]   Qingyu Zhang and Richard s. Segall," Web mining: a survey of current research,Techniques, and software", in the International Journal of Information Technology & Decision Making Vol. 7, No. 4 (2008) 683–720.

[3]   Q. Yang and X. Wu, 10 challenging problems in datamining research, Int. J Inform.Technol. Decision Making5(4) (2006) 597–604

[4]   Kosala and Blockeel, "Web mining research: A survey," SIGKDD:SIGKDD Explorations: Newsletter of the Special Interest Group (SIG) on Knowledge Discovery and Data Mining, ACM, Vol. 2, 2000

[5].   Virgilio Almeida, Azer Bestavros, Mark Crovella, and Adriana de Oliveira, " Characterizing reference locality in the WWW " , In IEEE International Conference in Parallel and Distributed Information Systems, Miami Beach, Florida, USA, December 1996.

[6].   http://www.cs.bu.edu/groups/oceans/papers/ Home.html.

[7].   http://www.thearling.com/text/dmwhite/dmwhite.htm

[8].   http://www.engr.sjsu.edu/~fayad/workshops/UDME07/cfp.php

[9].   http://www.data-mining-software.com/data_mining_history.htm

[10].   Raymond Kosala, Hendrik Blockeel," Web Mining Research: A

        Survey", In ACM SIGKDD, July 2000.

[11].   http://www.expertstown.com/web-mining/

[12].   Chen, M. S, Han, J. and Yu, P. S. "Data Mining: An overview from a database perspective", IEEE transaction on knowledge and data engineering, Vol. 08, No. 6, pp: 866-883.

MEDICAL IMAGE COMPRESSION USING REGION GROWING SEGMENATION

R.Arun, M.E(Ph.D)
Research scholar
M.S University

Dr.D.Murugan Asst.Prof
Department of Computer science & Engg
M.S University

Abstract:
The easy, rapid, and reliable digital transmission and storage of medical and biomedical images would be a tremendous boon to the practice of medicine. Patients in rural areas could have convenient access to second opinions. Patients readmitted to hospitals could have earlier imaging studies instantly available. Rather than waiting for others to finish with hardcopy films, medical and surgical teams collaborating on patient care could have simultaneous access to imaging studies on monitors throughout the hospital. This long-term digital archiving or rapid transmission is prohibitive without the use of image compression to reduce the file sizes.

As medical/biological imaging facilities move towards complete film-less imaging, compression plays a key role. Although lossy compression techniques yield high compression rates, the medical community has been reluctant to adopt these methods, largely for legal reasons, and has instead relied on lossless compression techniques that yield low compression rates. The true goal is to maximize compression while maintaining clinical relevance and balancing legal risk.

Now-a-days in medical field the digitized medical information such as computed tomography (CT), magnetic resonance imaging (MRI), generates increasingly important volumes of data is an important challenge to deal with is the storage, retrieval and transmission requirement**s** of enormous data, from one place to another place for urgent purpose including medical images. Compression is one of the indispensable techniques to solve this problem. In this paper we offer a lossless compression method with the segmentation for compression of medical images. In this method the medical image is segmented and compressed by wavelet method to increase the compression ratio and to store in a less space. Here we use the CT and MRI images and analyzed in detail.

Introduction:

Medical image compression:

There are two types of image compression: lossless and lossy. With lossless compression, the original image is recovered exactly after decompression. Unfortunately, with images of natural scenes it is rarely possible to obtain error-free compression at a rate beyond 2:1. Much higher compression ratios can be obtained if some error, which is usually difficult to perceive, is allowed between the decompressed image and the original image. This is lossy compression. In many cases, it is not necessary or even desirable that there be error-free reproduction of the original image. For example, if some noise is present, then the error due to that noise will usually be significantly reduced via some denoising method. In such a case, the small amount of error introduced by lossy compression may be acceptable. Another application where lossy compression is acceptable is in fast transmission of still images over the Internet.

Before the various image compression techniques are discussed, consider the motivation behind using compression. A typical 12-bit medical X-ray may be 2048 pixels by 2560 pixels in dimension. This translates to a file size of 10,485,760 bytes. A typical 16-bit mammogram image may be 4500 pixels by 4500 pixels in dimension for a file size of 40,500,000 (40 megabytes)! This has consequences for disk storage and image transmission time. Even though disk storage has been increasing steadily, the volume of digital imagery produced by hospitals and their new film less radiology departments has been increasing even faster. Even if there were infinite storage, there is still the problem of transmitting the images.

An image is a collection of measurements in two-dimensional (2-D) or three-dimensional (3-D) space. In medical images, these measurements or image intensities can be radiation absorption in X-ray imaging, acoustic pressure in ultrasound, or RF signal amplitude In MRI. If a single easurement is made at each location in the image, then the image is called a scalar image. With the growth of technology and the entrance into the Digital Age, the world has found itself amid a vast amount of information. Dealing with such enormous amount of information can often present difficulties. Digital information must be stored and retrieved in an efficient manner, in order for it to be put to practical use. Data compression is a fascinating topic when considered by it.

Segmentation:

It refers to the process of partitioning a digital image into multiple segments (sets of pixels, also known as super pixels). The goal of segmentation is to simplify and/or change the representation of an image into something that is more meaningful and easier to analyze. Image segmentation is typically used to locate objects and boundaries (lines, curves, etc.) in images. More precisely,

image segmentation is the process of assigning a label to every pixel in an image such that pixels with the same label share certain visual characteristics

Region growing methods:
The first region growing method was the seeded region growing method. This method takes a set of seeds as input along with the image. The seeds mark each of the objects to be segmented. The regions are iteratively grown by comparing all unallocated neighboring pixels to the regions. The difference between a pixel's intensity value and the region's mean, δ, is used as a measure of similarity. The pixel with the smallest difference measured this way is allocated to the respective region. This process continues until all pixels are allocated to a region.

Seeded region growing requires seeds as additional input. The segmentation results are dependent on the choice of seeds. Noise in the image can cause the seeds to be poorly placed. Unseeded region growing is a modified algorithm that doesn't require explicit seeds. It starts off with a single region A_1 – the pixel chosen here does not significantly influence final segmentation. At each iteration it considers the neighboring pixels in the same way as seeded region growing. It differs from seeded region growing in that if the minimum δ is less than a predefined threshold T then it is added to the respective region A_j. If not, then the pixel is considered significantly different from all current regions A_i and a new region A_{n+1} is created with this pixel.

Block Diagram of Region Growing Algorithms
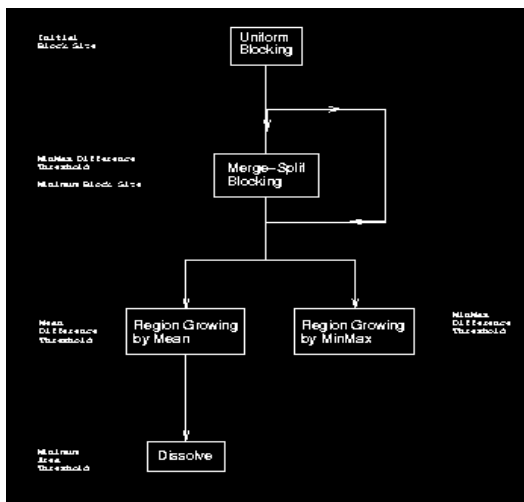
Compression Method:
3. Ezw Encoding
The EZW algorithm is based on four key concepts: 1) a discrete wavelet transform or hierarchical sub band decomposition, 2) prediction of the absence of significant formation across scales by exploiting the self-similarity inherent in images, 3) entropy-coded successive

approximation quantization, and 4) universal lossless data compression which is achieved via adaptive Huffman encoding. The EZW encoder was originally designed to operate on images (2D-signals) but it can also be used on other dimensional signals. The EZW encoder is based on progressive encoding to compress an image into a bit stream with increasing accuracy. This means that when more bits are added to the stream, the decoded image will contain more detail, a property similar to JPEG encoded images. Using an embedded coding algorithm, an encoder can

terminate the encoding at any point thereby allowing a target rate or target accuracy to be met exactly. Also, given a bit stream, the decoder can cease decoding at any point in the bit stream and still produce exactly the same image that would have been encoded at the bit rate

corresponding to the truncated bit stream. In addition to producing a fully embedded bit stream, EZW consistently produces compression results that are competitive with virtually all known compression algorithm on standard test images It is similar to the representation of a number

like π (pi). Every digit we add increases the accuracy of the number, but we can stop at any accuracy we like. Progressive encoding is also known as embedded encoding, which explains the E in EZW.

Embedded zerotree wavelet (EZW) algorithm
The embedded zerotree wavelet algorithm (EZW) is a simple, yet remarkable effective, image compression algorithm, having the property that the bits in the bit stream are generated in order of importance, yielding a fully embedded code. Using an embedded coding algorithm, an encoder can terminate the encoding at any point thereby allowing a target rate or target distortion metric to be met exactly. Also, given a bit stream, the decoder can cease decoding at any point in the bit stream and still produce exactly the same image that would have been encoded at the bit rate corresponding to the truncated stream. In addition to producing a fully embedded bit stream, EZW consistently produces compression results that are competitive with virtually all known compression algorithms.

The algorithm
The EZW output stream will have to start with some information to synchronize the decoder. The minimum information required by the decoder is the number of wavelet transform levels used and the initial threshold, if we assume that always the same wavelet transform will be used. Additionally we can send the image dimensions and the image mean. Sending the image mean is useful if we remove it from the image before coding. After imperfect reconstruction the decoder can then replace the imperfect mean by the original mean. This can increase the PSNR significantly.

The first step in the EZW coding algorithm is to determine the initial threshold. If we adopt bitplane coding then our initial threshold t_0 will be

$$t_0 = 2^{FLOOR\left(\log_2\left(MAX\left(\left|\gamma\left(x,y\right)\right|\right)\right)\right)}$$

Here MAX(.) means the maximum coefficient value in the image and $\gamma\left(x,y\right)$ denotes the coefficient. With this threshold we enter the main coding loop (I will use a C-like language):

```
threshold = initial_threshold;
do
{
  dominant_pass(image);
  subordinate_pass(image);
  threshold = threshold/2;
}
while (threshold>minimum_threshold);
```

We see that two passes are used to code the image. In the first pass, the *dominant pass*, the image is scanned and a symbol is outputted for every coefficient. If the coefficient is larger than the threshold a **P** (positive) is coded, if the coefficient is smaller than minus the threshold an **N** (negative) is coded. If the coefficient is the root of a zerotree then a **T** (zerotree) is coded and finally, if the coefficient is smaller than the threshold but it is not the root of a zerotree, then a **Z** (isolated zero) is coded. This happens when there is a coefficient larger than the threshold in the subtree. The effect of using the **N** and **P** codes is that when a coefficient is found to be larger than the threshold (in absolute value or magnitude) its two most significant bits are outputted (if we forget about sign extension).

Note that in order to determine if a coefficient is the root of a zerotree or an isolated zero, we will have to scan the whole quad-tree. Clearly this will take time. Also, to prevent outputting codes for coefficients in already identified zerotrees we will have to keep track of them. This means memory for book keeping.

Finally, all the coefficients that are in absolute value larger than the current threshold are extracted and placed without their sign on the subordinate list and their positions in the image are filled with zeroes. This will prevent them from being coded again.

The second pass, the *subordinate pass*, is the refinement pass. In [Sha93] this gives rise to some juggling with uncertainty intervals, but it boils down to outputting the next most significant bit of all the coefficients on the subordinate list. In [Sha93] this list is ordered (in such a

way that the decoder can do the same) so that the largest coefficients are again transmitted first. Based on [Alg95] we have not implemented this sorting here since the gain seems to be very small but the costs very high.

The main loop ends when the threshold reaches a minimum value. For integer coefficients this minimum value equals zero and the divide by two can be replaced by a shift right operation. If we add another ending condition based on the number of outputted bits by the arithmetic coder then we can meet any target bit rate *exactly* without doing too much work.

We can summarize the above with the following code fragments, starting with the dominant pass.

```
/*
 * Dominant pass
 */
initialize_fifo();
while (fifo_not_empty)
{
  get_coded_coefficient_from_fifo();
  if coefficient was coded as P, N or Z then
  {
    code_next_scan_coefficient();
    put_coded_coefficient_in_fifo();
    if coefficient was coded as P or N then
    {
      add abs(coefficient) to subordinate list;
      set coefficient position to zero;
    }
  }
}
```

Here we have used a FIFO to keep track of the identified zerotrees. If we want to enter this loop we will have to initialize the FIFO by "manually" adding the first quad-tree root coefficients to the FIFO. Depending on which level we start in the left of figure 2 this means coding and putting at least three roots in the FIFO. The call of code_next_scan_coefficient() checks the next uncoded coefficient in the image, indicated by the scanning order and outputs a **P**, **N**, **T** or **Z**. After coding the coefficient it is put in the FIFO. This will automatically result in a Morton scan order. Thus, the FIFO contains only coefficients which have already been coded, i.e. a **P**, **N**, **T** or **Z** has already been outputted for these coefficients. Finally, if a coefficient was coded as a **P** or **N** we remove it from the image and place it on the subordinate list.

This loop will always end as long as we make sure that the coefficients at the last level, i.e. the highest subbands (HH1, HL1 and LH1 in figure 2) are coded as zerotrees.

After the dominant pass follows the subordinate pass:

```
/*
```

```
 * Subordinate pass
 */
subordinate_threshold = current_threshold/2;
for all elements on subordinate list do
{
  if (coefficient>subordinate_threshold)
  {
    output a one;
    coefficient = coefficient-subordinate_threshold;
  }
  else output a zero;
}
```

If we use thresholds that are a power of two, then the subordinate pass reduces to a few logical operations and can be very fast.

Zerotree data structure

A wavelet coefficient x is said to be insignificant with respect to a given threshold T if $|x|<T$. The zerotree is based on the hypothesis that if a wavelet coefficient at a coarse scale is insignificant with respect to a threshold, then all wavelet coefficients of the same orientation in the same spatial location at the finer scale are likely to be insignificant with respect to the same threshold. More specifically, in a hierarchical subband system, with the exception of the highest frequency subbands, ever coefficient at a given scale can be related to a set of coefficients at the next finer scale of similar orientation. The coefficient at the coarse scale is called the *parent,* and all coefficients corresponding to the same spatial location at the next finer scale of similar orientation are called *children.* Similar, we can define the concepts *descendants* and *ancestors.*The data structure of the zerotree can be visualized in Figure ⌐. Given a threshold T to determine whether or not a coefficient is significant, a coefficient x is said to be an element of a *zerotree* for the threshold T if itself and all of its descendents are insignificant with respect to the threshold T. Therefore, given a threshold, any wavelet coefficient could be represented in one of the four data types: zerotree root (ZRT), isolated zero (IZ) (it is insignificant but its descendant is not), positive significant (POS) and negative significant (NEG).

(a) Zerotree data structure.   (b) Coefficients scaning order
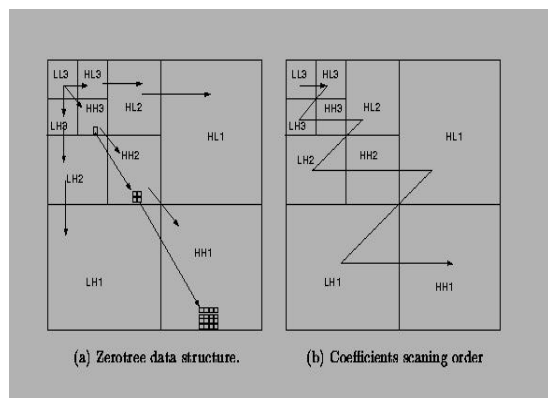
Dominant pass

Shapiro's algorithm creates rooted trees using a pixel of the LL subband for the root of each tree and a specific order of similarly positioned pixels from the other subbands for children. There are two types of passes performed: a dominant pass and a subordinate pass. The dominant pass finds pixel values above a certain threshold, and the subordinate pass quantizes all significant pixel values found in this and all previous dominant passes previous.

A dominant pass checks all trees for significant pixel values with respect to a certain threshold. The initial threshold is chosen to be one-half of the maximum magnitude of all pixel values. Subsequent dominant pass thresholds are always one-half the previous pass threshold. When an insignificant pixel value is found, and a check of all it's children reveals that they too are insignificant, then it is possible to encode that pixel and all it's children with one symbol, a zerotree root, in place of a symbol for that pixel and a symbol for each of that pixel's children, thus achieving compression. Pixel values found to be significant in the dominant pass are encoded with the symbol positive, for a value greater than zero, or negative, for a value less than zero, then those pixel values are added to a subordinate list for quantization, and the pixel value in the subband is then set to zero for the next dominant pass. Pixel values found to be insignificant in the dominant pass but with significant children are coded as isolated zeros. So, the dominant passes map pixel values to a four symbol alphabet which can then be further encoded by using an adaptive arithmetic coder.

Subordinate pass

After each dominant pass, a subordinate pass is then performed on the subordinate list which contains all pixel values previously found to be significant. The subordinate pass performs pixel value quantization which achieves compression by telling the decoder with a symbol roughly what the pixel value is instead of exactly what the pixel value is. Since the initial threshold is one-half the maximum magnitude of all pixel values for the first dominant pass, then in the first subordinate pass only two ranges are specified in which a significant pixel value could lie: the upper half of the range between the maximum pixel value and the initial threshold, or the lower half of the same range. A pixel value in the upper half of the range gets coded with the symbol upper (for upper part of the range), while a pixel value in the lower half gets coded with the symbol lower. A pixel value found to be in a particular range is quantized, from the decoders viewpoint, to the midpoint of that range. Upon subsequent subordinate passes the threshold has been cut in half and so there are twice as many ranges as the last subordinate pass plus two new ranges corresponding to the new lower threshold. By reading the subordinate symbol corresponding to a significant pixel and knowing the threshold, the decoder is able to determine the range in

which the pixel lies and reconstructs the pixel value to the midpoint of that range. Thus from the decoders viewpoint the rough estimate of a significant pixel's value is getting more refined and accurate as more subordinate passes are made. So, the subordinate passes quantize pixel values to a two symbol alphabet which then get encoded by using an adaptive arithmetic coder as described by Witten, Neal, and Cleary, thus achieving compression.

Decoding

What is needed for decoding an image compressed by Shapiro's algorithm is the initial threshold, the original image size, the subband decomposition scale and, of course, the encoded bit stream. The decoder then decompresses the arithmetically encoded files into symbol files, creates all the proper size subbands needed since it knows the subband decomposition scale and the original image size, and proceeds to undo the Shapiro compression since it knows the initial threshold and the subband scanning order.

An example

We use a two scale wavelet image as a simple to show the algorithm. The original image is shown in Figure.

(c) Initial image   (d) After DP 1   (e) After DP 2   (f) After DP 3
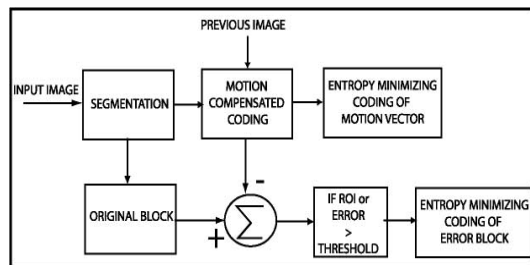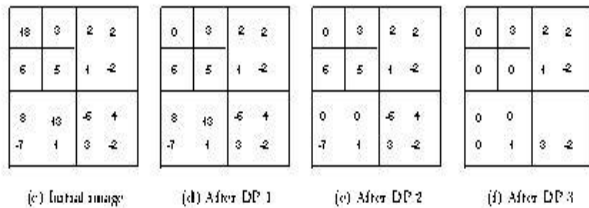
Conclusion:

In this paper we used the seeded region growing algorithm for segmentation for segmenting the medical image and EZW for compression method and the compression ratio is high and the segmentation
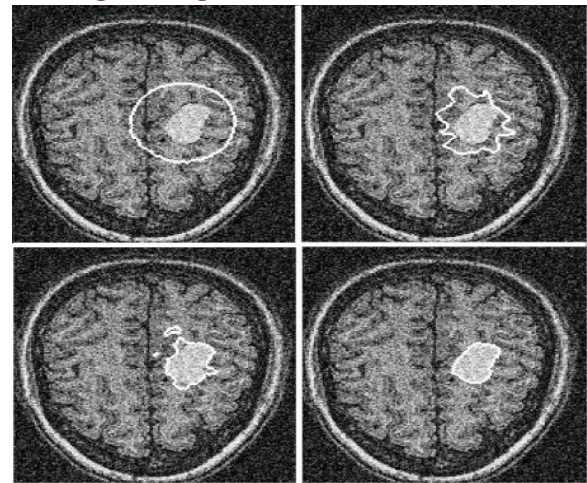
Test Image Compression Ratio

Image1	11.78 34.03
Image2	13.84 33.39

References:

[3]   A. Abu-Hajar and R. Shankar, "Enhanced Partial-EZW for

Lossless Image Compression" Acoustics, Speech and

Signal processing 2003, Proceedings (ICASSP '03)

[9]   Park, K., and Park, H.W.: 'Region-of-interest coding based on

set partitioning in hierarchical trees', IEEE Trans. Circuits Syst.

Video Technol., 2002, 12, (2), pp. 106–11

[3]   Yian-Leng Chang, Xiaobo Li, "Adaptive image

region-growing", IEEE Transactions on Image

Processing, vol.3, no.6, Nov. 1994, pp.868-72.

[4]   Rolf Adams and Leanne Bischof, "Seeded Region

Growing", IEEE Transactions on Image processing,

Vol.16, No.6, June, 1994, pp.641-47

[5]   Hojjatoleslami SA, Kittler J., "Region growing: a

new approach", IEEE Transactions of Image

Processing, vol.7, no.7, July 1998, pp.1079-84.

Security Enhanced Dynamic Routing Algorithm for Wireless Sensor Network

Ms. Nidhi Bansod

M.Tech 4th Sem
PIET, Nagpur

Abstract:

In this project we deal fully about the security which has become one of the major issues for data communication for wired and wireless networks. Different from the past work on the designs of cryptography and system infrastructure, a dynamic routing algorithm is proposed that could randomize delivery paths for data transmission. The algorithm is easy to implement and compatible with popular routing protocols, such as Routing Information protocol in wired networks and Destination sequenced distance vector protocol in wireless networks, without introducing extra control messages. An analytic study on the proposed algorithm is presented, and a series of simulation experiments are conducted to verify the analytic results and to show the capability of proposed algorithm. In the past decades, various security-enhanced measures have been proposed to improve the security of data transmission over public networks. Existing work on data transmission includes the designs of cryptography algorithms and system infrastructures and security enhanced routing methods. The main objective of the project is to propose a dynamic routing algorithm to improve the security of data transmission.

Keywords- Cryptography algorithms, Destination Sequenced Distance Vector routing protocol, security.

1.Introduction

Various security enhanced measures have been proposed to improve the security of data transmission over public data networks. Existing work on security enhanced data transmission includes the designs of cryptography algorithms and system infrastructures and security enhanced routing. Their common objectives are often to defeat various threats over the Internet, including eavesdropping, spoofing, hijacking etc. Among many well known designs for cryptography based systems, the IP security (IPSec) [23] and the secure socket layer (SSL) [21] are popularly supported and implemented in many systems and platforms. Although IPSec and SSL greatly improve the security level for data transmission, they unavoidably introduce substantial overheads [1], [7], [13], especially on gateway host and effective network bandwidth. For example the data transmission overhead is 5 cycles/byte over an intel pentium II with the Linux IP stack alone and the overhead increases to 58 cycles/byte when Advanced Encryption Standard (AES) [10] is adopted for encryption/decryption for IPSec. Another alternative for

security enhanced data transmission is to dynamically route packets between each source and its destination so that the chance for system break-in, due to successful interception of consecutive packets for a session. Intension of security enhanced routing is different from adopting paths between a source and a destination to increase the throughput of data transmission.

2. Table driven scheme

Destination-Sequenced Distance-Vector Routing (DSDV) is a table-driven routing scheme for ad-hoc mobile network based on the Bellmen-Ford algorithm. It was developed by C.Perkins and P.Bhagwat in 1994. The main contribution of the algorithm was to solve the Routing Loop problem. Each entry in the routing table contains a sequence number, the sequence numbers are generally even if a link is present; else, an old no is used. The no is generated by a destination, and the emitter needs to send out the next update with this no. Routing information is distributed between nodes.

Selection of Route

If a router receives new information, then it updates the latest sequence no. If the sequence no is the same as the one in the routing table then the route with better metric is used. Stale entries are those entries that have not been updated for a while. Such entries as well as the routes using those nodes as next hops are deleted.

3. Position based hybrid routing algorithm

The proposed algorithm PBHRA comes under position based algorithm class in hybrid main category. In the proposed algorithm the central node, in other words a master node is assigned as it directs the routing information in infrastructure wireless networks. When nodes are required to send data to a target node, they take the location of target node and the route to achieve it from master node. Accordingly they send their data through that route. At this stage, the proposed algorithm differs from infrastructure wireless networks since data is sent via central station in infrastructure wireless networks. However in proposed algorithm, the master node which behaves as if it is the central node helps only while finding the route to achieve the target.

3.1 Destination sequenced distance vector (DSDV) protocol

This routing method allows a collection of mobile computers, which may not be close to any base station and can exchange data along changing arbitrary paths of

interconnection, to afford all computers according to their numbers a (possibly multi-hop) path along which data can be exchanged. In addition our solution must remain compatible with operation in case where a base station is available. Packets are transmitted between the stations of the network by using routing tables which are stored at each station of the network. Each routing table at each of the stations lists all available destinations and the no of hops to each.

4. Security Goals:

In the ideal world, a secure routing protocol should, guarantee the integrity and authenticity, and availability of messages availability in the presence of adversaries of arbitrary power. Every eligible receiver should receive all messages intended for it and be able to verify the integrity of every message as well as the identity of sender.

In our view, protection against eavesdropping is not an explicit security goal of a secure routing algorithm. Secrecy is the most relevant to application data, and it is not the responsibility of a routing protocol to provide it. However, we do consider it the responsibility of a routing protocol to prevent eavesdropping caused by misuse of the protocol itself. Eavesdropping caused by the rerouting of a data flow should be prevented.

Similarly, we believe protection against the replay of data packets should not be a security goal of a secure routing protocol. This functionality is best provided at the application layer because only the application can accurately detect the replay of data packet (for example as opposed to retransmissions). In the presence of outsider adversaries, it is conceivable to achieve this idealized goals. However, in the presence of compromised or insider attackers, especially those with laptopclass capabilities, it is most likely that some if not all of this goals are not fully achievable. Rather, instead of complete compromise of the entire network,the best we can hope for in the presence of insider adversaries is graceful degradation.

4.1 Adaptive Routing:

Adaptive routing describes the capability of a system, through which routes are characterized by their destination, to alter the path that the route takes through the system in response to a change in conditions. The adaption is intended to allow as many routes as possible to remain valid (that is to have destination that can be reached) in response to the change. People using a transport system can display adaptive routing. For example if a local railway station is closed, people can alight from a train at a different station and use another method, such as a bus to reach their destination. The term is commonly used in data networking to describe the capability of a network to 'route around' damage, such as loss of a node or a connection between nodes so long as other path choices are available. There are several protocols used to achieve this:

1. RIP
2. OSPF
3. IS-IS
4. IGRP/EIGRP

4.2 Properties of DSDV protocol:

The DSDV protocol guarantees loop free paths to each destination. To see why this property holds, consider a collection of IV mobile hosts forming an instance of an ad-hoc style network. Further assume that the system is in steady state, i.e. routing tables of all nodes have already converged to the actual shortest paths. At this instant, the next node indicators to each destination induce a tree rooted at that destination. Thus , routing tables of all nodes in the network can be collectively visualized as forming IV trees, one rooted at each destination. In the following discussion, we'll focus our attention on one specific distance x and follow the changes occurring on the directed graph G(a) defined by nodes I and arcs (i, p;) where p: denotes the next-hop for destination x at node i. Operation of DSDV algorithm ensures that at every instant G(z) is loop-free, or rather, it is a set of disjoint directed trees directed. Each such tree is rooted either at z or at a node whose next-hop is nil. Since this property holds with respect to each destination z, all paths induced by routing tables of DSDV algorithm are indeed loop free at all instants.

Potentially a loop may form each time node i changes its next hop. This can happen in two cases. First, when node i detects that the link to the next hop is broken, the node resets p_i to nil. This action cannot form a loop involving i. The second scenario occurs when node i receives from one of its neighbors, a route to z, with sequence number s_k and metric m is selected to replace the current route it has through p_i. Let s_i denote the value of the sequence number stored at node i and di denote the distance estimate from i to z just prior to receiving route from k. i will change its next hop from p_i to k only if either of the following two happens.

1. The new route contains a newer sequence number i.e. $s_k > s_i$.
2. The sequence number s_k is same as s_i but the new route offers a shorter path to x i.e. $m < d_i$.
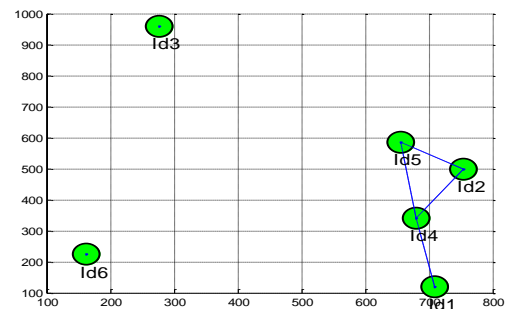
Results :
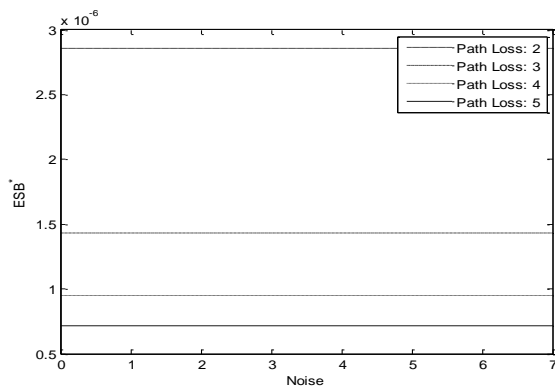

Fig. communication between nodes

Fig. Reduced path loss

Conclusion

In this study the proposed PBHRA algorithm is compared with table driven, on demand and position based algorithms in terms of normalized routing load, packet delivery fraction and end to end packet delay. It was observed from performance values that the PBHRA gives better results than table driven, on demand and position based algorithms especially in the case of high mobility. The PBHRA algorithm uses available bandwidth efficiently because of its high packet delivery fraction and low normalized routing overload. The algorithm is not affected with the number of nodes increased in the network. Further security can be achieved by reducing the time delay, path losses and collisions due to irregular acknowledgments.

References

[1] Abolhasan M, Wyosocki T, Dutkiewicz E (2004). A review of routing protocols for mobile *ad hoc* networks. *ad hoc* networks 1: 1-22.

[2]. Basagni S, Chiamtac I, Syrotiuk VR, Woodward BA (1998). A Distance Routing Effect Algorithm for Mobility (DREAM),Proceedings of the 4th International Conference on Mobile Computing and Networking pp. 76-84.

[3]. Corson S, Macker J (1999). Mobile Ad hoc Networking (MANET):Routing Protocol PerformanceIssuesandEvaluationConsiderations.IETF ;http://www.ietf.org/rfc/rfc2501.txt.

[4] Demirci R (2007). Similarity relation matrix-based color edge detection. Int. J. Elect. Commun. (AEU), 61: 469-478.

[5] Ehsan H, Uzmi ZA (2004). Performance Comparison Of *Ad Hoc* Wireless Network Routing Protocols. INMIC 2004; 0-7803-8680-IEEE.

[6] Hwang S, Chien C, Wang C (2005). A Novel GPS-Based Quorum Hybrid Routing Algorithm (GPS-QHRA) for Cellular-Based *Ad Hoc* Wireless Networks. J. Inform. Sci. Eng. pp. 1-21.

[7] Joe I, Batseli SG (2002). MPR-Based Hybrid Routing for Mobile Ad-Hoc Networks. Proceedings of the 27th Annual Conference on Local Computer Networks (LCN'02) IEEE Computer Society pp.7-12.

[8] Lin X (1999). GPS based localized routing algorithms for wireless Networks. Bsc Thesis. Ottawa-Carleton Institute for Computer Science School of Information Technology and Engineering pp. 25-29.

[9]. Perkins CE, Royer EM (1999). Ad-Hoc on Demand Distance Vector Routing. Proc. Of 2nd IEEE Wksp. Mobile Comput. Applic. pp. 90-100.

[10] Stajmenovic I (2002). Position Based Routing in *Ad Hoc* Networks.IEEE Commun. Magazine 7: 128-134.

[11] Watanabe M, Higaki H (2007). No-Beacon GEDIR: Location-Based Ad-Hoc Routing with Less Communication Overhead.International Conference on Information Technology (ITNG'07).

[12]. Wattenhofer R (2005). Algorithms for *ad hoc* and sensor Networks. Comp. Commun. 13: 1498-1504.

[13]. Y.-C. Hu, A. Perrig, and D. B. Johnson, "Wormhole detection in wireless ad hoc networks," Department of Computer Science, Rice University, Tech. Rep. TR01-384, June 2002.

[14] J. Hill, R. Szewczyk, A. Woo, S. Hollar, D. Culler, and K. Pister, System architecture directions for networked sensors," in *Proceedings of ACM ASPLOS IX*, November 2000.

3D modelling of the oldest olive tree of the world

Emmanuel Maravelakis*[(1)], Nikolaos Bilalis[(2)], Irini Mantzorou[(3)], Antonios Konstantaras[(4)], Aristomenis Antoniadis[(5)]

[(1)] Assistant Professor, Head of the Design & Manufacturing Laboratory,
Technological Educational Institute of Crete, Chania, Greece
marvel@chania.teicrete.gr, corresponding author
[(2)] Professor, Technical University of Crete
[(3)] Research Associate, Technical University of Crete
[(4)] Assistant Professor, Technological Educational Institute of Crete,
[(5)] Associate Professor, Technical University of Crete

Abstract
The Monumental Olive Tree of Vouves, known as the oldest olive tree in the World is an important part of our cultural heritage. Branches from this olive tree were used for the wreath bestowed upon the winners in the Olympic Games in Beijing and Athens and the winners of the Classic Marathon in Kalimarmaron Stadium. This ancient tree became an inspiration for sending messages of peace and hope worldwide. The process of developing a geometrically accurate 3D model of the Monumental Olive Tree of Vouves, using modern reverse engineering techniques is described in this paper and its complexity is analysed and compared to other scanned objects. The derived 3D model allows for a twofold employment: a) the creation of a virtual model for internet dissemination activities, and b) the enabling of enhanced possibilities for scientific study and analysis of the tree.

Keywords: oldest olive tree, terrestrial laser scanning, 3d tree model, complex tree physiognomy

1. Introduction
Our research aimed to examine the potential of reverse engineering technologies for developing a geometrically accurate 3D model of the Monumental Olive Tree of Vouves and to explore the enhanced new usages provided from the 3D model. Extensive literature and 3d model database review indicates that this is possibly the first application of 3D scanning and layered fabrication of any individual tree, especially with such complex physiognomy. A detailed virtual and physical model is produced allowing for the first time to accurately calculate the tree's volume and to produce its sections at any various heights enhancing upon conventional measuring techniques and mathematical applications in volume measuring [1,2]. In order to assess the complexity of the tree's physiognomy, quantitative geometry-driven complexity criteria have been incorporated, and the results are compared against various 3D scanned objects.

The archaeological importance of the Monumental Olive Tree of Vouves, known as the oldest olive tree of the world [3,4] gives added value to the virtual 3d model created, since it can be used in two ways: for the creation of a realistic virtual model for internet dissemination activities, and to enable enhanced possibilities for scientific study and analysis of the ancient tree. Further-more, since this is the first published 3D tree model these novel results can used as a benchmark to future similar studies.

1.1. The Monumental Olive Tree of Vouves
Within the settlement of AnoVouves, a small village in the island of Crete in Greece, there is an ancient olive tree, which, with the 603/1997 decision of the General Secretary of the Cretan District, has been declared a preserved monument of nature named as the Monumental Olive Tree of Vouves (figure 1). The aforementioned characterization of the olive tree arose because it exhibits "a particular aesthetic, ecological and historical interest". The vascular tree layout does not form a discrete straight line, as is usually the case with most trees, instead it appears in a form of helical bundles, a distinctive characteristic of untamed olive trees. Thus a sculptural sensation is being imparted in the trees' bole speculated to reminiscent sculptures of the great sculptor of the Italian Renaissance, Michael Angelo.

The tree's age cannot be determined with great precision, since it is not possible to apply the radioisotopes method, since, because of the tree's very old age, there is no remaining material left from the original core of the trees' bole. There is, though, a less accurate approach that is being performed, based upon comparative data of the size and the perimeter of the bole, which are directly related with a trees age, further supported by several other secondary elements for age verification. Greek and foreign literature reviews indicate that there is no mention of an olive tree with such a large perimeter. The existence of the tree in AnoVouves could be possibly associated with another discovery by the Classical Antiquities Ministry of two cemeteries aging back to the Geometric era, around 700_{BC}, which are in close proximity with it. Archaeological analysis showed that olive growing first became widespread in the Aegean in the Early Bronze Age [5,6] .
According to Wikipedia [3] and the Mother Nature Network [4] the Monumental Olive Tree of Vouves, is the oldest olive tree in the world and has an age between 2000 and 4000 years old. Furthermore the information spread from generation to generation and throughout the ages and has been preserved till nowadays, now spoken by us, regarding the legacy of the oldest olive tree known, is by itself another valuable element in support of its extremely old age. The reputation of the

Monumental Olive Tree of Vouves, led to the Olympic Committee decision for using the Branches from this olive tree for the wreath bestowed upon the winners in the Olympic Games in Beijing and Athens and the winners of the Classic Marathon in Kalimarmaron Stadium. This ancient tree became also an inspiration for sending messages of peace and hope worldwide.

Figure 1. The Monumental Olive Tree of Vouves   Figure 2. The inner cavity of the tree.

1.2 3D Preservation of Cultural Heritage

Cultural Heritage is playing a growing role in the European integration process, contributing to economic prosperity and creating jobs. But culture is a fragile and non-renewable resource. During the 20th century, it is considered that nearly 50% of Europe's tangible cultural heritage was lost. The combined impact of atmospheric pollution, urbanisation, excessive tourism, negligence and inappropriate restoration measures often results in irremediable changes and, in some cases, even the complete disappearance of major examples of immovable and movable heritage [7]. In order to tackle this problem, the last two decades, the ability to record the cultural components of a landscape in 3-dimensions has been employed by many archaeological surveyors [8,9]. Furthermore cultural heritage web sites and artefacts get a significant added value from high-resolution 3D models [10]. The technology of implementing 3D virtual models to web sites can be an important vessel for preservation, reconstruction, documentation, research and promotion of cultural heritage [11-14].

1.3 Current Approaches in 3D Tree Measuring and Analysis

A complete measuring procedure of an individual tree, includes the determination of many parameters such as age, stem diameter, diameter at breast height (dbh), height, canopy cover, leaf area and stand volume[15]. Age estimates are usually obtained by counting the number of annual rings in a stem function, or by using radiocarbon dating, but still there are many pitfalls with both of these methods [16,17]. More computerised techniques for age estimation are based on models of growth increment [18]. Conventional methods for measuring tree diameter include standard measuring tapes that are used to measure stem diameter by placing the tape around the circumference of the tree in different heights. Current efforts in estimating wood volume are focused on developing functions for stem volume and taper that allow estimates from simple measurements [1,2].

Recently the usage of Terrestrial Laser Scanners (TLS) has introduced very interesting approaches in 3D measuring and analysis of trees [19-22], but these methods are mainly focused on measuring forest structure [23,24] or canopy structure [25]. It still remains challenging to obtain accurate 3D reconstruction of individual trees [26]. A major problem in individual 3D Tree measuring is the difficulty in recreating a detailed virtual model of the tree, due to its complex structure. TLS methods and the new emerging non-contact measuring technologies, can provide a solution to this problem, since they have much higher resolution than the conventional field surveying methods [27,28].

2. Methodology

The bole of the Monumental Olive Tree of Vouves has a very complex shape, not only due to the helical bundles of the outer surface, but also due to the existence of a significantly large and complex inner cavity (figure 2). The reverse engineering approach comprises of three steps (figure 3):

- 3D data acquisition
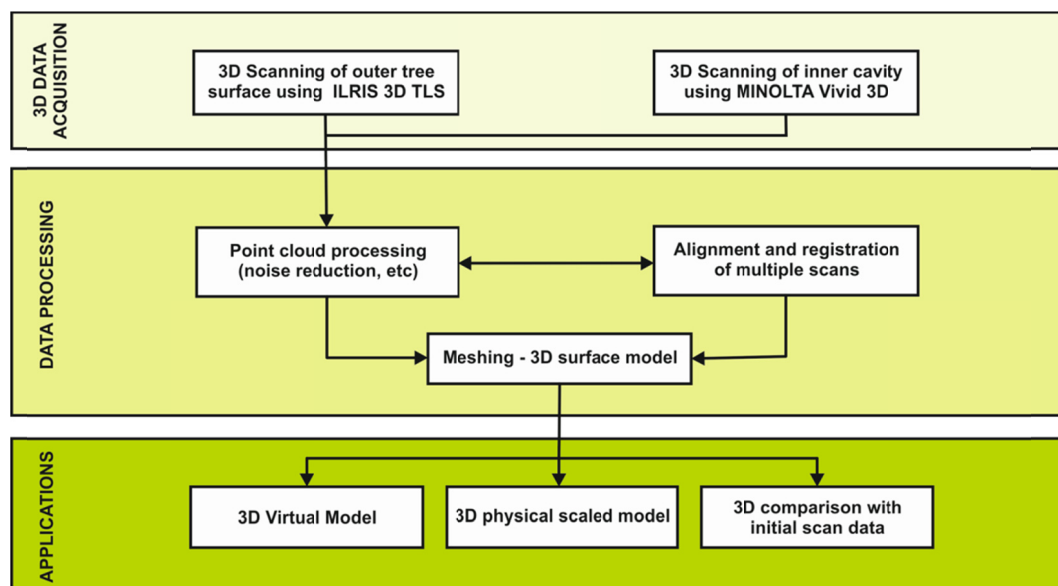- Data processing
- 3D model applications

Figure 3. The reverse engineering approach

Light detection and ranging (LiDAR) technology was used for obtaining information of the physiognomy of the outer surface of the tree. In particular an eye safe tripod mounted ILRIS-3D scanner (Optech Inc., Ontario) was used, which emits 2500 laser pulses per second across a horizontal and vertical field of view of 40° (figure 4). Since this scanner has a minimum scanning distance property of 3 meters, a close range non-contact 3D Minolta Vivid 910 digitizer (Konica Minolta, Tokyo) was used for the 3D data acquisition of the inner surface. Minolta Vivid 910 requires constant lightning to work properly, which made it necessary to carry out the scanning of the inner surface during the night.

Given the large size and complex geometry of the olive tree, the technique of multiple scans from different angles was employed, resulting in a total of 31 scans of the outer surface and 145 scans of the inner surface with a geometric accuracy of 0.5 cm. The choice of perspectives was done manually and the average scan range of ILRIS-3D was 6.3 meters, while the scanning range of Minolta Vivid 910 was much smaller, since the scanner was placed on the inside of the olive tree's cavity, where the space was limited.

Figure 4. 3D scanning of the outer surface of the trunk

The processing of the acquired 3D-data was done using the Geomagic Studio software. The first step was to prepare the different scans, eliminating the redundant data such as noise, objects from the background and even the foliage, until all that was left were the different scans of the trunk. Sampling and filtering were used in order to decrease the quantity of data without affecting the quality, reducing the average size of each scan from 22MB to 7MB.

The integration and alignment of the scans were conducted manually with an n-point registration, meaning that the number of common points selected on each scan were at least three. Because of the large number of the scans, they were divided into groups for easier use. The two main groups, which are the scans from the inner surface and the scans from the outer surface, were divided into sub groups, depending on the absolute position of the scans. The combined point cloud of the olive tree consisted of almost 14 million points which were subsequently reduced to 1,750,000, in this way enhancing the speed of the process. The procedure of aligning and merging the different scans was facilitated by the images captured by the integrated digital camera of ILRIS-3D.

3. The 3D Model of the Tree

The polygonal mesh created consisted of almost a million triangles, resulting in a good surface quality which revealed the complexity of the shape and texture of the tree trunk. Due to the particularity of the shape, there were certain blind spots that could not be scanned, creating holes on the surface that had to be filled. Similar anomalies appeared on the polygon mesh due to the noise which was not removed during the initial filtering. These anomalies showed up mainly in the areas near the crown and the roots of the olive tree where the removal of the noise created by the foliage and the weeds turned out to be challenging. These areas were treated by deleting the excessive triangles and filling the holes with smoother patches. Because of the bad visibility in these regions, assumptions were made based on the photos of the trunk concerning the shape and curvature of the fillings. The number of triangles that composed the final model was 1,200,000.

The complexity of a 3D model is closely related to a wide range of costs, in almost all phases of its lifecycle. These costs can include data acquisition or design costs, storage and transmission costs and computational and visualisation costs [29]. Many researchers also link complexity with manufacturing costs [30]. For this reason various criteria have been introduced to assess topological, morphological, combinatorial and representational complexity [29]. In this paper the shape complexity of the modelled tree was quantified using three geometry-driven criteria; the part volume ratio C_{PR}, the volume ratio C_{AR} and the thickness ratio C_{TR}[31]:

$$C_{PR} = 1 - \frac{V_p}{V_b}$$

$$C_{AR} = 1 - \frac{A_s}{A_p}$$

$$C_{TR} = 1 - \frac{T_{min}}{T_{max}}$$

whereV_p is the volume of the model, V_b is the volume of its boundary box, A_s is the surface of an imaginary sphere with volume equal to that of the model, A_p is the surface of the model and T_{min} and T_{max} the minimum and maximum thickness of the model respectively. The outcome from these criteria equations ranges between 0 and 1 with higher values indicating greater contribution to complexity. The weighted sum of these individual criteria is used to estimate the overall shape complexity factor C_F.

Table 1. Complexity criteria factors of the Monumental Olive Tree compared with various physical objects

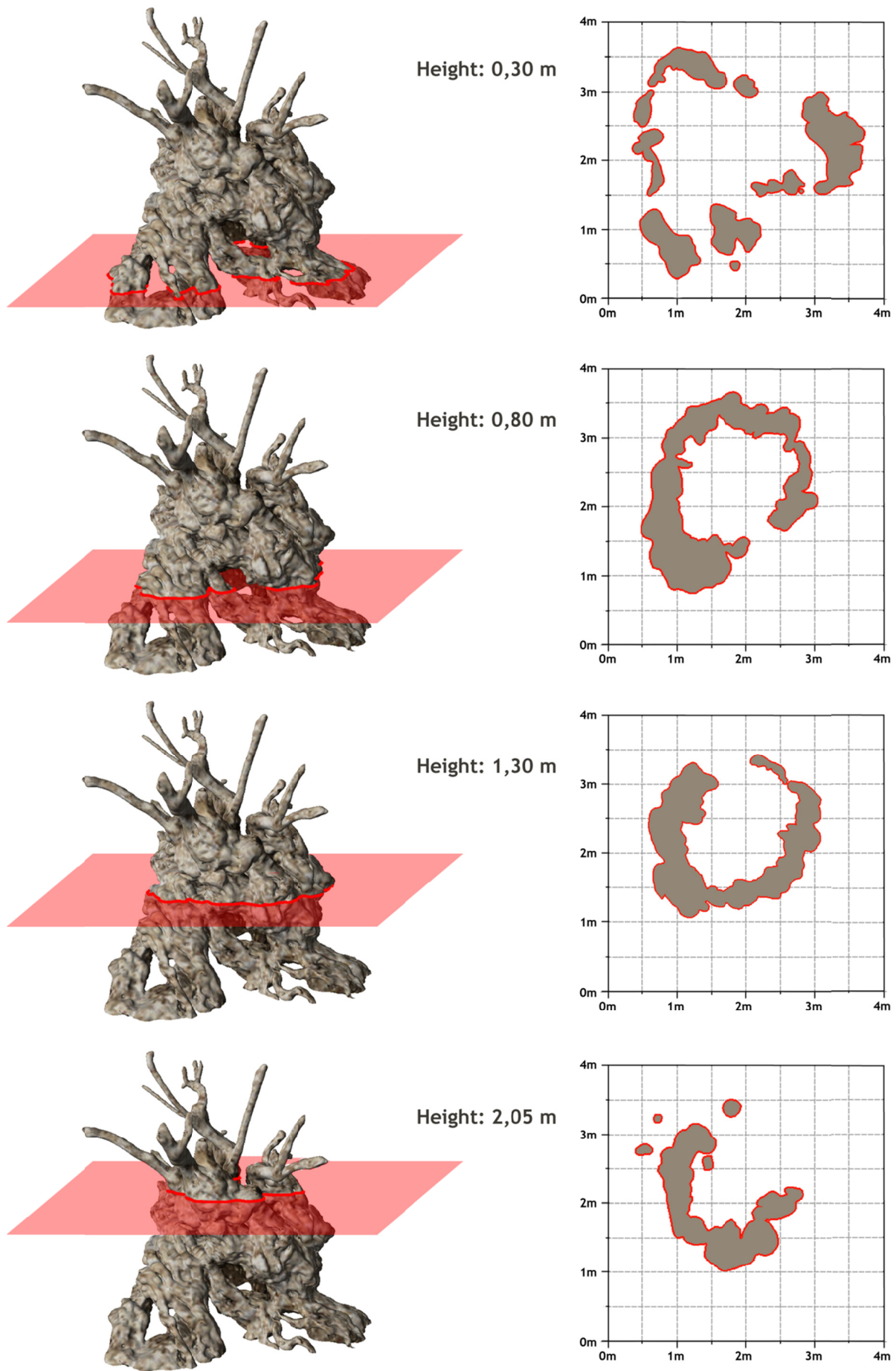|	Monumental Olive Tree	cube	sphere	wooden temple	ancient horse sculpture	musical instrument	human skull
V_p	4,67	1,00	4,19	2566,00	0,07	218,00	446,27
V_b	67,16	1,00	8,00	3122,00	0,95	1679,00	3776,16
C_{PR}	**0,93**	**0,00**	**0,48**	**0,18**	**0,92**	**0,87**	**0,88**
A_s	29,03	4,84	12,57	906,40	0,85	175,17	282,41
A_p	572,44	6,00	12,57	1855,00	1,85	380,77	1800,17
C_{AR}	**0,95**	**0,19**	**0,00**	**0,51**	**0,54**	**0,54**	**0,84**
T_{min}	0,05	1,00	1,00	1,13	1,22	1,13	0,85
T_{max}	2,55	1,00	1,00	5,52	5,22	5,52	7,80
C_{TR}	**0,98**	**0,00**	**0,00**	**0,80**	**0,77**	**0,80**	**0,89**
C_F	**0,95**	**0,06**	**0,16**	**0,49**	**0,74**	**0,74**	**0,87**

Figure 5. Detailed sections at different heights with a 0,5 cm accuracy

To further assess the complexity of the tree's physiognomy we compared these results with other physical objects scanned by our laboratory. In that aspect, to effectively investigate the relationship between the complexity and the physiognomy of the tree, the list of different physical objects used ranged from basic objects such as cube and sphere to more complex ones such as wooden temple, human skull etc. (table 1). The results indicated high values of complexity criteria factors for the Monumental Olive Tree of Vouves classing it towards the higher end of complexity among the selected objects.

The 3D model produced, introduced drastic improvements in tree analysis, compared with conventional, measuring tape based, tree analysis techniques. For example it was then possible to compute the volume of the trunk, which was 4.67 m^3, but also to produce detailed sections of the olive tree at any height with an accuracy between 12.92 mm (average positive error distance) and -5.96 mm (average negative error distance) (figure 5). From these sections the largest internal and external diameter at any height were calculated, which until now had only been estimated roughly. Some more significant measures calculated were the maximum inner and outer diameter at 1.3 m (Diameter at Breast Height - DBH), which were 2.01 m and 2.66m, respectively, the diameters at 0.9m DBH, which is 2.15m and 3.04m, respectively, as well as the longest distance between two points of the trunk at ground level, which is 3.95m.

In order for the olive tree- virtual model to be more realistic, five different color tones based on the real color of the trunk were projected on it, emphasizing its knobs and cavities. Also, lighter tones were used on the outer surface, while darker ones were used on the inner surface. After the color fitting was done, an animated gif was created for the Olive Museum's internet site using snapshots taken by rotating the trunk model around the perpendicular axis in equal degrees (figure 6). Finally an exact scaled replica of the Monumental Olive Tree of Vouves was manufactured (figure 7). The physical prototype was created by a Dimension Statasys 3D printer with a printing resolution of 0,245 mm per layer.

Figure 6. The 3D virtual model of the Monumental Olive Tree of Vouves

Figure 7.An exact scaled physical replica of the tree.

4. Discussion and Conclusions

To our knowledge this is the first detailed virtual model of an individual tree with such complex physiognomy. The archaeological importance of the Monumental Olive Tree of Vouves, known as the oldest olive tree of the world, gives added value to the virtual 3d model created, which can be used in two ways: for the creation of a realistic virtual model for internet dissemination activities, and to enable enhanced possibilities for scientific study and analysis of the ancient tree. Two different types of laser scanners were used in order to combine the outer and inner surface of the tree's bole. The processing of the obtained 3D data was done with commercially available reverse engineering software and produced a high quality 3D model result. Rough conventional inaccurate measuring techniques and mathematical applications, used by agricultural biotechnologist experts can this way be replaced with unlimited detailed measures of the ancient tree including accurate inner and outer diameters at any height and accurate computation of the trunk's volume. This methodology can be applied also to other important ancient trees, coming from the Wikipedia list of the oldest trees of the world. Future work includes re-scanning the tree's trunk after 5 years in order to calculate the tree's growth and provide valuable data to tree growth increment models, in order to make a more accurate calculation to the tree's actual age.

5. Acknowledgements

References

[1]   Avery, T. E. and Burkhart, H. E., 2002. Forest measurements. New York: McGraw-Hill.

[2]   West, P. W., 2004. Tree and forest measurement. Berlin: Springer-Verlag.

[3]   Wikipedia. (n.d.). Retrieved 2 21, 2011, from http://en.wikipedia.org/wiki/Olive_tree_of_Vouves

[4]   MNN – Mother Nature Network. Retrieved 2 21, 2011, from http://www.mnn.com/earth-matters/wilderness-resources/photos/the-worlds-10-oldest-living-trees/olive-tree-of-vouves

[5]   Renfrew, C., 1972. The Emerge of Civilisation. The Cyclades and the Aegean in the Third Millenium BC. London.

[6]   Riley, F., 2002. Olive oil production on bronze age Crete: Nutritional Properties, processing methods and storage life of Minoan olive oil. Oxford Journal of Archeology, 21(1), 63-75.

[7]   Chapuis, M., 2009. Preserving our heritage improving our environment - Volume I, 20 years of EU research into cultural heriatage. Brussels: European Commission - Directorate-General for Research.

[8]   Remondino F., Girardi S., Rizzi A., Gonzo L., 2009, 3D modeling of complex and detailed cultural heritage using multi-resolution data, Journal on Computing and Cultural Heritage (JOCCH), v.2 n.1, p.1-20.

[9]   Corns, A., and Shaw, R., 2009. High resolution 3-dimensional documentation of archaeological monuments & landscapes using airborne LiDAR. Journal of Cultural Heritage, 10(1), 72-77.

[10]   Guarnieri, A., Pirott, F., and Vettore, A., 2010. Cultural heritage interactive 3D models on the web: An approach using open source and free software. Journal of Cultural Heritage, 11, 350-353.

[11]   Bruno F., Bruno S., De Sensi G., Luchi M. , Mancuso S., Muzzupappa M., 2010, From 3D reconstruction to virtual reality: A complete methodology, Journal of Cultural Heritage 11, 42–49.

[12]   Scopigno R., Callieri M., Cignoni P., Corsini M., Dellepiane M., Ponchio F., Ranzuglia G., 2011, 3D models for Cultural Heritage: beyond plain visualization, IEEE Computer, 44, (7), 48-55.

[13]   Koller D. ,Frischer B., Humphreys G., 2009, Research challenges for digital archives of 3D cultural heritage models, Journal on Computing and Cultural Heritage v.2 n.3, p.1-17.

[14]   Maravelakis E., Andrianakis M, Psarakis K., Bolanakis N., Tzatzanis G., Bilalis N. and Antoniadis A., 2008. Lessons Learned from Cultural Heritage Digitisation Projects in Crete", In: Proceedings of the 14th International Conference on Virtual Systems and Multimedia, Nicosia, Cyprus, 152-156.

[15]   Newton, A. C., 2007. Forest Ecology and Conservation. Oxford: Oxford University Press.

[16]   Husch, B., Beers, T., and Kershaw, J., 2003. Forest mensuration. New York: Wiley.

[17]   Martínez-Ramos, M., and Alvarez-Buylla, E., 1999. How old are tropical forest trees? Trends in Plant Sciences, 3, 400-405.

[18]   Chambers, J. Q., and Trumbore, S. E., 1999. An age old problem. Trends in Plant Sciences, 4, 385-386.

[19]   Lovell, J.L., Jupp, D.L.B., Newnham, G.J., Culvenor, D.S., 2011. Measuring tree stem diameters using intensity profiles from ground-based scanning lidar from a fixed viewpoint. ISPRS Journal of Photogrammetry and Remote Sensing 66, (1), 46-55.

[20]   Koch, B. 2010, Status and future of laser scanning, synthetic aperture radar and hyperspectral remote sensing data for forest biomass assessment, ISPRS Journal of Photogrammetry and Remote Sensing 65 (6), 581-590.

[21]   Gärtner, H., Wagner, B., Heinrich, I., & C., D., 2009. 3D-laser scanning: a new method to analyze coarse tree root systems. For. Snow Landsc. Res., 82(1), 98-106.

[22]   Hopkinson, C., Chasmer, L., Young-Pow, C., and Treitz, P., 2004. Assessing forest metrics with a ground-based scanning lidar. Can. J. For. Res., 34, 573-583.

[23]   Miura, N., and Jones, S., 2010. Characterizing forest ecological structure using pulse types and heights of airborne laser scanning. Remote Sens Environ (114), 1069–1076.

[24]   Watta, P. and Donoghuea, D. 2005. Measuring forest structure with terrestrial laser scanning. International Journal of Remote Sensing, 27(7), 1437-1446.

[25]   Omasa, K., Hosoi, F. and Konishi, A., 2007. 3D lidar imaging for detecting and understanding plant responses and canopy structure. Journal of Experimental Botany, 58(4), 881-898.

[26]   Park, H., Lim, S., Trinder, J. and Turner, R., 2010. 3D surface reconstruction of Terrestrial Laser Scanner data for forestry. In:Geoscience and Remote Sensing Symposium (IGARSS), 2010 IEEE International, Honolulu, USA, 4366-4369.

[27] Bae, K. and Derek, D., 2008. A method for automated registration of unorganised point clouds. ISPRS Journal of Photogrammetry & Remote Sensing, 63(1), 36-54.

[28] Azernikov, S. and Fischer, A., 2008. Emerging non-contact 3D measurement technologies for shape retrieval and processing. Virtual and Physical Prototyping, 3(2), 85-91.

[29] Rossignac, J., 2005, Shape complexity, Visual Comput 21: 985-996, DOI 10.1007/s00371-005-0362-7.

[30] Valentan, B., Brajlih, T., Drstvensek, I. and Balic, J., 2006, Evaluation of shape complexity based on STL data. Joutanl of Achievements in Materials and Manufacturing Engineering, 17(1-2), 293-296.

[31] Durgesh, J. and Bhallamudi, R., 2010. Quantifying the Shape Complexity of Cast Parts. Computer-Aided Design & Applications, 7(5), 685-700.

"ANALYSIS AND COMPARISION OF IMAGE SEGMENTATION ALGORITHMS"

Mrs. Bharati R.Jipkate and Dr. Mrs. V. V. Gohokar
SSGMCE, Shegaon, Maharashtra-443101 (India)

Abstract—The image segmentation is a key process of the image analysis. The goal of image segmentation is to partition an image into a set of disjoint regions with uniform and homogeneous attributes such as intensity, color, tone or texture etc.There are various methods for segmentation. The main aim of this project is to compare the performance of image segmentation algorithms on real images .The influence of the variation in background, the object characteristics diversity and the noise is taken into consideration while comparing the methods.

Index Terms— Segmentation, segmentation methodssegmentation algorithms.

I. Introduction

Segmentation is the process of partitioning a digital image into multiple segments(set of pixels,also known as superpixels). The goal of segmentation is to simplify and/or change the representation of an image into something that is more meaningful easier to analyze. Image segmentation is typically used to locate objects and boundaries (lines, curves, etc.) in images. More precisely, image segmentation is the process of assigning a label to every pixel in an image such that pixels with the same label share certain visual characteristics.The result of image segmentation is a set of segments that collectively cover the entire image,or a set of contours extracted from the image(edge detection). Each of the pixels in a region are similar with respect to some characteristic or computed property, such as color,intensity, or texture.Adjacent regions are significantly different with respect to the same of intensity values: discontinuity and similarity.In the first category the approach is to partition an image based on abrupt changes in intensity,such as edges in an images.In the second category are based on partitioning an image into regions that are similar according to a set of predefine criteria.Thresholding,region growing, and region splitin and merging are example of method of this category.Image segmentation can be broadly classified into four different classes as follows [1-3]:-

i) Edge detection methods. ii) Thresholding and Histogram based methods. iii) Region based methods .iv) Cluster based methods.

2) Edge detection methods

An edge is the discontinuity in an image. An edge is the boundary between an object and the background, and indicates the boundary between overlapping objects. There are various algorithms for edge detection,few are discussed here.Sobel operator: For Better approximations of the gradients a Sobel operator is used. It looks for edges in both horizontal and vertical directions, and then combines the information into a single metric. The matrix coefficients are 0, 1,-1, 2 and -2.The Marr-Hildrethmethod:It is a gradient based operator which uses the Laplacian to take the second derivative of an image. The idea is that if there is a step difference in the intensity of the image, it will be represented in the second derivative by a zero crossing [5]: Canny Edge Detector:The Canny edge detector was released after Marr-Hildreth edge detector. Canny saw the edge detection problem as a signal processing optimization problem, so he developed an objective function to be optimized [4-6]. Fig1 shows segmentation by using sobel,Marr,canny edge detector.
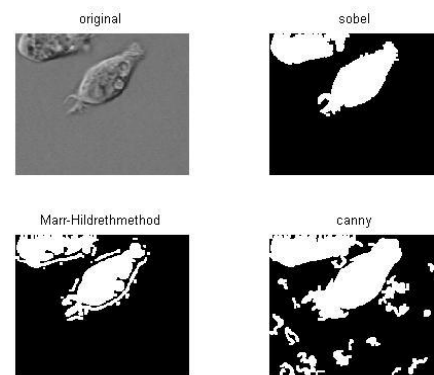
Fig1 .Edge based segmentation

3Thresholding and Histogram based methods

Histogram-based image segmentation techniques use the histogram to select the gray levels for grouping pixels into regions. In a simple image there are two entities: the background and the object. The background is generally one gray level and occupies most of the image. Therefore, its gray level is a large peak in the histogram. The object or subject of the image is another gray level, and its gray level is another, smaller peak in the histogram.

A thresholded image g(x, y) is defined as

$$g(x, y) = \begin{cases} 1, f(x, y) > T \\ 0, f(x, y) < T \end{cases}$$

Where 1 is object and 0 is background

When $T = T [f(x, y)]$, threshold is global

When $T = T [p(x, y), f(x, y)]$, threshold is local

When $T = T [x, y, p(x, y), f(x, y)]$, threshold is dynamic or adaptive

3.1 Fixed (or global) Thresholding algorithm:
 The threshold value is constant throughout the image.
Step1.   Select an initial estimate **T** to separate object from background.
Step2. Segment the image using **T**. This will producetwo groups of pixels. **G₁** consisting of all pixels withgray level values >=**T** and **G₂** consisting of pixels with values <**T.**
Step3. Compute the average gray level values mean1 and mean2 for the pixels in regions **G₁** and **G₂.**
Step4. Compute a new threshold value i.e. T = (1/2) (mean1 + mean2).
Step5. Repeat steps 2 through 4 until difference in **T** in successive iterations is smaller than a predefined parameter **T₀.**[26]
3.2 Optimal thresholding using Otsu's method: The criterion for Otsu is the minimization of the within-group variance of the two groups of pixels separated by the threshold. The between class variance is obtained by subtracting the within-class variance from the total variance of the combined distribution:

$\left|\sigma^2_{Between} (T) = \sigma^2 - \sigma^2_{within} (T)\right.$

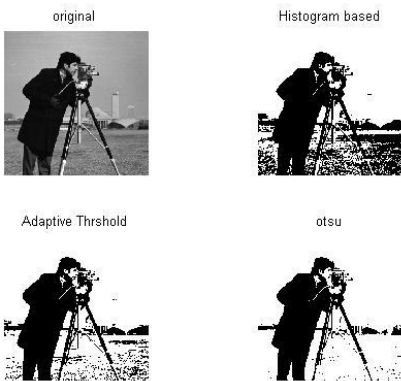Fig 2 shows comparison of histogram based and Otsu's method

Fig2 Threshold based segmentation

4 Region based methods

Region-based approaches that aim to detect regions satisfying a certain predefined homogeneity criterion.
4.1   Seeded region growing method[11]:The first region growing method was the seeded region growing method. Seed is a basic uniform region that belongs together.The seeds mark each of the objects to be segmented. The regions are iteratively grown by comparing all unallocated neighboring pixels to the regions. The algorithm is as follows

Step1. Find initial set of candidate pixels, calculate their fitness and put them into the priority queue.

Step2. While Queue is not empty –2a) Get candidate pixel with best fitness from queue.   2b) If (Candidate has more than one neighboring regions.) Then mark pixel as border region. Else Mark pixel with label of its neighboring region.

Step3. Identify new candidates among the neighbors of the pixel just processed, calculate their fitness and put them into the queue [11].
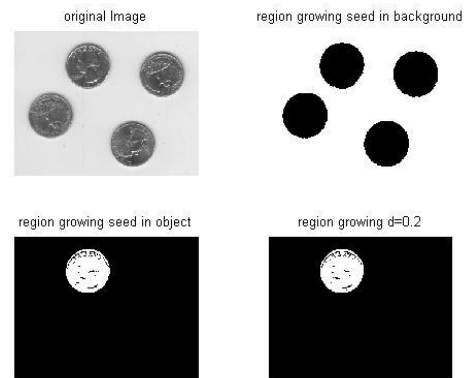
Fig3 Seeded region growing

Fig3 shows results of seeded segmentation,the effect of selecting the seed pixel on background and object is shown .

4.2 Split and Merge method:
Segments   image   by recursively dividing it into four equal blocks if   the variability in its pixels is greater than a certain amount. It merges the blocks depending on the similarity.

The algorithm is given below,
Step1**.** Split the given image into four disjoint quadrants any region R_i for which $P(R_i) = $ False
Step2**.**When no further splitting is possible, merge any adjacent regions $R_j$and R_k for which
$P(R_j \cup R_k) = $ True
Step3.   Stop when no further merging is possible[28].Figure 4 shows effect of   segmentation and the size of minimum block.Fig 4a has higher size of the minimum block as compared to figure 4b
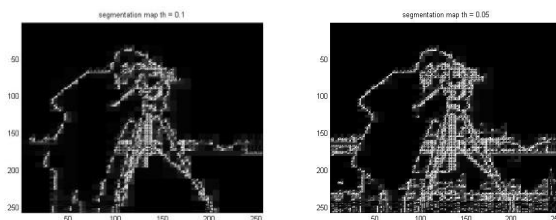
4.3 Marker-Controlled Watershed Segmentation:
Separating touching objects in an image is one of the more difficult image processing operations. The watershed transform is often applied to this problem. The watershed transform finds "catchment basins" and "watershed ridge lines" in an image by treating it as a surface where light pixels are high and dark pixels are low.The algorithm is
Step1**.** Compute a segmentation function. This is an image whose dark regions are the objects you are trying to segment.

Step2. Compute foreground markers. These are connected blobs of pixels within each of the objects.

Step3. Compute background markers. These are pixels that are not part of any object.

Step4. Modify the segmentation function so that it only has minima at the foreground and background marker locations.

Step5. Compute the watershed transform of the modified segmentation function.

Figure 5 shows the result of application of watershed algorithm ,

Fig5 Watershed Segmentation

5 Cluster based methods

Clustering is the problem of grouping similar objects together. Clustering is a process whereby a data set is replaced by **clusters** that "belong together".

5.1 K-means clustering:

It is an iterative Technique that is used to partition an image into *K* clusters**.**This algorithm aims at minimizing an *objective function*, in this case a squared error function. The objective function

$$J = \sum_{j=1}^{k} \sum_{i=1}^{n} \left\| x_i^{(j)} - c_j \right\|^2$$
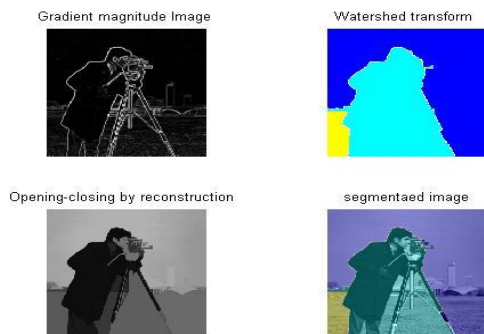
where $\left\| x_i^{(j)} - c_j \right\|^2$ is a chosen distance measure between a data point $x_i^{(j)}$ and the cluster centre c_j, is an indicator of the distance of the *n* data points from their respective cluster centers.The algorithm is as follows

Step1.Choose the number K of clusters either manually, randomly or based on some heuristic.

Step2.Generate K clusters and determine the cluster's center.

Step3**.** Assign each pixel in the image to the cluster that minimizes the variance between the pixel and the cluster center

Step4**.**Re-compute cluster centers by averaging all of the pixels in the cluster.

Step5**.**Repeat steps 3 and 4 until some convergence criterion is met

Figure6 shows segmentation in 2 and 3 clusters using this method
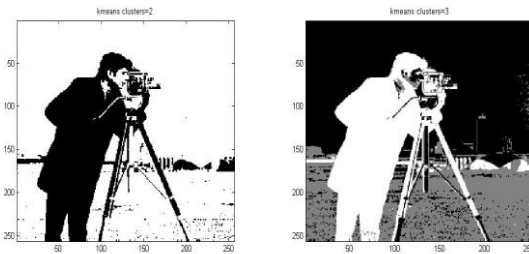
one piece of data to belong to two or more clusters. It is based on minimization of the following objective function:

$$J_m = \sum_{i=1}^{N} \sum_{j=1}^{C} u_{ij}^m \left\| x_i - c_j \right\|^2, \quad 1 \le m < \infty$$

The algorithm is as given below.

Step1. Choose a number of clusters in a given image.

Step2. Assign randomly to each point coefficients for being in a cluster.

Step3. Repeat until convergence criterion is met.

Step4. Compute the center of each cluster.

Step5. For each point, compute its coefficients of being in the cluster[17].

Fig7 shows the image segmented by c means algorithm

Fig7 C means

6. Conclusion

The paper compares various image segmentation algorithms .The algorithms are developed in MATLAM for analysis and comparison. Table 1 shows comparison of time required for segmentation for all these methods. Otsu's method is the least complex method. Watershed algorithm is the most complex algorithm but has advantages in segmenting images having occlusions

Method	Time
Global threh using otsu's	0.055485 sec
Marr-hildreth method	0.250379 sec
Canny edge detection	0.301408 sec
Sobel edge detection	0.427063 sec
Fuzzy c-means clustering	0.487124 sec
Split and merge method	1.286568 sec
K-means clustering	1.680861 sec
Watershed method	4.816477 sec
Seeded region growing	31.182382 sec

References

[1] Rafael C. Gonzalez, Richard E. Woods, Digital Image Processing 2nd, Prentice-Hall Inc, 2002

[2] Linda G. Shapiro and George C. Stockman,"Computer Vision", Prentice-Hall, 279-325, New Jersey, 2001

[3] Y. Zhang, "A survey on evaluation methods for image segmentation", Pattern Recognition, 29(8), 1996, 1335-1346.

[4] Jean Ponce, "Lecture 26: EdgeDetection II", 12/2/2004. http://www-cvr.ai.uiuc.edu /~ponce/fall04/lect26.ppt

[5] D. Marr and E. Hilreth. Theory of edge detection. In Proc. Royal Soc. Lond., volume B 207, pages 187--217, 1980.

[6] S. Price, "Edges: The Canny Edge Detector", July 4, 1996. http://homepages.inf.ed.ac.uk/rbf/CVonline/LOCAL_COPIES/MARBLE/low/edges/canny.htm

[7] R.Adams and L. Bischof, "Seeded region growing," IEEE Trans. On Pattern Analysis and Machine Intelligence, vol. 16, no. 6, pp. 641-647, 1994.

[] T.H. Cormen, C.E. Leiserson& R.L. Rivest. Intro.to Algorithms. The MIT Press, McGraw-Hill Book Company, 1990.

[28] T.Gevers and Smeulders, A. Combining Region Splitting and Edge Detection through Guided Delaunay Image Subdivision, Faculty of Mathematics Computer Science, University of Amsterdam, 1997.

[29] Dr.Teknomo, Kardi. K-Means Clustering Tutorials. http:\\people.revoledu.com\kardi\ tutorial\kMean\July 2007.

ANALYSIS OF SELF-EXITED INDUCTION GENERATOR FOR ISOLATED SYSTEM

ASHISH GUPTA
Department of Electrical Engineering,
Madhav Institute of Technology & Science, Gwalior, 474005, India

Dr. SULOCHANA WADHWANI
Department of Electrical Engineering,
Madhav Institute of Technology & Science, Gwalior, 474005, India[*]

Abstract

Self exited Induction generators are widely used in non conventional energy systems such as wind, micro/mini hydro, etc. The squirrel cage induction generator is simple, reliable, cheap, lightweight, ruggedness, and requires very little maintenance. This paper presents the self-excitation and modeling, steady-state, performance analysis and generating schemes of induction generators.

Keywords: self-exited induction generator; steady-state and performance analysis; generating schemes.

1. Introduction

An externally driven induction machine with an appropriate value of capacitor bank can be used as a generator [1]. This system is called self-excited induction generator (SEIG). The self-excited induction generators (SEIG) have been found suitable for energy conversion for remote locations. Such generators may be commonly used in the remote rural areas where it is not possible to draw from transmission lines. These machines can be used to meet the local demand of remote areas in the absence of a grid [2]. This system is called self-excited induction generator (SEIG). The SEIG has many advantages over the synchronous generator: brushless (squirrel cage rotor), reduced size, rugged and low cost. But the induction generator offers poor voltage regulation and its value depends on the prime mover speed, capacitor bank and load [3]. Use of an induction machine as a generator is becoming more and more popular for the renewable sources [4].

The paper is organized as follows. Section 2 presents the system Configuration. Steady-state and performance analysis is presented in Sections 3. Generating schemes of induction generators has been presented in Sections 4.

2. System Configuration

A SEIG is driven by prime mover. The generator supplies an isolated three-phase four-wire load. When an induction machine is driven at a speed greater than the synchronous speed (negative slip) by means of an external prime mover, the direction of induced torque is reversed and theoretically it starts working as an induction generator. From the circle diagram of the induction machine in the negative slip region [8], it is seen that the machine draws a current, which lags the voltage by more than 90. This means that real power flows out of the machine but the machine needs the reactive power. To build up voltage across the generator terminals, excitations must be provided by some means; therefore, the induction generator can work in two modes. In case of a grid-connected mode, the induction generator can draw reactive power either from the grid but it will place a burden on the grid or by connecting a capacitor bank across the generator terminals [6], [9]. For an isolated mode, there must be a suitable capacitor bank connected across the generator terminals. This phenomenon is known as capacitor self-excitation and the induction generator is called a "SEIG" [5]. Fig 1shows a schematic arrangement of self-Exited induction generator as a isolated system.
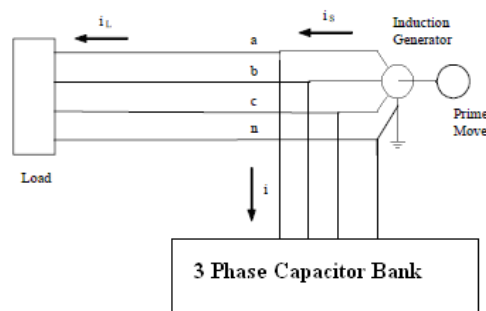

Fig. 1. Self exited induction generator system.

3. Steady-State and Performance Analysis

In the present paper, the standard steady state equivalent circuit of a SEIG with the usual assumptions considering the variation of magnetizing reactance with saturation as the basis for calculation. The equivalent circuit is normalized to the base frequency by dividing all the parameters by the p.u. frequency as shown in Fig 2.

The total current at node 'a' in the above figure can be written as
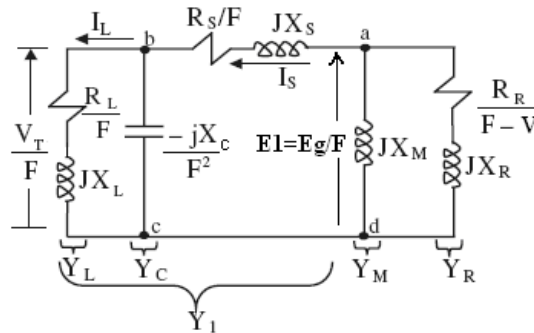
Fig. 2. Per-phase equivalent circuit oh a SEIG.

$$E_1(Y_1 + Y_M + Y_R) = 0 \qquad \text{---------------- (1)}$$

Therefore, under steady-state self-excitation, the total admittance must be zero,

$$(Y_1 + Y_M + Y_R) = 0 \qquad \text{---------------- (2)}$$

Where

$$Y_1 = \frac{(Y_C + Y_L)(Y_S)}{Y_C + Y_L + Y_S} \qquad\qquad Y_C = \frac{1}{-(jX_C/F^2)}$$

$$Y_L = \frac{1}{(R_L/F)} \qquad\qquad Y_S = \frac{1}{(R_S/F) + jX_S}$$

$$Y_M = \frac{1}{jX_M} \qquad\qquad Y_R = \frac{1}{\frac{R_R}{F-V} + jX_R}$$

By separating the real and imaginary components of equation (2) and putting separately equal to zero, two equations is obtained in term of machine parameters shaft speed and generated frequency.

$$G_0(F) = A_5F^5 + A_4F^4 + A_3F^3 + A_2F^2 + A_1F + A_0 = 0 \qquad \text{-------------- (3)}$$

$$H_0(V) = B_2V^2 + B_1V + B_0 = 0 \qquad \text{-------------- (4)}$$

The coefficients (A_0-A_5) and (B_0-B_2) of two characteristics equation are obtained by solving above two equation mathematically and given in appendix –I and X_M can be obtained from imaginary parts of equation (2) as

$$X_M = -1 \Big/ \left\{ \frac{X_R}{[R_R/(F-V)]^2 + X_R^2} + \frac{X_{ac}}{R_{ac}^2 + X_{ac}^2} \right\} \qquad \text{-------------- (5)}$$

Where

$$X_{ac} = X_s - X_{bc} \qquad\qquad R_{ac} = \frac{R_s}{F} + R_{bc}$$

$$X_{bc} = R_L^2 X_C/(F^2 R_L^2 + X_C^2) \qquad R_{bc} = R_L X_C^2/\left[F\left(F^2 R_L^2 + X_C^2\right)\right]$$

Now by solving the equivalent circuit of SEIG, the analysis of machine is simple and straight. Branch currents, terminal voltage input power and output power is computed as under:

$$I_S = \frac{E_g/F}{\frac{R_s}{F} + jX_S - \frac{jX_C R_L}{F^2 R_L - FX_C}} \qquad\qquad I_R = \frac{-E_g/F}{\frac{R_R}{F-V} + X_R}$$

$$I_L = \frac{-jX_C I_S}{R_L F - jX_C} \qquad\qquad V_T = I_L R_L$$

$$P_{in} = \frac{-3R_R F |I_R|^2}{F - V} \qquad\qquad P_{out} = 3|I_L|^2 R_L$$

4. Generating Schemes of Induction Generators

Depending upon the prime movers used (constant speed or variable speed) and their locations (near to the power network or at isolated places), generating schemes can be broadly classified as under:

- constant-frequency schemes
- constant- speed schemes
- variable-speed variable-frequency schemes

4.1. Constant frequency schemes

The variable-speed operation of wind electric system yields higher output for both low and high wind speeds [5]. This results in higher annual energy yields per rated installed capacity. Both horizontal and vertical axis wind turbines exhibit this gain under variable-speed operation. For constant frequency, shaft speed and magnetizing reactance will vary with the load and taken as variable and calculate using equation (4) & (5). These variations are shown in fig. 3 and fig. 4. The load range and speed regulation for constant frequency is summarized in Table 1.

Fig. 3. Variation of rotational speed with load.
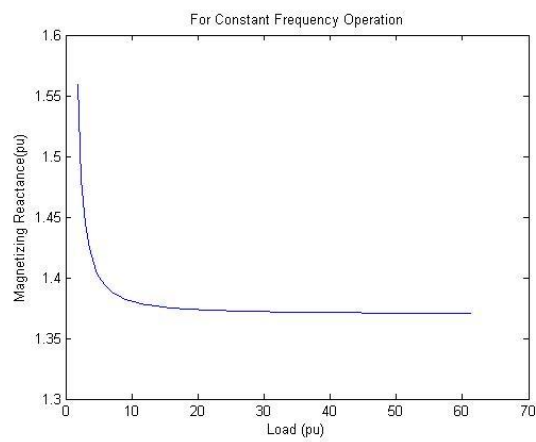
Fig. 4. Variation of magnetizing reactance with load.

Table 1. Load Impedance and Shaft Speed of SEIG with Constant Output Frequency.

Load impedance at unity power factor (pu value)	Shaft speed (pu value)	Output frequency (pu value)
1.80	1.0379	0.9
5.40	1.0105	0.9
10.20	1.0037	0.9
13.80	1.0016	0.9
21.00	0.9996	0.9
24.60	0.9991	0.9
29.40	0.9985	.09
33.00	0.9982	0.9
37.20	0.9979	0.9
39.60	0.9978	0.9
43.80	0.9976	0.9
52.80	0.9973	0.9
56.40	0.9972	0.9
61.20	0.9971	0.9

4.2. Constant speed schemes

To achieve constant speed operation, the generator should be driven by a fixed shaft speed turbine. In this scheme, the prime mover speed is held constant by continuously adjusting the blade pitch and/or generator characteristics [5]. An induction generator can operate on an infinite bus bar at a slip of 1% to 5% above the synchronous speed. Induction generators are simpler than synchronous generators. They are easier to operate, control, and maintain, do not have any synchronization problems, and are economical [6]. For constant shaft speed, generated frequency and magnetizing reactance

will vary with the load and taken as variable and calculate using equation (3) & (5). These variations are shown in fig. 5 and fig. 6. The load range and frequency regulation for constant speed is summarized in Table 2.
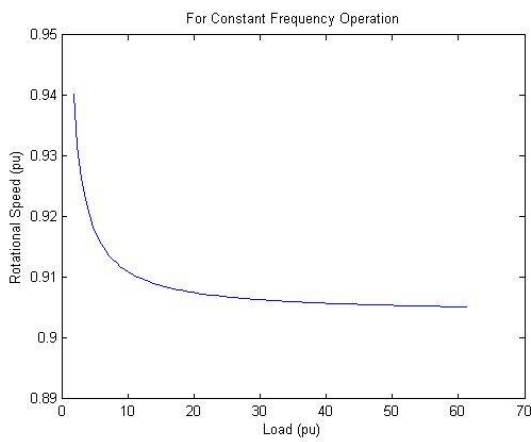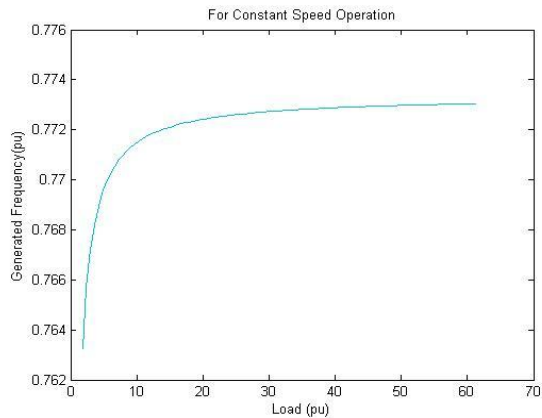

Fig. 5. Variations of Generated Frequency with Load   Fig. 6. Variation of Magnetizing Reactance with Load
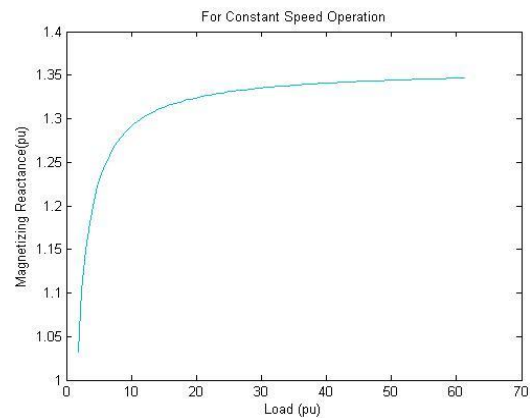
Table 2. Load Impedance and Output Frequency of SEIG with Constant Shaft Speed.

Load impedance at unity power factor (pu value)	Output frequency (pu value)	Shaft speed (pu value)
1.80	0.7632	0.95
5.40	0.7699	0.95
10.20	0.7715	0.95
13.80	0.7720	0.95
21.00	0.7725	0.95
24.60	0.7726	0.95
29.40	0.7727	0.95
33.00	0.7728	0.95
37.20	0.7728	0.95
39.60	0.7729	0.95
43.80	0.7729	0.95
52.80	0.7730	0.95
56.40	0.7730	0.95
61.20	0.7730	0.95

4.3. Variable speed variable frequency schemes

For variable speed corresponding to the changing derived speed, SEIG can be conveniently used for resistive heating loads, which are essentially frequency insensitive. This scheme is gaining importance for stand-alone wind power applications [4], [6]. In this operation generated frequency and magnetizing reactance will vary with the load and shaft speed both taken as variable and calculate using equation (3), (5). These variations are shown in fig. 7, fig. 8 and fig. 9.
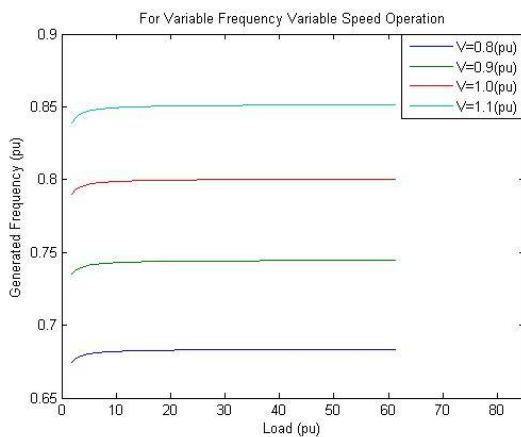
Fig. 7. Variations of Generated Frequency with Load   Fig. 8. Variation of Magnetizing Reactance with Load
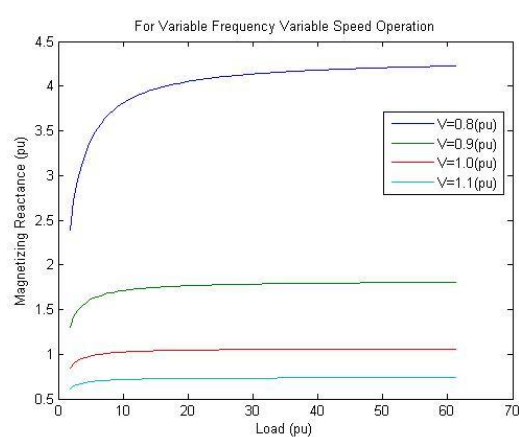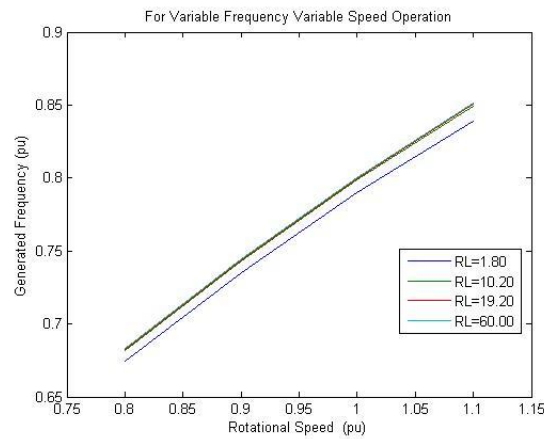
Fig. 9. Variations of Generated Frequency with Rotational Speed

5. Conclusions

Self Excited Induction Generators seem to be the right choice for remote windy locations for supplying power. It is found that proposed analysis results in to a estimation for generated frequency, magnetizing reactance and load variation at different condition. In this work many operating schemes of SEIG are discussed, which are useful to installing SEIG as an isolated systems provided low maintenance cost.

Analysis proposed may be helpful for researchers to think over the implementation of such generators successfully in windy remote locations and various mini and micro hydro plaint.

Nomenclatures

|	
R_S, R_R, R_M, R_L, R_C	P.U. stator, rotor, magnetizing, load and exciting resistances, respectively
X_S, X_R, X_M, X_L, X_C	P.U. stator, rotor leakage, magnetizing, load and exciting reactance respectively
Y_S, Y_R, Y_M, Y_L, Y_C	P.U. stator, rotor, magnetizing, load and exciting admittances, respectively
f_s	Synchronous frequency
F	P.U. frequency
V	P.U. rotational speed
E_g, V_T	P.U. air gap and terminal voltage, respectively
I_S, I_R, I_L	P.U. stator, rotor and load current per phase, respectively
P_{out}	Output electrical power
P_{in}	Input mechanical power
Z_c	Capacitor bank impedance

Appendix – I

Coefficients $(A_0 - A_5)$ of equation $G_0(F)$

$$A_0 = -VR_R \left(\frac{R_3}{R_L}\right)^2$$

$$A_1 = R_R \left(\frac{R_3}{R_L}\right)^2 + R_3 \left(\frac{R_R}{R_L}\right)^2 + V^2 R_3 \left(\frac{X_R}{R_L}\right)^2$$

$$A_2 = -2V R_3 \left(\frac{X_R}{R_L}\right)^2 - VR_R \left\{\left(\frac{R_S}{X_C}\right)^2 + \left(\frac{X_S}{R_L}\right)^2 - 2\left(\frac{X_S}{X_C}\right)\right\}$$

$$A_3 = R_R \left[\left(\frac{X_S}{R_L}\right)^2 + \left(\frac{R_S}{X_C}\right)^2 - 2\left(\frac{X_S}{X_C}\right)\right] + R_3 \left(\frac{X_R}{R_L}\right)^2 + R_S \left(\frac{R_R}{X_C}\right)^2 + V^2 R_S \left(\frac{X_R}{X_C}\right)^2$$

$$A_4 = -V \left[R_R \left(\frac{X_S}{X_C}\right)^2 + 2R_S \left(\frac{X_R}{X_C}\right)^2\right]$$

$$A_5 = R_R \left(\frac{X_S}{X_C}\right)^2 + R_S \left(\frac{X_R}{X_C}\right)^2$$

Where

$$R_3 = R_S + R_L$$

Coefficients ($B_0 - B_2$) of equation $H_0(V)$

$$B_0 = R_R F(R_{ac}{}^2 + X_{ac}{}^2) + R_{ac}(R_R{}^2 + F^2 X_R{}^2)$$
$$B_1 = -[R_R(R_{ac}{}^2 + X_{ac}{}^2) + 2F R_{ac} X_R{}^2]$$
$$B_2 = R_{ac} X_R{}^2$$

Appendix – II

The details of induction machine are:
- Specifications

3-phase, 4-pole, 60 Hz, star connected, squirrel cage induction machine
1kw, 380 V, 2.27A
- Parameters

The equivalent circuit parameters for the machine are

$R_S = 0.1$ $\qquad$ $X_S = 0.2$ $\qquad$ $R_R = 0.06$ $\qquad$ $X_R = 0.2$

Base values
Base voltage =219.3 V
Base current =2.27 A
Base Impedance=96.6 Ω
Base frequency=60 Hz
Base speed=1800rpm
The magnetization curve is represented mathematically as

$$\frac{E_g}{F} = 1.12 + .078X_M - 0.146X_M ; \qquad 0 < X_M < 3$$

References

[1] Bassett E.D. and Potter F.M., *"Capacitive Excitation for Induction Generators",* AIEE Transactions on Electrical Engineering, Vol. 54, pp. 540-545, May 1935.
[2] Joshi Dheeraj , Sandhu Kanwarjit Singh, Soni Mahender Kumar, *"Voltage Control of Self-Excited Induction Generator using Genetic Algorithm "* Turk J Elec Eng & Comp Sci, Vol.17, No.1, 2009, c_ T¨UB˙ITAK doi:10.3906/elk-0610-1.
[3] José Antonio Barrado1, Robert Griñó2 1 Departamento de Ingeniería Eléctrica, Electrónica y Automática ETSE, Universitat Rovira i Virgili Avinguda Països Catalans, 26. 43007 Tarragona (España) *"Analysis of voltage control for a self-excited induction generator using a three-phase four-wire electronic converter"*
[4] Bansal R. C., Bhatti T. S., and Kothari D. P., *"A bibliographical survey on induction generators for application of nonconventional energy systems,"* IEEE Trans. Energy Convers., vol. 18, no. 3, pp. 433–439, Sep. 2003.
[5] Jayadev T. S. , *"Windmills stage a comeback," IEEE Spectr.,* vol. 13, no. 11, pp. 45–49, Nov. 1976.
[6] Bansal R. C. , *"Three Phase Self Excited Induction Generator: An Overview,"* IEEE Trans. Energy Convers., vol. 20, no. 2, Jun. 2005.
[7] Joshi Dheeraj , Sandhu Kanwarjit Singh, *"Excitation Control of Self Excited Induction Generator Using Genetic Algorithm and Artificial Neural Network",*International journal of Mathematical Models and Methods in Applied Sciences issue 1, volume 3, 2009.
[8] Nagrath I. J. and Kothari D. P., *Electrical Machines*, 2nd ed. New York: Tata McGraw-Hill, 1997.
[9] Bansal R. C. , Kothari D. P., and Bhatti T. S. , *"Some aspects of grid connected wind electric energy conversion systems,"* in *Proc. 24th Nat. Renewable Energy Conversion*, Bombay, India, Nov.-Dec. 30–2, 2000.

Data Security Using LSB & DCT Steganography In Images

Deepak Singla[1], Rupali Syal[2]

Department of Computer Sci. & Engineering[1], Department of Information Technology[2]   PEC University of Technology, Sector-12 Chandigarh, India

Abstract

  Steganography is a technique of hiding information in digital media. In contrast to cryptography, it is not to keep others from knowing the hidden information but it is to keep others from thinking that the information even exists.In this paper, we propose a LSB & DCT-based steganographic method for hiding the data. Each bit of data is embedded by altering the least significant bit of low frequency DCT coefficients of cover image blocks. There are some techniques to utilizes the idea of SSB-4 technique in modifying the other bits (i.e, 1st , 2nd, 3rd and/or 4th), to obtain the minimum variation between the original and the modified coefficient. The experimental results show that this algorithm has better PSNR value and high capacity in comparison to other techniques such as LSB, modulus arithmetic, SSB4-DCT. It also maintains satisfactory security as secret message cannot be extracted without knowing the decoding algorithm. This is achieved using a Public Private key. It combined both feature of Steganography and cryptography.

Keywords: Authentication, Discrete Cosine Transform, Privacy, Steganography, Zigzag scanning.

1.   Introduction

   Security of information is one of the most important factors of information technology and communication. Security of information often lies in the secrecy of its existence and/or the secrecy of how to decode it. Cryptography techniques often use the worst approach assuming that only one of these two conditions holds [5]. It was created as a technique for securing the secrecy of communication. Various methods have been developed to encrypt and decrypt data in order to keep the message secret. Unfortunately, it is not enough to keep the content of the information/message secret, it may also be necessary to keep the existence of the information secret. The technique used to implement this, is called steganography.

   Steganography is the art of hiding information in plain sight. Looking at data in transmission it is very easy to detect if its encrypted or not. [28]. To hide information, straight message insertion may encode every bit of information in the image or selectively embed the message in noisy areas that draw less attention those areas where there is a great deal of natural color variation. The message may also be scattered randomly throughout the image. Redundant pattern encoding wallpapers the cover image with the message. A number of ways exist to hide information in digital images. We have concentrated on some techniques and methods which are divided into two types: Spatial Domain and Frequency Domain.

1.1. Spatial domain steganography

  Spatial domain techniques embed messages in the intensity of the pixels directly [6][7][8]. Least Significant Bit (LSB) is the first most widely used spatial domain steganography technique. It embeds the bits of a message in the LSB of the image pixels [9][10]. But the problem with this technique is that if the image is compressed then the embedded data may be lost. Thus, there is a fear for loss of data that may have sensitive information [11]. LSB has been improved by using a Pseudo Random Number Generator (PRNG) and a secret key in order to have private access to the embedded information [12]. The embedding process starts with deriving a seed for a PRNG from the user password and generating a random walk through the cover image that makes the steganalysis hard. Another recent improvement based on random distribution of the message was introduced by M. Bani Younes and A. Jantan [13]. Modulus arithmetic steganography proposed by Sayuthi Jaafar and Azizah A Manaf has calculated last four bits of each pixel by mod-16 operation. Then these bits are replaced with data bits [8]. In this the amount of the data that can be embedded is more but stego image has less PSNR value than LSB and SSB-4 techniques.

1.2. Frequency domain steganography

     In frequency domain, images are first transformed and then the message is embedded in the image [17][18][19]. When the data is embedded in frequency domain, the hidden data resides in more robust areas, spread across the entire image, and provides better resistance against statistical attacks. There are many techniques used to transform image from spatial domain to frequency domain. The most common frequency domain method usually used in image processing is the 2D discrete cosine transform [20][21]. In this technique the image is divided into 8×8 blocks and DCT transformation on each block is performed. DCT arranged the pixel of image according to their frequency value. The data bits are embedded in the low frequency coefficients of DCT. SSB-4 & DCT steganography proposed by Nedal M. S. Kafri and Hani Y Suleiman uses DCT approach with SSB-4 technique [21]. But in this stego image PSNR value is not so high. To improve it, a novel LSB & DCT based steganographic method for is proposed in this paper, which can not only preserve good image quality, but also

resist some typical statistical attacks.

2.   Proposed steganography method

The challenge in this work was to find a way to camouflage a secret message in an image without perceptible degrading the image quality and to provide better resistance against steganalysis process. Therefore, a combination of frequency domain by means of DCT and LSB technique of spatial domain steganography has been used to hide data. Two dimensional DCT converts the image block from spatial domain to frequency domain and then data bits are embedded by altering LSB of DCT coefficients is shown in fig.1.
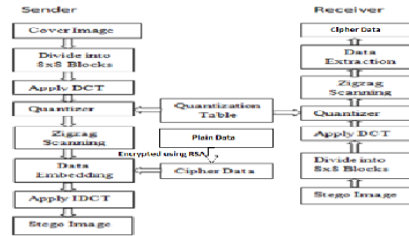
Figure: 1. Block diagram of LSB-DCT steganography

2.1. Discrete Cosine Transform

The image of size M×N is divided into 8×8 blocks and two dimensional (2-D) DCT is performed on each block. The DCT is calculated using equation 1:

$$F(u,v)=\frac{1}{4}C(u)C(v)\sum_{x=0}^{7}\sum_{y=0}^{7}f(x,y)\cos\left[\frac{\pi(2x+1)u}{16}\right]\cos\left[\frac{\pi(2y+1)v}{16}\right]$$ (1)

for x=0,..., 7 and y=0,..,7

$$\text{where } C(k)=\begin{cases}1/\sqrt{2} & \text{for } k=0 \\ 1 & \text{otherwise}\end{cases}$$

In DCT block lower frequency cofficents are at upper left positions and high frequency coefficients are lower right positions. Low frequency coefficients are of larger value than high frequency coeffcients. An example of a 8×8 block of DCT cofficient is shown in fig. 2.

Figure: 2.   DCT coefficient   Figure: 3.   Quantization Matrix

2.2. Quantization

The 8 x 8 block of DCT coefficients is compressed by quantization. A useful feature in this process is the image compression and quality is obtainable through selection of specific quantization table. The standard quantization matrix [27] is shown in fig. 3.

Quantization is achieved by dividing each element in the DCT coefficient block by the corresponding value in the quantization matrix, and the result is rounded to the nearest integer. As eye is not able to discern the change high frequency components so these can be compressed to larger extent. Lower right side components of quantization matrix are of high value so that after quantization high frequency components become zero.   The quantized DCT coefficients matrix P is computed by equation (2) and shown in fig. 4.

P (u, v) = F (u, v) / Q (u, v)   (2)

$$P = \begin{bmatrix} 10 & 4 & 2 & 5 & 1 & 0 & 0 & 0 \\ 3 & 9 & 1 & 2 & 1 & 0 & 0 & 0 \\ -7 & -5 & 1 & -2 & -1 & 0 & 0 & 0 \\ -3 & -5 & 0 & -1 & 0 & 0 & 0 & 0 \\ -2 & 1 & 0 & 0 & 0 & 0 & 0 & 0 \\ 0 & 0 & 0 & 0 & 0 & 0 & 0 & 0 \\ 0 & 0 & 0 & 0 & 0 & 0 & 0 & 0 \\ 0 & 0 & 0 & 0 & 0 & 0 & 0 & 0 \end{bmatrix}$$

$$\begin{bmatrix} 0 & 1 & 5 & 6 & 14 & 15 \\ 2 & 4 & 7 & 13 & 16 \\ 3 & 8 & 12 & 17 \\ 9 & 11 & 18 \\ 10 & 19 \\ 20 \end{bmatrix}$$

Figure: 4.Quantized DCT Block   Figure: 5.   Zigzag scan order

2.3. Zigzag Scanning

Although the DCT coefficients have been decorrelated by DCT transform to some extent, DCT coefficients in the same block are still not independent, which is called as intra-block correlation [16]. While neglecting the impact of block edge, the general trend in magnitude of the block coefficients in each block is non-increasing along *zigzag* scan order. After block DCT coefficients are arranged by zigzag scan pattern, dependencies among neighboring coefficients in both horizontal and vertical directions can be conveniently investigated [23]. For example, the sequence pairs (5,6) and (14,15) describe the correlations along horizontal direction, while the sequence pairs (2,3) and (10,20) describe correlations along vertical direction. Zigzag scan converts 8×8 block into 64 elements one dimensional array.

2.4. Data embedding

Data bits are concealed by altering the LSB of elements of zigzag array.
   a)   If data bit is '0', then make the DCT coefficient even or,
   b)   If the data bit is '1', then make the DCT coefficient odd.

2.5. Dequantization and inverse DCT

After embedding data zigzag array is again converted into 8×8 block. These blocks are dequantized and inverse DCT is performed. The entire 8×8 blocks are combined to form the stego image which is then sent to receiver. Complete embedding algorithm is given as follow:

Input: An M×N size cover image and data to be concealed.
Output: Stego image.
Step 1: Divide the cover image into 8×8 blocks. Step 2: Perform 2-D DCT on each block.
Step 3: Perform quantization on each block.
Step 4: Perform zigzag scan to convert 8×8 block into one dimensional array.
Step 5: Replace the LSB of DCT coefficients with data bits. Step 6: Convert 1-D zigzag array back to 8×8 block.
Step 7: Perform Inverse DCT on each block.
Step 8: Combine all the blocks to form stego image.

2.6. Extraction of secret message

The stego-image is received in spatial domain. Now stego image is divided into 8×8 blocks and DCT is performed on each block. Then scan the DCT block in zigzag way and extract the embedded data. Extraction algorithm is given as follows:

Input: Stego image.
Output: Secret message.
Step 1: Divide the stego image into 8×8 blocks.
Step 2: Perform 2-D DCT on each block.
Step 3: Perform quantization on each block.
Step 4: Perform zigzag scan to convert 8×8 block into one dimensional array.
Step 5: Check the DCT coefficient.
   a)   If DCT coefficient is even then data bit is 0 or,
   b)   If DCT coefficient is odd then data bit is 1.
Step 6: Concatenate the bits to obtain secret message and display it on screen.

2.7. Proposed Work

Our work also deals with the security of text messages at the time of sending it over the network. In our algorithm, we have used asymmetric key (RSA method) in cryptography which means public and private keys are needed to encrypt and decrypt the data. Encryption and decryption provide privacy. With RSA, message is encrypted using public and private keys of Sender and receiver. Encrypted message is hide into images using LSB & DCT.

3.   Experimental Results

Since the visual detection of stego images is depending on the nature of the image [24], so, varieties of image categories are utilized in the experiments. In order to have significant results. Images are divided into five categories: Tree, Dog, Monkey, Flower and Mountains. The experimental image data set consists of 60 JPEG images, 12 images for each category were used in experiments, which were taken by digital camera. We focused on short messages with length of 1500 bits because they are the most challenging to detect [24]. In addition to proposed steganography and cryptography techniques, for comparison purposes. In order to evaluate the quality of stego file/Images shown in fig. 6, generated by compared techniques.
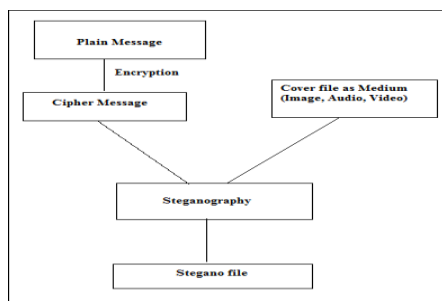
Figure: 6. stego files/Images

	PSNR Value			
	Modulus	*LSB-1st bit*	*LSB-4th bit*	*LSB-DCT*
Mountain.j	46.32	60.10	52.73	55.43
Dog.jpg	48.54	62.34	53.43	57.48
	47.69	61.34	51.85	55.78
Flower.jpg	48.64	63.46	52.57	56.51
Tree.jpg	47.33	63.59	52.41	57.44

Table 1. Comparative analysis of PSNR values of different steganography techniques

In this paper the stego image qualities are represented by Peak signal to noise ratio (PSNR). The implementations of the compared techniques (Modulus arithmetic (mod-16), 1- LSB, 4-LSB, and DCT with LSB) and the PSNR tests were carried out using MATLAB is a numerical computing environment and fourth-generation programming language. To calculate PSNR, first MSE is calculated using equation 3:

$$MSE = \frac{1}{mn} \sum_{i=0}^{m-1} \sum_{j=0}^{n-1} \|I(i,j) - K(i,j)\|^2$$

(3)

Where MSE is the Mean Squared Error of Original image (I) and stego image (K). Thereafter PSNR value is calculated using equation 4:

$$PSNR = 10.log_{10}\left(\frac{MAX_i^2}{MSE}\right) = 20.log_{10}\left(\frac{MAX_i}{\sqrt{MSE}}\right)$$

(4)

Where, MAX_i is the maximum pixel value of the image. In other words $MAX_i = 2^b - 1$, where b is the bit depth of the original image (e.g., MAX_i = 255 in the case of 8 bits depth grayscale images). PSNR computes the peak signal to noise ratio, in decibels, between two images. This ratio is used as a quality measurement between two images. The comparative analysis of PSNR value of different steganography technique, given in table 1, shows that LSB-DCT steganography has better image quality of stego image than other techniques.

4.   Discussion

The obtained experimental results is shown in fig 7. indicate that, the proposed method will be a good and acceptable steganogaphy scheme. Random steganography using LSB & DCT with asymmetric keys gives us more security than simple LSB & DCT method, where it is difficult to identify the hidden data in the stego image at specific location.

| Original Image | After Insertion Using LSB-1st bit Average (PSNR=64.59dB) | After Insertion Using LSB-4th bit Average (PSNR = 52.41 dB) | After Insertion Using LSB & DCT Average (PSNR=57.44 DB) |

Figure 7. Original tree Image,Stego Images Using 1-LSB,4-LSB and proposed scheme LSB and DCT Steganography

5. Conclusion

In this paper a mixed approach that applies the spatial domain with the frequency domain of steganography techniques and Asymmetric key cryptography. The idea is to utilize a significant bit of the DCT coefficients of a cover image to hide encrypted message bits. Thereafter, the information and the variation of the coefficients, affected by the embedding process, are spread in the stego image by utilizing the inverse of the DCT process. Steganography has its place in security.

References

[1]   DES Encryption Standard (DES), National Bureau of Standard (U.S.).Federal Information Processing Standards Publication 46, National Technical Information Service, Springfield, VA, 1997.

[2]   Daemen J., and Rijmen, V. "Rijndael: The Advanced Encryption Standard", Dr. Dobb's Journal, March 2001.

[3]   R. Rivest, A. Shamir, and L. Adleman, "A method for obtaining digital signatures and public-key cryptosystems". Communication of the ACM, pp. 120-126, 1978.

[4]   Pfitzmann, B. "Information hiding terminology", Proc. First Workshop of Information Hiding Proceedings, Cambridge, U.K., Lecture Notes in Computer Science, Vol.1174, pp. 347-350, 1996.

[5]   H & Wang, S, "Cyber warfare: Steganography vs. Steganalysis", Communications of the ACM, 47, pp.10-12, October 2004

[6]   Chan, C.K. and Cheng. L.M. "Hiding data inimage by simple LSB substitution. Pattern Recognition", 37, pp. 469 – 474, 2004.

[7]   Chang,C.C and Tseng, H.W. "A Steganographic method for digital images using side match". Pattern Recognition Letters, 25, pp. 1431 –

       1437, 2004.

[8]   Sayuthi Jaafar, Azizah A Manaf, Akram M Zeki, "Steganography Technique using Modulus Arithmetic", 9th International Symposium on Signal Processing and Its Applications, pp. 1 – 4, April 2007.

[9]   W. Bender, D. Gruhl, N. Morimoto, and A. Lu, "Techniques for Data Hiding", I.B.M. Systems Journal, 35(3-4): pp. 313-336, 1996.

[10]   N. Nikolaidis, and I. Pitas, "Robust Image Watermarking in the Spatial Domain", Signal Processing, 66(3), pp. 385-403, 1998

[11]   T. Morkel, J. Eloff, and M. Olivier, "An overview of image steganography", In Proceedings of the Fifth Annual Information Security South Africa Conference (ISSA2005), (Sandton, South Africa, Jun/Jul. 2005).

[12] J. Fridrich, M. Goljan, " Steganalysis of JPEG Images: Breaking the F5 Algorithm", Publisher: Springer Berlin, Heidelberg, Lecture Notes in Computer   Science, Vol. 2578, pp 310-323, 2003.

[13] M. A. Bani Younes, A. Jantan, "A New Steganography Approach for Image Encryption Exchange by Using the Least Significant Bit Insertion", IJCSNS, International Journal of Computer Science and Network Security, Vol. 8 No. 6, June 2008.

[14]   J. Rodrigues, J. Rios, and W. Puech "SSB-4 System of Steganography using bit 4", In International Workshop on Image Analysis for Multimedia WIAMIS, May, 2005.

[15]   J. Fridrich, and M. Goljan, "Practical steganalysis: state-ofthe-art", In Proceeding of SPIE Photonics West, Electronic Imaging 2002, volume 4675, pp. 1-13, 2002.

[16] Tu C. and Tran T D. "Context based entropy coding of block transform coefficients for image compression", IEEE Transaction on Image Processing, Vol.11, No.11, November, 2002.

[17]   Wenqiong Yu, "Blind Detection for JPEG Steganography", International Conference on Networking and Information Technology , pp. 128-132, July 2010.

[18]   Chung, K.L., Shen, C.H. and Chang, "A novel SVD- and VQ-based image hiding scheme".Pattern Recognition Letters, 22, pp. 1051 – 1058, 2001.

[19] Iwata M., Miyake K., and Shiozaki, "Digital Steganography Utilizing Features of JPEG Images", IEICE Transfusion Fundamentals, E87-A, 4, pp. 929 – 936,   2004.

[20]   M. Kharrazi06, H. Sencar, and N. Memon, "Performance study of common image steganography and steganalysis techniques," Communications of the   SPIE and IS&T, 15, No.4, pp. 1017-9909, Oct- Dec., 2006.

[21]   Nedal M.S. Kafari, Hani Y. Suleiman, "Bit-4 of Frequency Domain DCT Steganography Technique", FIRST NATIONAL CONFERENCE ON NETWORKED DIGITAL TECHNOLOGIES, PP. 286-291, 2009.

[22]   Dr. Ekta Walia, Payal Jain, Navdeep, "An Analysis of LSB & DCT based Steganography", Global Journal of Computer Science and Technology, Vol. 1, pp. 4-8, April, 2010.

[23]   Zhiping Zhou and Maomao Hui,   "Steganalysis for Markov Feature of Difference Array in DCT Domain", Proceedings of Sixth International

 Conference on Fuzzy Systems and Knowledge Discovery, pp. 581- 584 , Aug. 2009.

[24] L. Davidson, and P. Goutam, "Locating secret message in images", In ACM SIGKDD international conference on Knowledge discovery and data   mining, (Seattle, Washington, Aug.22-25. ACM 1-58113-888-1, 2004.

[25]   Gonzalez, R.C. and Woods, R.E., Digital Image Processing using MATLAB, Pearson Education, India,2006.

[26]   Jayaraman, S., Esakkirajan, S. and Veerakumar, T. Digital Image Processing, Tata McGraw Hill Education Private Limited, India, 2009.

[27]   www.vision.arc.nasa.gov/dctune/

[28]   S. Dickman, An Overview of Steganography, Research Report JMU-   INFOSEC-TR -2007-002, James Madison Univer- sity, July, 2007.

Implementation of AMBA AHB protocol for Wide Narrow BUS-SLAVE combination using VHDL

Varsha vishwarkama[1]   Abhishek choubey[2]   Arvind Sahu[3]

M.Tech, Rkdf-Ist,Bhopal   Hod (Ec) Rkdf-Ist,Bhopal   Asst.Prof.Tieit,Bhopal

Abstract-
The Advanced Microcontroller Bus Architecture (AMBA) is an open System-on-Chip bus protocol for high-performance buses on low-power devices. In this paper we implement a simple model of AMBA and use model checking and theorem proving to verify latency, arbitration, coherence and deadlock freedom properties of the implementation. Typical microprocessor and memory verifications assume direct connections between processors, peripherals and memory, and zero latency data transfers. They abstract away the data transfer infrastructure as it is not relevant to the verification. However, this infrastructure is in itself quite complex and worthy of formal verification. The Advanced Microcontroller Bus Architecture1 (AMBA) is an open System-on-Chip bus protocol for high-performance buses on low-power devices. In this report we implement a simple model of AMBA and verify latency, arbitration, coherence and deadlock freedom properties of the implementation. The verification is conducted using a model checker for the modal **µ**-calculus **Lµ**, that
has been embedded in the HOL theorem prover [3]. This allows results from the model checker to be represented as **HOL** theorems for full compositionality with more abstract theorems proved in HOL using a formal model theory of **Lµ** that we have also developed [4].

Keywords: AMBA, VHDL, ASB, APB, DMA, EDAROM, RAM, System-on chip.

1. Introduction- AMBA is an open specification that specifies a strategy on the management of the functional blocks that sort system on chip (SoC) architecture. It is a high-speed, high-bandwidth bus that supports multi master bus management to get the most out of system performance.

The AMBA specification defines three buses:

➢ Advanced High-performance Bus (AHB): The AHB is a system bus used for communication between high clock frequency system modules such as processors and on-chip and off-chip memories. The AHB consists of bus masters, slaves, an arbiter, a signal multiplexor and an address decoder. Typical bus masters are processors and DMA devices.

➢ Advanced System Bus (ASB): The ASB is also a system bus that can be used as an alternative to the AHB when the high-performance features of AHB are not required.
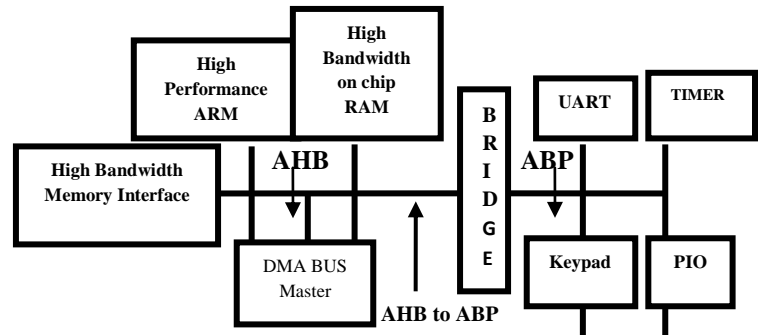
Fig 1 AMBA based microcontroller system

peripheral bus specialized for communication with low-bandwidth low-power devices. It has simpler interface and lower power requirements.

Designers can use either the AHB or the ASB in conjunction with the APB. The APB has a single bus master module that acts as a bridge between the AHB or ASB and the APB. The AMBA specification is hardware and operating system independent and requires very little infrastructure to implement. Figure 1 shows a typical AMBA-based microcontroller. We follow revision 2.0 of the AMBA specification.

2 AMBA APB- The APB is optimized for low power consumption and low interface complexity. It is used for connecting the high-band with system bus to low-bandwidth peripherals such as input devices. There is a single bus master, a single global clock and all transfers take two cycles. The bus master also acts as a bridge to the system bus, to which it can reconnect as a slave. The address and data buses can be up to 32 bits wide.

2.1 AMBA APB Specification-The operation of the APB consists of three stages, all of them are triggered on the rising edge of the clock:

1. IDLE. This is the initial and the default state of the bus when no transfer is under-way.

2. SETUP. The first stage of a transfer is a move to the SETUP state. The address, data and control signals are asserted during this phase but may not be stable. This stage always lasts for one clock cycle and then the operation moves to the ENABLE stage.

3. ENABLE. The address, data and control signals are stable during this phase. This phase also lasts one clock cycle and then moves to the SETUP or the IDLE stage depending on whether or not another transfer is required.

3 AMBA AHB- The AHB is a pipelined system backbone bus, designed for high-performance operation. It can support up to 16 bus masters and slaves that can delay or retry on transfers. It consists of masters, slaves, an arbiter and an address decoder. It supports burst and split transfers. The address bus can be up to 32 bits wide, and the data buses can be up to128 bits wide. As before, there is a single global clock. We choose to model the AHB rather than the ASB because the AHB is a newer design and also because it has been designed to integrate well with the verification and testing work flow.

3.1 AMBA AHB Specification-The operation of the AHB is too complex to be specified in terms of a few fixed stages. A simple transfer might proceed as follows (the list numbering below is not cycle accurate):

1. The AHB is in the default or initial state. No transfer is taking place, all slaves are ready and no master requires a transfer.
2. Several masters request the bus for a transfer.
3. The arbiter grants the bus according to some priority-scheduling algorithm.
4. The granted master puts the address and control information on the bus.
5. The decoder does a combinatorial decode of the address and the selected slave samples the address.
6. The master or the slave put the data on the bus and it is sampled. The transfer completes.

3.2 Granting bus access-The arbiter indicates which bus master currently the highest priority is requesting the bus by asserting the appropriate HGRANTx signal. When the current transfer completes, as indicated by HREADY HIGH, then the master will become granted and the arbiter will change the HMASTER **[3:0]** signals to indicate the bus master number. The arbiter changes the HGRANTx signals when the penultimate (one before last) address has been sampled. The new HGRANTx information will then be sampled at the same point as the last address of the burst is sampled.
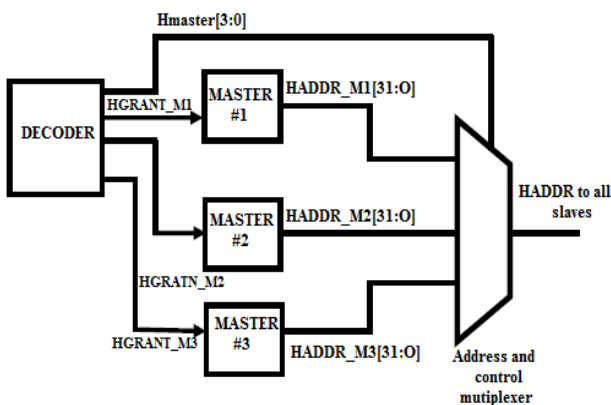
Fig. 3.1 HGRANTx and HMASTER signals are used in a system.

metal and the use of large on-chip memory blocks (such as Embedded DRAM) are driving factors which encourage the use of wider on-chip buses. Specifying a fixed width of bus will mean that in many cases the width of the bus is not optimal for the application. Therefore an approach has been adopted which allows flexibility of the width of bus, but still ensures that modules are highly table between designs.

The protocol allows for the AHB data bus to be *8, 16, 32, 64, 128, 256, 512 or 1024-*bits wide. However, it is recommended that a minimum bus width of 32 bits is used and it is expected that a maximum of 256 bits will be adequate for almost all applications. For both read and write transfers the receiving module must select the data from the correct byte lane on the bus. Replication of data across all byte lanes is not required.

3.4 AMBA AHB signal list -This section contains an overview of the AMBA AHB signals. All signals are prefixed with the letter H, ensuring that the AHB signals is differentiated from other similarly named signals in a system design.

Name	Source	Description
HCLK Bus clock	Clock source	This clock times all bus transfers. All signal timings are related to the rising edge of HCLK.
HRESETn Reset	Reset controller	The bus reset signal is active LOW and is used to reset.
HADDR [31:0]	Master	The 32-bit system addresses bus.
HTRANS [1:0]	Master	Indicates the type of the current transfer, which can be..
HWRITE Transfer direction	Master	When HIGH this signal indicates a write transfer and when LOW a read transfer.
HSIZE [2:0] Transferse	Master	Indicates the size of the transfer, which is typically byte (8-bit), halfword (16-bit) or word (32-bit).
HBURST [2:0]	Master	Indicates if the transfer forms part of a burst.
HPROT [3:0]	Master	The protection control signals provide additional information
HWDATA [31:0] Write data	Master	The write data bus is used to transfer data from the bus master to the bus slaves during write operations.
HSELx	Decoder	Each AHB slave has its own slave

Slave select		select signal and this signal indicates that the current
HRDATA	Slave	The read data bus is used to transfer data from bus slaves to the bus master during read operations.
HREADY Transfer done	Slave	When HIGH the HREADY signal indicates that a transfer has finished on the bus.
HRESP [1:8]	Slave	The transfer response provides additional information on the status of a transfer.

3.5 Implementing a wide slave on a narrow bus-A wide slave being implemented on a narrow bus. Again only external logic is required and hence predesigned or imported blocks can be easily modified to work with a different width of data bus. Bus masters can easily be modified to work on a wider bus than originally intended, in the same way that the slave is modified to work on a wider bus, by:

• Multiplexing the input bus

• Replication of the output bus
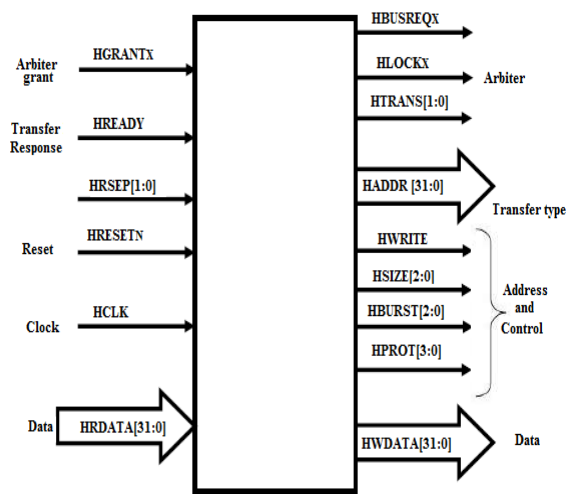
Fig.3.2 AHB bus master interface diagram

3.6 Implementing a narrow slave on a wider bus-A slave module, which has been originally designed to operate with a 32-bit data bus, can be easily converted to operate on a wider 64-bit bus. This only requires the addition of external logic, rather than any internal design changes, and therefore the technique is applicable to hard macrocells.

4 Results On Modelsim Using Xilinx Ise And Vhdl - The overall coding part can be writing on VHDL and simulate on ModelSim

4.1 Simulation Result of Slave 1-This simulation result contains the signal haddr =00100000, which shows that the master1 sending the address and control signals on the bus after the rising edge of the clock.Also the signal hlock1=1,the master1 requires locked access to the bus and no other master should be granted the bus until this signal is low.
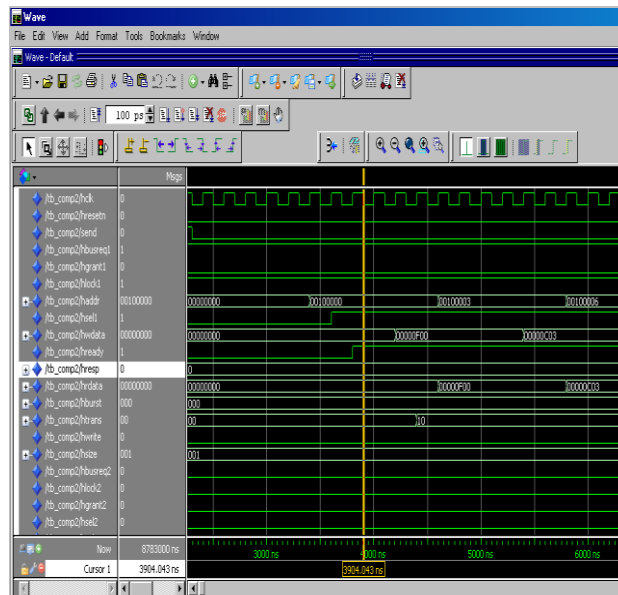
Fig.5.4 Simulation Result for the selection of slave1 and data transfer
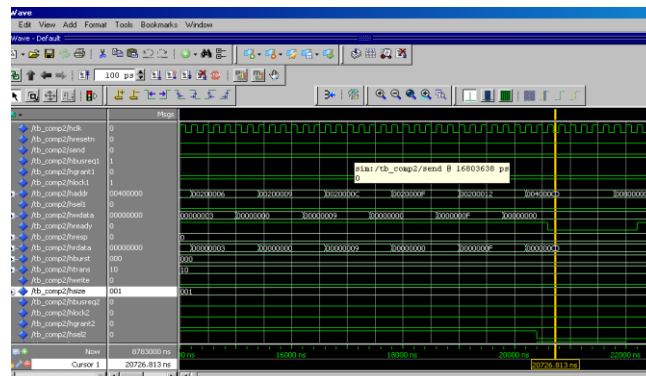
Fig.5.7 Simulation Result for wait state when hready=0

5. CONCLUSION - In this thesis we observe that the data transfer operation from one memory to another memory is fast as compared to serial communication by proposing the parallel communication in **AMBA AHB**. It also provides the opportunity to use master and slave up to 16 nos. and the data of every master is read and write simultaneously. In this implementation delay period is 4.33 ns and the clock period is 8.66 ns and frequency increases up to 115.401MHz..Here **AMBA AHB** supports the data transfer by reducing the time and increases the frequency of the bus to increase the system performance. The use of high capacity memory management with the **AMBA AHB** in this thesis successfully attempted to find the software solution for the problem of memory compliant in the microcontroller. The proposed implementation is capable of running in any PC with Xilinx and Modelsim EDA tools and FPGA board. This implementation able to sustain the external memory bandwidth, on which the CPU, on-chip memory and other direct memory access devices reside. This implementation supports external memory up to 2GB.

REFERENCES –

[1] "AMBA specification (Rev2.0)", ARM Inc.

[2] Hu Yueli,Yang Ben "Building an AMBA AHB compliant Memory Controller" in 2011.

[3] Ashutoshku.Singh, Anurag Shrivastava, G.S.Tomar" Design and Implementation of High Performance AHB Reconfigurable Arbiter for on-chip Bus Architecture "in 2011.

[4] Wei Chipin,Li Zhaolin,Zheng Qingwei,Ye Jianfei, Li Shenglong"Design of Configurable Multichannel Interrupt Controller "in 2010.

[5] Yi Zhiqiang, Li Yun"On Chip Bus Design for HDTV SOC Decoder" in 2010.

[6] Ramesh Bhakthatchalu, Deepthy G R, Shanooja S. "Implementation of Reconfigurable Open Core Protocol Complaint Memory System using VHDL" in 2010.

[7] Zhichao Zhang, Wuchen Wu "UART integration in OR1200 based SOC design" in 2010.

[8] Purvi D. Mulani "SOC Level Verification Using System Verilog" in 2009.

[9] Guoling Ma, Hu He "Design and Implementation of an Advance DMA Controller on AMBA-Based SOC "in 2009.

Host Based Information Gathering Honeypots for Network Security

M. Purushotham Reddy[1], K. Subba Reddy[2], M. Indra Sena Reddy[3], G. Sreenivasulu Reddy[4]

[1,4]Dept. of Computer Science and Engineering, VBIT, Proddatur, Kadapa, A.P, India.
[2, 3]Dept. of Computer Science and Engineering CSE, RGMCET , Nandyal, Kurnool (Dt), A.P, India.

Abstract

 Honeypots are an exciting new technology which is widely used in the areas of computer and Internet security that, allows us to turn the tables on the bad guys. It is a resource, which is intended to be attacked and computerized to gain more information about the attacker, and used tools. Compared to an intrusion detection system, honeypots have the big advantage that they do not generate false alerts as each observed traffic is suspicious, because no productive components are running in the system. The goal of *this* paper is to show the possibilities of honeypots and their use in research as well as productive environment.

Keywords: Levels of honeypots, Internet security, Network traffic, Firewall authentication.

1. INTRODUCTION

The concept of "honeypots" has been introduced in computing systems by Clifford Stoll in the late 80's. In the 'Cuckoo's Egg' [1], described the monitoring and tracking of an intruder. In the 90's, Cheswik implemented and deployed a real "honeypot" [2]. Bellovin discussed the very same year the advantages and problems related to its usage [3]. In 98, Grundschober and Dacier ([4, 5]) introduced the notion of "sniffer detector" , one of the various forms of what is called today a "honeytoken".   Lance Spitzner, a senior security architect for Sun Microsystems is the author of "Honeypots, Tracking hackers" [6]. "A honeypot is security resource whose value lies in being probed, attacked or compromised." [6, page 40] .This is the most common definition and many papers refer to it [7, 8]. However its precise meaning is not so clear. If we take a deeper look at it, we see that the definition can be decomposed as follows:

* One term: « a security resource »
* A subordinate description: "its value which lies in being probed, attacked or compromised" .

 This is the exact opposite of most production systems, which you do not want to be probed or attacked." [6, page 40] .In [6, page 42], the following example of a honeypot deployment is given: an old and unused server in the DMZ is closely watching any traffic to or from it. According to L.Spitzner, the server is here to "determine if there is any unauthorized activity happening within the DMZ". Can we reasonably call this machine a security resource? Furthermore, what happens if it logs nothing? According to lance Spitzner "if the system is never probed or attacked, then it has a little or no value". Reto Baumann, a Swiss engineer, discusses in [9] Lance Spitzner's interpretation. His definition slightly differs from the previous one: "A honeypot is a resource which pretends to be a real target. A honeypot is expected to be attacked or compromised. The main goals are the distraction of an attacker and the gain of information about an attack and the attacker." [9]

Many documents refer to Lance Spitzner's definition. Some of them adapt it to a more restrictive usage. This is the case of searchWebservices.com, a commercial portal on IT services. They suggest this one [10]: "A honeypot is a computer system on the Internet that is expressly set up to attract and "trap" people who attempt to penetrate other people's computer systems. (This includes the hacker, cracker, and script kiddy.) Maintaining a honey pot is said to require a considerable amount of attention and may offer as its highest value nothing more than a learning experience (that is, you may not catch any hackers)." [10] This definition is quite restrictive. First and foremost honeypots are not reserved to the Internet usage. They can be implemented to reveal internal attacks. In addition some of them are not 'expressively set up to attract'. One simple example consists in putting a basic Honeyd machine into the DMZ. It is likely to be scanned and attacked but it is not "expressly set op to attract people".

The niversity of Wisconsin-Platteville (http://www.uwplatt.edu/) as well as R.C. Barnett from the sourceforge.net web site ([11]) mentions the following definition:

"An Internet-attached server that acts as a decoy, luring in potential hackers in order to study their activities and monitor how they are able to break into a system. Honeypots are designed to mimic systems that an intruder would like to break into but limit the intruder from having access to an entire network. If a honeypot is successful, the intruder will have no idea that s/he is being tricked and monitored." [11] .Last definition we propose is suggested by the SANS Institute [12]. It appears in an article written by Michael Sink in April 2001: "The use of Honeypots and Packet Sniffers for Intrusion Detection" [13]:

"Within the realm of computer security, a honeypot is a computer system designed to capture all traffic and activity directed to the system. While honeypots can be set up to perform simple network services in conjunction with capturing network traffic, most are designed strictly as a "lure" for would-be attackers. Honeypots differ from regular network systems in that considerably greater emphasis is placed on logging all activity to the site, either by the honeypot itself or through the use of a network/packet sniffer. A honeypot is designed to look like something an intruder can attack to gain access to a given system." [13]

The problem with this definition is that it is rather verbose and vague. It characterizes honeypots from "regular network systems" as those that place "considerably greater emphasis on logging all activity". But many systems can be designed to capture traffic and activities. What does 'greater' exactly mean? A firewall which logs connections or an application that stores history may be considered as honeypot. The definition is very broad as many computer systems are collecting activities and traffic directed to them.

2. Honeypot Basics

A honeypot is a resource whose value is being in attacked and compromised. This means, that a honeypot is expected to get probed, attacked and potentially exploited.

Honeypot do not fix anything. They provide us additional, valuable information.

A honeypot is a resource, which pretends to be real target. A honeypot is expected to be attacked or compromised. The main goals are the distraction of an attacker and the gain of the information about the attack and the attacker.

Value of honeypots:

There are two categories of honeypots.

- Production honeypots
- Research honeypots

A production honeypot is used to help migrate risk in an organization while the second category, is meant to gather as much information as possible. These honeypots do not add any security value to an oraganition, but they can help to understand the blackhat community and their attacks as well as to build some better defenses against security threats. A properly constructed honeypot is put on a network, which closely monitors the traffic to and from the honeypot. This data can be used for a variety of purposes.

- Forensics: alyzing new attacks and exploits
- Trend analysis:look for changes over time of types of attacks,techniques,etc
- Identification: track the bad guys back to their home machines to figure out who they are.
- Sociology:learn about the bad guys as a group by snooping on email,IRC traffic,etc which happens to traverse the honeypot.

In general every traffic from and to a honeypot is unauthorized activity. All the data that is collected by a honeypot is therefore interested data. Data collected by the honeypot is of high value, and can lead to better understanding and knowledge which in turn can help to increase overall network security. One can also argue that a honeypot can be used for prevention because it can deter attackers from attacking other systems by occupying them long enough and bind their resources.

2.1 Low-involvement honey

A low-level involvement honeypot typically only provides certain fake services. In a basic form, these services could be implemented by having a listener on specific port.

In such a way, all incoming traffic can easily be recognized and stored. With such a simple solution it is not possible to catch communication of complex protocols. On a low-level honeypot there is no real operating system that attacker can operate on. This will minimize the risk significantly because the complexity of an operating system is eliminated. On the other hand, this is also disadvantage. It is not possible to watch an attacker interacting with operating system, which could be really interesting. A low-level honeypot is like one-way connection. We only listen, we do not ask any questions.
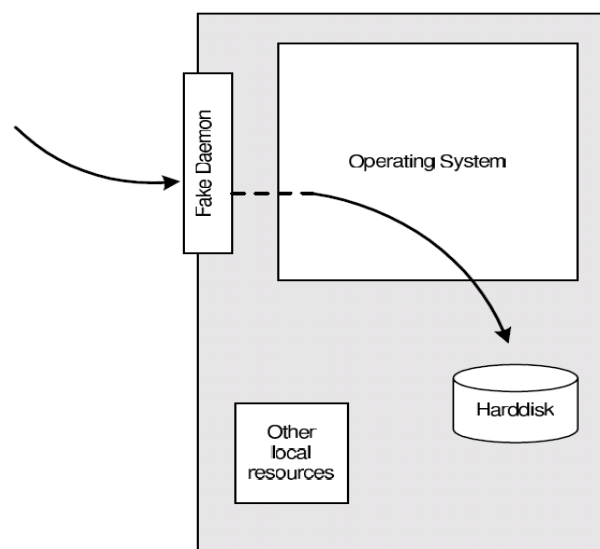
Figure 1. Low-involvement honeypot

2.2. Mid-involvement honeypot

A mid-involvement honeypot provides more to interact with but still does not provide a real underlying operating system. The fake daemons are more sophisticated and have deeper knowledge about the specific services they provide. At the same moment, the risk increases. The probability that attacker can find a security hole or vulnerability is getting bigger because the complexity of honeypot is increasing.

Through the higher level of interaction, more complexity attacks are possible and can therefore be logged and analysed. The attacker gets a better illusion of a real operating system. He has more possibilities to interact and probe the system. Developing a mid-involvement honeypot is complex and time consuming. Special care has to be taken for security check as all developed fake daemons need to be as secure as possible.
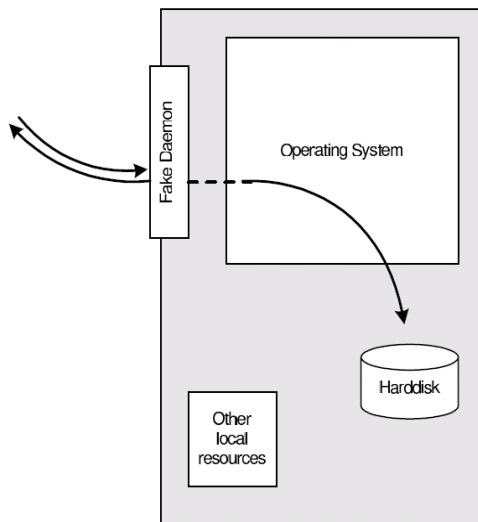
Figure 2. Middle level-involvement honeypot

2.3.High-involvement honeypot

A high-involvement honeypot has a real underlaying operating system. This leads to much higher risk as the complexity increases rapidly. At the same time, the possibilities to gather the information, the possible attacks as well as the attractiveness increase a lot. As soon as a hacker has gained access, his real work and therefore the interesting part begins.

A high-involvement honeypot is very time consuming. The system should be constantly under surveillance. A honeypot which is not under control is not of much help even become a danger or security hole itself. It is very important to limit a honeypot's access to local intranet, as the honeypot can be used by blackhats as if it was a real compromised system. Limiting outbound traffic is also important point to consider, as the danger once a system is fully compromised can be reduced.

By providing a full operating system to attacker, he has the possibilities to upload and install new files. This is where the high-involvement honeypot can show its strength, as all its actions can be recorded and analyzed.
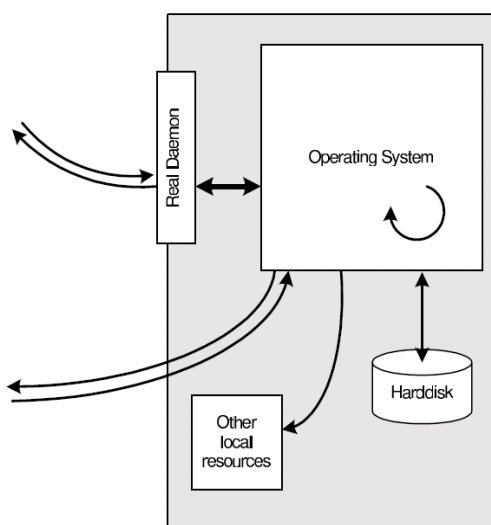
Figure 3. High level-involvement honeypot

	Low	Mid	High
Degree of involvement	low	mid	high
Real operating system	-	-	√
Risk	low	mid	high
Information gathering	connections	requests	all
Compromise wished	-	-	√
Knowledge to run	low	low	high
Knowledge to develop	low	high	mid-high
Maintenance time	low	low	very high

Figure 4. Details of honypot at different levels

Honeypot location:

A honeypot does not need a certain surrounding environment, as it is a standard server with no special needs. A honeypot can be placed anywhere a server could be placed. But certainly, some places are better for certain approaches as others.

A honeypot can be used on the Internet as well as the intranet, based on the needed service. placing a honeypot on the intranet can be useful if the detection of some bad guys inside a private network is wished. If the main concern is the Internet, a honeypot can be placed at two locations:

1. In front of firewalls(Internet)
2. DMZ
3. Behind the firewall(Intranet)

By placing the honeypot in front of firewall the risk for the internal works does not increases. A honeypot will attract and generate lot of unwished traffic like port scans or attack patterns. By placing a honeypot outside the firewall, such events do not get logged by the firewall and an internal IDS system will not generate alerts. Otherwise a lot of alerts would be generated on the firewall or IDS.

Probably the biggest advantage is that the firewall or IDS,as well as any other resources, have not to be adjusted as the honeypot is outside the firewall and viewed as any other machine on the external network. Running a honeypot does therefore not increase the dangers for the internal network nor does it introduce new risks.

The disadvantage of placing a honeypot in front of the firewall is that internal attackers cannot be located or trapped that easy. Placing a honeypot inside DMZ seems a good solution as long as the other systems inside the DMZ can be secured against the honeypot.Most DMZs are not fully accessible as only needed services are allowed to pass the firewall. In such a case, placing the honeypot in front of the firewall should be favored as opening all corresponding ports on the fire is too time consuming and risky.

A honeypot behind a firewall can introduce new security risks to the internal network, especially if the internal network is not secured against the honeypot through additional firewalls. This could be a special problem if the Ips are used for authentication. By placing the honeypot behind a firewall, it is inevitable to adjust the firewall rules if access from internet should be permitted. The biggest problem arises as soon as the internal honeypot is compromised by an external attacker. He gains the possibility to access the internal network through the honeypot.This traffic will be unstopped by the firewall as it is regarded as traffic to the honeypot only, which in turn is granted. Securing an internal honeypot is therefore mandatory, especially if it is a high-involvement honeypot. The main reason for placing a honeypot behind a firewall could be to detect internal attackers.

The best solution would be to run a honeypot in its own DMZ,therefore with a preliminary firewall. The firewall could be connected directly to the internet or intranet, depending on the goal. This attempt enables tight control as well as flexible environment with maximal security.
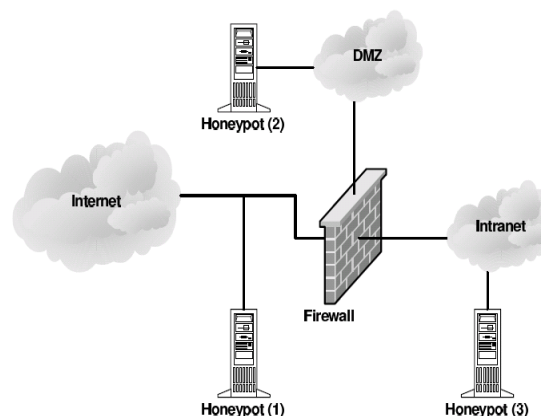
Figure 5. Firewalls involvement in honypot at different levels

3. HOST BASED INFORMATION GATHERING

This section will discussion possibilities that offer gain of information about ongoing on a honeypot by installing information gathering mechanisms on the honeypot itself.

Basic possibilities:
Information gathering facilities can basically be grouped into two categories; facilities that generates streams of information and facilities that offer the information to peek into the system and get the information about a certain state of the honeypot .

3.1. Microsoft windows
One could think the large amount of observed attacks on systems running ms windows operating system makes them ideal for the honeypot, but unfortunately the structure of these operating system makes the data gathering rather difficult. Until today the source code of the operating system of Microsoft is not freely available , which means that changes to the operating system are very hard to achieve.

B.Unix derivates:
Unix derivatives operating system offers interesting opportunities for deploying data gathering mechanisms since all of their components are available as source code.
Network based Information Gathering:Host based information gathering is always located at the host itself and is therefore vulnerable to detection and once detected it can also be disabled. Network based information gathering does not have to be located on the honeypot itself. It can also be implemented in an invisible way, as network traffic only gets analyzed but not manipulated. Network based information gathering is safer as it is harder to be detected and quiet impossible to disable.
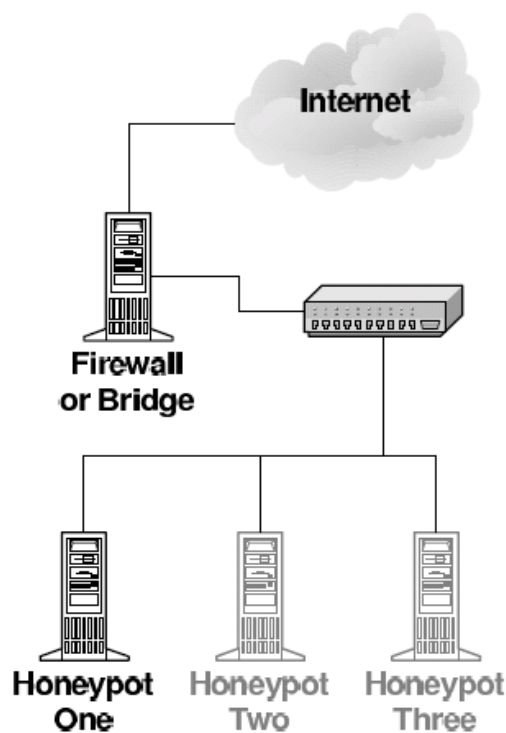
Figure 6. Firewall involvement in honypot

Dangers:
 Running a honeypot or honeynet is not something that should be underestimated- there are some dangers one must be aware of which basically are:
1.   Unnoticed takeover of the honeypot by an attacker
2.   Lost control over the honey pot installation.
3.   Damage done to third party.
Attractiveness:
Being the owner of a honeypot can be an interesting experience, but what if the members of the blackhat community do not find their way to the honeypot or, even more dramatically, are not interested in the honeyot at all. Another approach to lure attackers is the offering of the interesting services on the honeypot. Of course the question arises, what an interesting services is or what it should look like.

Advantages:

- Small Data sets→Honeypots only collect attack or unauthorized activity, dramatically reducing the amount of data they collect. Organizations that may log thousands of alerts a day may only log a hundred alerts with honeypots. This makes the data honeypots collect much easier to manage and analyze.
- Reduced False Positives→Honeypots dramatically reduce false alerts,as they only capture unauthorized activity.
- Catching False Negatives→Honeypots can easily identify and capture new attacks never seen before.
- Minimal Resources→Honeypots require minimal resources,even on the largest of networks.This makes them an extremely cost effective solution.
- Encryption→Honeypots can capture encrypted attacks.

Disadvantages:

- Single Data Point→Honeypots all share one huge drawback;they are worthless if no one attacks them. Yes,they can accomplish wonderful things,but if the attacker does not sent any packets to the honeypot,the honeypot will be blissfully unware of any unauthorized activity.
- Risk→Honeypots can introduce risk to your environment.As we discuss later,different honeypots have different levels of risk.Some introduce very little risk,while others give the attacker entire platforms from which to launch new attacks,Risk is variable,depending on how one builds and deploys the honeypot.

4. CONCLUSIONS

A honeypot is just a tool. How you use that tool is up to you. There are a variety of honeypot options, each having different value to organizations. We have categorized two types of honeypots, production and research. Production honeypots help reduce risk in an organization. Research honeypots are different in that they are not used to protect a specific oraganization. Instead they are used as a research tool to study and identify the threats in the Internet community. Regardless of what type of honeypot you use,keep in mind the 'level of interaction'. This means that the more your honeypot can do and the more you can learn from it, the more risk that potentially exists.You will have to determine what is the best relationship of risk to capabilities that exist for you.Honeypots will not solve an oraganization's security problems.Only best practices can do that.However,honeypots may be a tool to help contribute to those best practices.

5. References

1. C. Stoll, "Stalking the Wiley Hacker", Communications of the ACM, Vol. 31 No5. May 1988.
2. B. Cheswick, "An evening with Berferd in which a cracker is lured, endured and studied", Proc Winter USENIX Conference, San Francisco, Jan 20, 1992.
3. S. Bellovin, "There Be Dragons", Proc. of the Third Usenix Security Symphosium, Baltimore MD. Sept. 1992.
4. S. Grundschober, M. Dacier, "Design and Implementation of a Sniffer Detector", Recent Advances on Intrusion Detection Workshop (RAID98), 1998.www.raid-symposium.org/raid98/
5. S. Grundschober, "Sniffer Detector Report", Master Thesis, Eurecom Institute , June 1998, 50 pages, ref. Eurecom : CE-98/IBM/GRUN - Document number: 1914. Available on line: http://www.eurecom.fr/~nsteam/Papers/grundschober98.ps
6. L. Spitzner, "Honeypots: Tracking Hackers". Addislon-Wesley, ISBN from-321-10895-7, 2002.
7. E. Cole. Hackers Beware. New Riders Publishing 2001
8. R.Baumann. "White Paper: Honeypots". February 2002. Available on line: http://security.rbaumann.net/download/whitepaper.pdf
9. R. Baumann, C. Plattern. Honeypots, diploma thesis. Feb. 2002
10. Webservices commercial IT portal http://www.webservices.org/
11. Sourceforge home page: http://honeypots.sourceforge.net/
12. SANS Institute home page: http://ww.sans.org
13. M. Sink, « The Use of Honeypots and packet Sniffers for Intrusion Detection", Indiana University of Pennsylvania, April 2001. Available on line: http://www.lib.iup.edu/comscisec/SANSpapers/msink.htm

PULSE DIAGNOSIS BASED AUTOMATED DIAGNOSTIC SYSTEM

Mr. Bharat S. Shete[1*]
[1]Master of Technology. Department of Electronics
Rajarambapu Institute of Technology, Sakharale, M.S., India

Dr.Prof. A. B. Kakade[2]
[2]Asso. Prof. Department of Electronics
Rajarambapu Institute of Technology, Sakharale, M.S., India

Abstract- To diagnose disease, western medicine looks inside of patient's body using many devices such as MRI, city scan etc. but oriental medicine does not explore the root cause. Wrist is one of the best parts of our body to detect a pulse signal and in Ayurveda the wrist pulse has been used as a fundamental element for diagnosis. It has many properties and by perceiving these features, doctors can diagnose disease. Ayurveda is one of the most comprehensive healing systems in the world and has classified the body system according to the theory of Tridosha (vata, pitta, kapha) to overcome ailments. Diagnosis similar to the traditional pulse-based method requires a system of clean input signals, and extensive experiments for obtaining classification features. So we briefly describe our system of generating pulse waveforms and use various feature detecting methods to show that an arterial pulse contains typical physiological properties. By reading the signal from the sensors that are send to transmitters and amplifier and a DC (digitizer) for quantifying analog signal.

I. Introduction

Ayurveda is a traditional medicine and natural healing system in India. Pulse diagnosis instrument – "finding any disease using nadi pulse" is an automated system to find and dictate the disease and its related information of the human body.In ancient literatures, be it Ayurveda, Chinese, Unani, or Greek, pulse based diagnosis has its own unparalleled importance. The   organ   under   d istress is zeroed down by feeling the palpation from the three fingers (index, middle and ring) placed on the radial artery. These pulsations dictate the Physiological status of the entire human body. This is a tedious and inconvenient process and hence it takes years of practice to master this art Fig [1]. As a result this approach is
subjective in nature. The system is being evaluated by Ayurveda practitioners as an automated probable   disease output watcher. Fig [1] shows the Pulse diagnosis system followed by Ayurveda practitioners.
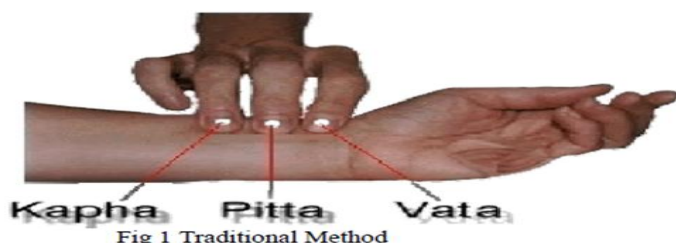

Fig 1 Traditional Method

Pulse has been ubiquitously accepted by modern clinicians as well. They examine the pulse using the method of trisection i.e. apply pressure until the pulse is maximal, and then vary pressure while concentrating on the phases of   the pulse. The arterial pulse variants (for example pulsus alternans, bisferiens pulse, bigeminal pulse) are basically used in detecting cardiac disorders. However, alternative medicine practitioners carefully examine pulses at different depths, each connected with a specific part of the body and each believed to register even the slightest physiological based changes. The main Objectives are: To provide a convenient and non-invasive computer aided device which will eliminate all the human errors performed manually by Indian medicine practitioners in the diagnosis of disease.Noi Kanipaan: Diagnose chronic diseases and other related information of the human body. To provide a device which is easy to use, uniform in diagnosis and by quick in response, which the performance will be based on accurate and quantitative information. Ayurveda meaning the 'science of life' believes that cosmos comprises of five basic elements - air, water, earth, fire and space. Human life is considered as a conglomeration of three humors (Vata, Pitta and Kapha), seven dhatus (tissues) and three mains (waste products). According to ancient literatures, any ailment in the body brings about a change in the constitution of these humors. These changes are then sensed by the fingers of a pulse examiner Fig [1]. In this paper we discuss our device, the three sensors of which simulate the human fingers to a large extent. In section II the instrumentall setup has been explained in detail. Section III describes the experiments conducted. The signal processing aspect has been dealt with in Section IV shows the results. References are drawn in Section V.

Ii. Automated Diagnose System
After the long literature study and discussion with the Ayurveda nadi practitioners we developed the electronic setup and nadi reading and dictate the probable disease from the readings that are read from the patients.
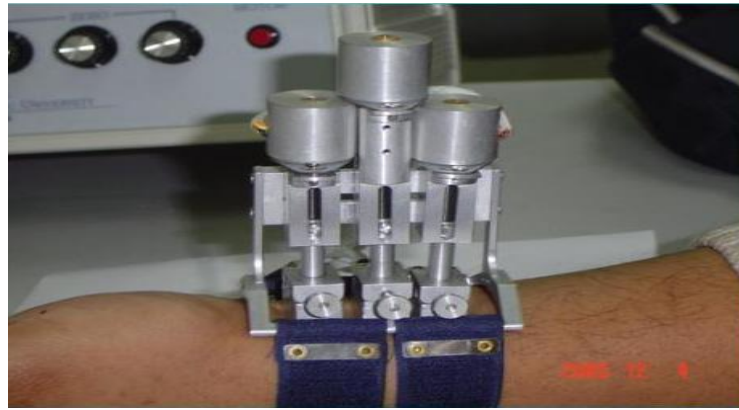
Fig 2 shows the setup of reading the (Vata, Pitta and Kapha)
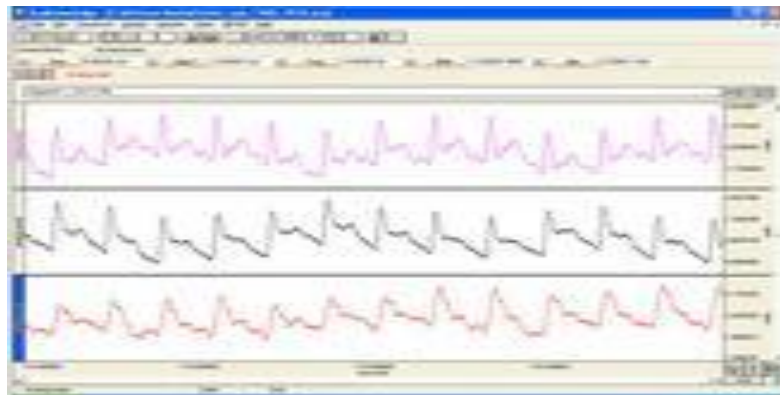
Fig 3 shows that our application plots the pulse graph per time.

1. Signals have been captured for a very small span of the (1-2 minutes) in most of the cases.
2. External pressure applied over the sensors varies while recording especially when a person holds them.
3. Motion artifacts become a reasonable consideration when the recordings are for a longer duration of time.
4. The system should remain steady and errors should not be incurred due to system malfunctioning. No noise should disrupt the nature of the signal.
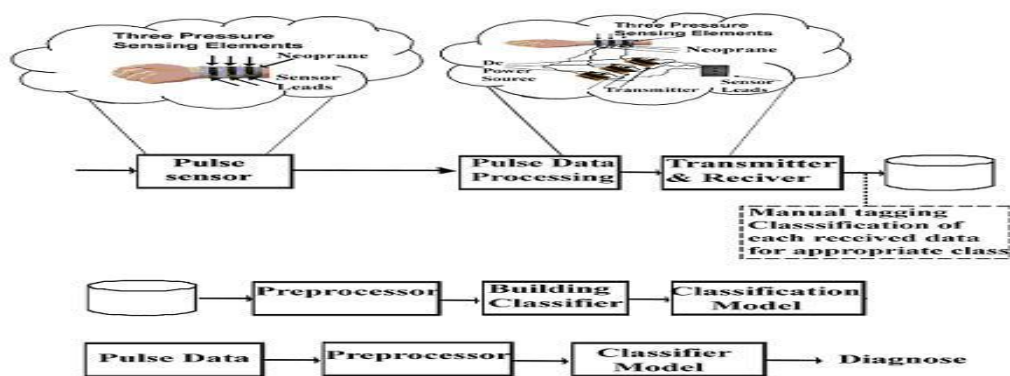
Fig 4 Block Diagram of Pulse diagnosis instrument.
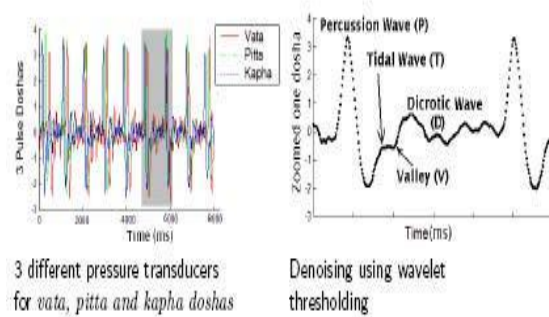
Fig 5 Sample Waveform

Our setup reads the amplified output from the electronic setup and digitizes the signal and the readings are observed by software DVSOFT. In our setup, we have tried to imitate the practitioner's fingers Fig(1). The system has three fingers like projections whose positions can be played with at the tip region to find out the best locations to capture the signal. Springs attached to them help in damping thus imitating the natural damping present due to muscles in the tip region of the practitioner's fingers (Fig 2). In our design, we proposed to use three identical piezo film based sensors to capture the waveform. The raw signal was filtered, amplified, and read by our software application then our DVSOFT software plots the graph according to the signals and dictates the probable disease and the ayurveda practioners can watch the graphs and perform prescribe the medicine for the patients.

Iii. Implementation

The system need to be test on over 200 students and people . We will chose 10 healthy volunteers to carry out the analysis. Here we are showcasing the variations of an individual when the signals were captured for the entire day.The volunteer was asked to relax for some time and the system was fixed on his wrist. The positions of the three sensors from which the signals were acquired correspond with the humor positions (Vata, Pitta and Kapha) in ayurveda. A pulse waveform is usually composed of important time domain features: percussion wave (P), tidal wave (T), valley (V) and dicrotic wave (D), as shown in Fig(5). These wave parts should be present in a standard pulse waveform with definite amplitude and time duration to indicate proper functioning of the heart and other body organs. These collected pulse waveforms are rich in harmonics and appear superior as compared to previously developed systems .Feature extraction followed by machine learning methods depend not only on clinician's experience but also on the
quality of the pulse waveforms. We e provide some of our normalized pulses from various patients with different disorders, and age groups for the three humors (Vata, Pitta and Kapha) .

We can observe variations in amplitudes, the rising & falling slopes, systolic & diastolic energies, velocities, and so on. We are developing algorithms that will be applied on these waveforms to distinguish major types of nadi defined in Ayurveda Fig (1). The pulse signals read by sensors should be able to provide reproducibility, accuracy and precision. In our system, we would like to check the reproducibility and completeness. In order to check the completeness of the acquired time series t, Nadi Readings was acquired with the same sensor but of a digitizer having an accuracy of 8-bit, 12-bit ,16-bit and 32-bit for same set of patients. The details captured by 8- bit digitizer were less as compared to the 12-bit. As there was no significant new information from 16-bit to 32-bit up gradation, we claim that all the details have been captured. In all the further experiments a digitizer having accuracy of 32- bit is used. In Ayurveda, the readings are sensed by the Ayurvedic practitioners at the wrist with varying pressure. At different applied pressures, different amplitudes, energies etc. are sensed which are then correlated with the body conditions. Further, traditionally in Nadi, the pulse has been classified simply as floating or sinking, according to whether the force exerted to detect the pulse is small or large [6]. We followed similar methodology of applying varying pressure using our system, and were able to confirm the desired behavior .

As the pressure of the sensor over the pulse increases, the amplitude of the pulse signal first increases, reaching a maximum, and then decreases. After a particular threshold value, the pulse dies. All these observations are consistent with the Ayurvedic literature [3]. At each pressure, the pulse gives different insights about the body. However at this point, we consider this finding to be only an appropriate observation which necessitates further investigation with more readings. Finally the signals are captured by the sensors and that read by our software application developed by Ayurvedic literature [1] with applied algorithms to plot the graph according to the three readings per time t.03

Iv. Conclusion And Future Work

We have a lot of proven records in ancient literature that there is not a single disease in the human body which cannot be diagnosed by examining the pulse. However, ancient medical practitioners had to totally rely upon years of clinical experience in order to come to any conclusive diagnosis. Clinicians today have limited examination of the pulse to its rate, rhythm and volume by virtue of which they hardly come to a concrete diagnosis based upon pulse alone. If there could be a system by which

the radial pulse could be critically examined just like the ancient ayurvedic practitioners and others, it could be one of the most useful tools in the field of non-invasive modern medical diagnosis of disease. Thus our system has potential to objectively measure and display the changes occurring in the radial artery in accordance with ayurvedic principles without having to undergo subjective interpretations. Future research will concentrate on the diagnosis of disease like (Cancer types and Sugar level) using our improved version of *an instrument*

References

[1] Dr. M. Sourirajan Ayurvedic Nadi Research fellow, "Nadi Vagadam nadiyum nooikanipum" published by Saraswathi Mahal Library Vol. 1 2000.

[2]   Nadi Tarangini: A Pulse Based Diagnostic System Aniruddha Joshi, Anand Kulkarni, Sharat Chandran, V. K. Jayaraman and B. D. Kulkarni

[3]   S. Upadhyay, Nadi vijnana (Ancient pulse science).

[4] Feng Yuanzhen,Chinese Journal of Biomedical Engineering, 1983.

[5] Y. Yoon, M. Lee, and K. Soh., "Pulse type classification by varying contact pressure," IEEE Engineering in Medicine and Biology Magazine, vol. 19, pp. 106–110., 2000.

[6] V.Lad, Secrets of the pulse: The ancient art of Ayurvedic pulse diagnosis. Motilal Banarasidas, Delhi 2005

[7] H. Wang and Y. Cheng, "A quantitative system for pulse diagnosis in traditional chinese medicine," IEEE EMBS, pp. 5676–5679, 2005

[8] Aniruddha Joshi, Anand Kulkarni, Sharat Chandran, V.K. Jayaraman and B.D. Kulkarni. Nadi Tarangini: A Pulse Based Diagnostic System .Proceedings of the 29th Annual International Conference of the IEEE EM

Application of ANN to Predict Liquefaction Potential

Vijay Kumar[1*], Kumar Venkatesh[2], R. P. Tiwari[3], Yeetendra Kumar[4]

[1,4]Research scholar, [2]Assistant Professor and [3]Professor.
Civil Engineering Department, Motilal Nehru National Institute of Technology, Allahabad, India Pin-211004.
Civil Engineering Department, Motilal Nehru National Institute of Technology, Allahabad, India, Pin-211004.

Abstract:
This study refers to the prediction of liquefaction potential of alluvial soil by artificial neural network models. To meet the objective 160 data sets from field and laboratory tests were collected for the development of ANN models. Initially these data sets were used to determine liquefaction parameters like cyclic resistance ratio and cyclic stress ratio by Idriss and Boulanger method to identify the liquefaction prone areas. Artificial neural network models were trained with six input vectors by optimum numbers of hidden layers, epoch and suitable transfer functions. Out of 160 data sets, 133 data sets were used for development of models and 27 datasets were used for validating the models. The predicted values of liquefaction potential by artificial neural networks models have been compared with Idriss and Boulanger method, which exhibits that trained artificial neural networks models are capable of predicting soils liquefaction potential adequately.

Keywords: Artificial Neural Network, Cyclic Resistance Ratio, Cyclic Stress Ratio, Idriss and Boulanger method, Liquefaction Potential.

1. Introduction:

Earthquake is kind of natural disaster, which occurs every year in the world. Engineers establish that soil comprising large amount of plastic fines has capability of liquefaction. Soil liquefaction is generally occurs in sand, silty sand and sandy silt soil [1]. Following conditions are required for liquefaction to occur:

- The soils must be submerged below the water table.
- The soil must be loose/soft to moderately dense/stiff.
- The ground shaking must be intense
- The duration of ground shaking must be sufficient for the soils to lose their shearing resistance.

 Liquefaction resistance of plastic soil due to earthquake causes seriously destroying of structures like buildings, bridges, highways etc. Soil grains are complex set of particles of different size, shapes and gradations. Ground motion during earthquake is influenced by and affects properties of ground. Under sufficient load soil exhibits plastic deformation due to combination of permanent slip of soil particles relative to one another. In any type of soil, when shearing stress subjected, the soil grains tend to rearrange into a more dense packing results decrease in volume, less space in voids and water in pore spaces is forced out [2]. If drainage of pore water is impeded, pore water pressures increase progressively with the shear load. This leads to transfer of stress from the soil skeleton to the pore water precipitating a decrease in effective stress and shear resistance of soil. If the shear resistance of the soil becomes less than the static, driving shear stress, the soil can undergo large deformations and is said to liquefy [3]. As the bearing capacity of soil to sustain foundation load is directly related to strength, liquefaction poses a serious hazard to structures and must be assessed in areas where liquefaction prone deposit exist [4]. Eight types of failure commonly associated with soil liquefaction in earthquakes are

- Buoyant rise of buried structures such as tanks.
- Failure of retaining walls due to increased lateral loads from liquefied backfill soil or loss of support from liquefied foundation soils.
- Flow failures of slopes involving very large down-slope movements of a soil mass.
- Ground oscillation where liquefaction of a soil deposit beneath a level site leads to back and forth movements of intact blocks of surface soil.
- Ground settlement, often associated with some other failure mechanism.
- Lateral spreads resulting from the lateral displacement of gently sloping ground.
- Loss of bearing capacity causing foundations failures.
- Sand boils, occur when water under pressure wells up through a bed of sand.

Generally, highly sensitive clays lose the strength substantially during earthquake excitation. Fine and uniform sands are more prone to liquefaction, as the pore pressure is dissipated more quickly in coarse sand; hence the chances of liquefaction are reduced in coarse sand deposits [5].
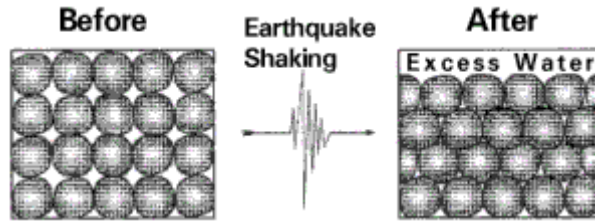
Fig. 1: pore water dissipated more quickly in sand

Due to the cost and the difficulty in acquiring undisturbed samples for analyses of liquefaction potential many empirical method based on in situ tests were developed, these are modified Seed's, Tokimatsu and Yoshimi (T-Y), Idriss and Boulanger (I-B) and new Japan Road Association (NJRA) methods etc. In these empirical methods I-B method is updated and modified version of simplified procedure so here we used I-B method. Field test data including the standard penetration test (SPT) have been used to develop liquefaction potential of soil by empirical method.

Now days a new technique called computational methods is being used frequently for the assessment of liquefaction potential as well as for the solution of various other engineering problems. Artificial neural network approach is one of them found suitable in the field of liquefaction potential assessment by various researchers like Goh, (1994); Goh, (1996); Wang and Rahman, 1999; Goh, (2002); Baziar and Nilipour, (2003); Neaupane and Achet, (2004); Baziar and Gharbani, (2005); Das and Basudhar, (2006); Hsu et al., (2006); Young-Su and Byung-Tak, (2006); Hanna et al., (2007); Rao and Satyam, (2007); Ramakrishnan et al., (2008); Farookhzad et al., (2010); Moradi et al., (2011) [6-13, 1, 14-17, 2, 18].

Current research is the effort of assessing liquefaction potential at the banks of river Ganga and Yamuna since alluvial soil is abundantly present in said areas. Soil strata on the bank of river Ganga and Yamuna mainly consists sandy and clayey soil at various depths. The upper part of strata contains major portion of silty soil and sandy silt enhancing probability. So there is a major chance of liquefaction occurrence in the upper soil zone at greater earthquake magnitude. Two different methods namely Idriss and Boulanger (I & B) and artificial neural network (ANN) modeling approach are used to find out liquefaction potential of soil. The developed ANN model could predict the liquefaction potential of soil.

1.1 Idriss and Boulanger method:

Geotechnical professionals generally investigate subsurface to evaluate the potential for liquefaction. The most common techniques using standard penetration test (SPT) blow count (commonly referred as to the "N-value") follows certain protocols:
1.   Estimation of the cyclic stress ratio (CSR) induced at various depths within the soil by the earthquake.
2.   Estimation of the cyclic resistance ratio (CRR) of the soil, i.e. the cyclic shear stress ratio which is required to cause initial liquefaction of the soil.
3.   Evaluation of factor of safety against liquefaction potential of in situ soils

Calculation of CSR:

Modus operandi by Idriss & Boulanger [20] for evaluation of CSR is same as "simplified method". Right after CSR calculated from the eqn.

$$\text{CSR} = \tau_{avg}/\sigma'_v = 0.65 \left(a_{max}/g\right)\left(\sigma_v/\sigma'_v\right)r_d \tag{1}$$

Value of CSR is adjusted for the moment magnitude M = 7.5. Accordingly the value of CSR is given as

$$(CSR)_{M=7.5} = CSR/MSF = 0.65\left(\sigma_v a_{max}/\sigma'_v\right)\frac{r_d}{MSF} \tag{2}$$

A new parameter r_d which could be adequately expressed as a function of depth and earthquake magnitude (M) was introduced and may be explain from following relations:

$$\ln(r_d) = \propto (z) + \beta(z)M \tag{3}$$

$$\propto (z) = -1.012 - 1.126 \sin\left(z/11.73 + 5.133\right) \tag{4a}$$

$$\beta(z) = 0.106 + 0.118 \sin\left(z/11.28 + 5.142\right) \tag{4b}$$

Where z is the depth in meters and M is moment magnitude. These equations were appropriated for depth z ≤ 34 m however for depth z > 34m; the following expression may be used:

$$r_d = 0.12 \exp(0.22M) \tag{5}$$

$CSR_{7.5}$ is the cyclic stress ratio for magnitude of 7.5 earthquakes, magnitude smaller or larger than 7.5, introduces a correction factor namely magnitude scaling factor MSF defined by the following equation given by [20]:

$$MSF = 10^{2.24}/M^{2.56} \tag{6}$$

Calculation of CRR:

Idriss and Boulanger [21] adjusted the equation of CRR for clean sands as follows

$$CRR = \exp\left\{\frac{(N_1)_{60cs}}{14.1} + \left(\frac{(N_1)_{60cs}}{126}\right)^2 - \left(\frac{(N_1)_{60cs}}{23.6}\right)^3 + \left(\frac{(N_1)_{60cs}}{25.4}\right)^4 - 2.8\right\} \qquad (7)$$

Subsequent expressions describes the way parameters in the above equation is calculated

$$(N_1)_{60cs} = (N_1)_{60} + (\Delta N_1)_{60} \qquad (8a)$$

$$(\Delta N_1)_{60} = \exp\left(1.63 + \frac{9.7}{FC} - \left(\frac{15.7}{FC}\right)\right) \qquad (8b)$$

$$(N_1)_{60} = C_N (N)_{60} \qquad (8c)$$

The variation of $(\Delta N_1)_{60}$ with FC, calculated using the eqn. (8c) is presented in fig. 2.
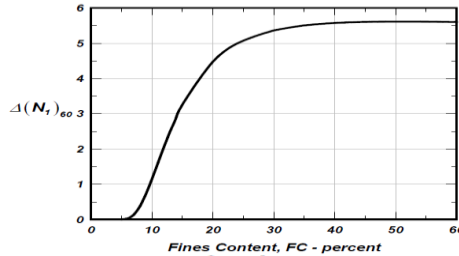
Fig. 2 Variation of $(\Delta N_1)_{60}$ with fines content

The use of equations in preceding articles provides a convenient means for evaluating the cyclic stress ratio required to cause liquefaction for cohesion-less soils with varying fines content.

Calculation of factor of safety:

If the cyclic stress ratio caused by an earthquake is greater than the cyclic resistance ratio of the in situ soil, then liquefaction could occur during the earthquake, and vice versa. The factor of safety (FOS) against liquefaction is defined as:

$$FS_{Liquefaction} = \frac{CRR}{CSR} \qquad (9)$$

Liquefaction is predicted to occur when FS≤ 1.0, and liquefaction predicted not to occur when FS > 1. The higher the factor of safety, the more resistant against liquefaction [22], however, soil that has a factor of safety slightly higher than 1.0 may still liquefy during the earthquake.

1.2 Overview of Artificial Neural Network:

Artificial neural network (ANN) consists of a large number of interconnected processing units known as biological neuron [9]. It is a soft computing approach that is inspired by the function and structural aspects of biological neurons. ANN is advanced and standard tools simulated by the mathematical model and computational model of the human brain and being used around the globe to find solutions to a wide variety of non-linear statistical data complications [15]. They are usually used to model complex relationship among inputs and targets to find patterns in datasets. Interconnections among neurons are established by weights, which are applied to all values passing through one neuron to another. The ANNs are arranged in three or more layers, one input layer, one or more hidden layers and one target layer. Each layer of neurons has connections to all the neurons in next layer. Each neuron receives an input signals from the previous neurons connected. Each of these connections has numeric weights associated with it.

Fig. 3: A two-layer feed-forward artificial neural network structure.

The signals from each input are then processed through a weighted sum of the inputs, and the processed output signal is then transmitted another neuron via a transfer of activation function. Once the network trained with sufficient number of datasets, it

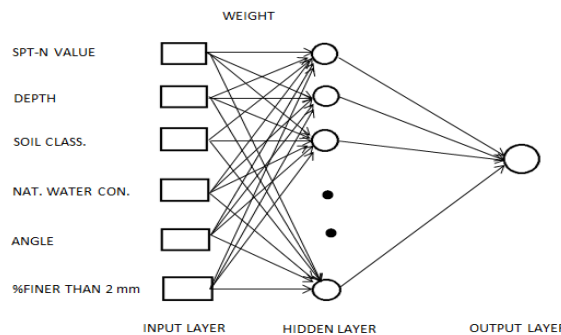can validate, the trained network required to make predictions for a new set of data that it has never been introduced during the previous phases [17]. Due to its multidisciplinary nature, ANN is becoming advanced and standard tool for accomplishment of their work. ANN model have also been used in the field of geotechnical engineering. A two layer feed-forward ANN structure is shown above in fig. 3.

Feed-forward back propagation technique:
In this section here we used Feed-forward back propagation technique. In this technique learning algorithm has two stages. In first stage, the inputs are forwarded from input layer to output layer. After computing the errors of each output between computed and desired output, in second stage information is send backward to the inputs which readjust the connecting weights in the hidden and output layer to minimize this error. The modification of the weights is carried out by using generalized delta rule [23].
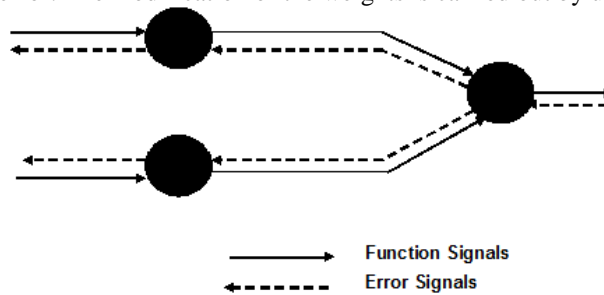
Fig. 4: Feed-forward back propagation network

Activation/Transfer function:
Though many activation functions exist, the most common is the sigmoid activation function, which outputs a number between 0 (for low input values) and 1 (for high input values). The resultant of this function is then passed as the input to other neurons through more connections, each of which are weighted [24]. Sigmoid transfer function is expressed as:

$$f(t) = \frac{1}{1+\exp{(-t)}} \qquad (10)$$
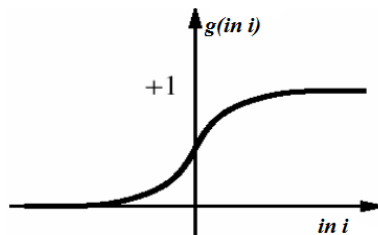
Fig. 5: Sigmoid transfer function.

2.   Development of ANN models:
To estimate liquefaction potential of sandy soil SPT tests on different stations were conducted as it is the most suitable site exploration test for sandy soil. Data collected from SPT tests were utilized to find out liquefaction potential through I & B method, further these data were used to develop ANN models. Output parameter that is occurrence of liquefaction in the ANN model is designed to answer in yes/no format based on I & B method. The soil properties found through SPT and other laboratory tests used as input vectors in ANN method is shown in table 1. The detailed methodology adopted is discussed under following sub-headings.

2.1 Experimental method:
Standard penetration test were conducted in order to collect bore-hole datasets. Disturbed and undisturbed soil specimen was collected from these bore-holes up to depth of 10 meters as well as SPT N-values were also determined at a regular interval of depth 1.5 m, disturbed soil samples were used to determine liquid limit; plastic limit; angle of internal friction; particle size finer than 2 mm, 0.075 mm and 0.002mm and undisturbed samples were used to find out natural water content, bulk unit weight. All experiments were conducted according to bureau of Indian standard's guidelines for soil testing.

Data modification:

Corrected SPT-N values were required to apply I & B method to calculate liquefaction potential hence standard method for SPT-N value correction was adopted as given by IS: 2131-1981. A brief discussion on corrected SPT-N value is discussed hereunder:

Correction for overburden pressure: N- value obtained from SPT test is corrected first which is either calculated by the equation:

$$N_1 = C_N \times N \tag{11}$$

C_N is correction factor obtained directly from the graph given in Indian Standard Code (IS: 3121-1981). (Fig. 6)
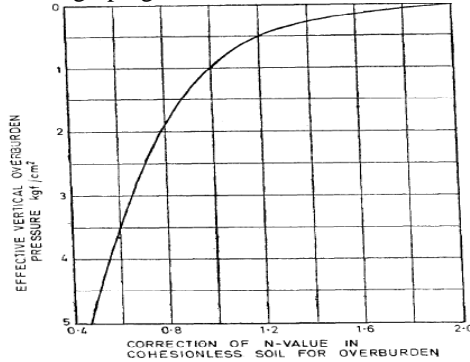
Fig. 6: Correction due to overburden pressure

It can also calculate from the formulae:

$$C_N = 0.77 \log_{10} \frac{2000}{p} \tag{12}$$

Where, p is effective overburden pressure in kN/m² [25].

Dilatancy correction: The values obtained in overburden pressure (N_1) shall be corrected for dilatancy if the stratum consist of fine sand and silt below water table for values of N_1 greater than 15 as under [26]:

$$N_c = 15 + 0.5(N_1 - 15) \tag{13}$$

Calculation of CSR value through I & B method is calculated for specific depth of water table and earthquake magnitude. Therefore CSR values were interpreted for different combination of depth and earthquake magnitude as shown below in table 1.

2.2 Network Architecture:

A total combination of 6 input variables comprising depth (z), SPT-N value (N), classification of soil, natural / field moisture content (w), angle of internal friction (φ) and particle size finer than 2 mm were used for ANN model development. Soil classification criteria were implemented by encoding soil class with a specific value keeping in view sand content in respective soil specimen. Table 3 illustrates soil encoding for different soil class [9]. A total of 160 datasets were used for training in which 27 datasets were reserved for validating the network. The boundaries for input and output parameters of the models are listed in Table 2. The input–output data of each ANN model were scaled to lie between 0 and 1 by using Eqn. (14).

$$\alpha = \frac{\alpha_{actual} - \alpha_{min.}}{\alpha_{max.} - \alpha_{min.}} \tag{14}$$

Where α_{norm} is the normalized value, α is the actual value, α_{max} is the maximum value and α_{min} is the minimum value.

ANN tool built in MATLAB (R2011a) software was used for all operations in which networks were trained with single or double hidden layers of varying numbers of neurons (2 to 20) were used in the analysis. Fig. 3 describes the way network were treated from given set of input and target parameters.

To identify its fundamental attributes a coding method was used for different depth of water table and earthquake magnitude, as such $W_X M_Y$ denotes W_X: depth of water table and M_Y: earthquake magnitude value. For each and every set of depth of water table and earthquake magnitude, we build different number of ANN architecture with varying hidden layer and number of neurons in each hidden layer. In this thesis, here we choose one and two hidden layers and neurons in hidden layer is varied up to 20. ANN architecture is simply denoted as N_X, which is varied from N_1 to N_{52}. Some of the liquefaction values obtained through selected ANN architecture for each network are discussed in subsequent literature.

3. Results and Discussion:

As mentioned above three water table depth and three earthquake magnitude values were considered for assessing liquefaction potential through I & B and ANN method. This resulted in total of nine set of liquefaction values through nine combinations of water table and earthquake magnitude values. Table 4-6 shows that liquefaction potential evaluated from I & B method and

computed by ANN models for the datasets which are reserved for validating. Calculation of errors between liquefaction potential by I & B method and ANN model is also shown in table 4-6.

Using the liquefaction values through I & B method and ANN (by validating the networks) method, graphs (fig. no. 6-14) were prepared for comparative analysis for these nine set of combinations of depth of water table and earthquake magnitude values however input vectors retained common in all ANN models (i.e. 6 number of inputs). For each nine set, we trained the network throughout the ANN architecture with varying epochs from 500 to 5000. Weights were randomly initialized. The numbers of hidden neurons are varied (4, 6, 8..... 20) and the generalization performance is reported in Table 2. Here we select four number of ANN architecture for each set those mean square error (MSE) is low and regression is high. After that, we calculate average absolute error for the selected ANN architecture and finally one model is selected on the basis of minimum average absolute error and high regression value. Absolute average error calculated for nine models is summarized in table no. 7.

From the graph, here we see that regression for validation is varied from 0.967 to 0.9969 and average absolute error is varied from 0.929% to 2.687%. An illustration of regression graph for network N_{21} is also shown in fig. 15. Moreover results obtained in occurrence/non-occurrence form of liquefaction for particular combination of depth of water table and earthquake magnitude values are as shown in table no. 4-6 for ANN method indicates closeness of predicted value to I & B method. In some cases like $W_3M_{7.5}$ serial no. 6, $W_4M_{7.5}$ serial no. 5 and 6, W_5M_7 serial no. 3, $W_5M_{7.5}$ serial no. 6 and W_5M_8 serial no. 13 are wrongly predicted by the respective model because of the ratio of CRR/ CSR is nearly equal to 1 .
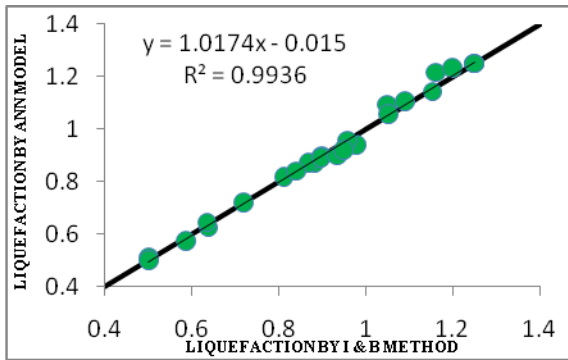

Fig. 6: Comparison study for W.T. 3m and M 7
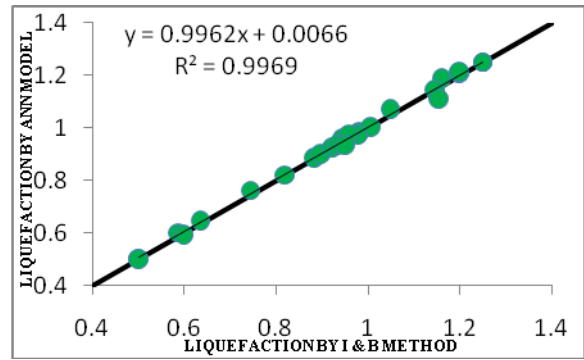

Fig. 9: Comparison study for W.T. 4m and M 7
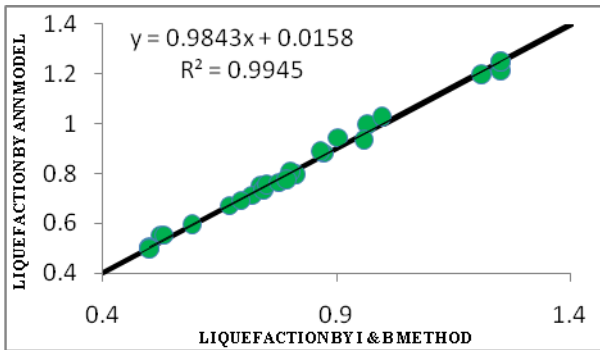
Fig. 7: Comparison study for W.T. 3m and M 7.5
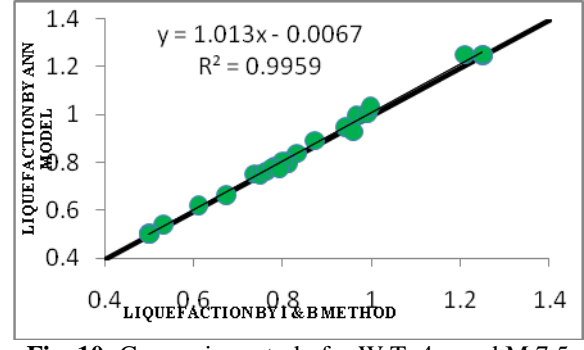
Fig. 10: Comparison study for W.T. 4m and M 7.5
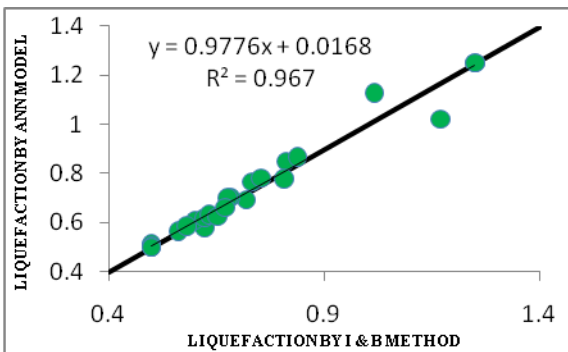
Fig. 8: Comparison study for W.T. 3m and M 8
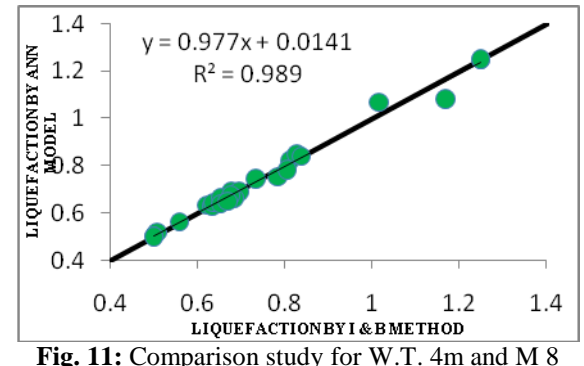
Fig. 11: Comparison study for W.T. 4m and M 8
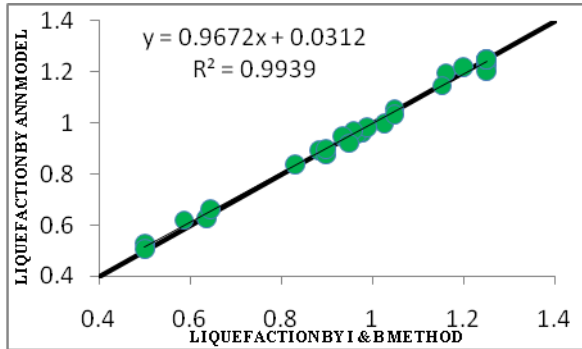
Fig. 12: Comparison study for W.T. 5m and M 7
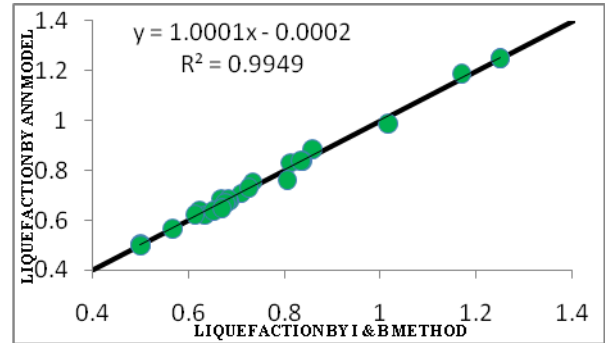
Fig. 14: Comparison study for W.T. 5m and M 8
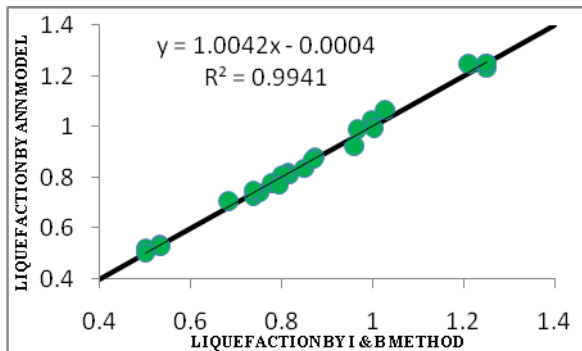
Fig. 13: Comparison study for W.T. 5m and M 7.5
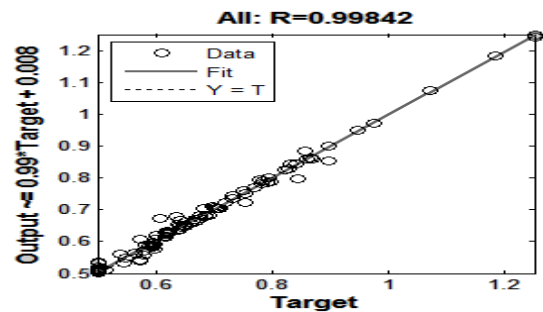
Fig. 15: Overall regression for Network N_{21}

4. Conclusions:

Artificial neural network have been developed for the assessment of liquefaction potential with field and laboratory datasets. This paper has established the usefulness of the ANN to model the complex relationship between the soil, seismic parameters and the liquefaction potential using in situ measurements based on SPT test. Coefficient of correlation values in all models are greater than 0.96 indicate satisfactory prediction capability of ANN models. Moreover, results obtained in occurrence/non-occurrence form of liquefaction for particular combination of depth of water table and earthquake magnitude values by ANN method indicates closer predictions compared to I & B method.

Field and Lab input parameters may directly be used as input vector for ANN models, which is simpler than the conventional methods to predict Liquefaction Potential. The prediction using ANN with SPT data had an overall success rate of ninety six percent resulting very effective and easily handle tool.

References:

[1]. S. Hsu, M. Yang, M. Chen, and J. Lin, Artificial Neural Network of liquefaction evaluation for soils with High Fines Content, 2006 international joint conference on neural networks, Canada. July 16-21 (2006) pp2643-2649.

[2]. F. Farrokhzad, A.J. Choobasti, and A. Barari, Liquefaction microzonation of Babool city using artificial neural network, 2010 Journal of king saud university (science) (2010).

[3]. H.B. Seed and I. M. Idriss, Summer Report on Ground Motions and Soil Liquefaction during Earthquakes, 1982 Earthquake Engineering Research Institute, Berkeley, California (1982).

[4]. Prasad, B.B., Fundamentals of soil dynamics and earthquake engineering by, PHI learning private limited, new delhi-110001, 2009.

[5]. Haykin, S., Neural Networks: A Comprehensive Foundation, 2nd edition, Prentice-Hall, Englewood Cliffs, NJ 1998.

[6]. A.T.C. Goh, Seismic liquefaction potential assessed by neural networks, 1994, *Journal of Geotechnical Engineering,* Vol. 120, No. 9, September, 1994, pp1467-1480.

[7]. A.T.C. Goh, Pile driving records reanalyzed using neural networks, J Geotech Engrg, ASCE 1996; 122(6) pp492–500.

[8]. J. Wang, and M.S. Rahman, A neural network model for liquefaction-induced horizontal ground displacement, 1999, Soil Dynamics and Earthquake Engineering. 18 (1999) pp555–568.

[9]. A.T.C. Goh, Probabilistic neural network for evaluating seismic liquefaction potential, 2002, Can. Geotech. J. (39) pp.219-232.

[10]. M.H. Baziar, N. Nilipour, Evaluation of liquefaction potential using neural-networks and CPT results, 2003, Soil Dynamics and Earthquake Engineering 23 (2003) pp631–636.

[11]. K.M. Neaupane, S.H. Achet, Use of backpropagation neural network for landslide monitoring: a case study in the higher Himalaya, 2004, Engineering Geology 74 (2004) pp213–226.

[12]. M.H. Baziar, A. Ghorbani, Evaluation of lateral spreading using artificial neural networks, 2005, Soil Dynamics and Earthquake Engineering 25 (2005) pp1–9.

[13]. S.K. Das, P.K. Basudhar, Undrained lateral load capacity of piles in clay using artificial neural network, 2006, Computers and Geotechnics 33 (2006) pp454–459.

[14]. K. Young-Su, and K. Byung-Tak, Use of Artificial Neural Networks in the Prediction of Liquefaction Resistance of Sands, 2006, Journal of Geotechnical and Geo-environmental Engineering ASCE (2006) pp1502-1504.

[15]. A.M. Hanna, D. Ural, and G. Saygili, Neural network model for liquefaction potential in soil deposits using Turkey and Taiwan earthquake data, 2007, Soil Dynamics and Earthquake Engineering 27 (2007a) pp521–540.

[16]. A.M. Hanna, D. Ural, and G. Saygili, Evaluation of liquefaction potential of soil deposits using artificial neural networks, 2007, International journal for computer-aided engineering and software, 24(1) (2007b) pp5-16.

[17]. K.S. Rao and D.N. Satyam, Liquefaction studies for seismic microzonation of Delhi region, 2007, Current science, vol. 92, no. 5 (10 march 2007), pp646-654.

[18]. D. Ramakrishnan, T.N. Singh, N. Purwar, K.S. Barde, Akshay, Gulati and S. Gupta, Artificial neural network and liquefaction susceptibility assessment: a case study using the 2001 Bhuj earthquake data, Gujarat, India, 2008, Comput Geosci (2008) 12: pp491-501.

[19]. G. Moradi, B.R. Khatiba, and M.H. Sutubadi, Determination of liquefaction potential of soil using $(N_1)_{60}$ by numerical modeling method, 2011, EJGE, vol. 16 (2011) pp407-417.

[20]. I.M. Idriss, and R.W. Boulanger, Semi-empirical procedures for evaluating liquefaction potential during earthquakes, 2006, Soil Dynamics and Earthquake Engineering. 26 (2006) pp115-130.

[21]. T. L. Youd, and I. M. Idriss, NCEER Workshop on Evaluation of Liquefaction Resistance of Soils, 1997, Nat. Ctr. for Earthquake Engg. Res., State Univ. of New York at Buffalo eds. (1997).

[22]. Youd et al., Liquefaction resistance of soils: summary report from the 1996 NCEER and 1998 NCEER/NSF workshops on evaluation of liquefaction resistance of soils, 2001, J. Geotech. Engg. Div.. ASCE, 127(10) (2001) pp817-833.

[23]. D.E. Rumelhart, G.E. Hinton, and R.J. Williams, "Learning Internal Representations by Error Propagation". In David E. Rumelhart, James L. McClelland, and the PDP Research Group, editors, Parallel Distributed Processing. Explorations in the Microstructure of Cognition, 1986, MIT Press, Volume 1: Foundations, pp318-364.

[24]. Krose, B. and Smagt, P.V.D., An introduction to neural networks, University of Amsterdam, Eighth edition, Nov-1996.

[25]. Terzaghi K., Peck R. B., and Mesri G., Soil mechanics in engineering practice (2nd Ed.), Wiley & Sons Inc., New York 1996.

[26]. Varghese, P.C. Foundation Engineering, prentice hall of India private limited, New Delhi – 110001, 2007.

Illustrations:

Table 1: Assumed water table and earthquake magnitude.

Depth of water table (m)	3	4	5
Earthquake magnitude (rector scale)	7.0	7.5	8.0

Table 2: Range of input and output parameters.

Input Parameters	minimum	maximum
depth (m)	0	10
SPT-N value	0	50
Soil classification	0	5
Natural water content	0.55	32.36
Angle of internal friction	12	33
Particle finer than 2 mm (%)	82.5	100
Liquefaction potential	0.5	1.25

Table 3: Soil class with respective number.

Soil description	Soil type number
Poorly graded sand (SP)	5
Silty sand (SM)	4
Very fine sand (ML)	3
Silty clay with low plasticity (CL)	2
Sandy clay with medium plasticity (CI)	1

Table 4: Comparison study about liquefaction potential for water table at 3m.

S. No.	Depth (z)	SPT-N value	For network W_3M_7				For network $W_3M_{7.5}$				For network W_3M_8			
			Lique. Pot. by I & B method		Lique. Pot. by ANN		Lique. Pot. by I & B method		Lique. Pot. by ANN		Lique. Pot. by I&B method		Lique. Pot. by ANN	
			ratio	status	ratio	status	ratio	status	ratio	status	ratio	status	ratio	status
1	1.5	12	0.882	Yes	0.873	Yes	0.737	Yes	0.753	Yes	0.737	Yes	0.579	Yes
2	3.0	22	1.161	No	1.215	No	0.966	Yes	0.996	Yes	0.966	Yes	0.848	Yes
3	4.5	20	0.868	Yes	0.87	Yes	0.718	Yes	0.713	Yes	0.718	Yes	0.609	Yes
4	3.0	19	1.049	No	1.095	No	0.873	Yes	0.882	Yes	0.873	Yes	0.766	Yes
5	4.5	26	1.09	No	1.106	No	0.902	Yes	0.943	Yes	0.902	Yes	0.78	Yes
6	3.0	23	1.199	No	1.234	No	0.997	Yes	1.028	No	0.997	Yes	0.867	Yes
7	4.5	21	0.899	Yes	0.898	Yes	0.744	Yes	0.735	Yes	0.744	Yes	0.62	Yes
8	6.0	29	1.052	No	1.056	No	0.865	Yes	0.889	Yes	0.865	Yes	0.692	Yes
9	1.5	12	0.897	Yes	0.891	Yes	0.75	Yes	0.755	Yes	0.75	Yes	0.633	Yes
10	3.0	16	0.978	Yes	0.939	Yes	0.814	Yes	0.796	Yes	0.814	Yes	0.702	Yes
11	4.5	18	0.811	Yes	0.816	Yes	0.671	Yes	0.671	Yes	0.671	Yes	0.563	Yes
12	6.0	16	0.638	Yes	0.625	Yes	0.525	Yes	0.552	Yes	0.525	Yes	0.501	Yes
13	3.0	28	1.25	No	1.25	No	1.209	No	1.199	No	1.209	No	1.128	No
14	4.5	19	0.84	Yes	0.84	Yes	0.695	Yes	0.691	Yes	0.695	Yes	0.584	Yes
15	6.0	19	0.719	Yes	0.721	Yes	0.591	Yes	0.597	Yes	0.591	Yes	0.51	Yes
16	1.5	25	1.25	No	1.25	No	1.25	No	1.214	No	1.25	No	1.022	No
17	3.0	50	1.25	No	1.25	No	1.25	No	1.25	No	1.25	No	1.25	No
18	1.5	14	0.958	Yes	0.958	Yes	0.801	Yes	0.806	Yes	0.801	Yes	0.701	Yes
19	3.0	16	0.933	Yes	0.899	Yes	0.777	Yes	0.763	Yes	0.777	Yes	0.625	Yes
20	1.5	13	0.949	Yes	0.921	Yes	0.793	Yes	0.777	Yes	0.793	Yes	0.661	Yes
21	3.0	20	1.153	No	1.143	No	0.959	Yes	0.935	Yes	0.959	Yes	0.779	Yes
22	4.5	50	1.25	No	1.25	No	1.25	No	1.25	No	1.25	No	1.25	No
23	1.5	7	0.635	Yes	0.645	Yes	0.531	Yes	0.552	Yes	0.531	Yes	0.511	Yes
24	3.0	7	0.587	Yes	0.574	Yes	0.5	Yes	0.507	Yes	0.5	Yes	0.501	Yes
25	4.5	8	0.5	Yes	0.508	Yes	0.5	Yes	0.501	Yes	0.5	Yes	0.5	Yes
26	7.5	5	0.5	Yes	0.501	Yes	0.5	Yes	0.5	Yes	0.5	Yes	0.5	Yes
27	9.0	5	0.5	Yes	0.5	Yes	0.5	Yes	0.5	Yes	0.5	Yes	0.5	Yes

Table 5: Comparison study about liquefaction potential for water table at 4m.

S. No.	Depth (z)	SPT-N value	For network W_4M_7				For network $W_4M_{7.5}$				For network W_4M_8			
			Lique. Pot. by I & B method		Lique. Pot. by ANN		Lique. Pot. by I & B method		Lique. Pot. by ANN		Lique. Pot. by I & B method		Lique. Pot. by ANN	
			ratio	status	ratio	status	ratio	status	ratio	status	ratio	status	ratio	status
1	1.5	12	0.882	Yes	0.887	Yes	0.737	Yes	0.752	Yes	0.623	Yes	0.633	Yes
2	3.0	22	1.161	No	1.187	No	0.966	Yes	0.996	Yes	0.812	Yes	0.82	Yes
3	4.5	20	0.98	Yes	0.983	Yes	0.811	Yes	0.805	Yes	0.678	Yes	0.689	Yes
4	3.0	19	1.049	No	1.071	No	0.873	Yes	0.892	Yes	0.734	Yes	0.743	Yes
5	4.5	26	1.197	No	1.207	No	0.991	Yes	1.008	No	0.829	Yes	0.847	Yes
6	3.0	23	1.199	No	1.213	No	0.997	Yes	1.032	No	0.839	Yes	0.839	Yes
7	4.5	21	1.006	No	1.002	No	0.832	Yes	0.838	Yes	0.696	Yes	0.691	Yes
8	6.0	29	1.146	No	1.143	No	0.942	Yes	0.947	Yes	0.783	Yes	0.753	Yes
9	1.5	12	0.897	Yes	0.9	Yes	0.75	Yes	0.749	Yes	0.634	Yes	0.63	Yes
10	3.0	16	0.978	Yes	0.974	Yes	0.814	Yes	0.796	Yes	0.684	Yes	0.662	Yes
11	4.5	18	0.921	Yes	0.925	Yes	0.762	Yes	0.763	Yes	0.637	Yes	0.644	Yes
12	6.0	16	0.744	Yes	0.76	Yes	0.612	Yes	0.619	Yes	0.509	Yes	0.518	Yes
13	3.0	28	1.25	No	1.25	No	1.209	No	1.249	No	1.017	No	1.068	No
14	4.5	19	0.945	Yes	0.958	Yes	0.782	Yes	0.783	Yes	0.654	Yes	0.665	Yes
15	6.0	19	0.818	Yes	0.82	Yes	0.672	Yes	0.663	Yes	0.559	Yes	0.563	Yes
16	1.5	25	1.25	No	1.25	No	1.25	No	1.245	No	1.17	No	1.081	No
17	3.0	50	1.25	No	1.25	No	1.25	No	1.25	No	1.25	No	1.248	No
18	1.5	14	0.958	Yes	0.973	Yes	0.801	Yes	0.806	Yes	0.677	Yes	0.673	Yes
19	3.0	16	0.933	Yes	0.934	Yes	0.777	Yes	0.778	Yes	0.653	Yes	0.638	Yes
20	1.5	13	0.949	Yes	0.934	Yes	0.793	Yes	0.774	Yes	0.67	Yes	0.65	Yes
21	3.0	20	1.153	No	1.109	No	0.959	Yes	0.929	Yes	0.807	Yes	0.781	Yes
22	4.5	50	1.25	No	1.25	No	1.25	No	1.25	No	1.25	No	1.25	No
23	1.5	7	0.635	Yes	0.645	Yes	0.531	Yes	0.539	Yes	0.5	Yes	0.502	Yes
24	3.0	7	0.587	Yes	0.599	Yes	0.5	Yes	0.506	Yes	0.5	Yes	0.5	Yes
25	4.5	8	0.6	Yes	0.592	Yes	0.5	Yes	0.501	Yes	0.5	Yes	0.5	Yes
26	7.5	5	0.5	Yes	0.501	Yes	0.5	Yes	0.5	Yes	0.5	Yes	0.5	Yes
27	9.0	5	0.5	Yes	0.5	Yes	0.5	Yes	0.5	Yes	0.5	Yes	0.5	Yes

Table 6: Comparison study about liquefaction potential for water table at 5m.

S. No.	Depth (z)	SPT-N value	For network W_5M_7				For network $W_5M_{7.5}$				For network W_5M_8			
			Lique. Pot. by I & B method		Lique. Pot. by ANN		Lique. Pot. by I & B method		Lique. Pot. by ANN		Lique. Pot. by I & B method		Lique. Pot. by ANN	
			ratio	status	ratio	status	ratio	status	ratio	status	ratio	status	ratio	status
1	1.5	12	0.882	Yes	0.892	Yes	0.737	Yes	0.727	Yes	0.608	Yes	0.637	Yes
2	3.0	22	1.161	No	1.195	No	0.966	Yes	0.989	Yes	0.832	Yes	0.83	Yes
3	4.5	20	1.025	No	0.999	Yes	0.849	Yes	0.835	Yes	0.702	Yes	0.707	Yes
4	3.0	19	1.049	No	1.056	No	0.873	Yes	0.88	Yes	0.743	Yes	0.753	Yes
5	4.5	26	1.25	No	1.225	No	1.027	No	1.065	No	0.857	Yes	0.884	Yes
6	3.0	23	1.199	No	1.218	No	0.997	Yes	1.027	No	0.856	Yes	0.84	Yes
7	4.5	21	1.049	No	1.032	No	0.868	Yes	0.87	Yes	0.724	Yes	0.731	Yes
8	6.0	29	1.25	No	1.202	No	1.003	No	0.995	No	0.803	Yes	0.837	Yes
9	1.5	12	0.897	Yes	0.875	Yes	0.75	Yes	0.74	Yes	0.635	Yes	0.619	Yes
10	3.0	16	0.978	Yes	0.964	Yes	0.814	Yes	0.817	Yes	0.653	Yes	0.676	Yes
11	4.5	18	0.966	Yes	0.955	Yes	0.799	Yes	0.803	Yes	0.666	Yes	0.687	Yes
12	6.0	16	0.829	Yes	0.836	Yes	0.682	Yes	0.705	Yes	0.575	Yes	0.567	Yes
13	3.0	28	1.25	No	1.249	No	1.209	No	1.247	No	1.084	No	0.988	Yes
14	4.5	19	0.987	Yes	0.983	Yes	0.817	Yes	0.81	Yes	0.688	Yes	0.684	Yes
15	6.0	19	0.897	Yes	0.899	Yes	0.738	Yes	0.749	Yes	0.627	Yes	0.623	Yes
16	1.5	25	1.25	No	1.249	No	1.25	No	1.233	No	1.074	No	1.187	No
17	3.0	50	1.25	No	1.25	No	1.25	No	1.25	No	1.25	No	1.25	No
18	1.5	14	0.958	Yes	0.971	Yes	0.801	Yes	0.809	Yes	0.697	Yes	0.669	Yes
19	3.0	16	0.933	Yes	0.949	Yes	0.777	Yes	0.778	Yes	0.65	Yes	0.639	Yes
20	1.5	13	0.949	Yes	0.921	Yes	0.793	Yes	0.769	Yes	0.657	Yes	0.649	Yes
21	3.0	20	1.153	No	1.145	No	0.959	Yes	0.922	Yes	0.795	Yes	0.762	Yes
22	4.5	50	1.25	No	1.25	No	1.25	No	1.25	No	1.25	No	1.25	No
23	1.5	7	0.635	Yes	0.628	Yes	0.531	Yes	0.533	Yes	0.511	Yes	0.504	Yes
24	3.0	7	0.587	Yes	0.619	Yes	0.5	Yes	0.521	Yes	0.505	Yes	0.501	Yes
25	4.5	8	0.644	Yes	0.661	Yes	0.533	Yes	0.529	Yes	0.504	Yes	0.501	Yes
26	7.5	5	0.5	Yes	0.53	Yes	0.5	Yes	0.502	Yes	0.5	Yes	0.5	Yes
27	9.0	5	0.5	Yes	0.507	Yes	0.5	Yes	0.502	Yes	0.5	Yes	0.5	Yes

Table 7: Details of errors and architecture for one of the best model.

model no.	W_3M_7	$W_3M_{7.5}$	W_3M_8	W_4M_7	$W_4M_{7.5}$	W_4M_8	W_5M_7	$W_5M_{7.5}$	W_5M_8
Network Name	N_{10}	N_2	N_4	N_{10}	N_{10}	N_{10}	N_{19}	N_{19}	N_{21}
Network Architecture	6-6-2-1	6-6-1	6-10-1	6-6-2-1	6-6-2-1	6-6-2-1	6-12-2-1	6-12-2-1	6-12-6-1
Avg. Abs. Error (%)	1.337	1.645	2.687	0.929	1.207	1.625	1.713	1.513	1.382
MSE $\times 10^{-4}$	1.5155	1.0687	1.8804	1.9927	1.5585	0.4467	2.7934	1.5633	0.222
epoch	4000	5000	1000	4000	2000	2000	4000	3000	2000
Regression	0.99553	0.99852	0.99851	0.99029	0.99757	0.99818	0.99441	0.99791	0.99842
Coeff. of correlation	0.9936	0.9945	0.9670	0.9969	0.9959	0.9890	0.9939	0.9941	0.9949

Development of Thermistor Linearization Circuit based on Modified 555 Timer using LabVIEW

Ayushi SRIVASTAVA[1], Vaishnavi A.R.S.N[2], Mahesh Prasad. M[3], Rama Rao.P[4], and K.V.L.Narayana[5]

[1,2,3,4,5] Department of Electronics and Instrumentation Engineering, GITAM University,
Rushikonda, Visakhapatnam-530 045, INDIA

Abstract:
Thermistors have high sensitivity which makes them suitable for various applications, but they exhibit a highly nonlinear resistance-temperature relationship which is exponential in nature. This nonlinearity is an important problem and a lot of research has been dedicated to correct it. In this paper a virtual instrument has been developed based on the modified 555 timer circuit using LabVIEW to obtain a linearized characteristic. The possibility of developing the proposed instrument as a temperature sensor with frequency as output has been investigated through simulation. It has been shown that the linearization of the thermistor characteristic is achieved by selecting the suitable parameters of the thermistor, the frequency determining elements and the control voltage of modified 555 timer circuit without connecting any additional elements. The experimentally obtained characteristics have a good match with the theoretically obtained characteristics through the investigations conducted in this paper. In a specific range of temperature the proposed circuit is characterized by high temperature stability, improved sensitivity and nonlinearity of about ±1% .

Keywords: Thermistor, Linearization, Modified 555, LabVIEW, Temperature Sensor, Data Acquisition.

1. Introduction

Negative temperature coefficient (NTC) thermistors are temperature sensors whose resistance decreases with increase in temperature. They are used for precise measurement of temperature in various fields like food, automobile, chemical industries and in medicine because of their high sensitivity, low cost and convenient physical shape. The NTC thermistors are composed of metal oxides. The most commonly used oxides are those of manganese, nickel, cobalt, iron, copper and titanium [1]-[3]. The fabrication of commercial NTC thermistors uses basic ceramics technology and continues today much as it has for decades. In the basic process, a mixture of two or more metal oxide powders are combined with suitable binders, are formed to a desired geometry, dried, and sintered at an elevated temperature. By varying the types of oxides used, their relative proportions, the sintering atmosphere, and the sintering temperature, a wide range of resistivity and temperature coefficient characteristics can be obtained.

Thermistors when used for temperature measurements, they are connected in circuits like voltage divider or bridge circuits. However, because of nonlinearity different methods are used to linearize the characteristic of thermistor [2], [3]. One of the methods is to connect passive element either in parallel or series to make the characteristic linear [4], [5]. The second method is to connect thermistors in circuits with logarithmic amplifiers [6]-[8]. The third method is to convert temperature to frequency where active elements are used [9]-[13]. Apart from these methods, computer methods for linearization are also used where lookup tables are used [14] ,[15].

National instruments developed Laboratory Virtual Instrument Engineering Workbench (LabVIEW). It is a graphical programming language used in a variety of industries for measurement, control, data analysis, data presentation [16], [17]. LabVIEW provides icons to manage and represent the user interface; it helps to develop a human-friendly front panel which can be customized according to our requirements for the analysis and design. In this paper LabVIEW is used for simulating the thermistor linearization circuit. LabVIEW is also used for real time data acquisition where the thermistor is interfaced with LabVIEW through a NI cDAQ 9174 card. A real time voltage value is acquired and is converted into resistance and temperature and this data is used in the simulation to get the linearized characteristic. Fig.1 shows the thermistor output acquisition system.

In this paper a virtual instrument has been proposed in which, the thermistor measures the temperature of a water bath and the measured value is interfaced with LabVIEW. This virtual instrument is designed with the help of LabVIEW .The thermistor circuit consists of a modified version of 555 timer which is used to linearize the characteristic of the thermistor. Utilizing the frequency determining parameters of circuit, thermistor parameters and the controlled voltage under a pre specified working temperature range, the thermistor characteristic has been linearized. A wider linearization range is obtained when thermistors with lower B values are used, such as V_2O_5 based thermistors. As we obtain frequency as the output, the signal has higher noise immunity.

2. Theoretical Background

For an NTC thermistor, the temperature dependence of the resistance R_T is exponential, as shown in Eq. (1)

$$R_T = R_0 \exp [B (1/T - 1/T_0)] \qquad (1)$$

Where R_0 is the zero-power resistance at a specific temperature T_0 in Kelvin, and B is the characteristic temperature of the material. B is the material constant (expressed in kelvins), which is determined by the activation energy q and he

Boltzmann's constant k with the dependence B = q/k [18]. The thermistor connection circuit uses the modified 555 timer circuit [19]. The proposed circuit of 555 timer is built on the laboratory using discrete electronic components. Fig. 2 shows the schematic of the circuit with the components that were used during the experiment. By controlling the input signal (Vcon), the output switching frequency (fs) is adjusted; an expression that describes the relationship between Vcon and fs is given by Eq. (2), where R_T is the thermistor and R_a and C_T are the frequency determining elements.

$$f_s = f(T) = \frac{1}{\ln\left|\frac{V_{cc}}{V_{con}} - 1\right|(C_T(2R_T + R_a))} \qquad (2)$$

$$f_s = f(T) = \frac{1}{\ln\left|\frac{V_{cc}}{V_{con}} - 1\right|(C_T(2R_{T25}e^{B(\frac{1}{T} - \frac{1}{298})} + R_a))} \qquad (3)$$

Where, R_{T25} is the resistance of the thermistor at 25°C, which together with B is given in the reference data of the thermistor of the manufacturer.

The graph of the transformation function given in Eq.3 and their first and second derivatives with respect to temperature T f' (T) and f" (T) are shown in Fig.3.

The above transformation function (3) contains an inflection point which is the extreme point of the first derivative and the corresponding value in the second derivative is zero. Around the inflection point, the changes for the first derivative are least and the characteristic of the measure can be treated as linearized in this range.

3. Experimental Results

NTC thermistors with different parameters have been selected to conduct the investigations. The V2O5-based thermistor has been used in the investigation and it has prepared using classical ceramic technology [20] in which the ceramic samples have been synthesized at a temperature of 660°C for 2 hrs. After being fired, the ceramic samples have been ground and cleaned in an ultrasonic basin. They have been coated with Leitsilber 200 (a silver solution in ethylene glycol and xylol) to form electrodes. The experimentally investigated thermistors [18], [19] are shown in Table 1.

3.1 Simulation of the proposed circuit characteristic for the thermistor linearization

For the simulation, LabVIEW software package has been used. The proposed circuit has been simulated with the virtual process having the temperature variation from 0°C to 120°C and the corresponding front panel diagram is as shown in Fig.4. A simulation of the proposed circuit characteristic is conducted for thermistors with the parameters given in Table 1 at Rτ= 1000Ω , Cτ=120 nF and Vcon=2V. The simulated results are shown in fig.5. According to the simulation results, the linearity in the widest range is observed for therm 1 (0°C to 120°C) which has the lowest value of B. The linearized segment for therm 2 is between 30°C to 120°C whereas for therm 3 it is above 90°C. To achieve linearized characteristic for therm 3, higher value of Rτ is used. The simulation result for all the thermistors when Rτ=6000Ω and Cτ=50nF is shown in fig.6. the characteristic shows linearization for therm 3 in the range around 40°C to 120°C.

3.2 Experimental investigation

The investigation of the temperature dependences is carried out using a water bath in the range from 0°C to 120°C. The experiment is carried out with the proposed circuit and thermistors with the parameters used same as simulations. The temperature is measured using a mercurial thermometer with precision of up to 0.5°and the resistance has been measured with the 4 digit TX3 true digital multimeter.

The output frequency and voltage of the proposed circuit insignificantly change with the change in temperature. The error from the temperature influence on the frequency output circuit for the thermistors is significantly small.

4. Conclusion

As a result of the investigations and the simulations conducted in this paper, the possibility of developing the virtual instrument as a temperature sensor based on the modified 555 with frequency as output and a linearized characteristic has been shown. The linearization of the transformation function is achieved without connecting additional elements to the circuit, but rather through a selection of a thermistor and the parameters of the frequency-determining circuit elements and the controlled voltage.

Following conclusions can be made on the basis of the obtained results.

1) A selection of a thermistor with a lower value of B leads to a wider linearized segment of the thermistor characteristic.

2) A specific frequency range of the output signal of the Thermistor can be selected through a change in the value of the frequency-determining capacitance Cτ of the timer, given the pre specified selected parameters of the thermistor and the frequency-determining resistance Rτ.

3) The sensitivity of the proposed instrument can be improved with the selection of control voltage preferably ranging from 0.5V to 2V.

References

1. K. Singh, N. D. Pandit, and C. Mande, "Effect of CuO as an impurity on the electrical properties of NiO−Mn2O3 NTC thermistor material," *J. Mater. Sci. Lett.*, vol. 1, no. 3, pp. 99–102, Mar. 1982
2. E. D. Macklen, *Thermistors*. London, U.K.: Electrochemical, 1979.
3. W. Heywang, Amorphe und polykristalline Halbleiter. New York: *Springer-Verlag,* 1984.
4. M. Diamond, "Linearization of resistance thermometers and other transducers," *Rev. Sci. Instrum.*, vol. 41, no. 1, pp. 53–60, Jan. 1970.
5. A. Burke, "Linearizing thermistors with a single resistor," *Electron.*, vol. 54, no. 11, pp. 151– 154, 1981.
6. A. A. Khan and R. Sengupta, "A linear temperature/voltage converter using thermistor in logarithmic network," *IEEE Trans. Instrum. Meas.*, vol. IM-33, no. 1, pp. 2–4, Mar. 1984.
7. A. A. Khan, "An improved linear temperature/voltage converter using thermistor in logarithmic network," *IEEE Trans. Instrum. Meas.*, vol. IM- 34, no. 5, pp. 635–638, Dec. 1985.
8. D. Patranabis, S. Ghosh, and C. Bakshi, "Linearizing transducer characteristics," *IEEE Trans. Instrum. Meas.*, vol. 37, no. 1, pp. 66–69, Mar. 1988.
9. D. K. Stankovic, "Linearized thermistor multivibrator bridges for temperature measurement," *IEEE Trans. Instrum. Meas.*, vol. IM-23, no. 2, pp. 179–180, Jun. 1974.
10. D. Stankovic and J. Elazar, "Thermistor multivibrator as the temperature-to-frequency converter and as a bridge for temperature measurement," *IEEE Trans. Instrum. Meas.,* vol. IM-26, no. 1, pp. 41–46, Mar. 1977.
11. B. Sundvist, "Simple, wide-range, linear temperature-to-frequency converters using standard thermistors," *J. Phys. E, Sci. Instrum.,* vol. 16, no. 4, pp. 261–264, Apr. 1983.
12. R. N. Sengupta, "A widely linear temperature to frequency converter using a thermistor in a pulse generator," *IEEE Trans. Instrum. Meas.*, vol. 37, no. 1, pp. 62–65, Mar. 1988.
13. S. Natarajan and B. B. Bhattacharyya, "Temperature-to-time converters," *IEEE Trans. Instrum. Meas.,* vol. IM-26, no. 1, pp. 77–79, Mar. 1977.
14. W. T. Bolk, "A general digital linearizingmethod for transducers," *J. Phys. E, Sci. Instrum.*, vol. 18, pp. 61–64, 1985.
15. W. Balzer, "Sensorkennlinien linearizieren," *Feinwerktechnik und Messtechnik*, no. 6, pp. 221–226, 1992.
16. Falcon, J.S. "LabVIEW State Diagram Toolkit for the Design and Implementation of Discrete-Event Systems", *2006 8th International Workshop* on 10-12 July 2006 Page(s):469 – 470
17. Akram, G.; Jasmy, Y.; "Numerical Simulation of the FDTD Method in LabVIEW", *Microwave Magazine,IEEE* Vol. 8, Issue 6, Dec. 2007 Page(s):90 – 99533
18. Zvezditza P. Nenova and Toshko G. Nenov, Member, IEEE ,"Linearization Circuit of the Thermistor Connection" *IEEE Trans Instrum Meas*., Vol. 58, NO. 2, Feb 2009.
19. J. Lam and P. K. Jain, "A novel valley fill high power factor electronic ballast with dimming feature and low crest factor—Part II. Controller circuit design," in Proc. *IEEE 2005 Ind. Electron. Soc. (IECON)*, pp. 820 825.
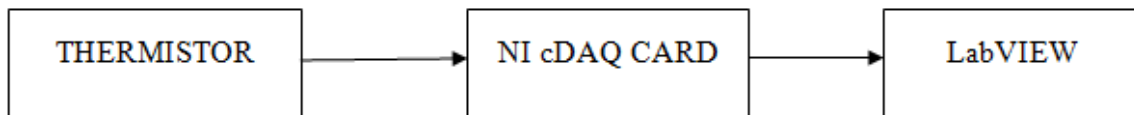
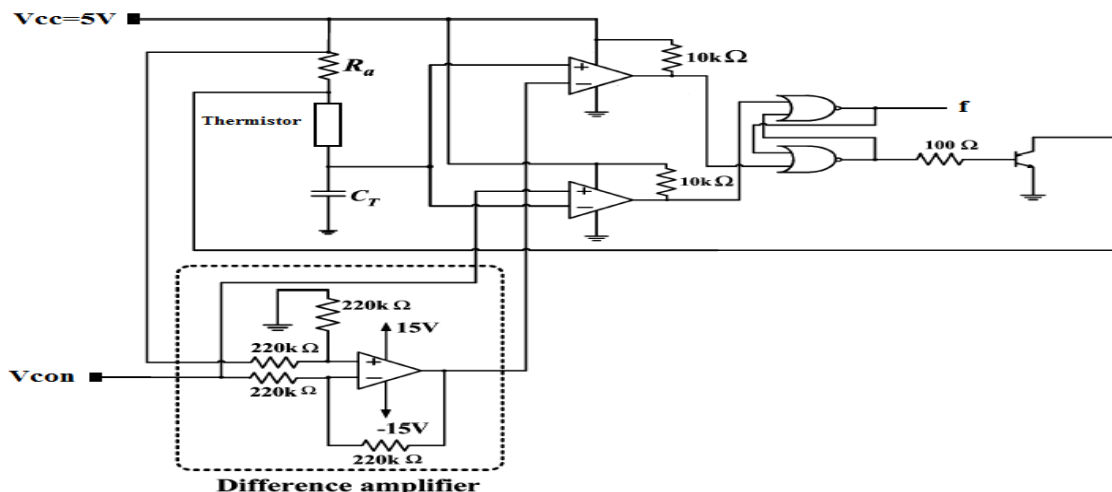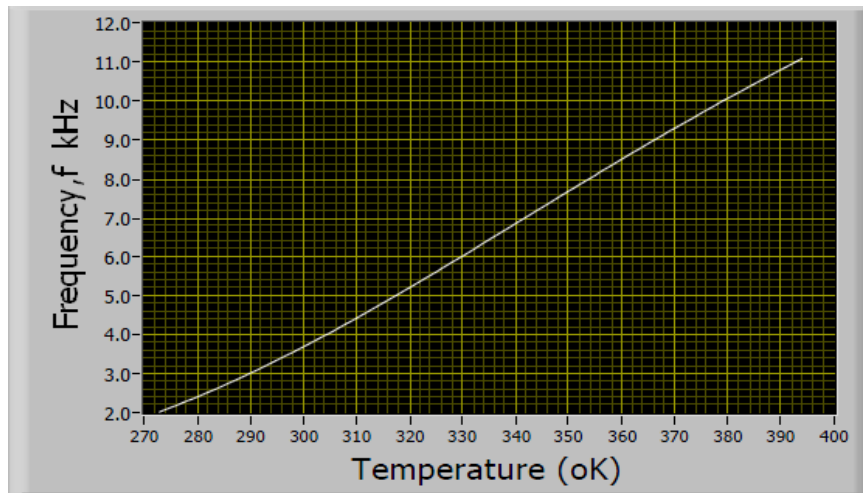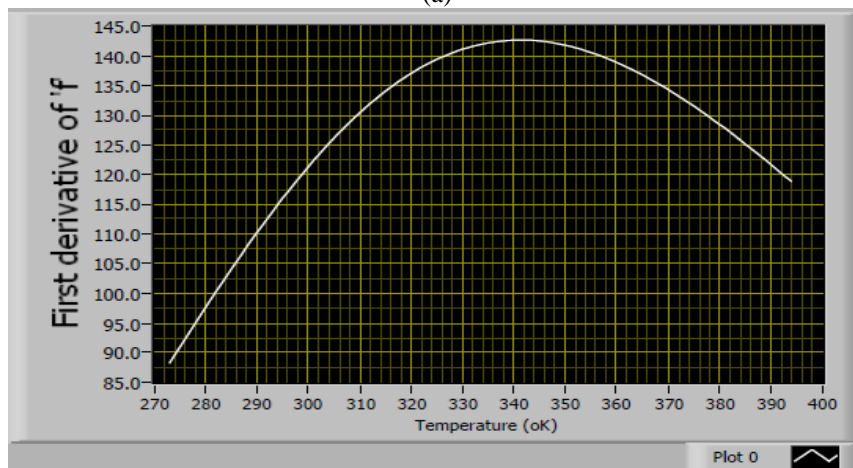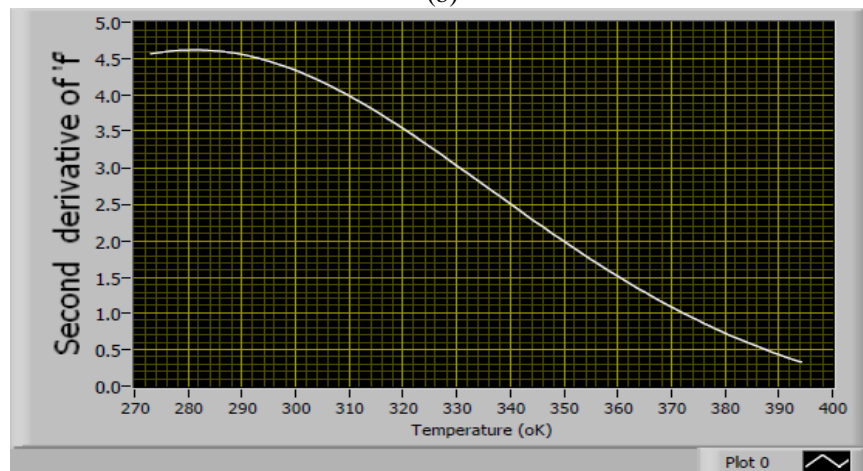**Fig.1.**Thermistor data acquisition system

Fig. 2. Modified 555 Timer

(a)

(b)

(c)

Fig.3. (a) connection circuit characteristic f =F (T). (b) First derivative. (c) Second derivative

Table 1. Thermistor parameters used for the simulations.

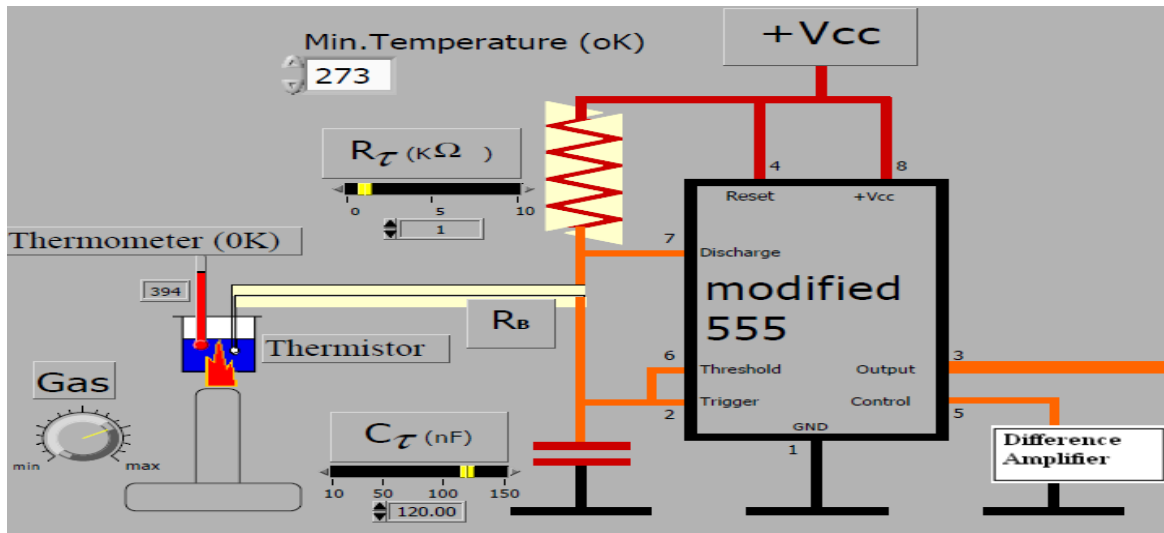| Thermistor	Material /Type	B25/85,K	Resistance at 25°C
Therm 1	V2O5	2109	2.4 kΩ
Therm 2	NTC thermistor Philips	3977	4.7kΩ
Therm 3	NTC thermistor Philips	4190	47kΩ

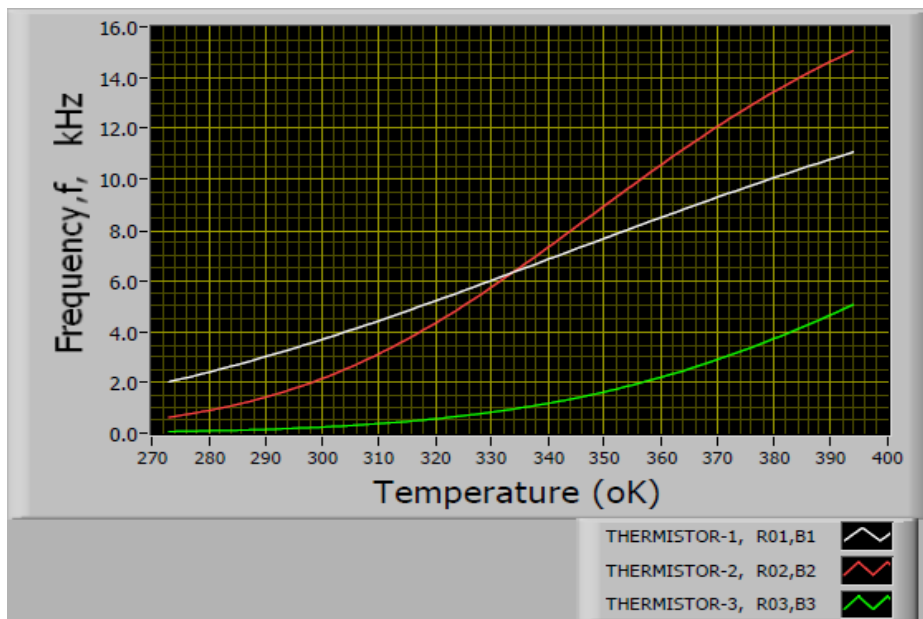**Fig.4**. Front panel diagram showing the connection of thermistor.

Fig.5. Simulated characteristic of thermistor (Rτ=1000Ω, Cτ=120nF)

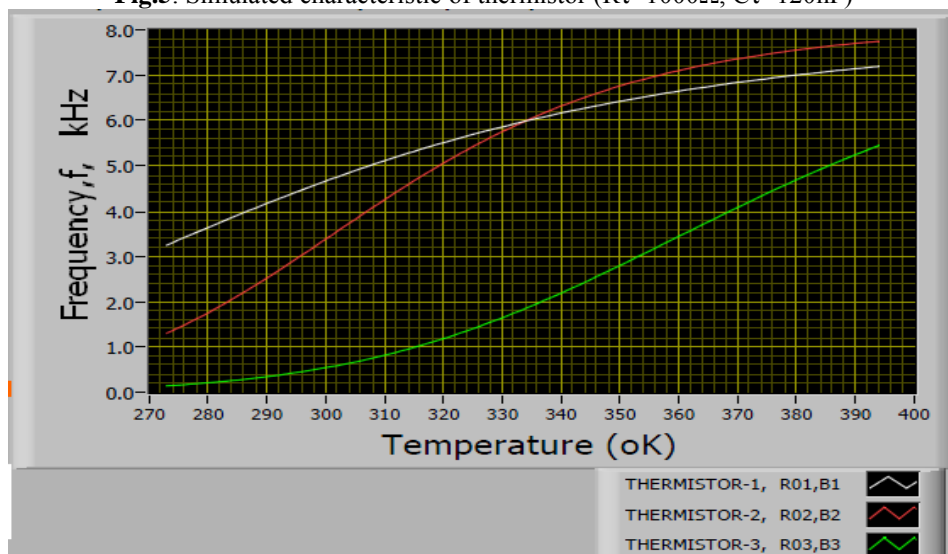**Fig.6.** Simulated characteristic of thermistor (Rτ=6000Ω, Cτ=50nF)

A Computer Program for Sizing and Performance Evaluation of Reciprocating Process Gas Compressors

Tonye K. Jack

Department of Mechanical Engineering, University of Port Harcourt, Port Harcourt, Nigeria

ABSTRACT

Delivering gas to final header storage tanks or end user locations require the use of pipelines and a means of transporting the gas through the lines. A gas compressor is employed satisfactorily to such needs. Gas compressor types vary (from the dynamic type to the positive displacement type) and which to apply for a particular service requirement will depend on the process conditions. For high pressure delivery, and low gas flow volume process conditions, the positive displacement type of reciprocating compressors is often the choice. Matching the compressor equipment manufacturer's available equipment designs to the various process conditions involves several parameters and requires a detailed selection process conducted by the Engineer. A computer program in Microsoft Excel ^{TM} to handle the selection process is described here, with the equations to develop one.

KEYWORDS COMPRESSORS, COMPRESSOR SELECTION, ENGINEERING WITH MICROSOFT EXCEL, GAS COMPRESSOR SIZING, PERFORMANCE EVALUATION OF COMPRESSORS, RECIPROCATING COMPRESSOR SELECTION.

1. INTRODUCTION

The standard practice in the industry application of compressors is to apply positive displacement Reciprocating type Compressors for low flows usually within limits of about 900 cubic metres per minute (m^3/min). Over and above this, the dynamic design Centrifugal type Compressors is the choice by most equipment owners. Reciprocating Compressor Equipment Manufacturers, design various sizes to meet with the variable process conditions. Designs are of two types - Single acting cylinder or a double acting piston. Single acting units are often applied in low gas power of less than 15 kW [1]. In the dual-acting design, compression occurs either when the piston moves on the inward stroke, toward the crankshaft, or outward stroke, away from the crankshaft. Thus, compression occurs on both sides of the piston. For better operational stability and to minimise dynamic loads in operation, a variant of the double-acting with opposed cylinder-piston connection of equal sizes, in pairs, arranged horizontally and connected to a common shaft called a Tandem cylinder arrangement, allows for load balancing. Such units are usually applied to handle larger gas compression requirements and are made up of two or more stages of compression, with each stage being a cylinder-piston connection.

Equipment Sizing or Selection for a Reciprocating Compressor is on a stage-by-stage evaluation basis. Important Considerations in such analysis as stated by [1, 2] will include amongst others:

a.   Temperature rise across a stage
b.   Frame or Piston rod loading
c.   Total pressure rise across a stage
d.   Valve design and losses

2. MATHEMATICAL RELATIONSHIPS FOR RECIPROCATING COMPRESSORS

2.1. Overall Compression ratio

$$r_c = \frac{P_2}{P_1} \qquad\qquad (1)$$

P_2 = Discharge or Final Delivery Pressure (bar)
P_1 = Suction Pressure (bar)

Knowledge of overall or total compression ratio, r_c, i.e. the ratio of the final delivery pressure to the initial suction pressure, is a guide to first estimation of the number of stages, with corrections being made based on temperature rise limitations. Neerken [1] advises to limit compression ratio for a stage to ≤ 3.5.

2.2. Gas Properties and Specific Heat Ratio

Gas for compression can be a single gas or a mixture made up of several gases. A gas analysis is usually conducted to determine mixture properties. A good program development guide is to have a stored database of critical properties of different gases as shown from the selection taken from [3]. Selection can then be made with a combo button. With knowledge of the percentage by volume of the gases, a mole percentage analysis can be conducted to obtain the final mixture properties. Gas Mixture analysis is handled by the method outlined in section 2.28.

The ratio of specific heats, k, is obtained from the table of specific heats at constant pressure taken at two temperature values [3].

$$k = \frac{C_p}{C_v} = \frac{C_{pmix}}{\left(C_{pmix} - 8.314\right)} \qquad (2)$$

C_p = Specific heat at constant pressure
C_v = Specific heat at constant volume
C_{pmix} = Gas mixture specific heat

Proper estimation of the value of the ratio of specific heats, k, should be based on average of the values at suction and discharge, k_{ave}. Linear interpolation and extrapolation is applied to obtain the mid-point and out of range value for temperature falling between and outside the ratios of specific heats, k, in the database. Thus,

$$k_{ave} = k_0 + \frac{T_{ave} - 0}{100}\left(k_{100} - k_0\right) \qquad (3)$$

Or

$$k_{ave} = \frac{C_{p-ave}}{C_{p-ave} - 8.314} = \frac{C_{p-0}}{C_{p-0} - 8.314} + \frac{T_{ave} - 0}{100}\left(\frac{C_{p-100}}{C_{p-100} - 8.314} - \frac{C_{p-0}}{C_{p-0} - 8.314}\right) \qquad (4)$$

Where, T_{ave} = Average temperature (K)

$$T_{ave} = \frac{T_d + T_s}{2} \qquad (5)$$

T_d = Discharge temperature (K)
T_s = Suction temperature (K)

Table 1: Gas .Critical Properties

Chemical Compound	Chemical Formula	Molecular Weight, Mw	Specific of heat ratio, k	Pc (bar)	Tc (0 ^{0}C)	Cp at 0 ^{0}C	Cp at 100 ^{0}C	Acentric Factor, w
Methane	CH4	16.04	1.31	46.4	191.1	34.5	40.13	0.0115
Ethane	C2H5	30.07	1.19	30.07	305.4	49.49	62.14	0.0908
Propane	C3H8	44.097	1.13	42.6	370	68.34	88.68	0.1454
Carbon Dioxide	CO2	44.01	1.3	73.8	304.1	36.04	40.08	0.225
Ethylene	C2H2	28.05	1.24	51.2	283.3	40.9	51.1	0.089

Source: Gresh [3]

2.3. Relative Density and Density of gas

$$\gamma_{sp.gr} = \frac{M_{w-gas}}{M_{w-air}} = \frac{\rho_{gas}}{\rho_{air}} \qquad (6)$$

2.4. Loss Factor

Frictional losses in the pistons and rings, piston rod packing, pulsations due to gas surge effects, and oscillations of valves are often accounted for using one of several methods. Scheel [2] suggest that estimates of Pulsation or Pulse Damper Loss be made in line with:

Pulsation or Pulse Damper Loss = 1% of absolute pressure at suction and discharge (7)

Mak [4] has provided a curve fit relationship of the Ludwig loss factor, L_o, curve as a function of the pressure ratio, given by equation (8):

$$L_0 = -0.002188\, r_c^7 + 0.05778\, r_c^6 - 0.6356\, r_c^5 + 3.7711\, r_c^4 - 13.036\, r_c^3 + 26.331\, r_c^2 - 29.019\, r_c + 14.929$$

$$(8)$$

The Scheel [2] method is applied in the program.

2.5. Approximate Compression Ratio per Stage

$$r_{c-stg.} = r_c^{\left(1/N_{stg}\right)} \qquad (9)$$

Where, $N_{stg.}$ = Number of stages
r_{c-stg} = compression ratio per stage

It was stated earlier that, Single cylinder applications are for low pressure ratios. For high pressure applications, multistage units are the choice to cope with the temperature variations required for efficient performance delivery. The overall compression and hence compression ratio is shared into a number of stages in line with equation (9) to allow for equal work in each stage. Such multistage units often have intercoolers between each stage [1, 5].

2.6. Suction Pressure per Stage

Accounting for the pulsation loss, the corrected suction pressure per stage is:

$$P_s = P_1 - PulsationLoss \qquad (10)$$

2.7. Approximate Discharge Pressure per Stage

$$P_{d-stg.} = \left(r_{c-stg.}\right)\left(P_s\right) \qquad (11)$$

2.8. Inter-stage Pressure Drop

$$P_{i-drop} \cong 0.1\left(P_{d-stg.}\right)^{0.7} \qquad (12)$$

Gas cooling between stages necessitates, making allowance for the pressure drop in the intercoolers [1]. In selecting compression ratios for a system unit, this is to be considered and adjustments made to computation of the actual discharge pressure in line with equation (12).

2.9. Actual Discharge Pressure

Actual discharge pressure will require that the inter-stage pressure drop be accounted for by adjusting the approximate discharge pressure which is a function of the adjusted suction pressure due to the pulsation losses, and the approximate stage compression ratio. This is given by equation (13):

$$P_{d-actual} = P_{d-stg.} + P_{i-drop} \qquad (13)$$

2.10. Actual Compression Ratio per Stage

$$r_{c-actual} = \frac{P_{d-actual}}{P_s} \qquad (14)$$

Optimum gas power is achieved when compression ratios in each of the stages are equal for multistage units. However, limits on the gas power capacity of individual cylinders, makes it impossible to obtain equal and hence, balanced compression ratios [6].

2.11. Suction Valve Loss Experienced in Filling Cylinder

$$\theta_s = \left(aU\right)^2\left[\frac{M_w}{10^4 T_1}\right] \qquad (15)$$

Where,

θ_s = Suction valve loss
a = Piston/valve area ratio
U = Average piston speed in metre per second (m/s)
M_w = Gas Molecular weight
T_1 = Suction temperature in Kelvin (K)

Scheel [2] gives Piston/Valve area ratio values between 8 and 12 for modern compressors. The Piston/valve area ratio is dependent on the pressures to be handled and valve opening lift, with higher pressures requiring lower valve lifts. Equally, lower Piston/valve area ratio requires a high lift valve. For good design practice [2] suggests an average value of 10. For air and lighter gases, a piston/valve area ratio of 13 is recommended.

2.12. Required Mean Pressure to Exhaust the Cylinder Displacement

$$\theta_d = \frac{\theta_s}{r_c^{\left(k-1/k\right)}} \qquad (16)$$

2.13. Average Piston Speed

$$U = 2NL \qquad (17)$$

U = Piston speed in metre per minute (m/min)
L = Piston Stroke, in metre (m)
N = Design rotating Speed, in RPM

2.14. Intrinsic Correction Factor

$$B = \frac{\left(1 + \theta_d\right)}{\left(1 - \theta_s\right)} \qquad (18)$$

The intrinsic correction factor, *B*, extends the normal compression ratio, r_c, to represent the actual effective, compression ratio, $r_{c-actual}$, within the cylinder [2].

2.15. Compression Efficiency

This is the ratio of adiabatic efficiency to mechanical efficiency and given by equation (19)

$$\eta_c = \frac{\left[r_c^{(k-1/k)} - 1 \right]}{\left[Br_c^{(k-1/k)} - 1 \right]} \qquad (19)$$

2.16. Suction Inlet Capacity to the Stage

$$Q_s = \frac{Q_{std.}}{60 \, x \, 24} \times \frac{P_{std.}}{P_s} \times \frac{T_s}{T_{std.}} \times \frac{Z_s}{1.0} \qquad (20)$$

Standard pressure and temperature have been set by the international committee on weights and measures [7]. For metric standards, the following values apply:

$P_{std.}$ = atmospheric pressure ≈ 1.01325 bar
$T_{std.}$ = standard temperature = 293.15 K (20 deg C)

These values are applied in the program.
This is also the standard adopted by the American Society of Mechanical Engineers (ASME) Power Test Codes Committee [7].
An alternate value adopted by other Engineering standardisation bodies such as the American Gas Association (AGA) is 288.15 K (15 deg C) [7].

$Q_{std.}$ = Inlet Capacity volume at *standard condition (scmd- standard cubic metre per day or m³/day)*
Q_s = Inlet Capacity volume at *inlet condition (m³/min)*
P_s = inlet pressure (bar)
T_s = inlet temperature (K)
Z_s = Compressibility at inlet

2.17. Mass Flow

The mass flow rate or weight flow of the gas is defined by the equation (21):

$$M = \frac{Q}{v} = \rho_{gas} Q \qquad (21)$$

Where,
M = Mass flow rate of gas (kg/min)
Q = Volume flow rate (m³/min)
v = Specific volume of gas (m³/kg) = $1/\rho_{gas}$

2.18. Specific Volume

$$v = \frac{ZRT}{P} \qquad (22)$$

Where,
Z = Gas Compressibility
R = Gas Constant = $8314/M_w$
M_w = Gas Molecular Weight

2.19. Adiabatic Head of Compression

$$H_{ad} = Z_{av} RT \left(\frac{k}{k-1} \right)_1 \left[r_c^{(k-1/k)} - 1 \right] \qquad (23)$$

H_{ad} = adiabatic head of compression (kN.m/kg)
Z_{av} = average gas compressibility at suction and discharge
Note that the adiabatic head equation (23) is also applied on a stage-by-stage basis.

2.20. Compression Power

$$GP = \frac{MH_{AD}}{\eta_C} \qquad (24)$$

GP = Compression Power or Gas Power (kW)

2.21. Volumetric Efficiency

$$\varepsilon_v = 0.97 - C_c \left[\frac{r_c^{(1/k)} - 1}{\left(Z_2 \big/ Z_1 \right)} \right] \qquad (25)$$

Volumetric efficiency, ε_v, defined as the amount of gas volume displaced with each stroke of the piston, decreases with an increase in compression ratio [2], [6].

The retained volume at the end of a piston stroke is the Cylinder clearance, C_c, expressed as a percentage of the swept volume and is usually provided by compressor equipment manufacturers. Scheel [2] gives a minimum clearance value of about 10 %. Suggested value is within the range of 10 % to 15 % for equipment selection purposes [1].

2.22. Cylinder Displacement Required

$$C_{dis} = \frac{Q_s}{\varepsilon_v} \qquad (26)$$

2.23. Cylinder Diameter

Cylinder diameter, *D*, is based on the area of the Head-end.

$$D = \sqrt{\left(\frac{4 A_{he}}{\pi} \right)} \qquad (27)$$

2.24. Area of Head-end

$$A_{he} = \frac{\pi D^2}{4} \qquad (28)$$

Where,
A_{he} = Area of Head-end (m^2)
D = cylinder diameter (mm or m)

2.25. Area of Crank-end

$$A_{ce} = A_{he} - \left(\frac{\pi d^2}{4} \right) \qquad (29)$$

Where,
d = piston rod size diameter (mm or m)
A_{ce} = Area of Crank-end (m^2)

2.26. Frame Load in Compression

Frame loads are the maximum permissible forces that can be sustained due to the pressures acting on the piston.

$$F_{LC} = P_d A_{he} - P_s A_{ce} \qquad (30)$$

F_{LC} = frame load in compression (N)

2.27. Frame Load in Tension

$$F_{LT} = P_s A_{he} - P_d A_{ce} \qquad (31)$$

F_{LT} = frame load in tension (N)

2.28. Compressibility Calculation by Redlich-Kwong Equation of State

The calculation of compressibility factor based on the Redlich-Kwong Equation of State (EoS) – Corresponding State Method can be defined by the functional relationship, $Z=f(T_r, P_r)$. Results were within reasonable accuracy. The Redlich-Kwong Corresponding State EoS is of the form given by Edmister [8]:

$$Z^3 - Z^2 + \left[\frac{\Omega_a P_r}{T_r^{2.5}} - \frac{\Omega_b P_r}{T_r} \left(1 + \frac{\Omega_b P_r}{T_r} \right) \right] Z - \frac{\Omega_a \Omega_b P_r^2}{T_r^{3.5}} = 0 \qquad (32)$$

Where,

Ω_a = 0.42748
Ω_b = 0.08664
P_r = Reduced pressure = P/P_c
T_r = Reduced temperature = T/T_c

P_c = Critical Pressure (bar)
T_c = Critical Temperature (K)

2.28.1. Solution to the Redlich-Kwong Cubic Compressibility Equation

A number of methods are available for solving cubic polynomial equations [7, 8]. The method of solution using Microsoft Excel ^{TM} is based on the built-in interpolation search solution methods – the Newton method and the Conjugate Gradient method. Noting that the equation (32) is written in a solution form, i.e. the left-hand side equals zero. Using the Solver Add-in option dialog box under the Tools menu, the desired constraints can be set as follows:

Set Target Cell:
Equal To:
Subject to: Guess value:

The Microsoft Excel ^{TM} Goal Seek option can also be applied as a solution method, with care being exercised to avoid having circular references – repeated recalculation of particular cell values as input and output.

2.28.2. Handling Gas Mixture

Gas Mixture analysis with the Redlich-Kwong Equation of State is conducted in line with the relations [8]:

$$\frac{T_{cm}}{P_{cm}} = \sum_{i}^{N} x_i \left(\frac{T_{ci}}{P_{ci}} \right) \tag{33}$$

$$\frac{T_{cm}^{2.5}}{P_{cm}} = \left[\sum_{i}^{N} x_i \left(\frac{T_{ci}^{1.25}}{P_{ci}^{0.5}} \right) \right]^2 \tag{34}$$

$$T_{cm} = \left\{ \frac{\left[\sum_{i}^{N} x_i \left(T_{ci}^{1.25} \middle/ P_{ci}^{0.5} \right) \right]}{\sum_{i}^{N} x_i \left(T_{ci} \middle/ P_{ci} \right)} \right\}^{2/3} \tag{35}$$

$$P_{cm} = \frac{T_{cm}}{\sum_{i}^{N} x_i \left(T_{ci} \middle/ P_{ci} \right)} \tag{36}$$

T_{cm} = Mixture Critical Temperature (K)
P_{cm} = Mixture Critical Pressure (bar)
T_{ci} = Individual gas Critical Temperature (K)
P_{ci} = Individual gas Critical Pressure (bar)
x_i = mol percent or percent by volume of each gas

3. PRACTICAL APPLICATION EXAMPLE WITH PROGRAM INPUT/OUTPUT

Estimate the sizing and performance requirements for a new compressor application in which 116808 m^3/day of a gas mixture is to be compressed in a 3-stage Reciprocating Compressor. The given data are:

Initial Suction Pressure = 14.3 bar absolute
Final Discharge Pressure = 130 bar absolute

Table 1: Example stage specification

	1st stage	2nd stage	3rd stage
Cylinder clearance (%)	15	15	15
Piston/Valve area ratio	10	10	10
Suction temperature (deg. C)	38	38	38

Design Requirements:
Initial suction pressure drop = 1%
Final pressure drop = 1%
Number of cylinders per stage = 1

Stroke length = 450 mm
Piston rod size = 12.5 mm
Desired operating speed = 277 rpm
The gas mixture consists of the following composition:

Table 2: A Gas Mixture Composition

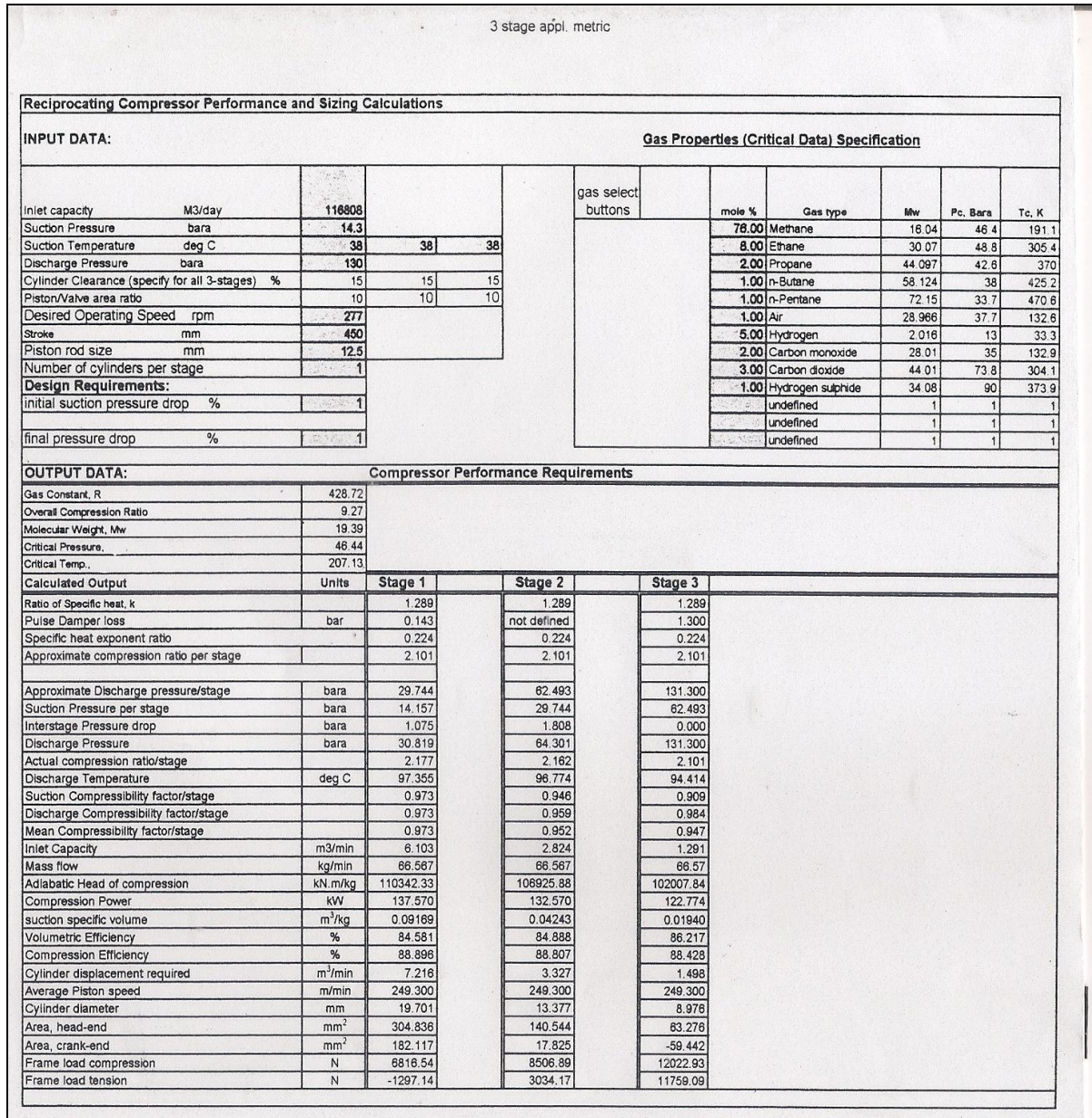| Component	mole percent (%)
Methane	76
Ethane	8
Propane	2
n-Butane	1
n-Pentane	1
Air	1
Hydrogen	5
Carbon Monoxide	2
Carbon dioxide	3
Hydrogen Sulphide	1

Figure 1. Microsoft Excel Program Screen Print-out Solution of input/output for the Example

4. CONCLUSIONS

The programmed solution method using Microsoft Excel (VBA) for the sizing and performance analysis calculations of reciprocating compressors is greatly simplified in handling the several parameters involved. What-if type of analysis can be conducted by changing certain variables such as suction pressure to fulfil limiting discharge pressure condition. The tedium with certain manual tasks in hand calculation is also eliminated.

5. REFERENCES

1.   R. F. Neerken, Keys to Compressor Selection, *Chemical Engineering*, 1979, pp. 17-33.

2.   Scheel, J. F., Gas Machinery, Gulf Publishing, Houston, 1972

3.   Gresh, T., Compressor Performance : Selection, Operation and testing of Axial and Centrifugal Compressors, Butterworth-Heinemann, 1991

4.   H. Mak, Handheld Calculator Program Helps Size New Reciprocating Compressors, *Oil & Gas Journal*, June 25, 1984, pp. 86-89

5.   Brown, R. N., Compressors: Selection and Sizing, Gulf Publishing, 2nd ed., 1997

6.   Ludwig, E. E., Applied Process Design for Chemical and Petrochemical Plants, Vol. 3, Gulf Publishing, Houston, 1993

7.   Avallone, E. A., ed., Baumeister III, T. ed., Sadagh, A. M. ed., Mark's Standard Handbook of Mechanical Engineers, 11th ed., 90th anniversary ed., McGraw-Hill, 2007, pp. -4:27

8.   Edmister, W. C., Applied Hydrocarbon Thermodynamics, Part 1 & 2, 1985

9.   Escoe, K., "Mechanical Design of Process Systems", Vol. 1 & 2, 1986

10.   Reid, R. C., Sherwood, T. K., The Properties of Gases and Liquids, McGraw Hill, 1966

11.   R. C. Reid, Derivative Compressibility factors, *Ind. & Eng. Ch*. Fundamentals, Nov. 1962

Author Information

Tonye K. Jack is a Registered Engineer, and ASME member. He worked on plant maintenance and rotating equipment in the Chemical Fertilizer industry, and on gas turbines in the oil and gas industry. He has Bachelors degree in Mechanical Engineering from the University of Nigeria, and Masters Degrees in Engineering Management from the University of Port Harcourt, and in Rotating Machines Design from Cranfield University in England. He was the Managing Engineer of a UK engineering software company, Alignagraphics. He is currently a University Teacher in Port Harcourt, Rivers State, Nigeria, teaching undergraduate classes in mechanical engineering. His research interests are on rotating equipment engineering, maintenance, engineering management, engineering computer programs, and applied mechanics.
He can be reached by

Active Contours, Gvf and Balloon Model

Abhinav Chopra[1], Seema Rawat[2], Praveen Kumar[3],

B.Tech (CS&E) - 4th Year[1,] Assistant Professor[2,3]
Amity University Noida[1, 2, 3]

Abstract: -
One of the substantial techniques in the field of digital image processing is image segmentation. It is excessively used in the field of medicine provides visual means for identification, inspection and tracking of diseases for surgical planning and simulation. Active contours or a snake is an image segmentation technique which is widely used for boundary detection. They are regarded as promising and vigorously researched model-based approach to computer assisted medical image analysis. However, its utility is limited due some problems caused in the traditional methods, i.e. Poor convergence of concavities and small capture range. This paper shows the application a new model for active contours, which comprises of the Balloon Model and the GVF model. This model helps in improving the detection quality of closed edges, thereby resolving the limitations of the traditional snake model.

Index Terms —Active contour models, balloon model, edge detection, gradient vector flow

1. Introduction

Segmentation is the process of splitting the image into several parts like objects (also called foreground or background. Active contours [1] or snakes provide an effective way of segmentation [2] of curves defined within the image domain that can move under the influence of external and internal forces. These forces are defined such that the snake will shrink wrap to an object boundary. This method is widely used in many applications, including motion tracking, edge detection and segmentation.

There are two types of active contour models in literature today: - *parametric active contours and geometric active contours* [3][4]. Our main focus here is on parametric contours. Parametric active contours synthesize parametric curves within an image domain and allow them to move towards desired features, usually edges. Typically the curves are drawn towards the edges by potential forces, which are defined to be the negative gradient of a potential function. Additional forces like the potential forces and pressure forces together comprise the external forces. There are also internal forces designed to hold the curve together (elastic forces) and to keep it from bending too much (bending forces).

There are two main difficulties we face during the parametric active contour algorithm. First, the active contours have difficulties progressing into boundary concavities. The second problem is that the initial contour must in general, be close to the true boundary or else it will predict an incorrect result. Most of the methods that are proposed to solve the above problems are ineffective in solving both issues and end up creating more difficulties.

In this paper we present two distinct models to help resolve the problems mentioned above. Firstly, the *balloon model* or the expanding snake model helps resolve the problem of small capture range. When the approximate boundary of an object is unknown the traditional model fails to provide accurate results, in such situations using the balloon model shows robustness. Secondly, the *gradient vector flow* (GVF) model[5] which forces active contours into concave regions. GVF is computed as a diffusion of the gradient vectors of a gray-level or binary edge map derived from the image. Since the external forces cannot be written as the negative gradient of a potential function, GVF snake is different from all other snake models used before.

The major advantages of using these models over the traditional model are that it can be initialized far from the boundary since it has a large capture range. And unlike pressure forces, it does not require prior knowledge about when to shrink or expand towards the boundary.

2. Literature survey

A. *Parametric snake model*

The contour [1] is defined in the (*x, y*) plane of an image as a parametric curve

$$\mathbf{v}(s) = (x(s), y(s))$$

Contour is said to possess energy (E_{snake}) which is defined as the sum of the three energy terms.

$$E_{snake} = E_{internal} + E_{external} + E_{constraint}$$

The energy terms are defined cleverly in a way such that the final position of the contour will have a minimum energy (E_{min}) Therefore our problem of detecting objects reduces to an energy minimization problem.

Internal Energy (E_{int}) depends on the intrinsic properties of the curve and is the sum of elastic energy and bending energy.

Elastic Energy ($E_{elastic}$) of the curve is treated as an elastic rubber band possessing elastic potential energy. It discourages stretching by introducing tension.

$$E_{elastic} = \frac{1}{2}\int_s \alpha(s)\,|\,v_s\,|^2\,ds \qquad\qquad v_s = \frac{dv(s)}{ds}$$

Weight $\alpha(s)$ allows us to control elastic energy along different parts of the contour. Considered to be constant α for many applications.

Bending Energy ($E_{bending}$): The snake is also considered to behave like a thin metal strip giving rise to bending energy. It is defined as sum of squared curvature of the contour.

β(s) plays a similar role to α(s). Bending energy is minimum for a circle.
Total internal energy of the snake can be defined as:-

$$E_{int} = E_{elastic} + E_{bending} = \int_s \frac{1}{2}(\alpha\,|\,v_s\,|^2 + \beta\,|\,v_{ss}\,|^2)ds$$

$$E_{bending} = \frac{1}{2}\int_s \beta(s)\,|\,v_{ss}\,|^2\,ds$$

External energy (E_{ext}) of the contour is derived from the image so that it takes on its smaller values at the function of interest such as boundaries. Define a function $E_{image}(x,y)$ so that it takes on its smaller values at the features of interest, such as boundaries.

Key rests on defining $E_{image}(x,y)$.

$$E_{ext} = \int_s E_{image}(v(s))ds$$

Energy and force equations: The problem currently on hand is to find a contour v(s) that minimize the energy functional

$$E_{snake} = \int_s \frac{1}{2}(\alpha(s)\,|\,v_s\,|^2 + \beta(s)\,|\,v_{ss}\,|^2) + E_{image}(v(s))ds$$

Using variational calculus and by applying Euler-Lagrange differential equation we get following equation

$$\alpha v_{ss} - \beta v_{ssss} - \nabla E_{image} = 0$$

Equation can be interpreted as a force balance equation.

$$F_{int} + F_{image} = 0 \qquad\qquad F_{ext} = -\nabla E_{image}$$

Each term corresponds to a force produced by the respective energy terms. The internal force F_{int} discourages stretching and bending while the external potential force F_{image} pulls the snake toward the desired image edges.
Solving the Euler equation:-
Consider the snake to also be a function of time i.e. $\quad v_t(s,t)$

$$\alpha v_{ss}(s,t) - \beta v_{ssss}(s,t) - \nabla E_{image} = v_t(s,t)$$

$$v_t(s,t) = \frac{\partial v(s,t)}{\partial t}$$

If RHS=0 we have reached the solution. On every iteration update control point only if new position has a lower external energy. Snakes are very sensitive to a false local minimum which leads to wrong convergence.

B.   Weakness of Traditional Snakes

<table>
<tr><td>(a)</td><td>(b)</td><td>(a)</td><td>(b)</td></tr>
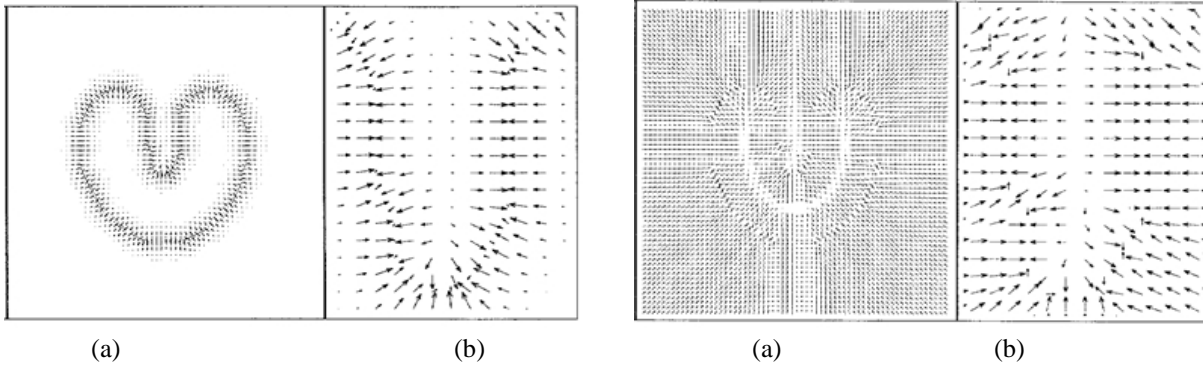</table>

Fig. 1 (a) traditional potential forces and (b) close-up   Fig. 2 (a) traditional distance forces and (b) close-up

An example of behavior of traditional snake is shown in fig. 3(b) and fig. 4(b). In fig. 4(b) we can see that it has boundary concavity on the side are left vacant. This snake formulation is a result of Euler's equation and we can see that it remains split across the concave region.

The reason for the poor convergence of this snake as seen in fig. 1(b) is because the forces point horizontally in opposite direction. Another weakness of the traditional snake model is that it has a limited capture range; this can be explained in fig. 1(b). The magnitudes of the external forces die out quite rapidly away from the object boundary. The boundary localization will become less accurate and distinct.

External forces are a negative gradient of a potential function that is computed using Euclidean distance map. These forces are referred to as distance potential forces so as to distinguish them from traditional potential forces The distance potential forces shown in fig. 2(a) have vectors with large magnitudes away from the object, explaining why the capture range is large for external force model. In fig.2 (b) the traditional potential forces are horizontally in opposite direction, which pulls the snake apart and not downward into the boundary concavity.Hence the problem of convergence is not solved by distance potential forces

3.   Balloon Model

The snake model originally introduced by Kass has been further developed by modified in recent years. The balloon model or the expanding snake mode [6] is one of the examples of this. Unlike, the traditional snake that shrinks wraps to the image boundary, this snake model expands outwards.

This model is based on an additional inflation force applied to give stable results. A snake which is not close to contours is not attracted by them. The curve behaves like a balloon which is inflated. When it passes by edges, will not be trapped by spurious edges and only is stopped when the edge is strong. The initial guess of the curve not necessarily is close to the desired solution. Pressure force is added to the internal and external forces.

The expansive behavior is achieved by modifying the values of f_x; f_y as followed,

$$f_x(x,y) = k_1 n(s) - k \frac{\nabla P_x}{\|\nabla P_x\|}$$
$$f_y(x,y) = k_1 n(s) - k \frac{\nabla P_y}{\|\nabla P_y\|}$$

where n(s) is the unit principal normal vector to the curve at point v(s), and k_1 is the amplitude of this force. k_1 and k are chosen such that they are of the same order, which is smaller than a pixel size and k is slightly larger than k_1 so an edge point can stop the Inflation force. The curve then expands and it is attracted and stopped by edges as before. The smoothing effect with the help of the inflation force then removes the discontinuity and the curve then passes through the edge.

4.   Gradient Vector Flow Snake

The overall approach is to use the force balance condition as a starting point to design the snake. This parametric curve thus formed is called GVF snake.

Gradient Vector Flow:- The GVF field is defined to be a vector field **:-**   V(x,y) = $(u(x,y), v(x,y))$

Force equation of GVF snake is, $\alpha v_{ss} - \beta v_{ssss} + V = 0$

V(x,y) is defined such that it minimizes the energy functional,

$$E = \iint \mu(u_x^2 + u_y^2 + v_x^2 + v_y^2) + |\nabla f|^2 |V - \nabla f|^2 \, dxdy$$

f(x,y) is the edge map of the image.
GVF field can be obtained by solving following equations

$$\mu \nabla^2 u - (u - f_x)(f_x^2 + f_y^2) = 0$$

$$\mu \nabla^2 v - (v - f_y)(f_x^2 + f_y^2) = 0$$

∇^2 Is the Laplacian operator.
The above equations are solved iteratively using time derivative of u and v. These equations provide further intuition behind the GVF formulation. We note that in the homogenous region the second term in both regions is zero because the gradient of f(x, y) is zero.

4. Results and Discussion

The Expanding snake model increases the capture range of an active contour. After its application we can see that the snake can move towards object boundary (fig. 4(b)) whereas in the case of the traditional snakes, they had a smaller capture range (fig. 3(b)).

(a)   (b)

(c)   (d)
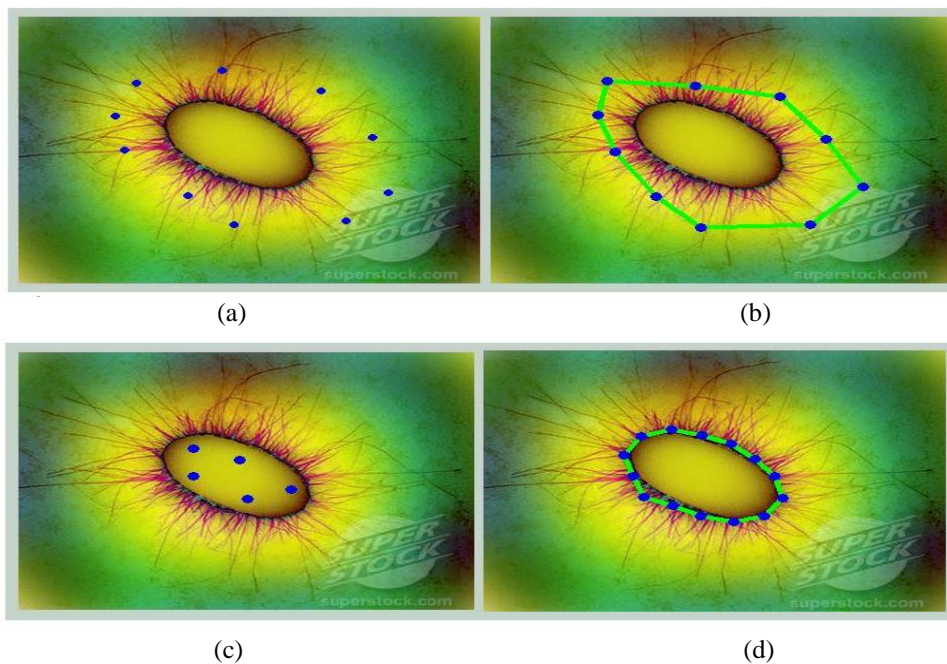
Fig3.(a) snake boundary using traditional snake , (b) small capture range of traditional snake, (c) snake boundary using balloon model and (d) problem of the small capture range resolved

The application of the GVF snake model shows that the snakes can move into boundary concavities (fig. 4(c)) as compared to the traditional snake model (fig. 4(b)).
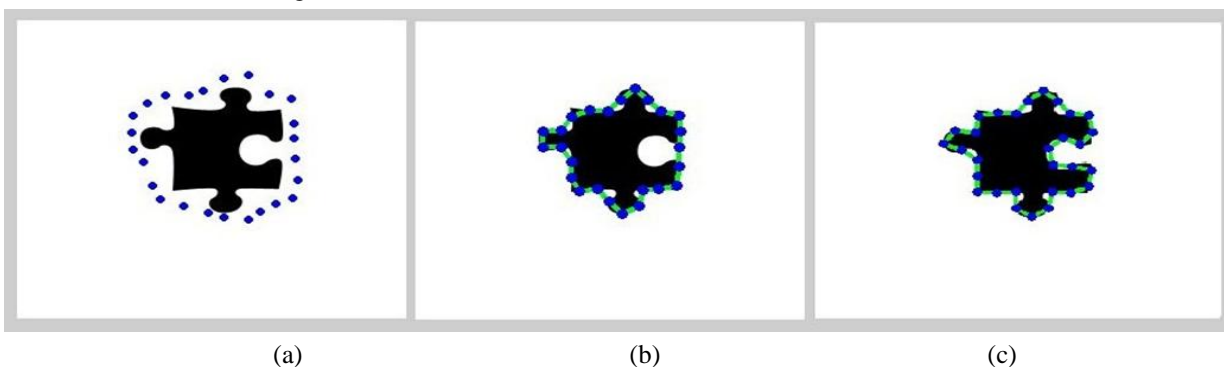

(a)   (b)   (c)
Fig4.(a) Convergence of a snake using, (b)traditional snakes and (c)using GVF snake

5. Conclusion

We have presented a model of deformation which can successfully deal with two of the major problems that are encountered in the traditional snake model thereby making it more efficient. Firstly, the Balloon Model which enables us to give an initial guess of the curve which in turn helps us to deal with the problem of small capture range. . Secondly, the application of the Gradient Vector Flow (GVF) model which successfully allows convergence to boundary concavities. This model provides a collective way of treating visual problems that were till now treated differently. We can also conclude that although the GVF snake model and the Balloon Model are both slower than the traditional snake model in the iteration process they provide us with much more accurate.

5. References

[1]   M. Kass, A. Witkin, and D. Terzopoulos, "Snakes: Active contour models," Int. J. Comput. Vis., vol. 1, pp. 321-331, 1987.

[2]   H. Tek and B. B. Kimia, "Image segmentation by reaction-diffusion bubbles," in Proc. 5th Int. Conf. Computer Vision, 1995, pp. 156-162.

[3]   V. Caselles, F. Catte, T. Coll, and F. Dibos, "A geometric model for active contours," Numer. Math., vol. 66, pp. 1-31, 1993.

[4]   R. Malladi, J. A. Sethian, and B. C. Vemuri, "Shape modeling with front propagation: A level set approach," IEEE Trans. Pattern Anal. Machine Intell., vol. 17, pp. 158-175,1995.

[5]   C. Xu and J. L. Prince, "Gradient vector flow: A new external force for snakes,"

[6]   L. D. Cohen and I. Cohen, "Finite-element methods for active contour models and balloons for 2-D and 3-D images," IEEE Trans. Pattern Anal. Machine Intell., vol. 15, pp. 1131-1147, Nov. 1993.

[7]   C. Davatzikos and J. L. Prince, "Convexity analysis of active contour models," in Proc. Conf. Information Science and Systems, 1994, pp.581-587.

[8]   J. L. Prince and C. Xu, "A new external force model for snakes," in Proc. 1996 Image and Multidimensional Signal Processing Workshop, pp. 30-31.

[9]   H. Tek and B. B. Kimia, "Image segmentation by reaction-diffusion bubbles," in Proc. 5th Int. Conf. Computer Vision, 1995, pp. 156-162.

[10]   P. M. Morse and H. Feshbach, Methods of Theoretical Physics. New York: McGraw-Hill, 1953.

[11]   A.K. Jain, Fundamentals of Digital Image Processing. Englewood Cliffs, NJ: Prentice-Hall, 1989

[12]   B. K. P. Horn and B. G. Schunck, "Determining optical flow, Artif.Intell" vol. 17, pp. 185-203, 1981.

[13]   S. N. Gupta and J. L. Prince, "Stochastic models for DIV-CURL optical flow methods," IEEE Signal Processing Lett., vol. 3, pp. 32-35, 1996.

[14]   R. Courant and D. Hilbert, Methods of Mathematical Physics, vol.

[15]   http://wibirama.com/ngaji/data/OpenCV/OpenCVHelp/ref/OpenCVRef_Cv.htm

[16]   http://nik.bmf.hu/vamossy/GepiLatas2007/9Activecontour/ snakeVZ. ppt

[17]   http://iacl.ece.jhu.edu/projects/gvf/

[18]   http://www.inf.uszeged.hu/~kato/teaching/emm/02-Snake.pdf

[19]   http://www.inf.uszeged.hu/~hpke/thesis.pdf

Communication between Host machine and the Host Bus Adapter over PCIE bus using Diagnostic window

Naveen G[1], Sheetal Kulkarni[2], Naresh Madhusudhana[3], K N Raja Rao[4]

[1]M.Tech Student, Digital Communication Engg. R V College of Engg. Bangalore-59
[2]M.Tech Student, Communication System Engg. R V College of Engg. Bangalore-59
[3]System Application Engineer, LSI India R & D India Private Limited Bangalore-102
[4]Professor, Dept. of Telecommunication Engg. R V College of Engg. Bangalore-59

Abstract

In this paper a study of the PCIE interface and the Host Bus Adapter is carried and demonstrated the communication between the HBA and the Host through a Diagnostic Window Access of PCIE. The API are written in java to access the DDR3 and flash memory on the HBA The diagnostic method is a back door mechanism to access the register and memory on HBA through PCIE. The flash memory is used to store the firmware from which the HBA becomes operational. The Flash memory is accessed and the following operation is carried out. The Flash erase, Flash read, Flash program and Flash QRY program is successfully demonstrated. The DDR3 Serial Presence Detect-SEEPROM is accessed using I2C protocol which is contains vital information about the timing parameter and the manufacturer information of DDR3 memory. The SPD data is used to initiate the training of any DDR3 chip and to make the DDR3 operational.

Keywords: DDR3, Flash Memory, HBA, PCIE.

Introduction

The steady increase in the huge volume of data and usage of internet application has motivated several organizations to carry out research in the area of data storage. The storage industry is moving at the faster pace to incorporate high end and high speed technologies in their designs to compete and increase their market size.

The communication is a taking drastic change in its speed and becoming more and more reliable. Sectors like banks, industries, scientific research organization, and social networking sites need huge storage network for data storage for different other applications and even that data should be secured by variety of different methods one such method is RAID (Redundant Array of Independent Disks). In order to communicate with storage network, needs an understanding of how the host communicates with device for example Host Bus Adapter residing on the PCIE (Peripheral Component Interconnect-Express) slot.

PCI Express [1] is the third generation high performance I/O bus that is used for communication between the peripheral devices in the applications such as the storage, communication and the computing platform at a rate of 2.5 Giga bits/second. PCIE implements the dual simplex link which implies that the data can be transmitted to from the device attached to the PCIE simultaneously.

Memory map in the host system
One of the major improvements the PCI Local Bus had over other I/O architectures was its configuration mechanism. In addition to the normal memory-mapped and I/O port spaces, each device on the bus has a configuration space. This is 256 bytes that are addressable by knowing the 8-bit PCI bus, 5-bit device, and 3-bit function numbers for the device (commonly referred to as the BDF bus/device/function). This allows up to 256 buses, each with up to 32 devices, each supporting 8 functions. A single PCI expansion card can respond as a device and must implement at least function number zero. The first 64 bytes of configuration space are standardized; the remainders are available for vendor-defined purposes. A portion of the PCIE configuration register memory map is illustrated in the figure 1.
During the boot process the host machine performs the PCIE Configuration cycles. During this cycle the device attached to the PCIE slot will be uniquely identified by the Bus ID, Device ID and Function ID. Host will allocate the bar register address. This address varies with the system or may change during different boot. The Bar register contain the host memory address from where the device connected will be accessed. Mem0 and Mem1 in a PCIE memory map contain the Base Address Register (BAR) to use in the PCIE memory cycle. BAR will be mapped to Program Inbound Memory (PIM).The size of the Mem1 BAR is programmable, and occupies the specified amount of the possible 2^64 bytes of PCI Memory address space. The entire region maps either to SHELL address space or to PLB Address space of the controller in the HBA connected. The host accessing the device memory map is illustrated in the figure 2.

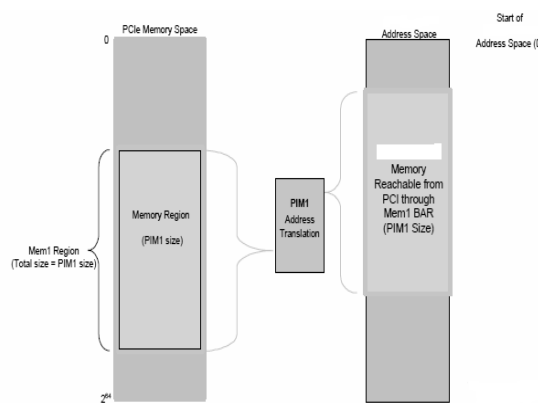Fig.1 A Portion of the PCIE configuration register memory map for Physical function 0

Fig.2 Host accessing the device memory map

PIM Register setup

 The PIM registers (Programmable Inbound Map) define a region in the PLB memory map that can be accessed by a corresponding region in the PCIE memory map. PIM0 uses PCI Memory BAR 0 and PIM1 uses PCI Memory BAR 1. By convention, PIM0 maps to the Messaging Unit registers contained in PCIE core. PIM1 is available to provide arbitrary PLB access to the host. i.e. BAR0 for messaging unit registers and BAR1 for PLB access of the device. The PIM registers are defined as a set of Address and Attribute Registers. The Address registers define an arbitrary PLB address to which PCI Slave transactions will be steered. The Attribute Register defines the operation state of the PIM window. The Host interaction with the Flash /DDR3 memory on HBA is illustrated in the figure 3.
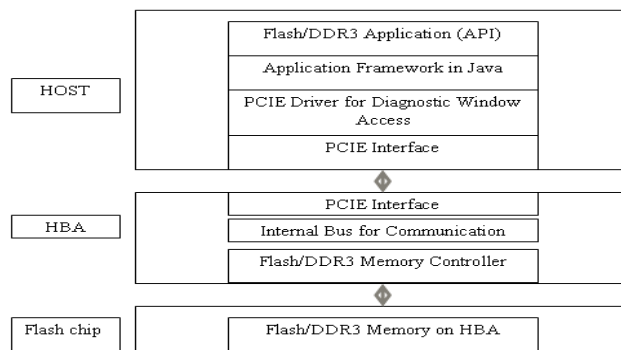

Fig 3: Host Interaction with the Flash /DDR3 Memory on HBA

Methodology

The methodology explains the mapping of the internal memory of HBA can be mapped to host memory

- Enable the Diagnostic Window.
- Use Mem0 to enable the access to diagnostic window. Here we are using PIM0 to configure PIM1.
- In diagnostic window we are writing to the PIM1 address low and PIM1 address high with the PLB base address low and PLB base address high of the region to be accessed.
- Use the Java API's to perform the register read/write, memory read/write operation.

Results and Discussion

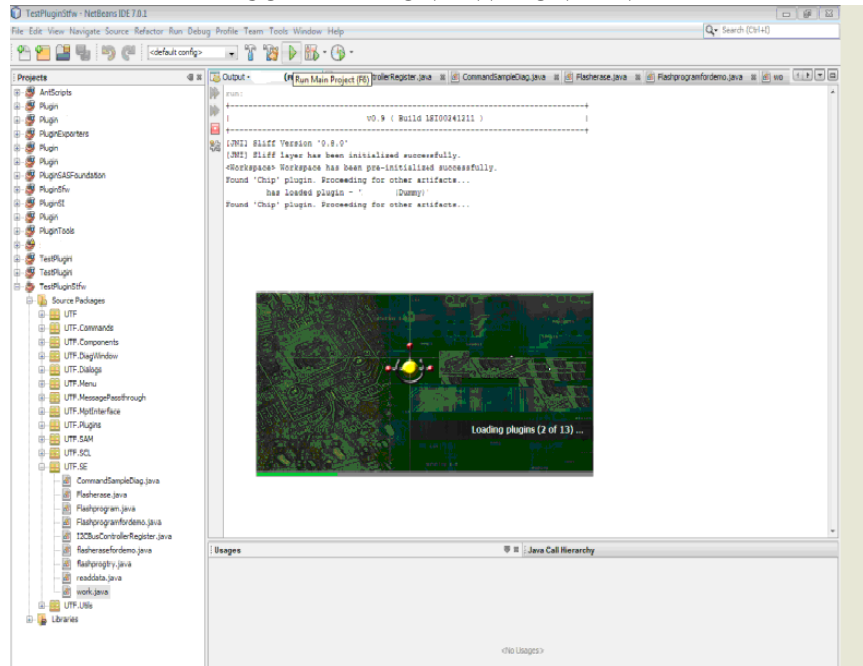**COMPILATION ENVIRONMENT**

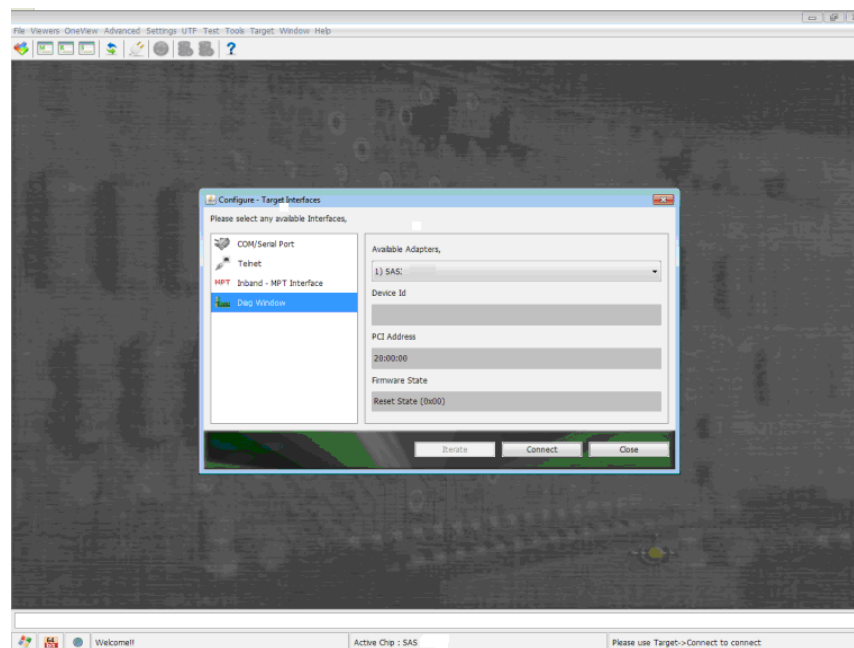Figure 4 Launching of DDR3/Flash Application

Figure 5 Listing of the device under Diag Window

Flash erase operation

Debug : The Given Command is utf se fler

(0xC20C2200) = 0x3370011F

(0xC20C2200) = 0x3371011F

Verbose : Chip erase successful

(0xFC000000) = 0xFF

All done....

Flash Read After Erase

Debug : File has been saved successfully to 'C:\Users\Administrator\Desktop\Flash Erase.html'

Debug : The Given Command is utf se flrd

Verbose : Readng data from flash memory

(0x0) = 0xFF

(0x1) = 0xFF

(0x2) = 0xFF

(0x3) = 0xFF

All done....

Flash Program

Debug : File has been saved successfully to 'C:\Users\Administrator\Desktop\Flash read after the erase.html'

Debug : The Given Command is utf se flprde

Verbose : Flash operation start

(0xC20C2200) = 0x3371011F

(0xC20C2200) = 0x3371011F

Verbose : Chip program in progress :0xFFFFFFAA

Verbose : Chip program in progress :0x55

Verbose : Chip program in progress :0xFFFFFFA0

Verbose : Chip program in progress :0x40

Read value is '0xBBCC

Verbose : 1st byte programmed

Read value is '0x4433

Verbose : 2nd byte programmed

Flash Read after Programming the region

Debug : File has been saved successfully to 'C:\Users\Administrator\Desktop\Program flash.html'

Debug : The Given Command is utf se flrd

Verbose : Readng data from flash memory

(0x0) = 0xCC

(0x1) = 0xBB

(0x2) = 0x33

(0x3) = 0x44

All done....

2. SPD read from DDR3

The first 12 location of SEEPROM is listed below

```
Verbose : Sequence transfer in progress....
The SEEPROM loc '0x0 0x92
The SEEPROM loc '0x1 0x10
The SEEPROM loc '0x2 0xB
The SEEPROM loc '0x3 0x2
Verbose : Recieve transfer in progress....
Verbose : Transmit transfer in progress....
Verbose : Sequence transfer in progress....
The SEEPROM loc '0x4 0x2
The SEEPROM loc '0x5 0x11
The SEEPROM loc '0x6 0x0
The SEEPROM loc '0x7 0x1
Verbose : Recieve transfer in progress....
Verbose : Transmit transfer in progress....
Verbose : Sequence transfer in progress....
The SEEPROM loc '0x8 0xB
The SEEPROM loc '0x9 0x52
The SEEPROM loc '0xA 0x1
The SEEPROM loc '0xB 0x8
```

The result described above shows the diag window method to access the controller memory and registers on the HBA.

Conclusion:

The host communication with the HBA using the diag window access (without firmware on HBA) is one of the methods widely helpful in the communication with HBA. This method establishes communication between the host and the HBA and is implemented in Java. The communication is demonstrated by performing operations on Flash/DDR3 memory in the HBA.

References

[1]   Ravi Budruk et.al. A text book on PCI Express System Architecture

[2]   Standard Development Group http//:www.pcisig.com

[3]   PCI Express 3.0 x 8 8GT/s Fusion MPT 2.0 Core Architecture Specification.

Routing Protocol for Indoor Monitoring Systems

Prof.Sudipta Bhadra, Prof.Sandipan Dutta and Prof.Tapan Chakrabarti

Department of Information Technology
Heritage Institute of Technology
Anandapur, Kolkata-700107, West Bengal, India

Abstract.
Extreme events like fire can cause massive damage to the indoor area. Damage occurs due to the extreme events can cause in life threatening conditions inside the indoor after that event. In such situation wireless sensor network (WSN) [1] based real time event driven indoor monitoring system is necessary to reduce the loss of human lives by identifying the source of the extreme events inside the hazardous indoor area. In this paper we present a routing protocol for a real time event driven indoor monitoring system which is use for selectively monitor the indoor area after an event occurred like fire. In case of fire the temperature recorded using temperature sensor of the stationary sensor motes as well as mobile sensor motes is very vital. Depending on the floor map of indoor, these sensor motes are placed permanently or temporarily. We need to gather sensed data with position information for tracking down the source of the extreme event based on sub area wise comparison of temperature of the total hazardous indoor area.

Keywords: Indoor Monitoring System, Routing protocol, Hazardous indoor area.

1. Introduction

Traditionally, indoor area monitoring systems were wire based. The sensors are placed at several vital points in the structure and connected to a central Data Acquisition Systems over a cable. For indoor area monitoring, the wired systems have lots of primary problems regarding installation and maintenance. Wired systems are not capable of real time event driven hazardous area monitoring. Wireless Monitoring System based on WSN have been used for numerous monitoring applications and suitable for real time event driven indoor area monitoring. A Real-time event driven indoor monitoring system (REIMS) requires the appropriate architecture for WSN topology as well as a suitable routing protocol.

Thus we effectively divide the complete monitoring system into four disjoint parts which are stitched together to make a complete REIMS system for indoor area.

- Localization
- Coverage technique
- Selective clustering routing protocol
- Event detection and data collection from deployment site

The routing protocol proposed by us covers the requirements of REIMS system .

The remainder of the paper is organized as follows. Section 2 describes related work.Section 3.1 describes the design view of REIMS. The implementation of the clustering-based routing protocol for REIMS is given in Section 3.2. Conclusion and future work is given in Section 4.

2. Prior Work

Wireless sensor networks which have been used for several monitoring applications. Foremost are the Habitat monitoring applications such as the great duck island experiment [2], studying the redwood tree macro scope project [3], Zebranet project [4] etc. Many WSN systems have been developed to support environment monitoring [5], object tracking [6], scientific observation [7], and so on. Wireless Sensor Network also provides an solution for indoor monitoring [8,9]. Thomas Schmid [10] describe an indoor environmental monitoring network based on WSNs. Won-Suk Jang used WSN technologies for condition monitoring of buildings [11]. A WSN system described in [12] was deployed in a number of residential and commercial buildings .W.S. Jang and W. M. Healy analyze WSN performance metric for indoor monitoring applications [13]. So, Wireless sensor networks are capable of real time event driven hazardous area monitoring.Routing protocol for those kind of REIMS is very important issue.

3. Design of REIMS

3.1. REIMS Architecture

Each node in the REIMS system is a Cricket motes consisting of an RF transceiver, a microcontroller, and other associated hardware. There are three types of REIMS nodes. They are stationary beacon node, mobile listener node and forwarder node. Stationary node and forwarder nodes are fixed reference points of the Cricket based localization system (nodes pre deployed at ceiling as per coverage algorithm). Forwarder node have same characteristic as stationary beacon node but it have no sensing responsibility. Main responsibility of the forwarder is data forwarding.

The flow of data is from all mobile sensor nodes towards the base station. Figure 1 gives the design view of the REIMS system. The three distinct modules named data collection performed by stationary beacon and mobile listener, data

aggregator performed by mobile listener and data forwarder performed by forwarder node are responsible for sensing, data fusion and data forwarding to the base station.
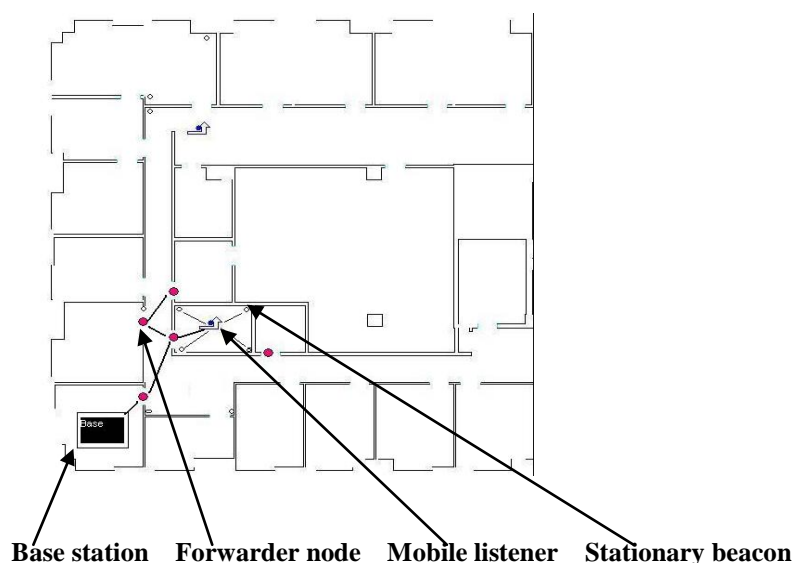

Base station   Forwarder node   Mobile listener   Stationary beacon

Fig. 1: Design View of the REIMS system

3.2.   Routing protocol of REIMS

Our dynamic WSN architecture with a selective clustering routing protocol designed specifically for our real-time event driven indoor monitoring system (REIMS) with the facility of selective monitoring.

According to the map of the indoor area all the nodes in the network are divided into clusters. There are three kinds of sensor nodes in the WSN: the stationary cluster member nodes , the mobile cluster head nodes and the communication backbone nodes.

Therefore the Dynamic WSN architecture we implement is divided into two parts. The first part is consisting of low transmission range, energy constrained stationary cluster member nodes(SCM) and high transmission range mobile cluster head nodes(MCH), which forms the data compilation network . The data compilation network , which is charged with the collection and transmission the sensed data.

The Second part is consisting of large transmission range communication backbone nodes(CB) to the base station, which forms the data communication network. The data communication network is the key to the communication with the base station, which is charged with the forwarding of the monitoring data to the base station and remote control instruction from base station.

In our proposed algorithms, we use four packets. They are as follows.

BEACON_DATA: This is a data packet from SCM to MCH which gives information of sensed data of a SCM. This packet has several fields such as SCM's Id, SCM's position(x,y and z co-ordinate) and sensed data value.

LISTENER_DATA: This is a data packet from MCH to CB which gives aggregated sensed data of MCH to CB. This packet has several fields such as MCH's Id, MCH's position(x,y and z coordinate) , MCH's aggregated sensed data value and MCH's destination Id.

FORWARDER_DATA: This is a data packet from CB to CB or Base station which gives information of aggregated sensed data of a particular MCH. This packet has several fields such as CB's destination Id, MCH's Id, MCH's position(x,y and z coordinate) and MCH's aggregated sensed data value .

DEST_SELECT: This is a data packet from CB to MCH or CB which gives information of level of CB. This packet has several fields such CB's Id and hop count of each CB node from the sink which indicates its level.

Our proposed selective clustering routing protocol has four algorithms for SCM, MCH, CB and Base station as mentioned bellow

---

Algorithm for SCM
1) Initialization of mode :Set mode=Beacon
2) After a random interval send BEACON_DATA packet (contain own id, position data and aggregated sensor data) and go to step 3.
3) Go to step 2.

Algorithm for MCH
1) Initialization of mode: Set mode=Listener, destination=NULL, HOPCOUNT = 1000, COUNT =0.
2) If packet received and type of the packet = DEST_SELECT then go to step 3 otherwise go to step 4.
3) Retrieve value of hop count field of DEST_SELECT packet. If value of hop count < HOPCOUNT then destination = value of CB's Id field of DEST_SELECT packet.
4) If packet received and type of the packet = BEACON_DATA then COUNT = COUNT +1. MCH aggregate sensor data of beacon with its own sensor data based on aggregator function (maximum sensed value) and go to step 5 otherwise go to step 2.
5) If COUNT > 10 and destination! =NULL then Set mode = Beacon and broadcast LISTENER_DATA packet (MCH's id , position data and aggregated sensor data) and then Set mode = listener and go to step 2 otherwise go to step 4.

Algorithm for CB
1) Initialization of mode: Set mode=Listener ,forwardmode = INITIAL, destination=NULL,HOPCOUNT = 1000,COUNT =0.
2) If packet received and type of the packet = DEST_SELECT then go to step 3 otherwise go to step 5.
3) Retrieve value of hop count field of DEST_SELECT packet. If value of hop count < HOPCOUNT then destination = value of Base station's or CB's Id field of DEST_SELECT packet then go to step 4.
4) If forwardmode = INITIAL then Set forwardmode = WORKING and Set mode = Beacon then go to step 9 otherwise go to step 5.
5) If packet received and type of the packet = LISTENER_DATA. Retrieve all information of LISTENER_DATA and go to step 6 otherwise go to step 7.
6) If value destination id field of LISTENER_DATA = own id then Set mode = Beacon and broadcast FORWARD_DATA packet (destination id, MCH's id, MCH's position data and MCH's aggregated sensor data) and then Set mode = listener and go to step 2.
7) If packet received and type of the packet = FORWARD_DATA. Retrieve all information of FORWARD_DATA and go to step 8 otherwise go to step 2.
8) If value destination id field of LISTENER_DATA = own id then Set mode = Beacon and broadcast FORWARD_DATA packet (destination id, MCH's id, MCH's position data and MCH's aggregated sensor data) and then Set mode = listener and go to step 2.
9) If FORWARD < 5 then broadcast DEST_SELECT packet with own id and hopcount field of DEST_SELECT = hopcount + 1 and go to step 10otherwise go to step 11.
10) Increase value of FORWARD by 1 and go to step 11.
11) Set mode = Listener and go to step 2.

Algorithm for Base station
1) Initialization of mode: Set mode=Beacon, basemode = INITIAL, destination=NULL,FORWARD =0.
2) If basemode = INITIAL and Set mode = Beacon then go to step 5 otherwise go to step 4.
3) If packet received and type of the packet = FORWARD_DATA. Retrieve all information of FORWARD_DATA and go to step 6 otherwise go to step 2.
4) Report data contained in the FORWARD_DATA packet (MCH's id, MCH's position data and MCH's aggregated sensor data) to the serial port then go to step 2.
5) If FORWARD < 5 then broadcast DEST_SELECT packet with own id and hopcount field of DEST_SELECT = 0 and go to step 6 otherwise go to step 7.
6) Increase value of FORWARD by 1 and go to step 8.
7) Set mode = Listener and basemode = WORKING and go to step 2.

---

4. Conclusion and Future Work

In this paper we proposed a routing protocol for a Real Time Event Based Indoor Monitoring system. This protocol proposes a new approach to fetch the data from the remote site using the mobile sensor nodes which has not been used earlier in other sensor network projects. A new approach of inverting nature of cricket motes from beacon to listener and listener to beacon in a rapid way has been done. Although our work focuses on event base monitoring of indoor environment, the routing protocol can be used in other places as well.

We plan to integrate all the different components of the system in near future . Deployment of sensors in an intelligent manner, need to be tackled. Issues such as rare events in the automation of the design are also required to handle. Thus rigorous testing before live use is needed.

5. Acknowledgements

6. References

[1]   L. M. Sun, J. Z. Li, Y. Chen and H. S. Zhu, "*Wireless Sensors Networks*," Tsinghua University Press, Beijing, 2005.

[2]   R. Szewczyk, A. Mainwaring , J. Polastre, J. Anderson and D. Culler. An analysis of a large scale habitat monitoring application In SenSys'04, Nov 2004.

[3]   G. Tolle, J. Polastre, R. Szewczyk, D. Culler, N. Turner, K. Tu, S. Burgess,T. Dawson, P. Buonadonna, D. Gay and W. Hong. A macroscope in the redwoods In SenSys'05, Nov 2005.

[4]   P. Zhang, C. M. Sadler, S. A. Lyon and M. Martonosi. Hardware design experiences in ZebraNet In SenSys'04, Nov 2004.

[5]   Mainwaring.A,Polastre.J,Szewcyk.R,Culler. D and Anderson. J 2002. Wireless sensor networks for habitat monitoring. In *Proceedings of the 1st ACM Workshop on Wireless Sensor Networks and Applications*.

[6]   Gui, C. and Mohapatra, P. 2004. Power conservation and quality of surveillance in target tracking sensor networks. In *Proceedings of the 10th ACM Annual International Conference on Mobile Computing and Networking*.

[7]   Xu, N., Rangwala, S., Chintalapudi, K. K., Ganesan, D., Broad, A., Govindan, P., and Estrine, D. 2004. A wireless sensor network for structural monitoring. In *Proceedings of the 2nd ACMInternational Conference on Embedded Networked Sensor Systems*.

[8]   A. Willing, "Wireless Sensor Networks: Concept, Challenges and Approaches," *Elektrotechnik & Informationstechnik*,Vol. 123, No.6, June 2006, pp. 224-231.

[9]   C. Adam and W. Jakub, "On Applications of WirelessSensor Networks," *Internet - Technical Development andApplications,* Springer, 2009, pp.91-99.

[10]   S. Thomas, D. F. Henri and V. Martin, "Sensor Scope:Experiences with a Wireless Building Monitoring Sensor Network," *Proceedings of the Workshop on Real-WorldWireless Sensor Networks,* Stockholm, 2005.

[11]   W. S. Jang, W. M. Healy and J. S. Miroslaw, "Wireless Sensor Networks as Part of a Web-Based Building Environmental Monitoring System," *Automation in Construction*,Vol. 17, No. 6, August 2008, pp. 729-736.

[12]   D. Tessa, G. Elena and B. James, "Wireless Sensor Networks to Enable the Passive House- Deployment Experiences," *Smart Sensing and Context,* Berlin Heidelberg:Springer, 2009, pp. 177-192.

[13]   W. S. Jang and W. M. Healy, "Wireless Sensor NetworkPerformance Metrics for Building Applications," *Energy and Buildings*, Vol. 42, No. 6, 2010, pp. 862-868.

Integrated Approach For Domain Dimensional Information Retrieval System By Using Neural Networks, CORBA, ORB.....

1.R. Kamalakar,
Incharge. Dept. of Computer Science, Satavahana University. Karimnagar,India.
2.P.Pradeep Kumar,
HOD,Dept.of Computer Science, VITS(N6),Karimnagar,JNTUH,India.
3.P.Sai Prasad ,
Asst.Professor,VITS(N6) Karimnagar,JNTUH,Andrapradesh,India.
4. M.Anjan Kumar,
Asst.Professor,VITS(N6) Karimnagar,JNTUH,Andrapradesh,India.

Abstract:
Search engines are the most commonly used type of tool for finding relevant information on the Internet. However, today's search engines are far from perfect. Typical search queries are short, often one or two words, and can be ambiguous therefore returning inappropriate results. A precise search engine adapted to professional environments which are characterized by a domain (e.g. medicine, law, sport, and so on). In our approach, each domain has its own terminology (i.e. a set of terms that denote its concepts: team, player, etc.) and it is organized along dimensions, such as person, location, etc.

The research work is focuses on personalization of information retrieval systems to achieve this we require one architecture that is to developed with immense ground knowledge on open source technologies and great Neural networks and Information retrieval system and there scope and existence. The architecture termed as ISA integrated service architecture.

General Terms—Information retrieval, domain dimensions, user interface, ISA, CORBA,ORB,NEURAL NETWORKS .

1. Introduction
1.1 Artificial Neural Networks
The term artificial intelligence was first coined in 1956, at the Dartmouth conference, and since then Artificial Intelligence has expanded because of the theories and principles developed by its dedicated researchers. Through its short modern history, advancement in the fields of AI have been slower than first estimated, progress continues to be made. From its birth 4 decades ago, there have been a variety of AI programs, and they have impacted other technological advancements

   A neural network is, in essence, an attempt to simulate the brain. Neural network theory revolves around the idea that certain key properties of biological neurons can be extracted and applied to simulations, thus creating a simulated (and very much simplified) brain. The first important thing to understand then, is that the components of an artificial neural network are an attempt to recreate the computing potential of the brain. The second important thing to understand, however, is that no one has ever claimed to simulate anything as complex as an actual brain. Whereas the human brain is estimated to have something on the order of ten to a hundred billion neurons, a typical artificial neural network (ANN) is not likely to have more than 1,000 artificial neurons. Artificial Intelligence is a combination of computer science, physiology, and philosophy.

   Before discussing the specifics of artificial neural nets though, let us examine what makes real neural nets - brains - function the way they do. Perhaps the single most important concept in neural net research is the idea of connection strength. Neuroscience has given us good evidence for the idea that connection strengths - that is, how strongly one neuron influences those neurons connected to it - are the real information holders in the brain. Learning, repetition of a task, even exposure to a new or continuing stimulus can cause the brain's connection strengths to change, some synaptic connections becoming reinforced and new ones are being created, others weakening or in some cases disappearing altogether.

A neuron may sum its inputs, or average them, or something entirely more complicated. Each of these behaviors can be represented mathematically, and that representation is called the transfer function. It is often convenient to forget the transfer function, and think of the neurons as being simple addition machines, more activity in equals more activity out. This is not really accurate though, and to develop a good understanding of an artificial neural network, the transfer function must be taken into account.

A Armed with these three concepts: Connection, strength   Inhibition/ Excitation , and the Transfer Function, we can now look at how artificial neural nets are constructed. In theory, an artificial neuron (often called a 'node') captures all the important elements of a biological one. Nodes are connected to each other and the strength of that connection is normally given a numeric value between -1.0 for maximum inhibition, to +1.0 for maximum excitation. All values between the two are acceptable, with higher magnitude values indicating stronger connection strength. The transfer function in artificial neurons whether in a computer simulation, or actual microchips wired together, is typically built right into the nodes' design.

Perhaps the most significant difference between artificial and biological neural nets is their organization. While many types of artificial neural nets exist, most are organized according to the same basic structure (see diagram). There are three components to this organization: a set of input nodes, one or more layers of 'hidden' nodes, and a set of output nodes. The input nodes take in information, and are akin to sensory organs. Whether the information is in the form of a digitized picture, or a series of stock values, or just about any other form that can be numerically expressed, this is where the net gets its initial data.
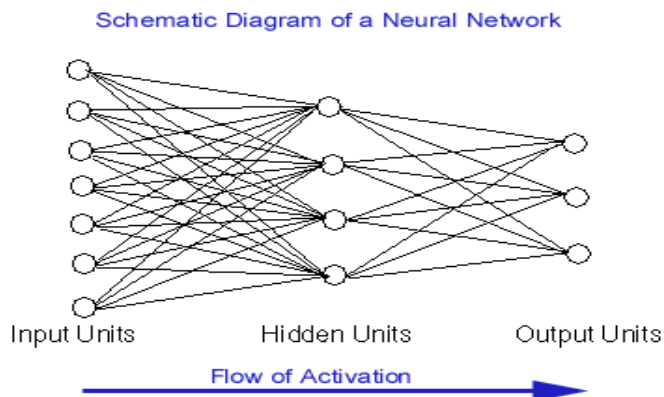
The information is supplied as activation values, that is, each node is given a number, higher numbers representing greater activation. This is just like human neurons except that rather than conveying their activation level by firing more frequently, as biological neurons do, artificial neurons indicate activation by passing this activation value to connected nodes.

After receiving this initial activation, information is then passed through the network. Connection strengths, inhibition/excitation conditions, and transfer functions determine how much of the activation value is passed on to the next node. Each node sums the activation values it receives, arrives at its own activation value, and then passes that along to the next nodes in the network (after modifying its activation level according to its transfer function). Thus the activation flows through the net in one direction, from input nodes, through the hidden layers, until eventually the output nodes are activated.

If a network is properly trained, this output should reflect the input in some meaningful way. For instance, a gender recognition net might be presented with a picture of a man or woman at its input nodes and must set an output node to 0.0 if the picture depicts a man, or 1.0 for a woman. In this way, the network communicates its knowledge to the outside world.

1.2 Information retrieval system

INFORMATION Retrieval Systems (IRS) are nowadays very popular, mainly due to the popularity of the Web. Most IRS on the Web (also called search engines) are not really domain-oriented: the same techniques are used to index any document. We think that there is a niche for domain-specific IRS

Schematic Diagram of a Neural Network

Input Units   Hidden Units   Output Units

Flow of Activation

2. Relevance Analysis

once the document domain is known, certain assumptions can be made and specific knowledge can be used. Users are then allowed to utilize much more precise queries than the usual small set of keywords in use for Web search engines. In professional environments, IRS should be able to process precise queries, mostly due to its use of a specific terminology, but also because the retrieved information is meant to be part of a user task (diagnose a disease, write a report, etc.).

 In professional environments, there is also a growing need for accessing information about specific domain documents in many languages and many types of media. In this paper, we present a precise search engine adapted to professional environments that are characterized by a domain (e.g. Medicine, Law, Sport, and so on). In our approach, each domain has its own terminology (i.e. a set of terms that denote its concepts) and it is organized along dimensions, such as *Person*, *Location*, etc.

 Dimensions, as described below, are defined by concepts and semantic relationships that represent a particular perspective or point of view on the corresponding domain. We mainly use the notion of domain dimension to *i*) precisely index document content and *ii*) implement an interactive interface that allows users to precisely describe his or her information need, and therefore precisely access a document collection. Our main goal through this system is to allow users fluid access to a digital library that contains documents belonging to specific domains, written in different languages, and using differnt medias. In particular, our system provides the user at all times with a feeling of control and understanding. It therefore provides a keyword search combined with a flexible navigation system. This combination allows a user to select a domain of his interest, build his query, expand and refine it, and select the language and the medias of the search results**.**

3. Domain Dimensions

We use domain dimensions for solving domain-specific precise queries that are characterized by a specialized terminology and a complex semantic structure. In this case, domain dimensions are used to extract the specialized vocabulary and therefore highlight the relevant elements that contribute to the description of a document (or query) semantic content. For example, through our dimension-based model, a journalist wishing to write a newspaper article can formulate his query as follows: "Give me documents dealing with the French General who created the security zone during the Balkans conflict". Our system is able to recognize domain dimensions and use them to precisely answer this query: *Person* (French General), *Location* (Balkans, security zone), *Event* (Balkans conflict).

4. Search Analysis

The main idea behind a search interface based on domain dimensions is quite simple. Rather than creating one large category hierarchy, we build a set of category hierarchies, each of which corresponds to a different dimension (facet) relevant to the domain described in the collection to be navigated. This representation is also known as hierarchical faceted categories. In dimension-based search interfaces, each domain has a set of dimensions and each dimension has a hierarchy of concepts. After the dimensions' hierarchies are designed, each document in the collection can be assigned to many concepts from the hierarchies. For example, in the medical domain, the dimension hierarchies can include *Human Anatomy* (Head, Brain, Femur, etc. with *part-of* relationships), *Pathology* (Cancer, fracture, lesion, etc., with is-a relationships), *Image Modality* (MRI, x-ray, ultrasound, etc., with is-a relationships) and so on. Thus, an *MRI* image describing a *fracture* of a *femur* might be assigned to (indexed by):

Anatomy > Musculoskeletal System > Skeleton > Bone and

Bones > Bones of Lower Extremity > Foot Bones > Leg Bones> Femur

*Pathology > Disorders of Environmental Origin > Wounds*

and Injuries > Fractures, Bone > Femoral Fractures

*Modality > Diagnostic Techniques and Procedures > Diagnostic*

Imaging > Magnetic Resonance Imaging

When a concept within a dimension hierarchy is selected within the interface, all documents that have been assigned to that concept are retrieved (and displayed). When concepts from different hierarchies are selected, the system builds a query that is a conjunct of disjuncts over the selected concepts and their sub concepts.
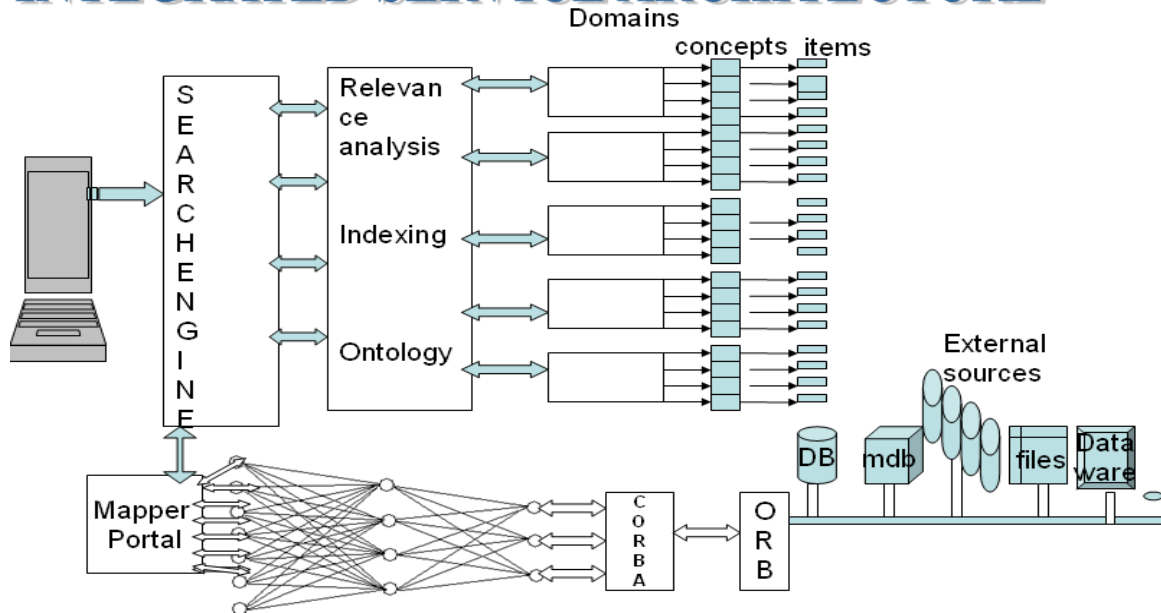
5.
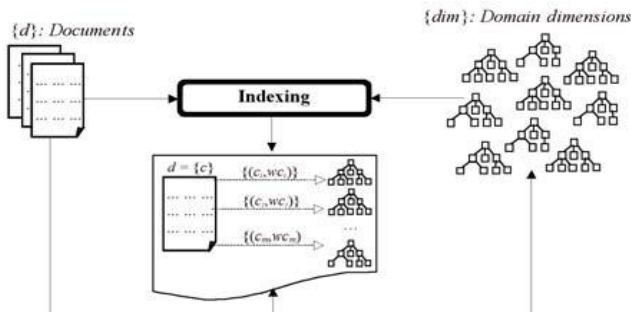
Document Indexing
The architecture of our system is presented in Figure 3.There are mainly three steps in our system design: *i*) defining the domain dimensions relevant to the given document collection; *ii*) multidimensional document indexing, which matches associate documents to the corresponding domain dimensions;

A. External Resources-Based Domain Dimension Definition
Our aim is to access a multimedia multilingual document collection through a dimensions-based search interface. Instead of using a specific indexing technique for each language and each media, we propose to use a unique technique for all documents independent of their languages or their media type. This technique is based on conceptual indexing that consists in representing documents (queries) by concepts instead of ambiguous descriptors (words extracted from text, features extracted from audiovisual information such as colour, shape, texture, motion, audio frequency, etc

6.Integrated Service Architecture

An ISA integrated service architecture is proposed to do the efficient information retrieval form multiple heterogeneous data sources. The efficency can be achieved by using the integrated technologies of Neural Networks and Object Resource Broker through CORBA.

The ISA architecture describes that the user can connect the search engine with own local resources to remote and search engine and there functionalities and comes under the domain of IRS. In previous sections we discussed the concept on relevance analysis and indexing with multiple domain dimensionalities .

Neural networks are the decision making tools and forwarding and back warding approaches when the desired date are to be fetched from the source by any neuron it will immediately sends to the MAPPER PORTAL . portal is a third party tool to integrate both environment for functional processing .

Why should I use corba and orbs?

The only the strait forward solution is that neutrability mean is an open source. By using orb's large immense features we can connect any type of data source like relational, object based, spatial, time series , file system and even data ware houses also. Due to implementation cost reduction and flexibility uses the orb.

The architecture implementation taken place and some important portion of integrations are carried on my work after success full implementation we will produce the results and dataset and constraint elaborately.

7. Conclusion

The research work is focuses on personalization of information retrieval systems to achieve this we require one architecture that is to developed with immense ground knowledge on open source technologies and great Neural networks and Information retrieval system and there scope and existence.

The architecture implementation taken place and some important portion of integrations are carried on my work after success full implementation we will produce the results and dataset and constraint elaborately.

8. References

1. Flexible building of specialized information retrieval systems application to the management of APL functions as a programming aid. Authors: Jean-Claude pages,Anne Mauboussin

2. Contemporary model and initiatives for information evalution. Systems: M.Anjan kumar, R.kamalakar**.** *Proceedings of the 63rd Internationalconference AMCM.2010*

3. "Neural networks with advanced bonding sectors ,"by M.ANJANKUMAR , R.KAMALAKAR .A.HUSSAIN in *Proceedings of the 3rdNationl Conference inf VITS(n6),knr Through ISTE CHAPTER ,2011*7.
4. Yee, K.P., Swearingen, K., Li, K., Hearst, M., "Faceted metadata for image search and browsing," in *CHI '03: Proceedings of the conference*
5. *on Human factors in computing systems*, ACM Press, pp. 401-408, 2003.
6. M¨akel¨a, E., Hyv¨onen, E., Saarela, S., "Ontogator - a semantic view based search engine service for web applications," in *International Semantic Web Conference*, pp. 847-860, 2006.
7. M¨akel¨a, E., Hyv¨onen, E., Sidoroff, T., "View-based user interfaces for information retrieval on the semantic web," in *ISWC-2005 WorkshopEnd User Semantic Web Interaction*, November 2005.
8. Sacco, G.M., "Research results in dynamic taxonomy and faceted searchsystems," in *DEXA Workshops*, IEEE Computer Society

AUTHORS PROFILES

1.

Kamalakar Ramineni is working as Lecturer at Satavahana University, Karimnagar, A.P, INDIA. He has received M.Sc Degree in Computer Science and currently pursuing Ph.D at Kakatiya University. His main research interest includes data retrieval process by using search engines.

2. Prof. P. Pradeep Kumar is working as a Professor and HOD to the dept. of CSE. In VITS(N6),JNTUH KARIMNAGAR. A.P. INDIA. He has eminent knowledge on multiple domains like data mining , mobile computing, and computational engineering, system engineering so on.

3.

P.Sai Prasad is working as Assistant Professor in VITS(N6),JNTUH KARIMNAGAR. A.P. INDIA.

He has received B.Tech degree in OSMANIA and M.Tech degree in

He has working under the research domain of data engineering. 4.

4

M.ANJAN KUAMR. Has received MCA In kakatiya university and M.Tech in JNTUH. Working in VITS(N6) Karimnagar.

He has the knowledge on the domains of Data Engineering, and Information retrieval systems and AI With machine learning tools.

He has 3 international publications and 4 national publications with good impact ratios

NODE PROGRESS IN CLUSTER COMPUTING

S.M.Krishna Ganesh[1] and A.SilesBalaSingh[2]

[1]Department of Computer Engineering, SJUIT, Tanzania,
[2]Department of Computer Engineering, SJUIT, Tanzania,

ABSTRACT
The system of cluster computing aims in distributing the process among the CPU to increase speed of processing. The server in the cluster performs the monitoring and load balancing of the clients. Here we aim to schedule the load of the client using a process scheduling node allocation based on the client capability, in a fashion that resembles a single node system. The algorithm can be implemented in any system that supports process migration. The objective is to improve the efficiency of load balancing and scalability in the cluster environment. The paper measures the performance of the algorithm on a MOSIX GRID with maximum of 60 nodes.
.

KEYWORDS: CLUSTER COMPUTING, CLUSTERING, LOAD BALANCING, MONITORING, PROCESS SCHEDULING.

1. INTRODUCTION

The cluster is a collection of interconnected stand-alone computers working together as a single, integrated computing resource consisting of many of the same or similar types of machine. A Cluster is a group of terminals or workstation attached to common control unit. We need to create a cluster with maximum number of nodes. It takes the advantage of non-local resources - using available computer resources on a wide area network. Overcoming memory constrain-single computers have very finite memory resources for large problems, using the memories of multiple computers may overcome this obstacle. The main feature in cluster environment with automatic resource discovery, pre-emptive process migration, and a priority scheme among migration in maximizing memory and/or disk performance among the cluster nodes we choose many workstations with peer architecture. Briefly, resource discovery is performed by an on-line information dissemination algorithm that maintains a distributed bulletin boardin order to provide each node with the latest information about the availability and the state of grid-wide resources. In the below figure it is shown that by a proper choice of the algorithm parameters, all the nodes can have nearly the same view of Cluster's resources.
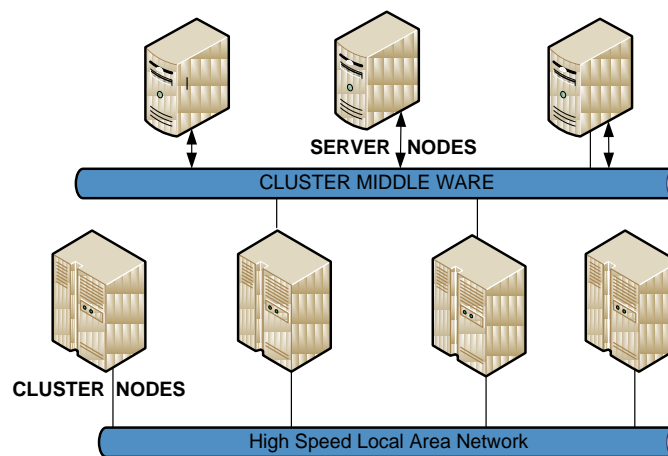

Figure1: The Cluster Environmental framework

2. Optimal Resource Constraint Scheduling (ORCS)

In computer science, a scheduling algorithm is the method by which threads or processes are given access to system resources, usually processor time. This is usually done to load balance a system effectively. The need for a scheduling algorithm arises from the requirement for most modern systems to perform multitasking, or execute more than one process at a time. Scheduling algorithms are generally only used in a time slice multiplexing. The reason is that in order to effectively load balance a system, the kernel must be able to suspend execution of threads forcibly in order to begin execution of the next thread. The proposed algorithm used may be as simple as Prior round-robin which is shown in figure 2. In which each process is given equal time (for instance 1 ms, usually between 1 ms and 100 ms) in a cycling list. So, process A executes for 1 ms, then process B, then process C, then back to process A. More advanced algorithms take into account process priority, or the importance of the process. This allows some processes to use more time than other processes. It should be noted that the kernel always uses whatever resources it needs to ensure proper functioning of the system, and so can be said to have infinite priority. In SMP systems, processor affinity is considered to increase overall

system performance, even if it may cause a process itself to run more slowly. This generally improves performance by reducing cache thrashing.
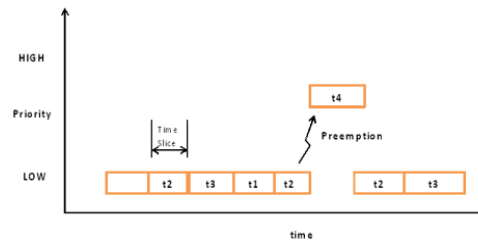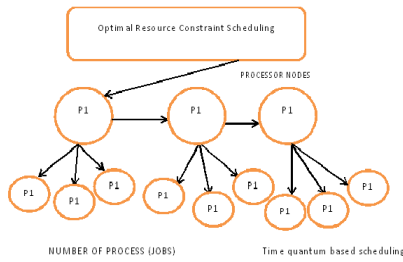

Figure 2: ORC Scheduling basic frame work   **Figure 3:** Process Preemption with priority

ORC Algorithm Steps:
1. Initially S_i = Max_100
2. Let r_i be the no of cluster nodes
3. The C_i be the capability of r_i
4. P_i be the no of process on r_i
5. $S_i/C_i * 100 = M_i \leftrightarrow \{M1, M2, \ldots \ldots Mn\}$
6. Max (M_i) is allotted with P_i
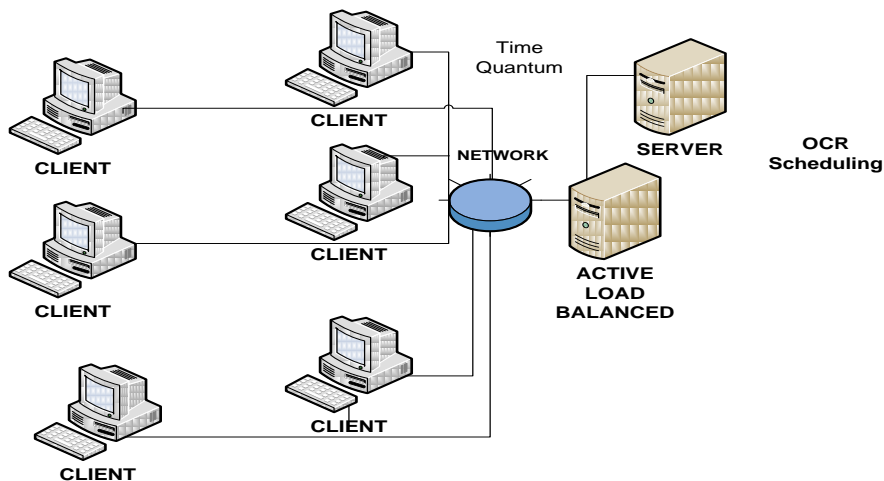7. The P_i exec: $= \Sigma P_i \in r_i \rightarrow M$

Figure 4: The Load Balancing scheme in cluster

    Let S_i be the server RAM with maximum memory which is utilized by the r_i number of cluster nodes effectively. The capacity of the nodes be C_i and is taken by dividing the RAM capacity and is utilized effectively. The maximum percentage is done with highest priority. Based on which the process are executed correspondingly to improve the scalability and load balancing. The simplest best-effort scheduling algorithms are round-robin, fair queuing (a max-min fair scheduling algorithm), proportionally fair scheduling and maximum throughput. If differentiated or guaranteed quality of service is offered, as opposed to best-effort communication, we use optimal resource constraint scheduling to improve the load balancing and scalability. Figure 3 below shows the OCR scheduling based on the time quantum compilation and pre-emption of process based on the priority. The main objective is to schedule the process dynamically among the clients by the server to improve the scalability and load sharing which could minimize the overhead. A scheduling algorithm which repeatedly runs through a list of users, giving each user the opportunity to use the central processing unit in succession. The existing scheduling may not be desirable if the size of the jobs or tasks are strongly varying. A process that produces large jobs would be favored over other processes. This problem may be solved by time sharing i.e. by giving each job a time slot or quantum (its allowance of CPU time), and interrupt the job if it is not completed by then. The job is resumed next time a time slot is assigned to that process. Thus the ORC improves the efficiency. Example: The time slot could be 100 milliseconds. If a job1 takes a total time of 250ms to complete, the priority scheduler will suspend the job after 100ms and give other jobs their time on the CPU. Once the

other jobs have had their equal share (100ms each), job1 will get another allocation of CPU time and the cycle will repeat. This process continues until the job finishes and needs no more time on the CPU

3. Performance Analysis of ORC Scheduling:

The process scheduling in cluster environment includes the round robin scheduling for the process to be distributed among the clients and the corresponding order is queued for execution. Thus the order of execution increases the performance of the load effectively shared across the network and the achieve the scalability. The tables below show the average waiting and turnaround time of the number of process in the total number of system executed correspondingly based on ORC algorithm. We consider a total of 5 systems and the maximum of 25jobs executed and minimal WT=10 and TT= 30 with high degree of accuracy. The ultimate aim is to improve the efficiency of the algorithm effectively and perform load balancing among the shared cluster nodes. The process in each processor is executed with high speed and the load of the server is distributed across the client effectively. The load balancing among the cluster nodes are distributed by the scheduling to reduce server load and improve the scalability of the systems effectively. This scheduling of the jobs to be run on the server is performed effectively. With improved efficiency and performance as shown in graph.

NODES	SYS1	SYS2	SYS3	SYS4	SYS5
AVG WT	3	6	14	20	22
AVG TT	21	32	43	54	65

SYSTEM 1: AVG WT= 13   AVG TT=23

NODES	SYS1	SYS2	SYS3	SYS4	SYS5
AVGWT	25	35	40	45	55
AVG TT	21	42	54	66	83

SYSTEM 2: AVG WT= 40   AVG TT=53

NODES	SYS1	SYS2	SYS3	SYS4	SYS5
AVG WT	24	44	65	85	107
AVG TT	32	64	87	106	141

SYSTEM 3: AVG WT=65   AVG TT=76

NODES	SYS1	SYS2	SYS3	SYS4	SYS5
AVG WT	32	63	96	129	159
AVG TT	44	78	110	137	171

SYSTEM 4: AVG WT=96   AVG TT=102

NODES	SYS1	SYS2	SYS3	SYS4	SYS5
AVGWT	43	77	121	155	204
AVG TT	56	103	130	167	204

SYSTEM 5: AVG WT= 112   AVG TT=132

NODES	SYS1	SYS2	SYS3	SYS4	SYS5
AVG WT	56	112	151	215	261
AVG TT	69	129	179	239	284

SYSTEM 6: AVG WT=159   AVG TT=178

Tables: Calculating the Average waiting time and Turnaround time

4. Experimental Study:

The experimental study here shows the process speed of execution and the corresponding turnaround time with high degree of efficiency. The Figure 5 shows the graph showing the process and the time of processing which indicates the speed of execution correspondingly. Table1: shows the corresponding waiting time and turnaround time of the process executed. By implementing this algorithm number of process on the node are scheduled effectively. This scheduling helps

to minimize the overload in the server and we increase the number of cluster nodes and their process being executed. The graph displays the increase in node and the corresponding process with increased performance. The graph displays comparison with FCFS, SJF and Round Robin Scheduling as follows

PROCESS	FCFS	SJF	RR
5	17	15	13
10	47	44	40
15	80	72	65
20	115	106	96
25	152	139	112
30	196	176	159

PROCESS	FCFS	SJF	RR
5	27	25	23
10	50	57	53
15	92	85	76
20	128	119	102
25	167	153	132
30	212	192	178

Table 1: Time showing the Waiting time of the running process   **Table2:** Time showing the Turnaround time running process

Figure 5: Graph showing the Process Vs Turnaround Time of processing
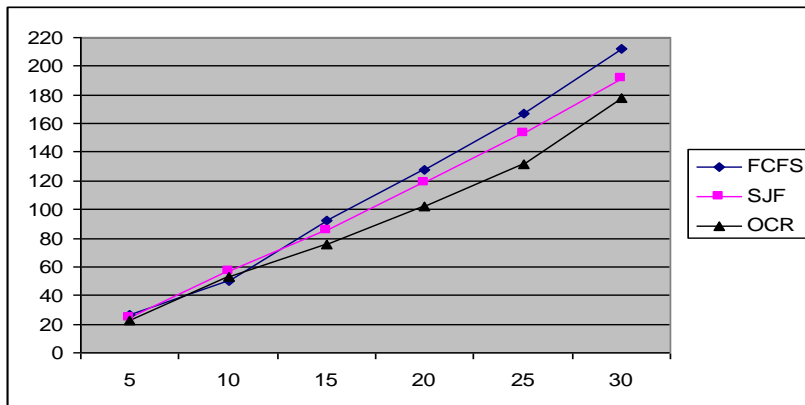
Figure 6: Graph showing the Process Vs Waiting Time of processing

CONCLUSIONS

The paper presented an on-line, resource sharing Algorithm for Node allocations in a cluster and its performance. First, we showed an algorithm for Excess allocations in which nodes, including unclaimed nodes, are proportionally allocated to users. Since in our model nodes are not shared by different users, the algorithm was extended to achieve a Temporal Node allocation by node circulations. In another extension, node allocations were based on a hierarchical tree. We implemented the algorithm on a running MOSIX Grid and measured its performance on a 60 node shared cluster. We tested cases with equal proportions, non-equal proportions, with node circulations, a hierarchical setup and in a flexible configuration. The result shows the performance evaluation of the running process and CPU utilization the work presented in this paper can be extended in several ways. First, our algorithm can be generalized to handle different resources, such as nodes with several CPUs (SMPs), nodes with different CPU speeds or different amounts of memory. Another possible extension is to support time-sharing of nodes,
.

REFERENCES

[1] A. C. Arpaci-Dusseau and D. E. Culler, "Extending Proportional-Share Scheduling to a Network ofWorkstations",PDPTA, 1997.

[2] A. Barak, A. Shiloh and L. Amar,(2005) "An Organizational Grid of Federated MOSIX Clusters", *CCGrid- 05,* Cardiff , 2005.

[3] J.F.C.M de Jongh,(2002) "Share Scheduling in Distributed Systems", *PhD Thesis*, Delft Tech. university, 2002.

[4] B. Dragovic,(2003) K. Fraser, S. Hand, T. Harris, A. Ho, I. Pratt, A. Warfield, P. Barham and R. Neugebauer, "Xen and the Art of Virtualization", *OSDI*, 2003.

[5] S.D. Kleban and S.H. Clearwater(2003), "Fair Share on HighPerformance Computing Systems: What Does Fair Really Mean?" *CCGrid-03*, 2003.

[6] K. Lai, L. Rasmusson, E. Adar, S. Sorkin, L. Zhang and B. A. Huberman(2004), "Tycoon: an Implementation of a Distributed Market-Based Resource Allocation System",*TR arXiv:cs.DC/0412038*, HP Labs, 2004.

[7] The Jemal H. Abawajy and S. P. Dandamudi (2000), "Distributed Hierarchical Co-ordination of Workstation Clusters,"IEEE PARELEC'2000, Trois-Rivierres, Quebec, Canada.

[8] S. P. Dandamudi and T.K. Thyagaraj,(1997), "A Hierarchical Processor Scheduling Policy for Distributed-Memory Multiprocessor Systems," In Proc. of HiPC'97, December 18-21, 1997, Bangalore, India.

[9] D. E. Bernholdt et. al(2000). A component architecture for high-performance scientific computing. to appear in Intl. J. High-Performance Computing Applications.

[10] E. Gabriel et al(2004). Open MPI: Goals, concept, and design of a next generation mpi implementation. In 11th European PVM/MPI Users' Group Meeting, 2004.

Authors

Mr. S.M.Krishna Ganesh has completed Masters of Technology Degree in Computer Science and Engineering at Kalasalingam University in the year 2009, Tamil Nadu, India.He is currently working as Lecturer in St. Joseph College of engineering and Technology,Dar Es Salaam, Tanzania, East Africa. He has 5 publications to his credit. He has guided more than 20 projects to final year B.E/B.Tech students with good industry and teaching experience. His areas of interests are Image Processing, Computer Networks, Neural networks and Bioinformatics.

Mr. A.Siles Balasingh working as Lecturer in St. Joseph University in Tanzania, East Africa. He has guided 12 projects for B.E final year students. His areas of interests are Computer Architecture, Computer Networks and security, and Ethical hacking.

A Two Bus Equivalent Method for Determination of Steady State Voltage Stability Limit of a Power System

B. Venkata Ramana, K. V. S. R. Murthy, P.Upendra Kumar, V.Raja Kumar

1. Associate Professor, LIET, Vizianagaram, AP, India
2. Associate Professor, GVPCOE, Visakhapatnam, AP, India
3. Associate Professor, LIET, Vizianagaram, AP, India
4. Assistant Professor, GITAM University, Visakhapatnam, AP, India

Abstract-
The problem of voltage instability is gaining more and more importance because of the unusual growth of power systems and insufficient or inefficient reactive power management. The voltage stability problem of a power system is associated with a rapid voltage drop due to heavy system load. Voltage reduction has a cumulative effect unless ample reactive power sources are available to regulate the voltage and maintain the reactive power balance. In this paper, simple and direct method of determining the steady state voltage stability limit of a power system at a particular load bus is implemented. The maximum permissible loading of a particular load bus is determined through a simplified Two-Bus equivalent model, called "Thevenin's Equivalent" of the original system. This method uses the base-case system information to find special Two-Bus equivalents of the system for analyzing the voltage stability problem. The effectiveness of this method is tested on a simple Two-Bus system and on the IEEE 14 Bus and IEEE 30 Bus systems and the results are compared with Newton- Raphson method. System performance is analyzed with and without a Static Var Compensator (SVC). The effects of load power factor and SVC rating on voltage stability limit are also studied. This method is very simple and does not require repetitive load flow simulations

Index Terms-Voltage Stability, Y-bus, Newton-Raphson Load Flow, Thevenin's Equivalent circuit, Q-V curves, Static Var Compensator (SVC)

I. Introduction

Power utilities are now forced to increase the utilization of existing transmission facilities to meet the growing demand without constructing new lines that are not only expensive but also environmentally unfriendly. Therefore transmission lines in a power systems are loaded more heavily than ever before to
avoid the capital cost of building new lines. A voltage collapse can take place in systems or subsystems and can appear quite abruptly.

When a system approaches the voltage collapse point, the voltage magnitude of some critical buses decreases rapidly with the increase of load. Controls or operators may not be able to prevent the voltage decay, sometimes may aggravate the situation, which results in voltage collapse. Voltage collapse has become an increasing threat to power system security and reliability. Many incidents of system blackouts because of voltage stability problems have been reported worldwide. Determination of steady state voltage stability limit is thus very important in order to operate the system with an adequate stability margin.

Nowadays, a proper analysis of the voltage stability problem has become one of the major concerns in power system operation and planning studies. The main reason for voltage instability in a power system is inadequate reactive power support at some critical buses. Voltage instability is a reactive power problem. The loading of a transmission network can be increased by maintaining proper voltage profile through injecting appropriate reactive power into the system. Unlike active power, it is very difficult to estimate the reactive power margin required to achieve a certain degree of voltage security.

When the voltage of a system starts to decrease, the current, and hence the reactive power loss in transmission lines and transformers, is increased. On the other hand, a decrease in voltage reduces the reactive power supply by the line charging and shunts capacitors. Thus the voltage reduction has a cumulative effect unless ample reactive power sources or some appropriate controls are available to regulate the voltage and maintain the reactive power balance.

Ii. Methodology

The phenomenon of voltage collapse on a transmission system, due to operation near the maximum transmissible power, is characterized by a fall in voltage, which is at first gradual and then rapid. The theoretical relationship between power transferred across a system and the receiving-end voltage follows an approximately parabolic shape. These curves are usually generated from the results of repetitive load flow simulations under modified initial conditions. Once the curves are generated, the voltage stability limit can easily be determined from the "nose" point of the curves.

The process of generating the curves is very time consuming, especially for a large system. However, the

computational time can significantly be reduced if the nose point can directly be determined without practically generating the curves. Direct determination of the nose point is possible if the power system can faithfully be represented by an equivalent Two-Bus system. The maximum loading capability of a particular load bus in a power system is determined through the Thevenin's equivalent circuit.

The Thevenin's equivalent circuits of all load buses are obtained in a single shot. Special care has been taken in modeling the generators to reflect actual operation, even for a change in operating conditions. This approach can provide very good results with less computation using the base-case system information. Note that the operating point of the generators at the verge of voltage stability may differ significantly from the base-case operating point. Thus, the Thevenin's equivalent circuit obtained at the base case with a conventional generator model may not represent a good equivalent circuit to determine the voltage stability limit unless some special care is taken in modeling the generators.

Iii. Fast Method For Finding Thevenin's Equivalent Circuit

A very fast approach to determine the Thevenin's equivalent circuits of all load buses in a single shot is implemented in the following sections. This approach uses the results of a single load flow solution and the system Z matrix. Both the load flow solution and the Z matrix are obtained by considering all the loads in the system. The voltage and impedance of the Thevenin's equivalent circuit are then obtained by slightly modifying the load flow solution and the diagonal elements of the Z matrix in order to nullify the effects of load impedance at the candidate bus.

Determination of the Thevenin's Impedance:
Let Z_{kk} be the k_{th} diagonal element of the Z matrix when all loads are considered. Our aim is to find the Thevenin's impedance Z_{th} of bus k when its load is ignored. These two impedances (Z_{kk} and Z_{th}) are shown in Fig 1.

It can be observed in the Fig 1 that

$$Z_{kk} = Z_k^L \text{ parallel with } Z_{th} = \frac{Z_k^L Z_{th}}{(Z_k^L + Z_{th})}$$

Here Z_k^L is the load impedance of bus k Thus, the Thevenin's impedance Z_{th} can readily be written as

$$Z_{th} = \frac{1}{\left(\frac{1}{Z_{kk}} - \frac{1}{Z_k^L}\right)} \qquad [1]$$
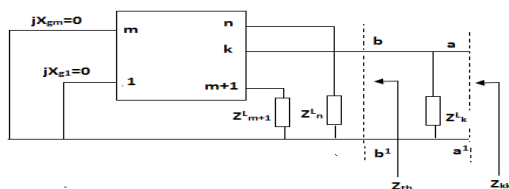

Fig 1. Thevenin's Impedance of Load Bus k.

Determination of the Thevenin's Voltage:

Let V_k be the voltage at bus k obtained from the load flow solution when all loads in the system are considered. The objective is to find the Thevenin's voltage V_{th} of bus k when its load is ignored. Fig 2 (a) and (b) shows the Thevenin's equivalent circuits of Fig 1at points aa' and bb', respectively.
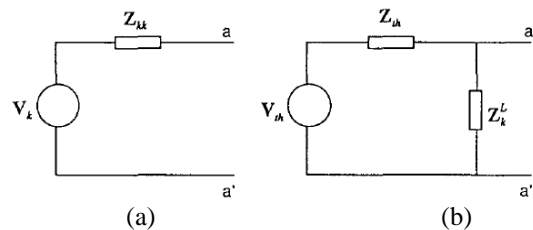

(a)   (b)
Fig. 2. Thevenin's Equivalent Circuits of Load Bus k

By comparing Figures 2 (a) and (b), the value of V_{th} can readily be written as

$$V_{th} = \left(1 + \frac{Z_{th}}{Z_k^L}\right)V_k \qquad [2]$$

Fig 2(b) represents the Thevenin's equivalent circuit of bus k and the maximum loading capability of this bus can be determined by varying the load impedance Z_k^L.

Iv. Voltage Stability Limit Of A Simple Two-Bus System

Consider a simple Two-Bus system as shown in Fig 3. The generator at bus 1 transfers power through a transmission line having an impedance of Z = R +jX to a load center at bus 2. Bus 1 is considered as a swing bus where both the voltage magnitude V2 and angle δ1, are kept constant.
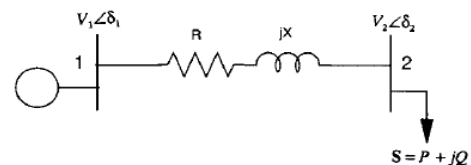

Fig 3. A simple Two-Bus system

For a given value of V_1 the relationship between the load voltage magnitude V_2 and the load power S = P +jQ can readily be written as

$$V_1 = V_2 + IZ = V_2 + I\sqrt{R^2 + X^2}$$

$$V_1^2 = V_2^2 + 2(RP + XQ) + \frac{P^2 + Q^2}{V_2^2}(R^2 + X^2) \qquad [3]$$

$$V_2^4 + [2(RP + XQ) - V_1^2]V_2^2 + [(R^2 + X^2)(P^2 + Q^2)] = 0$$

By assuming x = V_2^2, the above equation can be written in quadratic form as follows

$$a_1 x^2 + b_1 x + c_1 = 0 \qquad [4]$$

Where
$$a_1 = 1; \quad b_1 = 2(RP + XQ) - V^2 ;$$

$$c_1 = (R^2 + X^2)(P^2 + Q^2)$$

The positive voltage magnitudes of bus 2 can be obtained from the solution of equation [4] and are given by

$$V_2^2 = \frac{-b_1 \pm \sqrt{{b_1}^2 - 4a_1c_1}}{2a_1}$$

$$V_2^H = \sqrt{\frac{-b_1 + \sqrt{d}}{2a_1}} \qquad [5a]$$

$$V_2^L = \sqrt{\frac{-b_1 - \sqrt{d}}{2a_1}} \qquad [5b]$$

Where the discriminant 'd' is given by

$$d = b_1^2 - 4a_1c_1$$
$$d = V_1^4 + 4[2PQRX - (RP + XQ)V_1^2 - (R^2Q^2 + X^2P^2)] \qquad [6]$$

Here, V_2^H is called the high-voltage or stable solution while V_2^L is called the low-voltage or unstable solution. For zero load (P = Q = 0), V_2^H and V_2^L become V_1 and 0 respectively. As the load (at normal power factor) is increased from zero, V_2^H decreases while V_2^L increases. This process continues until a point is reached where both V_2^H and V_2^L become the same. This occurs when the value of d in equation [6] becomes zero. The load power for which $V_2^H = V_2^L$ is called the critical power and the corresponding voltage is called the critical voltage. It is said that the system has reached the voltage stability limit and it is not capable of transferring any additional power. For higher load power, the real solution of equation [4] (and hence the magnitude of V_2) will cease to occur because of the negative value of d.
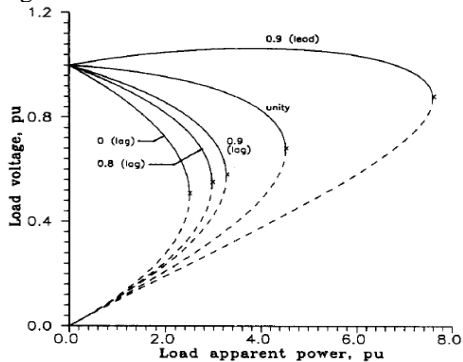

Fig 4. Variation of Load Voltage against the Load Apparent Power for various Power Factors

Typical variations of load voltage against the load apparent power for various power factors are shown in Figure 3.2 which is plotted for V1 = 1.0 p.u., R = 0.01 p.u. and X = 0.1 p.u. The high-voltage or stable solution is represented by full curves while the low-voltage or unstable solution is represented by broken curves. These two curves or voltages meet at the critical point. It can be observed in the figure that both the maximum load apparent power and critical voltage increase as the load PF changes from lagging to leading.

Critical Load Apparent Power:

Obviously, the condition of the maximum load apparent power (S_m) can be obtained by setting the value of d in Eq. (4) to zero. This gives the following quadratic equation:

$$a_2 S_m^2 + b_2 S_m + c_2 = 0 \qquad [7]$$

Where

$$a_2 = 4[RX\sin 2\theta - R^2\sin^2\theta - X^2\cos^2\theta]$$
$$b_2 = -4V_1^2(R\cos\theta + X\sin\theta) \qquad \text{and} \qquad c_2 = V_1^4$$

In deriving the above equation, it is considered that P = S cos θ and Q = S sin θ, where θ is the PF angle. The value of S_m can be obtained from the solution of above equation

$$S_m = \frac{V_1^2}{2} \frac{Z - (R\cos\theta + X\sin\theta)}{(R\sin\theta + X\cos\theta)^2} \qquad [8]$$

Here $Z = \sqrt{(R^2 + X^2)}$

V. Voltage Stability Limit Of A Simple Two-Bus System With S.V.C

This Section describes the technique of directly determining the voltage stability limit or noise point of the P- V curve of a simple Two-Bus system of Fig 5. The system transfers power from a generating station to a load center through a transmission line. A SVC of finite reactive power rating is also placed at the load center. The SVC is usually connected through a step down transformer as shown in Fig 5. It consists of a fixed capacitor C and a thyristor controlled inductor L. The reactive power of the SVC can be adjusted by controlling the firing angle of the thyristors.
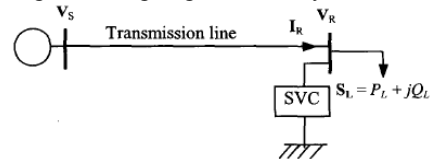

Fig 5. Single Line Diagram of a Simple Two-Bus System with SVC

When the load increases, the receiving end voltage of the line decreases and the SVC injects capacitive reactive power to boost the voltage. However, when the operation of the SVC hits the upper limit, it cannot adjust the reactive power anymore to maintain the desired voltage. Thus the load voltage decreases with further increase in load and the ultimate result is voltage collapse. It may be mentioned here that the voltage collapse may not occur until the operation of the SVC reaches the upper limit. For such an operation, the SVC can be represented by a fixed capacitive susceptance B_c

In this case, the current (I_R) at the receiving end of the line can be written as

$$I_R = \left(\frac{S_L}{V_R}\right)^* + jB_C V_R \qquad [9]$$

Here SL ($=P_L+jQ_L$) is the complex load and VR is the complex receiving end voltage. The sending end voltage Vs of the system can be written as

$$V_S = AV_R + BI_R \qquad [10]$$

Here A and B are the transmission line constants. In rectangular form, A and B can be expressed as

$$A = a_1 + ja_2 \text{ and } B = b_1 + jb_2 \qquad [11]$$

Using above the sending end voltage of equation can be written as

$$V_S = (a_1 + ja_2)V_R + (b_1 + jb_2)\left(\left(\frac{S_L}{V_R}\right)^* + jB_C V_R\right)$$

$$V_S = \left[c_1 V_R + (b_1\cos\theta + b_2\sin\theta)\frac{S}{V_R}\right] + j\left[c_2 V_R + \frac{S}{V_R}(b_2\cos\theta - b_1\sin\theta)\right] \qquad [12]$$

Where $c_1 = a_1 - b_2 B_c$ and $c_2 = a_1 + b_1 B_c$
In deriving equation [12], V_R is considered as a reference. Then

$$c_3 V_R^4 + c_4 V_R^2 + c_5 = 0 \qquad [13]$$

Where $c_3 = (c_1^2 + c_2^2)$

$c_4 = \{2S[(b_1 c_1 + b_2 c_2)\cos\theta + (b_2 c_1 - b_1 c_2)\sin\theta - V_S^2]\}$

$c_5 = S^2(b_1^2 + b_2^2)$

Note that equation [13] has four possible solutions but only the feasible solutions (real and positive) can be used to generate the P-V curve of the system.

The main objective is to directly determine the load apparent power at the nose point of the P-V curve without practically generating the curve. At the nose point or the same solution (stable and unstable) of load voltage magnitude, the coefficients of equation [11] must satisfy the following criterion

For critical value of Sm,

$$c_4^2 - 4c_3 c_5 = 0 \qquad [14]$$

The above non-linear equation can be expressed as

$$\int (S, \theta) = 0 \qquad [15]$$

$$S_m = \frac{c_7 \pm \sqrt{c_7^2 - 4c_6 c_8}}{2c_6}$$

Where

$c_6 = 4[(b_1 c_1 + b_2 c_2)\cos\theta + (b_2 c_1 - b_1 c_2)\sin\theta]^2 - (c_1^2 + c_2^2)(b_1^2 + b_2^2)$

$c_7 = -4V_S^2[(b_1 c_1 + b_2 c_2)\cos\theta + (b_2 c_1 - b_1 c_2)\sin\theta]$

$c_8 = V_S^4$

For a given load power factor angle θ, equation [15] can be expressed by a second order polynomial of load apparent power S and the feasible solution of the polynomial can be considered as the critical load apparent power Scr at the nose point of the P-V curve.

Vi. Test Cases And Simulation Results

In the NR method, the maximum apparent power loading of a load bus is determined by gradually increasing the power demand at the candidate bus in the original unreduced system until the method fails to converge in solving the load flow problem. As mentioned earlier, the maximum loading capability of a bus estimated by the Two-Bus method is slightly higher than the corresponding actual value because of the constant-impedance load model. Thus, the results obtained by the Two-Bus and NR methods and the actual value can be ranked as follows:

Results obtained by
NR method < Actual value < Two-Bus method

The IEEE-14 Bus System:
Using Newton-Raphson and Thevenin's (or Two–Bus) Equivalent circuit methods, Load Voltage versus Load Apparent Power curves are drawn for IEEE-14 Bus by varying Load apparent power at any bus and the Maximum Load Apparent Power values with both the methods are compared [Table 1]. Variation of Load Voltage against Load Apparent Power of 12 and 14 Buses of IEEE-14 Bus system with NR and Two-Bus methods is shown in Fig 6 and Fig 7. In this case, the system is first represented by an equivalent Two-Bus system.
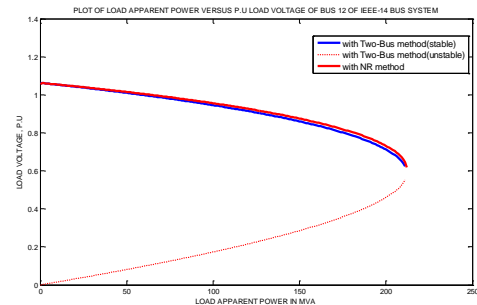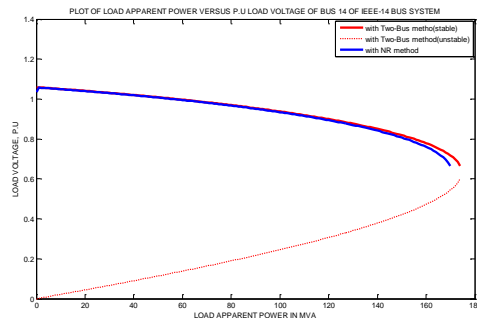

Fig 6. At Bus 12 of IEEE-14 Bus system

Fig 7. At Bus 14 of IEEE-14 Bus system

The critical load apparent power of the bus is then determined and the variation of critical load apparent power against the load power factor angle is shown in Fig 8. The voltage stability limit of bus 14 of the system is also determined from repetitive load flow simulations using Newton-Raphson method for comparison.

It can be noticed from Table 1 that the results (apparent power at the voltage collapse point) obtained by the load flow simulations (Newton-Raphson method) are slightly lower than the corresponding values found by the Two-Bus method and maximum error that observed at the 14 bus IEEE-14 Bus system is 3.6% at a load power factor of unity and when the system is equipped with SVC of 1.6 p.u.
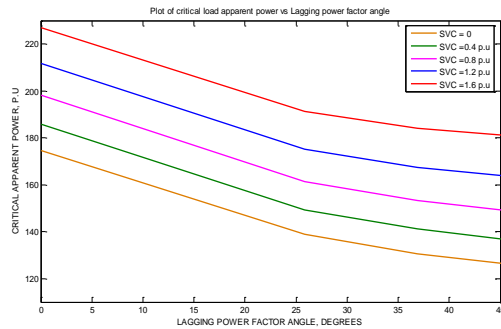

Fig 8. Variation of Critical Load Apparent Power of Bus 14 of IEEE-14 Bus System

Table 1
Comparison of Results obtained by Two-Bus and NR Methods of Bus14 of IEEE-14 Bus System

| Svc Value In P.U	Power Factor (Lagging)	Critical Apparent Power (MVA)		%Error
		Two-Bus Method	NR Method	
0	1	174.64	170	2.73
	0.9	138.84	136	2.09
	0.8	130.61	129	1.25
	0.7	126.21	124	1.79
0.4	1	185.77	181	2.64
	0.9	149.36	147	1.61
	0.8	141.09	139	1.50
	0.7	136.78	135	1.32
0.8	1	198.13	193	2.66
	0.9	161.42	159	1.52
	0.8	153.24	151	1.48
	0.7	149.12	147	1.44
1.2	1	211.82	205	3.32
	0.9	175.30	172	1.92
	0.8	167.41	165	1.46
	0.7	163.65	162	1.02
1.6	1	226.88	219	3.60
	0.9	191.32	188	1.77
	0.8	184.04	181	1.68
	0.7	180.90	179	1.06
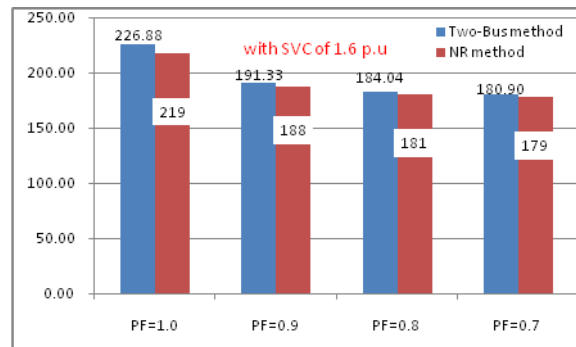
Fig 9. Variation of Critical Load Apparent Power of Bus 14 of IEEE-14 Bus System for different Power Factors with SVC of 1.6 p.u
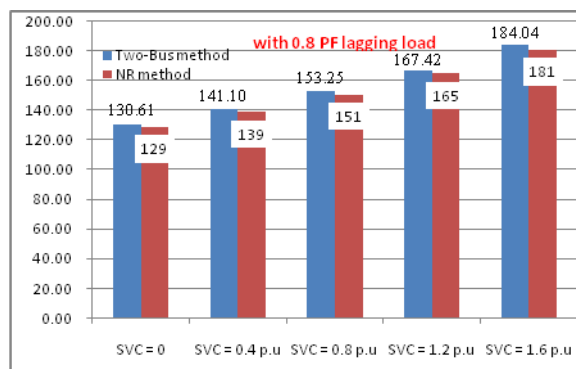

Fig 10. Variation of Critical Load Apparent Power of Bus 14 of IEEE-14 Bus System for different values of SVC with 0.8 PF Lagging Load

The IEEE-30 Bus System:

The load voltage versus load apparent power curves of 20and 24 buses of IEEE-30 Bus system are shown in Figures 11 and 12 respectively. From all these figures it is clearly shown that the critical apparent power at any load bus obtained by NR method and Two-bus methods are very
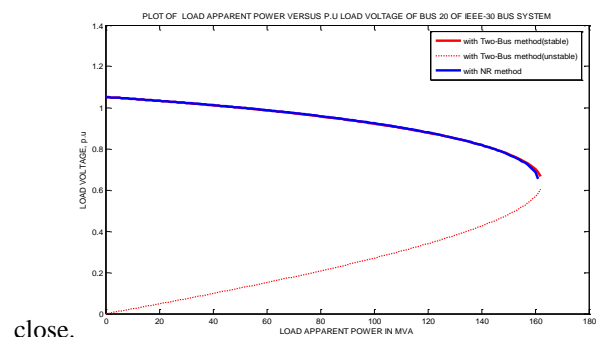

close.

Fig 11. AtBus 20 of IEEE -30 Bus System

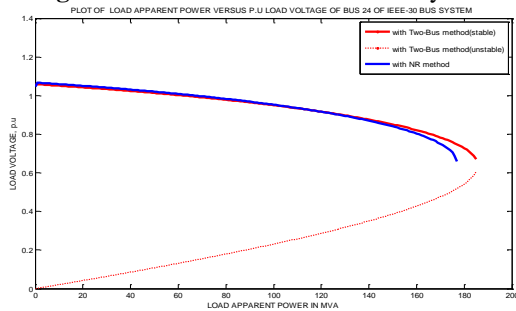PLOT OF LOAD APPARENT POWER VERSUS P.U LOAD VOLTAGE OF BUS 24 OF IEEE-30 BUS SYSTEM

Fig 12. At Bus 24 of IEEE -30 Bus   System

For the IEEE-30 Bus system, the voltage stability limit of bus 24 is determined. Table 2 summarizes the results obtained by the Two-Bus method as well as the repetitive load flow simulations. Maximum error that observed at the 24 bus IEEE-30 Bus system is 5.28% at a load power factor of unity and when the system is equipped with SVC of 1.6 p.u.
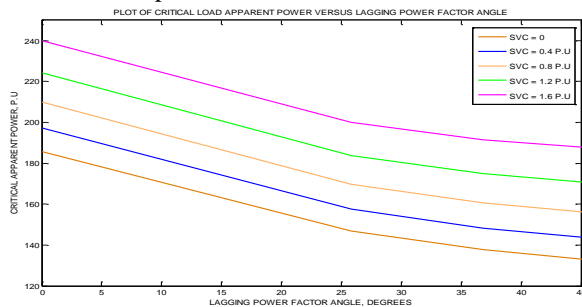

PLOT OF CRITICAL LOAD APPARENT POWER VERSUS LAGGING POWER FACTOR ANGLE

Fig 13. Variation of Critical Load Apparent Power against Load Power Factor Angle of Bus 24 of IEEE-30 Bus System for various values of SVC

Table 2

Comparison of Results obtained by Two-Bus and Newton-Raphson Methods of Bus 24 of IEEE-30 Bus System

| Svc Value In P.U	Power Factor (Lagging)	Critical Apparent Power (MVA)		%Error
		Two-Bus Method	NR Method	
0	1	185.69	177	4.90
	0.9	146.72	143	2.60
	0.8	137.70	135	2.00
	0.7	132.84	131	1.40
0.4	1	197.23	188	4.90
	0.9	157.45	153	2.90
	0.8	148.34	145	2.30
	0.7	143.52	142	1.07
0.8	1	210.06	200	5.03
	0.9	169.72	165	2.86
	0.8	160.62	157	2.30
	0.7	155.92	154	1.24
1.2	1	224.30	213	5.30
	0.9	183.81	179	2.68
	0.8	174.88	172	1.67
	0.7	170.46	168	1.46
1.6	1	240.05	228	5.28
	0.9	200.06	195	2.59
	0.8	191.57	188	1.89
	0.7	187.65	185	1.43
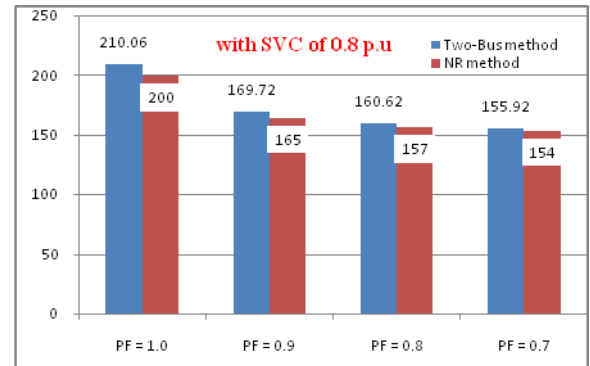
Fig 14. Variation of Critical Load Apparent Power of Bus 24 of IEEE-30 Bus System for different Power Factors with SVC of 0.8 p.u
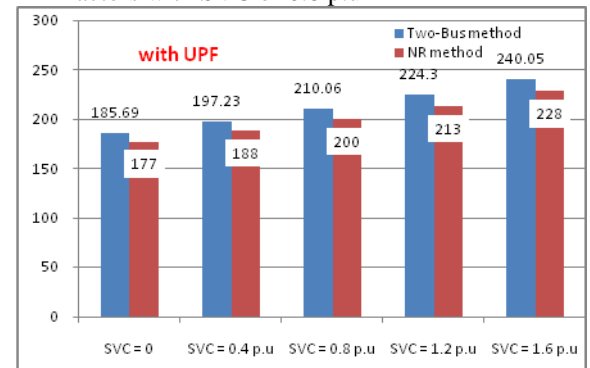

Fig 15. Variation of Critical Load Apparent Power of Bus24 of IEEE-30 Bus System for different values of SVC with UPF Load

Conclusion

A simple and fast method for analyzing the voltage stability problem of a general power system through a two-bus equivalent has been implemented. The generator model used in this project is very insensitive to the change in operating conditions. Thus the two-bus equivalents obtained at the base-case operating point through the Thevenin's theorem can be faithfully applied to determine the steady state voltage stability limit. Unlike the other methods, the Thevenin's equivalent circuits of all load buses are efficiently obtained in a single shot. This requires the results of the base-case load flow solution and computation of the Z matrix when all loads in the system are considered. A minor modification to the bus voltages and the diagonal elements of the Z matrix is required to exclude the effects of the load at the candidate bus.

Determination of the various quantities at the verge of voltage stability involves the solution of simple quadratic equations. The maximum demand at a load bus to ensure a minimum specified voltage can also be determined from the solution of another quadratic equation. This two-bus method has been tested on the IEEE 14-, and 30-Bus systems for a number of cases with and without SVC. The effects of the SVC rating and load power factor on the voltage stability limit are also studied in detail. The results obtained by this two-bus method are compared with those found by the conventional repetitive load flow simulations. Because of the constant-impedance model of the system load, the two-bus method provides slightly overestimated results at the verge of voltage stability. The convergence problem of the load flow method in the vicinity of the voltage collapse point is believed to be the main reason for the above discrepancy. The errors found in the simulation results are higher at the verge of voltage stability. Unlike the other methods, the two-bus method can provide much better and reliable results using the base-case system information with significantly less computation.

References

1. Haque, M.H., "Determination of steady state voltage stability limit of a power system in the presence of SVC" *IEEE Porto Power Tech Conference, $10^{th} – 13^{th}$ September, 2001,Porto, Portugal.*

2. Haque, M.H., "A fast method of determining the voltage stability limit of a power system", *Electric Power Systems Research, Vol. 32, 1995, pp. 35-43.*

3. Lof, P.A., Smed, T., Andersson, G. and Hill, D.J., "Fast calculation of a voltage stability index", *IEEE Trans. on Power Systems, Vol. 7, No. 1, 1992, pp. 54-64.*

4. Overbye, T.J. and DeMarco, C.L., "Improved technique for power system voltage stability assessment using energy methods", *IEEE Trans. On Power Systems, Vol. 6, No. 4, 1991, pp. 1446-1452.*

5. Overbye, T.J., Dobson, 1.D. and DeMarco, C.L., "Q-V curve interpretations of energy measures for voltage security", *IEEE Trans. on Power Systems, Vol. 9, No. 1, 1994, pp. 331-340.*

6. Canizares, C.A., "On bifurcations, voltage collapse and load modeling", *IEEE Trans. on Power Systems,Vol.10,N0., 1, 1995, pp. 512-522.*

7. Koessler, R.J., "Voltage instability/collapse – An overview", *IEE Colloquium on Voltage Collapse, Digest No.1997/101,1997,pp. 1/1 - 1/6.*

8. Chebbo, A.M., Irving, M.R. and Sterling, M.J.H.,"Voltage collapse proximity indicator: behavior and implications", *IEE Proc. - C, Vol. 139, No. 3, 1992, pp. 241-252.*

9. Gubina, F. and Strmcnik, B.,"A simple approach to voltage stability assessment in radial networks", *IEEE Trans. on Power Systems, Vol. 12, No. 3, 1997,pp. 1121-1 128.*

10. Vu, Khoi, Begovic, M.M., Novosel, D. and Saha, M.M., "Use of local measurements to estimate voltage stability margin", *IEEE Trans. on Power Systems,* Vol.14, NO. 3, 1999, pp. 1029-1035.

11. C.L. DeMarco and T.J. Overbye, "An energy based security measure for assessing vulnerability to voltage collapse", *IEEE Trans. Power Syst., 5 (1990),*419 - 427.

12. C.S. Indulkar, B. Viswanathan and S.S.Venkata, "Maximum power transfer limited by voltage instability in series and shunt compensated schemes for AC transmission systems", *IEEE Trans.Power Delivery, 4* (1989), pp.1246 -1252.

A Fast Gain Stage Suitable for High Performance Pipeline ADCs

Mohammad Nazaraliloo[1]
1. Islamic Azad University, Shabestar Branch , Shabestar, Iran

Saeid Masoumi [2]
2. Islamic Azad University, Tasouj Branch , Tasouj, Iran

Heydar Faraji [3]
3. Islamic Azad University, Khoy Branch , Khoy, Iran

Hasan Kalantari[4]
4. Islamic Azad University, Shabestar Branch , Shabestar, Iran

Abstract- A new circuit technique for voltage gain enhancement in CMOS op amp design suitable for low voltage and high speed operation is presented. In this paper, a new operational amplifier is presented that improves the specifications such as dc gain and speed virtually .To obtain these improvements, we have used the two important concepts of positive feedback and replica amplification.

Keywords: Replica amplification, positive feedback, Gain-Bandwidth-product (GBW), single stage amplifier

1. Introduction

Op Amps play an important role in many analog and mixed-mode applications. The rapid growth of high speed and high-resolution applications such as ADC and DAC's results in a necessary demand to the high speed and high gain amplifiers. The realization of high-gain amplifiers with large GBW in processes with decreasing supply voltage requires innovative circuit design techniques and advances in IC process technology. Since op amps are usually employed to implement feedback systems, the open-loop gain of an op amp determines the precision of the feedback system employing the op amp. With a very high dc gain needed for precision applications, four approaches for gain enhancement has received considerable attention for many years. One is based upon gain multiplication achieved by cascading two or more lower gain stages. Although high dc gains are achievable, the excess phase shift introduced by the cascading introduces serious compensation requirements which limit the high frequency performance of cascaded amplifiers in feedback applications. The second approach achieves gain enhancement by increasing the output impedance of a basic gain stage. This approach has proven most effective at achieving high gains and high GBW with favorable power dissipation (for medium accuracy). E. H. Armstrong, first time, in 1914, presented positive feedback [1] and this method, several times, was used in op-amps. Using positive feedback, dc gain can be increased a lot, but it simply, can make op-amp structures unstable. Also, this method can decrease output swing the same as negative feedback in active cascode op-amps [2]. Another commonly used gain enhancement technique is gain-boosting [3]. Very high gains are achievable with gain-boosting but it still requires one level of stacking of devices thereby making it difficult to operate with low supply voltages. The gain-boosting amplifier also adds its own poles, and reduces the speed of amplifier and consumes more power. Although negative impedance compensation offers potential for the most gain enhancement, low power dissipation, low voltage operation and excellent high frequency performance, the technique is seldom used commercially because of the high sensitivity of the gain to the negative compensating impedance inherent in existing negative impedance schemes. In 1993, a new concept as replica amplification was introduced [4]. This method is more suitable for low voltage and high performance applications such as data converters. We have designed an op amp by using this method.

2. Circuit design

2.1 Single Stage amplifier

The single stage amplifier having one pole is the simplest architecture imaginable. Because of its simplicity, it can be extensively analyzed and optimized by hand analysis. The single pole amplifier is also of a great deal of interest because of its inherent stability. The simple single pole architecture makes this amplifier the most attractive for high speed applications with low closed loop gain. We have improved the dc gain of single stage amplifier by using replica method. This method (replica) has a negligible effect on settling time of main amplifier [4].There is not any GBW limitation, in this method. Fig. 1a shows the single stage amplifier with active load in closed loop configuration. The dc-gain of this structure (intrinsic gain) in the 0.35 μ m CMOS process can be about 10 to 30 depend on devices size and input signal range. But by using negative impedance gain-enhancement (fig. 1b) we can increase the dc-gain (Av) of single stage amplifier a little, without any stability problems [5]. In this design gain enhancement by this technique is used to be 2. This structure has only one pole that's located in the output node. Therefore the speed of this circuit is high.

2.2 Replica Method:

Replica amplification is an ideal method for enhancing amplifiers dc-gain virtually, without any GBW limitation. This idea for the first time has been used in a two stage op amp structure [4]. Measurement results of fabricated circuit in [4] show the excellent improvements of replica method.

2.3 Proposed Circuit

Fig. 2 shows the complete schematic of the designed circuit. The total closed loop gain of this structure is designed to be one but with scaling the feedback capacitors (c1 and c2) we can achieve more different gains, especially for the residue amplifiers in the Pipeline ADC's. The structure is consists of a main and a replica amplifier. Output voltage and error (indeed error of a single stage amplifier) of replica amplifier can be estimated by:
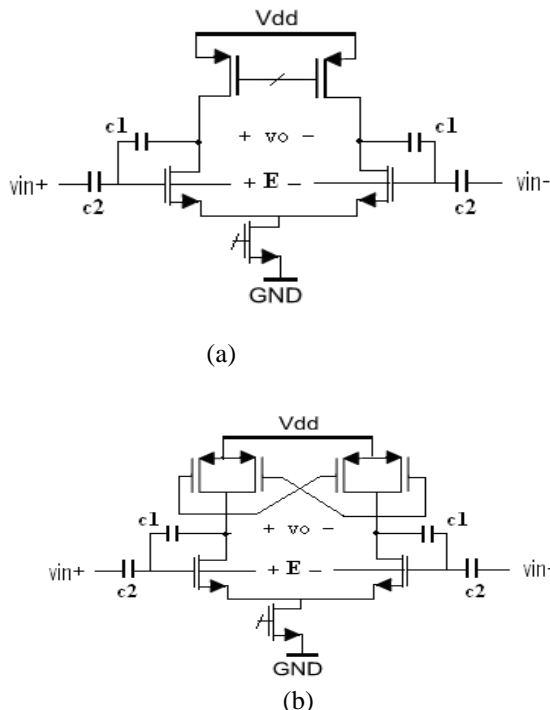

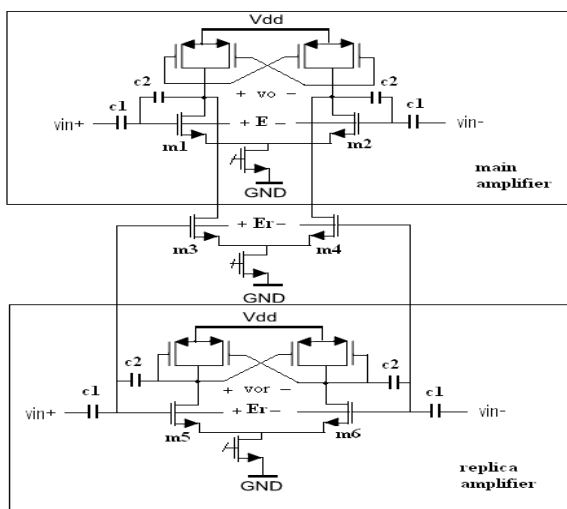(a)

(b)

Fig. 1: Simple single stage amplifiers.

Fig.2 Proposed design

$$V_{Or} = \frac{A_{Vr}.V_{in}}{(1 + A_{Vr})} \qquad (1)$$

$$E_r = \frac{V_{in}}{(1 + A_{Vr})} \qquad (2)$$

This error voltage appears in the gates of the input differential pair (m5, m6). The main idea is to amplify the error by using another differential pair (m3, m4) that is connected directly to the output nodes of main amplifier. The load of this differential pair is output impedance of main amplifier. The gain of this amplification (Av_s) can be equal to Av_r by scaling the size of the devices (m3, m4) as well. Using this method, output voltage of the main amplifier can reach to Vo_r only by replica amplifier

and an extra differential pair (m3, m4) (without any effect of the main amplifier). The main amplifier only corrects the difference of V_{in} and Vo_r (E_r) and decreases it to the final error (E). Assume Av_s is equal to Av_r, the total error of complete amplifier (E) that appears between the gates of input differential pair of the main amplifier is equal to:

$$E = \frac{E_r}{(1 + A_{Vm})} = \frac{V_{in}}{(1 + A_{vm}).(1 + A_{Vr})} \tag{3}$$

Where Av_m is the dc gain of the main amplifier. Hence the total error of the amplifier is reduced and the circuit can be more accurate. The speed improvement in this method has another reason too. The size of the feedback capacitors in the other gain enhancement methods (e.g. in the gain boosting method), must be large enough for capacitor matching (needed for desired accuracy), especially to compensate the parasitic capacitance effect of the gates of the input differential pair that alters the accuracy of the amplifier. And these large capacitors increase the settling time of the circuit. But in this design the feedback capacitors can be smaller, because each of the main or replica amplifiers needs less accuracy (half of the total desired accuracy). Using smaller feedback capacitors increase the speed of the circuit more and more. The circuit of Fig. 3 can be used for more precision. In this circuit the replica method is used twice so this topology can be more accurate if well designed, only by scaling the size of the devices (without any reduction in output impedance of the main amplifier). This configuration has never been reported yet. Using replica method for two times is another novel idea in this research. In this way instead of cascading or cascoding stages to achieve high dc gain that leads to speed reduction in the closed loop configuration, we can use more replica stages (replicating) to achieve more accuracy with a very small reduction in speed [4]. This speed reduction is only 20% that reported in [4] and can be reduced by scaling down of replica amplifier. In the circuit of fig.3, for every stage of the amplifier we can use the circuit of fig.1 (b) for more gain enhancement.
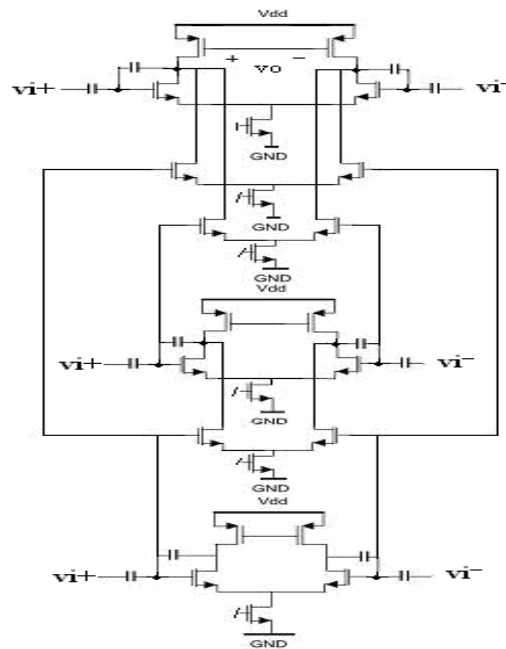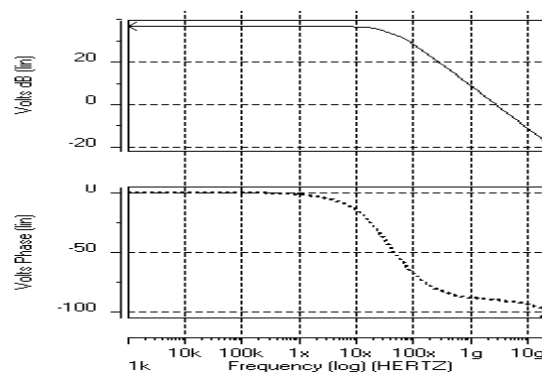

Fig. 3 More gain enhancement by replica method.

Fig.4 Ac response of single stage op-amp (circuit of fig. 1b)

3. Simulation results

The circuit of fig.2 is simulated by Hspice software using level 49 parameters (BSIM3v3). Fig.4 shows the AC response of designed amplifier (shown in fig.2). The step respons of circuit is shown in fig.5. The size of feedback capacitors is 0.5pF and a 0.5pF capacitive load is connected to the output nodes. Power dissipation of circuit is about 6mW.The settling time of the circuit for 0.1% error is less than 2nsec and that is depend on the amplitude of input signal, feedback and load capacitors size and bias currents 4]. Replica concept has been analyzed in detail in [4].

4. conclusion

A new circuit technique for voltage gain enhancement in CMOS op amp design suitable for low voltage and high speed operation is presented. In this paper, a new operational amplifier is presented that improves the specifications such as dc gain and speed virtually .To obtain these improvements, we have used the two important concepts of positive feedback and replica amplification. Indeed by using this method we can design an op-amp with accuracy of two stage op-amp but with speed of a one stage op-amp.
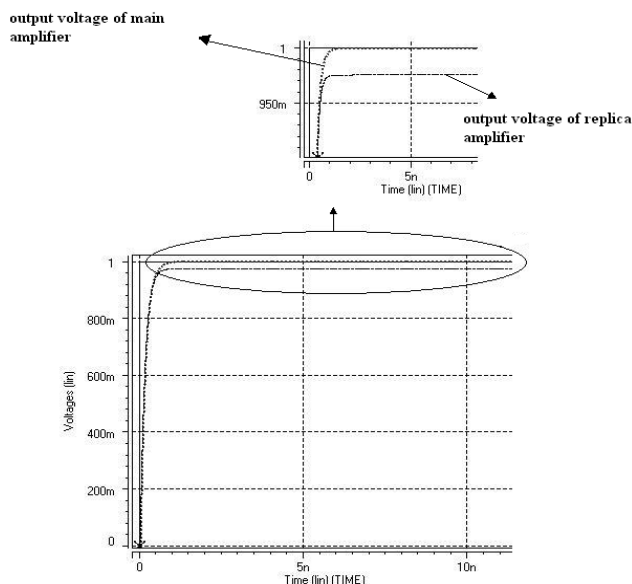

Fig.5 : Step response of proposed design.

Table 1: Op Amp Performance

Supply voltage	3.3v
process	0.35 μ m
Power Dissipation	$\approx$ 6mW
Load (pF)	0.5
0.1% error settling time In 1 volt step voltage	Less than 2 nsec
DC Open loop gain (virtual)	≈ 1000
Phase margin	$\approx 90^{0}$

5. References:

[1] E. H. Armstrong,"WIRELESS RECEIVING SYSTEM", U.S.   Patent 1 113 149, Oct. 6, 1914

[2] Carlos A. Laber and Paul R. Gray,"A Positive-Feedback Transconductance Amplifier with Applications to High-Frequency High- Q CMOS Switched- Capacitor Filters", IEEE J. Solid-State Circuits, VOL. 23. NO. 6, DECEMBER 1988, pp. 1370-1378.

[3] K. Bult and G. J. G. M. Geelen, "A fast-settling CMOS op amp for SC circuits with 90-dB dc gain," IEEE J. Solid-State Circuits, vol. 25, pp 1379-1 384, Dec. 1990.

[4] Paul C. Yu et al., A High-Swing 2-V CMOS Operational Amplifier with Replica-Amp Gain Enhancement, IEEE Journal of Solid-State Circuits, vol. 28, No. 12, pp. 1265-1272, Dec. 1993.

[5] R.Gregorian, Introduction to CMOS Op-Amps and Comparators.   John Wiley & Sons, 1999 .

Simulation of Wind driven currents for continental shelf of Golestan Province (Iran)

Saeed Sharbaty[*]

Faculty Member Dept. of fishery, Grogan University of Agricultural sciences & Natural Resource

Abstract

In this Investigation, three dimensional modeling of wind driven currents was done in the continental shelf of Golestan Province using MIKE 3 Model. In order to applying open boundary conditions in both western and northern borders, the results of implemented of two dimensional MIKE 21 model were used in the Caspian Sea. In implementation of MIKE 21 model, reanalysis data of NOAA satellite includes components of wind speed and pressure at sea level with 6 hours time intervals and variable in space and time, as well as input of major rivers and evaporation and Coriolis force is used. In the MIKE 3 HS model, the effects of Atrak, Gorganrood rivers and water exchange with the Gorgan Bay as source and sink has been considered. To applying wind effect on the continental shelf of Golestan Province, the data of Bandartorkaman synoptic station to become changed into the offshore wind. In order to verification of the results of the MIKE 3 model, the flow field measurements were used in two points of solution domain. The model results represented the high influence of wind action on the surface layers and in most cases; currents are along the dominant wind and in direction of southeast area. By moving towards deep area, currents go out from the solution area with the 180 degrees of phase difference from surface currents.

Key Words: Continental Shelf, Golestan Province, 3D Simulation, Wind Driven Currents.

1. Introduction

Sea currents due to their role in nutrients supplying are effective factors on biological primary productions in the water bodies. Therefore, the increasing of primary productions will cause to increasing secondary productions, catching and use of biological resources in the sea. On the other hands, sea currents are the main factors in the distribution of environmental pollutions and with sediments transporting caused to deformation coastal morphology. Knowledge of flow pattern is so necessary for marine structures and engineering projects. Today, utilizing of numerical models is obvious due to dramatic reductions in costs and time in order to simulating of marine phenomena such as current, sedimentation, wave, water level fluctuations and distribution of environmental pollutions. In recent years, MIKE 3 and MIKE 21 models have a special place among countries that is adjacent to the sea. In this investigation, three dimensional modeling of wind-driven flow pattern has been study in sea water of Golestan province (continental shelf zone). As an ecological case, this part of the Caspian Sea due to the low depth and appropriate water temperature is a suitable site for marine aquatic specially the Sturgeons, so that more than 46% of the share extracting of Iranian Sturgeons resources provided from this basin. However, some important ecosystems such as Gomishan wetland, Gorgan Bay and the Miankaleh peninsula, due to their neighboring with it received more effects of marine activities from this basin. Developing of pen cultures of fishes and shrimps in Golestan coats along side of industrial towns nearby this basin and civil projects to construction of Torkaman, Gaz and khajenafas ports and urban pollution brought via two major rivers (Gorgan Rude and Atrak) polluted this basin. There are many studies about hydrodynamic flow in the Caspian Sea and its surround, such as: Sharbaty [23, 24] Zounemat-Kermaniand; et al [29], Ibrayev; et al [6], Ghaffari; et al [5], Esmaeili; et al [4], Knysh; et al [8], Biabani [2], Nasimi; et al [19], Korotenko; et al [9], Panin; et al [20], Bannazadeh; et al [1], Sabbagh-Yazdi [22], Matthew; et al [18], Bondarenko [3], Kosarev [10], Klevtsova [7] and Lednev [11]. The continental shelf of Golestan with less than 0.5 degree gradient has maximum depth of 34 meter and mean depth of 8 meter. This basin with 90 kilometer length and 60 kilometer width, completely located on continental shelf zone. This basin bounded to Mazandaran province waters from west, Golestan province coasts from south and east-southern and Republic of Turkmenistan from northeastern part. The extent of this area is more than 5400 km^2 and its bottom sedimentation has marine and continent resource. The coastal zone of Golestan is so flat and smooth. The aim of this investigation is reaching to wind-driven flow pattern and velocity components (u, v, w) in three dimensional mode in different layers using MIKE 3 in continental shelf of Golestan province.

2. Material and Methods

This work is based on librarian studies, field measurement data performed by Ministry of Jihad-e-Agriculture, meteorology data in Bandartorkaman station, numerical-meteorological data of NOAA site and Implementation of MIKE 21 and MIKE 3 model.

2.1. Model Description, Main Equations and Numerical Formulation in MIKE 21 model

Due to lack of field measuring data of current and surface water elevation in two open boundaries in the solution domain in during 2001/07/20 to 2001/08/20, at first MIKE 21 model was implemented for the Caspian Sea. The hydrodynamic model in the MIKE 21 Flow Model is a general numerical modeling system for the simulation of water levels and flows in estuaries, bay and coastal areas. It simulates unsteady two-dimensional flows in one layer (vertically homogeneous) fluids and has been applied in a large number of studies. The effects of bottom friction stress, wind stress, water elevation for the open boundary condition, eddy viscosity, flood and dry, rivers inflow, precipitation and evaporation considered in MIKE 21 model [12, 13]. The governing equations are written as follows:

$$\frac{\partial \zeta}{\partial t} + \frac{\partial p}{\partial x} + \frac{\partial q}{\partial y} = \frac{\partial d}{\partial t} \qquad (1)$$

Momentum equation in x-direction:

$$\frac{\partial p}{\partial t} + \frac{\partial}{\partial x}\left(\frac{p^2}{h}\right) + \frac{\partial}{\partial y}\left(\frac{pq}{h}\right) + gh\frac{\partial \zeta}{\partial x} + \frac{gp\sqrt{p^2+q^2}}{c^2 h^2}$$

$$-\frac{1}{\rho_w}\left[\frac{\partial}{\partial x}(h\tau_{xx}) + \frac{\partial}{\partial y}(h\tau_{xy})\right] - \Omega_q - fv_x + \frac{h}{\rho_w}\frac{\partial}{\partial x}(p_a) = 0 \qquad (2)$$

Momentum equation in y-direction:

$$\frac{\partial q}{\partial t} + \frac{\partial}{\partial y}\left(\frac{q^2}{h}\right) + \frac{\partial}{\partial x}\left(\frac{pq}{h}\right) + gh\frac{\partial \zeta}{\partial y} + \frac{gq\sqrt{p^2+q^2}}{c^2 h^2}$$

$$-\frac{1}{\rho_w}\left[\frac{\partial}{\partial y}(h\tau_{yy}) + \frac{\partial}{\partial x}(h\tau_{xy})\right] + \Omega_p + fv_y + \frac{h}{\rho_w}\frac{\partial}{\partial y}(p_a) = 0 \qquad (3)$$

The following symbols are used in the equations:

$h(x, y, t)$ Water depth $(\zeta - d, m)$

$d(x, y, t)$ Time varying water depth (m)

$\zeta(x, y, t)$ Surface elevation (m)

$p, q(x, y, t)$ Flux densities in x-and y- directions (m³/s/m) = (uh, vh); (u,v) = depth Average velocities in x- and y- directions.

$C(x, y)$ Chezy resistance ($m^{1/2}/s$)

g Acceleration due to gravity (9.81 ms⁻²)

$f(V)$ Wind friction factor

$V, V_x, V_y(x, y, t)$ Wind speed and components in x- and y-directions (m/s)

$\Omega(x, y)$ Coriolis parameter, latitude dependent (s⁻¹)

$p_a(x, y, t)$ Atmospheric pressure (pa)

ρ_w Density of water (kg/m³)

x, y, z Space coordinates (m)

t time

$\tau_{xx}, \tau_{xy}, \tau_{yy}$ Components of effective shear stress

MIKE 21 HD makes use of a so-called Alternating Direction Implicit (A.D.I) technique to integrate the equations for mass and momentum conservation in the space-time domain. The equation matrices that result for each direction and each individual grid line are resolved by a Double Sweep (DS) algorithm [14].

2.2. MIKE 21 Model Setup

For making the bathymetry map of the Caspian Sea, the sheet map of the Caspian Sea with scale of 1:1500000 in WGS 1984 was used. The bathymetry included 63×117 rectangular grids with grid size 10 km in the both zonal and meridional directions

in Cartesian coordinate system. Since in the bottom topography modeling, the maximum depth in the Golestan continental shelf is less than 34 meter, in this work, all depths greater than 34 meter was considered equivalent to depths of 34 meters. Wind stress is an important factor to forming surface currents in the Caspian Sea. In this work, the wind data including wind speed (m/s) and wind direction (degree) components in 10 meter high from the sea surface and also surface pressure (hpa) was used as varying in space and time available from a re-analysis data of NOAA site (National Oceanic and Atmospheric Administration) [30]. The time step data was 6 hours (4-times daily) and the resolution was 2.5 degree latitude × 2.5 degree longitude, 63×117 rectangular local grid with grid size 10 km in the both zonal and meridional directions was considered. The wind friction in the sea surface is varying with wind speed, so in order to affect the wind friction factor with wind speed of variations we used smith and banks formula [28]:

$$f(v) = \begin{cases} f_0 & for \quad v < v_0 \\ f_0 + \dfrac{v - v_0}{v_1 - v_0}(f_1 - f_0) & for \quad v_0 \le v \le v_1 \\ f_1 & for \quad v > v_1 \end{cases} (4)$$

$$f_0 = 0.00013 \quad , \quad v_0 = 0 \quad m/s$$
$$f_1 = 0.0026 \quad , \quad v_1 = 30 \quad m/s$$

Where

$v_1, v, v_0:$ Are wind speed

$f_0, f_1:$ Wind friction parameter

Discharge of five main rivers to the Caspian Sea (Volga, Ural, Terek, Kura and Sefidrud) as source terms, water outflow to the Kara-Bogaz-Gol and evaporation as sink terms, the Coriolis forcing included in the model. Considering factors in MIKE 21 model briefly explain in table 1.
.

Table 1- considering factors in MIKE 21 model

Module Selection	Hydrostatic	Simulation Start Date	2001/07/20
Map Projection	Lat & long	Simulation End Date	2001/08/20
Time Step Range	4464	Max Courant Number	1.09
Time Step Interval (s)	600	Number of sources	5
Flooding & Drying Depth (m)	0.2 , 0.3	Number of sink	1
Initial Surface Elevation (m)	0	Evaporation (mm.day^{-1})	6
Precipitation (mm.day^{-1})	0	Eddy Viscosity (Smagorinsky Velocity Based) (m^2.s^{-1})	0.5
Resistance(Manning Number) (m$^{1/3}$.s^{-1})	32	Wind Conditions (m.s^{-1})	Varying in time and space

To verify the results of MIKE 21 model, flow pattern obtaining from MIKE 21 model compared to document reports in the reasonable resources (figs 2, 3). At the next step, mean velocity components $\bar{u}, \bar{v}$ and water level extracted as two profile series in west and north boundary (fig 1).
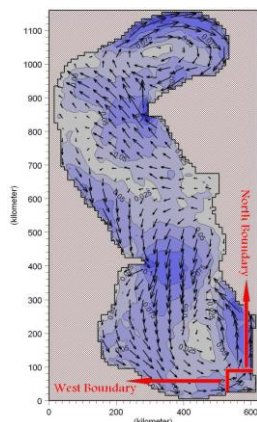
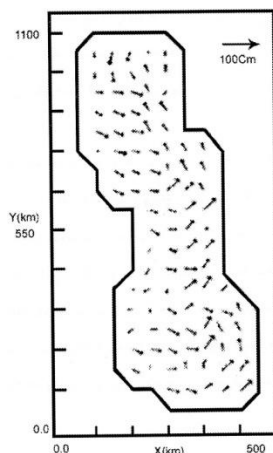**Figure 1- 2D flow pattern in the Caspian Sea by MIKE 21 model and location of west and north boundaries.**

Figure 2- main surface flow pattern of the Caspian Sea in the stationary mode by numerical model done by Bannazadeh (2002).
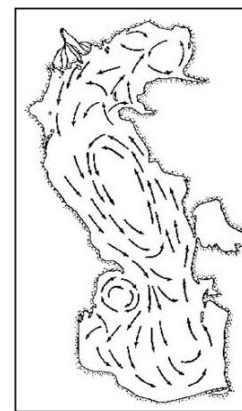
Figure 3- Scheme of the Caspian Sea currents by Ledinov (1943).

2.3. Model Description, Main Equations and Numerical Formulation in MIKE 3 Model

In this study, the MIKE 3 HD model was used for three dimensional simulation of flow pattern in the Golestan continental shelf. The hydrostatic (HS) model in MIKE 3 HD is a general numerical modeling system for simulation of unsteady three-dimensional flow in estuaries, bays and coastal areas as well as in lakes and oceans. It simulates flows taking into account bathymetry and external forcing such as meteorology, tidal elevations, currents and other hydrographic conditions [15, 16]. The mathematical foundation for the standard MIKE 3 HD engine is the mass equation and the Reynolds-averaged Navier-Stokes equation, including an artificial compressibility (ACM) due to the chosen numerical solution procedure. The hydrodynamic module of MIKE 3 makes use of the so-called Alternating Direction Implicit technique to integrate the equations for mass and momentum conservation in the space-time domain. The equation matrices, which result for each direction and each individual grid line, are solved by Double Sweep algorithm. These equations read [17] (only X-direction is shown for 2nd equation):

$$\frac{1}{\rho c_s^2}\frac{\partial P}{\partial t} + \frac{\partial u}{\partial x} + \frac{\partial v}{\partial y} + \frac{\partial w}{\partial z} = S_{MASS} \qquad (5)$$

$$\frac{\partial u}{\partial t} + \frac{\partial uu}{\partial x} + \frac{\partial uv}{\partial y} + \frac{\partial uw}{\partial z} + 2\omega\left(-v\sin(\phi) + w\sin(\phi)\sin(\lambda)\right) =$$

$$-\frac{1}{\rho}\frac{\partial P}{\partial x} + \frac{\partial}{\partial x}(2\upsilon_t\frac{\partial u}{\partial x}) + \frac{\partial}{\partial y}\left(\upsilon_t(\frac{\partial u}{\partial y} + \frac{\partial v}{\partial x})\right)$$

$$+\frac{\partial}{\partial z}\left(\upsilon_t(\frac{\partial u}{\partial z} + \frac{\partial v}{\partial z})\right) + u_{ss}S_{MASS} \qquad (6)$$

Where
ρ Density

c_s Speed of sound in water

u, v, w Velocities in x,y,z directions

ω Coriolis parameter

ϕ, λ Latitude, Longitude

υ_t Turbulent eddy viscosity

S_{MASS} Source/sink term with

$$S_{MASS} = \sum_{i_s=1}^{N_s} \delta(x - x_{s,i_s}, y - y_{s,i_s}, z - z_{s,i_s}) Q_{s,i_s}$$

δ Delta function of source/sink coordinates m^{-3}

$x_{s,i_s}, y_{s,i_s}, z_{s,i_s}$ Coordinates of source/sink NO. i_s

Q_{s,i_s} Discharge at source/sink NO. i_s , m^3/s

The differences between MIKE 3 HS and MIKE 3 ACM are:

A hydrostatic pressure assumption is applied, i.e. the vertical accelerations are assumed to be negligible. The vertical velocity w is assumed negligible, resulting in the removal of the secondary Coriolis term and the last diffusion term. The pressure is split up into two parts, the external pressure and the internal pressure. The external pressure is directly linked to the free surface, and the internal pressure is due to the density differences. The fluid is assumed incompressible, as opposed to the standard version of MIKE 3 HD. Consequently, the compressibility term in the mass equations is discarded.

$$\frac{\partial u}{\partial x} + \frac{\partial v}{\partial y} + \frac{\partial w}{\partial z} = S_{MASS} \qquad (7)$$

$$\frac{\partial u}{\partial t} + \frac{\partial uu}{\partial x} + \frac{\partial uv}{\partial y} + \frac{\partial uw}{\partial z} - 2\omega v \sin(\phi) = -\frac{1}{\rho}\frac{\partial P}{\partial x} + \frac{\partial}{\partial x}(2\upsilon_t \frac{\partial u}{\partial x})$$

$$+ \frac{\partial}{\partial y}\left(\upsilon_t(\frac{\partial u}{\partial y} + \frac{\partial v}{\partial x})\right) + \frac{\partial}{\partial z}\left(\upsilon_t(\frac{\partial u}{\partial z})\right) + u_{ss}S_{MASS} \qquad (8)$$

The external/internal pressure gradient force is given by:

$$\frac{1}{\rho}\frac{\partial P}{\partial x} = g\frac{\rho(\zeta)}{\rho}\frac{\partial \zeta}{\partial x} + \frac{g}{\rho}\int_z^\zeta \frac{\partial \rho}{\partial x}dz \qquad (9)$$

Where

g Acceleration due to gravity

ζ Surface elevation

In the ACM version of MIKE 3, the top horizontal layer containing the free surface is solved separately from, but not independently of, the underlying cells. The top layer is layer-integrated as opposed to the underlying cells. In the hydrostatic version of MIKE 3, the equations to be solved are in their layer-integrated form for both the top layer and the underlying cells. This is due to the solution procedure, where it is convenient to have the same formulation for all cells in each water column. Assuming that the horizontal velocities are constant over the layer thickness. The layer-integrated form of (7)-(8), with the pressure gradient force inserted, is:

$$\frac{\partial uh}{\partial x} + \frac{\partial vh}{\partial y} + w_{top} - w_{bot} =$$

$$P - E + \sum_{i_s} \delta(x - x_{s,i_s}, y - y_{s,i_s}) Q_{s,i_s} \qquad (10)$$

$$\frac{\partial uh}{\partial t} + \frac{\partial uuh}{\partial x} + \frac{\partial uvh}{\partial y} + (uw)_{top} - (uw)_{bot} - 2\omega vh\sin(\phi) =$$

$$- gh\frac{\partial \zeta}{\partial x} - \frac{g}{\rho}\int_{layer}\left(\int_{z'}^\zeta \frac{\partial \rho}{\partial x}dz'\right)dz + \frac{\partial}{\partial x}\left(2\upsilon_t h\frac{\partial u}{\partial x}\right) + \frac{\partial}{\partial y}(\upsilon_t h\left(\frac{\partial u}{\partial y} + \frac{\partial v}{\partial x}\right))$$

$$+ \upsilon_t(\frac{\partial u}{\partial z})_{top} - \upsilon_t((\frac{\partial u}{\partial z})_{bot} + u_{ss}\sum_{i_s} \delta(x - x_{s,i_s}, y - y_{s,i_s}) Q_{s,i_s} \qquad (11)$$

Where the sums represent all point source/sink in the considered layer, and precipitation and evaporation terms, P and E (m/s), have been expluded from the sum. The precipitation and evaporation terms is only included if the considered layer is the surface layer. The depth-integrated version of (10) is:

$$\frac{\partial \zeta}{\partial t} + \frac{\partial UH}{\partial X} + \frac{\partial VH}{\partial Y} = P - E$$
$$+ \sum_{i_s} \delta(X - X_{s.i_s}, Y - Y_{s.i_s}) Q_{s.i_s} \qquad (12)$$

With sum over all point source/sinks. The turbulence is modeled in terms of an Eddy Viscosity and a bed shear stress. In this study, we used mixed $1D - \varepsilon$, 2D Smagorinsky Turbulence model for determined horizontal and vertical eddy viscosity. The horizontal eddy viscosity is determined by Smagorinsky formula [27].

$$\upsilon_T = L^2 \sqrt{S_{ij}.S_{ji}} \qquad (13)$$

$$S_{ij} = \frac{1}{2}\left(\frac{\partial u_i}{\partial x_j} + \frac{\partial u_j}{\partial x_i}\right) \qquad (14)$$

u_i Are the velocity components in the x_i − directions. L Is a length scale and for the vertical direction, a 1D $k - \varepsilon$ model is applied.

$$\upsilon_T = C_\mu \frac{k^2}{\varepsilon} \qquad (15)$$

k The turbulent kinetic energy

ε The dissipation rate of turbulent kinetic energy

C_μ Is an empirical constant

The bed stress is specified in terms of a drag coefficient formulation according to the relation,

$$\frac{\tau_{bottom}}{\rho} = C_D u^* |u^*| \qquad (12)$$

τ_{bottom} Is the bottom shear stress

u^* The first computational speed encountered above the bottom.

C_D Is the drag coefficient.

When using the mixed $1D - \varepsilon$, 2D Smagorinsky closure model, the bed drag coefficient reads

$$\frac{\tau_{bottom}}{\rho} = C_D u^* |u^*| \qquad (16)$$

Z_b Is the vertical extent of the bottom grid cell

K Is von karmans constant

c_s Is bed roughness length scale

2.4. MIKE 3 Model Setup

In this study, due to lack of access to temperature and salinity field data in period of the modeling, the effects of these factors were negligible. To make the bathymetry model of Golestan continental shelf, the sheet map with scale of 1:100000 were used. Model area has to be rectangular in horizontal plane. A Cartesian coordinate system was selected and the model domain was divided into 60×90 square grids with a grid size of 1000 m. In order to calibration of the model and according to the depths of field measurements of flow velocity, the vertical grid spacing is chosen as 0.5 meter. After running the model for several times and changing some important calibration coefficients such as bottom friction and wind friction factor in surface, model was calibrated. For verification of the model, the current measurement data were used by Ministry of Jihad-e-Agriculture in southern part of the domain [21]. For evaluating the model results the Root mean square error formula was used to compare the percentage of errors (table 2).

Table 2- Comparing the results of modeling and field measurements, percent errors in the two situations.

Date	Station	lat (degree)	Long (degree)	Total depth (m)	Measurment depth (m)	Current Meter (m.s^{-1})	Model (m.s^{-1})	percent error
2001/08/01	B$_1$	36 55 00	54 02 18	1/9	0.4	0.1	0.09	0.1
					1.2	0.22	0.24	0.09
					1.6	0.24	0.19	0.2
	B$_3$	36 55 00	54 01 23	2/3	0.4	0.21	0.18	0.14
					1.4	0.2	0.21	0.05
					1.8	0.23	0.25	0.08

At the next stage and after the model calibration, according to the maximum depth of the basin (-34 meter), the vertical grid spacing chosen as 2 meter. Thus the model includes 17 separately vertical layers. In the present study, the results output of MIKE 21 for the Caspian Sea as a profile series including velocity components and water surface elevation in west and north boundaries as boundary conditions in two open boundaries of the basin in western and northern parts of it were used. In the period of the study, wind data including speed and direction as varying with time but constant in space for the Gorgan Bay were gathered from Bandartorkaman synoptic station after transform to offshore wind [26]. To implement the initial surface condition, the results of two dimensional modeling of the Caspian Sea was used. Mean discharge of Gorgan Rud and Atrak river included in the model as source terms. The Gorgan Bay located at the southeast part of the Golestan coastlines has an important role in forming the flow pattern in southeast part of the solution domain, so in this study the effects of water exchange between the Gorgan Bay and this basin was considered to modeling [25]. Table 3 shows the including factors in MIKE 3 model after calibration the model.

Table 2- considering factors in MIKE 3 model

Module Selection	Hydrostatic	Simulation Start Date	2001/07/20
Map Projection	WGS-1984-UTM-Zone-38N	Simulation End Date	2001/08/20
Time Step Range	4464	Max Courant Number	10/53
Time Step Interval (s)	600	Number of sources	2
Flooding & Drying Depth (m)	0.2 , 0.3	Number of sink	1
Initial Surface Elevation (m)	From file Dfs2 of MIKE 21	Evaporation (mm.day^{-1})	6
Precipitation (mm.day^{-1})	0	Turbulence model	$k-\varepsilon$ Mixed/Smagorinsky formula
Resistance (Manning Number) (m$^{1/3}$.s^{-1})	30	Wind Conditions (m.s^{-1})	Varying in time and space
Number of Vertical Layers	17	Apply Coriolis forcing	yes
Vertical grid spacing (m)	2	Boundary condition	data transfer (Velocity-dfs1)
Background salinity (psu)	13	Background temperature (^{0}c)	27
Warm-Up (day)	3	Number of computational points	437462

3. Discussion

It is necessary in MIKE 3 model to have useful boundary data to three dimensional simulating the wind-driven flow pattern. This basin has two open boundaries in western and northern parts. For extracting of water elevation and velocity components in the plan on the open boundaries, the results of MIKE 21 model were used in the Caspian Sea. MIKE 3 model was run after implemented the boundary conditions and transformed the coastal wind to offshore wind. The model results were verified in two points of the domain. Notice that the time step intervals in this simulation was 600 second and model was run for one month (2001/07/20 to 2001/08/20). In this section, mean monthly of MIKE 3 modeling results will be described.

3.1. Currents description in the coastal zone

Generally costal currents are along the coast and reciprocating in period of the simulation. In south part of the domain and above the Miankaleh peninsula currents almost are parallel to the peninsula and flow from west to east (fig 4). Model calculated maximum speed value about 0.45 m/s along these coasts. In west part of the coasts with moving from south to north, the speed values will be increased, such that maximum current speed in north coast is taking to 0.3 m/s. Flow pattern in the west coasts are depending to prevailing wind pattern and currents flow to the south along the north-south axis. Current speed with increasing the depth is decreased in shallow water in coastal zone because of the bottom friction and friction between adjacent layers. Golestan continental shelf divided in to northern and southern parts in order to estimating currents in the surface layer at the offshore areas. In surface layer of the northern part, currents mostly flow to southeast along the prevailing northwest wind. But in surface layer of the south part of the domain, currents affected by bottom topography and shifting their direction to the southeast in most of the time with maximum speed of 0.45 m/s.

3.2. Currents description in middle layer

Currents review in the middle layer in depth of 17 meter shows that this layer has much effectively from surface layer. Wind stress has a main role in forming of the current circulation in this layer. In northern part of this basin, currents deviated to the north and northwest. Maximum current speed in this layer was recorded in deeper parts of the continental shelf and is about 0.3 m/s. This high current speed was occurred because of the effect of high current speed in west open boundary that is effecting by fast and anticlockwise currents in the Caspian Sea. This layer at the southern part, getting a little effect from wind pattern in the surface layer and the current speed in this part is so low because this part is a shallow water zone and affected by bottom topography. Maximum current speed in this layer is about 0.1 m/s. Mean monthly of modeling results show that there is an anticlockwise ring in south part of this basin and in north part of it clockwise ring can be seen (fig 5).

3.3. Currents description in deep layer

In generally, current directions in depth of 28 meter are to the northwest. Such that current directions in these depths have about 180 degree phase difference with surface currents that mostly flow to the southeast. This occurrence indicated on outflow water in this depth from this basin. Maximum current speed in this part by affecting the bottom friction is about 0.14 m/s in this layer (fig 6).
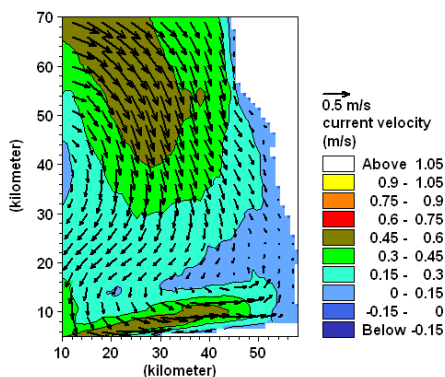

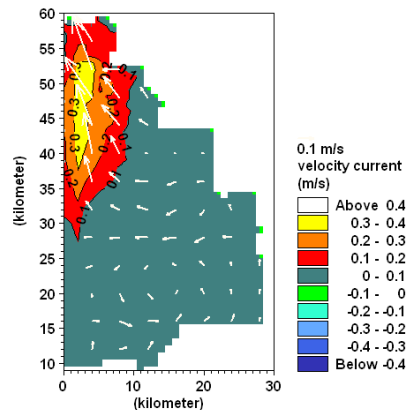**Figure 4- mean monthly flow pattern and velocity distributions in the surface layer.**

Figure 5- mean monthly flow pattern and velocity distributions in the middle layer (17 meter depth).
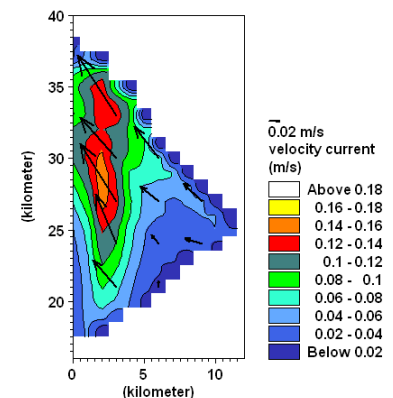
Figure 6- mean monthly flow pattern and velocity distributions in 28 meter depth.

4. Conclusion

The results in this study are a mean monthly from 2001/07/20 to 2001/08/20. To obtain better results, model must be implemented for at least one year period with including the effect of salinity and temperature variations. In this investigation because of lack of temperature and salinity field data in period of the modeling, the effect of these factors were negligible. Generally the modeling results are as follow:

1- In costal lines of Golestan continental shelf, currents are along the coast and reciprocating. This result is completely matched to two dimensional modeling by MIKE 21 model that was done by Rahimpoor Anaraky (2005) [22]. Due to effective bed friction in coastal lines, surface current speed in these areas is lower than offshore surface currents.

2- Modeling results of the middle layer show that there is an anticlockwise ring in southern part of this layer and in northern part of it clockwise ring can be seen. The effects of north and west open boundaries and prevailing wind pattern have an important role to forming these rings.

3- Current direction in deep part of the basin is to the northwest has about 180 degree phase difference with surface currents. This occurrence indicated on outflow water in this depth from this basin.

Reference

1. Bannazadeh M.R, Bidokhti A.A, Kherandish M, Hosseni H.F (2002). A Three-Dimensional Model of the Caspian Sea. J. Esteghlal, 21(1):207-220. (In Persian)

2. Biabany M (2008). A Study of Wind – driven Circulation by a three dimensional Numerical Model in the Amir Abad Region. Islamic Azad University, M.S Thesis, pp. 76.

3. Bondarenko A.L (1993). Currents of the Caspian Sea and formation of salinity of the Water of the north part of the Caspian Sea. Moscow, Nauka, pp.122. (In Russian)

4. Esmaeili M, Azarmsa A, Karami A.kh (2009). Long shore Currents Simulation using Mike21 Numerical Model, Case Study: Kiashahr area. J. Earth and space physics, 35(2):139-156. (In Persian)

5. Ghaffari P, Chegini V (2009). Acoustic Doppler Current Profiler Observations in the southern Caspian Sea: shelf currents and flow field off Freidoonkenar Bay. Iran Ocean Sci. Discuss, 6:3019–3053.

6. Ibrayev R. A, Zsoy E. O, Schrum C, Sur H. I (2010). Seasonal variability of the Caspian Sea three dimensional circulation, sea level and air-sea interaction. Ocean Sci Discuss, 6:1913-1970.

7. Klevtsova N.D (1967). Sea current regime near east coast of the middle and south Caspian basin. Proceeding of Hydro-meteo observatory of Baku, 3: 44-49. (In Russian)

8. Knysh V. V, Ibrayev R. A, Korotaev G. K, Inyushina N. V (2008). Seasonal Variability of Climatic Currents in the Caspian Sea Reconstructed by Assimilation of Climatic Temperature And Salinity into the Model of Water Circulation. SSN 0001-4338, J. Atmospheric and Oceanic Physics, 44(2):236–249.

9. Korotenko K. A, Mamedov R. M, Kontarb A. E, Korotenko L. A (2004). Particle tracking method in the approach for prediction of Oil slick transport in the sea: modelling oil pollution resulting from river input. J. Marine System, 48:159–170.

10. Kosarev A.N (1990). The Caspian Sea, Structure and water Dynamics. Moscow, Nauka. (In Russian)

11. Lednev V.A (1943). Currents of the northern and central parts of the Caspian Sea. Nauka, Moscow. (In Russian)

12. Manual of MIKE 21 FLOW MODEL Hydrodynamic Module, Scientific Documentation, Danish Hydraulic Institute (DHI Software), 58pp, 2007.

13. Manual of MIKE 21 FLOW MODEL, Hydrodynamic Module, step-by-step training guide, Danish Hydraulic Institute (DHI Software), 42 pp, 2007.

14. Manual of MIKE 21 FLOW MODEL, Hydrodynamic Module, User Guide, Danish Hydraulic Institute (DHI Software), 90 pp, 2007.

15. Manual of MIKE 3 FLOW MODEL, Coastal Hydraulic and Oceanography Hydrodynamic Module, Hydrostatic Version, Scientific Documentation, Danish Hydraulic Institute (DHI Software), 2007.

16. Manual of MIKE 3, Coastal Hydraulic and Oceanography Hydrodynamic Module, Scientific Documentation, Danish Hydraulic Institute (DHI Software), 2007.

17. Manual of MIKE 3, Coastal Hydraulic and Oceanography Hydrodynamic Module, User Guide, Danish Hydraulic Institute (DHI Software), 2007.

18. Matthew C. W, Roderick T, Tatsu I (2001). Hydrodynamic and Dispersion Modeling for the Azeri, Chirag, Gunashi Field Offshore Baku. Azerbaijan, CLIENT URS Dames & Moore, Project Number ASA 01-007, pp. 47.

19. Nasimi S, Ghiasi R (2006). A three-dimensional model of water circulation and temperature structure in the Caspian Sea. J. Earth Space Phys, 32:21-35.

20. Panin G. N, Dzuyba A. V (2003). Current variations in the wind speed vector and the rate of evaporation from the Caspian Sea surface. Water Res, 30: 177-185.

21. Rahimipour Anaraki H (2005). Investigation of Hydrodynamic of currents and prediction of Erosion and Sedimentation Pattern in Groan Bay-Iran. Soil Conservation and Watershed Management Research Institute, 84/322:1-48. (In Persian).

22. Sabbagh-Yazdi S.R (2002). Investigation of Coriolis Forces on the Caspian Sea Currents Using a Two Dimensional Numerical Model. 4th International of Coasts, Ports and Marin Structures (ICOMPAS 2002), Ramsar, Iran. (In Persian)

23. Sharbaty S (2012). 3-D Simulation of Wind-Induced Currents Using MIKE 3 HS Model in the Caspian Sea, Canadian Journal on Computing in Mathematics, Natural Sciences, Engineering and Medicine, Vol. 3, No. 3, pp. 45-54.

24. Sharbaty S (2012). comparison if MIKE 3 MODEL and Princeton Ocean MODEL in Wind driven Current patterns under same condition for the Caspian Sea, Canadian Journal on Computing in Mathematics, Natural Sciences, Engineering and Medicine, Vol. 3, No. 3, pp. 60-66.

25. Sharbaty S, Imanpoor M.R, Gorgin S, Hosseini S (2010). The first phase of simulation studies of short-term sea currents in the Gorgan Bay. Research Report, Gorgan University of Agricultural Sciences and Natural Resources, 89-2-257, 41 pp. (In Persian)

26. Shore Protection Manual, (1984), U.S. Army Engineer Waterways Experiment Station, Washington, D.C., U.S. Government Printing Office, Vol.2.

27. Smagorinsky j (1963). General circulation Experiments with the primitive equations. Monthly weather review, Vol.91, pp: 91-164.

28. Smith S.D, Bank G (2007). Variation of the sea drag coefficient with wind speed. Quart. Journal of Met. Soc. Vol.101, PP. 665-673.

29. Zounemat-Kermani M, Sabbagh Yazdi S.R (2010). Conjunction of 2D and 3D Modified Flow Solvers for Simulating Spatio-Temporal Wind Induced Hydrodynamics in the Caspian Sea. Journal of Ocean Sci. 45(2):113-128.

30. http://www.cdc.noaa.gov

ULTRA LOW POWER MODULO $2^n + 1$ MULTIPLIER USING GDI

Pavankumar Reddy S
Dept Of Ece
Srm Univesity

Mrs.N.SARASWATHI
Assistant Prof. (S.G)
Dept Of Ece
Srm Univesity

Gnanavargin Rokkala
Assistant Professor
Dept Of Ece
Aditya Engineering College

Abstract:
Modulo $2^n + 1$ multiplier is one of the critical components in applications in the area of digital signal processing, data encryption and residue arithmetic that demand high-speed and low-power operation. Ultra low power and low area modulo $2^n + 1$ multiplier is designed using the GDI technology. modulo $2^n + 1$ multiplier has three major functional modules including partial products generation module, partial products reduction module and final stage addition module. The partial products reduction module is completely redesigned using the novel compressors and the final addition module is implemented using a new less complex sparse tree based inverted end-around-carry adder. The resulting modulo $2^n + 1$ multiplier is implemented in GDI cell technology and compared both qualitatively and quantitatively with the existing hardware implementations.

Keywords: Modulo multipliers, Residue Number System (RNS), Compressors, Sparse Tree Adder, GDI technology

I. Introduction
Modulo arithmetic has been widely used in various applications such as digital signal processing where the residue arithmetic is used for digital filter design [1, 2]. Also, the number of wireless and internet communication nodes has grown rapidly. The confidentiality and the security of the data transmitted over these channels have becoming increasingly important. Cryptographic algorithms like International Data Encryption Algorithm (IDEA) [5, 6, 7, 8] are frequently used for secured transmission of data.

In IDEA there are three major components that's decide the overall power area and performance. They are modulo 2^n addition, bitwise-xor and modulo $2^n + 1$ multiplier. Modulo 2^n addition and bitwise-xor will take less time and easy to implement improving the area and power efficiency of the modulo $2^n + 1$ multiplication operation leads to significant decrease in area and power consumption of the IDEA cipher.

Here we introducing new low power design technique called GDI (Gate-Diffusion-Input) technology Instead of CMOS technology. The modulo multiplier has three major blocks partial product generation, partial product reduction, and final stage addition. The partial product reduction block use the GDI EXOR gates this the area of the partial product block which will reduced to 65%

of the area. In the partial product generation blocks we will use GDI based AND and OR gates.

II. COMPRESSORS
A. GDI Vs CMOS:
A new low power design technique that solves most of the problems known as Gate-Diffusion-Input (GDI) is proposed [17]. This technique allows reducing power consumption, propagation delay, and area of digital circuits. The GDI method is based on the simple cell shown in Figure.1. A basic GDI cell contains four terminals – G (common gate input of nMOS and pMOS transistors), P (the outer diffusion node of pMOS transistor), N (the outer diffusion node of nMOS transistor), and D (common diffusion node of both transistors)
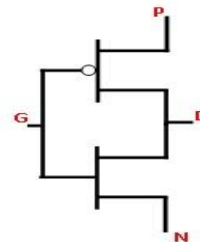

Fig.1 basic gdi cell

B. Description of compressors:
A (p,2) compressor[8,9] with p inputs $X_1, X_2, \ldots X_p$ and two output bits Sum and Carry along with carry input bits and carry output bits is governed by the equation:

$$\sum_{i=1}^{p} X_i + \sum_{i=1}^{p} (c_{in})_i = sum + 2\left(carry + \sum_{i=1}^{p} (c_{out})_i\right)$$

For example, a (5:2) compressor takes five inputs and two carry inputs and generates a Sum and Carry bit along with two carryout bits. Diagrams of 5:2 and 7:2 compressors are shown in Fig. 2 & 3. Are designed using the GDI multiplexers.

The Boolean equation of carry generator block is given by

$$O = (X_1 + X_2)X_3 + X_1 X_2$$

TABLE:1 different operations using GDI

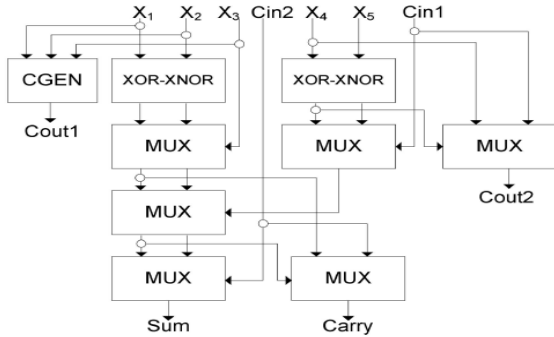| N	P	G	D	Function
0	B	A	A'B	F1
B	1	A	A'+B	F2
1	B	A	A+B	OR
B	0	A	AB	AND
B	A	S	S'A+SB	MUX
0	1	A	A'	NOT

FIG 2 5:2 compressor

FIG 3 7:2 compressors

Iii. Algorithm For Implementation Of Modulo $2n+1$ Multiplier

The algorithm for computation of X·Y mod $2^n + 1$ is described below. From the architectural characteristic comparisons, the algorithm presented in is considered as the best existing algorithm for the computation of X·Y mod $2^n + 1$ in the literature. Hence, this algorithm is used for the proposed implementation of the modulo multiplier. According to the algorithm it takes two n+1 bit unsigned numbers as inputs and gives one n+1 bit output. The proposed implementation can be adapted to IDEA cipher, in which the mod $2^n + 1$ multiplication module takes two n-bit inputs and gives one n-bit output, by assigning the most significant bits of the inputs zeros and neglecting the most significant bit of the output Let $/A/ B$ denote the residue of A modulo B. Let X and Y be two inputs represented as X=$X_n X_{n-1} \ldots X_0$ and Y=$y_n y_{n-1} \ldots y_0$ where the most significant bits x_n and y_n are '1' only when the inputs are 2^n and 2^n respectively. X·Y mod $2^n + 1$ can be represented as follows:

$$P = |X.Y|_{2^n+1} = \left| \sum_{i=0}^{n} x_i 2^i . \sum_{j=0}^{n} y_i 2^i \right|_{2^n+1} = \left| . \sum_{i=0}^{n} \left(\sum_{j=0}^{n} p_{i,j} 2^{i+j} \right) \right|_{2^n+1}$$
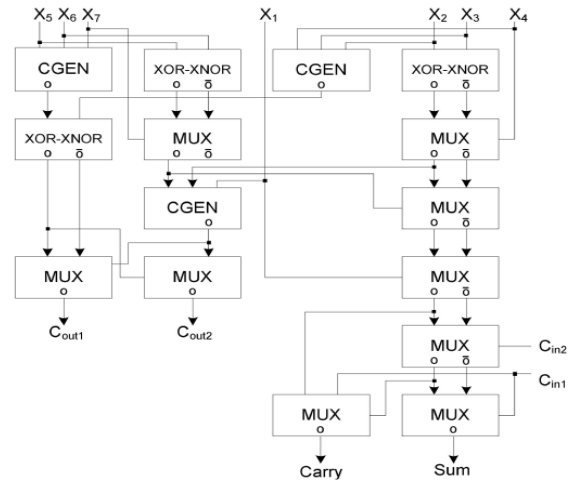
The n×n partial product matrix in Fig. 6 is derived from the initial partial product matrix in Fig. 4, based on several observations. First observation is, the initial partial product matrix can be divided into four groups A, B, C and D in which the terms in only one group can be different from '0'. Groups A, B, D and C are different from '0', if inputs (X,Y) are in the form of (0Z,0Z),(1Z,0Z),(0Z,1Z) and (10. . .0,10. . .0) respectively (here 'Z' is a 16-bit vector). Hence the four groups can be integrated into a single group by performing logical OR operation (denoted by v) instead of adding the bits arithmetically. Logical OR operation is performed on the terms of the groups B, D and A in the columns with weight 2^n up to $2^{2n} - 2$ and on the two terms of the groups B and D with weight $2^{2n} - 1$ (the ORed terms of the groups B and D are represented by q_i, where $q_i = p_{n,i} V p_{i,n}$). Since $|2^{2n-1}|_{2^n+1} = 2^{n-1}+1$, the term with weight $2^{2n} + 1, p_{n-1}$, can be substituted by two terms q$n-1$ in the columns with weight 2^{n-1} and 1, respectively, and ORed with any term of the group A there. Moreover, since $|2^{2n}|_{2^n+1}=1$, the term $p_{n,n}$ can be ORed with p0,0. The modified partial product matrix is shown in Fig. 5. Second observation is repositioning of the partial product terms in the modified partial product matrix, with weight greater than 2^{n-1} based on the following equation:

$$\left| s2^t \right|_{2^n+1} = \left| -s2^{|t|_n} \right|_{2^n+1} = \left| (2^n + 1 - s)2^{|t|_n} \right|_{2^n+1} = \left| \bar{s}2^{|t|_n} + 2^n 2^{|t|_n} \right|_{2^n+1} \cdots (1)$$

Equation (1) shows that the repositioning of each bit results in a correction factor of $2^n 2^{|t|_n}$. In the first partial product vector, there is only one such bit and in the second partial product vector 2 bits need to be repositioned and so on. Hence the correction factor for the entire partial product matrix would be:

$$COR1 = |2^n(2^n - n - 1)|_{2^n+1} \cdots (2)$$

The n×n partial product matrix along with the equation (2) results in n+1 operands. These partial product terms can be reduced into two final summands Sum array and Carry array using a Carry Save Adder (CSA) array. Suppose the carry out bit at i^{th} stage of CSA is c_i with weight 2n, this carryout can be reduced into:

$$|c_i 2^n|_{2^n+1} = |-c_i|_{2^n+1} = |2^n + \bar{c_i}|_{2^n+1}$$

Therefore the carry output bits at the most significant bit position of each stage can be used as carry input bits of the next stage. In an n-1 stage CSA array in areproduced n-1 such carry out bits. Hence there will be a second correction factor. And the overall correction factor using this algorithm is:

$$COR2 = |2^n(n-1)|_{2^n+1} \ldots\ldots(3)$$

The final correction factor will be the sum of COR1 and COR2. The constant '3' in equation (5) will be the final partial product.

$$COR = COR1 + COR2$$

$$= |2^n(n-1) + 2^n(2^n - n - 1)|_{2^n+1} \ldots(4)$$

$$= |2^n(2^n - 2)|_{2^n+1} = 3 \ldots (5)$$

Iv. Proposed Implementation Of The Mod 2n+1 Multiplier

The proposed implementation of the modulo multiplier consists of three modules. First module is to generate partial products, second module is to reduce the partial products to two final operands and the last module is to add the Sum and Carry operands from partial products reduction to get the final result.

A. Partial products generation

From the above $n \times n$ partial product matrix (shown in Fig. 6), it is possible to observe that the partial product generation requires AND, OR and NOT gates. The most complex function of partial product generation module is $\overline{p_{n-1,n-1} V q_{n-2}}$ where $p_{i,j} = a_i b_j$ and $q_i = p_{n,i} V p_{i,n}$.

B. Partial products reduction

The partial product reduction unit is the most important module which mainly determines the critical path delay and the overall performance of the multiplier. Hence this module needs to be designed so as to get minimum area and consume less power.

In the partial products reduction module, the $n \times n$ partial product matrix and the constant 3(i.e., correction factor) need to be added to produce the final sum and carry vectors. Zimmerman demonstrated that (*Sum+Carry*+1) modulo $2^n + 1$ (final stage addition module) can also be

calculated by (*Sum + Carry*) modulo 2^n using inverted End-Around-Carry (EAC) adders, where *Sum* and *Carry* are *n*-bit vectors generated by the partial products reduction module. Modulo 2^n inverted EAC adders have a regular structure that can be easily laid out for efficient VLSI implementation. Hence, instead of directly adding the correction factor of 3 to the $n \times n$ partial product matrix in the partial products reduction module, an intermediate correction factor of 2 has to added to the $n \times n$ partial product matrix to save a constant 1 for the final stage addition module. Since there is a saved constant 1 available in the final stage addition module, modulo 2^n inverted EAC adder can be used instead of the complex modulo $2^n + 1$ adder.
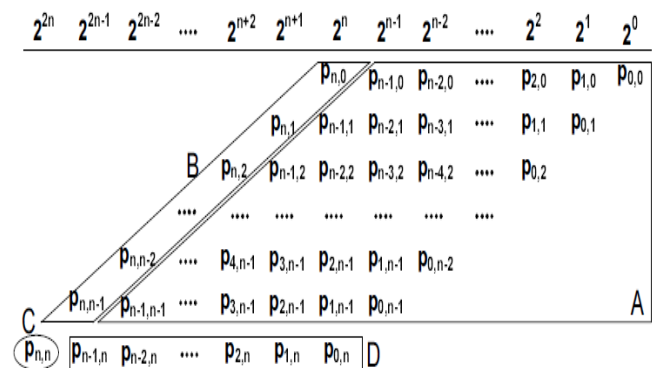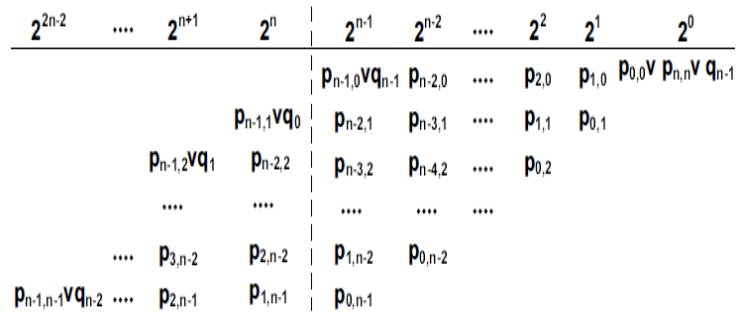

Fig-4: normal partial products

Fig 5: modified partial product matrix

Table 1: final partial product matrix

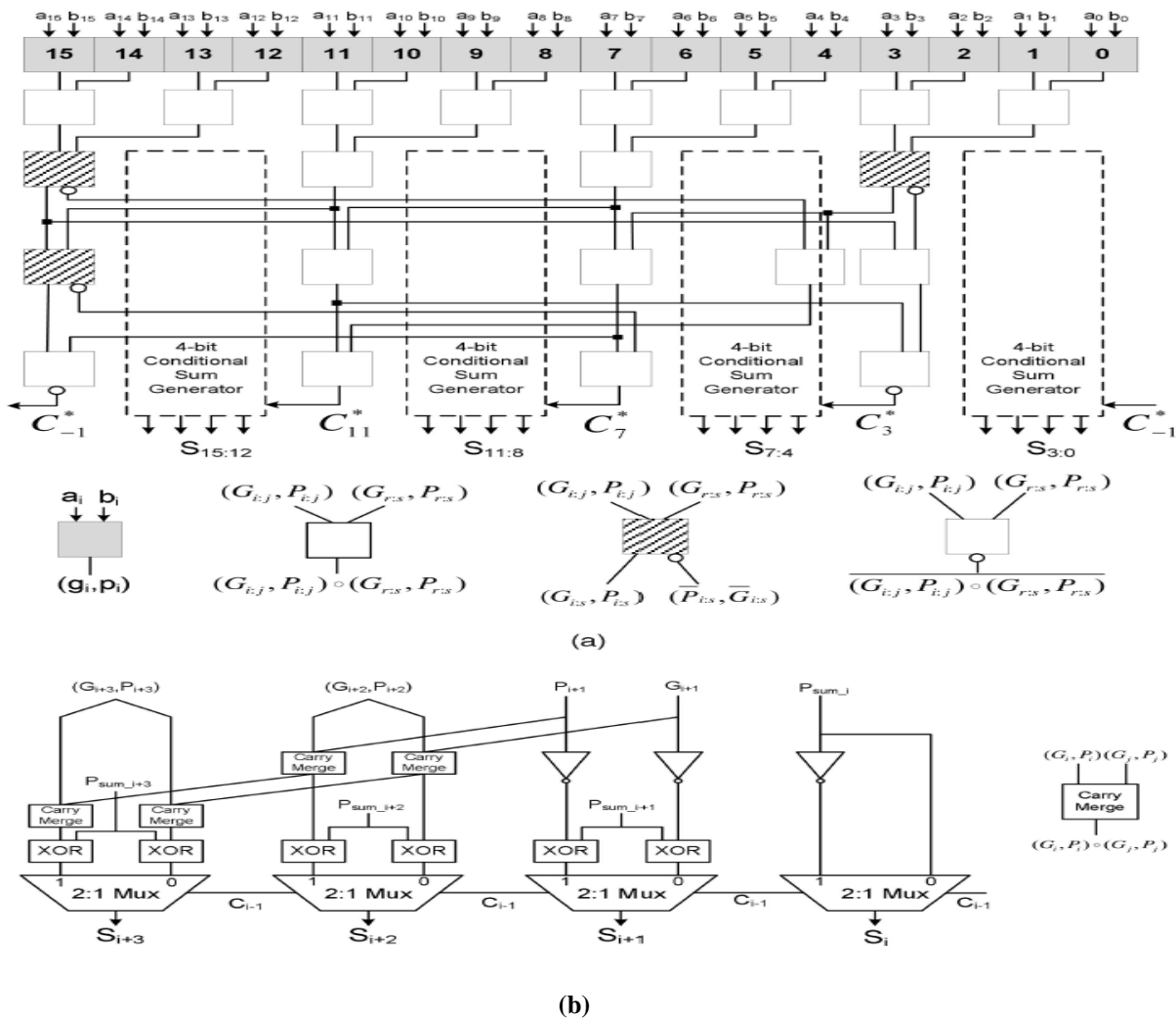| 2^{n-1}	2^{n-2}	2^{n-3}		2^2	2^1	2^0
$pp_0 = p_{n-1,0}{}^V q_{n-1}$	$p_{n-2,0}$	$p_{n-3,0}$		$p_{2,0}$	$p_{1,0}$	$p_{0,0}{}^V q_{n-1}{}^V p_{n,n}$
$pp_1 = p_{n-2,1}$	$p_{n-3,1}$	$p_{n-4,1}$		$p_{1,1}$	$p_{0,1}$	$\overline{p_{n-1,1}{}^V q_0}$
$pp_2 = p_{n-3,1}$	$p_{n-4,2}$	$p_{n-5,2}$		$p_{0,2}$	$\overline{p_{n-1,2}{}^V q_1}$	$\overline{p_{n-2,2}}$
....	....	....	....	....	....	....
$pp_{n-2} = p_{1,n-2}$	$p_{0,n-2}$	$\overline{p_{n-1,n-2}{}^V q_{n-3}}$		$\overline{p_{4,n-2}}$	$\overline{p_{3,n-2}}$	$\overline{p_{2,n-2}}$
$pp_{n-1} = p_{0,n-1}$	$\overline{p_{n-1,n-1}{}^V q_{n-2}}$	$\overline{p_{n-2,n-1}}$		$\overline{p_{3,n-1}}$	$\overline{p_{2,n-1}}$	$\overline{p_{1,n-1}}$

FIG 7 : (a) 16-bit Sparse-tree-based Inverted EAC adder and (b) 4-bit conditional sum generator.

Along with the constant 2, the *n* partial products should be added to produce the final *n*-bit Sum and Carry vectors. In a single stage of the Carry Save Addition, series of *n* full adders take 3 input operands and produce two *n*-bit output vectors. To add *n+1* input operands, *n*-1 Carry Save Addition stages are required in the partial products reduction module. As the first partial product is the constant 2, in the first stage of the *n*-1 CSA stages, half adders can be used instead of full adders except for the for the second bit. The *n*-1 stage CSA can be implemented using *n* full adders in each column of the *n*-1 stages. In this regular implementation, series of full adders in the CSA adder columns can be replaced by the proposed GDI EXOR-based compressors that take the same number of inputs, which leads less power implementation of the multiplier. For example, for a modulo $2^8 + 1$ multiplier the existing CSA design uses 7 full adder stages in a single column to reduce the 9 partial products, the same reduction can be done by more efficient designs based on the proposed compressors.

In the proposed compressor-based architecture, use of suggested compressors not only reduces power consumption but also the area of the circuit. For example, the full adder implementation requires fifteen full adders in series in any column for a modulo 2^{16+1} multiplier. However, these fifteen full adders can be replaced by two 7:2 compressors, one 5:2 compressor and two 3:2 compressors .

V. Final stage addition

In binary addition operation, the critical path is determined by the carry computation module. Among various formulations to design carry computation module, parallel prefix formulation [18] is delay effective and has regular structure suitable for efficient hardware implementation. The binary addition of two numbers using a parallel prefix network is done as follows: $A = a_{n-1}a_{n-2}.....a_1a_0$ and $B = b_{n-1}b_{n-2}.....b_1b_0$ be two weighted input operands to the network. The generate bit (g_i) and the propagate bit (p_i) are defined as $g_i = a_i \ AND \ b_i$ and $p_i = a_i \ OR \ b_i$ and these generate bits can be associated using the prefix operator as follows:
$(g_i, p_i) \cdot (g_{i-1}, p_{i-1}) =$
$(g_i + p_i \cdot g_{i-1}, p_i * p_{i-1}) (g_{i:i-1}, p_{i:i-1})$

Where + is logical OR operation and * is logical AND operation. The carryout's (C_i) for all the bit positions can obtained from the group generate ($C_i^* = G_i^*$) where
$(G_i, P_i) = (g_i, p_i) \cdot (g_{i-1}, p_{i-1}) \cdot .....(g_1, p_1) \cdot (g_0, p_0)$.

The function of End around Carry (EAC) adder is to feed back the carryout of the addition and add it to the least significant bit of the sum vector. Similarly, in inverted End Around Carry adders, the carryout is inverted and fed

back to the least significant bit of the sum vector. The parallel prefix-network-based Inverted EAC [19] adder achieves the addition of the input operands by recirculating the generate and the propagate bits at each existing level in $log_2 n$ stages. Let $C_i^*(G_i^*)$ be the carry at bit position i in the inverted EAC, this can be related to G_i as follows:

$$(G_i^*, P_i^*) = \begin{cases} \overline{(g_{n-1}, p_{n-1})} \ for \ i = -1 \\ (g_i, p_i) \cdot \overline{(g_{n-1:i+1}, p_{n-1:i+1})} \\ \quad for \ n-1 \ge i \ge 0 \end{cases}$$

$$.....................(5)$$

In the above equation $\overline{(G_i^*, P_i^*)} = (\overline{G}, P)$ where

$$(G_i, P_i) = (g_i, p_i) \cdot (g_{i-1}, p_{i-1}) \cdot ..... (g_1, p_1) \cdot (g_0, p_0)$$
and

$$(G_i, P_i) = (g_{n-1}, p_{n-1}) \cdot (g_{n-2}, p_{n-2})$$

$$\cdot ..... (g_{i+2}, p_{i+2}) \cdot (g_{i+1}, p_{i+1})$$

In some cases, it is not possible to compute (G_i^*, P_i^*) In $log_2 n$ stages, then in these cases, the equations in (5) are transformed into the equivalent ones as shown in (7) by using the following property [19]: suppose that $(G^x, P^x) = (g, p) \cdot \overline{(G, P)}$ and $(G^y, P^y) = \overline{((\overline{g}, \overline{p}) \cdot (G, P))}$

$G^x = g + p\overline{G} = \overline{\overline{g} + \overline{p}G}$.....(6) Therefore $G^x = G^y$ and in (2), P^y is computed as p.P. To implement the parallel prefix computation efficiently, these transformations have to be applied j number of times recursively on $(G_i, P_i) \cdot \overline{(G_{n-1:i+1}, P_{n-1:i+1})}$ using the fallowing relation:

$$n - 1 - i + j = \begin{cases} n, if \ i > \frac{n}{2} - 1 \\ \frac{n}{2}, if \ i \le \frac{n}{2} - 1 \end{cases} \quad ....(7)$$
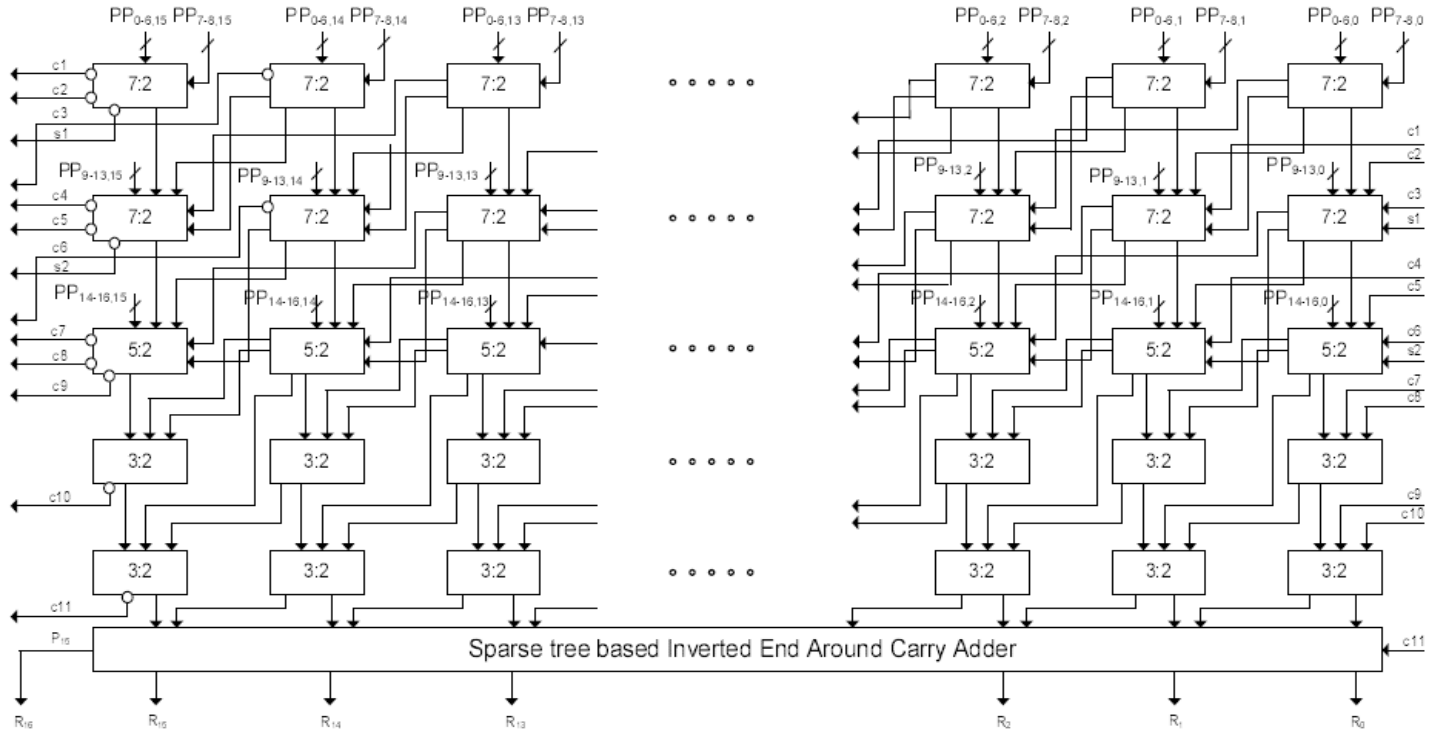
\

Fig 8 : proposed implimentation of modulo $2^{16}+1$ multiplier using compressors with GDI technology

The new carryout's can be computed using the following equation:

$$(G_i^*, P_i^*) =$$

$$\begin{cases} \overline{(g_{n-1}, p_{n-1})} & for\ n = - \\ \overline{(\overline{P_i}, \overline{G_i})} \bullet (g_{n-1:i+1}, p_{n-1:i+1}) & for\ n-1 \ge i \ge 0 \end{cases}$$

$$\dots\dots(8)$$

Hence, the transformations used above to achieve the parallel prefix computation in $log_2 n$ stages result in more number of carry merge cells and thereby adding more number of interstage wires. Parallel prefix adders suffer from excessive interstage wiring complexity and large number of cells, and these factors make parallel prefix based adders inefficient choices for VLSI implementations. Therefore, a novel sparse-tree-based EAC and inverted EAC adders are used as the primitive blocks in this work.

In sparse-tree-based inverted EAC adders, instead of calculating the carry term Gi for each and every bit position, every Kth (K=4,8 . .) carry is computed. The value of K is chosen based on the sparseness of the tree,

generally for 16 and 32-bit adders, K is chosen as four. The higher value of K results in higher value of noncritical path delay compared to critical path delay of O($log_2 n$) which should not be the case. The proposed implementation of the sparse-tree-based Inverted End Around Carry Adder (IEAC) is explained below clearly for 16-bit operands. For a 16-bit sparse IEAC with sparseness factor (i.e., K) equal to four, the carries are computed for bit positions -1,2,3 and 11. Here, bit position -1 corresponds to the inverted carryout $(\overline{(G_{15}, P_{15})})$ of the bit position 15. The carryout equation for the 16-bit sparse tree IEAC are as fallows

$$C_{-1}^* = \overline{(G_{15}, P_{15})}$$
$$= \overline{(g_{15}, p_{15}) \bullet (g_{14}, p_{14}) \bullet \dots (g_1, p_1) \bullet (g_0, p_0)}$$
$$C_3^* = (G_3, P_3) \bullet \overline{(G_{15:4}, P_{15:4})}$$

$$= (g_3, p_3) \bullet \dots \bullet (g_0, p_0) \bullet \overline{(g_{15}, p_{15}) \bullet \dots \bullet (g_4, p_4)}$$

$$C_7^* = (G_7, P_7) \bullet \overline{(G_{15:8}, P_{15:8})}$$

$$= (g_7, p_7) \bullet \dots \bullet (g_0, p_0) \bullet \overline{(g_{15}, p_{15}) \bullet \dots \bullet (g_8, p_8)}$$

$$C_{11}^* = (G_{11}, P_{11}) \bullet \overline{(G_{15:12}, P_{15:12})}$$

$$= (g_{11}, p_{11}) \bullet \ldots \bullet (g_0, p_0) \bullet \overline{(g_{15}, p_{15}) \bullet \ldots \bullet (g_{12}, p_{12})}$$

Fig. 7 shows the finalized 16-bit sparse tree Inverted EAC adder. From Fig. 7, we can observe that all the carryouts are computed in $log_2 n$ stages with less number of carry merge cells and reduced interstage wiring intensity. The implementation of the sparse-tree-based EAC is similar to IEAC shown in Fig. 7, except the carry is not inverted.

The Conditional Sum Generator (CSG) shown in Fig. 2C is implemented using ripple carry adder logic, and two separate rails are run to calculate the carries $C_{i+1}^*, C_{i+2}^*, C_{i+3}^*$ and C_{i+4}^* assuming the input carry C_i^* as 0 and 1. Four 2:1 multiplexers using the carry C_i^* from sparse tree network as one-in-four select line generate the final sum vector. The conditional sum generator is shown in Fig. 7b. The final sum is generated in log2n stages in IEAC sparse tree adder with less number of cells and less interstage wiring. Hence, this approach results in low power and smaller area while providing better performance.
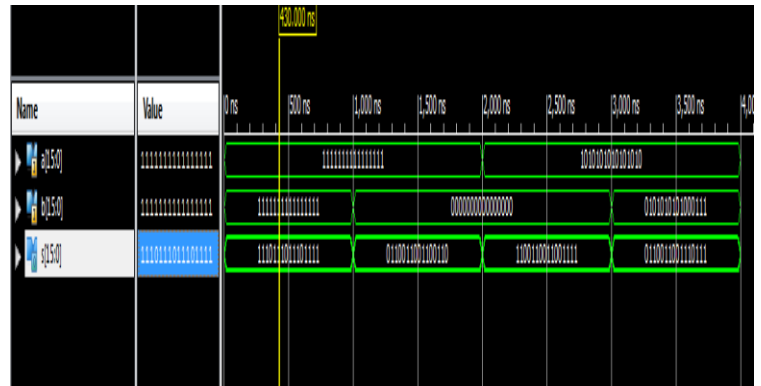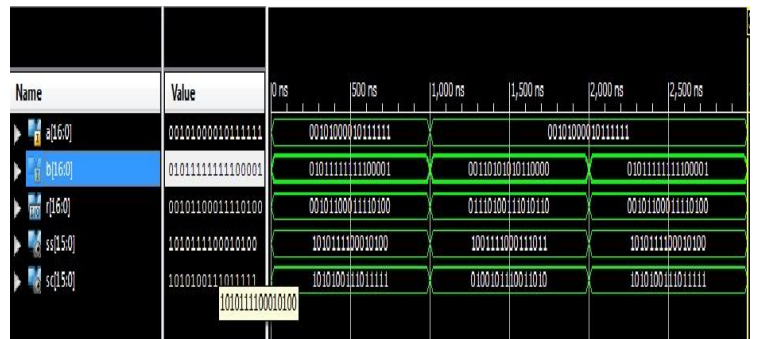
VI. SIMULATION RESULTS:

7:2 compressor:

5:2 compressor:
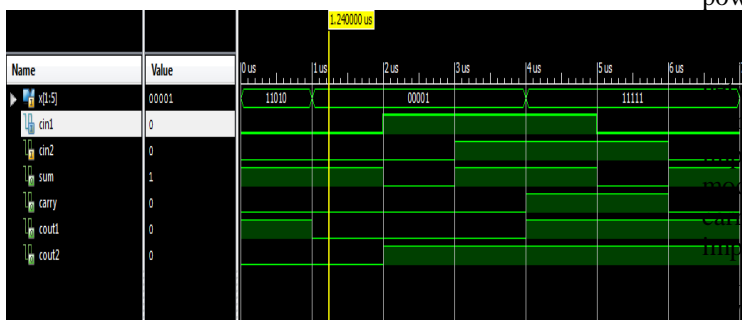
Spare tree adder:

Final output :

V. CONCLUSIONS:

An ultra low power implementation of the modulo $2^n + 1$ multiplier is presented in this paper. The proposed novel implementation takes advantage of newly designed low power compressors using GDI technology and sparse tree based Inverted End-Around-Carry (EAC) adders. The proposed design of the modulo $2^n + 1$ multiplier uses compressors in the partial products reduction stage, the use of the GDI compressors in place of CMOS compressors resulted in considerable improvements in terms of area and power. An efficient sparse tree based inverted EAC adder in final stage addition, which has less wiring complexity sparse carry merge cells compared to parallel prefix work based implementations. The proposed multiplier is pared with the most efficient modulo $2^n + 1$ multiplier ementations available in the literature. The unit gate model analysis and EDA-based parametric simulation are carried out on the proposed implementation and the existing implementations to clearly demonstrate and verify potential efits from the proposed design. The proposed multiplier erified to outperform the existing implementations with respect to three major design criteria (i.e., area and power).

REFERENCES

1. Zimmermann, R., Curiger, A., Bonnenberg, H., Kaeslin, H., Felber,N., and Fichtner, W. "A 177 Mb/s VLSI implementation of the international data encryption algorithm", IEEE J. Solid-State Circuits, 1994, 29, (3), pp. 303-307

2. Zimmerman, R., "Efficient VLSI implementation of modulo ($2n \pm 1$) addition and multiplication" IEEE trans. Comput., 2002, 51, pp. 1389- 1399.

3. Sousa, L., and Chaves, R., "A universal architecture for designing efficient modulo $2n + 1$ multipliers", IEEE Trans. Circuits Syst. I., 2005, 52, pp. 1166-1178.

4. Efstathiou, C., Vergos, H.T., Dimitrakopoulos, G., and Nikolos, D., "Efficient diminished-1 modulo $2n + 1$ multipliers", IEEE Trans. Comput., 2005, 54, pp. 491-496.

5. Vergos, H.T.; Efstathiou, C., "Design of efficient modulo $2n + 1$ multipliers", IET Comput. Digit. Tech., 2007, 1, (1), pp. 49-57.

6. R. Zimmermann and W. Fichtner., "Low power logic styles: CMOS versus pass-transistor logic" IEEE J. Solid- State Circuits, vol. 32, pp. 1079-1090, July 1997.

7. Veeramachaneni, S.; Avinash, L.; Rajashekhar Reddy M; Srinivas, M.B., "Efficient Modulo ($2k \pm 1$) Binary to Residue Converters System on- Chip for Real-Time Applications" The 6th International Workshop on Dec. 2006 pp.195 - 200.

8. C-H Chang, J Gu, MZhang "Ultra low-voltage lowpower CMOS 4-2 and 5-2 compressors for fast arithmetic circuits " IEEE J. Circuits and Systems I, Volume: 51, Issue: 10 pp: 1985- 1997,2004

9. Rouholamini, M.; Kavehie, O.; Mirbaha, A. P.; Jasbi, S.J.; Navi, K., "A New Design for 7:2 Compressors" Computer Systems and Applications, 2007. AICCSA '07. IEEE/ACS International Conference on 13-16 May 2007 Page(s):474 – 478

10. Mathew, S.; Anders, M.; Krishnamurthy, R.K.; Borkar, S.; "A 4-GHz 130-nm address generation unit with 32-bit sparse-tree adder core" In IEEE Journal of Solid-State Circuits, Volume 38, Issue 5, May 2003 Page(s):689 - 695.

11. Zhongde Wang, Graham A. Jullien, William C. Miller., "An efficient tree architecture for modulo $2n +1$ multiplication" VLSI Signal Processing 14(3): 241-248 (1996).

12. P. Kogge and H. S. Stone., "A parallel algorithm for the efficient solution of a general class of recurrence equations" IEEE Trans. Comput., vol. C-22, pp. 786-793, Aug 1973.

13. Sklavos N and Koufopavlou O, "Asynchronous Low Power VLSI Implementation of the InternationalData Encryption Algorithm" proc. of 8th IEEE International Conference on Electronics,

Circuits 346 and Systems (ICECS'01) (Malta 2-5 September 2001) Vol. III pp 1425-1428

14. A. Curiger et. al., "VINCI: VLSI Implementation of the New SecretkeyBlock Cipher IDEA", Proc. of the Custom Integrated Circuits Conference, San Diego, USA, May 1993

15. Yan Sun, Dongyu Zheng, Minxuan Zhang, and Shaoqing Li "High Performance Low-Power Sparse-Tree Binary Adders" 8th International Conference on Solid state and Integrated Circuit Technology, ICSICT 2006.

16. Haridimos T. Vergos, Costas Efstathiou, Dimitris Nikolos: "Diminished- One Modulo 2n+1 Adder Design" IEEE Trans. Computers 51(12): 1389-1399 (2002)

17. A. Morgenshtein, A. Fish, I. A. Wagner. Gate Diffusion Input (GDI) – A Novel Power Efficient Method for Digital Circuits: A Design Methodology. 14th ASIC/SOC Conference, Washington D.C., USA, September 2001.

18. P. Kogge and H.S. Stone, "A Parallel Algorithm for the Efficient Solution of a General Class of Recurrence Equations," IEEE Trans. Computers, vol. 22, no. 8, pp. 786-793, Aug. 1973.

19. H.T. Vergos, C. Efstathiou, and D. Nikolos, "Diminished-One Modulo 2n+1 Adder Design," IEEE Trans. Computers, vol. 51, no. 12, pp. 1389-1399, Dec. 2002.

IMPLEMENTATION OF COMBINATIONAL CIRCUITS USING TERNARY   MULTIPLEXER

Sweta Giri
Dept of ece
Srm univesity

Mrs.N.Saraswathi
Assistant Prof. (S.G)
Dept Of ece
Srm Univesity

Abstract
This is the paper presenting a novel method for defining, analyzing and implementing the basic combinational circuitry with less number of ternary multiplexers. Multilplexer is used as basic building block to realize all the combinational and sequential circuitry providing complete, concise, implementation-free description of the ternary function involved. This shows the potential of VHDL modeling and simulation which can be applied to Ternary switching circuits for verifying its functionality and timing specifications. This is the method which is used in analyzing the complex ternary functions and reduction of gate count

Keyword:- Gate count, Multivalued logic, Reability-unreability model ,VHDL, Ternary switching levels.

1.   Introduction
In the Multi-valued logic, a many-valued logic is a propositional calculus in which there are more than two truth values. Traditionally, there was only two possible values (i.e. "true" and "false").An obvious extension to classical two values logic is an n-valued logic for n greater than 2. The most popular in the literature are the three valued logic, the finite value with the more than three values and the infinite (e.g. Fuzzy logic) logics. The paper emphasis on the three valued logic which has three values (true ,false and intermediate) mathematically. Nowadays, VLSI us the technology which is used for the realization of MVL circuits in order to bring their full potential into many of the operational circuits. Three valued logic has many more advantages over the binary logic. It is possible for the ternary logic to reduce the computation steps, complexity of interconnect, chip area and chip delay. In this logic, higher information carried by the each line offers better utilization of the transmission channels. Serial and serial-parallel operations can be carried out faster and also gives efficient error detection and correction codes when the ternary logic is applied. Section 2 covers the preliminaries to ternary logic to recognize and to bring out its importance. In Section 3, ternary switching algebra with the basic operation of T-gates and its conceptual laws and theorems are presented. Design of combinational and sequential circuits with minimum number of multiplexers are presented in section 4. Section 5 gives the conclusion with future work.

2. Preliminaries Of Ternary Logic
The ternary logic (also called three-valued or trivalent logic and abbreviated 3VL) is a promising alternative to the conventional binary logic design technique. It is possible for ternary logic to achieve simplicity and energy efficiency in digital design since the logic reduces the complexity of interconnects and chip area, in turn reducing the chip delay. It offers better utilization of transmission channels because of the higher
information content carried by each line, also gives more efficient error detection and correction codes and possess potentially higher density of information storage. In principle, MVL can provide a means of increasing data processing capability per unit chip area. Furthermore, serial and serial-parallel arithmetic operations can be carried out faster if the ternary logic is employed. One of the main advantages of ternary logic is that it reduces the number of required computation steps. Since each signal can have three distinct values, the number of digits required in a ternary family is $\log_3 2$ times less than that required in binary logic. It is assumed that ternary-logic elements can operate at a speed approaching that of the corresponding binary-logic elements. However, if the ternary and binary logic gates are used to take advantage of their respective merits, performance could be significantly improved because ternary logic gates are good candidate for decoding block since it requires less number of gates while binary logic gates are a good candidate for fast computation modules. Thus, ternary design technique combined with the conventional binary logic gate design technique also provides an excellent speed and power consumption characteristics in data path circuit such as full adder and multiplier.
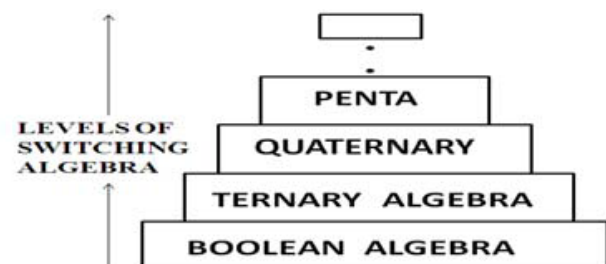

Fig1: Levels of switching algebra

3. Ternary Switching Algebra
Ternary has the logic levels '0' corresponding to logic-0 in binary (also called zero element or low voltage), '1' corresponding to an intermediate stage (also called Meta stable state) and '2' corresponds to logic-1 in binary (also called universal element or high voltage). The intermediate state can be metaphorically thought of as either true or false. The binary logic is limited to only

two states '1' and '0', where as MVL is a set of finite or infinite number of values. In a standard CMOS process, the three supply voltages are vdd, vdd/2 and ground. Ternary logic gates are the basic building blocks in realizing combinational and sequential logic functions. The implementation is based around (bipolar transistors, MOSFETs etc.) a basic switching elements, which is referred to as T-Gates . The Ternary gate called T-gate qualifies as a universal element in several different senses. Firstly, it should be logically complete with simple operation. Secondly, it should be easily implemented with its straightforward construction. Thirdly, it should possess two essential elements that must be embodied in any logic gate, namely, logic-value thresholding and logic-signal connection of switching . This functional completeness of T-gate is the property of a set of compositions which enables one to synthesize any arbitrary switching function within a particular class. There are several algebras available for the design of ternary switching functions among which, the Post and the Modular algebra have the advantages of similarity with ordinary algebra.
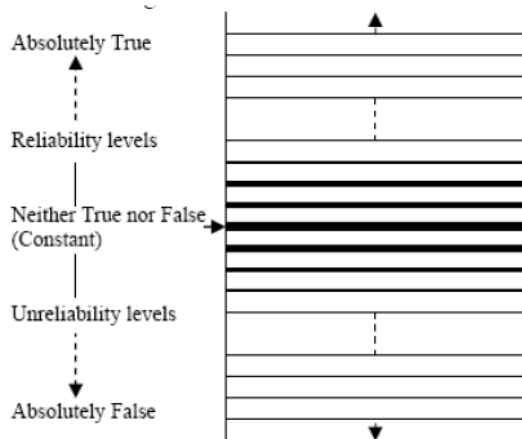

Fig 2: Truth table decision based on Reability-Unreability model

4.Design And Verification Of Ternary Circuits

This is the paper in which 3:1 MUX is taken as a basic building block to explore the realization of circuits with minimum number of ternary 3:1 MUX . Ternary K map method is the concept for the implementation of the ternary function minimization.

A.DESIGN OF THE BASIC GATES

For designing the ternary multiplexers, we start with the basic gates and design of decoder which are building blocks for any circuitry. The basic building gates are Ternary Inverter, Ternary OR (TOR), Ternary AND (TAND) and Ternary XOR (TXOR) which is symbolized and represented as given in Fig and Equations respectively .

$$STI = \overline{X^1} = 2 - X$$
$$PTI, NTI = \overline{X^i} = \begin{cases} i \ if \ X \neq i \\ 2 - i \ if \ x \neq i \end{cases}$$

A general ternary inverter (GTI) is a basic unary operator with one input *x* and three outputs. Therefore, the implementation of ternary inverter requires three inverters namely negative ternary inverter (NTI), standard or simple ternary inverter (STI) and positive ternary inverter (PTI) forming an operator set that is complete in logic sense. This basic ternary inverter is used for constructing ternary AND/NAND, ternary OR/NOR etc. The VHDL Modeling is used for unary functions as well as shown the simulation results.
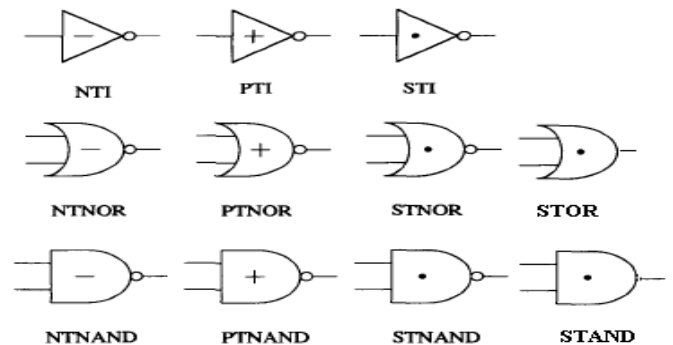

Fig3: Symbol for the basic gates

Table 4.1. Function Table For Ternary Inverter

X	$\overline{X^0}(NTI)$	$\overline{X^2}$(PTI)	$\overline{X^1}(STI)$
0	2	2	2
1	0	2	1
2	0	0	0

It can be proved that the complement or negation of literals (Xi) give the following observed which are helpful in reduction of ternary gates during implementation. The negation is defined and represented as shown

$$X^2 = \overrightarrow{\overline{X^{01}}} \& X^{01} = \overrightarrow{X^2}$$
$$X^1 = \overrightarrow{\overline{X^{02}}} \& X^{02} = \overrightarrow{X^1}$$
$$X^0 = \overrightarrow{\overline{X^{12}}} \& X^{12} = \overrightarrow{X^0}$$
$$\vec{0} = 2 \& \vec{2} = 0$$

This observed result is used to show the reduction in gate count and also in simplification of ternary function. The operation of addition (+) and multiplication (.) on L, which can be called Ternary OR (TOR) and Ternary AND (TAND) respectively, represent two multiple input operators. It is represented by following equations and tabulated as shown in Table 3 and Fig.5 and 6. Logic Sum or TOR:

X1+X2+…+Xn=MAX(X1,X2,…,Xn)

Logic Product or TAND:

X1 . X2 ….. Xn =MIN(X1,X2,…,Xn)

Similarly, TNAND is

$$\overline{X1.X2.X3\ldots.Xn} = \min\overline{X1.X2.X3\ldots\ldots.Xn}$$

TNOR is

$$\overline{X1 + X2 + X3\ldots.+Xn} = \min\overline{X1 + X2 + X3\ldots\ldots.+Xn}$$

Clearly (L, +,.) is a distributive lattice with zero element(0) and universal element(2). Thus the following laws hold for any x, y, z ∈L:

Idempotent: X+X=X   X . X=X

Commutative: X+Y=Y+X   X. Y=Y. X

Associative: (X+Y)+Z=X+(Y+Z)
                  X . (Y . Z)= (X . Y) . Z

Absorption: X+ X . Y =X   X . (X+Y) = X

Distributive: X+Y . Z= (X+Y) . (X+Z)
                  X. (Y+Z)=X. Y+X.Z

It is evident that laws of identity elements, holds here.

X + 0 = X
X • 0 = 0
X + 2 = 2
 X ≠ 0)
X+1 = 1(for cases X ≠ 2) & 2(for x=2) X • 2 = X
X • 1= 1(for cases DeMorgan's Theorem holds for ternary logic when the three types of inverters are used.)

$$\overline{(X+Y)^0} = \overline{X^0}.\overline{Y^0}$$
$$\overline{(X.Y)^0} = \overline{X^0} + \overline{Y^0}$$
$$\overline{(X+Y)^1} = \overline{X^1}.\overline{Y^1}$$
$$\overline{(X+Y)^1} = \overline{X^1} + \overline{Y^1}$$
$$\overline{(X+Y)^2} = \overline{X^2}.\overline{Y^2}$$
$$\overline{(X.Y)^2} = \overline{X^2} + \overline{Y^2}$$
$$\overline{\overline{X}1^1} = X$$

Ternary Ex-OR function is mod-3 addition of ternary numbers. Modulo 3 sum is the sum of two integers ignoring the carry digits in the addition. Modulo-3 addition is an important function, since so many redundant code techniques use half-adding functions . It is denoted and expressed as given in Fig.7 and Table 4.

$$X + Y = MODSUM (X ,Y) = (X + Y)\bmod 3$$

Ternary functions of one or more variables may be represented in truth table or K-map form or algebraically in canonical form as a product of sum or sum of product. According to Expansion theorem [21], any ternary function f(Xl,X2,...,Xn) may be generated from (Xl,

X2,...,Xn) by means of (+), (.) and the unary functions X^0, X^1, X^2 as given below:

$$f(Xl,X2, ..., Xn) = 2 \bullet F2(Xl,X2 \ldots Xn) + 1 \bullet F1(Xi,X2,\ldots,xn) + 0 \bullet F0(Xl,X2 \ldots Xn)$$

i.e., $f = 2 \bullet F2 + 1 \bullet F1 + 0 \bullet F0$

where F_K equals 2, when value of the function f equals k, otherwise, it is 0. Applying equations to the above equation, the function may be represented by $f = F2+1 \bullet F1$ for canonical Sum of Product form and $f= F2 \bullet (1+ F1)$ for canonical Product of Sum form

B. Design Of 3:1 Ternary Multiplexer

A ternary multiplexer is a combinational circuit that selects one of the 3n input lines based, on a set of n selection lines and directs it to a single output line. The design of 3x1 multiplexer (MUX) is as presented in Fig.11 and operates as given in Table 5. In this paper, 3x1 MUX is taken as a basic building block to explore the realization of 9x1 MUX, 27x1 MUX, Half Adder, Half Subtractor, Full Adder, Full Subtractor, Multiplier, 1-bit Comparator, 1-bit and 2-bit Position shifter ,Ripple carry Adder and position shifter.
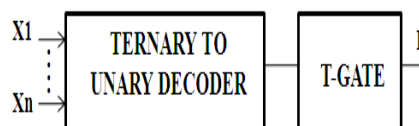

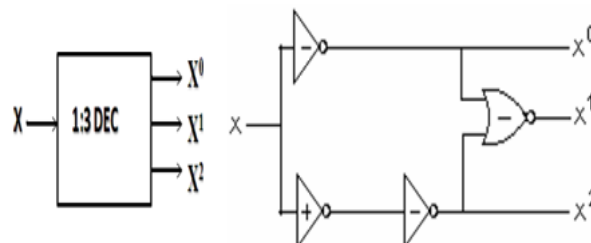
Fig 4: Implementation of the Ternary function
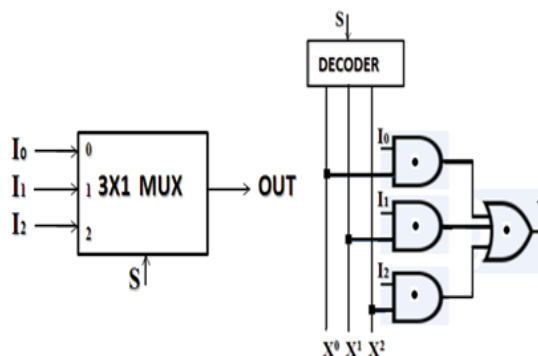

Fig 5: Block Diagram of 1:3 Decoder

Fig 6: Block Diagram of 3:1 Multiplexer

C. Design Of 9:1 Mux Using 3:1 Mux

A 9x1 MUX is built using four 3x1 MUX as shown in Fig.11(a). A 9x1 MUX has 2 select lines to give an output among 9 inputs as given in Table VI and Fig.11(a) shows the simulation result for structural coding.
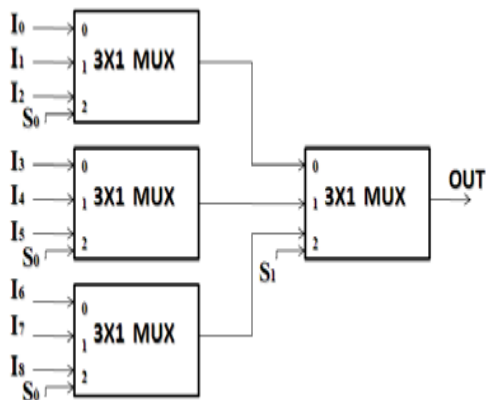
Fig 7: Block Diagram of 9:1 Multiplexer

Table 4.2 of 9:1 mux

S1	S0	OUT
0	0	I0
0	1	I1
0	2	I2
1	0	I3
1	1	I4
1	2	I5
2	0	I6
2	1	I7
2	2	I8

D.Design Of Half Adder And Half Subtractor Using 3:1 Mux

Ternary half adders (HA) is a circuit that adds two bits and generates a sum and carry using Modulo-3 addition. There are two inputs and two outputs and, consequently, two decoders are required. The half adder functions as shown in Table 7 can be realized as given in Fig.13(a-c) using 3x1 MUX.
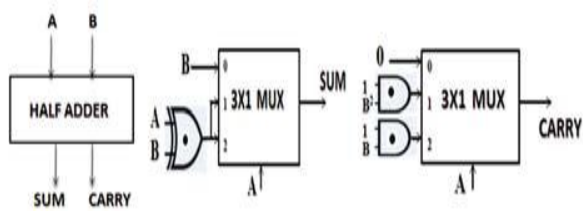

Fig 8: Block Diagram of Half Adder
Table 4.3: for half adder

A	B	SUM	CARRY
0	0	0	0
0	1	1	0
0	2	2	0
1	0	1	0
1	1	2	0
1	2	0	1
2	0	2	0
2	1	0	1
2	2	1	1

Ternary half subtractor (HS) is a circuit that will subtract one from the other number (i.e., A-B) and generate a difference and borrow using ternary logic. The half subtractor function is as shown in Table 8 and can be realized as given in Fig.14(a-c) using 3x1 mux.
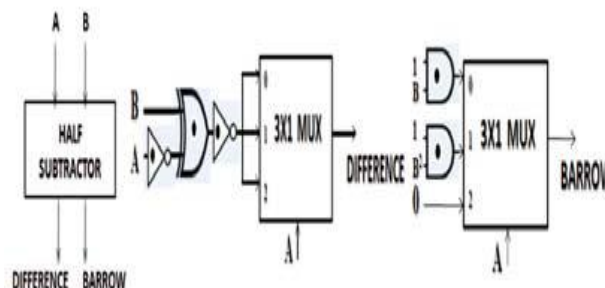

Fig 9: Block Diagram of Half Subtractor

Table 4.4: for half subtractor

A	B	DIFF	BORROW
0	0	0	0
0	1	2	1
0	2	1	1
1	0	1	0
1	1	0	0
1	2	2	1
2	0	2	0
2	1	1	0
2	2	0	0

E.   DESIGN OF FULL ADDER AND FULL SUBTRACTOR USING 3:1 MUX

A full adder (FA) is a circuit that will add three bits and generates a sum and a carry. Fig. shows the design of full adder realization with 3x1mux .

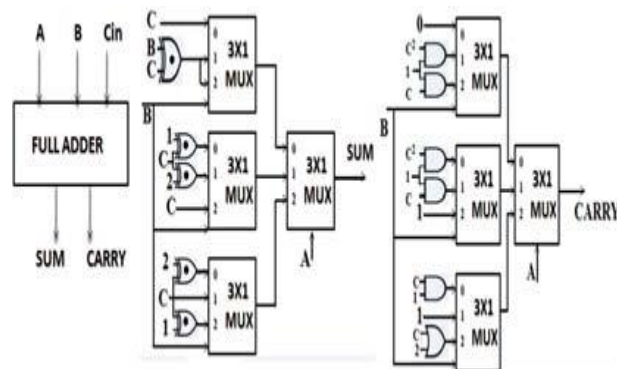

Fig 10: Block Diagram of Full Adder

Full subtractor (FS) is a circuit that will subtract three bits (i.e., (A-(B-Bin)), and generates a difference and a borrow. Fig. shows the design of full subtractor realization with 3x1mux .
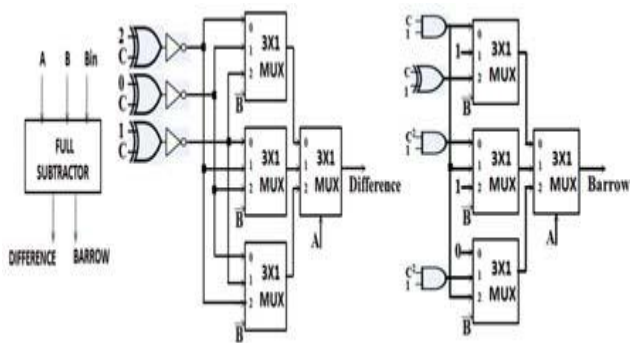
Fig 11: BLOCK Diagram of Full Subtractor

F. DESIGN OF 27:1 MUX USING 3:1 MUX

3x1 MUX is taken as a basic building block to explore the realization of 27x1 MUX in which we have the three selection lines.

G. DESIGN OF 1 BIT MULTIPLIER

A multiplier multiplies two bits and generates the product. Truth table for multiplier is shown in Table 11 and Fig.17(a-b). The gate count of multiplier is

$fp+fc=7+2=9.$
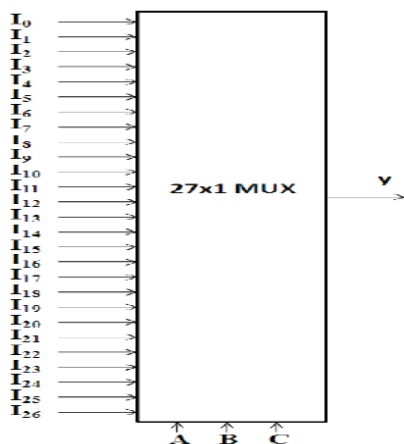$fp = A^2B^1 +A^1B^2 +1.(A^1B^1+A^2B^2)$
$fc = 1.(A^2B^2)$
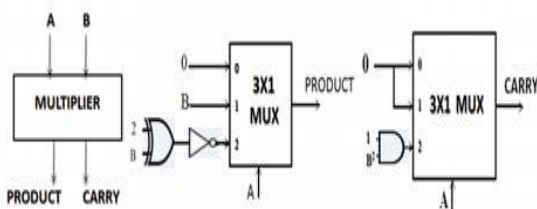

Fig 12: Block Diagram of 27:1 Mux

Fig 13: Block Diagram of 1 Bit Multiplier

H. Design Of 1 Bit Comparator

A magnitude comparator is a combinational circuit that compares two bits A & B and determines their relative magnitudes. The comparison of two bits is an operation that determines if one number is greater than, less than or equal to other number as Fig.19(a-b) and Table 12 shows the design of 1-bit comparator which gives

$Y=f(A>B)$ when en=0, $Y=f(A=B)$ when en=1and

$Y=f(A<B)$ when en=2

$f(A>B) = A^1B^0 +A^2B^0 +A^{2B^-}B^1 = A^O B^0+A^2B^1$

$f(A=B) = A^0B^0+A^1B^1 +A^2B^2$

$f(A<B) = A^0B^1+A^0B^2+A^1B^2 = A^0B^0+ A^1B^2$
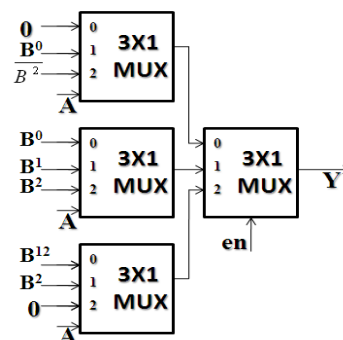
Fig 14: Block Diagram of 1 Bit Comparator

Fig4:5: for 1 Bit comparator

A	B	A>B	A=B	A<B
0	0	0	1	0
0	1	0	0	1
0	Z	0	0	1
1	0	1	0	0
1	1	0	1	0
1	Z	0	0	1
Z	0	1	0	0
Z	1	1	0	0
Z	Z	0	1	0

I.Design Of 1 & 2 Bit Position Shifter

The shifter circuit is as designed in Fig.21 and Table 15 which shifts the bits of an n input vector by 1–bit position to the right. It fills the vacant position on the left side with zero. If S=0, the input is loaded as output which is said to work in parallel mode, if S=1, the input is shifted by one bit position and if S =2, the input is shifted by two-bit positions padded by zeros in the left position. The more versatile shifter circuit will be able to shift by more bit positions at a time. If the bits that are shifted out are placed into the vacated positions on the left, then the circuit effectively rotates the bits of the input vector by a specified number of bit positions
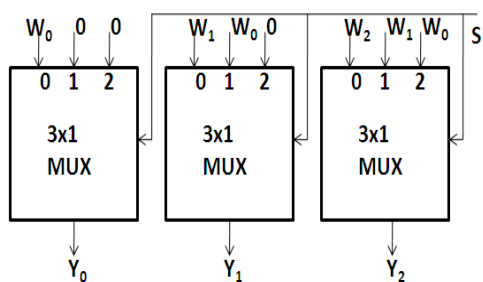
Fig 15: Block Diagram of 1 & 2 Bit Position Shifter

J.Design Of Ripple Carry Adder

Two binary words, each of n bits, can be added using ripple carry adder as shown in Fig.21 (a). The carry input is connected to the least significant bit and the carry output of each full adder is connected to carry input of the next most significant FA. It is a typical example of iterative circuit which is slow, since in the worst case a carry must propagate from least significant FA to the most significant one.

K.Design Of Carry Save Adder Using 3:1 Mux

Carry save adder computes the sum of 3 or more n-bit numbers which gives the sequence of partial sum and carry bits.

Fig 16: Block Diagram of Ripple carry Adder

Fig 17: Block Diagram of Carry save Adder

5.Simulation Results:

5.1 3:1 multiplexer:

5.2 9:1 multiplexer:

5.3 full adder:

5.4 full subtractor:

5.6 1-bit multiplier:
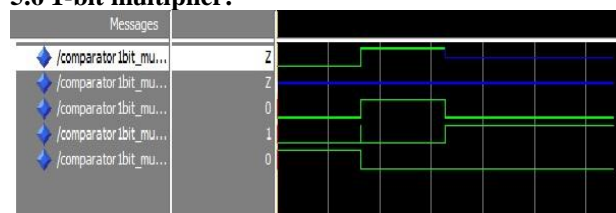
5.7 position shifter

5.8 1-bit comparator:

5.9 carry save adder:

6. Conclusion

The ternary logic is a promising alternative to the conventional binary logic design technique. The ternary and binary logic gates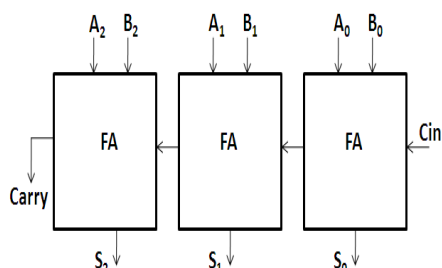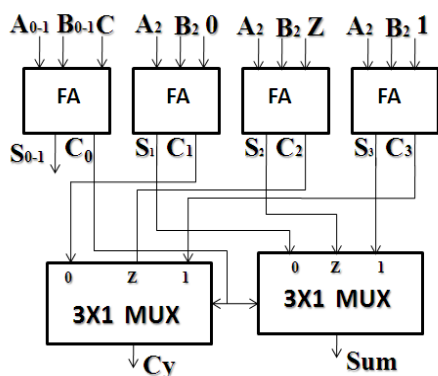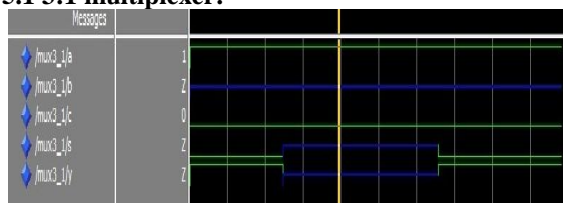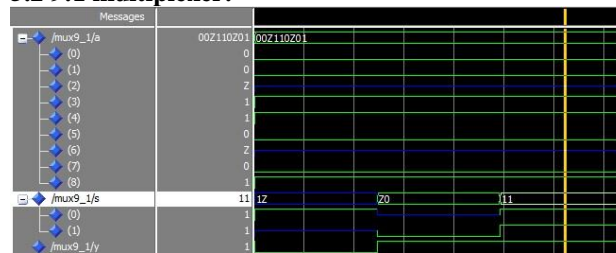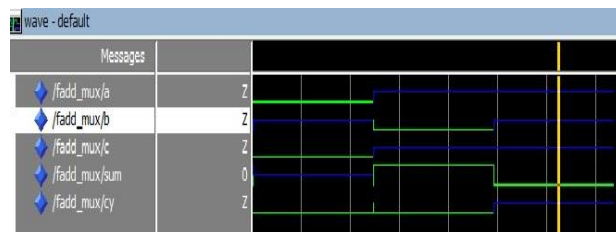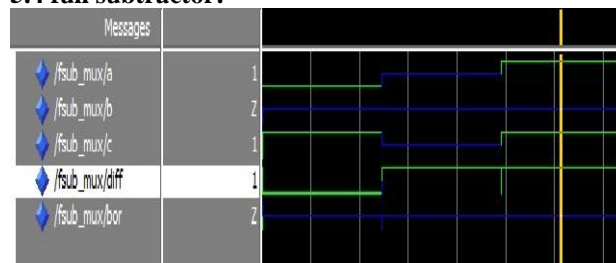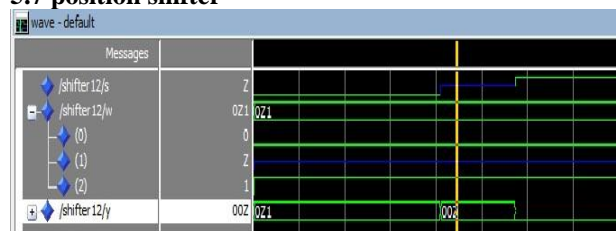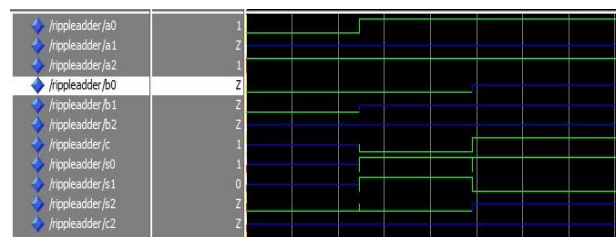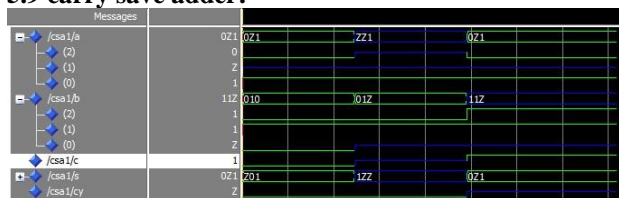 can be used to take advantage of their respective merits, to improve performance in terms of computation speed and power consumption. Expanding the existing logic levels to higher levels higher processing rates could be achieved. In this paper, we have implemented a technique to reduce the gate count. The main advantages of the ternary logic is that it reduces the power 50% as compare to the ternary logic and also reduces the computation steps, chip area and chip delay. Thus, ternary logic gate design technique combined with the conventional binary logic gate design technique also provides an excellent speed and power consumption characteristics in data path circuit such as full adder and multiplier. VHDL simulator has been used to simulate MVL Systems which provide enough information to verify functionality and timing specifications.

References

[1] http://www.embedded.com/columns/netcentricview/13100886?_requestid=133447

[2] http://en.wikipedia.org/wiki/Ternary_logic

[3] K. C. Smith. (1981): The Prospects for Multivalued Logic: A Technology and Applications View, *IEEE Transactions on Computers*, Vol. C-30, Issue.9, pp.619-634.

[4] Sheng Lin et al. (2009): CNTFET-Based Design of Ternary Logic Gates and Arithmetic Circuits, *IEEE Trans. On Nanotechnology*, Vol. PP, Issue.99, pp.1-1.

[5] S.L.Hurst. (1984): Multivalued logic - Its status and its future, *IEEE Trans .on Computers,* vol. C-33, pp. 1160-1179.

[6] Raymond E.Miller. (1966): Switching Theory, Vol. I, John Wiley & Sons, pp.8-9.

[7] D. Venkat Reddy et. al (2008): Sequential Circuits In The Framework Of (2n+1)-ary Discrete Logic, *IJCSNS International Journal of Computer Science and Network Security*, Vol.8 No.7, July, pp.175-181.

[8] Marek Perkowski (2006): Introduction to multivalued logic.Available as: http://web.cecs.pdx.edu/~mperkows/temp/JULY/2006.Introduction-to-MV-logic.ppt

[9] A.P. Dhande et. al. (2005): Design And Implementation Of 2 Bit Ternary ALU Slice, 3rd International Conference, Sciences of Electronic (SETIT), *IEEE Transc.*, pp.1-11.

[10] K.C. Smith. (1988): Multiple-Valued Logic, A Tutorial and Appreciation, Survey & Tutorial Series, *IEEE Transc*. *In computers*,Vol.21, Issue.4, pp.17-27.

[11] H.T. Mouftah. (1975): Three-valued logic and its implementation with COS/MOS integrated circuits, D.Sc. thesis, Laval University, Quebec, Canada.

[12] H.T. Mouftah. (1975): A Study On The Implementation Of Three-valued Logic, University of Toronto, Toronto, Ontario, Canada, pp.123-126., Monograph .

[13] D. I. Porat, "Three-valued digital systems", *PROC. IEE Inst. Elect Eng,* Vol. 116, No. 6, JUNE 1969, pp.947-954.

[14] R. P. Hallworth and F. G. Heath, "Semiconductor Circuits For Ternary Logic", The Institution of Electrical Engineers, Monograph No. 482 E, *IEEE trans.*,VOL. 109, PART C.,Nov. 1961, pp.219-225.

[15] Richard F.Tinder, "Engineering Digital Design", Second Edition, Academic Presss,2000.

[16] Neil H.E.Weste,David Harris, Ayan Banerjee, "CMOS VLSI Design",A circuit and systems perspective, third Edition, pearon Education,2007.

[17] John F.Wakerly, "Digital Design, principles & practices, third edition, prentice Hall of India Private Limited (EEE),2005.

[18] Nazeih M.Botros, "HDL Programming VHDL and verilog",dreamtech press, 2006.

[19] Stephen Brown and Zvonko Vranesic, "Fundamentals of Digital Logic with Verilog Design", second edition, Tata McGraw-Hill Publishing Company Limited, New Delhi,2008.

HYBRID PARTICLE SWARM OPTIMIZATION BASED REACTIVE POWER OPTIMIZATION

[1]Vivek Kumar Jain, [2]Himmant Singh

[1, 2] Department of Electrical Engineering, Madhav Institute of Technology and Science, Gwalior (M.P.), India

Abstract— in this paper, a solution to reactive power optimization problem with a Hybrid particle swarm optimization (PSO) approach. The algorithm changed the stochastic initialization and adopted a principle of particle searching by itself. Several particles in feasible solutions were used to lead swarms motion and update the performance of the proposed hybrid approach is demonstrated with the IEEE-30and IEEE-57 bus systems and also the performance of this hybrid PSO is compared with that of particle swarm optimization, genetic algorithm and evolutionary programming. The performance of the proposed method is compared with the previous approaches reported in the iterative. The performance of hybrid PSO seems to be better in terms of solution quality and computational times.

Keywords— reactive power optimization, particle swarm optimization, evolutionary programming, and hybrid approach and loss minimization.

I. INTRODUCTION

The problem of reactive power optimization is directly concerned not only with service quality and reliability of supply, but also with economy and security of the power systems. Therefore, the power system reactive power optimization problem result directly influences the power system stability and power quality. [2] The reactive power can be controlled in order to improve the voltage profile and minimize the system loss. Generally, some load bus voltage might violate their upper or lower limits during system operation due to disturbances and/or system configuration changes. The power system operator can alleviate this situation and voltages can be maintained within their permissible limits by reallocating reactive power generation in the system. This means by adjusting generator voltages, transformer taps and switch-able VAR sources (capacitors/reactors). [1] Generally, HPSO has a more global searching ability at the start of the run and a local search near the end of the run. Therefore, while solving problems with more limited optima, there are more possibilities for the PSO to discover local optima at the end of run. However, the reactive power optimization problem does have these properties itself. For these reasons, a reliable global approach to power system optimization problems would be of considerable value to power engineering society. Moreover, they did not consider the cost aspect of the problem. Only the sensitivity to voltage has been used for solving the difficulty [3].The purpose of reactive power optimization is to minimize the system loss or other optimum performance indices, subjecting to security and operation constraints. There are many solutions for it, such as linear programming, nonlinear programming, secondary programming, sensitive analysis, and mixed integer planning [10-7]. These methods are generally based on some presumptions and have some defects. With the development of artificial intelligent optimization technologies, the stochastic methods of global searching and optimization have attracted many interests, and have been applied in power system reactive power optimization. In [5], methods based on PSO, GA, Tabu search and fuzzy control, expert system, and neural network, are proposed with demonstration of good results. This paper proposes a hybrid approach to the reactive power optimization (RPO) problem. Particle Swarm Optimization (PSO) is one of the evolutionary computation (EC) technique based on swarm intelligence. It is sensitive to the tuning of its parameters and has a flexible mechanism to explore a global optimum point within a short calculation time [8]. By employing the PSO initially the solution quality improves rapidly; later on obtaining the further improvement is very difficult and most of the computation time is spend over obtaining small improvements. The hybrid Particle swarm optimization (PSO) [4-6] methods both under the category of Evolutionary Algorithms have been implemented independently as optimization techniques in the present paper, the authors propose a very new come near for the solution of the reactive power optimization (RPO) problem based on hybrid Particle swarm optimization (PSO) on an IEEE 30-bus power system and a practical 57- bus power system. Simulation results show that the proposed hybrid approach converges to better solutions much faster than the previous reported approaches.

II. PROBLEM FORMULATION

The reason of the RPO is to reduce the system real power Losses. The general RPO with standard power system circumstance can be formulated [12] as follows: The objective function is represented as:

$$P_L = \sum_{i=1}^{nl} loss\ k \tag{1}$$

Where,

$P_L = network\ real\ power\ loss$

nl = number of line

The reactive power optimization (RPO) problem is subjected to the following constraints
*(*A)The Power constraint equations:

The power loss is a non-linear function of bus voltages, which are functions of control variables. The minimization predicament is subject to operating constraints [12], which are limits on various control variables (the inequality constraints) and power flow constraints (the equality constraints).

Equality constraints:

$$P_i - V_i \sum_{i=1}^{N_B} V_j \left(G_{ij} \cos \theta_{ij} - B_{ij} \sin \theta_{ij} \right) = 0, \quad i \, \varepsilon \, N_{B-1} \tag{2}$$

$$Q_i - V_i \sum_{i=1}^{N_B} V_J \left(G_{ij} \sin \theta_{ij} - B_{ij} \cos \theta_{ij} \right) = 0 \quad i \, \varepsilon \, N_{PQ} \tag{3}$$

Where,

V_i = Voltage magnitude at bus I

V_j = Voltage magnitude at bus j

P_i, Q_i = Real and reactive powers injected into network at bus i

G_{ij}, B_{ij} = Mutual conductance and susceptance between bus i and bus j

Q_{gi} = Reactive power generation at bus i

$N_B - 1$ = Total number of buses excluding slack bus

N_{PQ} = Number of PQ buses

θ_{ij} = Voltage angle difference between bus i and bus j

Inequality Constraints:

In the control variables, the generator bus voltages (AVR operating values) are taken as continuous variable; the transformer tap settings are taken as discrete variable and shunt susceptance values are taken as binary variable. The load bus voltages and reactive power generation Q_g are taken as state variables.

Continuous control variable:

$$V_i^{min} \leq V_i \leq V_i^{max} \quad ; \quad i \varepsilon N_B \tag{4}$$

Discrete Control variable:

$$t_k^{min} \leq t_k \leq t_k^{max} \quad ; \quad i \varepsilon N_T \tag{5}$$

State Variables:

$$Q_{ci}^{min} \leq Q_{ci} \leq Q_{ci}^{max} \; ; \; i \, \varepsilon \, N_c \tag{6}$$

$$Q_{gi}^{min} \leq Q_{gi} \leq Q_{gi}^{max} \quad ; \quad i \, \varepsilon \, N_g$$

$$|s_1| \leq |s_1^{max}| \tag{7}$$

$$S_l \leq S_l^{max} \quad ; \quad l \varepsilon N_l \tag{8}$$

Where,

t_k = Tap setting of transformer at branch k

Q_{Ci} = Reactive power generated by i^{th} capacitor bank

Q_{gi} = Reactive power generation at bus i

S_l = Apparent power flow through the ith branch

N_B = Total number of buses

N_T = Number of tap-setting transformer branches

N_c = Number of capacitor banks

N_g = Number of generator buses

State variable are restricted by adding them as a quadratic consequence terms to the objective function. Therefore the equation (1) is changed to the following form:

$$Min. F_T = f + K_v \sum_{i=1}^{Npq} \left(V_i - V_i^{lim}\right)^2 + K_q \sum_{i=1}^{Ng}\left(Q_{gi} - Q_{gi}^{lim}\right)^2 + K_f \sum_{i=1}^{Nb}\left(S_l - S_l^{lim}\right)^2 \tag{9}$$

Where K_v, K_q and K_f are the penalty factors for the bus voltage limit violations, generator reactive power limit violations and line flow violations respectively.

$$X_i^{lim} = X_i^{max} \; if \; X_i > X_i^{max}$$

$$X_i^{lim} = X_i^{min} \; if \; X_i < X_i^{min}$$

$$F = \frac{K}{F_T} \tag{10}$$

Where k is a large constant this is used to amplify $1/F_T$ the value of which is usually small, so that the fitness value of the chromosome will span a wider range. The objective function of the target power system is calculated using load flow calculation with the above mentioned equality and inequality constraint.

III. PARTICLE SWARM OPTIMIZATION APPROACH

PSO algorithm, originally introduced by Kennedy and Eberhart (1995). Similar to evolutionary algorithm, the PSO technique conducts searches using a population of particles, corresponding to individuals. Each particle represents a candidate solution to the reactive power optimization (RPO) problem. In a HPSO system, particles change their positions by flying around in a multidimensional search space until a relatively unchanged position has been encountered, or until computational boundaries are exceeded. In social science context, a PSO system combines a social –only model and a cognition-only model. The social-only component suggests that individuals ignore their own experience and adjust their behavior according to the successful beliefs of the individual in the neighborhood. On the other hand, the cognition-only component treats individuals as isolated beings. A particle changes its position using these models. [1-3] The PSO system simulates the knowledge evolvement of a Social organism, in which *N* individuals, a potential Solution to a problem is represented as a particle flying in D-dimensional search space, with the position vector $X_i = (X_{i1}, X_{i2}, X_{i3}, \ldots \ldots X_{iD})$ and velocity $V_i = (V_{i1}, V_{i2}, V_{i3}, \ldots \ldots V_{iD})$ Each particle records its best previous position (the position giving the best fitness value) as $P_{besti} = P_{besti_1}, P_{besti_2}, \ldots P_{best_{id}}$ called personal best position. The global version of the PSO keeps track of the overall best value (g^{best}), and its location, obtained thus far by any particle in the population. At each iteration, each particle competes with the others in the neighborhood or in the whole population for the best particle (with best fitness value among neighborhood or the population) with best position $g_{besti} = g_{best\,i_1}, g_{besti_2} \ldots \ldots g_{best_{id}}$ called global best position. Then utilize those reminiscences to regulate their own velocity and position of each particle can be calculated as shown in the following formulas:

$$V_{id} = w_i v_{id}^k + C_1 rand_1 + C_2 rand_2 \left(g_{bestid} - X_{id}^k\right) \tag{11}$$

$$X_{id} = X_{id} + V_{id} \tag{12}$$

where i is the number of iteration; C1and C2are the cognitive and social components that are the acceleration constants responsible for varying the particle velocity towards P_{best} and g_{best}, respectively; rand and Rand are two random numbers within (0, 1); and the parameter W is the inertia weight introduced to accelerate the convergent speed of the PSO [4].The particle swarm optimization algorithm is simple in concept easy to implement and computational efficient.

The weighting function is usually utilized in the above equation (11):

$$w_i = w_{max} - \frac{w_{max} - w_{min}}{iter_{max}} \times iter \tag{13}$$

Where,

w_{max} =initial weight

w_{min} = final weight

I_{ter} = current iteration

$Iter_{max}$ = maximum iteration

Using the above equation (13), a certain velocity which gradually gets close to p_{best} *and* g_{best} can be calculated. The current position can be modified by equation (12). The right hand side of Equation (11) consists of three terms. The first term is the previous velocity of the agent. The second term and third terms are utilized to change the velocity of agent. Without second third terms, the agent will keep on flying in the same direction until it hits the boundary. It's to explore new areas and, therefore, first term corresponds to diversification in the search procedure. On other hand, without the first term, velocity of the flying agent is only determined by using its current position and best position in history. It keeps track of its coordinates in hyperspace which are associated with its previous best fitness solution, and also of its counterpart corresponding to the overall best value acquired thus far by any other particle in the population. Vectors are taken as presentation of particles since most optimization problems are convenient for such variable presentations. In fact, the fundamental principles of swarm intelligence are adaptability, diverse response, proximity, quality, and stability. It is adaptive corresponding to the change of the best group value [6, 13]. The allocation of responses between the individual and group values ensures a diversity of response. The agents will try to converge to their p_{best} *and* g_{best} therefore, the terms correspond to intensification in the search procedure.

IV. HPSO ALGORITHM PROCEDURE

Step 1: Initialization of the parameters
Step 2: arbitrarily set the velocity and location of each and every one particles.
Step 3: calculate the robustness of the preliminary particles by conducting Newton-Raphson power flow analysis results. Pbest of e ach particle is set to preliminary position. The preliminary best evaluation value among the particles is set to gbest.
Step 4: revolutionize the velocity and position of the particle according to the equations (11) to (13).
Step 5: Select the best particles come into mutation operation according to (14).
Step 6: If the location of the particle violates the limit of variable, set it to the limit value.
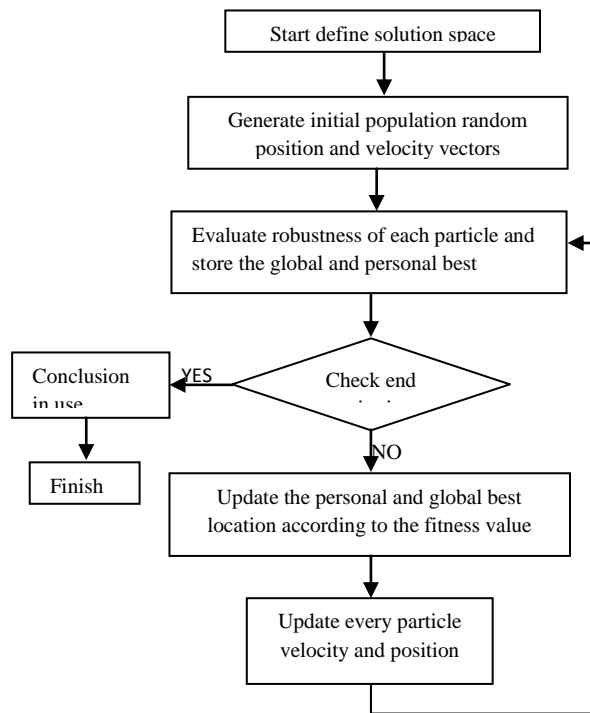
Fig-1 Flow Chart for PSO

Step 7: Compute the fitness of new particles. If the fitness of each character is better than the previous pbest the current value is set to pbest value. If the best pbest is better than gbest, the value is set to be gbest.
Step 8: The algorithm repeats step 4 to step 7 awaiting the meeting criteria is met, usually a satisfactorily good fitness or a greatest quantity of iterations.

The advantages of PSO more than other established optimization techniques can be summarized as follows:

(1) PSO uses probabilistic evolution system and not deterministic regulations. Hence, PSO is a kind of stochastic optimization algorithm that can search a complicated and unsure area. This makes PSO more bendable and roust than predictable methods.

(2) PSO uses payoff (presentation guide or purpose function) in sequence to guide the search in the difficulty breathing space. Therefore, PSO can without difficulty arrangement with non-differentiable objective functions. Moreover, this property relieves PSO of assumptions and approximations, which are often necessary by fixed optimization models.

(3) Separate Genetic Algorithm (GA) and other heuristic algorithms, PSO has the elasticity to control the balance between the global and local examination of the explore space. This single characteristic of a PSO overcomes the rash meeting difficulty and enhances the explore ability.

(4) PSO is a population-based search algorithm this property ensures PSO to be a lesser amount of subject to receiving gripped on limited minima and different the established methods, the solution excellence of the future advance don't rely on the initial people. Preparatory wherever in the search space, the algorithm ensures the meeting to the most favorable explanation [14, 15].

V. TEST RESULTS AND ANALYSIS

The process described above was implemented using the FORTRAN language and the residential software Program was executed on a 450 MHz Pentium III PC. The Hybrid particle swarm optimization based reactive power optimization problem was implemented using MATLAB code was executed on a PC. The proposed algorithm was run minimization of real power loss as the objective function [3]. The IEEE 30-bus system has 6 generator buses, 24 loads buses and 41 transmission lines of which four branches are (6-9), (6-10) , (4-12) and (28-27) - are through the tap setting transformers. The IEEE 57-bus system has 7 generator buses, 50 load buses and 80 transmission lines of which 17 branches are with tap setting transformers. The real power settings are taken from [1]. The lower voltage magnitude limits at all buses are 0.95 p.u. and the upper limits are 1.1 for all the PV buses, 0.05 p.u. for the PQ buses and the reference bus for IEEE 30-bus and IEEE 57-bus system. To obtain the most favorable values of the control variables, the HPSO based algorithm was run Maximum no. of generations: 50

PSO based parameters

Maximum no. of generations   :   60
Population size   :   30
W_{max} :   0.9
W_{min} :   0.4
C_1 :   2
C_2 :   2

The effectiveness of the PSO algorithm has been demonstrated through solution of reactive power optimization problem in, IEEE 30-bus test system and IEEE 57-bus system.

TABLE 1. Comparison of simulation results of RPO with Other methods for IEEE-30 bus systems

	PSO	GA	EP	**HPSO**
$P_{loss \ (MW)}$	4.52	4.71	4.92	4.472

TABLE 2. Comparison of results of reactive power Optimization for IEEE30 and IEEE-57 bus systems

Compared item	IEEE-30 bus	IEEE-57 bus
best	4.4240	26.5731
worst	4.4769	26.6754
average	4.6497	26.6132

TABLE 3: comparison of best and worst results in IEEE30, 57 and IEEE 118- bus systems

Loss(MW)	**IEEE-30 bus**	**IEEE-57 bus**	**IEEE-118 bus**
best	4.32	26.5760	135.51
worst	4.46	26.6390	137.17
average	4.37	26.6128	136.42

VI. CONCLUSIONS

The performance of the expectations method recognized through its estimation on the IEEE 30-bus and IEEE 57- bus power system shows that HPSO is able to undertake global search with a fast convergence rate and a characteristic of robust computation. From the reproduction learning, it has been found that HPSO converges to the global optimum. The optimization strategy is all-purpose and can be used to other power system optimization problems as well. Table(2,3)gives the best and the worst solutions obtained using particle swarm optimization(PSO) and genetic algorithm(GA) .reproduction consequences shows that the particle swarm optimization(PSO) and genetic algorithm(GA) based reactive power optimization (RPO)algorithm is able to improve profile along with minimization in power scheme. This new strategy can adequately utilize the historical in sequence in PSO algorithm. In addition, to intensify the refined search ability in restricted region, local search procedure is employed and hybridized with PSO algorithm. Based on the above constraints management procedure and restricted explore method, the HPSO algorithm model is proposed for reactive power optimization (RPO) difficulty. The computational results verify its good presentation in terms of solution excellence, computational cost as well as the meeting stability.

Acknowledgement

References

[1] Haibo Zhang, Lizi Zhang, Fanling Meng, "Reactive Power Optimization Based on Genetic Algorithm", Proceedings of International Conference on Power System Technology, POWERCON '98. 1998, Vol. 2, pp. 1448 –1453

[2] W.N.W Abdullah, H. Saibon A.AM Zain, "Genetic Algorithm for Optimal Reactive Power Dispatch", Proceedings of International Conference on Energy Management and Power Delivery, 1998. Vol. 1, 3-5 Mar 1998, pp. 160-164.

[3] Luss, R. and Jaakola, T.H.I. 1973 Optimization by direct search and systematic reduction of the size of the search region American Institute of Chemical Engineering Journal, (1973)760-766.

[4] A. I.Selvakumar and K. Thanuskodi,"Anti predatory particle swarm optimization solutionto non convex economic dispatch problems", Electric Power System Research, Vol. 78, No. 1, Jan. 2008, pp. 2 -10.

[5] Venkatesh, B.; Sasadivam, G.; Abdullah Khan [M]. "Towards on-line optimal reactive power scheduling using ANN memory model based method", Power Engineering Society 1999 Winter Meeting, IEEE, Volume 2, 31 Jan-4 Feb 1999 Page(s):844 - 848 vol.2

[6] J. Kennedy and R.C. Eberhart, "Particle swarm optimization", IEEE Int. Conf. Neural Networks, Perth, Australia, 1995

[7] DAS D B, PATVARDHAN C. "Reactive Power Dispatch with a Hybrid Stochastic Search Techniques", Electric Power Energy System, 2002, 24(9): 731-736

[8] Liang, J.J., Qin, A.K Suganthan P.N. and Baskar S.,2004 Particle swarm optimization algorithms with novel learning strategies IEEE International Conference on. Systems, Man and Cybernetics, (2004) 3659-3664

[9] Shonkwiler, R., Mendivil, F. and Deliu, A. "Genetic Algorithms for the I-D Fractal Inverse Problem". Proceedings of the 4th International Conference on Genetic Algorithms and Their Applications, pp: 495-501. University of California, San Diego, 1991

[10] Bjelogrlic M, Calovic M S, Ristanovic P, et al. Application of Newton's optimal power flow in voltage/reactive power control [J]. IEEE Trans on power system, 1990, 5(4): 1447-1454.

[11] B. Bhattacharyya and S.K. Goswami, "SA based genetic algorithm for reactive power optimization", The Journal of CPRI, Vol. 3, No. 1, pp. 59-64, Sept. 2006.

[12] Abdul Rahaman, K.H. Shahidehpour, S.M.1993 A fuzzy based optimal reactive power control IEEE Transactions on power System, 8(1993) 662-670.

[13] H.D. Chiang, J.C. Wang, O. Cockings, and H.D. Shin,"Optimal capacitor placements in distribution systems: part 2: solution algorithms and numerical results", IEEE Trans. Power Delivery, Vol. 5, No. 2, pp. 634-641, April 1990.

[14] Golhdberg, D.G. "Genetic Algorithm in search optimization and machine learning" , Addison Wesley: reading, M.A. 1989.

[15] K.-P. Wang, L. Huang, C.-g. Zhou, and W. Pang, "Particle Swarm Optimization for Traveling Salesman Problem," In Proceedings of the Second International Conference on Machine Learning and Cybernetics. Vol. 5, pp. 1583-1585, 2003.

Renewable Energy Sources- The Ultimate Source of Survival & Management of resources

1. Prof. Chavan Dattatraya K
Professor, Mechanical Engineering Dept., MMCOE, Pune -52
Pune University, Maharashtra, India
PhD scholar, JJT University, Rajasthan
2. Prof. L. S Utpat
Professor, Mechanical Engineering Dept., MMCOE, Pune-52
Pune University, Maharashtra, India
3. Prof. Dr. G. S. Tasgaonkar
Professor, Mechanical Engineering Dept., ZES, DCOE, Narhe, Pune
Pune University, Maharashtra, India
4. Sandeep Shinde, Patil Sameer G.
Graduate Students   MMCOE, Pune

Abstract: Energy is the primary and most universal measure of all kinds of work by human beings and nature. Whatever happens in the world is only the expression of flow of energy in either of its forms. Out of the known World petroleum reserves, only a part may be technically economically feasible to explore. This fact, coupled with the present and expected consumption rates implies that these reserves may not last beyond the next 30 years. For India, the situation could be even more difficult. Given limited reserves, present known stocks may not last even 10 years at the current consumption rate.

At one end, the rapid industrialization has led to increased use of fossil fuels such as coal, oil etc, to meet its power and steam requirement. For which, the developing nations like India are paying huge import bills putting stress on economy. At other end, a naturally available energy sources such as solar, wind, biomass, biogas etc are not effectively used. India has potential to generate 45,000 MW from wind energy, 19,000 MW from biomass energy, 15,000 MW from small hydro projects. In addition to it the urban areas in India produce @ 30 millions of solid waste and 4400 Million cubic meters of liquid waste every year. The same can be exploited to generate power and meet a part of the ever increasing demand of urban areas.

Therefore, the need of the hour is to conserve petroleum by its judicious use, substituting it by
other resources wherever techno-commercially feasible and restricting its use only to the essential needs. In this paper we will see that even though the resources are depleting, but we cannot stop using them, therefore we will explore the data through which we can understand how the renewable sources of energy can be used and applied effectively.

Key words: Energy, Renewable, Solar energy, Wind energy, Biogas, Geothermal energy etc;

1 Introduction:
Currently the energy requirement of the world is fulfilled by the conventional resources, the percentage of the currently used sources can be seen from the table below:

S.No.	Sources	Available in (%)
1.	Oil	31
2.	Coal	26
3.	Natural Gas	19
4.	Hydro Electricity	6
5.	Firewood & Crop waste	12

Table 1: Currently used conventional sources

The development of infrastructure is an important factor to sustain economic growth. The power sector is one of the most important constituents of infrastructure. The achievement of energy security necessitates diversification of our energy resources and the sources of their supply, as well as measures for conservation of energy. So far, we were dependent on conventional sources of energy like thermal, hydro (large hydro) and nuclear. Fortunately, India is blessed with the third largest coal supplies in the world, although not of the best quality but we cannot use them indefinitely. The increasing prices for petroleum products, projection that petroleum resources would be exhausted in a relatively short period of time and the use of fossil fuel resources for political purposes will adversely affecting worldwide economic and social development. The impact of the energy crisis is particularly felt in developing countries like India, where an ever-increasing percentage of national budgets earmarked for development must be diverted to the purchase of petroleum products. After independence large hydroelectric projects have been executed, some of them

are still under construction and some have been planned for future. The inherent drawbacks associated with large hydro are; large gestation period, large area along with vegetation has to be submerged, shifting of people etc. from the sites. Political and environmental implications have made planners to think for some other alternative to the large hydro. For nuclear power plants also there is a problem of getting proper fuel, processing and safety from radiations. In addition, global warming caused largely by green-house gas emission from fossil fuel generating systems is also a major concern. To overcome the problems associated with conventional sources of energy, most countries including India have shifted their focus to develop non-conventional renewable sources of energy. Among these resources are solar energy, wind, geo thermal energy, biomass and small hydropower. 263 districts in 16 states and one Union Territory have so far been covered under the Integrated Rural Energy Programme of government of India, which aims at providing a cost effective energy mix of non-conventional sources to meet the energy need of the rural areas. With the various initiatives taken by the government, a healthy power sector would emerge in the country which would pave the way for fast industrialisation, growth in agricultural production, rural development and a better quality of life through non-conventional renewable energy sources.
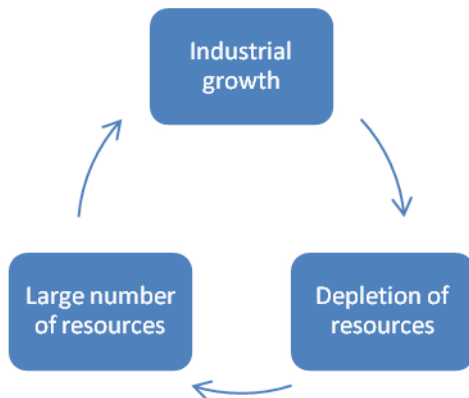
Chart 1 : relationship between industrial growth & resources
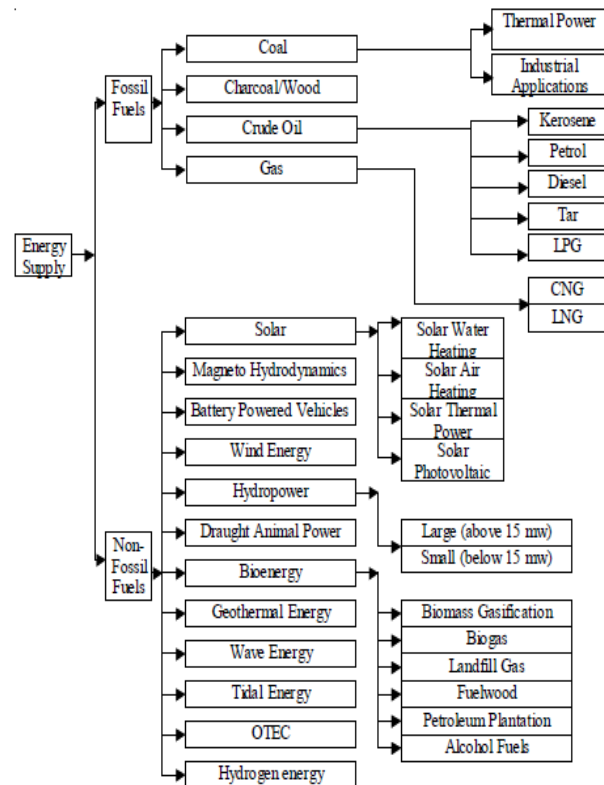
Chart 2 : current sources of energy

2. Renewable Energy Scenario:

In India the potential of renewable energy source is about 81.200 MW out of which only 5594 MW i.e. 6.9% has been harnessed so far. The potential and capacity harnessed so far is given in Table 1 [1]. India's need for power is growing at a prodigious rate, annual electricity generation and consumption in India have both nearly doubled since 1990, and it's projected 2.6% (low end) to 4.5 % (high end). Annual rate of increase for electricity consumption (through 2020) is the highest for any major country. India is currently the seventh greatest electricity consuming country (accounting for about 3.5% of the world total annual electricity consumption) but will soon overtake both Germany and Canada in that regard. India now faces an electricity shortages conservatively estimated at 11% and as high as 18% during peak demand periods

Sl. No.	Renewable Energy Sources	Potential (MW)	Potential harnessed so far (MW)
1.	Wind	45,000	2980
2.	Small Hydro Up to (25 MW)	15,000	1693
3.	Biomass	3,500	727
4.	Gasifiers	16,000	62
5.	Urban & industrial Waste	1700	46.5
6.	Solar Photo Voltaic (S.P.V.)	20/SQ km	86
	TOTAL	81,200	5,594

Table 2: Potential and Installation of Renewable Energy Systems

3. Renewable Energy Technologies

3.1 Solar Energy

Solar energy has the greatest potential of all the sources of renewable energy and if only a small amount of this form of energy could be used, it will be one of the most important supplies of energy specially when other sources in the country have depleted energy comes to the earth from the sun. This energy keeps the temperature of the earth above than in colder space, causes current in the atmosphere and in ocean, causes the water cycle and generate photosynthesis in plants. The solar power where sun hits atmosphere is 10^{17} Watts, whereas the solar power on earth's surface is 10^{16} Watts. The total worldwide power demand of all needs of civilization is 10^{13} Watts. Therefore the sun gives us 1000 times more power than we need. If we can use 5% of this energy, it will be 50 times what the world will require [3]. Electricity can be produced from the solar energy by photovoltaic solar cells, which convert the solar energy directly to electricity. The most significant applications of photovoltaic cell in India are the energisation of pump sets for irrigation, drinking water supply and rural electrification covering street lights, community TV sets, medical refrigerators and other small power loads.

3.2 Wind Energy

Wind energy, which is an indirect source of solar energy conversion, can be utilized to run windmill, which in turn drives a generator to produce electricity. Wind can also be used to provide mechanical power such as for water pumping. In India generally wind speeds obtainable are in the lower ranges. Attempts are, therefore, on the development of low cost, low speed mills for irrigation of small and marginal farms for providing drinking water in rural area. The developments are being mainly concentrated on water pumping wind mill suitable for operation in a wind speed range of 8 to 36 km per hour. In India high wind speeds are obtainable in coastal areas of Saurashtra, western Rajasthan and some parts of central India [5]. Among the different renewable energy sources, wind energy is currently making a significant contribution to the installed capacity of power generation, and is emerging as a competitive option. India with an installed capacity of 3000 MW ranks fifth in the world after Germany, USA, Spain and Denmark in wind power generation. Energy of wind can be economically used for the generation of electrical energy. Wind energy equipment are modular in nature and the investment requirement for these equipments as compared to conventional energy equipments is not large and the industry is able to attract private investment thereby reducing the burden on the encourages such investment.

3.3 Biomass and Biogas Energy

The potential for application of biomass, as an alternative source of energy in India is large. We have plenty of agricultural and forest resources for production of biomass. Biomass is produced in nature through photosynthesis achieved by solar energy conversion. As the word clearly signifies Biomass means organic matter. In simplest form, the process of photosynthesis is in the presence of solar radiation. Biomass energy co-generation programme is being implemented with the main objective of promoting technologies for optimum use of country's biomass resources and for exploitation of the biomass power generation potential, estimated at 19500 MW. The technologies being promoted include combustion, gasification and cogeneration, Either for power in captive or grid connected modes, or for heat applications.

3.4 Ocean Thermal Energy Conversion

This is also an indirect method of utilizing solar energy. A large amount of solar energy is collected and stored in tropical oceans. The surface of the water acts as the collector for solar heat, while the upper layer of the sea constitutes infinite heat storage reservoir. Thus the heat contained in the oceans, could be converted into electricity by utilizing the fact that the temperature difference between the warm surface waters of the tropical oceans and the colder waters in the depth is about 20 – 25 K. Utilization of this energy, with its associated temperature difference and its conversion into work, forms the basis of ocean thermal energy conversion (OTEC) systems. The surface water, which is at higher temperature, could be used to heat some low boiling organic fluid and the vapours of which would run a heat engine. The exit vapour would be conduced by pumping cold water from the deeper regions. The amount of energy available for ocean is replenished continuously. All the systems of OTEC method work on a closed routine cycle and use low boiling organic fluids like ammonia, Propane, R – 12, R – 22 etc.

3.5 Tidal Energy

The tides in the sea are the result of the universal gravitational effect of heavenly bodies like sun and moon on the earth. Due to fluidity of water mass, the effect of

this force becomes apparent in the motion of water, which shows a periodic rise and fall in levels which is in synthesis with the daily cycle of rising and setting of sun and moon. This periodic rise and fall of the water level of sea is called tide. These tides can be used to produce electrical power which is known as tidal power. When the water is above the mean sea level, it is called flood tide and when the level is below the mean sea level, it is called ebb tide. To harness the tides, a dam is to be built across the mouth of the bay. It will have large gates in it and also low head hydraulic reversible turbines are installed in it. A tidal basin is formed, which gets separated from the sea by dam. The difference in water level is obtained between the basin and sea. By using reversible water turbines, turbines can be run continuously, both during high tide and low tide. The turbine is coupled to generator, potential energy of the water stored in the basin as well as energy during high tides used to drive turbine, which is coupled to generator, generating electricity.

3.6 Geo Thermal Energy

This is the energy, which lies embedded with in the earth. According to various theories the earth has a molten core. The steam and the hot water comes naturally to the surface of the earth in some locations of the earth. Two ways of electric power production from geothermal energy has been suggested. In one of these heat energy is transferred to a working fluid which operates the power cycle. This may be particularly useful at places of fresh volcanic activity, where the molten interior mass of earth vents to the surface through fissures and substantially high temperatures, such as between 450 to 550^{0}C can be found. By embedding coil of pipes and sending water through them can be raised. In the other, the hot geothermal water and or steam is used to operate the turbines directly. At present only steam coming out of the ground is used to to generate electricity, the hot water is discarded because it contains as much as 30% dissolved salts and minerals and these cause serious rust damage to the turbine.

3.7 Small Hydropower

Energy from small hydro is probably the oldest and yet, the most reliable of all renewable energy sources. The term 'small hydro' has a wide range in usage, covering schemes having installed capacities from a few kW to 25 MW. In India small hydro schemes are further classified as micro hydro up to 100 kW plant capacity, mini hydro from 101 kW to 2000 kW and small hydro up to 25000 kW plant capacity. The advantage of this resource is that it can be harnessed almost everywhere in India from any nearby stream or canal – in the most environmentally benign manner, and without encountering any submergence, deforestation or resettlement problems which are generally encountered in the development of large hydro power development. Small hydropower development can reduce the load on conventional sources

of energy. Small hydro technology is mature and proven. Civil works and installation of equipment involve simple processes, which offer ample employment opportunities to local people and use locally available material. Gestation period is also short. Simple and proven design concepts suit local conditions. The development of small-scale hydropower in India started almost in the pace with the world's first hydroelectric installation in 1882 at Appleton USA. The 130 KW installations in Sidrapong (Darjeeling) in the year 1897 was the first installation in India. The other installations were Shivasamundram at Mysore (2000 kW).

3.8 Hydrogen Energy and Fuel Cells

In recent years hydrogen has been receiving worldwide attention as a clean and efficient energy carrier with a potential to replace liquid fossil fuels. Significant progress has been reported by several countries including India in the development of hydrogen energy as an energy carrier and an alternative to fossil fuels. Serious concerns relating to energy security. Depleting fossil fuel reserves, green house gas emissions and air quality are driving this global transformation effort towards a hydrogen-based economy. Hydrogen has high-energy content, when burnt, it produces only water as a by-product and is, therefore, environmentally benign. At present hydrogen is available as a by-product from several chemical processes, plants or industries.

4.Steps Towards Energy Anagement:

India's Energy Balance

Source: U.S. Energy Information Administration
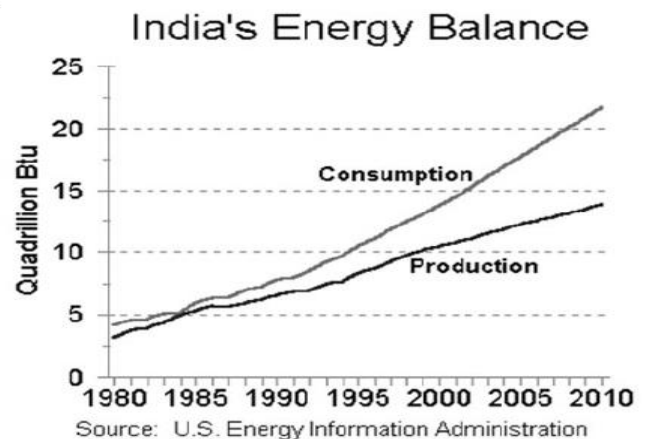
Taking the overview of these forecasts it is observed that in each and every area demand is
more and the supply is less. If this situation persists no conventional source will remain to supply
energy.
The draft renewable energy policy of the Govt. of India sets the following targets to be achieved.

- 30 million more households to have improved cook stoves

- 3 million more family-size biogas plants to be set up 5 million solar lanterns
- Decentralized electricity, including village grid tail-end injection systems, to be provided to one-quarter of these villages in the following manner, through power plants with an average installed capacity of 100 kW per plant:
- 500 solar photovoltaic plants
- 2000 biomass gasifier-based power plants
- 1000 small hydro power plants
- 2 million solar home systems
- 5 million square metres of collector area for low-temperature solar water-heating systems,

5 . Conclusions

1. The renewable sources are cost effective, user-friendly, so that they can easily beat the fossil fuels
2. By promoting renewable energy sources we can avoid, Air pollution, soil pollution and water pollution
3. Country's Economy will increase
4. Due to technological advancement vehicles are made with improved fuel efficiency and also perfect hybrid vehicle are made
5. Throughout the year these sources are available without affecting the Environment

6 .References

1. Solar Energy
- By Suhas P. Sukhatme

2. Non-Conventional Energy Sources
- By G. D. Rai

3. Non-Conventional Energy Sources – Principles, prospects and progress
- By K. M. Mital

4 Annual Report, 2004-2005, Ministry of Non-Conventional Energy Sources, Govt. of India, New Delhi, 2005.

5 Sharma M.P., Saini R.P., "SPV based electrification of remote rural area", National Symposium on recent advances in RET's, Shivaji University Kolhapur, Aug 13-14, 2002

6 www.wikipedia.com/non-conventionalresources.Php

Fast Fractal Image Compression Scheme

Hitashi[1] and Sugandha Sharma[2]

[1] Research Scholar, Indo Global College, Punjab (India)
[2] Deptt. of CSE, Indo Global College, Punjab (India)

Abstract. Compression and decompression tools of digital image has become a significant aspect in the storing and transferring of digital image. Fractal image compression technique is recently used to compress images. The main problem with fractal image compression is that it takes a lot of computational time for searching blocks (domain block and range block) and then compares these blocks. There are many optimization techniques which are used to improve efficiency of fractal image compression. Some of these are particle swarm optimization, ant colony optimization and biogeography based optimization. In this paper the technique of biogeography based optimization (BBO) is applied for fractal image compression (FIC).With the help of this evolutionary algorithm effort is made to reduce the search complexity of matching between range block and domain block. The main drawback of FIC is that it involves more computational time due to global search. In order to improve the computational time and also the satisfactory quality of the decoded image, BBO algorithm is proposed. Investigational outcome show that the BBO is a better method than the traditional comprehensive search method in terms of encoding time. Results are calculated from wavelet based fractal image compression than BBO is applied over it to decrease the encode time and get better visual quality of image. In this paper compression time (encoding time) of fractal image compression is reduced.

Keywords: fractal image compression, biogeography based optimization (BBO), encoding time, suitability index variables (sivs).

1. Introduction

Compression and decompression tools of digital image has become a significant aspect in the storing and transferring of digital image. Most of the methods in use can be classified under the head of lossy compression. This implies that the reconstructed image is always an estimate of the original image. Fractal image coding introduced by Barnsley and Jacquin is the outcome of the study of the iterated function system developed in the last decade [1]. Because of its high compression ratio and simple decompression method, many researchers have done a lot of research on it. But the main drawback of their work can be related to large computational time for image compression.

The science of biogeography can be traced to the work of nineteenth century naturalists such as Alfred Wallace and Charles Darwin. In the early 1960s, Robert MacArthur and Edward Wilson began working together on mathematical models of biogeography, their work culminating with the classic 1967 publication The Theory of Island Biogeography [4].

Mathematical models of biogeography describe how species migrate from one island to another, how new species arise, and how species become extinct. The term "island" here is used descriptively rather than literally. That is, an island is any habitat that is geographically isolated from other habitats. We therefore use the more generic term "habitat" in this paper [4]. Geographical areas that are well suited as residences for biological species are said to have a high habitat suitability index (HSI) [4]. Features that correlate with HSI include such factors as rainfall, diversity of vegetation, diversity of topographic features, land area and temperature. The variables that characterize habitability are called suitability index variables (sivs). Sivs can be considered the independent variables of the habitat, and HSI can be considered the dependent variable. Habitats with a high HSI tend to have a large number of species, while those with a low HSI have a small number of species. Habitats with a high HSI have a low species immigration rate because they are already nearly saturated with species. Therefore, high HSI habitats are more static in their species distribution than low HSI habitats. By the same token, high HSI habitats have a high emigration rate; the large number of species on high HSI islands has many opportunities to emigrate to neighboring habitats. Habitats with a low HSI have a high species immigration rate because of their sparse populations. However if a habitat's HSI remains low, then the species that reside there will tend to go extinct, which will further open the way for additional immigration. Due to this, low HSI habitats are more dynamic in their species distribution than high HSI habitats. A good solution is analogous to an island with a high HSI, and a poor solution represents an island with a low HSI. High HSI solutions resist change more than low HSI solutions. [4]

The goals of this paper is to study BBO and apply it on fractal image compression to reduce the compression time (encode time) and improve the picture quality. First give a general presentation of the new optimization method called BBO. This is done by first studying natural biogeography, and then generalizing it to obtain a general-purpose optimization algorithm. Section 2 reviews the ideas and mathematics of fractal image compression section 3 discusses biogeography and how BBO can be used to formulate a general optimization algorithm, section 4 discuss algorithm which is applied over fractal image compression to improve its efficiency(i.e. decrease encode time), section 5 and section 6 discusses experimental result calculated over image.

2. Fractal Image Compression

Fractal image compression is based on the local self-similarity property in a nature images. The fundamental idea is coming from the Partitioned Iterated Function System (PIFS). Suppose the original gray level image *f* is of size *m* * *m*. Let the range pool *R* be defined as the set of all non-overlapping blocks of size *n*n* of the image *f*, which makes up $(m/n)^2$ blocks. For obeying the Contractive Mapping Fixed-Point Theorem, the domain block must exceed the range block in length. Let the domain pool *D* be defined as the set of all possible blocks of size *2n* * *2n* of the image *f*, which makes up $(m-2n + 1)^2$ blocks. For *m* is 256 and *n* is 8, the range pool *R* is composed of (256/8) *(256/8) =1024 blocks of size 8 *8 and the domain pool *D* is composed of (256-16 + 1) *(256-16 + 1) = 58081 blocks of size 16*16. For each range block *v* from the *R*, the fractal affine transformation is constructed by searching all of the domain blocks in the *D* to find the most similar one and the parameters representing the fractal affine transformation will form the fractal compression code for *v*. To execute the similarity measure between range block and domain block, the size of the domain block must be first sub-sampled to 8*8 such that its size is the same as the range block *v*. Let *u* denote a sub-sampled domain block. The similarity of two image blocks *u* and *v* of size *n*n* is measured by mean square error (MSE) defined as

$$MSE = \frac{1}{mn} \sum_{i=0}^{m-1} \sum_{j=0}^{n-1} \lfloor I(i,j) - K(i,j) \rfloor^2 \tag{1}$$

The primary tool used in describing images with iterated function systems is the affine transformation. This transformation is used to express relations between different parts of an image. Affine transformations can be described as combinations of rotations, scaling and translations of coordinate axes in n-dimensional space [9]. For example, in two dimensions a point (x, y) on the image can be represented by (xn, yn) under affine transformation.

In this paper wavelet based fractal image compression is used to compute result. Wavelet transform is used to decompose the original image to various frequency subbands in which the attributes can be extracted from the wavelet coefficients belonging to different sub-bands. The distribution of wavelet   coefficients can be used in context-based multi scale classification of document image [5].

3. Biogeography

Fig. 1 illustrates a model of species abundance in a single habitat [4]. The immigration rate λ and the emigration rate μ are functions of the number of species in the habitat. Consider the immigration curve. The maximum possible immigration rate to the habitat is I, which occurs when there are zero species in the habitat. As the number of species increases, the habitat becomes more crowded, fewer species are able to successfully survive immigration to the habitat, and the immigration rate decreases.

The largest possible number of species that the habitat can support is S_{max} at which point the immigration rate becomes zero. Now consider the emigration curve. If there are no species in the habitat then the emigration rate must be zero. As the number of species increases, the habitat becomes more crowded, more species are able to leave the habitat to explore other possible residences, and the emigration rate increases. The maximum emigration rate is E, which occurs when the habitat contains the largest number of species that it can support. The equilibrium number of species is S_0 at which point the immigration and emigration rates are equal. However, there may be occasional excursions from S_0 due to temporal effects. Positive excursions could be due to a sudden spurt of immigration (caused, perhaps, by an unusually large piece of flotsam arriving from a neighboring habitat), or a sudden burst of speciation (like a miniature Cambrian explosion). Negative excursions from could be due to disease, the introduction of an especially ravenous predator, or some other natural catastrophe.

It can take a long time in nature for species counts to reach equilibrium after a major perturbation [7], [8]. We have shown the immigration and emigration curves in Fig. 1 as straight lines but, in general, they might be more complicated curves. Nevertheless, this simple model gives us a general description of the process of immigration and emigration. The details can be adjusted if needed.
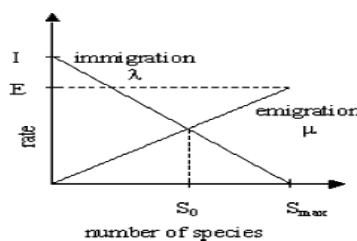

Fig. 1. Species model of a single habitat based on [6]

3.1 Biogeography-based optimization (BBO) in this section, we discuss how the biogeography theory can be applied to optimization problems with a discrete domain.

3.1.1   Migration

Suppose that we have a problem and a population of candidate solutions that can be represented as vectors of integers. Each integer in the solution vector is considered to be an SIV. Further suppose that we have some way of assessing the goodness of the solutions. Those solutions that are good are considered to be habitats with a high HSI, and those that are poor are considered to be habitats with a low HSI. HSI is analogous to "fitness" in other population-based optimization algorithms (GAs, for example). High HSI solutions represent habitats with many species, and low HSI solutions represent habitats with few species. We assume that each solution (habitat) has an identical species curve (with E=1 for simplicity), but the S value represented by the solution depends on its HSI. in Fig. 2 represents a low HSI solution, while S_2 represents a high HSI solution. $S_{1\ in}$ Fig. 2 represents a habitat with only a few species, while S_2 represents a habitat with many species. The immigration rate λ_1 for S_1 will, therefore, be higher than the immigration rate λ_2 for S_2. The emigration rate μ_1 for S_1 will be lower than the emigration rate μ_2 for S2. We use the emigration and immigration rates of each solution to probabilistically share information between habitats. With
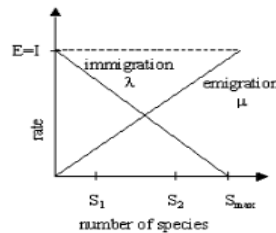

Fig. 2. Illustration of two candidate solutions to some problem. S_1 is a relatively poor solution, while S_2 is a relatively good solution [6].

probability P_{mod}, we modify each solution based on other solutions. If a given solution is selected to be modified, then we use its immigration rate λ to probabilistically decide whether or not to modify each suitability index variable (SIV) in that solution. If a given SIV in a given solution S_i is selected to be modified, then we use the emigration rates μ of the other solutions to probabilistically decide which of the solutions should migrate randomly selected SIV to solution S_i.

The BBO migration strategy is similar to the global recombination approach of the breeder GA [4] and evolutionary strategies in which many parents can contribute to a single offspring, but it differs in at least one important aspect. In evolutionary strategies, global recombination is used to create new solutions, while BBO migration is used to change existing solutions.

3.1.2 Mutation

Cataclysmic events can drastically change the HSI of a natural habitat. They can also cause a species count to differ from its equilibrium value (unusually large flotsam arriving from a neighboring habitat, disease, natural catastrophes, etc.). A habitat's HSI can, therefore, change suddenly due to apparently random events. We model this in BBO as SIV mutation, and we use species count probabilities to determine mutation rates. By looking at the equilibrium point on the species curve of Fig. 2, we see that low species counts and high species counts both have relatively low probabilities. Medium species counts have high probabilities because they are near the equilibrium point.

Each population member has an associated probability, which indicates the likelihood that it was expected a priori to exist as a solution to the given problem. Very high HSI solutions and very low HSI solutions are equally improbable. Medium HSI solutions are relatively probable. If a given solution has a low probability, then it is surprising that it exists as a solution. It is, therefore, likely to mutate to some other solution. Conversely, a solution with a high probability is less likely to mutate to a different solution.

3.2 Differences among BBO and Other Population-Based Optimization Algorithms

In this section, we point out some of the characteristic of BBO. First, we note that although BBO is a population-based optimization algorithm it does not involve reproduction or the generation of "children." This clearly distinguishes it from reproductive strategies such as GAs and evolutionary strategies.

BBO also clearly differs from ACO, because ACO generates a new set of solutions with each iteration. BBO, on the other hand, maintains its set of solutions from one iteration to the next, relying on migration to probabilistically settle in those solutions.

BBO has the most in ordinary with strategies such as PSO and DE. In those approaches, solutions are maintained from one iteration to the next, but each solution is able to learn from its neighbors and adapt itself as the algorithm progresses. PSO represents each solution as a point in space, and represents the change over time of each solution as a

velocity vector. However, PSO solutions do not change directly; it is rather their velocities that change, and this indirectly results in position (solution) changes. DE changes its solutions directly, but changes in a particular DE solution are based on differences between other DE solutions. Also, DE is not biologically motivated. BBO can be contrasted with PSO and DE in that BBO solutions are changed directly via migration from other solutions (islands). That is, BBO solutions directly share their attributes (SIVs) with other solutions. It is these differences between BBO and other population- based optimization methods that may prove to be its strength.

4. Implementation of BBO algorithm in fractal image compression

The BBO algorithm in fractal image compression can be formally applied as:

1. Reduce the search space for FIC.
2. The classifier partition all of blocks in domain pool and range pool into 2 classes according to wavelet coefficient.
3. Initialize the BBO parameters. This means deriving a method of mapping problem solutions to SIVs and habitats
4. Initialize a random set of habitats, each habitat corresponding to a potential solution
5. Define HSI, Smax, immigration rate (λ) and emigration rate(μ).
6. Calculate MSE in each iteration of every range block and domain block.
7. Calculate probability of each domain block and range block based on MSE of each domain and range block.
8. If probability come above a predefined value immigrate that block in high HSI, else in low HSI.
9. Goto step 6 for next iteration.
10. If no domain is left then:
    (i)   Stop the process.
          Else:
    (i)   Go to step 6.

    End

$$Pi(n + 1) = Pi(n) = r_1(PHSIi - Xi) + r_2((H_{hsi}) - Xi) \tag{3}$$
$$Xi(n + 1) = Xi(n) + Pi(n + 1). \tag{4}$$

The i_{th} block is represented as Xj = (x1, x2, x3, · · · , xj). The best probability of each domain and range block is recorded and represented as PHSI$_i$ = (PHSI1, PHSI2, PHSI3, · · · , PHSIj). The probability of the block among all the values in that iteration is considered as H$_{hsi}$. The probability for block 'i' is represented as Pj = (P1, P2, P3, · · · , Pj). Based on equation (3), (4) species(in our case domains) can migrate to habitat having high HSI. This is done on the basis of high probability value.[13]

5. Implementation of BBO based FIC

In a typical run of the BBO, for every range block, an initial population of random values which correspond to the top left coordinates of domain blocks and its isometry are generated. Each random value corresponds to the location of the domain block and is used to evaluate the domain block and find the MSE. The domain block with the minimum MSE in the BBO is identified and its coordinates are noted as PHSI values. Each Block keeps track of its coordinates in habitat which are associated with the fittest solution it has achieved so far. The P$_i$ domain of each block at iteration is updated according to Eq.(5) .

$$P_i = \begin{cases} Xi & fi(n) < fi(n-1) \\ HSIi(n-1) & otherwise \end{cases} \tag{5}$$

Where fi(n) is the Mean Squared error (MSE) value between the range block and selected domain block in the present iteration. The probability and block value are updated using Eq. (3) and Eq. (4) in each iteration. The application of BBO involves repeatedly performing two steps:[13]
• The calculation of the objective function (MSE) for each of the block in the current population 'i'.
• The biogeography optimization then updates the block coordinates based on Eq. (3) and Eq. (4)

6. System investigated

In this paper a Gray level image of 512×512 size with 256 Gray levels is considered. A Range block of size 4×4 and Domain blocks of size 8×8 are considered. The domain blocks are mapped to the range block by affine transformations and the best domain block is selected. The PSNR considered in this work are given by:

Table 1 Image compressed with FIC (wavelet Based)

Image	Encode Time(sec)	Compressed image size(bytes)	Compression Ratio	MSE	PSNR(db)
Pirate	292.5440	199280	1.496	61.5985	30.2351
Mandrill	278.5600	224161	1.329	130.2591	26.9827

Table 2 Image compressed with BBO applied on FIC

Image	Encode Time(sec)	Compressed Image size(bytes)	Compression Ratio	MSE	PSNR(db)
Pirate	227.9690	208646	1.428	108.6298	27.77
Mandrill	225.0830	174377	1.709	339.3875	22.83

7. Results and discussions

This work is carried out in MATLAB 7.10.0 version on Pentium-dual core processor with 1.86 GHz and 1 GB RAM and the original image is classical 512×512 pirate and mandrill image coded with 8 bits per pixel. A random population of points is generated and each point is evaluated in the following manner. The point is converted into its corresponding binary value and the first 16 bits are utilized to locate the top left corner of domain block and next 3 bits are used to find the isometry to be applied to the selected domain block. Tab. 2 shows the comparison of BBO based FIC with the traditional exhaustive search method. It can be seen from the table that the visual quality and encoding time with the proposed technique has been improved as compared with the traditional method. Fig. 7 and Fig. 8 show the reconstructed images using FIC with BBO as search algorithm along with the original images of pirate and mandrill after 32 iterations.

Note down visual quality of image is much better with BBO as compared to FIC. Also encode time decreases after applying BBO optimization. Image compressed with BBO optimization is much close to original one, but with FIC distortion comes in the image.

Figure 3 and 4 original images Pirate.gif (298146) and Mandril.gif (298097 bytes)

Figure 5 and 6 images compressed with FIC pirate.gif (199280 bytes) and mandrill.gif (224161 bytes)

Figure 7 and 8 compressed images after applying BBO on FIC pirate.gif (208646 bytes) and mandrill.gif (174377 bytes)

8. References:

[1]. M. Barnsley, A. Jacquin, "Application of recurrent iterated function system to images," Proceedings of SPIE 3, vol. 1001, pp.122–131, 1998.

[2]. D. Simon, "A Probabilistic Analysis of a Simplified Biogeography-Based Optimization Algorithm," IEEE, pp. 1604-1616, 2009.

[3]. J. Li and R. M. Gray, "Context-based multiscale classification of document images using wavelet coefficient distributions," IEEE Transactions on Image Processing, vol. 9, pp. 1604-1616, 2000.

[4]. D. Simon, "Biogeography-Based Optimization," IEEE, vol. 12, no. 6, pp. 702-713, 2008.

[5]. Y. Chakrapani, K. Soundarararajan, "Implementation of fractal image compression employing particle swarm optimization," World Journal of Modelling and Simulation, vol. 6, no. 1, pp. 40-46, 2010.

[6]. Jacquin, "Fractal image coding a review," IEEE, vol. 81, pp. 212–223, 1993.

[7]. Wallace, "The Geographical Distribution of Animals," Boston, MA: Adamant Media Corporation, pp. 201-206, 2005.

[8]. Jacquin, "Image coding based on a fractal theory of iterated contractive image transformation," IEEE Transactions on Image Processing, pp.18–30, 1992.

[9]. Y. Lin and W. Chen, "Fast Search Strategies for Fractal Image Compression," JISE 28, pp. 17-30, 2012.

[10]. Y. Chakrapani, K. Soundarararajan, "Implementation of fractal image compression employing artificial neural Networks," World Journal of Modelling and Simulation, pp. 287-295, 2008.

Analysis Of Flow Induced Vibration In Superheater Tube Bundles In Utility Boilers Using Computational Method

Aditya Kumar Pandey[*], L.A.Kumaraswamidhas and C.Kathirvelu

Department of Mechanical Engineering, National Institute of Technology, Tiruchirappalli -620015, Tamilnadu, India

Abstract
Flow induced vibration in tube bundles subjected to cross flow has been known for a long time. In boilers, tube bundles carrying steam or water are subjected to cross flow of flue gases. This flow causes external forces which may generate vibrations and sound in the boiler during their regular operation. These vibrations can result in tube thinning at support points and consequent leakage or damage to tubes, damage to structural attachments as well as insulation cladding provided around the enclosure. Hence, it is required to predict the occurrence of flow induced vibrations early-on and address the problem. This paper focuses on the flow induced vibration phenomenon of vortex shedding and acoustic resonance in horizontal Low Temperature Superheater (LTSH) tube bundles in utility boilers at full load operation. Computational fluid dynamics tools have been used to perform the flow analysis. The results have been used to predict the occurrence of vortex shedding and acoustic resonance phenomenon and to calculate the amplitude of vibration. Validation has been conducted as per experimental results and confirmed that the methodology adopted holds suitable. The sources of error and their effect on the model in deviation of the conditions from the actual ones have also been discussed.

Keywords: Acoustic resonance, Flow induced vibration, Low temperature super heater, Vortex shedding

1. Introduction

Flow induced vibration for tubes subjected to cross-flow have been a subject of investigation the world over. In boilers, tube bundles carrying steam or water are subjected to cross flow of flue gases. This flow causes external forces which may generate vibrations and sound in the boiler during their regular operation. These vibrations can result in tube thinning at support points and consequent leakage or damage to tubes, damage to structural attachments as well as insulation cladding provided around the enclosure. It could lead to forced shutdown of boiler to replace the damaged components. Hence, it is required to predict the occurrence of flow induced vibrations early-on and address the problem to avoid forced outages. Physical measurement of the vibrations in the tube bundles by measuring probes is difficult in the running boiler due to high temperature. So, there is a need to evaluate vibrations in affected regions theoretically. Computational Fluid Dynamics tools have been found appropriate to perform the flow analysis. Owing to recent improvements in Computational Fluid Dynamics, simulation and flow analysis for tube bundles is now practicable for industrial purposes. Schroder and Gelbe [2] performed two and three dimensional CFD simulation of flow-induced vibration excitation in tube bundles. Dhamangaonkar et. al [5] performed CFD analysis to simulate flow in a typical 250 MW coal fired utility boiler. This paper focuses on the flue gas flow distribution in the in the Low Temperature Super Heater (LTSH) tube bundles situated in second pass of a utility boiler (Figure 01) and the phenomenon of flow induced vibration. Commercially available computational fluid dynamics tools have been used to model the flow domain and perform the flow analysis. GAMBIT has been used for modeling and FLUENT for flow analysis. The phenomenon of vortex shedding and acoustic resonance has been found to occur in the boiler.
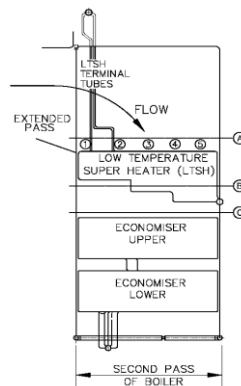

Figure 1: Boiler second pass with reference location for velocity and displacement measurement

2. Vortex Shedding And Acoustic Resonance

When fluid flows perpendicular to tube bundle staggered or inline, the most common phenomenon is the formation and shedding of vortices in the wake beyond the tubes. [2] The vortex shedding phenomenon can be characterized by a non dimensional parameter known as Strouhal number 'S_u', which gives relation between Vortex Shedding Frequency 'f_v', diameter of tube 'D' and velocity of the flow 'v' as,

$$S_u = f_v.D/v \qquad [1]$$

The value of Strouhal number is based on tube spacing in bundles and diameter of tubes. In this paper, the value of Strouhal number $S_u = 0.31$ and 0.27 based on charts by Chen and Fitzhugh respectively have been considered. [3][4]

The vortex shedding causes a harmonically varying force on the tube perpendicular to the normal flow of the fluid. It is a self excited vibration. If the Vortex Shedding Frequency 'f_v' coincides with the Natural Frequency of vibration of the tubes 'f_n', resonance occurs and tubes vibrate, leading to tube leakages and structural damages. The condition is :

$$0.8f_n < f_v < 1.2f_n \qquad [7]$$

Another mechanism associated with vortex shedding is the acoustic resonance. Acoustic resonance may take place when vortex shedding frequency coincides with Acoustic Frequency 'f_a' of standing waves in the enclosure. The condition is given as,

$$0.8f_a < f_v < 1.35f_a \qquad [8]$$

The acoustic frequency due to gas flow in the passage considering width of boiler 'L_a', effective speed of sound in bundles' C_{eff}' , and acoustic modes 'n' is given by the relation,

$$f_a = n. C_{eff}/2.L_a \qquad [12]$$

The effective speed of sound through the tube bundles, is related to speed of sound in the empty passage 'C' and the solidity ratio of the tube bundle 'σ' by the relation,

$$C_{eff} = C/(1+\sigma) \qquad [12]$$

3. Methodology

In this paper, flow induced vibration mechanisms described above have been studied for LTSH tube bundles. For this, the 3D flow domain of boiler enclosure with LTSH has been modeled in GAMBIT and analyzed in FLUENT to study the flow distribution. A 2D model of cross-section of LTSH tube bundle has also been made to study the flow distribution inside the tube bundle. Velocity of flue gases obtained from the flow analysis has been used to calculate f_v. A comparison of fv with f_n and f_a has been made to predict the vortex shedding phenomenon. Validation was conducted as per site measured values and confirmed that the methodology adopted holds suitable.
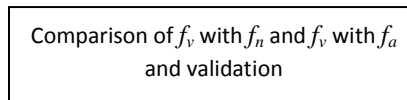
Comparison of f_v with f_n and f_v with f_a
and validation
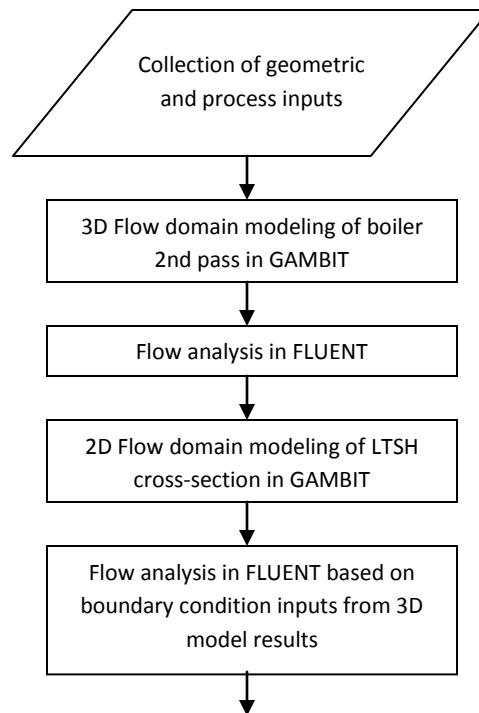
Figure 2: Flow chart for approach followed

3.1 3D Model for second-pass of boiler

A 3D model of boiler second-pass pass up to LTSH has been developed in GAMBIT for a typical 210MW utility boiler. The LTSH tube bundle is a dense arrangement of tubes which makes it difficult to be meshed with the limiting computing resources. For ease of computation, porous media approach has been used. The LTSH terminal tubes and LTSH tube bundle have been modeled as volumes of equivalent dimensions and declared as porous block. The Inertial Resistance (I.R) and porosity for the porous block has been calculated from the original LTSH model. Pressure Drop (PD) across tubes and velocity for calculation has been considered as per the design criterion. Tetrahedral elements have been used to mesh the model as shown in Figure 03. Flue gas has been taken as the fluid medium. The 3D model has been analyzed with velocity inlet and pressure outlet boundary conditions and k-ε has been used as the turbulence model.
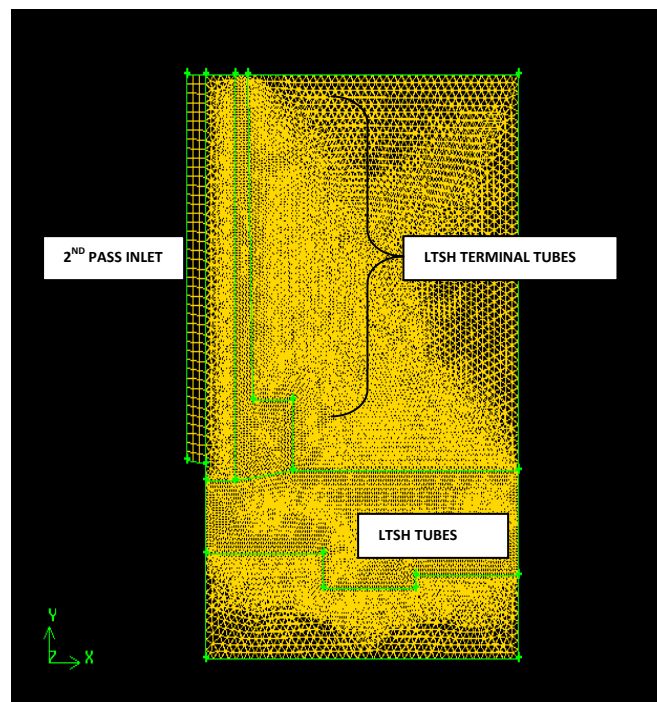

Figure 03: Meshed flow domain with porous components

3.2 2D Model for cross-section of LTSH

   The cross-section of LTSH tube bank has been modeled in 2D as shown in Figure 04. First and last three rows of tubes have been modeled and porous media approach has been used for the space in between. The face at inlet, outlet and porous zone has been meshed with quadrilateral elements and the faces with tube cross-section have been meshed with triangular elements as shown in Figure 05. The velocity profiles obtained from the 3D model at five locations above LTSH as shown in Figure 01 have been used as inlet boundary condition and pressure as outlet boundary condition. Flue gas has been taken as the fluid medium and k-ε had been used as the turbulence model.
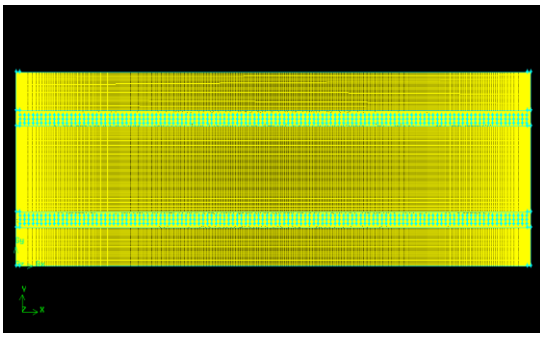
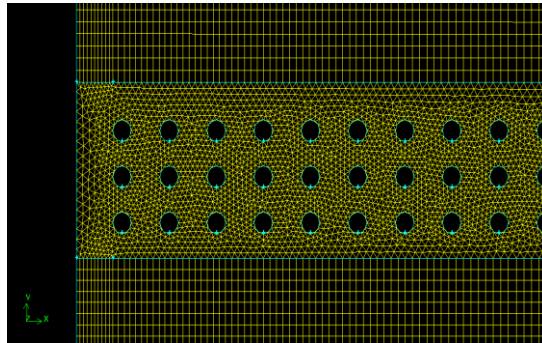**Figure 04:** Meshed 2D model of LTSH cross section

Figure 05: Meshed quad and tri elements

4. Results And Discussions

The flue gas flow changes direction as it flows from extended pass to LTSH tube bundles. The extended pass is tapered. Due to this, the flow enters with a sharp turn in the second pass of boiler. As it is evident from the velocity contour shown in Figure 06, a certain degree of separation occurs in the lower side and the flow distribution cannot be uniform over the transverse direction of the section. As a result, no uniform velocity distribution can occur at the top of LTSH. It can be said that, these tube bundles will be subjected to varying flow along the depth of boiler second pass. Figure 07 shows the variation of average velocity at the inlet of LTSH along the depth at aforementioned locations.
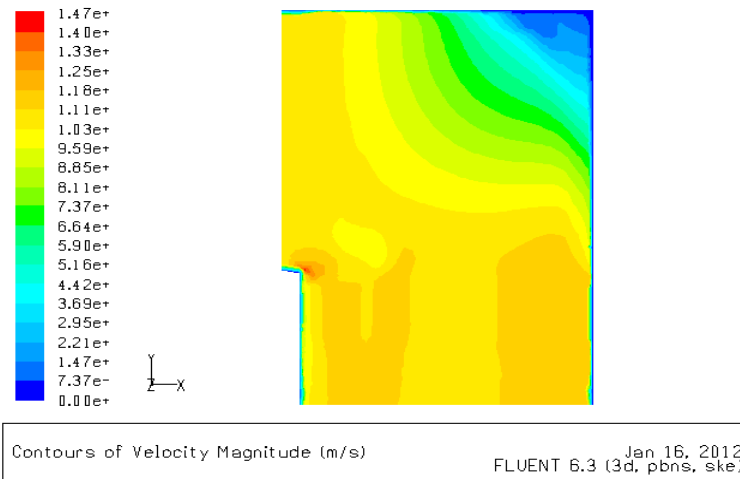
Figure 06: Velocity contour at mid-plane of second pass of boiler
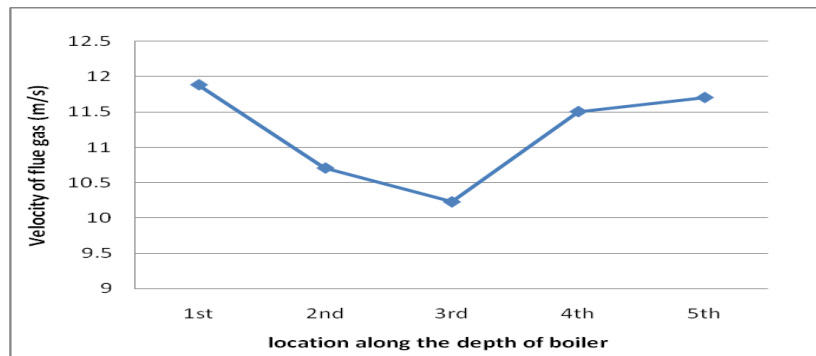
Figure 07: Variation of flue gas velocity at different locations above LTSH along the depth of boiler

To address this non-uniform flow distribution, the velocity profile has been captured at the above five locations along the depth of boiler from the analysis. These velocity profiles serve as inlet boundary condition to the 2D model of cross-section of LTSH. The typical flow pattern obtained for the 2D model of LTSH cross section in Figure 08, shows confined tube wakes as

pointed out by Ziada [6]. The flow dynamics in the flow lanes would be expected to dominate the development of the velocity fluctuations within the tube bundle.

Figure 08: Typical velocity contour through LTSH cross-section

The average velocities at LTSH outlet obtained from the 2D model analysis has been used to predict the vortex shedding frequency. Table 03 shows the calculated vortex shedding frequency. Table 04 gives the value of natural frequency and acoustic frequency for the first five modes. Comparing vortex shedding frequency according to Chen's criterion with tube natural frequency and acoustic frequency it has been found that tub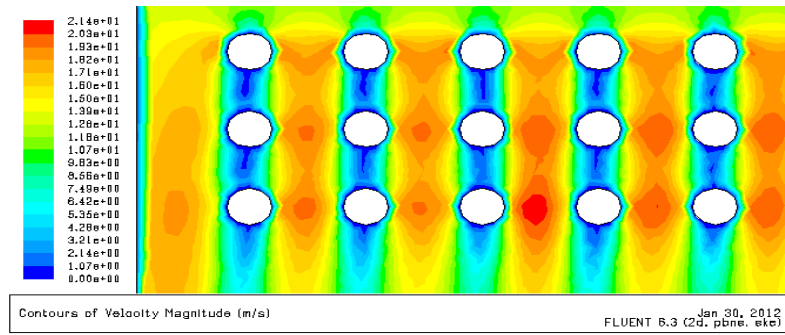e vibration is possible in 2nd mode. It could increase further at higher load and decrease if the boiler is operated at lower loads. Acoustic resonance is possible at higher nodes. According to Fitzhugh criterion tube vibrations may occur in 2nd mode and acoustic resonance is possible at higher nodes.

Table 03: Average velocity at five locations along depth of boiler and vortex shedding frequency

Location from second pass wall (Fig.01)	Vortex shedding frequency, f_v Chen's criterion (Hz)	Vortex shedding frequency, f_v Fitzhugh criterion (Hz)
1st	82.83	72.14
2nd	74.60	64.98
3rd	71.26	62.07
4th	80.18	69.83
5th	81.56	71.05

Table 04: Natural and acoustic frequency for first five nodes

Modes	Natural frequency, f_n (Hz)	Acoustic frequency, f_a (Hz)
1st	36.50	18.93
2nd	100.62	37.8
3rd	197.27	56.7
4th	326.11	75.72
5th	487.15	94.65

Physical measurement of the vibrations in the tube bundles by measuring probes is difficult in the running boiler due to high temperature. So, actual measurement of amplitude of vibrations was performed at the structures outside the boiler enclosure. The amplitude of vibrations in the tubes has been calculated, based on the flow velocity, at reference elevations A, B & C as shown in Figure 01. [12] A comparison has been shown between the tube vibration calculated and vibration data measured at the left and right hand side of boiler structure side in Figure 09. The difference in the calculated and measured values could be attributed to reasons like; (i) Actual measurement performed at outer structure of boiler and not on tube surface (ii) Porous media approach (iii) Geometry errors. However, on careful observation, it can be seen that the trend of predicted vibrations are more or less similar to the trend of site measured values.
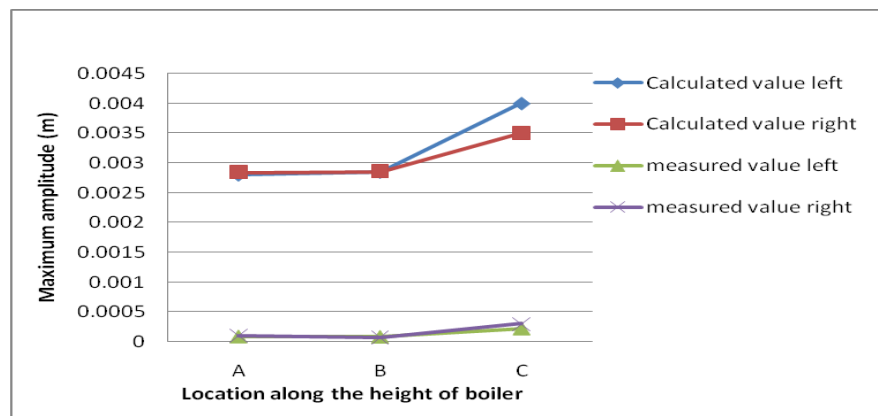
Figure 09: Predicted and measured amplitude of vibration**.**

Tube vibrations can be reduced to within limits by either reducing the cross-flow velocity or increasing the tube natural frequency or suppressing the standing waves. Reducing the cross-flow velocity of flue gas is directly linked to desired steam output parameters and needs careful considerations. By providing additional supports and baffles in between tubes or by removing tubes, the tube natural frequency can be changed and acoustic standing waves can be suppressed.

5.   Conclusion

   In this paper flow induced vibration phenomenon has been studied for horizontal Low Temperature Superheater (LTSH) tube bundles in utility boilers at full load operation. Flow analysis has been performed using commercial software FLUENT and the results have been used to predict the occurrence of vortex shedding and acoustic resonance phenomenon for LTSH. From the analysis, it has been observed that LTSH receives varying flow distribution along the depth of boiler. The phenomenon for vortex shedding and acoustic resonance has been observed in the boiler. The trend of calculated vibration amplitude at reference elevations has been found to be similar to the site measured values. The sources of error and their effect on the model in deviation of conditions from the actual ones have been discussed. The model can be used to predict vortex shedding and acoustic resonance phenomenon at different operating loads by changing the boundary conditions. Thus an optimum operating load range could be predicted for the boiler to operate avoiding vortex shedding and acoustic resonance phenomenon.

References
1.   R.D.Blevins, 1990 "Flow Induced Vibration", 2nd ed., Van Nostrand Reinhold, New York
2.   K. Schroder, H.Gelbe, 1999, "Two and Three-dimensional CFD-simulation of flow-induced vibration excitation in tube bundles", Chemical Engineering and Processing 38, pp. 621-629.
3.   Y.N.Chen, 1968, "Flow-Induced Vibration and Noise in Tube-Bank Heat Exchangers Due to Von Karman Streets," Trans ASME, Jour. of Engineering for Industry, Vol 1, pp. 134-146.
4.   J.S.Fitzhugh, 1973, "Flow-induced vibration in heat exchangers," Symposium on Vibration Problems in the Industry, Kasurck, United Kingdom, pp.10-12.
5.   P.R.Dhamangaonkar, S.R.Kajale, M.R.Nandgaonkar, Abhishek Deshmukh, Aditya Deshmukh, Swaroop Thakur, 2011, "Use of Cold Air Velocity Test (CAVT) to Locate Erosion Prone Zones in Pulverized Coal Fired Utility Boiler", Proceedings of the World Congress on Engineering, Vol III, WCE 2011, London, U.K
6.   Samir Ziada, 2006, "Vorticity shedding and acoustic resonance in tube bundles", Journal of the Brazilian Society of Mechanical Sciences and Engineering, Vol 28 no.2 Rio de Janeiro
7.   H.G.D.Goyder, 2002, "Flow-induced Vibration in Heat Exchanger", Institution of Chem Engg, Trans IChemE, Vol 80,Part A
8.   R.D.Blevins, M.M.Bressler, 1987, "Acoustic resonances in heat exchangers Part II: Prediction and suppression of resonance", Journal of Pressure Vessel Technology 109, pp.282-288
9.   V.Ganapathy, 1987, "Avoid Heat Transfer Equipment Vibration", Hydrocarbon Proc.
10.   M.J.Pettigrew, C.E.Taylor, 2003, "Vibration analysis of shell-and-tube heat exchangers: an overview- Part 2: vibration
11.   response, fretting-wear, guidelines, Journal of Fluids and Structures, pp.485-500
12.   W.J.Deane, L.J.Cohan, 1965, "Solution of Acoustical Standing Wave Vibration in Utility Steam Generators", Pacific Coast Electrical Association Engineering and Operating Conference, Los Angeles
13.   T. Kuppan, "Heat Exchanger Design Handbook", Marcel Dekker, Inc., New York, 2000, pp.423-461
14.   V.Ganapathy, "Applied Heat Transfer", Pennwell Books, Tusla, Okla, .82, pp.630-658
15.   Y.N.Chen, W.C.Young, 1973, "Damping Capability of the Tube Bank against Vortex-Excited Sonic Vibration in the Fluid Column", Design Engineering Technical Conference, Cincinnati, Ohio

Air Pollution reduction in metal industry using residual gas and natural gas combustion.

K Sridhar*[a], J Abbas Mohaideen[b]

K Sridhar, Research Scholar, Sathyabama University, No. 166, Temple Street, R.V.Nagar, Kodungaiyur, Chennai-119
[a] Research Scholar, Sathayabama University, Chennai, India
[b] Principal, Mamallan Institute of Technology, Chennai, India

Abstract:
Air pollution is the effect of atmosphere getting filled with toxic chemicals, particulate matter, or biological materials that cause harm or discomfort to humans or other living organisms, or damaging the environment. Basic air pollutants found in an industrial belt are CO, NO_x, SO_x, HC and PM. These pollutants are dispersed throughout the atmosphere in concentrations depending on the point of origin.

The aim of this paper is to study the effect of gases generated from coal used in a steel plant the combustion of Natural gas and coke oven gas (residual gases from steel plant blast furnace) results in pollutants. The residual gases of blast furnace and coke oven are characterized by reduced lower heating values(LHV) and high content of carbon monoxide (CO), Carbon dioxide (CO_2), Nitrogen(N_2) and Hydrogen sulphide (H_2S). Combustion of these fuels leads to increased emission of pollutants. Formation of these pollutants are influenced by excess O_2 of combustion, the case with less excess air (10%) was numerically simulated on a steam generator furnace. The study was done in a 230MW, water-tube boiler having vertically aligned burners. It defines the temperature, NO, CO and SO_2 distribution in the combustion chamber. The simulation results were compared with the actual boiler furnace measurements (corresponding to 25% excess air).

Key-Words - NO formation, SO_2 yield, Coke-oven gas, Low temperature corrosion, LHV.

Introduction

The air we breathe is polluted majorly by burning fossil fuels like oil, coal, natural gas and also during the manufacture of chemicals. Millions of people live in areas where urban smog, tiny particles and toxic pollutants pose serious health concerns. Rapid industrialization is a major factor contributing towards growing air pollution problem. Air pollutants [1,2,3,4,5,6] threatens not only the health of human beings and other living things but also our planet. Invisible pollutants in air create smog and acid rain causes cancer or other serious health effects, diminish the protective ozone layer in the upper atmosphere, greenhouse effect and contribute to the greatest potential for world climate change besides causing property damage.

The iron and steel industry uses coal as the main source of energy. Some of the coal is converted to coke oven gas during the production of coke and in blast-furnace gas where iron ore is reduced with coke to metallic iron. These gases may be recovered and used as fuel in various installations. This combustion raises a variety of problems such as high emission of NO_x due to the high amount of nitrogen in the blast-furnace gas, high emission of SO_2 due to the high amount of Hydrogen sulphide (H_2S) in the coke-oven gas and relatively high CO_2 emission, if compared with other hydrocarbon fuels like natural gas. This paper studies the ways to combat pollution by burning 2 different fuels separately and as a mixture.

Materials And Methods

The combustion of the two artificial fuels (coke gas and blast-furnace gas) in the furnace of 230 MW boiler is made simultaneously with the combustion of natural gas. The two artificial fuels have a reduced heating value compared to that of natural gas. The volumetric composition of the fuels can be seen in Table 1. The furnace of the boiler is made of two identical chambers consisting of four coaxial jets. Starting from the axis of symmetry, it is composed of a natural gas central jet, surrounded by an air flow, followed by a coke gas or blast-furnace gas flow and air at the periphery.

The burners are displayed on the walls of the furnace in the following way: on the upper level the burner fuelled with natural gas burners, and at the lower level, the burner fuelled with coke-oven gas and natural gas, on the lateral wall are arranged vertically the two burners fuelled with blast-furnace gas and natural gas.

Table 1: Characteristics of gas fuels.

	Analysis vol. %		
	Blastfurnace	Cokeoven	Natural gas
Carbon dioxide, CO_2	17.98	3.03	-
Oxygen, O_2	0.21	0.689	-
Carbon monoxide, CO	21.21	8.498	-
Hydrogen, H_2	6.9	51.158	-
Methane, CH_4	0.3	21.068	99.3
Ethane, C_2H_6	-	1.683	-
Hydrogen sulphide, H_2S	0.3	6.174	-
Nitrogen, N_2	53.1	7.7	0.7
Lower heating value, kJ/Nm^3	3431	17166	35523

The air jet is swirled i.e., it goes tangentially into the air box. The burners are designed to operate combined with natural gas/oil and coke-oven gas or blast furnace gas. The flow, combustion and pollutant formation has been done with the exit of the jets from the burner (air and fuels), from their interaction area. The Table 2 lists the operation conditions of the investigated furnace boiler. This investigation has been made to visualize the flame of each burner and the flames interaction for the whole furnace to emphasize the correlation between the parameters of thermogas dynamics and the pollutant formation.

Table 2.   Natural gas operating conditions

Natural gas flow rate, Nm^3/h	658
Air flow rate, Nm^3/h	6645.8
Air temperature, °C	260
Excess air, %	10

Coke-oven & blast-furnace operating conditions

Coke-oven gas flow rate, Nm^3/h	10000
Blast-furnace gas flow rate, Nm^3/h	3500
Air flow rate, Nm^3/h	7283/16404
Air temperature, °C	260
Excess air, %	10

Furnace operating conditions

Number of natural gas burners	2
Number of coke-oven burners	1
Number of blast-furnace gas burners	2
Static pressure, atm	1
Temperature of walls, °C	380

The experiment has been done to analyze the pollution characteristics of flows inside the boiler furnace. The operating parameters include the excess air, combustion air, temperature and air jet swirl angle as refered in Table3.

Table3:

Parameter	Natural Gas	Mixture Gas(Coke oven +Blast furnace gas)	Natural Gas + Mixture gas
Sox ppm	12	50	20
NOx ppm	5	38	7
CO ppm	50	120	75
PM nJ/m3	100	180	110
Excess Air %	15	15	15

It is clear from the results that in the increasing demand of Natural gas as a main source of fuel which is scarce in supply, a combination of Natural gas and Mixture gas(coke oven and blast furnace gas) can be used to combat all the emissions and particularly the NOx emissions to the tune of 90%. The burners are fed with this combination gas instead of depending solely on natural gas and also the steel industry produces coke oven and blast furnace gases.

NO_x are formed or destroyed during the combustion process by two separate reaction processes, which are classified as thermal NO and prompt NO. Thermal NO is formed by oxidation of atmospheric and fuel molecular nitrogen at relatively high temperatures in fuel lean environments, and has a strong temperature dependence. The prompt NO is formed by combination of molecular nitrogen in the air and fuel with fuel in fuel-rich conditions. Many investigations have shown that the prompt NO contribution to total NO from stationary combustors is small[3]. The thermal NO process is described by the Zeldovich mechanism [5].

In cases when excess air is more, SO_2 gets converts into SO_3. The presence of SO_3 in the burning gases leads to the increase of dew point of the gases. The risk of reaching this temperature is that, when burning gases cross the surface of the air preheater, leads to low temperature corrosion. Besides the demand for Green House Gases reduction due to Global warming, industries have to abide by the National and International regulations.

The legislation stipulates a maximum emission for furnace supplied with gas fuel, 350 mg/Nm^3 for NOx and 35mg/Nm^3 for SO_2 for new installations, and a maximum emission of 1700 mg/Nm^3 for NO_x and 350 mg/Nm^3 for SO_2 for old installations. These concentrations are related to excess oxygen in burning gases of 3%. To respect these limits we must deal with organizing the combustion or treating the burning gases. The selection of an alternative is determined by cost and the efficiency of the polluting emission reduction.

NO_x formation during the combustion process in gas fired boiler occurs mainly through the oxidation of N_2 from the combustion air and from the fuel. The formation of NO is an extremely complicated problem due to many parameters that influence its formation. The main parameters are the flame temperature, the concentration of N_2 and O_2 in flame (determined by the excess air), the concentration of N_2 in fuel, the burner's construction (combustion air swirl angle) and the organization of combustion (staged combustion). Carbon monoxide is formed during combustion because of either [1] inadequate supply of oxygen, or insufficient values of the three *T*'s, which are the Temperature, Time or Turbulence.

Turbulence is characterized by,
 (i) poor mixing of fuel and air;
 (ii) insufficient residence time to complete combustion;
(iii) quenching of combustion gases.

During combustion of fuels which is having sulphur, or hydrogen sulphide, SO_2 is produced (typically 1–3%). Under certain conditions SO_2 is being transformed into SO_3, which at lower temperatures, reacts with water vapour forming sulphuric acid [10]:

$$SO_3 + H_2O \leftrightarrow H_2SO_4$$
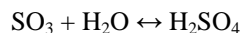
If the temperature of flue gases, containing H_2SO_4 and H_2O vapours decreases below the dew point, it results in condensation and the sulphuric acid solution formed is highly corrosive on the heat exchanger metal surfaces, in which the low-temperature corrosion appears. The numerical calculation of NO & CO is a three dimensional problem that involves combustion, turbulence and the heat transfer. By all means, among the cheapest solutions to reduce NO_x emission is an efficient way of combustion ratios and improvement in the burner design. As the excess air in the furnace influences NO, CO and SO_3 formation this paper presents the results of the co-combustion of natural gas with blast furnace gas with reduced excess air than the actual one (10% instead of 25%).

Results And Discussions

The operational mode with reduced excess air (10% instead of actual 15%) was investigated. The results are given for the furnace exit. The temperature distribution and the concentrations distribution of O_2, CO and SO_2 are shown in the vertical sections which go through the axes of the burners. The heat that is released by gases combustion is emphasized by the distribution of temperatures.

The maximum of temperature (2000°C) is situated in the area where the jets of the coke-oven gas and blast-furnace gas burners interact. Near each burner's air inlets, temperature is lower (about 850°C) due to the fact that combustion is poor in fuel. This non-uniformity of the thermal field disappears at the furnace exit. The predicted temperature at furnace exit (1330°C) is a little higher than that measured temperature for 15% excess air (1295°C). The predicted concentrations of CO

are high in the areas where the flame is rich in fuel, and the jets of the blast furnace gas and the coke- oven gas burners. The maximum concentration of CO is 1.96 to 10.1% (mass) and it gradually decreases towards 01.64·10-1% (mass) as CO mixes and reacts with O_2 in the upper area of the furnace. The high concentrations of CO influence both the temperature of the

mixture and the concentrations of O_2 and CO_2. It was expected an increase in CO concentration is due to the reduced excess air. Even with less excess air the CO concentration is low, almost equal to that corresponding to 15% excess air. From a value of 23 % (mass) at the outlet of each burner, the O_2 concentration reaches a value of 2.35% after combustion is completed. At the exit of the furnace, the O_2 concentration is 0.015% (mass), which means that there is an adequate amount of excess air in the furnace.

The presence of oxygen in the post-combustion area is undesirable because it leads to the increase of the conversion rate of SO_2 into SO_3 and eventually to the occurrence of the boiler's low temperature corrosion phenomenon. With less excess air in furnace it is expected a lower conversion rate. The coke-oven gas burner have an average content of SO_2 of $2300 mg/Nm^3$, which means that its value is higher than the one stipulated by environmental norms.

The NO formation occurs during the burning process and the main mechanism of formation is the thermal one. That is emphasized by the high concentrations of NO in the zones with high temperatures of the flame (260-330 ppm) and low concentrations of NO in the zones with low temperature (50- 120 ppm). Mixing within the furnace results in an average NO value of 270 ppm ($554 mg/Nm^3$) at the furnace exit, corresponding to an O_2 concentration of 1.5 % (vol.). If we recalculate the NO emission for a concentration of O_2 of 3%, we obtain a value of $608 mg/Nm^3$. This value of the predicted NO concentration is higher than the value stipulated by emission norms , but is lower than that corresponding to 15% excess air ($753 mg/Nm^3$).

Conclusion

The study provides insight on the correlation the effect of excess air on emissions like CO, SO_2 and NO_x. The results have shown that the decrease in excess air from 25 to 10% results in an increased exit temperature, almost the same CO and SO_2 concentrations and increase in reduction of NO_x concentrations. As the SO to SO_2 conversion rate depends on O_2 concentration it is expected a decrease of SO_2 concentration and therefore an alleviation of low-temperature corrosion of the steam boiler surfaces (air preheater, flue gas channels) is expected. Although the reduction of air excess leads to a reduction of pollutant concentrations, the pollutant emissions are slightly higher which can be reduced further by using techniques like flue gas recirculation, change in aerodynamic conditions in the furnace and burner design.

References

[1]   A. Buekens, Control of carbon monoxide and volatile organic compounds, including condensation, in Pollution Control Technologies, [Eds. Bhaskar Nath, and Georgi St. Cholakov], in Encyclopedia of Life Support Systems (EOLSS), 2005.

[2]   O. Gicquel, L. Vervisch, G. Joncquet, B. Labegorre, N. Darabiha, Vol 82, Nr. 8, , pp. 983-991

[3]   M. A. Habib, M. Elshafei, M. Dajani, 2008 Vol 37, pp. 12–23.

[4]   R.J. Heinson, R.L. Kabel, Sources and control of air pollution, Prentice- Hall, Inc., Upper Saddle River, NJ 1999.

[5]   S.C. Hill, L.D. Smoot, 2000, Vol 26, pp. 417–458.

[6]   G. Löffler, R. Sieber, M. Harasek, H. Hofbauer, R. Hauss, J. Landauf, 2006, Vol 85, pp. 513–523.

[7]   M. Marinescu, D. Stanciu, 2007, pp. 99-101.

[8]   X. Paubel, A. Cessou, D. Honore, L. Vervisch, R. Tsiava, 2007, Vol 31, pp. 3385–3392.

[9]   F. Pen, J.M. Blanco, 2007, Vol 27, pp. 2153–2158.

[10]   D. R. Schneider, Ž. Bogdan, 2007, Vol 27, pp. 1944–1950.

[11]   J. Warnatz, U. Maas, R. W. Dibble, Combustion–Physical and Chemical Fundamentals, Modeling and Simulation, Experiments, Pollutant Formation, Springer, Berlin, 1996

Deque Automata for all classes of Formal languages

B. Asha latha[1]

Department of computers
SRKIT Engineering
Vijayawada Andhra Pradesh
(India)

T.Vishnupriya[2]

Department of Electronics
SRKIT Vijayawada, Andhra
Pradesh (India)

N.Himabindu[3]

Department of computers
Pottisriramulu College of
Engineering ,Vijayawada, Andhra
Pradesh (India)

Abstract: The purpose of computation involves solving problems by communicating them to a computational model by means of a suitable language .A number of languages have been developed for this purpose. To recognize these languages some computational models has been developed and they are finite state machine, push down automata, queue automata and turing machines. But these machines are restricted to only one specific formal languages like regular, context free ,etc. In this paper we proposed a machine called a Dequeue automaton that is capable of recognizing different classes of automata. We also shown that the simulation results from the Deque automata.

Keywords: Formal languages, Finite automata, PDA ,TM.

I. Introduction

A finite automaton was the first abstract model as well as the mathematical model of digital computers. It is very powerful model of computation. It can recognize and accept regular languages. But finite automata have limited memory(states) which prevents them accepting Context free languages .Since memory is a limitation of finite automata ,a memory element is added as a stack, in order to made finite automata a powerful machine and to accept Context free languages. That new type of computational model is known as a Push down automata.PDA is similar to finite automata except that it has an extra memory unit stack. Stack is defined as a data structure where insertion and deletion of any element is possible only at one end called top of the stack.[1].

The automata with queue memory was constructed in a similar way as the PDA, however the new type of memory of QA is queue. The definition of queue automata is similar to that of PDA. The difference concerns the type of memory. The main advantage of QA is it is equivalent to Turing machine. That is a TM can be simulated by a QA that keep a copy of the TM's contents in its queue at all times with two special marks. One for the end of TM's head position and one for the end of the tape. Its transitions simulate those of the TM by running through the whole queue, popping off each of its symbols and re-enqueing either the popped symbol or near the head position. A queue machine can be simulated by a TM but more easily by a multi tape TM which is known to be equivalent to a normal single-tape machine.

But the PDA is not able to recognize the Context sensitive languages and Recursively Enumerable languages. To recognize the Context sensitive languages and Recursively Enumerable languages another automaton that is Turing machine was developed. The following table summarizes each class of the formal language and its corresponding automaton that recognizes it.

II. Categories of languages and Automaton

S.NO	Formal language	Automaton
1	Regular language	Finite automaton
2	Context free language	Non deterministic Push down automaton
3	Context sensitive and Recursively enumerable languages	Turing machine
4	Context free languages	Queue Automaton

Table: 1 Different types of Automaton

Every regular language is Context free, every context free language, not containing empty string is context sensitive and every recursive language is recursively enumerable. These are all proper inclusions, meaning that there exists recursively enumerable languages which are not context sensitive ,context sensitive languages which are not context free and context free languages which are not regular.
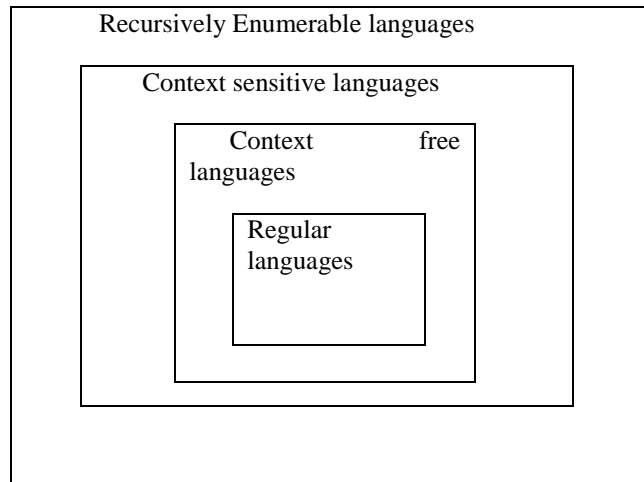
Fig : 1 Categories of languages

II. Deque computational model

The Deque Automaton is an extension of Queue automaton .It uses double ended queue as a memory element. The Dequeue is auxiliary storage element ,that contains list of items from a finite alphabet 'ζ' where the alphabets can be read ,inserted, or deleted from the both ends of the queue. That is we can perform the three operations namely reading, inserting, deleting from the front end as well as rear end of the deque. The main advantage of the Dequeue automaton is all the formal languages can be recognized by using it.

III Defining the automata

A deque automata is a hex-tuple machine. we can define it mathematically as

$$M=(Q,\textstyle\sum, \zeta,\delta,S,F)$$

Where Q=non empty set of finite state (s)

∑=non empty set of input alphabet

ζ=deque alphabet

(δ)=transision function

S=Starting state

F=Final state

III. Operations of Deque

Consider the expression (p,a,α ….β), (q,γ…θ) ε δ ,where {p,q} ε Q

αε ∑

α,β ε ζ

We can describe the above expression as if the automata are in the state

'p' with' α' as the front element and' β' as the back element of the Deque and reading the current input symbol from the tape as 'a' ,then the machine enters into a state 'q' by changing the alphabets of the que as α=γ or β=θ .If the machine is non deterministic then there is possibility that a=e (empty string).There is always a chance that p=q [2] There are six basic operations involved with the deque.

1.PUSH R: Pushing the input alphabet from the right of the deque

Examples:
((p,a,e) ,(q,a)) <= PUSH R means pushing the symbol 'a' on an empty deque from its right.

((p,a,a),(q,aa)) <= PUSH R means pushing the symbol 'a' on' a' into the deque from its right

((p,a,b),(q,ba)) <= PUSH R means pushing the symbol 'a' on' b' into the queue from its right

((p,b,a),(q,ab)) <= PUSH R means pushing the symbol 'b' on 'a' into the deque from its right

((p,b,b),(q,bb)) <= PUSH R means pushing the symbol 'b' on' b' into the deque from its right

Where {p,q}εQ

{a,b}ε∑

2.PUSH L: Pushing the input alphabet from the left of the deque

Examples:
((p,a,e),(q,a)) <=PUSH L means, pushing the symbol 'a' on an empty deque from its left

((p,a,a),(q,aa)) <=PUSH L means pushing the symbol 'a' on' a' into the deque from its left

((p,a,b),(q,ab)) <=PUSH L means pushing the symbol 'a' on' b' into the deque from its left

((p,b,a),(q,ba)) <=PUSH L means pushing the symbol 'b' on' a' into the deque from its left

((p,b,b),(q,bb)) <=PUSH L means pushing the symbol 'b' on' b' into the deque from its left

Where {p,q}εQ

{a,b}ε∑

3.POP R: removing or deleting an item from the right of the deque

Examples:
((p,u,a),(q,e)) <= POP R , delete the symbol 'a' from right of the deque

((p,u,ab),(q,a)) <= POP R , delete the symbol 'b' from right of the deque

((p,u,ba),(q,b)) <= POP R , delete the symbol 'a' from right of the deque

((p,u,b),(q,e)) <= POP R , delete the symbol 'b' from right of the deque

Where   {p,q}εQ

u ε∑*

{a,b}εζ

4.POP L : Removing or deleting an item from the left of the queue

Examples:
((p,u,a),(q,e)) <= POP L ,means delete the symbol 'a' from the left of the deque

((p,u,ab),(q,b)) <= POP L means delete the symbol 'a' from the left of the deque

((p,u,ba),(q,a)) <= POP L, means delete the symbol 'b' from the left of the deque

((p,u,b),(q,e)) <= POP L, means delete the symbol 'b' from the left of the deque

((p,u,e),(q,e)) <= POP L, means no symbol is present deque to delete and 'q' is the halting state.

5.SENSE R : Read the character from the input tape on the right of the current position of read head.

6.SENSE L:Read the input symbol on the left of the current position of the reading head.

IV. Representation of the deque

We can represent the transitions of the deque by following the notation Q X $\sum$* X ζ* where the first component is the machine state, second component is the input symbols, and the third component is the alphabets of deque reading from left to right. For example

Consider the notation (p,abc,ABC) 'p' is the present state 'abc' is the input string to be read,'ABC' is the content of the deque read from front to rear.

V. Deriving the other models from Deque

1. Queue automata from Deque: If we want to perform queue automata on deque we have to made some assumptions and these assumptions are restrict the use of deque operations only to PUSH L,POP R, and SENSE R.

Example: $L=a^n b^n$ (n>0) the instantaneous descriptions are as follows

$((q_0,a,e),(q_1,a))$ <=SENSE R,PUSH L

$((q_1,a,a),(q_1,a))$ <=SENSE R,PUSH L

$((q_1,b,a),(q_2,e))$ <=POP R

$((q_2,u ,e),(q_3,e))$ <=POP R

Where Q= $\{q_0, q_1, q_2, q_3\}$

$\qquad$ $\sum=\{a,b\}$

$\qquad$ $\zeta=\{a\}$

$\qquad$ S=q_0

$\qquad$ F=q_3

2. Push down automata from deque: If the deque is compelled to use only PUSH L, POP L, SENSE R then the deque can be   treated as PDA. Let take the same example $L=a^n b^n$(n>0) The instantaneous descriptions are as follows

$\qquad$ $((q_0,a,e),(q_1,a))$ <= SENSE R,PUSH L

$\qquad$ $((q_1,a,a),(q_1,a))$ <= SENSE R,PUSH L

$\qquad$ $((q_1,b,a),(q_2,e))$ <= POP L

$\qquad$ $((q_2,u ,e),(q_3,e))$ <= POPL

Where Q= $\{q_0, q_1, q_2, q_3\}$

$\qquad$ $\sum=\{a,b\}$

$\qquad$ $\zeta=\{a\}$

$\qquad$ S=q_0
$\qquad$ F=q_3

3. Finite automata from the Deque automata: In finite automata there are two cases, the first case is DFA and the second Case is NFA. Every finite automata can be viewed as a Deque automata having no operation on the deque.

Let M=(Q,$\sum$,ζ,δ,q_0,F) be a DFA

M^I=(Q,$\sum$,ζ,δ^I,q_0,F) be aDeque automata

Case :1 To accept languages accepted by the DFA, the transition function δ^1 is defined as

$$\delta^1 = \{ ((p,u,e),(q,e)) : (p,u,q) \; \varepsilon \; \delta \}$$

Example : consider the regular language that accept three successive zeros

The transitions are (δ) : (q_0, 1) = (q_0)

(q_0,0) = (q_1)

(q_1,0) = (q_2)

(q_2,0) = (q_3)   Here q_3 is the final state.

Case : 2 Any NFA can be converted to an equivalent DFA and the DFA is derived from the Deque automata.

4. Turing machine from the Deque automata : To derive Turing machine from the deque we need to perform all operations of Deque .Let us consider an example L= $a^n b^n c^n$,and the

instantaneous descriptions are as follows

($(q_0$,a,e),(q_1,a))   <=SENSE R,PUSSH L

($(q_1$,a,a),(q_1,a))   <=SENSE R,PUSH L

($(q_1$,b,a),(q_2,b))   <= SENSE R ,PUSH R

($(q_2$,b ,b),(q_2, b))   <= SENSE R,PUSH R

($(q_2$,c,a&b),(q_3,e))   <= POP L and POP R

($(q_3$,u ,be (q_4, b))   <= POP L and POP R   here q_4 is the final state

VI.Conclusions
In this paper from deque automata how remaining automatas are derived is described. The simulation results for all formal languages are also shown.

VII. Future scope
Researches are going on with deque of deque to find the intersection between the deque   automata

References
[1].   *Introduction to automata theory languages and computation by ULLAMAN*
[2].   Bhattacharjee, A.,and Debnath, B.K.,"Queue Automata ".

Numerical Solution of Heat and Mass Transfer with thermal radiation and MHD Boundary layer flow over a Stretching Surface with Suction/Injection

Navneet joshi[1] ̧ Manoj Kumar[2] and Sandeep K. Budhani[3]

Abstract

In this research the researchers studied and made an analysis to the effects of suction/Injection, MHD and thermal radiation on mass transfer characteristics over stretching surface. The magneto hydrodynamic flow over a stretching surface with heat and mass transfer, chemical reaction, radiation has been studied. The system of non-linear differential equations has been obtained and transformed in to set of ordinary differential equations with the help of similarity transformation for the governing flow. This set of ODEs has been solved and results have carried out for different values of the various physical parameters involved in the problem. The results showing the effect of various physical parameters on velocity temperature and concentration profiles have been obtained and presented graphically. The velocity decreases with increasing effect of magnetic parameter while with the increase in radiation parameter, the velocity increases. The mass and momentum transport in laminar boundary layer on moving, stationary and linearly stretching surface has important applications in polymer industry and electrochemistry.

Key Words: Heat and Mass Transfer, MHD flow, chemical reaction, Radiation, Runge-Kutta method with shooting echnique.
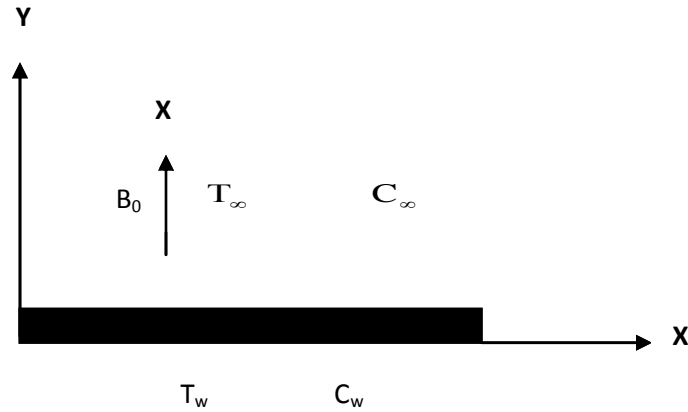
1. Department of Mathematics, Graphic Era Hill University, Sattal Road, Bhimtal (Nainital).
2. Department of Mathematics, Statistics &Computer Science G.B. Pant University of Agriculture and Technology, Pantnagar-263 145 Uttarakhand, India
3. Department of Computer Scienc, Graphic Era Hill University, Sattal Road, Bhimtal (Nainital).

Introduction

The boundary-layer flow over a continuously stretching surface moving with a certain velocity in an otherwise quiescent fluid medium is an often-encountered flow in many engineering processes. There are lots of applications in industries such as the hot rolling, wire drawing, glass fiber production and so on [1]–[3]. The pioneer work in this area was done by Sakiadis [4], [5]. He described the boundary layer assumptions and governing equations of the problem, and the boundary-layer flow on a continuously stretching surface with a certain speed was investigated. His work was further verified by Tsou et al. [6] experimentally. At the same time, the thermal boundary layer for this flow configuration with constant wall temperature was also discussed [6]. For these investigations, the boundary conditions on the surface were extended by other researchers [7]–[11].Fang [12] studied the influence of property variation on the boundary layers of a stretching surface. The effect of thermal radiation on the heat transfer over a nonlinearly stretching sheet immersed in an otherwise quiescent fluid has been studied by Bataller [13]. Exact solution of mass transfer over a stretching surface with chemical reaction and suction/ injection has been studied by Hassan [14]. Joshi and Kumar [15] described the combined effect of chemical reaction, radiation and MHD on mixed convection heat and mass transfer along a vertical moving surface. The purpose of this investigation is to study the effects of MHD, convection and radiation over a stretching surface.

Mathematical Formulation

The steady, laminar, incompressible and viscous fluid on a continuous stretching surface with MHD, convection and radiation has been considered. The fluid properties are assumed to be constant in a limited temperature range. The concentration of diffusing species is very small in comparison to other chemical species, the concentration of species far from the surface. The chemical reactions are taking place in the flow and all physical properties are assumed to be constant. The x-axis runs along the continuous surface in the direction of the motion and the
y-axis is perpendicular to it. Under Boussinesq approximation the equations governing the flow are:

$$\frac{\partial u}{\partial x} + \frac{\partial v}{\partial y} = 0 \tag{1}$$

$$u\frac{\partial u}{\partial x} + v\frac{\partial u}{\partial y} = v\frac{\partial^2 u}{\partial y^2} - \frac{\sigma B_0^2}{\rho}u \tag{2}$$

$$u\frac{\partial T}{\partial x} + v\frac{\partial T}{\partial y} = \frac{k}{\rho C_p}\frac{\partial^2 T}{\partial y^2} - \frac{1}{\rho C_p}\frac{\partial q_r}{\partial y}$$

$$(3)$$

$$u\frac{\partial C}{\partial x} + v\frac{\partial C}{\partial y} = D\frac{\partial^2 C}{\partial y^2} - k_1(C - C_\infty) \tag{4}$$

where u, v are the velocity components along x and y directions, v is the kinematics viscosity, k is the thermal diffusivity, β is the volumetric coefficient of expansion for heat transfer, ρ is the density, σ is the electrical conductivity of the fluid, g is acceleration due to gravity, T is the temperature, T_∞ is the temperature of the fluid far away from the surface, C_∞ is the concentration of the fluid far away from the surface, D is the molecular diffusivity, k_1 is the first order chemical reaction, with the boundary conditions:

$$u = Ax \qquad v = v_w \qquad T = T_w \qquad C = C_w \qquad \text{at y=0} \tag{5}$$

$$u = 0 \qquad T = T_\infty \qquad C = C_\infty \qquad \text{as y=}\infty \tag{6}$$

Introducing the similarity variables and non-dimensional parameters:

$$\eta = y\sqrt{\frac{A}{v}} \qquad \psi = \sqrt{Av}xf(\eta) \qquad \theta(\eta) = \frac{T - T_\infty}{T_w - T_\infty} \qquad \varphi(\eta) = \frac{C - C_\infty}{C_w - C_\infty}$$

Where , $\quad v = -\sqrt{Av}f(\eta)$

$$M = \frac{\sigma B_0^2}{\rho A}, \qquad u = Axf'(\eta), \qquad S_c = \frac{v}{D},$$

$$P_r = \frac{v}{\alpha}, \qquad R = \frac{4\sigma\sigma_\infty^3}{kx}, \qquad L = \frac{k_1 S_c}{A} \tag{7}$$

Where Pr is Prandal number, L is chemical reaction parameter, M is magnetic parameter and Sc is Schmidt number. The values of Grashof number for heat transfer and mass transfer are Gr and Gc respectively.
Using equation (7), equations (2), (3) and (4) reduce to:

$$f''' + ff'' - (f')^2 - Mf' = 0 \tag{8}$$

$$\frac{1}{P_r}\left(1 + \frac{4}{3}R\right)\theta'' + f\theta' = 0 \tag{9}$$

$$\varphi'' + fS_c\varphi' - L\varphi = 0 \tag{10}$$

The corresponding initial and boundary conditions are:

$$f' = 1, \quad f = f_w, \qquad \theta = 1, \qquad \varphi = 1, \quad \text{at} \qquad \eta = 0$$
$$f' = 0, \qquad\qquad\quad \theta = 0, \qquad \varphi = 0 \quad \text{as} \qquad \eta = \infty \tag{11}$$

Results and discussion

The non-linear ordinary differential equations (8)-(10) with boundary conditions (11) have been solved by using fourth order Runge-Kutta method with shooting technique for various values of physical parameters. The effects of these parameters on the velocity, temperature and concentration profiles have been analyzed with the help of graphical representation through figures 1-8. Figures 1, 2 and 3 show that the velocity decreases with an increase in magnetic parameter, Schmidt number and Prandal number respectively. Figures 4 shows that the velocity increases with an increase in radiation parameter and heat and mass transfer parameter.The temperature increases with an increase in the radiation parameter as shown in figure 5. Figures 6 and 7 show that the concentration decreases with an increase in chemical reaction parameter, and Schmidt number. The temperature decreases with increasing values of the Prandal number as shown in figure 8. There is no significant effect seen in velocity for chemical reaction parameter and in temperature for Schmidt number, chemical reaction parameter and magnetic parameter.
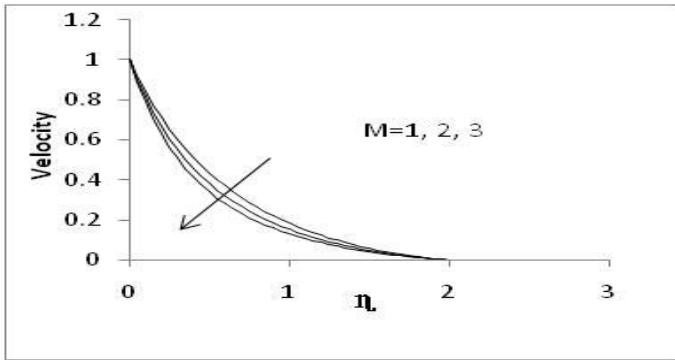

Figure. 1. Velocity profile with Magnetic parameter for Gr=1, Gc=1, R=0.5, Pr=0.71, Sc=0.2, L=0.2
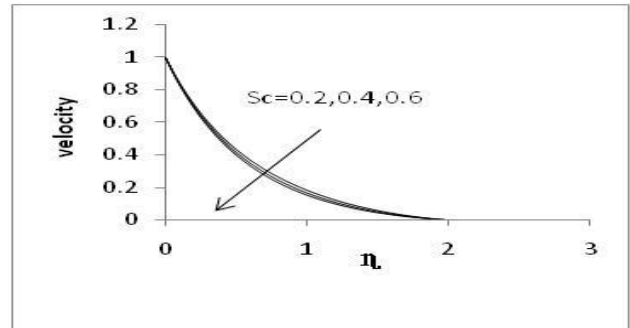

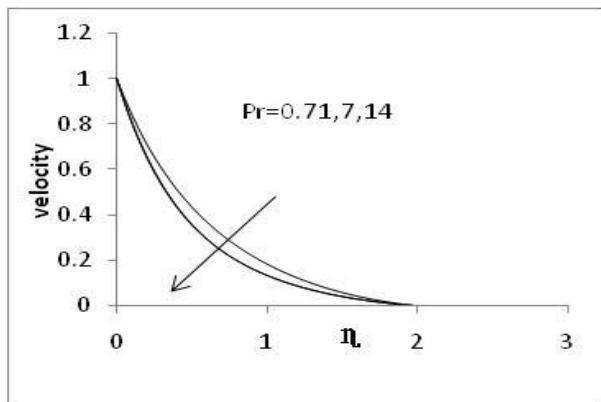**Figure. 2. Velocity profile with Schmidt number for M=1, Gr=1, Gc=1, R=0.5, Pr=0.71, L=0.2**

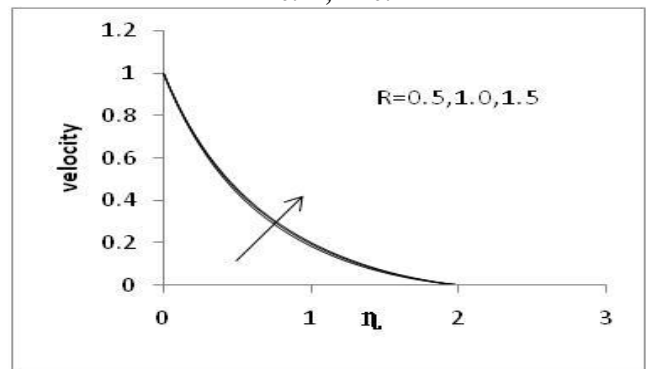**Figure3.Velocity profile with Prandtl**

Figure4. Velocity profile with

number for M=1, Gr=1, Gc=1, R=0.5, Sc=0.2, L=0.2

Radiation parameter for M=1, Gr=1, Gc=1, Pr=0.71, Sc=0.2, L=0.2

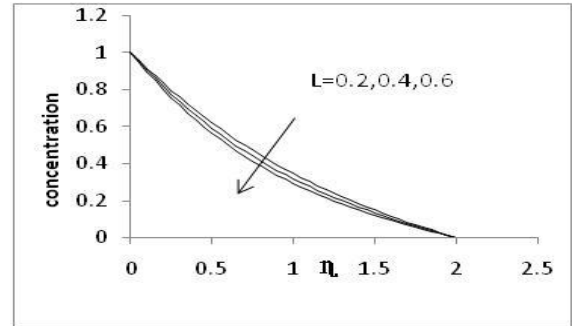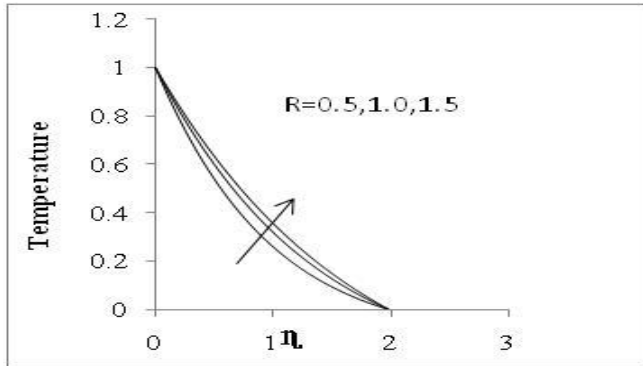**Figure5.Temperature profile with Radiation parameter for M=1, Gr=1,Gc=1, Pr=0.71, Sc=0.2, L=0.2**

Figure6. Concentration profile with Chemical reaction parameter for M=1, Gr=1,Gc=1,R=0.5, Pr=0.71, Sc=0.2,
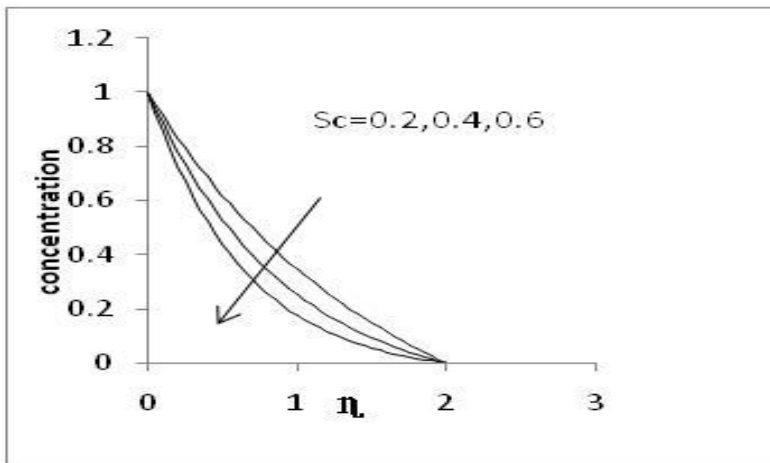

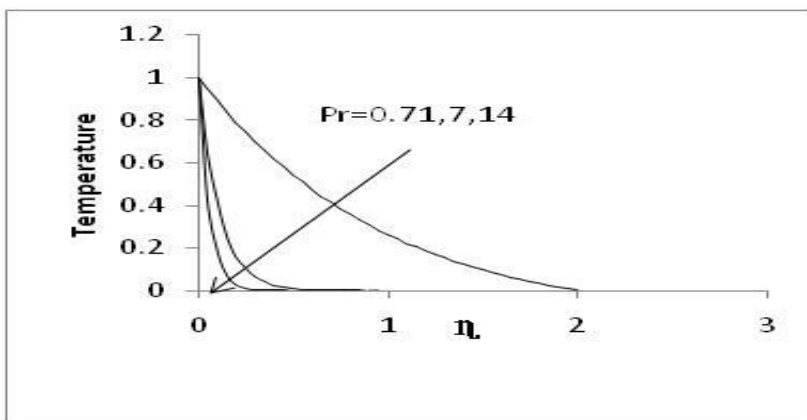**Figure7. Concentration profile with Schmidt number for M=1, Gr=1,Gc=1, R=0.5, Pr=0.71, L=0.2,**

Figure8. Temperature profile with Prandal number for M=1,Gr=1,Gc=1, R=0.5,Sc=0.2, L=0.2,

References

[1]   Altan, T., Oh, S., Gegel, H.: Metal forming fundamentals and applications. Metals Park: American Society of Metals 1979.

[2]   Fisher, E. G.: Extrusion of plastics. New York: Wiley 1976.

[3]   Tadmor, Z., Klein, I.: Engineering principles of plasticating extrusion. Polymer Science and Engineering Series. New York: Van Nostrand Reinhold 1970.

[4]   Sakiadis, B. C.: Boundary-layer behavior on continuous solid surface: I. Boundary-layer equations for two-dimensional and axisymmetric flow. J. AIChe 7, 26–28 (1961).

[5]   Sakiadis, B. C.: Boundary-layer behavior on continuous solid surface: I. Boundary-layer equations for two-dimensional and axisymmetric flow. J. AIChe 7, 221–225 (1961).

[6]   Tsou, F. K., Sparrow, E.M., Goldstain, R.J.: Flow and heat transfer in the boundary layer on a continuous moving surface. Int. J Heat Mass Transfer 10, 219–235 (1967).

[7]   Dutta, B. K., Roy, P., Gupta, A. S.: Temperature field in flow over a stretching sheet with uniform heat flux. Int. Comm. Heat Mass Transfer 12, 89–94 (1985).

[8]   Grubka, L. J. Bobba, K. M.: Heat transfer characteristics of a continuous stretching surface with variable temperature. ASME J. Heat Transfer 107, 248–250 (1985).

[9]   Chen, C. K., Char, M. I.: Heat transfer of a continuous stretching surface with suction and blowing. J. Math. Anal. Appl. 135, 568–580 (1988).

[10] Ali, M. E.. The effect of variable viscosity on mixed convection heat transfer along a vertical moving surface. *International Journal of Thermal Science*. 45: 60-69 (2006) .

[11] Elbashbeshy, E. M. A.: Heat transfer over a stretching surface with variable surface heat flux. J. Phys. D: Appl. Phys. 31, 1951–1954 (1998).

[12] Fang, T.: Influences of fluid property variation on the boundary layers of a stretching surface. *Acta Mechanica*. 171,105-118(2004).

[13] Bataller, R.C.: Similarity solutions for flow and heat transfer of a quiescent fluid over a nonlinearly stretching surface. *Mater*.Process.Technol. 203,176-183(2008).

[14] Hassan,A.M, El-Arabawy.: Exact Solutions of Mass Transfer Over a Stretching Surface with Chemical Reaction and Suction/Injuction. *Journal of Mathematics and statistics* 5(3):159-166(2009).

[15] Joshi, N. Kumar, M.: The combined effect of chemical reaction, radiation MHD on mixed convection heat and mass transfer along a vertical moving surface. *Applications of Applied Mathematics* 5, 1631-1640 (2010).

DESIGN OF PULSE TRIGGERED FLIP FLOP USING PULSE ENHANCEMENT SCHEME

A.Selvakumar[1]   T.Prabakaran[2]

[1]P.G Student/VLSI Design, SNS College of Technology, Coimbatore, Tamilnadu.
[2]Associate Professor, Dept. of ECE, SNS College of Technology, Coimbatore, Tamilnadu.

Abstract

For the past several years, much progress has been made in Low power VLSI Design .In This paper ,a novel low-power pulse Triggered flip- flop design is presented. First, the pulse generation control logic an AND function, is removed from critical path to facilitate a faster discharge operation. A simple two-transistor AND gate design is used to reduce the circuit complexity. Second, a conditional pulse-enhancement technique is devised to speed up the discharge along the critical path only when needed. As a result, transistor sizes in delay inverter and pulse-generation circuit can be reduced for saving. Various post layout simulation results based on UMC CMOS 90-nm technology reveal that the proposed design features the best power-delay-product performance in four FF designs under comparison.

Keywords: Flip flop, low power and pulse-triggered

I Introduction

Flip-Flops (FFs) are the basic storage elements used extensively in all kinds of digital designs. In particular, digital designs nowadays often adopt intensive pipelining techniques and employ many FF-rich modules. It is also estimated that the power consumption of clock system, which consists of clock distribution networks and storage elements, is as high as 20%-45% of the total system power[1]. In recent VLSI's, a clocking system, including clock interconnections and flip flops. This is partially because the activation ratio of a clock system is unity. In this clocking system power, 90% is consumed by the last branches of the clock distribution network which derive directly F/F's and the F/F's themselves. P-FF has been considered a popular alternative to the conventional master-slave based FF in the application of high speed operations[2]. High performance flip flops are key elements in the design of contemporary high-speed integrated circuits. In these circuits, high clock frequencies are generally gained by using a fine grain pipeline in which only few logic levels are inserted between pipeline stages. In this paper, we will present a novel low-power implicit-type P-FF design featuring a conditional pulse-enhancement scheme. Three additional transistors are employed to support this feature. In spite of a slight increase in total transistor count, transistors of the pulse generation logic benefit from significant size reductions and the overall layout area is even slightly reduced.

II Implicit-Type P-FF Design With Pulse Control Scheme
Conventional Implicit-Type P-Ff Designs:

1. ip-DCO

Some conventional implicit-type P-FF designs, which are used as the reference designs in later performance comparisons, are first reviewed. A state-of-the-art P-FF design, named ip-DCO, is given in Fig 1(a) [6]. It contains an AND logic-based pulse generator and a semi-dynamic structured latch design. Inverters I5 and I6 are used to latch data and inverters I7 and I8 are used to hold the internal node. The pulse generator takes complementary and delay skewed clock signals to generate a transparent window equal in size to the delay by inverters I1-I3. Two practical problems exist in this design. First, during the rising edge, nMOS transistors N2 and N3 are turned on.
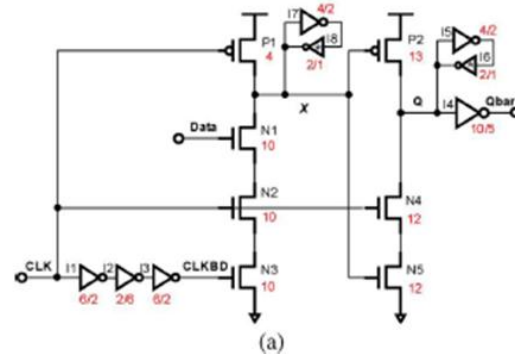
Fig. 1(a) ip-DCO

2. Mhllf:

An improved P-FF design, named MHLLF Fig.1 (b) MHLLF, by employing a static latch structure presented in [10]. Node is no longer pre charged periodically by the clock signal. A weak pull-up transistor P1 controlled by the FF output signal Q is used to maintain the node level at high when Q is zero. This design eliminates the unnecessary discharging problem at node. However, it encounters a longer Data-to-Q (D-to-Q) delay during "0" to "1" transitions because node is not pre-discharged. Larger transistors N3 and N4 are required to enhance the discharging capability. Another drawback of this design is that node   becomes floating when output Q and input Data

both   equal
to "1". Extra DC power emerges if node X is drifted from an   intact
"1".

Fig. 1(b) MHLLF

3. SCCER:
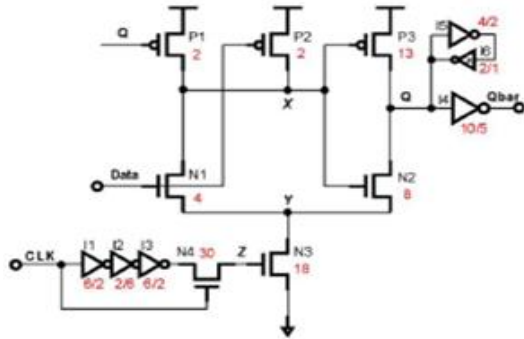
A refined low power P-FF design named SCCER using a conditional discharged technique [9], [8]. In this design, the keeper logic (back-to-back inverters I7 and I8 in Fig. 1(a) is replaced by a weak pull up transistor P1 in conjunction with an inverter I2 to reduce the load capacitance of node [8]. The discharge path contains nMOS transistors N2 and N1 connected in series. In order to eliminate superfluous switching at node, an extra nMOS transistor N3 is employed. Since N3 is controlled by Q_fdbk, no discharge occurs if input data remains high. The worst case timing of this design occurs when input data is "1" and node   is discharged through four transistors in series, i.e., N1 through N4, while combating with the pull up transistor P1. A powerful pull-down circuitry is thus needed to ensure node can be properly discharged.
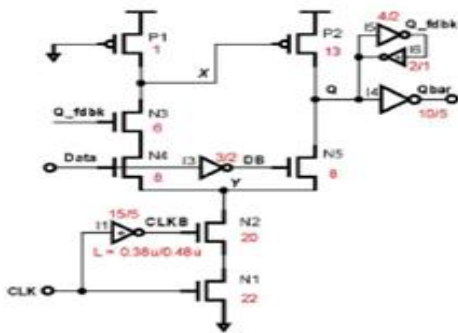

Fig. 1(c) SCCER

This implies wider N1 and N2 transistors and a longer delay from the delay inverter I1 to widen the discharge pulse width.

III Simulation Results

A simulation window appears with inputs and output. The power consumption is also shown on the right bottom portion of the window. If you are unable to meet the specifications of the circuit change the transistor sizes. Generate the layout again and run the simulations till you achieve your target delays. Depending on the input sequences assigned at the input the output is observed in the simulation.

To demonstrate the superiority of the proposed design, post layout simulations on various P-FF designs were conducted to obtain their performance figures. These designs include the three P-FF designs shown in Fig. 1 (ip-DCO [6], MHLLF [9], SCCER [10]), another P-FF design called conditional capture FF (CCFF) [7], and two other non-pulse-triggered FF designs, i.e., a sense-amplifier-based FF (SAFF) [2], and a conventional transmission gate-based FF (TGFF). The target technology is the UMC 90-nm CMOS process. The operating condition used in simulations is 500 MHz/1.0 V. Since pulse width design is crucial to the correctness of data capturing as well as the power consumption, the pulse generator logic in all designs are first sized to function properly across process variation. All designs are further optimized subject to the tradeoff between power   and   D-to-Q   delay,   i.e., minimizing the product of the two terms.
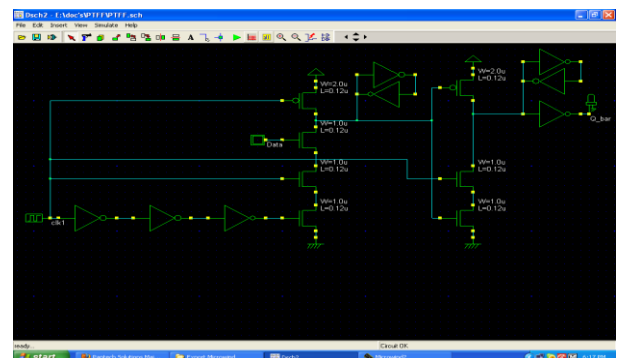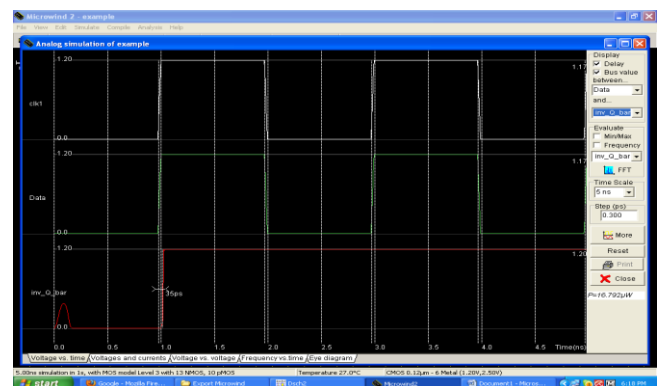

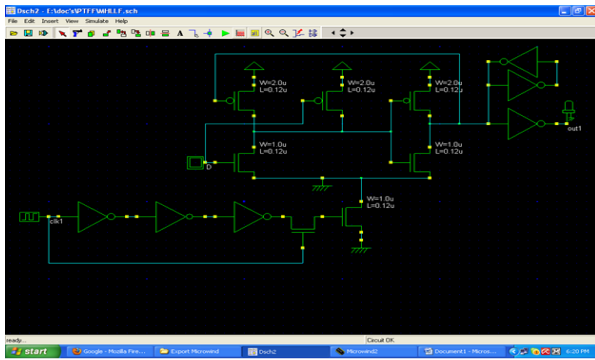**Fig. 2**(a) ip-DCO in Microwind

Fig. 2(b) ip-DCO waveform in Microwind

Fig. 2(c) **MHLLF** in Microwind
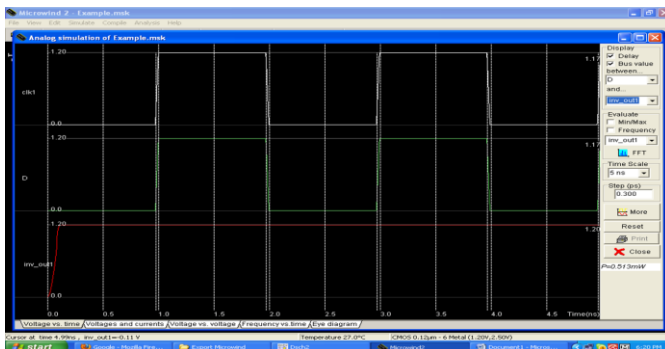

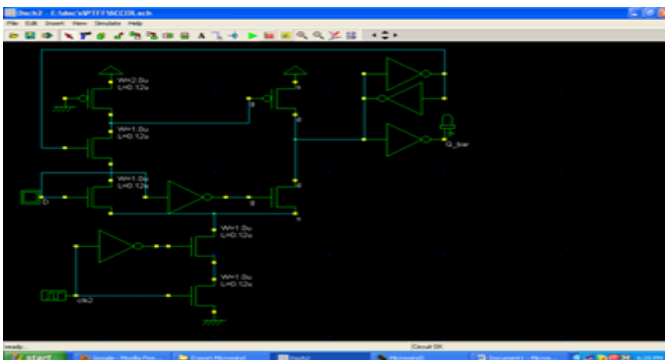**Fig. 2**(d) **MHLLF** waveform in Microwind

Fig. 2(e) SCCER in Microwind
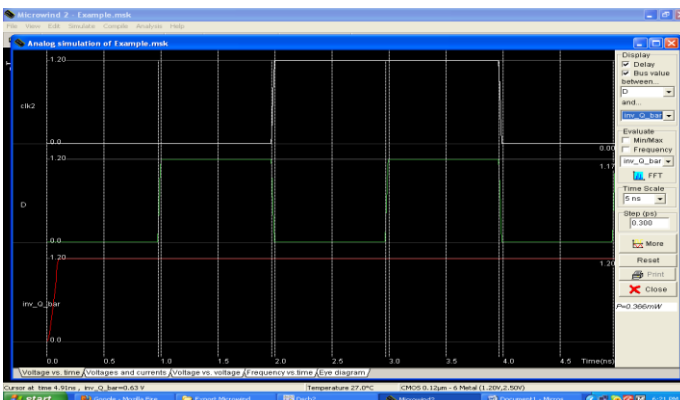
Fig. 2(f) SCCER waveform in Microwind

These are the simulation block and its results of ip-DCO, MHLLF and SCCER in Microwind.

IV Comparison Table

P-FF	ip-DCO	MHLLF	SCCER
No of transistors/lay out area(μm^2)	23/91.88	19/93.02	17/80.07
Average power(μw)	42.20	35.96	36.27
Optimal power delay product	4.22	4.89	3.19

Table: 1 Comparison of designed methods

From the designed methods the various parameters are tabulated and compared. With this comparison results the SCCER performed better than other two designed methods.

V Conclusion

In this paper, the various Flip flop design like, ip-DCO, MHLLF and SCCER are discussed. These were been also designed in Wicrowind tool and those result waveforms are also discussed. The comparison table also added to verify the designed methods. With these all results SCCER performed better than ip-DCO and MHLLF designs.

VI Future work

To improve the performance design of the P-Flip flop, The Pulse enhancement scheme will be designed and also these results will be discussed with the existing pulse trigger Flip Flop.

References

[1] H. Kawaguchi and T. Sakurai, "A reduced clock-swing flip-flop (RCSFF) for 63% power reduction," IEEE J. Solid-State Circuits, vol.33, no. 5, pp. 807-811, May 1998.

[2] A. G. M. Strollo, D. De Caro, E. Napoli, and N. Petra, "A novel high speed sense-amplifier-based flip-flop," IEEE Trans. Very Large Scale Integr. (VLSI) Syst., vol. 13, no. 11, pp. 1266-1274, Nov. 2005.

[3] H. Partovi, R. Burd, U. Salim, F. Weber, L. DiGregorio, and D. Draper, "Flow-through latch and edge-triggered flip-flop hybrid elements," in IEEE Tech. Dig. ISSCC, 1996, pp. 138-139.

[4] F. Klass, C. Amir, A. Das, K. Aingaran, C. Truong, R. Wang, A. Mehta, R. Heald, and G. Yee, "A new family of semi-dynamic and dynamic flip flops with embedded logic for high-performance processors," IEEE J. Solid-State Circuits, vol. 34, no. 5, pp. 712-716, May 1999.

[5] S. D. Naffziger, G. Colon-Bonet, T. Fischer, R. Riedlinger, T. J. Sullivan, and T. Grutkowski, "The implementation of the Itanium 2 microprocessor," IEEE J. Solid-State Circuits, vol. 37, no. 11, pp.1448-1460, Nov. 2002.

[6] J. Tschanz, S. Narendra, Z. Chen, S. Borkar, M. Sachdev, and V. De, "Comparative delay and energy of single edge-triggered and dual edge triggered pulsed flip-flops for high-performance microprocessors," in Proc. ISPLED, 2001, pp. 207-212.

[7] B. Kong, S. Kim, and Y. Jun, "Conditional-capture flip-flop for statis- tical power reduction," IEEE J. Solid-State Circuits, vol. 36, no. 8, pp.1263-1271, Aug. 2001.

[8] N. Nedovic, M. Aleksic, and V. G. Oklobdzija"Conditional precharge techniques for power-efficient dual-edge clocking," in Proc. Int. Symp. Low-Power Electron. Design, Monterey, CA, Aug. 12-14, 2002, pp. 56-59.

[9] P. Zhao, T. Darwish, and M. Bayoumi, "High-performance and low power conditional discharge flip-flop," IEEE Trans. Very Large Scale Integr. (VLSI) Syst., vol. 12, no. 5, pp. 477-484, May 2004.

[10] C. K. Teh, M. Hamada, T. Fujita, H. Hara, N. Ikumi, and Y. Oowaki, "Conditional data mapping flip-flops for low-power and high-perfor-mance systems," IEEE Trans. Very Large Scale Integr. (VLSI) Systems, vol. 14, pp. 1379-1383, Dec. 2006.

AUGMENTED REALITY ON GPS NAVIGATION (ARGPS)

Murugavel. KN[1]

[1](Asst. Professor, Department of Computer Science and Engineering,
Birla Institute of Technology-UAE Campus, CIIHE, Ras Al Khaimah, UAE)

Abstract

Augmented Reality is a new and upcoming field of technology aimed at providing information to the user via Optical methods. It consists of portable hardware and light software that enable the user to get extra information about his environment that would generally require a desktop computer or some form of a handheld device. Augmented Reality GPS Navigation is a conceptual project that is aimed at creating an Augmented Reality Interface and implementing a GPS based navigation application.

Keywords –Gult, Xact, Glew, Glee, Glaux, Ar.

I. INTRODUCTION

WHAT IS AUGMENTED REALITY

Augmented reality (AR) is a term for a live direct or indirect view of a physical real-world environment whose elements are *augmented* by virtual computer-generated imagery. It is related to a more general concept called mediated reality in which a view of reality is modified (possibly even diminished rather than augmented) by a computer. As a result, the technology functions by enhancing one's current perception of reality. In the case of Augmented Reality, the augmentation is conventionally in real-time and in semantic context with environmental elements, such as sports scores on TV during a match. With the help of advanced AR technology (e.g. adding computer vision and object recognition) the information about the surrounding real world of the user becomes interactive and digitally usable. Artificial information about the environment and the objects in it can be stored and retrieved as an information layer on top of the real world view.

Augmented reality research explores the application of computer-generated imagery in live-video streams as a way to expand the real-world. Advanced research includes use of *Head Mounted Displays (HMD)*[2] and *Virtual Retinal Displays*[6] for visualization purposes, and construction of controlled environments containing *any number of sensors and actuators*.

II. USES OF AUGMENTED REALITY

Augmented Reality is a group of technologies that provide the user with information about the environment via optical manipulation. It allows the user to have more accurate and detailed information about the object or scene

they are looking at. In a day where information exchange must be fast, accurate and easily available, augmented reality is crucial in delivering the said information in an easy, user friendly method without the need of a handheld device[8] or personal computer.

Potential uses of Augmented Reality include:

- **Advertising:** Marketers started to use AR to promote products via interactive AR applications. For example, at the 2008 LA Auto Show, Nissan unveiled the concept vehicle Cube and presented visitors with a brochure which, when held against a webcam, showed several versions of the vehicle. In August 2009, Best Buy ran a circular with an augmented reality code that allowed users with a webcam to interact with the product in 3D[7].

- **Support with complex tasks:** Complex tasks such as assembly, maintenance, and surgery can be simplified by inserting additional information into the field of view. For example, labels can be displayed on parts of a system to clarify operating instructions for a mechanic who is performing maintenance on the system.AR can include images of hidden objects, which can be particularly effective for medical diagnostics or surgery. Examples include a virtual X-ray view based on prior tomography or on real time images from ultrasound or open NMR devices[5]. A doctor could observe the fetus inside the mother's womb.

- **Navigation devices:** AR can augment the effectiveness of navigation devices for a variety of applications. For example, building navigation can be enhanced for the purpose of maintaining industrial plants. Outdoor navigation can be augmented for military operations or disaster management. Head-up displays or personal display glasses in automobiles can be used to provide navigation hints and traffic information. These types of displays can be useful for

airplane pilots, too. Head-up displays are currently used in fighter jets as one of the first AR applications. These include full interactivity, including eye pointing.

- **Industrial Applications:** AR can be used to compare the data of digital mock-ups with physical mock-ups for efficiently finding discrepancies between the two sources. It can further be employed to safeguard digital data in combination with existing real prototypes, and thus save or minimize the building of real prototypes and improve the quality of the final product.

- **Military and emergency services:** AR can be applied to military and emergency services as wearable systems to provide information such as instructions, maps, enemy locations, and fire cells.

- **Prospecting:** In the fields of hydrology, ecology, and geology, AR can be used to display an interactive analysis of terrain characteristics. Users could use, and collaboratively modify and analyze, interactive three-dimensional maps.

- **Art:** AR can be incorporated into artistic applications that allow artists to create art in real time over reality such as painting, drawing, modeling, etc. One such example of this phenomenon is called Eye-writer that was developed in 2009 by Zachary Lieberman and a group formed by members of Free Art and Technology (FAT), Open Frameworks and the Graffiti Research Lab to help a graffiti artist, who became paralyzed, draw again.

- **Architecture:** AR can be employed to simulate planned construction projects.

- **Sightseeing:** Models may be created to include labels or text related to the objects/places visited. With AR, users can rebuild ruins, buildings, or even landscapes as they previously existed.

- **Collaboration:** AR can help facilitate collaboration among distributed team members via conferences with real and virtual participants. The Hand of God is a good example of a collaboration system.

- **Entertainment and education:** AR can be used in the fields of entertainment and education to create virtual objects in museums and exhibitions, theme park attractions (such as Cadbury World), and games (such as ARQuake[9] and The Eye of Judgment).

- **Music:** Pop group Duran included interactive AR projections into their stage show during their 2000 *Pop Trash* concert tour. Sydney band Lost Valentines launched the world's first interactive AR music video on 16 October 2009, where users could print out 5 markers representing a pre-recorded performance from each band member which they could interact with live and in real-time via their computer webcam and record as their own unique music video clips to share via YouTube.

III. FUTURE POSSIBILITES

Expanding a PC screen into the real environment: program windows and icons appear as virtual devices in real space and are eye or gesture operated[4], by gazing or pointing. A single personal display (glasses) could concurrently simulate a hundred conventional PC screens or application windows all around a user.

Virtual devices of all kinds, e.g. replacement of traditional screens, control panels, and entirely new applications impossible in "real" hardware, like 3D objects interactively changing their shape and appearance based on the current task or need[3].

Enhanced media applications, like pseudo holographic virtual screens, virtual surround cinema, virtual 'holodecks' (allowing computer-generated imagery to interact with live entertainers and audience)

Replacement of cell phone and car navigator screens: eye-dialing, insertion of information directly into the environment, e.g. guiding lines directly on the road, as well as enhancements like "X-ray"-views[5].

Virtual plants, wallpapers, panoramic views, artwork, decorations, illumination etc., enhancing everyday life. For example, a virtual window could be displayed on a regular wall showing a live feed of a camera placed on the exterior of the building, thus allowing the user to effectually toggle a wall's transparency[6].

With AR systems getting into mass market, we may see virtual window dressings, posters, traffic signs, Christmas decorations, advertisement towers and more. These may be fully interactive even at a distance, by eye pointing for example.

Virtual gadgetry becomes possible. Any physical device currently produced to assist in data-oriented tasks (such as the clock, radio, PC, arrival/departure board at an airport, stock ticker, PDA, PMP, informational posters/fliers/billboards, in-car navigation systems, etc.) could be replaced by virtual devices that cost nothing to produce aside from the cost of writing the software. Examples might be a virtual wall clock, a to-do list for the day docked by your bed for you to look at first thing in the morning, etc.

Subscribable group-specific AR feeds. For example, a manager on a construction site could create and dock instructions including diagrams in specific locations on the site. The workers could refer to this feed of AR items as they work. Another example could be patrons at a public event subscribing to a feed of direction and information oriented AR items.

AR systems can help the visually impaired navigate in a much better manner (combined with a text-to-speech software).

Computer games which make use of position and environment information to place virtual objects, opponents, and weapons overlaid in the player's visual field.

IV. DESIGN

GLUT simplifies the implementation of programs using OpenGL rendering. The GLUT application programming interface (API) requires very few routines to display a graphics scene rendered using OpenGL. The GLUT API (like the OpenGL API) is stateful. Most initial GLUT state is defined and the initial state is reasonable for simple programs. The GLUT routines also take relatively few parameters. No pointers are returned. The only pointers passed into GLUT are pointers to character strings (all strings passed to GLUT are copied, not referenced) and opaque font handles.

The GLUT API is (as much as reasonable) window system independent. For this reason, GLUT does not return *any* native window system handles, pointers, or other data structures. More subtle window system dependencies such as reliance on window system dependent fonts are avoided by GLUT; instead, GLUT supplies its own (limited) set of fonts. For programming ease, GLUT provides a simple menu sub-API. While the menu support is designed to be implemented as pop-up menus, GLUT gives window system leeway to support the menu functionality in another manner (pull-down menus for example).

Two of the most important pieces of GLUT state are the *current window* and *current menu*. Most window and menu routines affect the *current window* or *menu* respectively. Most callbacks implicitly set the *current window* and *menu* to the appropriate window or menu responsible for the callback. GLUT is designed so that a program with only a single window and/or menu will not need to keep track of any window or menu identifiers. This greatly simplifies very simple GLUT programs.

GLUT is designed for simple to moderately complex programs focused on OpenGL rendering. GLUT implements its own event loop. For this reason, mixing GLUT with other APIs that demand their own event handling structure may be difficult. The advantage of a built in event dispatch loop is simplicity.

GLUT contains routines for rendering fonts and geometric objects; however GLUT makes no claims on the OpenGL display list name space. For this reason, none of the GLUT rendering routines use OpenGL display lists. It is up to the GLUT programmer to compile the output from GLUT rendering routines into display lists if this is desired.

GLUT routines are logically organized into several sub-APIs according to their functionality.

The sub-APIs are

Initialization: Command line processing, window system initialization, and initial window creation state are controlled by these routines.

Beginning Event Processing: This routine enters GLUT's event processing loop. This routine never returns, and it continuously calls GLUT callbacks as necessary.

Window Management: These routines create and control windows.

Overlay Management: These routines establish and manage overlays for windows.

Menu Management: These routines create and control pop-up menus.

Callback Registration: These routines register callbacks to be called by the GLUT event processing loop.

Color Index Color-map Management: These routines allow the manipulation of color index color-maps for windows.

State Retrieval: These routines allow programs to retrieve state from GLUT.

Font Rendering: These routines allow rendering of stroke and bitmap fonts.

Geometric Shape Rendering: These routines allow the rendering of 3D geometric objects including spheres, cones, icosahedrons, and teapots[3].

V. ARTOOLKIT

ARToolKit is a C and C++ language software library that lets programmers easily develop Augmented Reality applications. Augmented Reality (AR) is the overlay of virtual computer graphics images on the real world, and has many potential applications in industrial and academic research.

One of the most difficult parts of developing an Augmented Reality application is precisely calculating the user's viewpoint in real time so that the virtual images are exactly aligned with real world objects. ARToolKit uses computer vision techniques to calculate the real camera position and orientation relative to marked cards, allowing the programmer to overlay virtual objects onto these cards. The fast, precise tracking provided by ARToolKit should enable the rapid development of many new and interesting AR applications[1].

ARToolKit is a software *ToolKit* like GLUT. It furnishes predefined functions that you need to call in a specific order for developing an AR program. But you can also use different parts of the ToolKit separately. ARToolKit[1] supports multiple platforms, while attempting to minimise library dependencies without sacrificing efficiency. ARToolKit uses OpenGL for the rendering part, GLUT for the windows/event handler aspect and hardware-dependent video library and standard API on each platform (e.g. win32 in Windows).

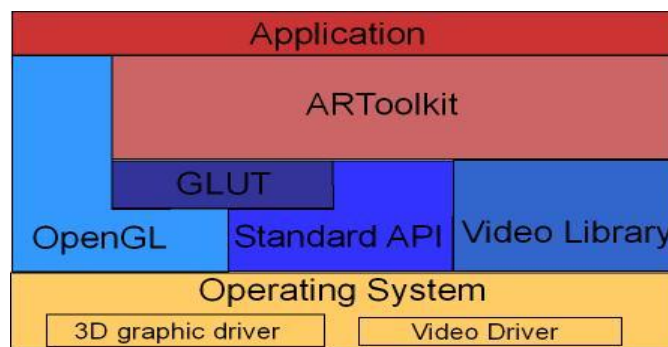Figure.1 summarizes the relationship between Application, ARToolKit and dependent libraries.

Figure 1: ARToolKit Architecture

VI. STRUCTURE

This section provides a better description of the main elements of ARToolKit[2].

The ARToolKit library consists of four modules:

- **AR module:** core module with marker tracking routines, calibration and parameter collection.

- **Video module:** A collection of video routines for capturing the video input frames. This is a wrapper around the standard platform SDK video capture routines.

- **Gsub module:** A collection of graphic routines based on the OpenGL and GLUT libraries.

- **Gsub_Lite module:** Replaces GSub with a more efficient collection of graphics routines, independent of any particular windowing toolkit.

The next figures show the hierarchical structure of ARToolKit and relation with dependencies libraries.
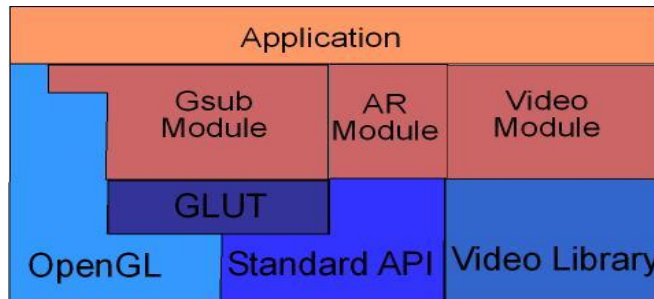
Figure 2: Hierarchical structure of ARToolKit using Gsub Module
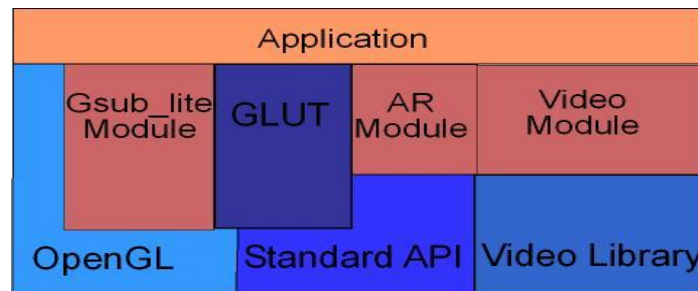
Figure 3: Hierarchical structure of ARToolKit using Gsub_Lite Module

The modules respect a global *pipeline metaphor* (video->tracking->display), so the user can easily replace any module with another (like gsub with Open Inventor renderer).
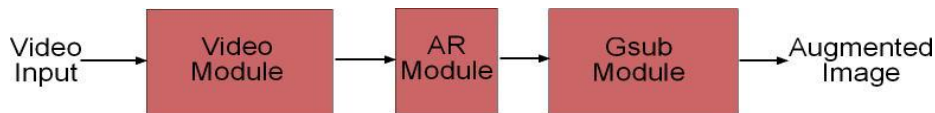
Figure 4: Main ARToolKit pipeline

VII. DATA TYPES

ARToolKit manipulates a lot of different kinds of variable. Internally, it uses global variables that restrict re-entrant part of the code. Otherwise, standard multi-argument interface are used based on a data-flow approach.

ARToolKit uses different image formats between different modules. Figure 4 summarises all the different formats supported. Some formats are only available on certain platforms or with certain hardware.
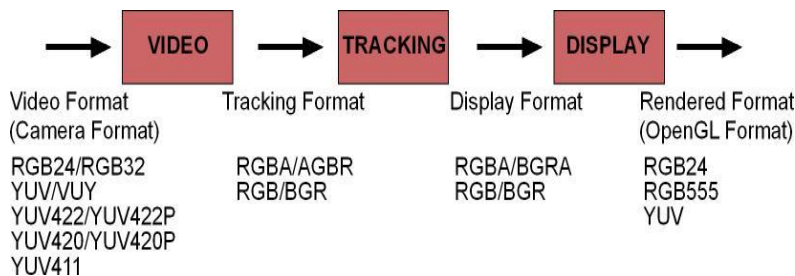
Figure 5: ARToolKit data-flow

VIII. PATTERN RECOGNITION ALGORITHM
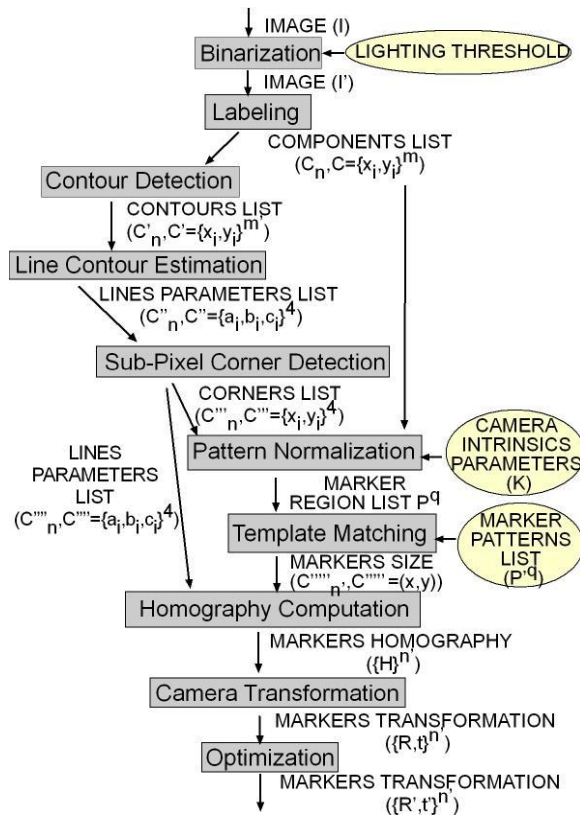
IX. THE WORKING OF THE APPLICATION
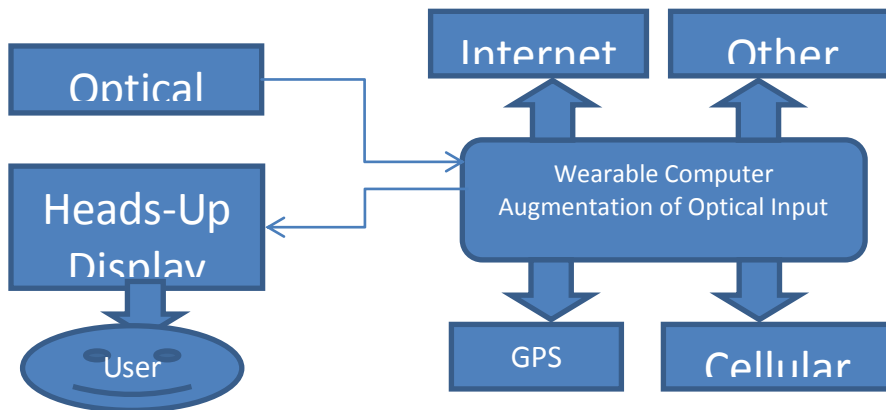
The Video module consists of the DirectX webcam library which is implemented by ARToolkit. The application opens a video stream to the webcam and captures video frame-by-frame and also displays it on the HUD. Each frame gets searched by the application for a pattern. If a pattern is present, it gets recognized and the display function associated to the pattern is called.

The GUI module is responsible for displaying all data to the HUD. It consists of OpenGL functions that enable creation of virtual objects as well as modification of the video window

The GPS device gets the co-ordinates and sends it to the application. Here, the co-ordinates are displayed on the screen as well as sent to the MAP application.

The Map application is an independent application utilizing C++ and Developers Image Library (DevIL). It gets the GPS co-ordinates and displays it on a map loaded from the hard disk.

X. LIST OF ABBREVIATIONS

➢ NMEA: National Marine Electronics Association.
➢ XACT: XInput and the Cross-platform Audio Creation Tool
➢ ARB: Architecture Review Board
➢ GLEW: OpenGL Extension Wrangler Library
➢ GLEE: OpenGL Easy Extension Library
➢ GLAux: OpenGL Auxiliary Library
➢ GLUT: OpenGL Utility Toolkit

XI. CONCLUSION

During the course of the project we have learned how to use an integrated developer environment (IDE) to create a standalone application. The OpenGL library, a major graphical library used in the mainstream market to create graphical applications for all sorts of platforms was successfully utilized to create the Heads up display interface as well as to display the video captured from the webcam. Pattern recognition was successfully implemented using ARToolkit's native library functions. The theory behind it was examined and understood. A new pattern was created and successfully recognized by the software. GPS was interfaced using a COM port, but due to closed source restrictions of certain libraries, we were unable to utilize it in the application. Source code using the library has been added to the application but it is defunctionate due to the library restrictions. The Map module has been successfully created and implemented as an independent application and utilizes the OpenGL and DevIL image libraries.

REFERENCES
Journal Papers:

[1] ARToolkit. http://www.hitl.washington.edu/research/ zhared_space

[2] Fuchs, Henry and Jeremy Ackerman. "Displays for Augmented Reality: Historical Remarks and Future Prospects." In *Proc. International Symposium on Mixed Reality,* pp.31-41, Yokohama, Japan, March 9-11, 1999.

[3] T. Kanade, et. al, "Virtualized reality: digitizing a 3D time-varying event as is and in real time," *Proc. Int'l Symp. Mixed Reality (ISMR '99). Mixed Reality-Merging Real and Virtual Worlds,* Yokohama, Japan, 9-11 Mar. 1999, pp. 41-57.

[4] Murray, Janet. *Hamlet on the Holodeck: The Future of Narrative in Cyberspace.* New York: Simon and Schuster, 1997.

[5] N. Navab, A. Bani-Hashem, M. Mitschke. "Merging Visible and Invisible: Two Camera-Augmented Mobile C-arm (CAMC) Applications," *Proc. 2nd Int'l Workshop Augmented Reality. (IWAR '99).* San Francisco, 20-21 Oct. 1999, pp. 134-141.

[6] H.L. Pryor, T.A. Furness, E. Viirre. "The Virtual Retinal Display: A New Display Technology Using Scanned Laser Light," *Proc. 42nd Human Factors Ergonomics Society.* Chicago, 5-9 Oct. 1998, pp. 1570-1574.

[7] R. Raskar, G. Welch, W-C. Chen, "Table-top spatially-augmented realty: Bringing physical models to life with projected imagery," *Proc. 2nd Int'l Workshop Augmented Reality. (IWAR '99).* San Francisco, 20-21 Oct. 1999, pp. 64-71.

[8] J. Rekimoto, "NaviCam: A Magnifying Glass Approach to Augmented Reality," *Presence: Teleoperators and Virtual Environments,* vol. 6, no. 4, Aug. 1997, pp. 399-412

[9] B. Thomas, et. al., "ARQuake: An Outdoor/Indoor Augmented Reality First Person Application," *Proc. 4th Int'l Symp. Wearable Computers. (ISWC 2000).* Atlanta, 16-17 Oct. 2000, pp. 139-146.

Issues Involved In Speech To Text Conversion

Er. Jaspreet Kaur*, Er. Nidhi**, Ms. Rupinderdeep Kaur***

*Department of Computer Science, SVIET, Banur
**Department of Computer Science, SVIET, Banur
***Department of Computer Science, Thapar University, Patiala

Abstract

This document presents various Speech Recognition issues in Indian script. STT synthesis is an online application to convert the speech into the text form. The term "voice recognition" is sometimes used to refer to recognition systems that must be trained to a particular speaker—as is the case for most desktop recognition software. Recognizing the speaker can simplify the task of translating speech. Speech recognition is the process of converting an acoustic waveform into the text similar to the information being conveyed by the speaker. Speech is the most natural way of communication. It includes the fundamentals of speech recognition & different issues like commands by using hyperlink, effectiveness, overlapping speech, low signal to noise ratio, homonyms.

1) Introduction

Speech is a natural mode of communication for people. We learn all the relevant skills during early childhood, without instruction, and we continue to rely on speech communication throughout our lives. Speech recognition is the ability of a machine or program to identify words and phrases in spoken language and convert them to a machine-readable format. Generally, transfer of information between human & machine is accomplished via keyboard, mouse etc. But human can speak more quickly instead of typing. Speech input offers high bandwidth information & relative ease of use. Speech recognition applications include call routing, speech-to-text, voice dialing and voice search. Speech recognition is a solution which refers to technology that can recognize speech without being targeted at single speaker such as a call center system that can recognize arbitrary voices. Speech recognition applications include voice user interfaces such as voice dialing (e.g., "Call home"), call routing (e.g., "I would like to make a collect call")[1,2] .

2) Punjabi Language

Punjabi is an Indo-Aryan language spoken by inhabitants of the historical Punjab region (north western India and in Pakistan). Punjabi is the modern form of Gurmukhi (in India) or Shahmukhi (in Pakistan).Gurmukhi means "from the mouth of the Guru"[3]. According to the Ethnologue[4] 2005 estimate, there are 88 million native speakers of the Punjabi language, which makes it approximately the 10th most widely spoken language in the world. In India, Punjabi is one of the 22 languages with official status in India. It is the first official language of Punjab (India) and Union Territory State Chandigarh and the 2nd official language of Haryana, Himachal Pradesh and Delhi. In Pakistan, Punjabi is the provincial language of Punjab(Pakistan) the second largest and the most populous province of Pakistan.

2.1 Character Set For Punjabi

Punjabi fonts containing the entire Punjabi character set, with simple input. It includes Vowels, Consonants & Auxiliary signs as follows [5]:

2.1.1 Vowels

There are nine vowel phonemes in Punjabi. They are vowels making only one sound. All consonants use the vowel. Table 1 shows the vowels.

	Vowel Sign		Name of vowel	
1.	Invisible		ਮੁਕਤਾ	muktā
2.	T		ਕੰਨਾ	kannā
3.	f		ਸਿਹਾਰੀ	sihārī
4.	ी		ਬਿਹਾਰੀ	bihārī
5.	ੁ		ਅੰਕੜ	auṅkaṛ
6.	ੂ		ਦੁਲੈਂਕੜ	dulaiṅkaṛ
7.	ੇ		ਲਾਂਵਾਂ	lāṃvāṃ
8.	ੈ		ਦੁਲਾਂਵਾਂ	dulāṃvāṃ
9.	ੋ		ਹੋੜਾ	hōṛā
10.	ੌ		ਕਨੌੜਾ	kanauṛā

Table 1

2.1.2 Consonants
Punjabi language consists of 41 consonants. Consonants list of Punjabi language is written in Fig 2.

ੳ ਅ ੲ ਸ ਹ
ooraa airaa eeree sassaa haahaa
ਕ ਖ ਗ ਘ ਙ
kakkaa khakkhaa gaggaa ghaggaa ganggaan
ਚ ਛ ਜ ਝ ਞ
chachchaa chhachhchhaa jajjaa jhajjaa yannyaan
ਟ ਠ ਡ ਢ ਣ
tainkaa thatthaa daddaa dhaddaa naanaa
ਤ ਥ ਦ ਧ ਨ
tattaa thatthaa daddaa dhaddaa naanaa
ਪ ਫ ਬ ਭ ਮ
pappaa phapphaa babbaa bhabbaa mammaa
ਯ ਰ ਲ ਵ ੜ
yayyaa raaraa lallaa vavvaa raaraa
ਸ਼ ਖ਼ ਗ਼ ਜ਼ ਫ਼
shashshaa khakkhaa gaggaa zazzaa faffaa

Fig 2

2.1.3 Auxiliary Signs
It serves to add a nasal sound to a particular vowel. These signs are represented in Fig 3.
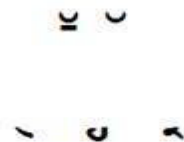
ੰ ੱ

ਂ ੍ ਁ

Fig 3

3) Fundamentals of Speech Recognition

Speech recognition is a multileveled pattern recognition task, in which acoustical signals are examined and structured into a hierarchy of subword units (*e.g.* phonemes), words, phrases, and sentences. Each level may provide additional temporal constraints, *e.g.* known word pronunciations or legal word sequences, which can compensate for errors or uncertainties at lower levels. This hierarchy of constraints can best be exploited by combining decisions probabilistically at all lower levels, and making discrete decisions only at the highest level[6]. The structure of a standard speech recognition system is illustrated in Fig 4.
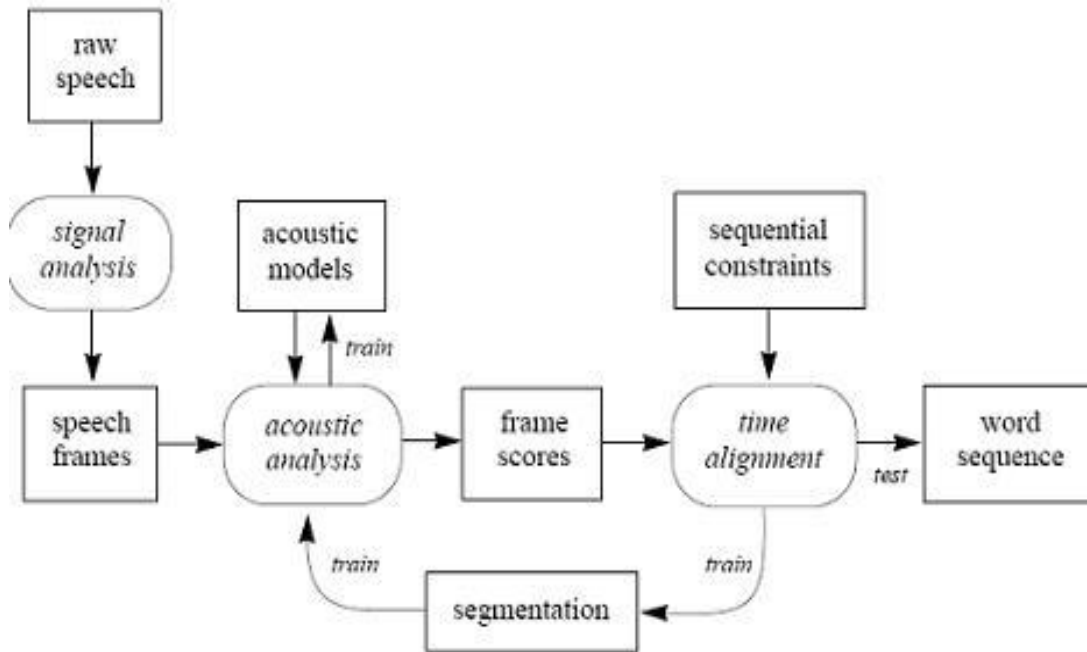
Fig 4. Structure of a standard speech recognition system.

4) Different issues

The various key issues were seen in speech to text convertor for English language using some online softwares. While speaking, the vocal tract of human being can vary widely in terms of their accent, pronunciation, articulation, roughness, nasality, pitch, volume, and speed. All these sources of variability make speech recognition, even more than speech generation, a very complex problem. So, these issues or the problem may be avoided in our STT for Punjabi language. We can work out for improving our STT convertor by taking into consideration following points :

4.1 Commands By using Hyperlink

We can apply the commands by using the hyperlinks, when we speak any command as given in our database, then it helps to open the link by navigating to that link.

4.2 Speaker dependence vs. independence

By definition, a speaker dependent system is intended for use by a single speaker, but a speaker independent system is intended for use by any speaker. Speaker independence is difficult to achieve because a system's parameters become tuned to the speaker(s) that it was trained on, and these parameters tend to be highly speaker-specific.

4.3 Effectiveness

The effectiveness of the speech recognition system can be described when a group of people speak the same speeh and we get the same output as matched by some of people *i.e.* if we consider 10 people to speak the same speech and only 6-7 of them are matched and give the same result. It shows that how effective our speech recognition system is.

4.4 Adverse Conditions

A system's performance can also be degraded by a range of adverse conditions. These include environmental noise (*e.g.* noise in a car or a factory); acoustical distortions (*e.g.* echoes, room acoustics); different microphones (*e.g.* close-speaking, omnidirectional, or telephone); limited frequency bandwidth (in telephone transmission); and altered speaking manner (shouting, whining, speaking quickly, *etc*.).

4.5 Low signal-to-noise ratio

The program needs to "hear" the words spoken distinctly, and any extra noise introduced into the sound will interfere with this. The noise can interrupt the user from a number of sources, including loud background noise in an office environment. Users should work in a quiet room with a quality microphone positioned as close to their mouths as possible. Low-quality sound cards, which provide the input for the microphone to send the signal to the computer, often do not have enough shielding from the electrical signals produced by other computer components.

4.6 Overlapping of speech

There are so many systems which have difficulty separating simultaneous speech from multiple users(like in group discussion). If we try to employ recognition technology in conversations or meetings where people frequently interrupt each other or talk over one another, you're likely to get extremely poor results.

4.7 Homonyms

Homonyms are two words that are spelled differently and have different meanings but sound the same. "There" and "their," "air" and "heir," "be" and "bee", "hair" and "hare", "bear" and "beer" are all examples. There is no another way for a speech recognition program to differentaite between these words based on sound alone. However, extensive training of systems and statistical models that take into account word context can greatly improved their performance.

5) Conclusion

In order to solve these issues we have to improve our speech to text convertor and improve recognition rate for Punjabi words. In some cases we have found some ambiguity problems and efficient methods should be followed to remove the ambiguity problem. To get best speech synthesis rate, database of system should be modified so that our speech recognition engines suits our requirements. A number of methods can be followed to build an effective and efficient database of proposed system.

6) References

1. *Kuldeep Kumar, R. K. Aggarwal " HINDI SPEECH RECOGNITION SYSTEM USING HTK"* , International Journal of Computing and Business ResearchISSN (Online) : 2229-6166 Volume 2 Issue 2 May 2011

2. Jurafsky, D and Martin, J H (2009) *Speech and Language Processing,* Pearson Education, New Delhi, India.

3. Dinesh Kumar, Neeta Rana "Speech Synthesis System for Online Handwritten Punjabi Word: An Implementation of SVM & Concatenative TTS", *International Journal of Computer Applications (0975 – 8887)Volume 26– No.2, July 2011*

4. In India And 70 million in Pakistan Punjabi language at *Ethnologue* (16th ed., 2009)

5. Rajiv K . Sharma, Dr. Amardeep Singh "Segmentation of Handwritten Text in Gurumukhi Script" , International Journal of Image Processing

6. Fundamental Of Speech Recognition, "http://www.learnartificialneuralnetworks.com/speechrecognition.html"

RANDOMIZED ROUTES FOR SECURE DATA TRANSMISSION USING WIRELESS SENSOR NETWORKS

C.Muthuramalingam, A.Karthikeyan, R.Bharathiraj, M.Muthukummaar, S.Edwin Raja

P.S.R Engineering College, Sivaksi

ABSTRACT

Compromised node and denial of service are two key attacks in wireless sensor networks (WSNs). In this paper, we study data delivery mechanisms that can with high probability circumvent black holes formed by these attacks. We argue that classic multipath routing approaches are vulnerable to such attacks, mainly due to their deterministic nature. So once the adversary acquires the routing algorithm, it can compute the same routes known to the source, hence, making all information sent over these routes vulnerable to its attacks. In this paper, we develop mechanisms that generate randomized multipath routes. Under our designs, the routes taken by the "shares" of different packets change over time. So even if the routing algorithm becomes known to the adversary, the adversary still cannot pinpoint the routes traversed by each packet. Besides randomness, the generated routes are also highly dispersive and energy efficient, making them quite capable of circumventing black holes. We analytically investigate the security and energy performance of the proposed schemes. We also formulate an optimization problem to minimize the end-to-end energy consumption under given security constraints. Extensive simulations are conducted to verify the validity of our mechanisms.

Introduction
1.1   Scope of the Project
The main objective of this project is to provide security to the data transmission between source and destination sensor nodes by using ECDH security algorithm and, to avoid black holes.

1.2   WIRELESS SENSOR NETWORK
A **wireless sensor network (WSN)** consists of spatially distributed autonomous sensors to monitor physical or environmental conditions, such as temperature, sound, vibration, pressure, humidity, motion or pollutants and to cooperatively pass their data through the network to a main location. The more modern networks are bi-directional, also enabling control of sensor activity. The development of wireless sensor networks was motivated by military applications such as battlefield surveillance; today such networks are used in many industrial and consumer applications, such as industrial process monitoring and control, machine health monitoring, and so on.

The WSN is built of "nodes" – from a few to several hundreds or even thousands, where each node is connected to one (or sometimes several) sensors. Each such sensor network node has typically several parts: a radio transceiver with an internal antenna or connection to an external antenna, a microcontroller, an electronic circuit for interfacing with the sensors and an energy source, usually a battery or an embedded form of energy harvesting. A sensor node might vary in size from that of a shoebox down to the size of a grain of dust, although functioning "motes" of genuine microscopic dimensions have yet to be created. The cost of sensor nodes is similarly variable, ranging from a few to hundreds of dollars, depending on the complexity of the individual sensor nodes. Size and cost constraints on sensor nodes result in corresponding constraints on resources such as energy, memory, computational speed and communications bandwidth. The topology of the WSNs can vary from a simple star network to an advanced multi-hop wireless mesh network. The propagation technique between the hops of the network can be routing or flooding.

1.3 Application of WSN:

1.3.1 Area monitoring
Area monitoring is a common application of WSNs. In area monitoring, the WSN is deployed over a region where some phenomenon is to be monitored. A military example is the use of sensors to detect enemy intrusion; a civilian example is the geo-fencing of gas or oil pipelines.

When the sensors detect the event being monitored (heat, pressure), the event is reported to one of the base stations, which then takes appropriate action (e.g., send a message on the internet or to a satellite). Similarly, wireless sensor networks can use a range of sensors to detect the presence of vehicles ranging from motorcycles to train cars.

1.3.2 Air pollution monitoring
Wireless sensor networks have been deployed in several cities (Stockholm, London or Brisbane) to monitor the concentration of dangerous gases for citizens. These can take advantage of the ad-hoc wireless links rather than wired installations, which also make them more mobile for testing readings in different areas. There are various architectures that can be used for such applications as well

as different kinds of data analysis and data mining that can be conducted.

1.3.3 Machine health monitoring
Wireless sensor networks have been developed for machinery condition-based maintenance (CBM)as they offer significant cost savings and enable new functionalities. In wired systems, the installation of enough sensors is often limited by the cost of wiring. Previously inaccessible locations, rotating machinery, hazardous or restricted areas, and mobile assets can now be reached with wireless sensors.

1.3.4 Water/wastewater monitoring
There are many opportunities for using wireless sensor networks within the water/wastewater industries. Facilities not wired for power or data transmission can be monitored using industrial wireless I/O devices and sensors powered using solar panels or battery packs and also used in pollution control board.

3 Proposed System:
In this scheme a randomized multipath routing algorithm that can overcome the above problems. In this algorithm, multiple paths are computed in a randomized way each time an information packet needs to be sent, such that the set of routes taken by various shares of different packets keep changing over time. As a result, a large number of routes can be potentially generated for each source and destination. To intercept different packets, the adversary has to compromise or jam all possible routes from the source to the destination, which is practically not possible. Because routes are now randomly generated, they may no longer be node-disjoint. However, the algorithm ensures that the randomly generated routes are as dispersive as possible, i.e., the routes are geographically separated as far as possible such that they have high likelihood of not simultaneously passing through a black hole. Considering the stringent constraint on energy consumption in WSNs, the main challenge in our design is to generate highly dispersive random routes at low energy cost. By reducing hop count energy conservation can be avoided.

Advantages
• Purely random propagation (PRP), it utilizes only one-hop neighborhood information and pro-vides baseline performance

• Directed random propagation (DRP), it utilizes two-hop neighborhood information to improve the propagation efficiency, leading to a smaller packet interception probability

• Non repetitive random propagation (NRRP), scheme records all traversed nodes to avoid traversing them again in the future.

• Multicast tree-assisted random propagation (MTRP) it tries to propagate shares in the direction of the sink, making the delivery process more energy efficient.

Hardware and Software Specification: Processor: 1.4GHz Pentium IV Processor
• RAM : 128 MB
• Hard Drive : 10GB
• Operating System: Windows XP / Linux.
• Tools : ns-allinone-2.28.
• Pre-Request Software : Cygwin.
• Languages : Tcl/Tk, OTcl, C++.

Assumptions
The following simplifying assumptions are made in order to implement the mobile agent model.

1. Instead of sending the actual agent code along with data and execution stack, only a reference to the agent's OTcl object is sent. Thus, the actual sizes of agent's code, data and executi on state are required to be set as parameters of an agent. So it is assumed that all these parameters are known.

2. It is assumed that the servers, whose services are desired, are known in advance.

3. It is also assumed that the number of bytes required for request and reply in each interaction is known.

4. The processing time for an agent (if not explicitly specified for a specific scenario) and also the time for marshalling and unmarshalling are assumed to increase linearly with the total size of the agent.

5. The marshalling factor (marshalling ti me per unit byte) and time required for an agent's creation is assumed to be known.

6. The selectivity (Strasser pg. 18) of the mobile agent, defined as a factor by which the mobile agent reduces the size of the reply by remote processing, is also assumed to be known (if applicable).

7. No assumption is made about the underlying communication facilities for migrating agents. Any communication models including RPC, RMI, CORBA etc. can be utilized. But no such models are currently implemented in NS.

8. TCP is used as an underlying transport layer protocol. UDP may also be used here but the above choice is made only for the sake of performance analysis under reliable conditions.

9. As the principle aim of implementing this model is performance analysis of mobile agents, no consideration is given to the security matters in mobile agent systems. Thus, no security overhead is assumed.

10. Although implementation is bas ed upon an entry-point migration (Brewington pg. 15) (weak migration mainly using IBM's Aglets API), it is assumed to be equally applicable to t he study of agent systems with other types of migration using appropriate values for the model parameters. For example, while studying st rong migration, one can account for the size of agent's current execution stack, which can be otherwise considered as zero for weak migration.

Deciding the Inheritance Structure of the Model
In order to implement the basic behavioral model of mobile agent, the main objects required are a mobile agent itself and a context or a place where mobile agents can execute on a given node. Here, context is responsible for creating mobile agent and also for providing each and every facility required by the agent like dispatching to other node, loading and processing the incoming agent, registering, disposing etc. It uses the existing communication facilities for mobile agent migration. Thus, a context must be implemented on top of the transport layer facilities. Just like the real world systems, NS applications are implemented on top of the transport layer agents. Any simulated application is required to implement the Application interface provided in NS. Thus the mobile agent's context is required to implement this Application interface. Though context is implemented as an application, the mobile agent system model can be easily utilized for building real world applications on top of it.

System Architecture And Description

4 Wireless Channels
IEEE 802.11g/b wireless nodes communicate with each other using radio frequency signals in the ISM (Industrial, Scientific, and Medical) band between 2.4 GHz and 2.5 GHz. Neighboring channels are 5 MHz apart. However, due to the spread spectrum effect of the signals, a node sending signals using a particular channel will utilize frequency spectrum 12.5 MHz above and below the center channel frequency. As a result, two separate wireless networks using neighboring channels (for example, channel 1 and channel 2) in the same general vicinity will interfere with each other. Applying two channels that allow the maximum channel separation will decrease the amount of channel cross-talk and provide a noticeable performance increase over networks with minimal channel separation.

4.1 Wireless Sensor Network:
- Rapidly deployable, self configuring.
- No need for existing infrastructure.
- Wireless links.
- Senor nodes are mobile, topology can be very dynamic.
- Nodes must be able to relay traffic since communicating nodes might be out of range.

4.1.1 Sensor node usage areas:
The main two characteristics are mobility and multihop.
- Military scenarios
- Sensor networks
- Rescue operations
- Students on campus
- Free Internet connection sharing Conferences

4.1.2 Mechanisms required in a Senor Networks:
- Multihop operation requires a routing mechanism designed for mobile nodes.
- Internet access mechanisms.
- Self configuring networks requires an address allocation mechanism.
- Mechanism to detect and act on, merging of existing networks.
- Security mechanisms.

4.1.3 Routing protocol requirements:
- Self starting and self organizing
- Multi-hop, loop-free paths
- Dynamic topology maintenance
- Rapid convergence
- Minimal network traffic overhead
- Scalable to large networks

5 AES

5.1 Explanation:
The Advanced Encryption Standard (AES) specifies a FIPS-approved cryptographic algorithm that can be used to protect electronic data. The AES algorithm is a symmetric block cipher that can encrypt (encipher) and decrypt (decipher) information. Encryption converts data to an unintelligible form called cipher text; decrypting the cipher text converts the data back into its original form, called plaintext. The AES algorithm is capable of using cryptographic keys of 128, 192, and 256 bits to encrypt and decrypt data in blocks of 128 bits.

6 Conclusion
By analyzing and simulating the results have shown the effectiveness of the randomized dispersive routing in combating CN and DOS attacks. By appropriately setting the secret sharing and propagation parameters.The packet interception probability can be easily reduced by the new algorithms which is at least one order of magnitude smaller than approaches that use deterministic node-disjoint multipath routing. At the same time, we have also verified that this improved security performance comes at a

reasonable cost of energy. Specifically, the energy consumption of the proposed randomized multipath routing algorithms is only one to two times higher than that of their deterministic counter-parts. The proposed algorithms can be applied to selective packets in WSNs to provide additional security levels.

References

1. Ansgar Kellner, Kerstin Behrends, Dieter Hogrefe (2010) "Simulation Environments for Wireless Sensor Networks" TECHNICAL REPORT,IFI-TB-2010-04,JUNE 2010.

2. Sabitha Ramakrishna and T.Thyagarajan (2009) "Energy Efficient Medium Access Control for Wireless Sensor Networks" IJCSNS International Journal of Computer Science and Network Security,VOL.9 No.6,June 2009.

3. Zoran S. Bojkovic, Bojan M. Bakmaz, and Miodrag R. Bakmaz (2008) "Security Issues in Wireless Sensor Networks" INTERNATIONAL JOURNAL OF COMMUNICATIONS, Issue 1, Volume 2, 2008.

4. A.Vijay kumar, T. Naveen, and B. Thirupathi (2011) "Secure Data Collection in Wireless Sensor Networks Using Randomized Routes" ARPN Journal of systems and software, Volume 1 No.5,August 2011.

5. Noor Zaman and Azween B Abdullah (2011) "Different Techniques Towards Enhancing Wireless Sensor Network (WSN) Routing Efficiency and Quality of service (QoS)" World Applied Sciences Journal 13(4);789-805,2011.ISSN 1818-4952 IDOSI publications,2011.

6. T. Claveirole, M.D. de Amorim, M. Abdalla, and Y. Viniotis,"Securing Wireless Sensor Networks Against Aggregator Compromises,"IEEE Comm. Magazine, vol. 46, no. 4, pp. 134-141, Apr.2008.

7. B. Vaidya, J.Y. Pyun, J.A. Park, and S.J. Han, "Secure Multipath Routing Scheme for Mobile Ad Hoc Network," Proc. IEEE Int'l symp. Dependable, Autonomic and Secure Computing, pp. 163-171, 2007.

8. R. Mavropodi, P. Kotzanikolaou, and C. Douligeris, "SecMR-a Secure Multipath Routing Protocol for Ad Hoc Networks," Ad-Hoc Networks, vol.5, no. 1, pp. 87-99, Jan. 2007.

9. P. Papadimitratos and Z.J. Haas, "Secure Data Communication in Mobile Ad Hoc Networks," IEEE J. Selected Areas in Comm., vol. 24, no. 2, pp. 343-356, Feb. 2006.

10. W. Lou and Y. Kwon, "H-Spread: A Hybrid Multipath Scheme for Secure and Reliable Data Collection in Wireless Sensor Networks" IEEE Trans. Vehicular Technology, vol. 55, no. 4, pp. 1320-1330, July 2006.

LOW POWER WITH IMPROVED NOISE MARGIN FOR DOMINO CMOS NAND GATE

[1]Pushpa Raikwal, [2]V. Neema, [3]S. Katiyal

[1,3]School of electronics DAVV, Indore, Madhya Pradesh, India
[2]Institute of Engineering and Technology, DAVV, Indore, Madhya Pradesh, India

ABSTRACT

With the advancement in semiconductor technology, chip density and operating frequency are increasing, so the power consumption in VLSI circuits has become a major problem of consideration. More power consumption increases packaging cost and also reduces the battery life of the devices. So it has become necessity of the VLSI circuits to reduce the dynamic as well as the static power consumption. To reduce leakage power it is necessary to increase the threshold voltage of the circuit. In this paper to reduce the leakage power AVL (Adaptive Voltage Level) circuit technique and Body biasing technique are used. Our paper proposes a technique for reducing power dissipation of CMOS VLSI design while simultaneously improving the noise immunity.

Keywords: AVL circuit technique, CMOS, Noise immunity, VLSI circuit.

INTRODUCTION

It is important to introduce low-power design techniques and to reduce the package size during the circuit normal mode of operation. More power consumption also reduces the battery life of the devices. Therefore reducing power dissipation during operation has become a critical objective in today's VLSI circuit designs. So special cooling equipment is necessary to remove excessive heat produced during circuit operation. Power consumption in CMOS circuits can be dynamic or static. Dynamic power dissipation takes place due to switching activities because of short circuits current and charging and discharging of load capacitances. Static power consumption is another type of power dissipation in CMOS circuits. Leakage currents with sub-threshold source-to-drain leakage, reverse bias junction band-to-band tunneling, gate oxide tunneling, and other current drawn continuously from the power supply cause static power dissipation [7].

Today, the necessity of portable systems and simultaneously improvement in battery performance depicts the power consumption is major factor in CMOS VLSI design parameters [3]. To reduce dynamic power dissipation it is necessary to reduce the supply voltage of the circuit, reduction of supply voltage after a certain limit affects the performance of the circuit, to maintain circuit performance of the circuit it is necessary to decrease the threshold voltage as well, but it leads to leakage power dissipation. Leakage power can be reduced by increasing the threshold voltage [5]. In this paper to reduce the voltage applying to the load circuit, we suggest the use of AVL (Adaptive Voltage Level) circuit technique. AVL circuit is controlled by sleep control signal. The advantage of using AVL circuit is that the load circuits can operate quickly when they are in active mode due to the increase in drain-source current as the AVL circuit supplies the maximum drain-source voltage Vds to the on-MOSFETS through on-switches. On the other hand, during standby mode, it supplies a slightly lower voltage through the weakly-on switches [2]. Hence the sub-threshold leakage current of the off-MOS transistors decrease and the standby power gets reduced. It also produces high noise immunity. When we applied voltage to the substrate of a MOSFET it affects the threshold voltage of a MOSFET as well. The voltage difference between the source and the substrate, V_{BS} also affects the width of the depletion layer and due to changes in the charge in depletion layer voltage across the oxide also get changed. Therefore the expression for the threshold voltage is given by:

$$V_T = V_{FB} + 2\phi_F + \frac{\sqrt{2\varepsilon_s q N_a (2\phi_F + V_{SB})}}{C_{ox}}$$

The threshold difference due to an applied source-substrate voltage can therefore be expressed by:

$$\Delta V_T = \gamma(\sqrt{(2\phi_F + V_{SB})} - \sqrt{2\phi_F})$$

Where γ is the body effect parameter given by:

$$\gamma = \frac{\sqrt{2\varepsilon_s q N_a}}{C_{ox}}$$

Substrate biasing provides an effective circuit-level technique for varying threshold voltage and to enhance the performance of the circuit.

This paper gives emphasis on low power design as well as improved noise margin for domino NAND gate technique. Among different dynamic logic circuit techniques, domino logic technique is mostly used because it provides less delay and its area consideration, but it has less tolerance to noise and its static power consumption is high. So in this paper we have applied AVL circuit technique and body bias technique to overcome both of these problems.

STANDARD DOMINO NAND GATE

A standard domino NAND gate is as shown in Figure 1. A standard Domino NAND gate consists of one p-type transistor and an n-type dynamic logic block. During pre-charge phase the output node of the dynamic CMOS stage is pre-charged to high logic level [4]. During evaluation phase, the output node of the dynamic CMOS stage is either discharged to a low level or it remains high, means that, the output node may be selectively discharged through the n-type logic block depending upon whether there is a path exist to the GND or not. It depends upon the inputs of the NMOS logic block. If a path to ground is not formed during the evaluation phase, means there is no conducting path exist to the ground, we get the high logic level at the output. If inputs to the n-type logic blocks are such that it makes a conducting path to the ground, output will be low.
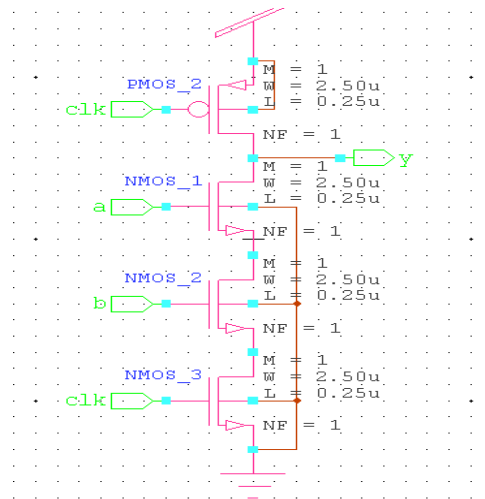

Figure 1 Domino NAND GATE

AVL NAND GATE

In this circuit AVL circuit is connected above the Domino NAND gate. AVL circuit contained one p-MOSFET and two series connected n-MOSFETS, which will reduce the voltage applying to the load circuit. AVL circuit is controlled by sleep (slp) control signal [1]. When sleep signal is low, the p-MOSFET is on, while series connected n-MOSFETs are off. During this operation, we get the full voltage out of the AVL circuit. When sleep signal make transition from low to high, this will turn-on series connected n-MOSFETs, and turn-off p-MOSFET, Thus, the drain-to-source voltage (Vdsn), of the off n-MOS in load circuit (domino NAND gate) can be expressed as

$$Vdsn = VDD - 2v$$

Where v is a voltage drop of the series connected single n-MOSFET and Vdsn can be changed by changing the number of series connected n-MOSFETs. If Vdsn decreases this will increase the barrier height of the off n-MOS [6], therefore it will decrease the drain induced- barrier-lowering (DIBL) effect and, consequently, increase Vthn. This result in a decrease in the sub threshold current of the n-MOS, therefore the leakage current through the gate decreases.
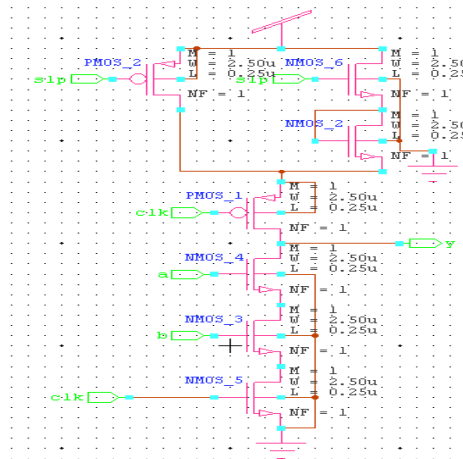
Figure 2 AVL NAND GATE

BODY BIAS NAND GATE

Domino logic gates are frequently employed in high performance circuits for high speed and area efficiency. As supply voltage is reduced, delay increases, unless threshold voltage Vth is also decreased. Substrate biasing provides an effective circuit-level technique for varying threshold voltage. Here substrate of NMOS is connected to the clock and PMOS is connected to Vdd, which increases the threshold voltage that in turn reduces the leakage current.
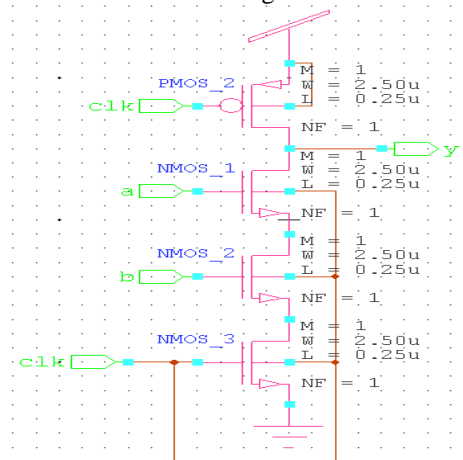
Figure 3.Body Bias NAND GATE

NAND GATE USING PROPOSED TECHNIQUE

In this method we have taken Domino NAND gate with both of the techniques, AVL circuit technique and body biasing technique. Here AVL circuit is connected above the NAND gate. For applying body bias technique, the substrate of PMOS is connected to Vdd and the substrate of NMOS is connected to the clock. Our proposed method will reduce the power consumption through the gate. Simulations of all the circuits are performed using Tanner EDA Tools 180 nm technology. The advantage of using AVL circuit is that load circuit will operate very fast when they are in active mode due to increase in drain source current but in stand by mode due to less drain source voltage, threshold voltage will increase which reduces the leakage current, of the circuit [1].
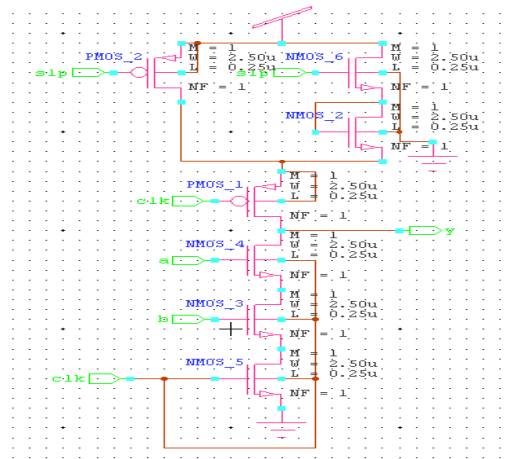
Figure 4.Proposed NAND GATE

Parameters Observation

The parameters observations of different techniques are as follow:

Technique	Dynamic power dissipation In mili watts	Leakage Power in pico watts	Evaluation Delay in Pico seconds	Noise margin in volts (NMH)	Noise margin in volts (NML)
Domino NAND gate	0.087	140.73	25.99	1	0.5
AVL NAND gate	0.068	162.20	37.58	1	0.5
Body Bias NAND gate	0.081	176.95	25.81	1.2	0.85
Proposed NAND gate	0.052	130.70	36.42	1.6	0.85

Table 1.Parameters observation
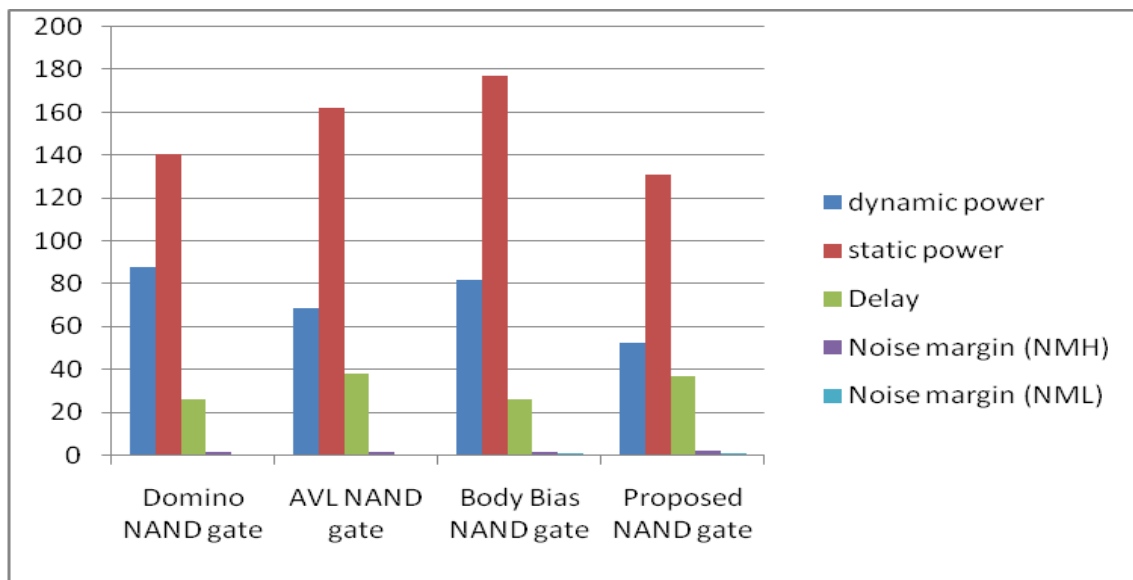
Figure 5. Comparison of power consumption, delay and noise margin

SIMULATION RESULTS

The output of the domino NAND GATE is shown below

Figure 6 Domino NAND GATE

The output of the AVL NAND GATE is shown below

Figure 6.AVL NAND GATE

The output of the body bias NAND GATE is shown below

Figure 7.Body bias NAND GATE

The output of the proposed NAND GATE is shown below

Figure 8.Proposed NAND GATE

CONCLUSION

In this paper we have designed Domino NAND gate with AVL circuit technique and body bias technique, and comparison has been carried out with standard domino NAND gate, AVL NAND gate and body bias NAND gate.
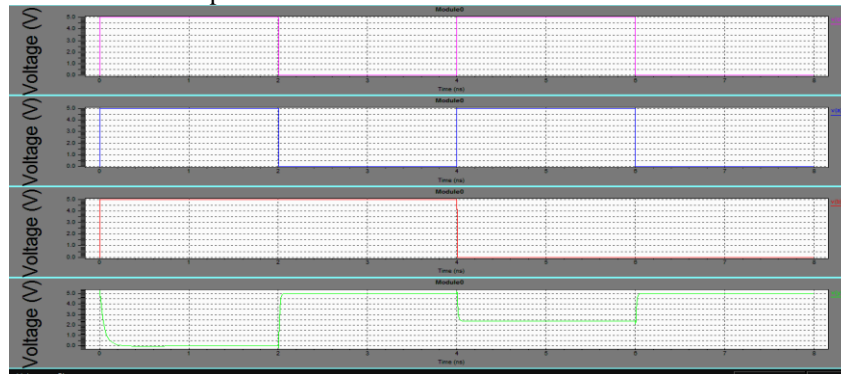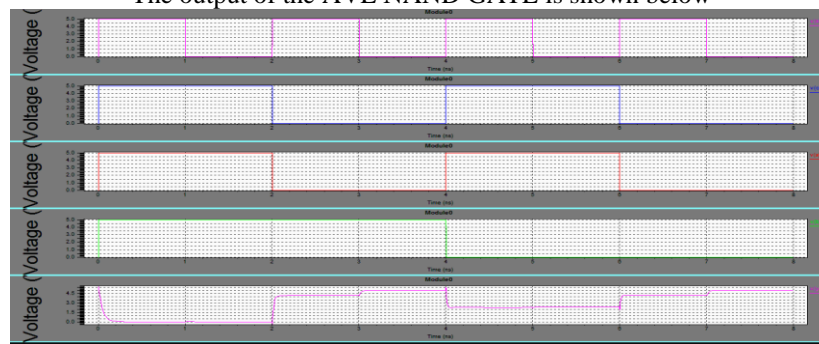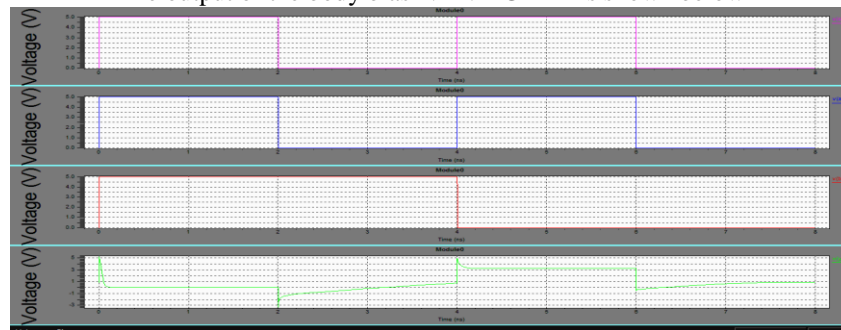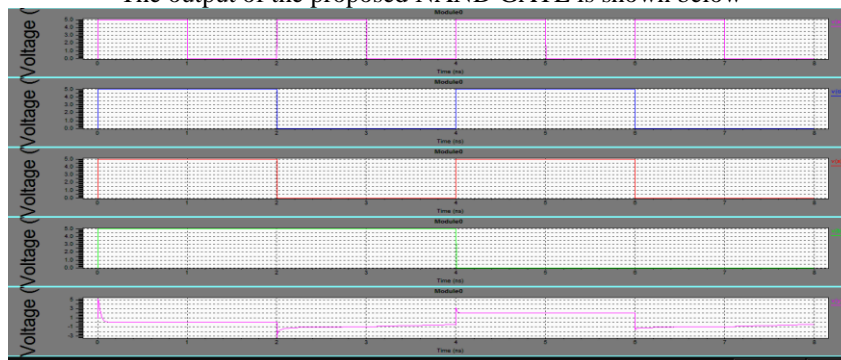
Simulation results shows that our proposed circuit technique consumes less dynamic as well as static power than other three techniques. The other benefit of proposed technique is its high noise immunity as compare to other technique.

In this dissertation we can say that our proposed NAND gate consumes less power and gives high noise margin.

REFERENCES

[1] H. Mangalam and K. Gunavathi, "Domino Logic Circuit with Reduced Leakage and Improved Noise Margin",International Journal of Applied Engineering Research ISSN 0973-4562 Volume 2, Number 4 (2007), pp. 585–593.

[2] Suman Nehra, K.G.Sharma, Tripti Sharma and Prof.B.P.Singh," High Performance VLSI Design Using Body Biasing in Domino Logic Circuits" -International Journal of Technology And Engineering System(IJTES):Jan – March 2011- Vol.2.No.2.

[3] Sreenivasa Rao.Ijjada, Ayyanna.G , G.Sekhar Reddy, Dr.V.Malleswara "PERFORMANCE OF DIFFERENT CMOS LOGIC STYLES FOR LOW POWER AND HIGH SPEED",International Journal of VLSI design & Communication Systems (VLSICS) Vol.2, No.2, June 2011.

[4] Kang, S. and Y. Leblebici. CMOS Digital Integrated Circuits: Analysis and Design. The McGraw-Hill Companies, Inc.: New York. 1996, pp 383-384.

[5] Gholamreza Karimi1, Adel Alimoradi2" Multi-Purpose Technique to Decrease Leakage Power in VLSI Circuits" Canadian Journal on Electrical and Electronics Engineering Vol. 2, No. 3, March 2011.

[6] Tadayoshi Enomoto, Yoshinori Oka, Hiroaki Shikano, and Tomochika Harada Chuo University, Faculty of Science and Engineering, Tokyo, Japan enomoto@ise.chuo-u.ac.jp" A Self-Controllable-Voltage-Level (SVL) Circuit for Low-Power, High-Speed CMOS Circuits, ESSCIRC 2002,pp 412-414.

[7] Shervin Sharifi, Javid Jaffari, Mohammad Hosseinabady, Ali Afzali-Kusha, and Zainalabedin Navabi, Electrical and Computer Engineering Department Faculty of Tehran, Iran "Simultaneous Reduction of Dynamic and Static Power in Scan Structures". Proceedings of the Design, Automation and Test in Europe Conference and Exhibition (DATE'05)-2005.

AUTHORS PROFILE

Pushpa Raikwal pursuing M.Tech(Embedded Systems) School of Electronics, Devi Ahilya University, Indore (M.P.).

Dr.Vaibhav Neema He completed Ph.D. in Low Power CMOS Digital Circuit design from Institute of Engineering and Technology, Devi Ahilya University, Indore (MP) then he did Mater degree of Technology (M.Tech.) in Microelectronics from Punjab University Chandigarh, India. under supervision of Dr. Sanjiv Tokekar development of low power design techniques as broad area of research from Institute of Engineering & Technology, Devi Ahilya University Indore India. He is also Assistant Professor in Electronics & Telecommunication Engineering Department Institute of Engineering & Technology, Devi Ahilya University Indore India. He has having more than nine years of teaching experience with various prestigious University/Institutes of India. He has more than 20 research publication in various pre-reviewed journal and conferences. He also chaired a technical session in ICEDSA'2010 held in Malaysia.

Dr.Sumant Katiyal is Professor in School of Electronics,h Devi Ahilya Univerity, Indore (M.P.) India. He has more than 26 years of experience in teaching and research. His current area of research includes VLSI technology and Design of Embedded Systems. He has published more than ninety five papers in National and International Journals/Conferences.

Batch Signature for Mixed Signals in Wireless Networks

Battula Sudheer Kumar[1] (M.Tech)
P. Anjaiah[2] M. Tech
C.V.S.R College of Engineering, JNTU
C.V.S.R College of Engineering, JNTU

Abstract
In wireless networks interference is considered has a major problem. So, in order to avoid the interference we use the technique called mixing signal (Network Coding). The problem here is there are vulnerable to possible malicious attacks. i.e., if any of the intruder knows the information of other signal in the mixed signal they can be decoded easily. In order to resolve this problem we are proposing a good secure network coding scheme batch signature for mixed signal. So with the above network coding scheme we are providing a security to the signal.

Keywords: Batch Signature, Pollution Attack, RSA, Network Coding.

1. Introduction

   All Wireless networks have been designed using the wires network as the blueprint. The design abstracts the wireless channel as a point-to-point link, and graft wired network protocol onto the wireless environments. For Example, routing uses shortest path protocols, routers forward packets but don't modify the data, and reliability relies on retransmission. The design has worked well for wired networks, but less so for the unreliable and unpredictable wireless medium.

   A main distinguishing feature of a wireless network compared with a wired network is its broadcast nature, in which the signal sent by a node will reach all its destination neighboring nodes [1]. The signal will collide, if a neighbor apart from the target node is receiving data from more than one node at the same moment then the required signal will get cracked, which results in communication crash. In conventional or traditional wireless networks, this crash of signals may cause communication failure if no division technique is adopted. This will corrupt the system performance, which include packet loss rate and energy effectiveness.

   In order to avoid interference problem we use mixing of signals are also called as (Network Coding Technique).
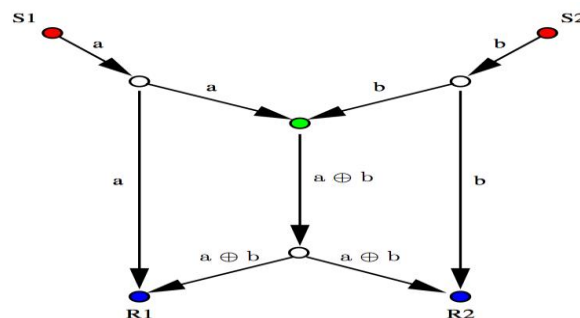
Fig: 1 Example of Network Coding

   Network coding is described using the famous butterfly example [2]. Consider the network in Fig 2, where source S_i wants to deliver the signal a_i to both R_1 and R_2 and source S_2 wants to send the signal b_i to the same receivers. Assume all links have a capacity of one message per unit of time. If routers only forward the message they receive, the middle link will be a bottleneck, which for every time unit, can either deliver a_i to R_1 or b_i to R_2. In contrast if the router feeding the middle link XORs the two signals and sends a_i b_1 as shown in the figure, both receivers obtain two signals in every time unit. Thus, network coding allows the routers to mix the bits in forwards the mixed signal, as a single signal. At the receiver side we use signal recovery algorithm which will recover the useful signal from the mixed signal with already known information of the other signal and decrypt the signals thus the way we can get the original signal with out damaging the signal.

   But the problem here is, if any intruder knows the information of other signal they can recover the original signal from mixed signal. So, In order to resolve this security issue we are proposing the Batch Signature for Mixed Signal. This scheme is based on the recently network coding technique which was first proposed by Ahlswede et al. [4] and Li et al. [5]. The rest of this paper explains about the Background, Batch signature overview, Limitations and Conclusion.

2. Background

The idea underlying batch signature in network coding is we can provide the security for the signal that is going to be recovered. In traditional mixed signal or network coding the intruder can decode the signal and get the useful signal easily if he knows the information of other signal [6]. To avoid this problem this paper proposes a scheme known as batch signature for mixed signal in wireless networks. A batch RSA digital signature scheme in which a signer can sign signals for multiple recipients simultaneously, with this scheme even if the intruders knows the information of other signal also he cannot decode the signal [7]. Batch RSA scheme will takes the three inputs to decrypt the original signal the first one is batch cipher text and second one is private key and third one is the information of other signal.

3. Batch Signature Overview

The network coding based applications are vulnerable to possible malicious pollution attacks. The batch signature [8] schemes have been well-recognized as the most effective approach to address this security issue. The pollution attack can be defined as that a malicious intermediate node can inject junk packets into the network to pollute the output, and further contaminate the entire downstream, preventing proper decoding. Formally, we describe the pollution attacks as follows. If any of the intruders as modified the signal or packet of the mixed signal then one invalid packet can destroy or corrupt the entire signal. So in order to provide the security we propose batch signature for network coding.
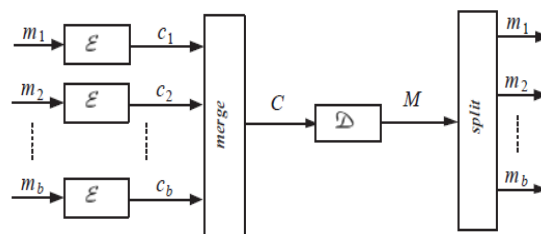
Fig: 2 Example of Batch Encryption & Decryption

Our scheme of wireless networks is shown in Fig. 2, where the source terminals $S_1, S_2 ..S_n$ intend to transmit signals $m_1, m_2 .. m_b$ to the receiver R1. In our scheme, at encryption side each signal is encrypted using public keys using RSA, after that each individual encrypted signal $c_1, c_2.. c_b$ is going to mix(merge) and form a single signal called as encrypted mixed signal C, using the technique called network coding. At decryption side this encrypted mixed signal C, will received by the receiver and decrypt the signal using their private key and gets the mixed signal M and then decode the signals $m_1, m_2.. m_b$ from the mixed signal using the signal recovery algorithm[9].

The Algorithm for batch cipher in Mixed Signals as follows
1. It takes a prime number as a security parameter to generate Public key and private key for encryption and decryption
2. Encrypt the each signal m1,m2..mn and sends the cipher signal to the reciever
3. Intermediate node takes the cipher text and merges as a single signal using a network coding techniwue and sends to the reciever.
4. At the receiver side decrypt the mixed signal (Cipher signal) .
5. Finally split the signal from the mixed signal using the signal recovey algorithm to get the actual signal.

4. Limitations

S.No	Security Strength
1.	Information Theoretic
2.	Equivalent to RSA
3.	Equal to the strength of crypto algorithm
4.	Not information theoretically secure but secure enough for the application
5.	Single point of failure

Table 1: Limitations of Scheme under Study

Ideally a good secure network coding scheme should consume less time and resources of the network, not be vulnerable, have ease of implementation and have good security strength.

5. Conclusion

In this paper, we have proposed an efficient security scheme for network coding against pollution attacks. The proposed scheme is using the Batch RSA for its signature with this secure communication is possible with out loss of rate. So, this scheme can achieve high efficiency and security in packet signature, and meet the important and emerging requirements for securing network coding.

6. References

Journals:
[1] S. Y. R. Li, R. W. Yeung, and N. Cai, "Linear network coding," IEEE Trans. Inf. Theory, vol. 49, no. 2, pp. 371–381, Feb. 2003.
[2] J. Zhang, P. Fan, and K. B. Letaief, "Network coding for efficient multicast routing in wireless ad-hoc networks," IEEE Trans. Commun., vol. 56, no. 4, pp. 598–607, Apr. 2008.
[3] D. Charles, K. Jain, and K. Lauter, "Signatures for Network Coding," Proc. 40th Annual Conf. on Inform. Sci. and Syst. (CISS '06) (Princeton, NJ, 2006), pp. 857–863.
[4] R. Ahlswede, N. Cai, S. Y. R. Li, and R. W. Yeung, "Network information flow," *IEEE Trans. Inf. Theory*, vol. 46, no. 4, pp. 1204–1216, Jul. 2000.
[5] S. Y. R. Li, R. W. Yeung, and N. Cai, "Linear network coding," *IEEE Trans. Inf. Theory*, vol. 49, no. 2, pp. 371–381, Feb. 2003.
[6] Jing Dong, Reza Curtmola, and Cristina Nita-Rotaru, "Secure network coding for wireless mesh networks: Threats, challenges, and directions, vol. 32, no. 2, pp. 121–125, Nov. 2009.
[7] Sudheer kumar and Shruthi Reddy, "Mixed signal based transmission in mixed layers for high throughput wireless network,"*Elixir online journal''vol-3*, pp. 7382–7385, Mar. 2012.
[8] A. Fiat, "Batch RSA," Crypto'89, pp.175-185, 1989, See also Journal of Cryptology, 10(2):75-88, 1997.
[9] R. Johnson, D. Molnar, D. Song, D. Wagner, Homomorphic signature schemes, Proceedings of RSA, Cryptographer's Track. LNCS 2271 (2002).

Books:
[10] T. S. Rappaport, presented at the Wireless Communications Principles and Practice 2nd edition.

Sudheer Kumar Battula
Received the Bachelor's degree from Aurora's Scientific and Technological Institute affiliated to JNTU Hyderabad University in 2009. I'm currently pursuing my Masters from the *Anurag* Group of Institutions affiliated to JNTU Hyderabad University in Computer Science & Engineering department.

P. Anjaiah
Received the Bachelor's degree from Aurora's engineering college bhongir, affiliated to JNTU Hyderabad University in 2004. Received M.Tech degree from SIT, jnt university,. in 2006. Currently working as a Asst. Professor in *Anurag* group of institutions affiliated to JNTU in C.S.E.

Sinusoidal PWM Based Modified Cascaded Multilevel Inverter

*M.Murugesan, R.Sakthivel, E. Muthukumaran and R.Sivakumar

Assistant Professor,
Department of Electrical and Electronics,
V.S.B Engineering College,
NH 67, Covai Road, Karudayampalayam post,
Karur-639 111

Abstract

In this paper, an H-bridge inverter topology with reduced switch count technique is introduced. This technique reduces the number of controlled switches used in conventional multilevel inverter. To establish a single phase system, the proposed multilevel inverter requires one H-bridge and a multi conversion cell. A multi conversion cell consists of three equal voltage sources with three controlled switches and three diodes. In conventional method, twelve controlled switches are used to obtain seven levels. Due to involvement of twelve switches the harmonics, switching losses, cost and total harmonic distortion are increased. This proposed topology also increases the level to seven with only seven controlled switches. It dramatically reduces the complexity of control circuit, cost, lower order harmonics and thus effectively reduces total harmonic distortion.

Keywords- Cascaded Multilevel Inverter, H-bridge Inverter, Total Harmonic Distortion, Sinusoidal Pulse Width Modulation. Insulated Gate Bipolar Transistor.

I. Introduction

Numerous industrial applications have begun to require higher power apparatus in recent years. Some medium voltage motor drives and utility applications require medium voltage and MW power level. Therefore high power and medium voltage inverter has recently become a research focus. As far as conventional two level inverter is concerned, it exhibits many problems when used in high power applications [1]-[2].

Multilevel inverters have been gained more attention for high power application in recent years which can operate at high switching frequencies while producing lower order harmonic components. A multilevel inverter not only achieves high power ratings, but also enables the use of renewable energy sources. Renewable energy sources such as photovoltaic, wind and fuel cells, which can be easily interfaced to a multilevel inverter system for high power applications. There are several topologies such as diode clamped multilevel inverter or neutral point clamped inverter, flying capacitor based multilevel inverter, and cascaded multilevel inverter [3]. The main disadvantage still exists in diode clamped multilevel inverter topology, which restricts the use of it to the high power range of operation. Moreover flying capacitor based multilevel inverter also exhibits a disadvantage including more number of capacitors [4]. The first topology introduced is the series H-bridge design, in which several configurations have been obtained. This topology consists of series power conversion cells which form cascaded H- bridge multilevel inverter and power levels will be scaled easily. An apparent disadvantage of this topology is large number of controlled switches. The proposed topology for multilevel inverter has seven levels associated with a seven number of power switches. In this proposed topology sinusoidal pulse width modulation technique is used.

Ii. Cascaded Multilevel Inverter

The general structure of cascaded multilevel inverter for a single phase system is shown in Figure 1. Each separate voltage source V_{dc1}, V_{dc2}, V_{dc3} is connected in cascade with other sources via a special H-bridge circuit associated with it. Each H-bridge circuit consists of four active switching elements that can make the output voltage either positive or negative polarity; or it can also be simply zero volts which depends on the switching condition of switches in the circuit. This multilevel inverter topology employs three voltage sources of unequal magnitudes. It is fairly easy to generalize the number of distinct levels [5],[6]. The S number of sources or stages and the associated number of output level can be written as follows

$$N_{level} = 2S + 1 \tag{1}$$

For example if S=3, the output wave form has seven levels ($\pm 3V_{dc}$, $\pm 2V_{dc}$, $\pm 1V_{dc}$ and 0). The voltage on each stage can be calculated by using the equation,

$$A_i = 1V_{dc}(i = 1,2,3\dots) \tag{2}$$

The number of controlled switches used in this topology is expressed as,

$$N_{switch} = 4S \tag{3}$$

The output voltage of the multilevel inverter is given as,

$$V_o = A_1 + A_2 + A_3 \tag{4}$$

Where A_1, A2 and A_3 are DC voltage sources.

The advantages of cascaded multilevel inverter are modularized layout and packaging. This enables the manufacturing process to be done more quickly and cheaply. The drawback of this topology needs a separate DC source for each of H-bridge and involves high number of semiconductor switches.
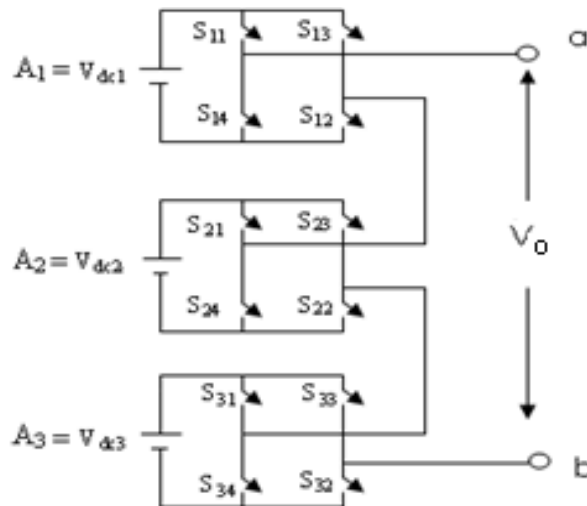
Figure 1: Topology for cascaded Multilevel Inverter
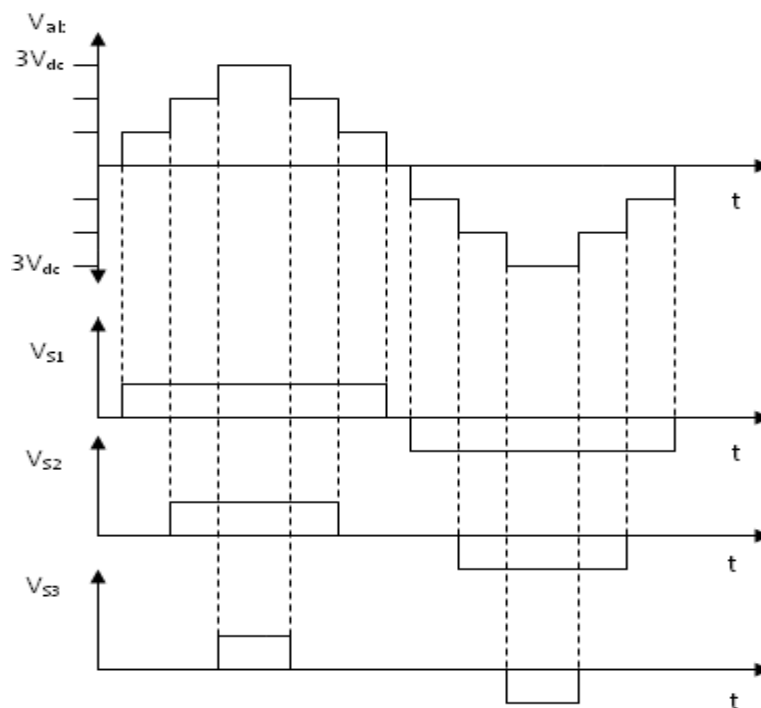
Figure 2: Typical output waveform for cascaded multilevel inverter

Figure 2 shows the typical output voltage waveform of a seven level cascaded multilevel inverter with three separate DC sources.

Iii. Modified Cascaded Multilevel Inverter

The general structure of a proposed cascaded multilevel inverter is shown in Figure 3. This inverter consists of a multi conversion cell and an H bridge. A multi conversion cell consists of three separate voltage sources (V_{dc1}, V_{dc2}, V_{dc3}), each source connected in cascade with other sources via a circuit consists of one active switching element and one diode that can make the output voltage source only in positive polarity with several levels. Only one H-bridge is connected with multi conversion cell to acquire both positive and negative polarity. By turning on controlled switches S1 (S2 and S3 turn off) the output voltage $+1V_{dc}$ (first level) is obtained. Similarly turning on of switches S1, S2 (S3 turn off) $+2V_{dc}$ (second level) output is produced across the load. Similarly $+3V_{dc}$ levels can be achieved by turning on S1, S2, S3 switches as shown in

Table I. The main advantage of proposed modified cascaded multilevel inverter is seven levels with only use of seven switches. The S number of DC sources or stages and the associated number output level can be calculated by using the equation as follows,

$$N_{level} = 2S + 1 \tag{5}$$
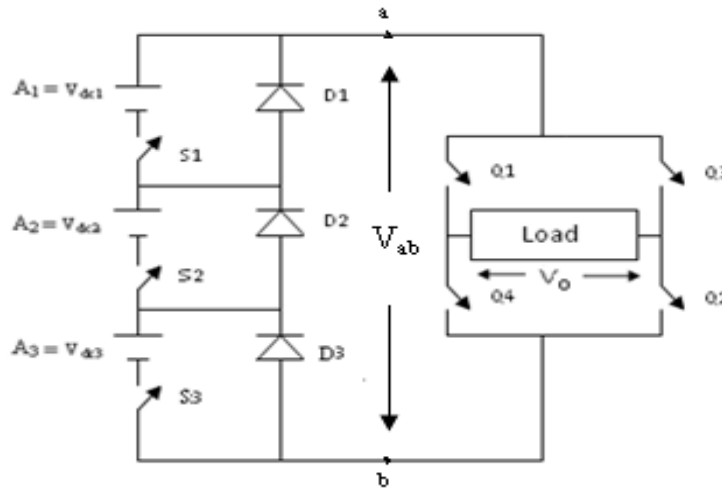
Figure 3: Topology for modified cascaded multilevel inverter

For an example, if S=3, the output wave form will have seven levels ($\pm 3V_{dc}$, $\pm 2V_{dc}$, $\pm 1V_{dc}$ and 0). Similarly voltage on each stage can be calculated by using the equation as given,

$$A_i = 1V_{dc} (i = 1, 2, 3 \dots) \tag{6}$$

The number switches used in this topology is given by the equation as follows,

$$N_{switch} = 2S + 4 \tag{7}$$

Table I: Basic Operation of Proposed Multilevel Inverter

S. No	Multiconversion Cell		H-Bridge		Voltage levels
	On switches	Off switches	On switches	Off switches	
1	S1, S2, S3	D1,D2,D3	Q1,Q2	Q3,Q4	+3V$_{dc}$
2	S1, S2, D3	S3, D1,D2	Q1,Q2	Q3,Q4	+2V$_{dc}$
3	S1, D2, D3	S2, S3, D1	Q1,Q2	Q3,Q4	+1V$_{dc}$
4	D1, D2, D3	S1, S2, S3	Q1,Q2	Q3,Q4	0
5	S1, D2, D3	S2, S3, D1	Q3,Q4	Q1,Q2	-1V$_{dc}$
6	S1, S2, D3	S3, D1,D2	Q3,Q4	Q1,Q2	-2V$_{dc}$
7	S1, S2, S3	D1,D2,D3	Q3,Q4	Q1,Q2	-3V$_{dc}$

The switching table for modified cascaded multilevel inverter is shown in Table I. It depicts that for each voltage level, only one of the switches is in ON condition among the paralleled switches. Multi conversion cell converts DC voltage into a stepped DC voltage, which is outputted as a stepped or approximately sinusoidal AC waveform by the H-bridge inverter. In this H-bridge, for positive half cycle, switches Q1 and Q2 will be turned on, similarly for negative half cycle switches Q3 and Q4 must be in ON condition. Figure 2 shows the typical output voltage waveform of a seven level cascaded multilevel inverter with three separate DC sources.
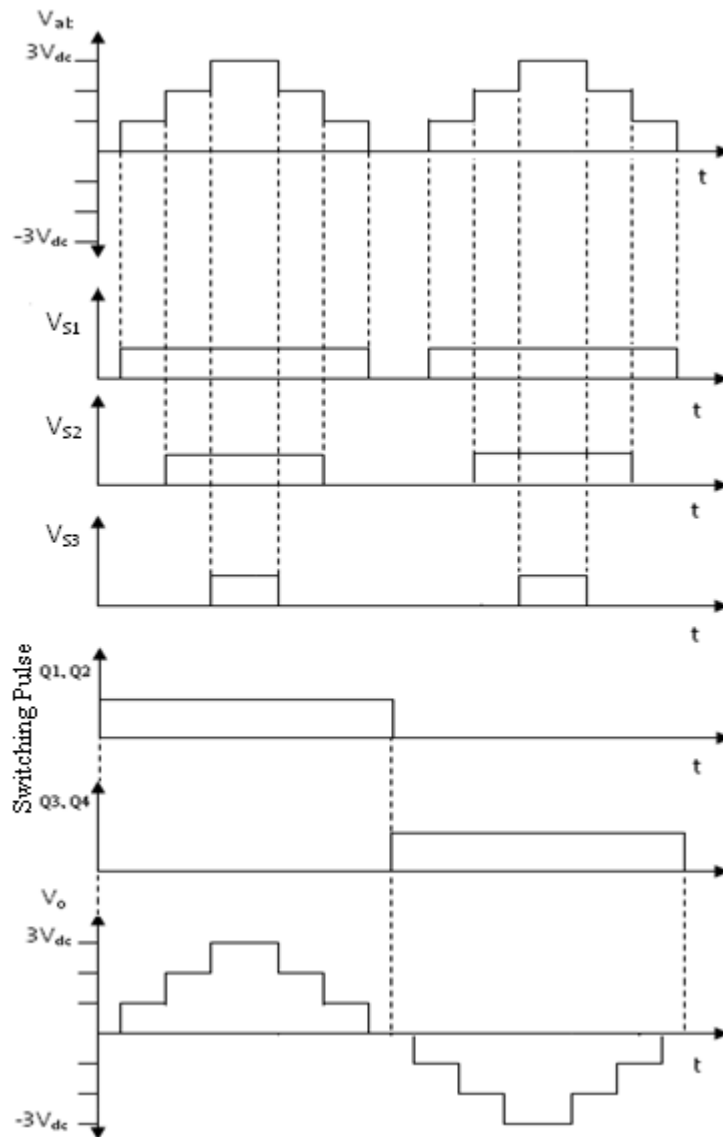
Figure 4: Typical output voltage waveform of a modified cascaded multilevel inverter

Iv. Pwm For Harmonics Reduction

PWM technique is extensively used for eliminating harmful low-order harmonics in inverters. In PWM control, the inverter switches are turned ON and OFF several times during a half cycle and output voltage is controlled by varying the pulse width. SPWM techniques are characterized by constant amplitude pulses with different duty cycle for each period. The width of this pulses are modulated to obtain inverter output voltage control and to reduce its harmonic content. Sinusoidal pulse width modulation is the mostly used method in motor control and inverter application [7].In order to verify the ability of the proposed multilevel inverter topology to synthesize an output voltage with a desired amplitude and better harmonic spectrum, programmed SPWM technique is applied to determine the required switching angles. It has been proved that in order to control the fundamental output voltage and eliminate 'n' harmonics, 'n+1' equations are needed. The method of elimination will be presented for 7-level inverter such that the solution for three angles is achieved. The Fourier series expansion of output voltage waveform using fundamental frequency switching scheme as follows

$$V_o(\omega t) = \sum_{n=1,3,5}^{\infty} \frac{4V_{dc}}{n\pi} (\cos(n\theta_1)) + \cos(n\theta_2) + \cdots + \cos(n\theta_K))\sin(n\omega t)$$

(8)

Where K is the number of switching angle required for 7 level inverter. Ideally, for a given fundamental voltage V_1, it is required to determine the switching angles $\theta_1, \theta_2,..., \theta_K$ so that output voltage $V_o(\omega t)=V_1\sin(\omega t)$ and a specific higher harmonics of $V_n(n\omega t)$ are equal to zero. According to the three phase theory in balanced three phase system third order harmonic is cancelled. The switching angles can be found by solving the following equations

$$\cos(\theta_1) + \cos(\theta_2) + \cos(\theta_3) = m$$
$$\cos(5\theta_1) + \cos(5\theta_2) + \cos(5\theta_3) = 0$$

$$\cos(7\theta_1) + \cos(7\theta_2) + \cos(7\theta_3) = 0 \qquad (9)$$

Where modulation index, $m = \dfrac{V_1}{\left(\frac{4V_{dc}}{\pi}\right)}$

One approach to solve the set of nonlinear transcendental equations (9), is to use an iterative method such as the Newton-Raphson method [8]. In contrast to iterative methods, the approach here is based on solving polynomial equations using the theory of resultants which produces all possible solutions [9]. The transcendental equations characterizing the harmonic content can be converted into polynomial equations. Then the resultant method is employed to find the solutions when they exist. These sets of solutions have to be examined for its corresponding total harmonic distortion (THD) in order to select the set which generate the lowest harmonic distortion (mostly due to the 11th and 13th harmonics). The computed THD in percent is defined by

$$THD\% = \frac{\sqrt{V_3^2 + V_5^2 + V_7^2 + \cdots + V_{19}^2}}{V_1^2} \times 100 \qquad (10)$$

Transforming the transcendental equations (9) into polynomial equations using the change of variables and the trigonometric identities

$$x_1 = \cos\theta_1, x_2 = \cos\theta_2, \; x_3 = \cos\theta_3, x_4 = \cos\theta_4,$$
$$x_5 = \cos\theta_5, \; x_6 = \cos\theta_6, x_7 = \cos\theta_7 \qquad (11)$$
$$\cos(5\theta) = 5\cos\theta - 20\cos^3\theta + 16\cos^5\theta$$
$$\cos(7\theta) = -7\cos\theta + 56\cos^3\theta - 112\cos^5\theta + 64\cos^7\theta \qquad (12)$$

To transfer (9) into the equivalent conditions

$$p_1(x) = x_1 + x_2 + x_3 + -m = 0$$
$$p_5(x) = \sum_{i=1}^{7} (5x_i - 20x_i^3 + 16x_i^5) = 0$$
$$p_7(x) = \sum_{i=1}^{7} (-7x_i + 56x_i^3 - 112x_i^5 + 64x_i^7) = 0 \qquad (13)$$

System (12) is a set of three polynomial equations in three unknowns x_1, x_2, and x_3, where x=(x_1, x_2, x_3,) and the angles condition must satisfy $0 \le x_1 \le x_2 \le x_3 \le 1$. Polynomial systems are also considered to compute the solutions of the harmonic elimination equations by iterative numerical methods which give only one solution [10]. In contrast, this system of polynomial equations will be solved using resultant such that all possible solution of (9) can be found. A systematic procedure to do this is known as elimination theory and uses the notion of resultants. The details of this procedure can be found in [10].

V. Simulation Result Analysis

The performance of the proposed modified cascaded multilevel inverter for induction motor drive is verified through the simulation results. It can be seen from Figure 3 input voltages for each succeeding voltage source is same. Figure 5 shows the simulation diagram of three phase modified cascaded multilevel inverter for induction motor drive. From that multilevel inverter seven level can be easily achieved by making the switching pulse sequences as shown in Figure 6 and Figure 7. Figure 8 and 9 shows the output voltage waveform of single phase line to ground and line to line voltages of the proposed inverter. Figure 10 and 11 shows the output voltage waveform of three phase line to ground and line to line voltages of the proposed inverter In this phase voltage is 220V and line voltage is 400V for seven level. Figure 12 and 13 shows the MATLAB simulation output waveform of speed and torque curve of induction motor. From the speed and torque curves, it is concreted that rated speed quickly achieved within 0.4 msec and the torque is quickly settled at 0.45 msec. Figure 14 shows the stator current waveform of induction motor. Therefore the proposed multilevel inverter can be used for variable speed drive application, which can be obtained by varying the frequency of multilevel inverter. From the FFT analysis it can be inferred that when the number of levels are increased, the harmonics and total harmonic distortion is reduced. Figure 15 shows THD value of proposed seven level inverter and it is 11.98%.
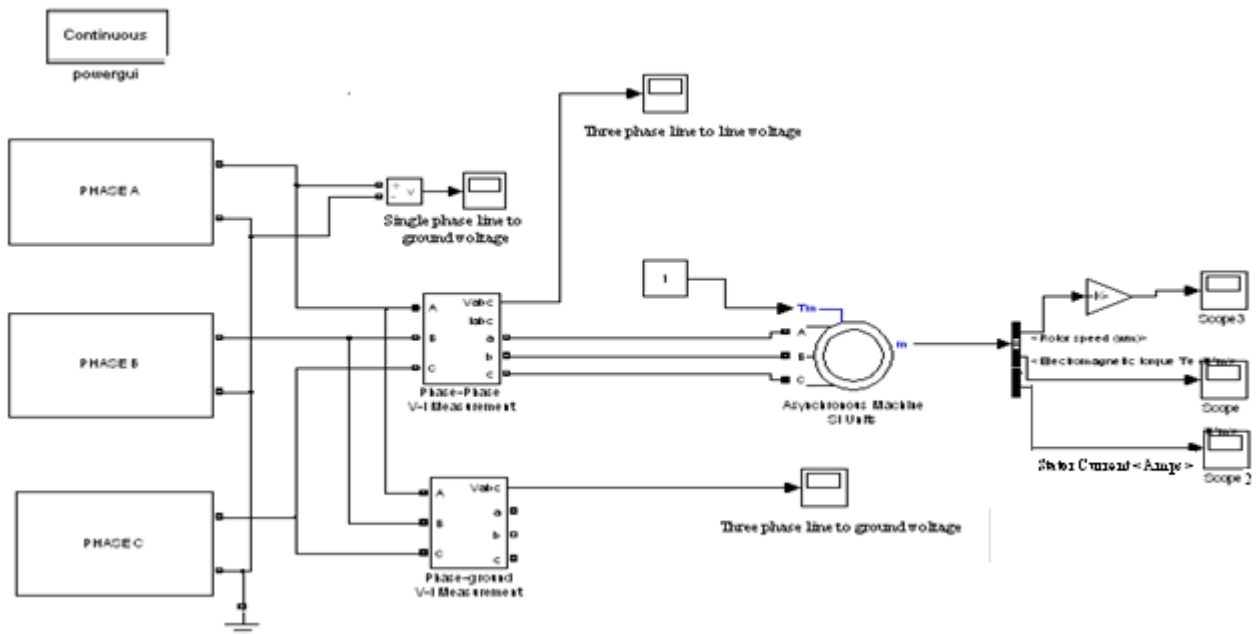
Figure 5: Simulation diagram for modified cascaded multilevel inverter for induction motor drive
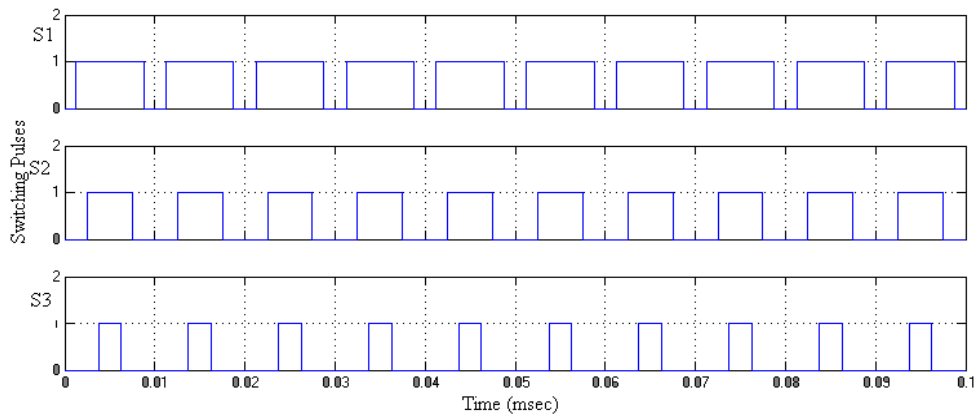
Figure 6: Switching pulses for Switches S1, S2, S3, S4, S5 and S6
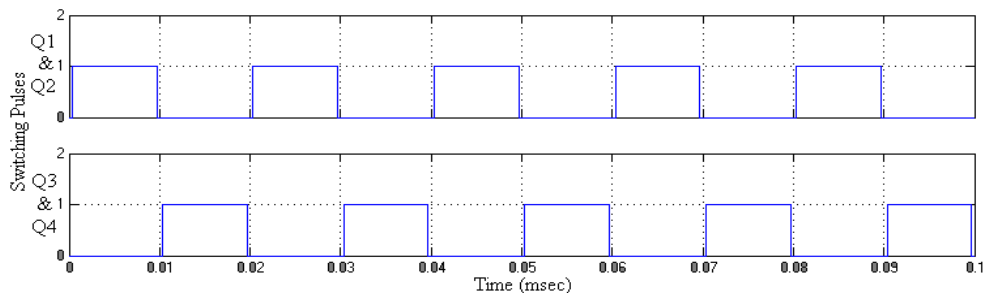
Figure 7: Switching pulses for Switches Q1-Q2 and Q3-Q4
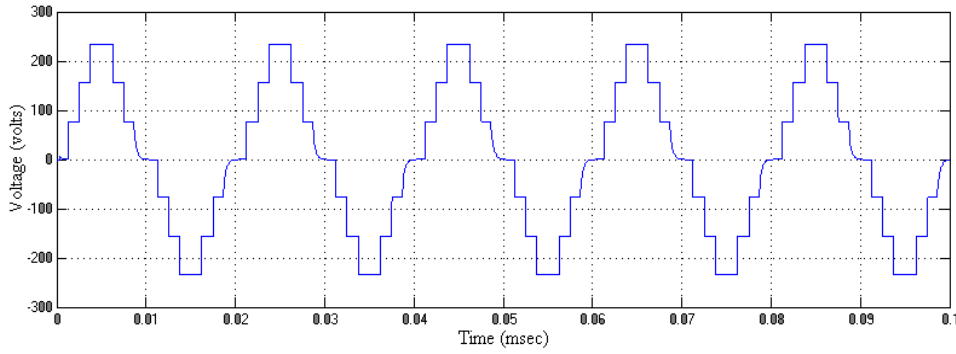
Figure 8: Single phase to ground output voltage waveform for modified cascaded multilevel inverter
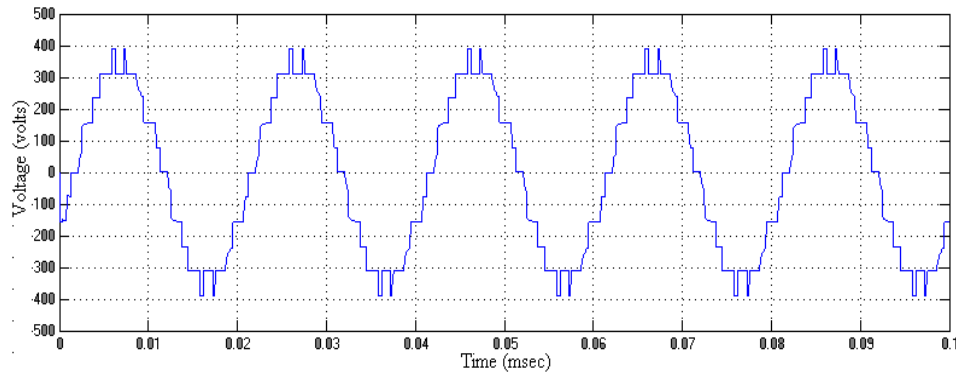
Figure 9: Single phase to phase output voltage waveform for modified cascaded multilevel inverter
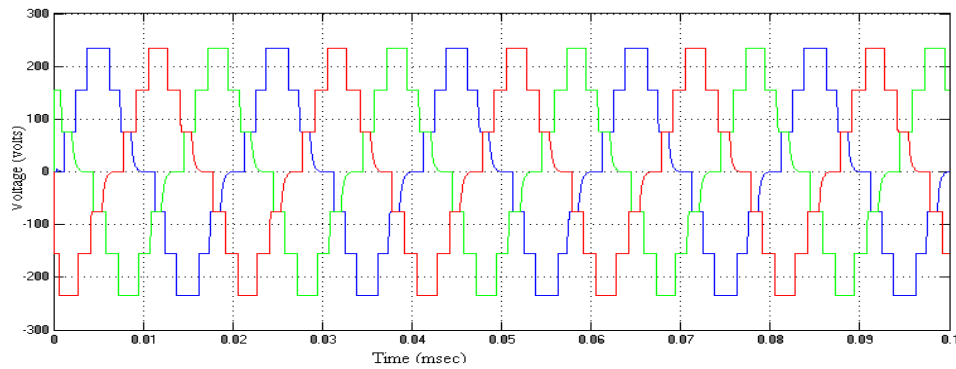
Figure 10: Three phase line to ground output voltage waveform of f modified cascaded multilevel inverter
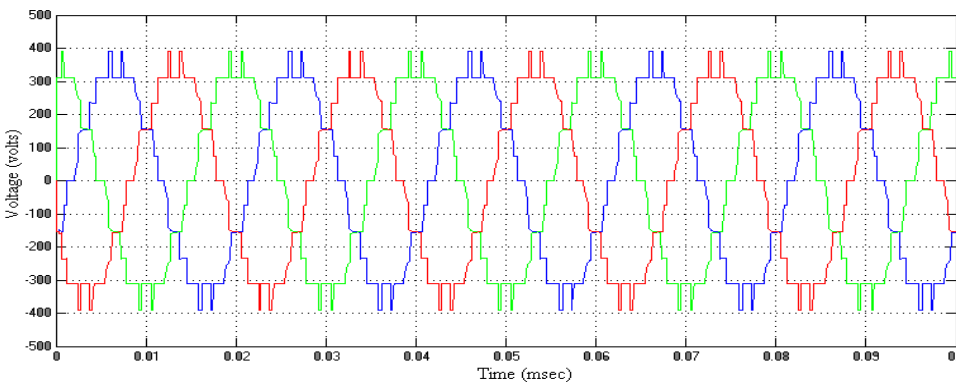
Figure 11: Three phase line to line output voltage waveform for modified cascaded multilevel inverter
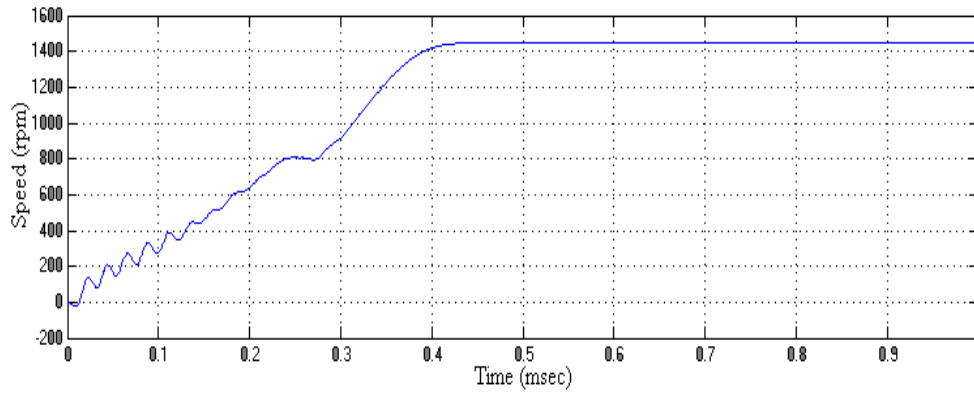
Figure 12: Speed curve of modified cascaded multilevel inverter fed induction motor drive
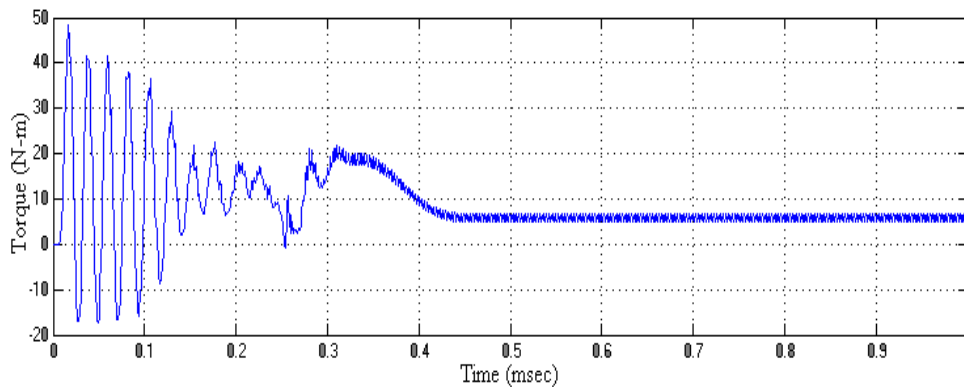
Figure 13: Torque curve of modified cascaded multilevel inverter fed induction motor drive
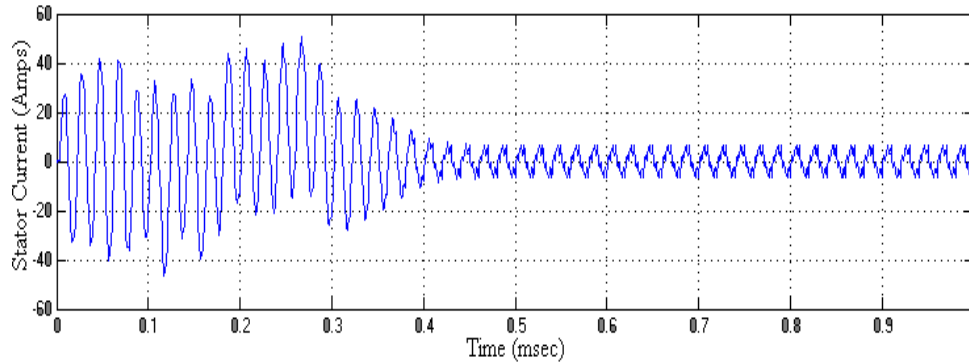
Figure 14: Stator current waveform of modified cascaded multilevel inverter fed induction motor drive
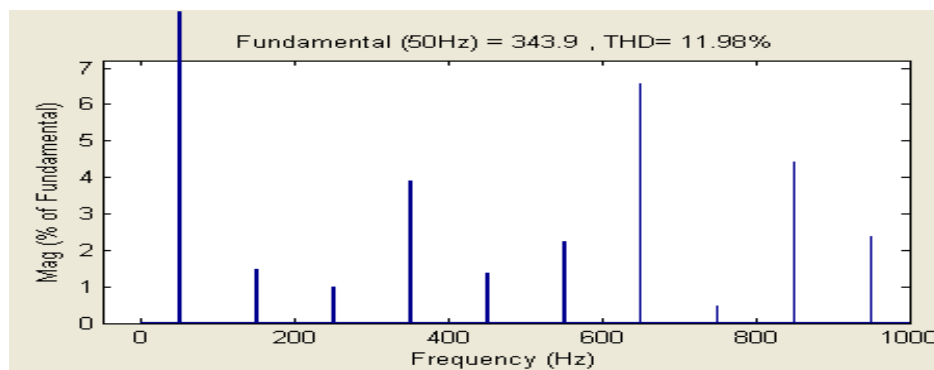
Figure 15: FFT analysis for seven level modified cascaded multilevel inverter

Vi. Comparison Results

Table II shows that the modified cascaded multilevel inverter involves only seven switches whereas conventional inverter comprises twelve switches, but in both cases input voltage at each stage and output level are same. Therefore the proposed modified cascaded multilevel inverter has less switching losses, simple control circuit and less complexity than conventional cascaded multilevel inverter.

Table II. Comparison of cascaded and modified cascaded multilevel inverter

S.No	Name of Topo logy	Voltage level on each stage(S)	Number of output level	Number of switches used	Number of switches for seven level
1	Cascaded Multilevel inverter	$1V_{dc}$	2S+1	4S	12
2	Modified Cascaded Multilevel inverter	$1V_{dc}$	2S+1	S+4	7

Vii. Experimental Verification

Simulation of modified cascaded multilevel inverter output voltage is verified by single phase hardware prototype. Hardware prototype includes seven switches. Among those, three MOSFETs and three diodes are made available for a multi conversion cell. This cell consists of three power stages. In each power stage, one MOSFET (IRF250) and one diode are used as main switches, which are connected in modified configuration. Each stage is supplied by a symmetrical DC source. A PIC 16F877 microcontroller is used as the main processor, which provides gate logic signals. According to microcontroller control signal MOSFET gate terminal is turned on and off. Output of the inverter terminal is connected to R load. Hardware result of proposed multilevel inverter is exposed in Figure 14. The resultant voltage of seven level cascaded multilevel inverter is 9 volts, with frequency of 50 Hz. The hardware block diagram and prototype of modified cascaded multilevel inverter for a single leg are shown in Figure 15 and 16.
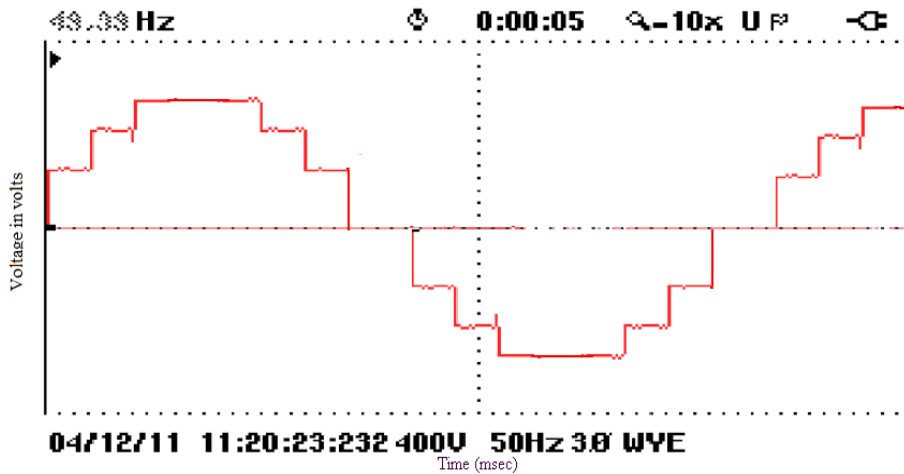
Figure 14: Hardware output waveform for modified cascaded multilevel inverter
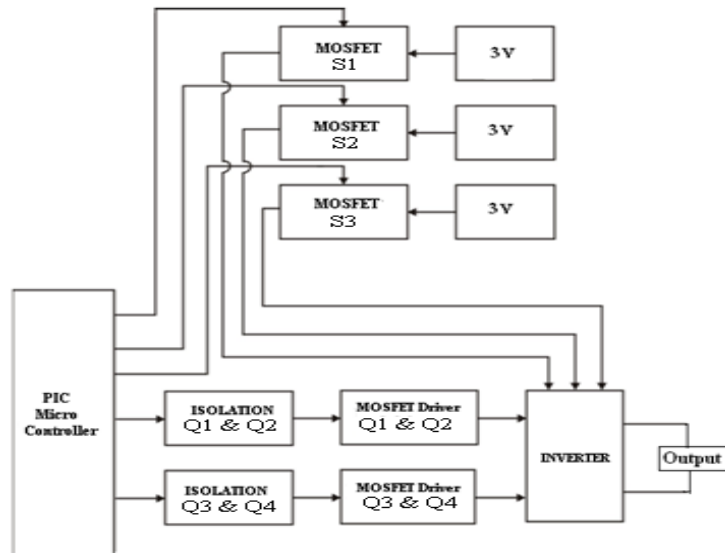
Figure 15: Block diagram for modified cascaded multilevel inverter
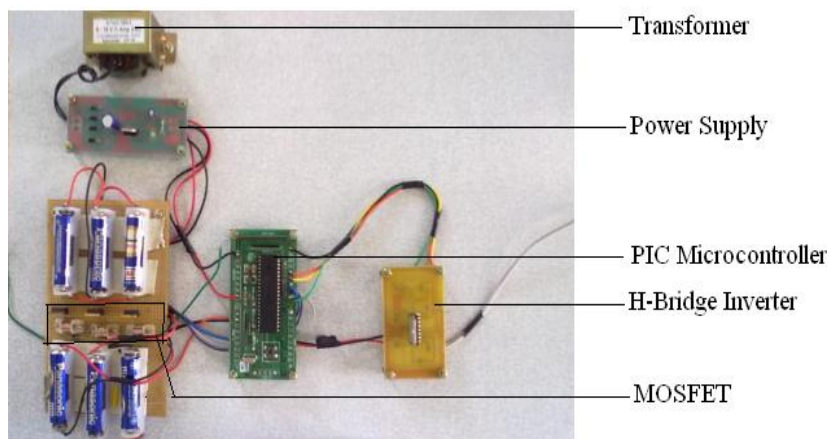
Figure 16. Experimental setup of modified cascaded multilevel inverter

Viii. Conclusion

This paper revealed that proposed modified multilevel inverter topology with reduced number of switches can be implemented for industrial drive applications. This multilevel inverter structure and its basic operations have been discussed elaborately. A detailed procedure for calculating required voltage level on each stage has been conversed. As conventional seven level inverter involves twelve switches, it increases switching losses, cost and circuit complexity The proposed inverter engages only seven switches with three didoes, which reduces switching losses, cost and circuit complexity. Moreover it effectively diminishes lower order harmonics. Therefore effective reduction of total harmonics distortion is achieved.

Appendix

Motor Details
Rotor Type: Wound
Nominal Power: 3730 W
Voltage: 420 Volts
Frequency: 50 Hz
Stator Resistance: 1.115Ω
Stator Inductance: 0.005974Ω
Rotor Resistance: 1.083Ω
Rotor Inductance: 0.005947Ω

References
Journals:
1. L.G.Franquelo, "The age of multilevel converters arrives", IEEE Industrial Electronics Magazine", Vol.2, No.2, pp 28-39, June 2008
2. J.Rodriguez, J.S.Lai and F.Z.Peng, "Multilevel inverters: Survey of topologies, controls, and applications", IEEE Trans. Ind .Appl. Vol.49, No.4, pp.724-738, Aug 2002
3. Z.Du, L.m.Tolbert, J.N.Chiasson, and B.Opineci, "A cascaded multilevel inverter using a single dc power source", in Proc. IEEE APEC, pp.426-430, 2006
4. Fang Zheng Peng "A Generalized Multilevel Inverter Topology with Self Voltage Balancing", IEEE Trans. Ind .Appl., Vol.37, No.2, March/April 2001
5. K.A.Corzine, M.W. Wielebski, F.Z Peng, and J.Wang, "Control of cascaded multilevel inverters", IEEE Trans. Power Electron., Vol.19, No.3, pp.732-738, May 2004
6. K.A. Corzine, F.A.Hardick, and Y.L.Familiant, "A cascaded multilevel inverter H-Bridge inverter utilizing capacitor voltage source", Proceeding of the IASTED International Conference, Power and Energy Systems, pp.290-295, Feb.24-26, 2003
7. B. Ismail, S. T. "Development of a Single Phase SPWM Microcontroller-Based Inverter" First International Power and Energy Conference PEC, Putrajaya, Malaysia: IEEE, Nov, 28-29, 2006.
8. H.S. Patel and R.G. Hoft, "Generalized Techniques of Harmonic Elimination and Voltage Control in Thyristor Inverters: Part I – Harmonic Elimination", IEEE Trans. Ind.Appl., 3, pp. 310-317, 1973.
9. J.N. Chiasson, L.M. Tolbert, K.J. Mckenzie and Z. Du, "Control of a Multilevel Converter Using Resultant Theory", IEEE Transactions Control System Theory, Vol. 11, No.3, pp. 345-354, 2003.
10. J.N. Chiasson, L.M. Tobert, K.J. McKenzie and Z. Du, "A Unified Approach to Solving the Harmonic Elimination Equations in Multilevel Converters", IEEE Trans. Power Electron., Vol.19, No.2, pp. 478-490, 2004.

Biography

M.Murugesan was born in Anthiyur on December 27, 1986. He is graduated in 2009 from Anna University, Chennai. He is post graduated M.E Power Electronics and Drives during 2011 from Anna University. He is currently working as Assistant professor at V.S.B Engineering College. His area of interest involves in Power Electronics, inverter, modeling of induction Motor. He is an ISTE life member. He has published more than 12 papers.

R.Sakthivel received his Bachelor degree in Electrical and Electronics engineering from Madras University, Chennai, in the year 2002, and Masters in power electronics and drives from Anna University, Chennai in the year 2007. He is currently working as a Assistant professor in the Department of Electrical and Electronics Engineering, at V.S.B. Engineering college, Karur. His research area includes Semiconductor devices, Inverters, Machine design and Drives & controls.

E.Muthukumaran received his Bachelor degree in Electrical and Electronics engineering from National Engineering College, Kovilpatti, in the year 2009, and Masters in power systems engineering from K.L.N College of Engineering, Madurai in the year 2011. He is currently working as Assistant professor in the Department of Electrical and Electronics Engineering, at V.S.B. Engineering college, Karur. His research interests are Power System Stability, Inverters, Neural Networks and Fuzzy logic applications to power system.

R.Sivakumar was born in Madurai on June 4, 1979. He is graduated in 2000 from M.K.University, Madurai and post graduated in 2011 at Anna University of technology, Trichy. He is currently working as Assistant professor in the department of EEE at VSB engineering College, Karur from April 2006. His research area involves inverter and modeling of wind turbine. He is an ISTE life member.

A Comparative Analysis Of Two Position Based Hybrid Routing Algorithms Over MANETs.

Mr. Chethan Chandra S Basavaraddi [1], Smt. Geetha N.B. M.Tech [2],

Department of Computer Science, University B.D.T. College Of Engineering Davangere–577004, Karnataka
Visvesvaraya Technological University, Belgaum, Karnataka - India.
Ph: 09916704280, 09844508359, India.

Abstract

Mobile ad hoc networks (MANETs) are autonomously self-organized networks without infrastructure support. In a mobile ad hoc network, nodes move arbitrarily; therefore the network may experience rapid and unpredictable topology changes. Here each node participating in the network acts as host and a router and therefore must forward packets for other nodes. Because nodes in a MANET normally have limited transmission ranges, some nodes cannot communicate directly with each other. Hence, routing paths in mobile ad hoc networks potentially contain multiple hops, and every node in mobile ad hoc networks has the responsibility to act as a router. Researches in this area are mostly simulation based, and in this paper we will be analyzing the performance of DWI-PBHRA routing protocol with the PBHRA. In the performance evaluation of the protocol, the protocols are tested under the realistic conditions including evaluating performance when applied to variable pause times and constant number of nodes we perform extensive simulations using NS-2 simulator.

Keywords: Hybrid routing, Extended battery life, Manet, Position Based Routing, Ad-Hoc Networks, Mobility.

1. Introduction

In recent years, the study of *mobile ad hoc networks (MANETs)* has attracted a lot of interest, mainly from the networking community. A significant part of the research has focused on routing, which is particularly challenging in MANETs due to their dynamic nature [8], and requires algorithms that work in a fully distributed way, are able to self-organize, and show robust and adaptive behaviour. As a result, a number of MANET routing protocols have been designed [7], [3]. However, due to the costs and technological difficulty of setting up real and large MANET test beds, most of this research is carried out in simulation.

These simulations are usually based on simplified scenarios, where nodes move randomly in an open area, and rely on idealized models of physical phenomena such as interference. Recently, experiences with real world test beds [2] have lead to an awareness that results from such simplified simulation scenarios do not reflect well the performance that can be expected in reality. There is therefore now a lot of interest in simulation studies that reflect more complex, realistic situations. In this paper, we investigate the distinctive properties in terms of limitations such as the mobility patterns, and data patterns, and we study how they affect the effectiveness of the two routing algorithms.

2. Related Works

Extensive research has been done in modeling mobility for MANETs. In this section, we mainly focus on experimental research in this area. Much of the initial research was based on using random waypoint as the underlying mobility model and Constant Bit Rate (CBR) [5] traffic consisting of randomly chosen source-

destination pairs as the traffic pattern. Routing protocols were mainly evaluated based on the following metrics: packet delivery ratio (ratio of the number of packets received to the number of packets sent) and routing overhead (number of routing control packets sent). However, in this paper we focus on the impact of mobility models on the performance of MANET routing protocols, so our two observations regarding to discuss the effect of movement mobility speed of the nodes to evaluate the performance of the two Geographic Position Based Routing Algorithms, using NS- 2[11] simulator considering the problem from a different perspective, using the simulation with varying number of movement speed at an invariable pause time which should be zero under weakest case because a longer pause time of the node may be insignificant for mobile Ad-hoc network with frequently and fastly moving nodes, based on the routing load and the connectivity of three typical routing protocols of ad-hoc networks with the different simulation model and metrics like (mobility speed, simulation times, connectivity sources).

2.1 Routing Protocols for Ad-hoc Networks

To compare and analyze mobile ad-hoc network routing protocols, appropriate classification methods are important. Classification methods as Figure 1 help researchers and workers on mobile wireless ad-hoc protocols and designers to understand distinct characteristics of a routing protocol and find its relationship with others [13].
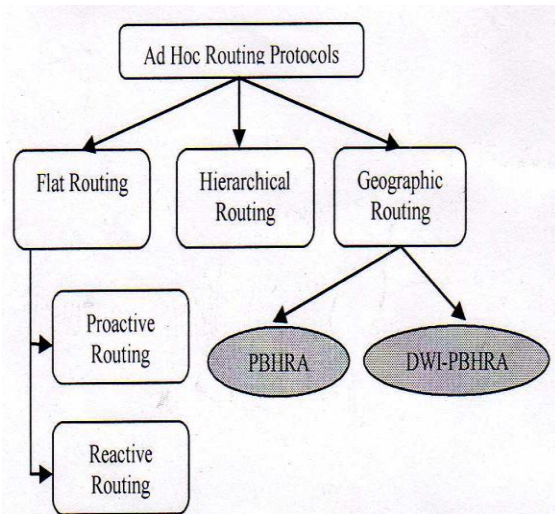
Fig 1: Classification of the Routing Algorithm.

2.2 Mobile Ad-Hoc Networks MANETs

In order to facilitate communication within the network, a routing protocol is used to discover routes between nodes. The primary goal of such an ad-hoc network routing protocol is correct and efficient route establishment between a pair of nodes so that messages may be delivered in a timely manner. Route construction should be done with a minimum of overhead and bandwidth consumption. An Ad-hoc routing protocol is a convention or standard that controls how nodes come to agree which way to route packets between computing devices in a MANET. In ad hoc networks, nodes do not have a priori knowledge of topology of network around them, they have to discover it. The basic idea is that a new node announces its presence and listens to broadcast announcements from its neighbors. The node learns about new near nodes and ways to reach them, and announces that it can also reach those nodes. As time goes on, each node knows about all other nodes and one or more ways how to reach them.

3. Summary Of Routing Models For Simulation

In mobile Ad hoc Network the routing can be categorized into three categories namely, proactive routing, reactive routing and hybrid routing. Many proactive protocols stem from conventional link state routing. On-demand routing, on the other hand, is a new emerging routing philosophy in the ad hoc area. It differs from conventional routing protocols in that no routing activities and no permanent routing information is maintained at network nodes if there is no communication, thus providing a scalable routing solution to large populations. His category of protocols combines the best features of the proactive and the reactive categories. Nodes within a certain distance from the node concerned, or within a particular geographical region, are said to be within the routing zone of the given node. For routing within the zone the proactive approach is used and for the nodes that are located beyond the zone a reactive approach is used. Here we will discuss the two models which will use some of the table driven or proactive and on-demand reactive routing concepts. Although these two models comes under Hybrid protocols they differ from the other hybrid protocols as this two comes under the Geographical position based routing algorithms which are interested in localized nodes. Localization is realized by GPS that is use to determine the geographical position of the nodes. The position change occurs due to nodes mobility.

3.1 The PBHRA Model

Routing algorithm called position based hybrid routing algorithm (PBHRA) [9] was developed to optimize bandwidth usage of ad hoc networks. In the PBHRA algorithm, a central node, in other words a master node is assigned as it is in infrastructured wireless networks and directs the routing information. When nodes require sending data to a target node, they take the location of target node and the route to achieve it from master node. Accordingly, they send their data through that route. At this stage, the PBHRA differs from infrastructure wireless networks since data is sent via central station in infrastructured wireless networks. However in this algorithm, the master node behaving as if it is central node helps only while finding the route to achieve the target. The main goal of PBHRA is effective use of bandwidth by reducing the routing overload. Additionally, the other goals of the algorithm are to extend battery life of the mobile devices by reducing the required number of operations for route determination and to reduce the amount of memory used.

3.1.1. Working steps of algorithm

The detailed working steps of the algorithm are these: (a) The first node that stands up, while network is firstly started is assigned as master node. If two nodes are opened at the same time and two master nodes form, these nodes compare MAC addresses in the first packets that they took from each other and the node whose MAC address has higher value decides not to be the master node. The details of master determining process are given in the following section. (b) Master node broadcasts packets in regular intervals and declares to the other nodes in the network that it is the master node. These packets are called "master node announcement packet (map)".(c) The nodes excluding master node send "update packets (up)" to master node. In these packets there is information about the geographical position of nodes (as x, y, z coordinates), rest of battery life as percentage and node density. There are destination address, source address and id area in the update packet. Id area is used for in order to update the related line of position information matrix that master node will form.

The receiver address is the current address of the node that sent updating data. Sender node increases id area in

the packet each update. In this format of updating information is processed as a row element in P matrix kept on master node. If updating information is taken from the same node formerly id values are compared. The packet that has higher id value is recorded and follow former record is changed.

$$P = \begin{pmatrix} x_1 & y_1 & z_1 & b_1 & d_1 & id_1 \\ x_2 & y_2 & z_2 & b_2 & d_2 & id_2 \\ \ldots\ldots\ldots\ldots\ldots & \ldots \\ \ldots\ldots\ldots\ldots\ldots.. \\ x_k & y_k & z_k & b_k & d_k & id_k \end{pmatrix} \ldots(1)$$

(d) Master node forms position information matrix by using packets that come from other nodes. There are position information as (x_i, y_i, z_i), battery life as b_i, density d_i and node update sequence number id_i in the columns of this matrix called P matrix. The row numbers of the matrix are equal to number of nodes. This matrix for k-node network is given in (1).

$$l_{i,j} = \sqrt{(x_j - x_i)^2 + (y_j - y_i)^2 + (z_j - z_i)^2} \ldots (2)$$

(e) Master node calculates the distance of each node to each other by using the first, second and third columns of P matrix that is given in (1). It makes this process by using the (2). In the result of this, q square matrix that's dimension is equal to number of nodes in the network. M distance matrix for k-node network is obtained as given (3).

$$M = \begin{pmatrix} l_{1.1} & l_{1.2} & \ldots & l_{1.k} \\ l_{2.1} & l_{2.2} & \ldots & l_{2.k} \\ \ldots\ldots\ldots\ldots. & \ldots\ldots \\ \ldots\ldots\ldots\ldots.. \\ l_{k.1} & l_{k.2} & \ldots & l_{k.k} \end{pmatrix} \ldots(3)$$

The diagonal of M will be zero as the distance of every node to itself is zero. Also with a condition i _ j, the distance between i and j and the distance between j and i are the same, thus the matrix M will be symmetrical matrix. Therefore the upper triangular part of matrix M will only be calculated. The lower triangular part of M will be filled by upper triangle. As a result of this, the computational time, which is an important factor for battery life of a node, is reduced. (f) The node in the center of the network is determined. The total of row elements of M distance matrix given in (3) are derived and transferred to column matrix T that is given in (4). The number of the row that has the smallest element of T matrix is equal to the number of the node that is in the center of the network.

$$T = [\, t_1 \ t_2 \ t_3 \ \ldots \ t_k \,] \ldots(4)$$

Where

$$t1 = \sum_{n=1}^{k} l_{n.1} \ldots(5)$$

(g) New master node candidate is the node that is in the center of the network. Master node asks candidate master node if it can be the new master node. If the answer is positive, it sends the whole routing information that it keeps on itself to the new master node and also it declares new master and its position information to the other nodes. If the answer is negative, the second central node for the T matrix is the new master candidate. The same processes are realized for this node. Candidate node can refuse to be the master node because of low battery life or high density.

(h) New master node sends broadcast packets to the network relating to being master node. The updating packets that will come from other nodes are collected in P matrix as the former master node did. New master node repeats the steps between a to h.

(i) The other nodes send event based updating packets to the master node when they changed their position, their battery life got under threshold level and their density increased. Thanks to id value sent in P matrix related to that node. Because other nodes send id value that is one bigger than the former in the update packet they sent.

(j) According to this algorithm, normal nodes requisition from master node path information to destination node when they want to send a data to any destination. Master node assigns a cost value to the intermodal borders with fuzzy logic by using M matrix and P matrix when a request relating to a destination comes to itself. In this way a graph consisted of nodes and borders forms. G matrix is formed in order to keep the cost values of graph. The forming of G matrix will be handled in the next section. (k) Master node supplies an optimization in order to found the path between source and destination with the least cost over the formed graph. The shortest path, in other words the path has lowest cost is determined by using Dijkstra or Bellman Ford algorithm.

(l) Master node declares the result got from j and k steps to the node which requested path and related node send its data using this path. When any node will demand routing path from master node, it sends a "route request packet (rqp)" to the master node. Master node sends "route reply packet (rrp)" to the node which requested a route. Master node answers to the node that is the owner of request by determining most optimum path to the destination node from the source node and replacing an optimization on graph structure that is formed when master node received route request packet.

(m) If master node goes far from central position or battery life falls down a threshold, it transfers the mastership to other node, which has minimum row total value in M. Nodes decide to be a master node or not in

accordance with battery lives and densities. In the case of master node's closure with any reason, a "secondary master" node is assigned in order not to make network stay without a master. This assignment process is made by the master node. Master node selects the nearest node to itself as the secondary master. It sends the routing information that it holds on itself to the secondary node in certain periods. The frequency of data sending to the secondary master is four times of the interval of master node broadcast packet sending

(n) The other nodes do not hold information belonging to whole nodes and do not make any process related to routing. But they hold "master node packet" that comes from master node in their memories.

Figure 2 shows the flow chart of the algorithm whose detailed steps were given.

3.1.2. Determining role of master node

According to PBHRA algorithm, there are three roles for a node in the network. These are master, secondary master and normal node. The process of determining secondary master's role is determined by master node. For this reason, a node has to know whether it is a master node or a normal node. Determining of being a master is realized with following steps:

(a) A node in the network waits for 30 second after it stands up

(b) Did the node receive master node announcement packet (map) in this period?

c) If the answer step b is yes; (c1) Did it receive one map, or more maps than once?

(c1a) If it receives one map, it records at its memory the address and position of node from which it receives a packet as master node. Thus, it decides itself that it is a Signal

.normal node. c1b) If it receives maps more than once, it compares the address in the packets received. It records the one with low address and its position into its memory as master node. It decides that it is a normal node itself.

(c2) It sends an update packet

(up) containing its position to master node whose address is stored in memory.

(d) If the answer of 2nd step is No; (d1) There is no master node in the network. It decides that it is a master node itself; (d2) It broadcasts maps for period of 30 seconds.

e) Finish.
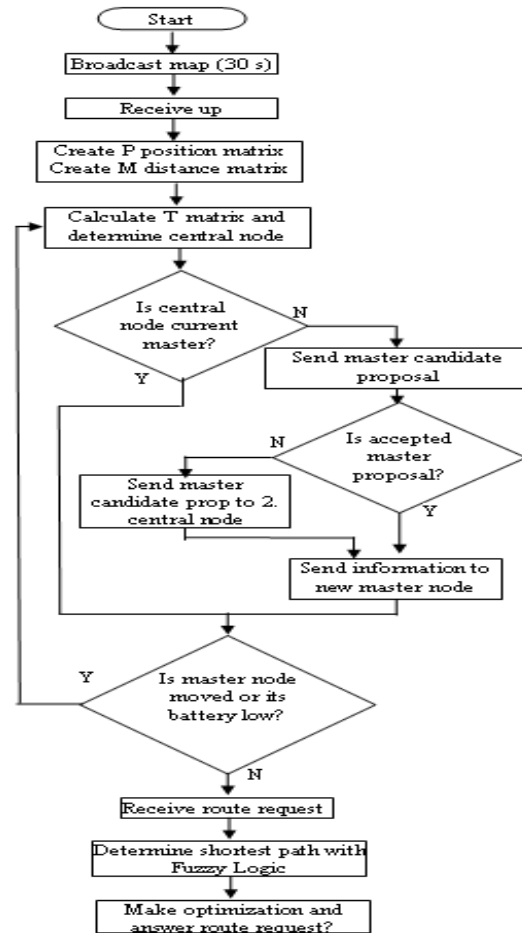
Figure 2. Flow chart of PBHRA algorithm

3.2 The DWI-PBHRA Model

The distributed workload implied approach to the PBHRA is the work with the goal of monitoring the mobility in the network and the other goals where to reduce the energy consumption for communication, reduce the routing overhead and making the network more reliable. The central nodes, in other words a primary (Brain) and secondary (Heart) nodes are assigned as it is in infrastructured wireless networks and directs the routing information. When nodes require sending data to a target node, they take the location of target node and the route to achieve it from brain node. Accordingly, the data is send through that route. The heart node is newly implemented to monitor the networks mobility by broadcasting frequent alive packets in the network. And the algorithm provides the network with the recovery mechanism, for unexpected crashes of Master, making the network more reliable.

4. Design Of The Experiment

The Algorithms to be analyzed for routing need to be experimented under the carefully designed routing traffic base configuration and network scenario, and to vary the node density and mobility at a time to stress the network

in different directions. Careful selection of these control parameters enables us to assess and isolate the effect of network size, with fixed application traffic CBR. In addition, design of the base condition, network topology, and routing are to be taken into account the real networks for which the results should be applicable.

4. 1 Mobility Setup

A mobility model [10] should attempt to mimic the movements of real Mobile Networks. Changes in speed and direction must occur and they must occur in reasonable time slots. For example, we would not want Mobile Networks to travel in straight lines at constant speeds throughout the course of the entire simulation because real Mobile Networks would not travel in such a restricted manner. There is several mobility models supported, nodes in the simulation set up move according to a model that is well known as the "random waypoint" model. The movement scenario files we used for each simulation are characterized by a pause time. Each node begins the simulation by remaining stationary for pause time seconds. It then selects a random destination in the 500m x 500m space and moves to that destination at a speed distributed uniformly between 0mps and a maximum speed of 10mps. Upon reaching the destination, the node pauses again for pause time seconds, selects another destination, and proceeds there as previously described, repeating this behavior for the duration of the simulation. Each simulation ran for 200 seconds of simulated time. We ran our simulations with movement patterns generated for a fixed pause time of 30 Seconds.

4.2 Traffic Setup

A traffic generator named Cbrgen was developed to simulate constant bit rate sources in NS-2, act as the important parameter of our simulation to compare the performance of each routing protocol. We chose our application traffic sources to be constant bit rate (CBR) sources. When defining the parameters of the communication model, we experimented with sending rates of 1.2 packets per second and packet sizes of 512 bytes to observe the consistency.

4.3 Effect of Unvarying Pause Time

Pause time can be defined as time for which nodes waits on a destination before moving to other destination. We used a constant pause time as a parameter as it is measure of mobility of nodes. Low pause time means no de will wait for less time thus giving rise to high mobility scenario.

5. Simulation Results And Performance

This section presents a comparative analysis of the performance metrics generated from all simulations, evincing general and relevant aspects of the evaluated routing protocols in the diversity of network mobility levels that can occur over the Position Based Hybrid

Routing Algorithm, and Distributed Workload implied Position Based Hybrid Routing Algorithm. Considering the diversity of routing protocols user mobility levels (20, 40, 60, 80, and 100 m/s). Performance metrics that have been proposed for the performance evaluation of an ad-hoc network protocol. The following metrics are applied to comparing the protocol performance. Some of these metrics are suggested by the MANET working group for routing protocol evaluation [6].

Packet delivery fraction ratio: The ratio between the number of data packets originated by the "application layer" CBR sources and the number of data packets received by the CBR sink at the final destination [1], [12].

Routing packet overhead: Routing Packet overhead RPO is the total number of transmissions routing packets transmitted during the simulation. For packets sent over multiple hops, each transmission of the packet (each hop) counts as one transmission [4].

Packet loss ratio: The ratio of the data packets originated by the sources failure to deliver to the destination.

5.1 Analysis Based on Energy Consumed by Cluster-heads

The Energy consumed by the cluster heads were compared for both the algorithms under the diversity of routing protocols user mobility levels, and the results shown in the Figure 3 suggests that in the DWI-PBHRA model the cluster heads consumed lesser energy compare to the PBHRA at any mobility levels.
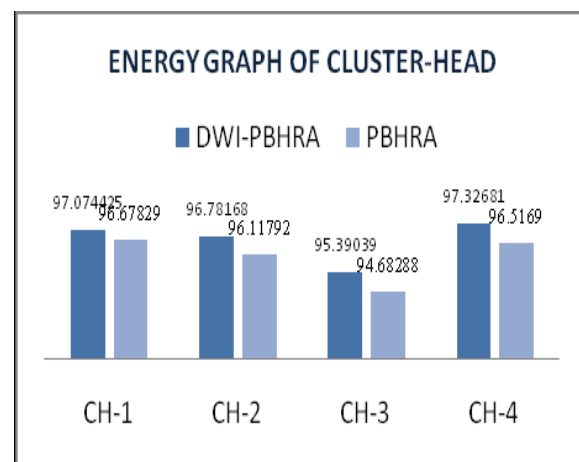

Fig 3: Energy Graph of Cluster-Head

5.2 Analysis Based on Packet Routing Overhead

The routing packet overhead is the packets need to be transferred to make a connection for communication, and from the results of the simulation the DWI-PBHRA performed better with less packet routing overhead in the network at the various levels of the mobility.
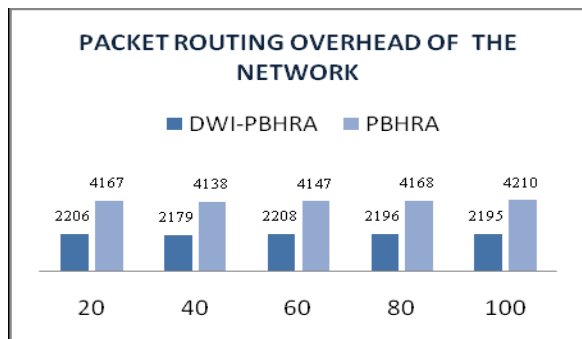
Fig 4: Packet Routing Overhead of the Network

The Figure 4 is the graph with the x axis for variable pause time and the y axis is for the no of packets for the network to establish and connection to be made for the transfer of the data in the network. This analysis was made under the fixed simulation setup where the simulation was made for 200secs.

6. Performance Analysis

Performance analysis has done for the pause time with packets received, pause time with consumed energy. During the simulation it was found that a change in the pause time affects the energy consumption and packet delivery fractions in the network. Every time the network needs to be monitored and every hop need to reliable for transfer of data hence topology changes frequently need new routes for data transfer. It was found that for more mobility or short pause time was not managed well in the infrastructure less network where the infrastructure based network with central control were more capable of handling large networks better in high mobility. Here our proposed scheme has given better results in terms of packed delivery fractions as well as energy savings.

7. Conclusion

The area of ad-hoc networking has been receiving increasing attention among researchers in recent years, as the available wireless networking and mobile computing hardware bases are now capable of supporting the promise of this technology. Over the past few years, a variety of new routing protocols targeted specifically at the ad-hoc networking environment have been proposed, but little performance information on each protocol and node tailed performance comparison between the protocols has previously been available. This paper has presented a comparing performance of two Position Based routing algorithms that comes under the hybrid routing algorithm category, include the properties of table driven and on demand protocols and are usually interested in localized nodes. For routing packets between wirelesses mobile hosts in an ad-hoc network PBHRA and DWI-PBHRA using a network simulator like NS-2 with scenario consist of fixed network size, number of nodes and movement speed in a range of 0 to 10 at

variable pause time. The General observation from the simulation: The Distributed workload implied position based routing algorithm which was developed with the goal of monitoring the mobility of the network that it achieved by introduction of heart node and its pulses, The Performance got a difference because of the distribution of the work among the member, Brain and Heart nodes. Whereas the master node in the Position base Hybrid routing algorithm had more overload of routing and giving central control, the reliability was there in the new approach of brain and heart with its recovery mechanism from crash of Master. The Results showed the distributed workload implied position based hybrid routing algorithm outperformed the position based hybrid routing algorithm for the energy consumption by cluster head, packet Routing overhead, and packet delivery fraction.

References

[1] C. E. Perkins, E. M. Royer, S. R. Das, and M. K. Marina, "Performance comparison of two on-demand routing protocols for Ad Ho c networks," *IEEE Personal Communications Magazine Special Issue on Ad hoc Networking* , vol. 8, pp. 16-28, Feb. 2001.

[2] C. Tschudin, P. Gunningberg, H. Lundgren, and E. Nordstrom, "Lessons from experimental MANET research," *Ad Hoc Networks Journal*, vol.3, no.2, pp.221− 233, 2005.

[3] E.Royerand, C. K. Toh, "A review of current routing protocols for ad hoc mobile wireless networks," *IEEE Personal Communications*, 1999.

[4] J. Bro ch, D. Johnson, and D. Maltz, The Dynamic Source Routing Protocol for Mobile Ad Hoc Networks, *IETF Internet Draft*, Dec. 1998. (http://www.ietf.org/internetdrafts/ draft-ietfmanet-dsr-01.txt)

[5] Kevin Fall and Kannan Varadhan, "ns notes and documentation". *The VINT project, UC Berkeley*, LBL, USC/ISI, and Xerox PARC, May 1998.

[6] L. Layuan, Y. Peiyan, and L. Chunlin, "Performance evaluation and simulations of routing protocols in Ad ho c networks," *Computer Communications*, vol. 30, pp. 1890- 1998, 2007.

[7] M. Abolhasan, T. Wysocki, and E. Dutkiewicz, "A review of routing protocols for mobile ad hoc

networks," *Ad Hoc Networks*, vol.2, pp. 1–22, 2004.

8]   N. H. Vaidya, "Mobile Ad ho c networks routing, mac and transport issues*," Proceedings of the IEEE International Conference on Computer Communication* INFOCOM, 2004.

[9]   Resul Kara ,Ibrahim Ozcelik and Huseyin Ekiz (2010). Anew routing algorithm in MANETs: Position based hybrid routing. *Scientific research and essays* Vol. 5(3), pp. 328-238.

[10]   T. Camp, J. Boleng, and V. Davies, "A survey of mobility mo dels for Ad ho c network research," Wireless Communications & Mobile Computing (WCMC), *Special issue on Mobile Ad Hoc Networking, Research, Trends and Applications*, Sep. 2002.

[11]   The Network Simulator - NS-2. (http://www.isi.edu /nsnam/ns/index.html).

[12]   Y. Wang, V. C. Giruka, and M. Singhal, "A truthful geographic forwarding algorithm for Ad ho c networks with selflsh nodes*," Proceedings of the International Journal of Network Security*, Nov. 2007.

[13]   Yasser Kamal Hassan, Mohamed Hashim Ab d El-Aziz, and Ahmed Safwat Ab d El-Radi, "Performance Evaluation of Mobility Speed over MANET Routing Protocols" *International Journal of Network Security*, Vol.11, No.3, pp.128-138, Nov. 2010.

[14]   Boukerche A, El-Khatib K, Xu L, Korba L (2005) An efficient secure distributed anonymous routing protocol for mobile and wireless ad hoc networks. Computer Communications, Volume 28, Issue 10:1193–1203

[15]   Moaveninejad K, Song W-Z, Li X-Y (2005) Robust position-based routing for wireless ad hoc networks. Ad Hoc Networks, Volume 3, Issue 5:546–559

[16]   Rango FD, Gerla M, Marano S (2006) A scalable routing scheme with group motion support in large and dense wireless ad hoc networks. Computers&Electrical Engineering, Volume 32, Issues 1–3:224–240

[17]   Ghosh RK, Garg V, Meitei MS, Raman S, Kumar A, Tewari N (2006) Dense cluster gateway based routing protocol for multi-hop mobile ad hoc networks. Ad Hoc Networks, Volume 4, Issue 2:168–185

[18]   Wang Y-H, Chao C-F (2006) Dynamic backup routes routing protocol for mobile ad hoc networks. Information Sciences, Volume 176, Issue 2:161–185

[19]   Ahn CW (2006) Gathering-based routing protocol in mobile ad hoc networks. Computer Communications, Volume 30, Issue 1:202–206

[20]   Eisbrener J, Murphy G, Eade D, Pinnow CK, Begum K, Park S, Yoo SM, Youn J-H (2006) Recycled path routing in mobile ad hoc networks. Computer Communications, Volume 29, Issue 9:1552–1560

[21]   Song J-H, Wong VWS, Leung VCM (2007) Secure position-based routing protocol for mobile ad hoc networks. Ad Hoc Networks, Volume 5, Issue 1:76–86

Author Profile:

Mr. Chethan Chandra S Basavaraddi : pursuing M.Tech (CS) from Department of Computer Science, University B.D.T. College Of Engineering Davangere–577004, Karnataka. Visvesvaraya Technological University, Belgaum, Karnataka   - India.
Ph: 09916704280, 09844508359, India.

Smt. Geetha N.B. M.Tech : Asst. Professor,   Department of computer Science, University B.D.T. College Of Engineering Davangere–577004, Karnataka, India..
Ph:09480794017

Smt. Anitha G. BE,ME : Chairperson, Department of computer Science, University B.D.T. College Of Engineering Davangere–577004, Karnataka, India.

Database Architecture with Row and Column stores
Mrs G.Prisilla Jayanthi

ABSTRACT:
Data warehouses perform better with Column Stores as they involve analytical applications like reporting from the information present in them. However, there are reports other than the Informational reports that business organizations need. *Real-time* reports, called the Operational Reports are needed.
Operational reporting differs from informational reporting in that its scope is on day-to-day operations and thus requires data on the detail of individual transactions. It is often not desirable to maintain data on such detailed level in the data warehouse and the update frequency required for operational reports. Therefore, a Hybrid Row-Column database architecture is proposed. An OLTP database architecture that serves the conventional OLTP load out of a row-store database and serves operational reporting queries out of a column-store database which holds the subset of the data in the row store required for operational reports. The column-store is updated within the transaction of the row database; hence OLTP changes are directly reflected in operational reports.
The project done with SAP AG have been studied and the results of are described here. The described solution for Operational Reporting was implemented in SAP Business ByDesign and SAP Business Warehouse.
Row and Column stores along with their applications have been briefed. Then Operational Reporting is described as being different from Informational Reporting and the need for Operational reporting is identified. As the Hybrid Row-Column Database Architecture for Operational reporting solution was implemented in SAP Business ByDesign and SAP Business Warehouse, SAP Business ByDesign, TREX and MaxDB have been discussed briefly.

Informational And Operational Reporting:

Informational Reports are summary reports usually containing past information. These reports help the top or middle management in making long-term decisions.

Operational Reports are detailed reports and are real-time. They help front-line operations personnel in making very short term detailed decisions.

Informational Reports are used strategically whereas operational reports are used tactically by the corporation. Middle management uses informational reports in order to make long-term decisions. In an informational report, the details are almost irrelevant, but the summarizations are everything. Examples of Informational reporting include monthly sales trends, annual revenue, regional sales by product line for the quarter, industry production figures for the year, number of employees by quarter and weekly shipping costs by carrier. The decisions that these kinds of reports support are longer term and tend to be strategic [1]. However, informational reports are not the only reports needed by organizations for decision making. Reports on day-to-day operations are also needed for small-term decision making. These reports are called operational reports and the activity is Operational Reporting.

Operational Reporting is about details. It is typically used by the front-line operations personnel. Very short-term, detailed decisions are made from operational reports. Operational Reporting is designed to support the detailed day-to-day activities of the corporation at the transaction level. In operational reporting, detail is much more important than summary. In fact, in operational reporting, summary information is often irrelevant. Examples of operational reporting include daily account audits and adjustments, daily production records, flight-by-flight traveler logs and transaction logs. The kinds of decisions made from these reports are very detailed, immediate decisions are made under the line-manager level .

Why Operational Reporting?

Operational Reporting is also called "Enterprise Reporting" or "Transactional Reporting" . Operational Reporting is made up of detailed information, organized to meet the needs of each area of business or function (eg: report turnover of a period type of a client or product portfolio composition of orders by geographical area or branch, retail cost structure of a particular department, the average cost resources per cost center).

The operational reporting provides a thorough and detailed management process for each center of responsibility (focusing for example, on revenues of individual products / divisions or costs related to each cost center).

It is a tool for those responsible for operational functions of the company and commercial production, always useful to have financial data under control (revenues, costs and margins of its areas) both indicators efficiency of processes .

One example of operational reporting is planning activities, for example when trying to forecast sales for products offered. Such planning is important to estimate cash-flow and to drive manufacturing planning in order to cater for the expected

demand. This plan will then be tracked against actual sales and will frequently be updated [4]. Often there are requirements to look at the sales data on intra-day basis to support decisions related to production planning or financial planning.

Data Warehousing or OLTP Store?

The fact that operational reporting is real-time and very different from informational reporting makes it difficult to choose from row-stores and column-stores. Data warehousing appears to be an obvious option since reporting is involved hence column stores can be considered. However, the real-time nature of the queries makes (OnLine Transaction Processing)OLTP database also a viable option making us consider row-stores also.

Row stores store the content by row. They are suitable for OLTP. An OLTP database is designed to record hence they are *write-optimized.* A row-oriented implementation of a DBMS stores every attribute of a given row in sequence, with the last entry of one row followed by the first entry of the next.

Column stores store the content by column. They better suit the (OnLine Analytical Processing)OLAP applications and the data warehouse. A data warehouse is a database that is designed for facilitating querying and analysis. Often designed as OLAP systems, these databases contain read-only data that can be queried and analyzed far more efficiently as compared to regular OLTP application databases. Hence they are *read-optimized.*

Row-stores can be emulated as column-stores using mechanisms like Vertical Partitioning, Index-only Plans and Materialized Views but it is seen that none of them perform as well as column-stores do on data warehouses. Thus, column stores are more efficient than row-stores when it comes to data retrieval, analysis and informational reporting.

The fact that operational reporting is real-time and very different from informational reporting makes it difficult to choose from row-stores and column-stores. Data warehousing appears to be an obvious option since reporting is involved hence column stores can be considered. However, the real-time nature of the queries makes OLTP database also a viable option making us consider row-stores also.

Row stores store the content by row. They are suitable for OLTP. An OLTP database is designed to record hence they are *write-optimized.* A row-oriented implementation of a DBMS stores every attribute of a given row in sequence, with the last entry of one row followed by the first entry of the next.

Column stores store the content by column. They better suit the OLAP applications and the data warehouse. A data warehouse is a database that is designed for facilitating querying and analysis. Often designed as OLAP systems, these databases contain read-only data that can be queried and analyzed far more efficiently as compared to regular OLTP application databases. Hence they are *read-optimized.*

Row-stores can be emulated as column-stores using mechanisms like Vertical Partitioning, Index-only Plans and Materialized Views but it is seen that none of them perform as well as column-stores do on data warehouses. Thus, column stores are more efficient than row-stores when it comes to data retrieval, analysis and informational reporting.

Using an OLTP store for Operational Reporting:
Though operational reporting is real-time, the operational reporting queries are relatively long-running in comparison to pure OLTP workloads resulting in resource contention as the locks of long-running queries block the short-running ones. Also, it is well known that the OLTP data model is not optimized for reporting.

Using a DW for Operational Reporting:
What happens to the data warehouse environment if you try to force all reports out of the data warehouse? Some consequences are:
- The data warehouse is forced to be designed to the lowest level of granularity of the corporation. This may or may not be an acceptable design constraint.
- Update will need to be done in the data warehouse. While this can usually be done in the DBMS that manages the data warehouse, this in many ways runs contrary to the way data warehouses operate.
- The timing of adjustments and transactions being entered and reflected inside the data warehouse becomes an issue, usually to the detriment of other operations occurring inside the data warehouse.

In short, the constraints placed on the data warehouses are not positive when operational reporting is done on the data warehouses [1].

Real-time DW Architectures:
The general architecture of data warehouses is well known. The characteristics defined by Inmon, i.e. that data in a warehouse must be subject-oriented, integrated, time-variant, and non-volatile, led to an architecture separating operational and analytical data. Data in OLTP systems is organized according to the relational model, i.e. data is highly normalized in order to ensure consistency and to run day-to-day according to the dimensional model, using for example, the star or the snow-flake schema. The reason for this is mainly the wish to achieve the best query performance for both OLTP and OLAP.

The data warehouse contains an ETL processor which extracts data from various OLTP sources into a staging area, where data transformations for cleansing and integration are applied. Once this process has been completed, the ETL processor stores the data according to a dimensional data storage paradigm, so that an OLAP engine can run queries against this dimensional data store.

With the proliferation of (Business Intelligence)BI technologies, this general architecture has been extended with concepts such as data marts or Operational Data Stores (ODS). Data marts aim at decentralizing warehouses in order to optimize performance around certain subject areas. The downside is that in data mart architectures, the data warehouse cannot provide a consolidated view on all data relevant for strategic decision making in an enterprise, which was the original intent of data warehouses. ODSs store OLTP data, often using an integrated schema, i.e. the ETL steps of data mapping and cleansing are applied before moving data into an ODS. The result is increased timeliness of the data on which reporting can be done, as well as the possibility to work on line-item level incase the ODS is modeled that way. It remains, however, an expensive operation to refresh the ODS. One possibility to optimize timeliness of operational data being available in an OLAP environment would be to shorten the intervals between ETL runs to a minimum. The main disadvantage of such *Microbatch* approaches is the resource consumption of the frequent ETL runs: The ETL process should only run in a defined batch window, because the query performance of the warehouse is dramatically affected during ETL processing time.

To enable less resource-intensive ETL processing, architectures have been proposed that move the data transformation outside of the ETL process. Instead, the transformations are done in the warehouse after extraction and loading. Such processing is called ELT, respectively. Also, *push architectures* for ETL have been proposed in order to replace bulk processing with the handling of deltas on a business or database transaction level. Kimball further suggests separating historical data from recent data in a warehouse. The recent data is constantly copied into the so-called *real-time partition* using the push approach described above. In doing so, the data warehouse can still be optimized for queries on historical data, while recent events in an enterprise are also recorded in the warehouse.

TABLE 1: REAL-TIME DATAWAREHOUSE ARCHITECTURE

Architecture	Working	Usage	Limitation(s)
ODS	Stores copy of the OLTP data using an integrated schema	Reporting can be done with data of increased timeliness	High granularity but no up-to-date data Refreshing ODS with updates is a very expensive operation
ODS Microbatch	Configure ETL process to run in very short intervals	ETL process should run in a defined batch window	Resource consumption of frequent ETL runs dramatically affect the query performance
Push Architecture (ELT)	Data transformations are moved outside the ETL process. Transformations are done in the datawarehouse after extraction and loading	Handles deltas on a business or database transaction level	Resource intensive High granularity but no up-to-date data
Virtual ODS (Pull-oriented architecture)	Queries are redirected against OLTP system	*Inmon* argues that Virtual ODS architectures are of limited use when the data in the source systems is not integrated.	Affects performance of OLTP system

The notion of virtual ODS, as opposed to the traditional, physical ODS describes a pull-oriented OLAP architecture which gathers the requested information at query run-time. The ODS is virtual in the sense that it translates data warehousing queries into downstream queries to OLTP or third-party systems without persisting any data. Inmon argues that virtual ODS architectures are of limited use when the data in the source systems is not integrated. This is due to the fact that virtual ODS systems do not provide ETL transformations at run-time, which would be necessary to provide for data integration. The reason is that ETL transformations are costly and there is, thus, a trade-off between the extent of functionality offered in a virtual ODS and the response times experienced by end-users [1]. The 'ETL'comes from **'Extract, transform, and load'**- the ETL tools were created to improve and facilitate data warehousing.

SAP:

SAP stands for Systeme, Andwendungen, Produkte in der Datenverarbeitung (in German) . SAP, the company was founded in Germany in 1972 by five ex-IBM engineers.

SAP is the leading Enterprise Information and Management package worldwide. Use of this package makes it possible to track and manage, in real-time, sales, production, finance accounting and human resource in an enterprise.

Traditional computer information systems used by many businesses today have been developed to accomplish some specific tasks and provide reports and analysis of events that have already taken place. Examples are accounting general ledger systems. Occasionally some systems operate in "real-time" mode, that is have up to date information in them and can be used to actually control events. A typical company has many separate systems to mange different processes like production, sales and accounting. Each of these systems has its own database and seldom passes information to other systems in a timely manner.

SAP takes a different approach. There is only one information system in an enterprise, SAP. All applications access common data. Real events in the business initiate transactions. Accounting is done automatically by events in sales and production. Sales can see when products can be delivered. Production schedules are driven by sales. The whole system is designed to be real-time and not historical.

SAP structure embodies what are considered the "best business practices" .

SAP BI Accelerator:

SAP's Business Intelligence Accelerator is a product that's all RAM based, and generally geared for multi-hundred-gigabytes data marts. The basic design is a compression-heavy column-based architecture, evolved from SAP's text-indexing technology TREX.

SAP TREX:

When TREX updates an index, it rewrites the majority of the index files. If the indexes are large this process can take a long time and generate a high system load.

TREX allows you activate a *Delta Index* in order to speed up the update. The delta index is a separate index that TREX creates in addition to the main index. The main index and its delta index only differ TREX-internally. Outside TREX they form a unit.

If the delta index is activated changes flow into the delta index. Because, the delta index is smaller than the main index, fewer documents are affected by the update. The delta index can therefore be updated more quickly.

The delta index only speeds up the update if it is kept small. If it becomes too large, it no longer improves performance. When it reaches a certain size you have to integrate it in the main index. You can integrate the delta index manually or configure TREX so that TREX regularly integrates it automatically. TREX creates a new delta index automatically when the integration of the previous delta index is complete.

The integration process involves TREX rewriting all main index files. The duration of the integration process depends on the size of the main index.

The index server cannot index new documents during the integration of the delta index. This has the following effects:

- If indexing takes place with a queue server, the queue server retains the documents until the integration process has been completed. Then the queue server transmits the documents to the index server.
- If indexing takes place without a queue server, the application can continue to send indexing requests to the index server. However, the index server only processes them after the completion of the integration process. This means that it takes longer for indexing requests to be processed and for the application to receive the relevant response [7].

SAP MaxDB

SAP MaxDB is the database management system developed and supported by SAP AG. It has its focus on the requirements of SAP customers and SAP applications and can be used as a less expensive alternative to databases from other vendors for your own or third-party applications as well. It is a competitive database management system for medium to large server configurations and also a convincing offering for a desktop or laptop database management system, as SAP MaxDB is very easy to install and operate.

The key benefits of SAP MaxDB are its many built-in self-administering features. SAP MaxDB is available for the most prominent operating system/hardware platforms Microsoft Windows, Linux, and Unix .
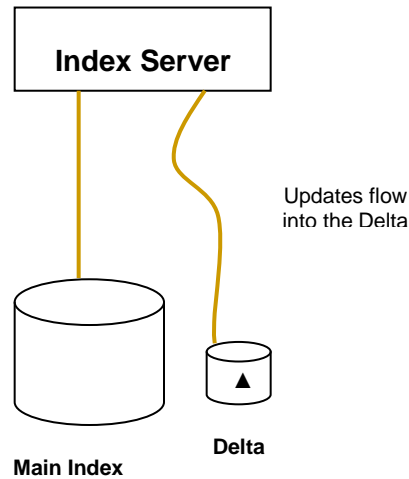
Figure 1: TREX Index Server

SAP Business ByDesign

Business ByDesign is a SAP application software suite. The software is a software-as-a-service (SaaS) product and is remarkable in its overall product breadth.
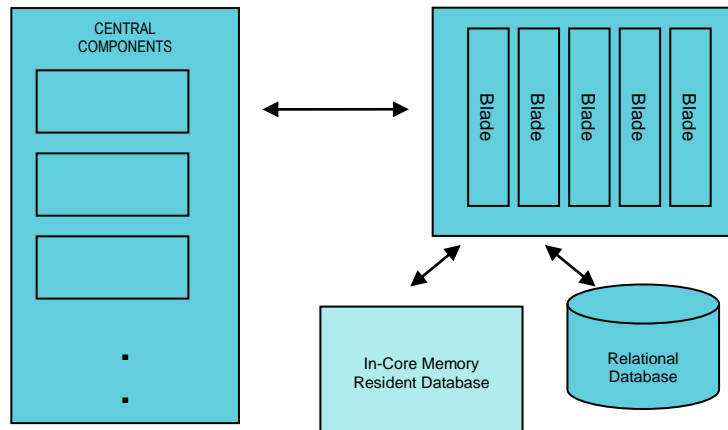
Figure 2: SAP Business ByDesign Technical Architecture

Originally, SAP could support approximately 20 concurrent users per blade. Today, the company believes it can support 150-200 concurrent users/blade.

SAP has created a number of "central components". These are data and processing constants that do not change because of a single customer. Think of these components as containing functionality and tables to support: tax calculations, printing services, knowledge management and more.

Next, SAP has moved customer-specific data to a relational database. This database is stored on a more traditional disk storage device. Alternatively, SAP is also ramping up its use of in-core, memory resident technology .

ARCHITECTURE OF THE HYBRID SYSTEM:
In this architecture for operational reporting no replication into a data warehouse occurs, but data is accessed directly in the transactional system when queried.
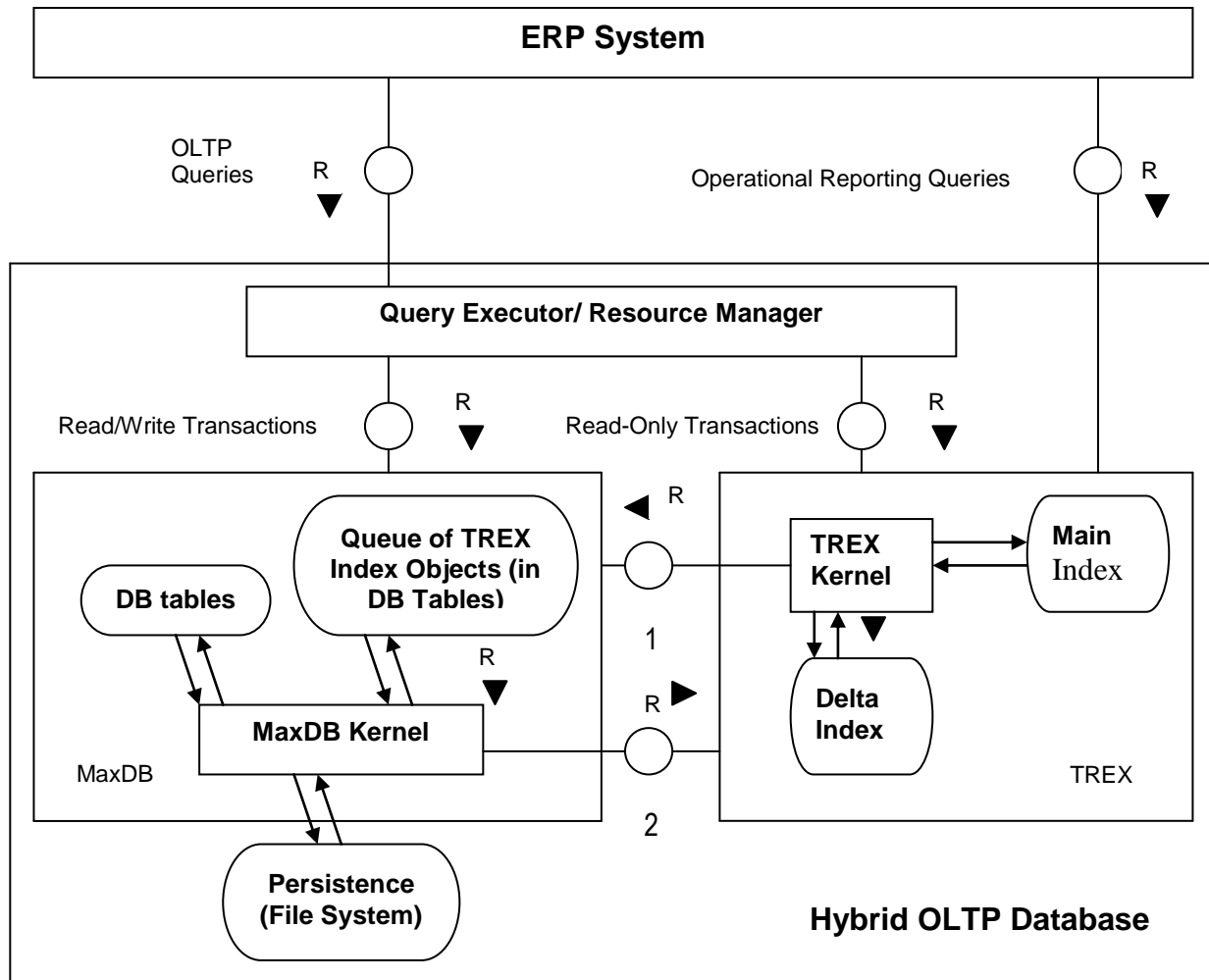
Figure 3: Hybrid Database Architecture

This architecture consists of both a row-oriented database for the entity-oriented OLTP operations (i.e "full-row" queries) and a column-oriented database to handle the operational reporting queries. SAP MaxDB is discussed as the row-oriented database, since it is the database underlying SAP Business ByDesign. It fully supports ACID. As the column-oriented database SAP's Text Retrieval and Information Extraction engine (TREX), which is the engine underlying SAP BIA, is used that answers operational reporting in Business ByDesign. TREX has originally been developed as a text search engine for indexing and fast retrieval of unstructured data. The figure shows how TREX is integrated with MaxDB and how read and write access is distributed between TREX and MaxDB.

Requests that change data or insert new data are handled by MaxDB, which ensures the ACID properties. The MaxDB kernel stores the changes in the database tables and manages so-called "queue tables" for TREX. Those queue tables containing information about data that is relevant for operational reporting and that has been updated or inserted in MaxDB. TREX is notified about the changes and can update its own data with the help of the queue tables. This happens within the same database transaction using on-update and on-insert triggers, which are created inside MaxDB when the system is configured. The triggers fire stored procedures which forward the queries to TREX. Accordingly, TREX and MaxDB share a consistent view of data.

Queries for operational reporting and some read-only transactions go directly to TREX. TREX manages its data in so-called *main indexes*. The main index holds a subset (i.e. the OLTP data that must be available for operational reporting) of the database tables in MaxDB, except that the schema is flattened and the data is stored column-wise. Since the main index is highly optimized for read access, TREX holds a delta index to allow fast retrieval while concurrently updating its data set. All updates and inserts taken from the queue tables are collected in the delta index. When responding to a query, data in the delta index as well as the main index is accessed and the results are merged together in order to provide a consistent view of the entire data set compared with the data base tables of MaxDB. The delta index is not compressed to allow for fast writes, while it must be able to provide a reasonable read performance. In the current implementation delta indexes are organized as a B-tree in memory. It is important that delta indexes do not grow larger than a certain size limit, since the read time from the delta index should not exceed the read times from the main index of a given table (main and delta index are read in parallel). Upon reaching a certain size or pre-defined intervals the delta index is merged with the main index. To do so, a copy of the index is created in memory along with a new, empty delta index for that copied index. The queries coming in during the merge will be run against this structure. In particular, the new delta index that receives all inserts and updates during the merge. After the merge of the original delta index and the main index, the new delta index becomes the delta index for the merged index. The copy of the original main index in memory is now discarded. This procedure for merging a delta index with a main index ensures that neither read nor write accesses to delta index with a main index ensures that neither read nor write accesses to TREX are blocked during merge time.

In the prototypical implementation, MaxDB was extended to serve as the primary persistence for the TREX indexes (i.e. tables), as opposed to using the standard file system persistence of TREX. The reason is that in case of a disaster both MaxDb and TREX can be recovered to a valid state using MaxDB's recovery manager. Therefore, the queue tables in MaxDB also serve as a recovery log for the TREX delta indexes. A possible direction for future research would be to conceptually move the delta index in the column store completely into the row store.

VIRTUAL CUBE:
A virtual cube allows for seamless consumption of operational reports from a data warehouse environment. From a data warehouse perspective the consumption is seamless because the same interface is provided as for a standard cube.

Figure provides a high level view of the target architecture. The analytical engine accesses data through the virtual cube. The virtual cube provides the same interface for analysis as standard cubes in a data warehouse. This includes navigation along various levels of hierarchy (i.e. drill-down and roll-up) as well as slicing and dicing along different dimensions. In the prototypical implementation, a virtual cube that is plugged into the OLAP engine of SAP BI was created. In consequence, all reporting front-ends supported by SAP BI can be used to launch queries against the OLTP data.
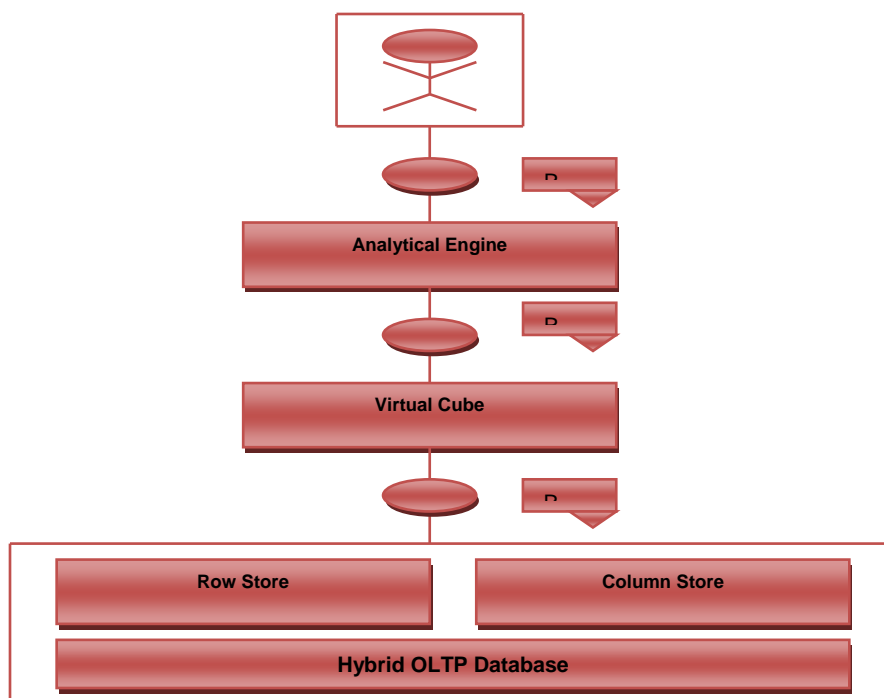
Figure 4: Virtual Cube

In comparison to traditional cubes in a warehouse, the virtual cube does not store any data. Instead, it is a collection of functions that are executed during the run-time of a report. The operational reporting queries from the reporting front-end are sent to the OLAP engine, which then executes OLAP queries against the virtual cube. The latter transforms the incoming queries into queries against TREX.

While the strategy for obtaining the best response times for operational reporting is to push as much as computation as possible down to TREX, predicate filtering on attributes is handled by the OLAP engine of SAP BI in the prototypical implementation. While it would technically be possible to push filtering down to the TREX layer, the result filtering capabilities of OLAP engine are used due to some of the particularities of TREX's query API that would have required to implement a more elaborate query rewriter between the OLAP engine and TREX.

Discussions:

There are many tools, techniques and software available helping in Operational Reporting by generating operational reports and making the real-time information flow across the different departments of an organization. SAP is itself a business suite which helps in this.

The aim of this study was not to identify or compare these tools or software but to identify which database architecture (row or column store) would better suit Operational Reporting. And the study concludes that row-stores or column-stores, if used individually, have their own disadvantages. Further, the study suggests that A Hybrid Row-Column Database Architecture would be needed for Operational Reporting.

References:

http://www.dbms2.com/2006/09/20/saps-bi-accelerator/

http://help.sap.com/saphelp_nw04s/helpdata/en/2a/c4a74046033813e10000000a155106/frameset.htm

http://www.sdn.sap.com/irj/sdn/maxdb?rid=/webcontent/uuid/400cac68-a958-2910-0b9e-a15a67fd4b06

http://blogs.zdnet.com/sommer/?p=735

http://www.information-management.com/issues/20000701/2349-1.html

http://www.rossmorrissey.com/uv

http://www.tagetik.com/resources/glossary/operational-reporting

http://www.vldb.org/conf/2008/workshops/WProc_BIRTE/p7-schaffner.pdf

http://www.onestopsap.com/introduction/1.asp

TENSOR PAIRS FOR FERROTOROIDAL MOMENT

M.Vijaya Laxmi
PhD scholar
Department of Engineering Mathematics
Andhra University, Visakhapatnam

Prof.S.UMA DEVI
Professor
Department of Engineering Mathematics
Andhra University, Visakhapatnam

Abstract:
The form of Physical property tensors invariant under point groups and their Subgroups can determine the basis for the classification of domain pairs in ferroic Crystals. In a ferroic Crystal containing two or more equally stable domains of the same structure but of different spatial orientation, macroscopic tensorial physical properties that are different in domains, determine a tensor distinction of the domains. In this paper, we have calculated the ferrotoroidic tensor pairs, using double Coset decomposition of all 324 ferroic Species, taking 32 grey groups as prototypic point groups.

Key Words: Ferroic point group. Ferrotoroidic, Grey group, Prototypic point group, tensor pairs , toroidal moment.

Introduction:
A Ferroic phase transition is a phase transition of a crystalline structure from a phase of higher point group symmetry G to a phase of lower point group symmetry F. In the lower symmetry phase there are $n = |G| / |F|$, single domain states S1, S2 …… Sn. Where |G| and |F| denote the number of elements in G and F. A ferroic Crystal contains two or more equally stable domains of volumes of the same homogeneous crystalline structure but of the different spatial orientations.

Tensor distinction had been discussed by Aizu [1] subsequently Litvin have extended and evaluated tensor distinction by magnetization, polarization and strain in a ferroic phase transition and also included tenor distinction by toroidal moment. Here ferrotoroidic tensor pairs for all 324 ferroic species by using double coset decomposition are calculated. A crystal, regarded as a thermodynamic system, any physical property can be defined by a relation between two measurable quantities.

A Crystal is an anisotropic medium, means that the response of a Crystal to an external 'force' depends not only on the magnitude of that force but also on its orientation relative to the Crystal axes. Domain states may be distinguished by the values of components of certain spontaneous macroscopic tensorial properties. Ferrotoroidic type with toroidal moment "av" for all 324 ferroic species are calculated, taking grey group as the prototypic point group since "a" have no effect on ordinary 32 point groups. So, we have consider grey groups, Here "V" denotes a polar Vector; "a" denotes zero rank tensors that change sign under time inversion. A magnetic toroidal moment represents a vector like electromagnetic multipole moment which breaks both space and time reversal symmetries simultaneously. Magnetic toroidal moment in solids have increased attention due to its potential relevance in the context of multiferroic materials and magneto electric coupling. The toroidal moment is ideally suited to discuss magneto structural or magneto electric coupling, it has been proposed as the primary order parameter for the low temperature phase transition from a ferroelectric into a simultaneously ferroelectric and ferromagnetic. This means that ferrotoroidicity is the fundamental form of ferroic order, equivalent to ferromagnetism, ferroelectricity, and ferroelasticity. A theoretical analysis of magnetic toroidal moments in periodic system, in the limit the toroidal moments are caused by a time and space reversal symmetry breaking arrangement of localized magnetic dipole moments. The toroidal property is exhibited in the crystals $BaNIF_4$, $LICOPO_4$, $GaFeo_3$, and $BIFeo_3$. All these materials have been discussed in context of multiferroics, magneto-electric coupling or ferrotoidics, by observation of ferrotoroidic domins in this material using nonlinear optical techniques. The material $LICOPO_4$ crystallizes in the oliving structure with in the orthorhombic space group Pnma, it is originally believed that magnetic moments of the four Co ions in the Unit Cell are antiferromagnetically aligned along the orthorhombic direction.

G is one of the 32 Crystallographic point group and 1^1 is a group consisting of identity and time inversion R_2. The direct product of G and 1^1, which is designated by $G1^1$ is known as grey group and 32 point groups in which R_2 does not occur explicitly nor in combination with Symmetry operations are known as ordinary point groups. The 58 groups in which R_2 Occurs implicitly are known as magnetic variants of the 32 ordinary point groups. The 32 ordinary and 58 magnetic Variants are known as magnetic point groups. Shubnikov (1951) discussed point groups are 122, where the ordinary point groups are 32, the grey groups are 32 and the magnetic point groups are 58.

Every time Symmetry point group is a prototypic point group.

Let H be a point group of an orientation state "S" and a subgroup of prototypic point group $G1^1$. Then H is called the ferroic point group. All different ways in which the elements of the ferroic point group correspond to the elements of the Prototypic point groups gives so many possible species and they are denoted by $G1^1$ FH.

Representative Tensor Pairs:

Let G be the prototypic point group of the crystal and H be the ferroic point group of the one of the domains. $H^{(i)}$, i= 1, 2 …q, denote the point groups of each of the domains with $H^{(1)}$ = H. Let T denote a spontaneous physical property tensor which arises in the low symmetry phase of the crystal. Denote by $T^{(i)}$, i = 1,2………q, the specific form of the tensor T characterizing each of the q domains, and denote $T^{(1)}$ = T.

All pairs of tensors having the same mutual relationship can be considered as a single class of tensor pairs and are called a class of crystallographically equivalent tensors pairs (Litvin and Wike, 1989). A single tensor pair, called a representative tensor pair is chosen from each class to represent the mutual relationship between all tensor pairs in that class.

All ordered tensor pairs could be partitioned into classes of crystallographically equivalent tensor pairs. Two tensor pairs $(T^{(i)}, T^{(j)})$ and $(T^{(i1)}, T^{(j1)})$ are said to be crystallographically equivalent with respect to G and to belong to the same class of ordered tensor pairs, if there is an element g of G such that $(T^{(i)}, T^{(j)}) = (gT^{(i1)}, gT^{(j1)})$ that is, if $T^{(i)} = g\ T^{(i1)}$ and $T^{(j)} = g\ T^{(j1)}$.

Let Gτ denote the stabilizer of T in G, this subgroup Gτ of G is the set of all elements g of G which leave T invariant i.e. gT=T. If Gτ =H then T is a full physical property tensor and there are q_T = q distinct forms of the tensor T i.e. each of the few domains is characterized by distinct form of the tensor T. If H is a subgroup Gτ then T is a partial physical property tensor and there are qτ ≤ q distinct forms of the tensor T by $T^a_{(d)}$ a = 1,2,……..qτ and choose $T_d^{(1)} = T^{(1)} = T$.

All ordered distinct tensor pairs $(T_d^{(a)}, T_d^{(b)})$ could be partitioned into classes of crystallographically equivalent ordered distinct tensor pairs in the same manner as $(T^{(i)}, T^{(j)})$. The number of classes ordered distinct tensor pairs is same as the number of classes of tensor pairs (Litvin and Wike 1989).

Let G be the prototypic point group, H is the ferric point group and T is the specific form of the physical property tensor T that keeps H invariant. The number N of crystallographically equivalent ordered distinct tensor pair classes is equal to the number of double cosets in the double coset decomposition of G with respect to $G_τ$.

$G = G_τ E\ G_τ + G_τ g_1 G_τ +……. G_τ g_N G_τ$

Where Gτ is the stabilizer of T in G and g_k , k= 1,2,……N are the double coset representatives . Tables of the coset and double coset decomposition of the 32 cyrstallographic point groups with respect to one of the each set of conjugate sub groups were given by janovee and Dvorakova (1974).

Litvin S.Y and Litvin (1990) have tabulated the representative tensor pairs (T, g_k T) for all classes of tensor pairs for all point groups G and sub groups H and all physical property tensor T of rank 0,1and 2.

Example: Ferrotoroidic tensor pairs for the ferroic species: $4/m1^1F2^1$

Consider the ferroic species $4/m1^1F2^1$, where $4/m1^1$ is prototypic point group and 2^1 is a ferroic point group and the stabilizer Gτ is $2^1/m$. The number of distinct tensor pair classes are 4 .The double coset decomposition of $4/m1^1$ with respect to the stabilizer $2^1/m$ is given by

$G = 4/m1^1 = (2^1/m)\ E\ (2^1/m) + (2^1/m)\ C^+_{4z}\ (2^1/m) + (2^1/m)\ R_2\ (2^1/m) + (2^1/m)\ R_2\ C^+_{4z}\ (2^1/m)$

Since form, $2^1/m$ ferroic point groups, the stabilizer is $2^1/m$ so that decomposition is w.r.t to $2^1/m$ is for these groups

Table 1: ferrotoroidic tensor pairs for ferroic species $4/m1^1\ F\ 2^1$; $4/m1^1\ Fm$; $4/m1^1\ F\ 2^1/m$

S No	Prototypic point group, G	Ferroic Point group, H	Stabilizer	Double coset elements	Tensor Pairs
1	$4/m1^1$	2^1 m $2^1/m$	$2^1/m$	E, C^+_{4z}, R_2, $R_2\ C^+_{4z}$	$(T_1, T_2, O)\ (T_1, T_2, O)$; $(T_1, T_2, O)\ (-T_2, T_1,\ O)$; $(T_1, T_2, O)\ (-T_1, -T_2, O)$; $(T_1, T_2, O)\ (T_2, -T_1,\ O)$

Table 2 gives the list of all the Tensor pair representatives of toroidic physical property tensors. In the below mentioned table 2 the 2nd column represents Prototypic point group "G", 3rd column represents the ferroic point group "H" , 4th column represents the Stabilizer GT, 5th column represents the Double Coset elements and 6th column represents the Tensor Pairs.

Table 2

S No	Prototypic Point Group G	Ferroic Point Group H	Stabilizer $G\tau$	Double Coset elements	Tensor Pairs
1.	1^1	1	1	E , R_2	$(T_1,T_2,T_3)(-T_1,-T_2,-T_s)$; $(T_1,T_2,T_3)(T_1,T_2,T_3)$
2.	$\bar{1}1^1$	1	$\bar{1}^1$	E , R_2	$(T_1,T_2,T_3)(-T_1,-T_2,-T_3);(T_1,T_2,T_3)(T_1,T_2,T_3)$
3.	21^1	1	1	E ,C_{2z}, R_2 , $R_2 C_{2z}$	$(T_1,T_2,T_3)(-T_1,-T_2,T_3);(T_1,T_2,T_3)(-T_1,-T_2,-T_s)$ $(T_1,T_2,T_3)(T_1,T_2,T_3);(T_1,T_2,T_3)(T_1,T_2,-T_3)$
	21^1	2	2	E , R_2	$(0,0,T_3)(0,0,-T_3);(0,0,T_3)(0,0,T_3)$
	21^1	2^1	2^1	E , R_2	$(0,0,T_3)(0,0,-T_3);(0,0,T_3)(0,0,T_3)$
4	$m1^1$	m	m	E,R_2	$(T_1,T_2,T_3)(-T_1,-T_2,-T_3)$
	$m1^1$	m^1	m^1	E,R_2	$(T_1,T_2,T_3)(-T_1,-T_2,-T_3)$
5.	$2/m1^1$	$\dfrac{1}{\bar{1}^1}$	$\bar{1}^1$	E, R_2 ,C_{2z} ,$R_2 C_{2z}$	$(T_1,T_2,T_3)(-T_1,-T_2,-T_3);(T_1,T_2,T_3)$ $(-T_1,-T_2,-T_3)$; (T_1,T_2,T_3) $(-T_1,-T_2,T_3);(T_1,T_2,T_3)$ $(T_1,T_2,-T_3)$
	$2/m1^1$	$\begin{array}{c}2\\m^1\\2/m^1\end{array}$	$2/m^1$	E,R_2	$(T_1,T_2,T_3)(-T_1,-T_2,-T_3)$
	$2/m1^1$	$\begin{array}{c}2^1\\m\\2^1/m\end{array}$	$2^1/m$	E,R_2	$(T_1,T_2,0)(T_1,T_2,0)$;$(T_1,T_2,0)(-T_1,-T_2,0)$
6	2221^1	1	1	$E,C_{2X},C_{2Y},C_{2Z},$ $R_2C_{2X},R_2C_{2Y},$ $R_2C_{2Z},$ R_2	$(T_1,T_2,T_3)(-T_1,-T_2,-T_3);(T_1,T_2,T_3)$ $(-T_1,-T_2,-T_3)$; (T_1,T_2,T_3) $(-T_1,-T_2,T_3);(T_1,T_2,T_3);(-T_1,-T_2,-T_3);$ $(T_1,T_2,T_3);(-T_1,T_2,T_3);(T_1,T_2,T_3);(T_{-1},T_2,T_3);$ $(T_1,T_2,T_3);(T_1,T_2,-T_3);(T_1,T_2,T_3)(T_1,T_2,T_3)$
	2221^1	2^1	2^1	$E,R_2,C2Y,R_2C2Y$	$(T_1,T_2,0)(-T_1,-T_2,0);$ $(T_1,T_2,0)(-T_1,T_2,0);$ $(T_1,T_2,0)(-T_1,-T_2,0);$ $(T_1,T_2,0)(T_1,T_2,0)$
7	$mm21^1$	$\begin{array}{c}2\\mm2\end{array}$	mm2	E,R_2	$(0,0,T_3)(0,0,-T_3);(0,0,T_3)(0,0,T_3)$
	$mm21^1$	m	m	E,C_{2Z} ,R_2,R_2C_{2Z}	$0, T_2,T_3)(0, -T_2,T_3);(0, T_2,T_3)(0, -T_2,-T_3);$ $(0, T_2,T_3)(0, T_2,-T_3);(0, T_2,T_3)(0, T_2,T_3)$
	$mm21^1$	m^1m2^1	m^1m2^1	E,R_2	$(0, T_2,0)(0, -T_2,0);$ $(0, T_2,0)(0, T_2,0)$
8.	$mmm1^1$	$\dfrac{1}{\bar{1}^1}$	$\bar{1}^1$	$E,C_{2X},C_{2Y},C_{2Z},$ $R_2C_{2X},R_2C_{2Y},$ R_2C_{2Z}	$(T_1,T_2,T_3)(T_1,-T_2,-T_3);(T_1,T_2,T_3)(-T_1,T_2,-T_3);$ $(T_1,T_2,T_3)(-T_1,-T_2,T_3);(T_1,T_2,T_3)(-T_1,-T_2,-T_3);$ $(T_1,T_2,T_3)(-T_1,T_2,-T_3);(T_1,T_2,T_3)(T_1,-T_2,T_3);$ $(T_1,T_2,T_3)(T_1,T_2,-T_3)$
	$mmm1^1$	$\begin{array}{c}2\\m^1\\2/m^1\\2^12^12\\mm2\\mmm^1\end{array}$	mmm^1	E,R_2	$(0,0,T_3)(0,0,T_3)$;$(0,0,T_3)(0,0,-T_3)$
	$mmm1^1$	$\begin{array}{c}2^1\\m\end{array}$			$(T_1,T_2,0)(T_1,T_2,0)$;$(T_1,T_2,0)(-T_1,-T_2,0)$

	$2^1/m$ m^1m2^1	m^1m2^1		E,R_2	
9.	41^1	1	1	E,C^+_{4z}, C^-_{4z}, C_{2Z} R_2 $R_2C^+_{4z}$, $R_2C^-_{4z}$ R_2C_{2Z}	$(T_1,T_2,T_3)(-T_2,T_1,T_3);(T_1,T_2,T_3)(T_2,-T_1,T_3);$ $(T_1,T_2,T_3)(-T_2,-T_1,T_3);(T_1,T_2,T_3)(-T_2,T_1,-T_3);$ $(T_1,T_2,T_3)(T_2,-T_1,-T_3);(T_1,T_2,T_3)(-T_2,T_1,-T_3);$ $(T_1,T_2,T_3)(T_1,T_2,-T_3);(T_1,T_2,T_3)(T_1,T_2,T_3);$
	41^1	$\dfrac{2}{4}$	4	E,R_2	$(0,0,T_3)(0,0,T_3);$ $(0,0,T_3)(0,0,-T_3)$
	41^1	2^1	2^1	E,R_2,C^+_{4z}, $R_2C^+_{4z}$	$(T_1,T_2,0)(-T_1,-T_2,0);$ $(T_1,T_2,0)(-T_2,T_1,0);$ $(T_1,T_2,0)(T_2,-T_1,0);$ $(T_1,T_2,0)(T_1,T_2,0)$
10.	$\overline{4}1^1$	1	1	E,S^-_{4Z}, S^+_{4Z}, C_{2Z} ,R_2, $R_2S^-_{4Z}$, $R_2S^+_{4Z}$, R_2C_{2Z}	$(T_1,T_2,T_3)(T_1,T_2,T_3);$ $(T_1,T_2,T_3)(T_2,-T_1,-T_3);(T_1,T_2,T_3)(-T_2,T_1,-T_3);$ $(T_1,T_2,T_3)(-T_1,-T_2,T_3);(T_1,T_2,T_3)(-T_1,-T_2,-T_3);$ $(T_1,T_2,T_3)(-T_2,T_1,T_3);(T_1,T_2,T_3)(T_2,-T_1,T_3);$ $(T_1,T_2,T_3)(T_1,T_2,-T_3)$
	$\overline{4}1^1$	$\overline{\dfrac{2}{4^1}}$	$\overline{4}^1$	E,R_2	$(0,0,T_3)(0,0,T_3);$ $(0,0,T_3)(0,0,-T_3)$
	$\overline{4}1^1$	2^1	2^1	$E,S^+_{4Z},R_2, R_2S^+_{4Z}$	$(T_1,T_2,0)(T_1,T_2,0);$ $(T_1,T_2,0)(-T_2,T_1,0);$ $(T_1,T_2,0)(-T_1,-T_2,0);$ $(T_1,T_2,0)(T_2,-T_1,0)$
11.	$4/m1^1$	$\overline{\dfrac{1}{1^1}}$	$\overline{1}^1$	E, C^-_{4Z}, C_{4Z} C_{2Z} R_2, R_2 C^+_{4Z}, R_2 C^-_{4Z}, R_2 C_{2Z}	$(T_1,T_2,T_3)(-T_1,-T_2,-T_3); (T_1,T_2,T_3)(-T_2,T_1,T_3);$ $(T_1,T_2,T_3)(T_2,-T_1,-T_3);(T_1,T_2,T_3) (T_1,T_2,T_3);$ $(T_1,T_2,T_3)(T_2,-T_1,T_3);(T_1,T_2,T_3)(-T_2,T_1,-T_3);$ $(T_1,T_2,T_3)(T_1,T_2,-T_3), (T_1,T_2,T_3)(-T_1,-T_2,T_3)$
	$4/m1^1$	2 m^1 $2/m^1$ 4 $\overline{4}^1$ $4/m^1$	$4/m^1$	E,R_2	$(T_1,T_2,T_3)(T_1,T_2,T_3);(T_1,T_2,T_3)(-T_1,-T_2,-T_3)$
c.	$4/m1^1$	2^1 m $2^1/m$	$2^1/m$	E, C^+_{4z}, R_2, $R_2C^+_{4z}$	$(T_1,T_2,0)(-T_2,T_1,0); (T_1,T_2,0)(T_2,-T_1,0);$ $(T_1,T_2,0)(-T_1,-T_2,0); (T_1,T_2,0)(T_1,T_2,0);$
12.	4221^1	1	1	E, C^+_{4z}, C^-_{4z}, C_{2Z}, C_{2x}, C_{2y}, C_{2a}, C_{2b}, R_2, $R_2 C^+_{4Z}$, $R_2 C^-_{4Z}$, $R_2 C_{2Z}$, $R_2 C_{2x}$, $R_2 C_{2y}$,$R_2 C_{2a}$,$R_2 C_{2b}$	$(T_1,T_2,T_3)(T_1,T_2,T_3)$ $(T_1,T_2,T_3)(-T_2,T_1,T_3) ; (T_1,T_2,T_3)(T_2,-T_1,T_3) ;$ $(T_1,T_2,T_3)(-T_1,-T_2,-T_3);(T_1,T_2,T_3)(T_1,-T_2,-T_3);$ $(T_1,T_2,T_3)(-T_1,T_2,-T_3);(T_1,T_2,T_3)(T_2,T_1,-T_3) ;$ $(T_1,T_2,T_3)(-T_2,-T_1,-T_3);(T_1,T_2,T_3)(T_2,-T_1,-T_3);$ $(T_1,T_2,T_3)(-T_2,T_1,-T_3);(T_1,T_2,T_3)(T_2-T_1,-T_3);$ $(T_1,T_2,T_3)(-T_1,T_2,T_3);(T_1,T_2,T_3)(T_1,-T_2,T_3);$ $(T_1,T_2,T_3)(-T_2,-T_1,T_3);(T_1,T_2,T_3)(T_2,T_1,T_3)$
	4221^1	2 $2^12^1 2$ 4 42^12^1	42^12^1	E,R_2	$(T_1,T_2,T_3)(T_1,T_2,T_3) ;(T_1,T_2,T_3)(-T_1,-T_2,-T_3)$
	4221^1	2^1	2^1	E, C^+_{4z} ,c_{2x},c_{2a},R_2, $R_2C^+_{4z}$, $R_2 c_{2x}$, $R_2 c_{2a}$	$(T_1,T_2,0) (T_1,T_2,0);$ $(T_1,T_2,0)(-T_2,T_1,0); (T_1,T_2,0)(T_1,-T_2,0);$ $(T_1,T_2,0)(T_2,T_1,0); (T_1,T_2,0)(-T_1,-T_2,0);$ $(T_1,T_2,0)(T_2,-T_1,0); (T_1,T_2,0)(-T_1,T_2,0);$ $(T_1,T_2,0)(-T_2,T_1,0)$

13	$4mm1^1$	2 mm2 4 4mm	4mm	E, R_2	$(0,0,T_3)$ $(0,0,T_3)$;$(0,0,T_3)(0,0,-T_3)$
	$4mm1^1$	2^1	2^1	$E, C^+_{4z}, R_{2,} R_2$ $C^+_{4z}, R2, \sum_x,$ $R_2, \sum_{da.}$	$(T_1,T_2,0)(-T_2, T_1,0); (T_1,T_2,0)(T_2, -T_1,0);$ $(T_1,T_2,0)(-T_1,-T_2,0); (T_1,T_2,0)(T_1,T_2,0);$ $(T_1,T_2,0)(T_1,T_2,0)(-T_2, T_1,0)$
	$4mmm1^1$	m (x)	m	$E, C^+_{4z}, C^-_{4z}, C^-_{2z},$ $R_{2,} R_2 C^+_{4z,} R_2 C^-_{4z,} R_2 C_{2z,}$	$(0, T_2,T_3)(-T_2,0, T_3);(0, T_2,T_3)(T_2,0, T_3);$ $(0, T_2,T_3)(0, T_2,-T_3);(0, T_2,T_3)(0, -T_2,T_3);$ $(0, T_2,T_3)(T_2,0, -T_3);(0, T_2,T_3)(-T_2,0, -T_3);$ $(0, T_2,T_3)(0, T_2, T_3);(0, T_2,T_3)(0, -T_2, -T_3);$
	$4mm1^1$	$m^1 m 2^1$	$m^1 m2^1$	$E, C^+_{4z}, R_{2,} R_2$ $C^+_{4z,}$	$(0, T_2,0)(, -T_2,0, 0); (0, T_2,0)(T_2,0, 0);$ $(0, T_2,0) (0, T_2, 0); (0, T_2,0) (0, -T_2,0)$
14	$\bar{4}2m1^1$	2(P) m $2^12^12(p)$ mm2 $\bar{4}^1$ $\bar{4}^12^1m$	$\bar{4}^12^1m$	E, R_2	$(0,0,T_3)(0,0,T_3);(0,0,T_3)(0,0,-T_3)$
	$\bar{4}2m1^1$	2(s)	2	$E, C_{2z} ,s^+_{4z},R_2,$ $R_2C_{2z,} R_2 s^+_{4z,}$	$(T_1,0,0,) (-T_1,0,0); (T_1,0,0,) (0,T_1,0);$ $(T_1,0,0,) (T_1,0,0); (T_1,0,0,) (0,-T_1,0);$
	$\bar{4}2m1^1$	$2^1(s)$	2^1	$E, C_{2z} ,s^+_{4z},R_2,$ $R_2C_{2z,} R_2 s_{4z,}$	$(T_1,0,0,) (-T_1,0,0); (T_1,0,0,) (0,T_1,0);$ $(T_1,0,0,) (T_1,0,0); (T_1,0,0,) (0,-T_1,0);$ $(0, T_2,T_3)(0, T_2,T_3);(0, T_2,T_3)(0, -T_2,T_3);$ $(0, T_2,T_3)(-T_2,0,-T_3);(0, T_2,T_3)(0, -T_2, -T_3);$ $(0, T_2,T_3)(0, T_2,-T_3);(0, T_2,T_3)(T_2,0, -T_3)$
15.	$4/mmm1^1$	1 $\bar{1}^1$	$\bar{1}^1$	$E, C^+_{4z}, C^-_{4z}, C_{2z},$ $C_{2x} ,C_{2y} , C_{2a} ,$ $C_{2b} ,R_2,$ $R_2 C^+_{4z,} R_2 C^-_{4z,}$ $R_2 C_{2z,} R_2C_{2x}$ $,R_2C_{2y} , R_2C_{2a} ,$ R_2C_{2b}	$(T_1,T_2,T_3)(T_1,T_2,T_3);$ $(T_1,T_2,T_3)(-T_2,T_1,T_3);(T_1,T_2,T_3)(T_2,-T_1,T_3);$ $(T_1,T_2,-T_3)(-T_1,-T_2,T_3);(T_1,T_2,T_3)(T_2,T_1,-T_3);$ $(T_1,T_2,T_3)(-T_2,-T_1,-T_3);(T_1,T_2,T_3)(-T_1,-T_2,-T_3);$ $(T_1,T_2,T_3)(T_2,-T_1,-T_3);(T_1,T_2,T_3)(-T_2,T_1,T_3);$ $(T_1,T_2,T_3)(T_1,T_2,-T_3);(T_1,T_2,T_3)(-T_2,-T_1,T_3);$ $(T_1,T_2,T_3)(T_2,T_1,T_3);(T_1,T_2,T_3)(T_1,-T_2,-T_3);$ $(T_1,T_2,T_3)(-T_1,T_2,T_3);(T_1,T_2,T_3)(-T_1,T_2,-T_3);$ $(T_1,T_2,T_3)(T_1,-T_2,T_3)$
	$4/mmm1^1$	42^12^1 4mm $\bar{4}2^1m$ $4/m^1mm$ $\bar{4}$ $4/m^1$ 2(p) $m^1(p)$ $2/m^1(p)$ $2^12^1 2(p)$ $2^12^1 2(s)$ mm2(p) $m^1m2^1(ps)$ 4 $mmm^1(p)$	$4/m^1mm$	E, R_2	$(0,0,T_3)(0,0,T_3)$;$(0,0,T_3)(0,0,-T_3)$

16.	31^1	1	1	E, C^+_3, C^-_3 $R_2 c^+_3$, $R_2 c^-_3$	$(T_1,T_2,T_3)(T_1,T_2,T_3);(T_1,T_2,T_3)(-T_2,T_1,-T_2,T_3);$ $(T_1,T_2,T_3)(-T_1,+T_2,-T_1,T_3);(T_1,T_2,T_3)(-T_1,-T_2,-T_3)$ $(T_1,T_2,T_3)(T_2,-T_1,+T_2,-T_3);$ $(T_1,T_2,T_3)(T_1,-T_2,+T_1,-T_3)$
	31^1	3	3	E,R_2	$(0,0,T_3)(0,0,-T_3);(0,0,T_3)(0,0,T_3)$
17.	$\overline{3}1^1$	$\frac{1}{1^1}$	$\overline{1}^1$	E,$R_{2,}$ c^+_3, c^-_3, R_2 c^+_3, $R_2 c^-_3$	$(T_1,T_2,T_3)(-T_2,T_1,-T_2,T_3);$ $(T_1,T_2,T_3)(-T_1,+T_2,-T_1,T_3);$ $(T_1,T_2,T_3)(T_1,T_2,T_3);(T_1,T_2,T_3)(T_2,-T_1,+T_2,-T_3);$ $(T_1,T_2,T_3)(T_1,-T_2,T_1,-T_3)$
	$\overline{3}1^1$	3 $\overline{3}^1$	$\overline{3}^1$	E,R_2	$(0,0,T_3)(0,0,T_3);(0,0,T_3)(0,0,-T_3)$
18	321^1	2	2	E,C^+_3,R_2, $R_2 C^+_3$	$(0, T_2 ,0,)(-T_2,-T_2,-0);(0, -T_2 ,0)(T_2,T_2,-0);$ $(0, T_2 ,0,)(0, T_2 ,0,);(0, T_2 ,0,)(0, -T_2 ,0,)$
	321^1	2^1 3 32^1	32^1	E,R_2	$(0,0,T_3)(0,0,T_3);(0,0,T_3)(0,0,-T_3)$
19	$3m1^1$	m	m	E,C^+_3,R_2, $R_2 C^+_3$	$(\frac{(T_1+T_2)}{2},0,T_3),(0,\frac{(T_1+T_2)}{2},T_3);$ $(\frac{(T_1+T_2)}{2},0,T_3),(\frac{-(T_1+T_2)}{2},0,-T_3);$ $(\frac{(T_1+T_2)}{2},0,T_3),(0,-\frac{(T_1+T_2)}{2},T_3)$ $(\frac{(T_1+T_2)}{2},0,T_3),(\frac{(T_1+T_2)}{2},0,T_3)$
	$3m1^1$	m^1	m^1	E,C^+_3,R_2, $R_2 C^+_3$	$(0, T_2 ,0,)(-T_2,-T_2,-0);(0, T_2 ,0)(0,-T_2,-0);$ $(0, T_2 ,0,)(T_2, T_2 ,0,);(0, T_2 ,0,)(0, T_2 ,0,)$
	$3m1^1$	3 3m	3m	E,R_2	$(0,0,T_3)(0,0,-T_3);(0,0,T_3)(0,0,T_3)$
20	$\overline{3}m1^1$	2 m^1 $2/m^1$	$2/m^1$	E,C^+_3,R_2, $R_2 C^+_3$	$(T_1,T_2,0)(T_2, T_2,0);$ $(T_1,T_2,0)(-T_2, -T_2,0);$ $(T_1,T_2,0)(-T_1, -T_2,0);$ $(T_1,T_2,0)(T_2, T_2,0)$

Similarly, ferrotoroidic tensor pairs for all 324 ferrotoroidic Ferroic species are calculated using the above procedure, here tensor pairs for 108 ferroic spices are given table 2 and rest of the tables are available with the authors.

3. Conclusions:
D.B. Litvin has calculated tensor distinction of domains in ferroic crystals in this paper the ferrotoroidic tensor pairs are calculated using double coset decompastion for all the 324 ferrotoroidic ferroic species,where 32 grey groups are the prototypic point groups.

References:
1.   Aizu, k. 1970.phys. Review P.754.
2.   Aizu, k. 1974.J phys.Japan, 36, P.1273.

3. Arthur.S.Nowick, crystal properties via group theory.
4. Bhagavantam.S(1966) "Crystal symmetry and physical properties" academic press London.
5. Bradly C.J and Cracknels A.P 1972
6. D.B. LITVIN act a. Crst., A64:316-320(2008)
7. D.B. LITVIN Ferri electrics, 376. 158-167 (2008)
8. D.B. LITVIN Eue.phys.J.B71, 315-320(2009)
9. D.B. LITVIN,Phase Transitions, Vol 84. 804-809(2011)
10. Janovec.V Czech phys.J.B22, p.974,1972
11. Janovec.V and D.B. LITVIN act a. Crst., A62:98-102,2006
12. Janovec, Group analysis of domains and domain pairs phys.J.22, 974-994(1972)
13. Nye,J.F Physical properties of crystals
14. Wooster W.A "tensor and group theory for the physical property tensors of crystals"
    Clearendon press 1973.

Seasonal Variation Of Ground Water Quality And Its Suitability For Drinking In And Around Tiptur Town, Tumkur District, Karnataka, India: A WQI Approach.

S.B.Basavaraddi[1], Heena Kousar[2], E.T .Puttaiah [3]

[1]Departmentof Environmental Science, Kuvempu University. Shankargatta-577451 Karnataka India
[2]Departmentof Environmental Science, Kuvempu University. Shankargatta-577451 Karnataka
[3] Vice Chancellor Gulbarga University. Gulbarga, Karnataka
Mob: 9916704280

Abstract

A water quality index provides a single number that expresses over all water quality at certain location and time based on several water quality parameters. The objective of an index is to turn complex quality data in to information that is understandable and useable by the public. Seven most important physico- chemical parameters such as PH, Total dissolved solids Total hardness, Calcium, Magnesium, Chloride and Nitrate were taken for the calculation of WQI of ground water to assess the impact of pollutants due over exploitation, Domestic sewage, mining operation, agriculture ,human activities on ground water quality. The water quality index values for the ground water ranged between 83.9-138.5 during pre monsoon and 67.91 -130.5 during Post monsoon season. In the present investigation the quality of water was found to be good in all the sampling locations in tiptur town and surrounding areas.

Key words: Water quality index, physicochemical parameters, Human activities, complex quality data, Public.

1. Introduction

Water is indispensable and one the precious natural resource of our planet. Ground water is an important natural source of water supply all over the world. Its use in irrigation ,industries and domestic usage continues to increase where perennial surface water source are absent (Mariappan et al 2005). The modern civilization, over exploitation, rapid industrialization and increased population have lead to fast degradation of our environment(K .Murali; 2011). To meet the rising demand it is imperative to recognize the fresh water resources and also to find out remedial methods for improvement of water quality (Ch Maruthi Devi et al ;2011).The quality of water may depend on geology of particular area and also vary with depth of water table and seasonal changes and is governed by the extent and composition of the dissolved salts depending upon source of the salt and soil , subsurface environment.

The development of growing regions in developing countries is allied several social, economical ,environmental and technical aspect of concern area along

with the study of available, sustainable resources for civilization. Among all; Ground water is the one of the vital resources confined everlasting. In the context of quality and quantity ; ground water fluctuates in variably in its own which reflects the time to time status of ground water as a whole for the region (Neeraj D et al ;2010).

A number of indices have been developed to summarize water quality data in an easily expressed under the stood format .The WQI which was first developed by Horton in the early 1970s is basically a mathematical; Means Of Calculating a Single value from multiple test results .The Index results represents the levels of water quality in a given water aquifers and lakes, river or stream. After Horton a number of workers all over the world developed WQI based on rating of different water quality parameters. Basically a WQI attempt to provide a mechanism for presenting water accumulatively derived. Numerical expression defining a certain level of water quality (Miller et al ;1986). The different analyzing water data based on rank of observations and factor analysis (Shoji et al ;1966,Harkin;1974).For the evaluation of water quality; WQI was applied to river water as well as coastal (Dojlido et al ,1994, Gupta et al 2003 and Avvannavar and shrihari,2007)

A water quality index is a means to summarize large amounts of water quality data into simple terms (eg good, excellent, moderate,, poor) for reporting to management and public in a consistent manner (Aswani Kumar et al ;2009).The objective of the present study is to investigate the water quality of ground water in and surrounding areas of tiptur town ,tumkur district ,Karnataka,India. The index produces a number between 0 for worst water quality and 100 for best water quality (saffron et al ,2001).

2. Study Area

Karnataka state is situated in the southern peninsular India. Tiptur town is about 75km from Tumkur district. It covers an area of 785 sq km having 13°, 16' north latitude 76°, 29' east longitude and an altitude of 850.30 meter above

the sea level. The average temperature ranges from 11°in winter and 38° during summer. The average rain fall of Tiptur town is 503 mm.

TIPTUR TALUK
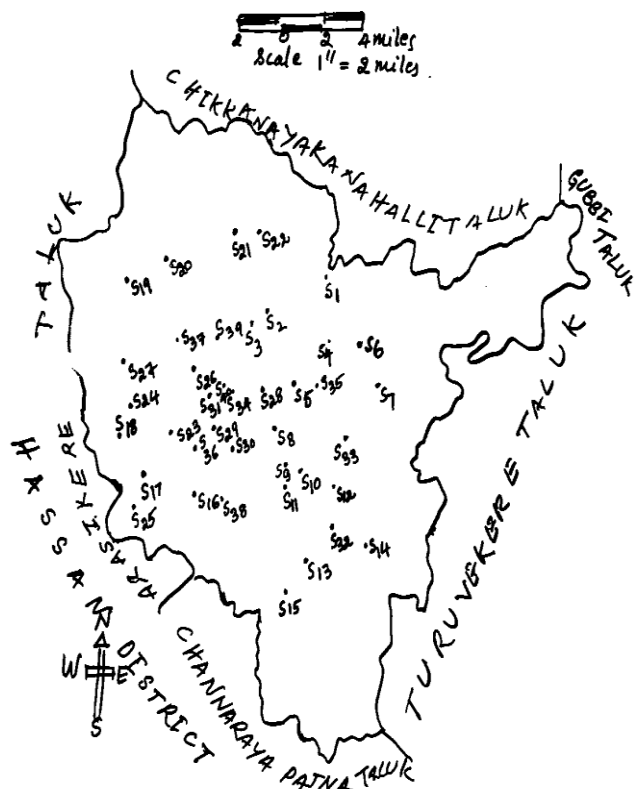
3. Material and Methods

Water samples were collected once every month from 50 locations in and around tiptur town during Pre monsoon and post monsoon. A WQI was calculated for Average values of the parameter in both seasons.

3.1. Analytical Methods

The parameters like Temperature, PH, total dissolved solids, were noted immediately at the spot using water analyzer kit (Global make). In the laboratory, the other parameters like, Total hardness, chloride, calcium ,Magnesium and Nitrate ion was done by volumetric analysis using standard methods given in APHA (1998) ,Eaton et al (1998) and Trivedy and Goel 1986).

Water quality index was calculated for average values of parameters for pre monsoon and post monsoon. It was done considering important physico-chemical properties using central public Health Environmental engineering organization (CPHEEO) 1991 and Indian council of medical research (ICMR,1975),BIS and IS10500 standards

WQI was obtained by weight arithmetic index method as given below.

Water quality index $(QWI) = q_i w_i$

Where q_i is water quality rating .

$q_i = (Va- Vi) /(Vs- Vi) *100$

Va- Actual value of the parameter present in water sample.

Vi -ideal value.

Vs-Standard value

$Wi = K/Sn$ where Wi = unit weight.

K(constant) = $1 / 1/Vs_1 + 1/Vs_2 + 1/Vs_3 + ------(1/Vsn)$.

Where **Sn** –standard value.

4. Result and discussion

The results of study are given in the table (1) and (2) . PH of water is influenced by geology of the area, buffering capacity of water (Achutha Nair et al ; 2005). If the water has PH less < 7 may cause tuberculation and corrosion ,while higher the values may produce in crustation, sediment deposit and difficulties in chlorination for disinfection of water .(Ch .Marthi Devi et al 2011). In the present study PH in all the sampling locations varied between 6.63 to 7.73 during pre monsoon and 7.02 to 8 during post monsoon. The permissible limit of PH value of drinking water specified as 6.5 to 8.5 as per IS 10500 standards and the values were acceptable.

TDS is an important parameter for drinking water and other uses. Water with high solid content is of inferior palatability and may produce unfavorable physiological reaction in the transient consumer (Abudul Jameel; 2002). In the study TDS was found in range of 213 to1427 mg/L during pre monsoon and 310 to 1670 mg/ L (Tadasur, S16)during post monsoon. The permissible level of TDS is specified as 500 to 1500 mg/L as per WHO /ICMR standard.

Total hardness varied between 100 mg/L to 1180mg/L in pre monsoon and 280 mg/L to 720 mg/L in post monsoon .Total hardness of water is characterized by content of calcium and magnesium salts. Calcium was 8 mg/L to 153 mg/L in pre monsoon season compared to post monsoon 24 mg/L and 128mg/L specially (S23) other wise in the most of the sampling locations calcium and Magnesium concentration are well with in the ICMR /BIS standard.

Chloride concentration in all the sampling locations ranged between 52mg/l 330 mg/L and except for sampling locations S23 ,340mg/L and S25 , 400mg/L in pre monsoon and 50mg/L to 250 mg/L in the post monsoon ,were with in the WHO limits. Chloride concentration imparts salty taste and higher value produces laxative effect on consumers

Nitrate varied between 4mg/L to 56mg/during pre monsoon season and 10 mg/L 72 mg/L. Nitrate was found more than 45mg/L in 20% of sampling locations. But as per BIS standards. Regular consumption of nitrate >45mg/L may cause Blue baby disease or Methaemoglobinaemia in infants.(K. Murali et al ; 2011).

Water quality index (WQI) is one of meaningful approach for ground water and all other type of water like river, lake and surface water quality analysis (Eaton A.D ,Clescer and Green beg A E , 1998). The value of WQI in all sampling locations was reported to approach 100 and some

samples > 100, indicating that the water suitable for human use.

On the basis of the WQI the quality of water is categorized from very Bad to Excellent (Tiwari and Mishra, 1985) table-3. According to water quality index (WQI). The water in all sampling locations range between good and excellent category in tiptur town and surrounding areas. Hence the ground water in and around tiptur town is suitable for pot ability as well as irrigation purpose.

Physico –chemical Parameters Pre monsoon season in and around tiptur town.Table-1

	Smapling Stations	PH	TDS	TH	Ca+2	Mg+2	Cl-	No3	WQI
S1	Eralagre	7.48	622	240	39	34.6	160	10	89.42
S2	Chikkmarppanahalli	7.14	720	175	74	2.37	220	20	85.74
S3	Doddamarppanahalli	6.98	213	310	8	70.4	52	10	87.25
S4	Ramenahalli	6.96	780	315	83	26.1	305	29	92.54
S5	Huchgondnahalli	7.35	620	285	51	38.2	165	4	88.55
S6	Karadi	7.12	680	205	68	8.54	270	26	88.03
S7	Kuppalu	6.24	640	195	57	12.79	180	49	83.91
S8	Gorgondanahalli	6.88	1387	222	92	1.87	440	48	94.42
S9	Hedagarahalli	6.8	914	100	69	17.5	187	21	85.09
S10	Bedagarahalli	6.89	994	502	90	67.3	305	56	107.69
S11	Aldahalli	7.12	534	530	53	96.5	156	5	98.24
S12	Kannugatta	7.02	447	400	27	80.7	125	55	103.2
S13	Sugur	7.01	400	390	23	80.7	94	24	95.03
S14	Kodihalli	6.98	1020	270	91	10.3	240	31	90.72
S15	Machegatta	7.12	340	570	13	130.5	76	10	101.66
S16	Tadasur	6.8	1367	660	108	94.7	330	27	107.95
S17	Gurgadahalli	7.06	600	350	49	55.2	174	15	91.60
S18	Siddapura	7.1	260	310	11	68.6	78	10	88.64
S19	Honnavalli	6.63	960	510	99	63.8	260	25	97.39
S20	Potarihalli	6.82	594	260	50	32.8	100	15	84.20
S21	Byrapura	7.05	600	500	24	106.8	125	37	104.53
S22	Halenahalli	6.92	894	770	32	167.5	225	16	112.56
S23	Madenoor	6.8	1367	1180	131	207.1	340	51	138.54
S24	Bidaregudi	7.12	480	480	19	105	115	19	99.79
S25	Shivara	6.98	1427	750	153	89.3	400	46	117.95
S26	Manakikere	7.06	847	335	44	54.6	185	47	99.25
S27	Nagatihalli	6.99	813	670	56	128.7	195	50	115.35
S28	Idenahalli	6.99	574	415	35	79.5	183	34	99.11
S29	Marangere	6.9	633	390	56	60.7	171	27	94.68
S30	Anagondanahalli	7.1	527	560	29	118.4	114	24	104.4
S31	Madihalli	7.68	528	630	22	139.6	99	24	113.76
S32	Nagaragatta	7.11	600	625	27	135.4	170	3	103.38
S33	Echoor	6.9	867	600	64	106.8	205	47	110.23
S34	Kanchegatta	7.45	586	400	47	68.6	127	25	99.98
S35	Kotanayakanahalli	7.28	567	485	42	92.3	172	14	100.31
S36	Lingadahalli	7.3	687	510	45	96.5	152	30	105.54
S37	Gudigondanahalli	7.12	467	490	24	104.4	155	46	106.87
S38	Rangapura	7	673	750	43	156	100	15	110.39
S39	Sarathavalli	7.35	360	305	18	63.1	85	25	94.48
S40	Kobredoddayyanna Palya	7.46	586	550	33	113.5	110	10	104.16
S41	Gandhi Nagar	7.73	380	260	13	55.25	75	12	93.050
S42	Chamundeshwari	6.93	740	600	39	122	151	28	106.10

	Badavane								
S43	Sharada Nagar	7.28	514	610	30	129.9	110	15	106.47
S44	Vidya Nagar	7.32	567	370	15	80.7	115	24	97.86
S45	H.B.Colony	6.9	620	495	36	98.4	120	28	100.29
S46	Govina Pura	7.3	1173	1000	32	223.4	151	10	126.14
S47	Shankarappa Layout	7.14	994	970	20	223.4	273	12	124.54
S48	Manjunatha Nagar	7.66	414	400	18	86.2	73	5	97.43
S49	Vinayaka Nagar	6.86	1014	920	30	205.2	265	10	118.50
S50	Kote	7	893	460	32	92.3	235	14	97.75

Physico -chemical Parameters   post monsoon season in and around tiptur town. Table 2

	Smapling Stations	PH	TDS	TH	Ca+2	Mg+2	Cl	No3	WQI
S1	Eralagre	7.67	770	290	32	51	110	20	96.27
S2	Chikkmarppanahalli	7.24	950	300	24	58	100	50	100.15
S3	Doddamarppanahalli	7.82	690	300	26	57	130	20	98.42
S4	Ramenahalli	7.28	1250	310	32	56	170	48	101.52
S5	Huchgondnahalli	7.72	470	400	34	51	60	10	93.78
S6	Karadi	7.84	350	300	35	60	100	20	67.9
S7	Kuppalu	7.06	1090	310	24	76	200	58	77.6
S8	Gorgondanahalli	7.42	1410	600	64	107	240	20	104.85
S9	Hedagarahalli	7.26	900	350	48	56	90	25	110.2
S10	Bedagarahalli	7.39	1190	350	32	65	230	60	95.97
S11	Aldahalli	8	280	400	32	77.7	60	20	107.65
S12	Kannugatta	7.71	240	340	30	64	70	10	103.59
S13	Sugur	7.85	550	590	40	119	110	50	95.37
S14	Kodihalli	7.3	950	400	57	62	50	20	119.27
S15	Machegatta	7.14	310	490	56	85	70	10	96.99
S16	Tadasur	7.3	1670	700	80	121	290	52	96.48
S17	Gurgadahalli	7.39	650	500	80	73	160	20	121.9
S18	Siddapura	7.7	500	280	56	34	100	42	102.4
S19	Honnavalli	7.02	1000	520	88	73	200	35	99.98
S20	Potarihalli	7.2	720	360	32	68	95	15	102.37
S21	Byrapura	7.2	510	600	40	121	110	45	93.64
S22	Halenahalli	7.25	970	580	51	110	200	15	111.9
S23	Madenoor	7.08	1320	500	96	63	220	52	105.63
S24	Bidaregudi	7.61	490	700	29	152	80	25	108.26
S25	Shivara	7.18	1390	400	56	63	110	52	116.22
S26	Manakikere	7.3	1260	500	64	57	90	42	104.89
S27	Nagatihalli	7.29	490	560	32	116	120	45	103
S28	Idenahalli	7.3	770	400	66	57	180	20	111.16
S29	Marangere	7.3	1050	500	32	102	100	25	97.46

S30	Anagondanahalli	7.49	590	560	32	116	80	15	104.57
S31	Madihalli	7.87	520	540	40	107	70	10	105.84
S32	Nagaragatta	7.4	240	620	8	146	100	35	107.09
S33	Echoor	7.49	500	610	40	124	140	42	113.08
S34	Kanchegatta	7.6	710	500	88	68	160	20	114.93
S35	Kotanayakanahall	7.51	1000	490	80	70	170	45	104.38
S36	Lingadahalli	7.54	710	500	35.2	100	95	25	109.79
S37	Gudigondanahalli	7.3	600	460	40	87	120	40	106.13
S38	Rangapura	7.14	910	630	40	129	70	10	105.14
S39	Sarathavalli	7.55	500	450	56	75	90	20	105.07
S40	Kobredoddayyan na Palya	7.37	670	650	44	131	80	20	*101.43*
S41	Gandhi Nagar	7.87	1440	600	32	126	150	45	110.12
S42	Chamundeshwari Badavane	7.39	1340	600	34	125	200	58	120.99
S43	Sharada Nagar	7.5	640	500	32	102	90	45	119.53
S44	Vidya Nagar	7.32	720	460	128	34	140	60	110.46
S45	H.B.Colony	7.11	430	480	40	92	100	40	107.8
S46	Govina Pura	7.37	1110	680	90	110	220	62	103.7
S47	Shankarappa Layout	7.56	1060	610	48	119	250	72	122.07
S48	Manjunatha Nagar	8	410	700	32	150	70	70	124.47
S49	Vinayaka Nagar	7.4	1080	720	96	116	240	62	130.50
S50	Kote	7.09	900	480	56	83	180	48	124.23

Water quality range based on WQI Table-3

WQI	Quality of water
90-100	Excellent
70-90	Good
50-70	Moderate
25-50	Bad
0-25	Very Bad

Drinking water standards

Parameters mg/L	IS -10500,1991	BIS	ICMR
PH	6.5-8.5	6.5-8.5	7-8.5
TDS	500	500-1500	500-1500
Hardness	300-600	500	300-600
Calcium	75—200	75	75-200
Magnesium	30-100	50	50
Chloride	250-1000	250-600	250-1`000
Nitrate	45	45	20-100

Graph
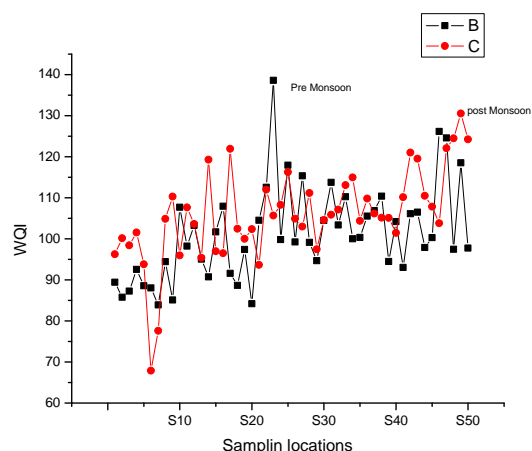
Conclusion

In the present study WQI was the main tool for analyzing the over all quality of different parameters assessing water quality by index number between $0 \geq 100$. The investigated parameters were with the ICMR/BIS standards, except at few sampling locations. The WQI calculated ranged between 70 to > 100 in both the seasons. But out of the 50 samples 75%were indexed > 100.The investigation under the present study revealed that the ground water quality in tiptur town and its surrounding areas is good in its quality for drinking ,Domestic use and agriculture.

Acknowledgements

Reference

1. APHA 1998 ;Standard methods for the examination of water and waste water ,16th Edition ;American public Health Association, Washington D C.
2. Achutha Nair ; G ,Al-Mariami, Jalal Ahemed Bojuari ;Muftab. A and Premkumar. K ;2005.Assessment of the well water quality of Benghaziliya IJEP ,25 ;481-489.
3. Ch Maruthi Devi and T .Usha Madhuri A study on Ground water Quality in Pakistan district and its suitability for drinking nept ,vol 10 No -3,pp 481-483;2011.
4. K Murli R D , Swasthik and R. Elangovan ; Assessment of ground water quality in coimbatore south Taluk ,coimbatore District,India. A WQI approach ,vol 10 No 4 pp 521-524 ;2011.
5. Eaton,A d, Clescer, L.s and Green berg A E 1998 Standard methods for examination of water and waste water American public health Association 1820th ED Washington USA.
6. Trivedy ,R .K and Goel P .K ; chemical and Biological Methods for pollution studies ; Environmental Publications ,Karad ,India.
7. Abdul Jameel A ,2002 Evaluation of drinking water quality in Tiruchirapalli ,India J of Env Health ,44 ; 108 -112.
8. Mariappan ;V ,Prabakaran P ; Rajan M R and Ravichahandran A. D , 2005 ;A systametic study of water quality index among the physic chemical characteristic of ground water in and around Thanjavur Town . IJEP ,25 ; 551-555.
9. Sawant R S , et al 2011 ;Grund water quality of Gadhinglaj Tahsil of Maharastra.,vol 10 No-4 pp. 613-616.
10. Subin M P et al 2011, The study of water Quality of Tripunithura ,a city suburb of Ernakulam District in Kerala, India. Vol 10, No 4 pp. 583-588.

Author Profile:

S B Basavaraddi M.sc,M.Phil,,

Research Scholar (Environmental Science),

Associate Professor of Physics,

Kalpatru Science College, Tiptur,

Tumkur-District, Karnataka-572202.

Department of Environmental Science,

Kuvempu University. Shankargatta,

-577451 Karnataka India.

Integration of GIS and Artificial Neural Network for prediction of Ozone Concentration in Semi-rural areas of Rawalpindi and Islamabad

Sheikh Saeed Ahmad[1]∗, Neelam Aziz[1], Madiha Ejaz[2] and Muhammad Tahir Ali Shah[3]

[1]Department of Environmental Sciences, Fatima Jinnah Women University, Rawalpindi, Pakistan
[2]Department of Computer Sciences, Fatima Jinnah Women University, Rawalpindi, Pakistan
[3]Department of Agriculture, Allama Iqbal Open University, Islamabad, Pakistan

Abstract:

Ozone is one of the most effective pollutants in lower atmosphere. Concentration of ozone in atmosphere reveals its impact on plants, human and on other organic materials. Many techniques had been used in past to calculate the concentration of ozone with the help of other environmental factors like wind, humidity, rainfall, temperature and etc. Prediction models like artificial neural network have gained much reputation in calculating accurate results with learning data. This paper shows a study of integration of predicted ozone concentration from neural network and GIS. The study initiated with data collection from the study area. The collected data is then fed to neural network as training data to get the concentrations of ozone with input variables temperature, humidity and rainfall. The study shows the great dependence of ozone concentration upon environmental factors. Finally the results are spatially interpolated with the help of GIS.

Keywords: Artificial Neural Network Model (ANN), Climatic Variables, Geographic Information System (GIS), Inverse Distance Weighted (IDW), Rawalpindi and Islamabad, Pakistan, Semi-rural areas, Tropospheric ozone concentration,

1. Introduction

The presence of ozone molecule in ozone layer saves earth life from harmful damage by absorbing 97-99% of harmful radiations from sun. Whereas same ozone molecule present in lower atmosphere of earth is declared harmful air pollutant. Ozone in lower atmosphere has major impact on plants, vegetation, animals and most of human respiratory diseases. Many studies have shown a significant correlation between ozone levels and respiratory illness [1]. The emission of the pollutant is directly proportional to nature of industrial and urban activities. So relationship between different other pollutants and meteorological factors can be used to determine ozone level. Many approaches have been made for such purpose. Such approaches can be linear or non linear. Multiple linear regression, principal component regression, quantile regression, among others, are a few examples of linear models [2][3] and, on the other hand, artificial neural networks are the nonlinear models most commonly used [4][5]. One idealistic approach would be to make a deterministic model that depends on chemical processes and atmospheric movements. Other approach is Empirical Kinetic Modeling Approach EKMA that is used for designing emission control strategies [6]. Abdul-Wahab developed a statistical empirical model from measured ambient air quality data, which was based on obtaining the functional relationship between the ozone level and various independent variables by using a stepwise multiple regression procedure [7]. Multiple linear regression is used to obtain a linear input output model for a given data set. If the functional relationship is non-linear, then one or more other inputs can be transformed first into a non-linear form. There are many non-linear multivariate statistical methods which are used to approximate any non-linear relationship; but the assumption of functional dependency is a serious drawback of such methods. [8] Artificial neural network is the so far the strongest approach that is known for developing predictive model without any assumptions and are able to handle multivariable problems. Predictions from ANN were proven more accurate when contrasted with applied linear regression analysis techniques [9] and regression models [10]. Artificial neural networks learn even a complex relationship between different independent variable while the processing on neurons took place [11] and have ability to develop non-linear relationships [12]. ANNs are widely used in environmental problems and their accuracy of prediction has been proven [13, 14, 15, 16]. The multiplayer perceptron, first application of ANN was developed in Slovenia and was aimed at predicting SO2 levels. [14]. ANN can also be applied to predict ozone concentration [17, 18]. Ruiz-Suarez used neural network models for short-term forecasting of ozone in a selected spot of Mexico City [19]. Yi and Prybutok used feed-forward neural network model for predicting ozone concentrations in an urban area with four vehicle emitted pollutants variables carbon dioxide, nitric oxide, nitrogen dioxide, and oxides of nitrogen and three meteorological variables temperature, wind speed, and wind direction[20] . Abdul-Wahab and Al-Alawi used neural network for the Assessment and prediction of tropospheric ozone concentration Levels in Khaldiya region of Kuwait. Thirteen variables CH_4, NMHC, CO, CO_2, NO, NO_2, SO_2, temperature, relative humidity, wind speed, wind direction, solar radiation and dust were selected as input and Ozone as output [21]. Study

of Elkamel illustrated the successful use of a neural network to predict ozone concentrations using both meteorological and chemical data near an industrial area in Kuwait [22]. Hence artificial neural network proved best for prediction of ozone concentration. Detailed descriptions on the use of ANNs in environmental modeling can be found in Maier and Dandy [23]

1.1. What is Artificial Neural Network

An artificial neural network is a system based on the operation of biological neural networks i.e. emulation of biological neural system. The basic constituent of neural network is neutrons that are arranged in different layers known as input, hidden and output layer also known as architecture of neural network. It is a directed graph where a vertex corresponds to a neuron and an edge to a synapse.
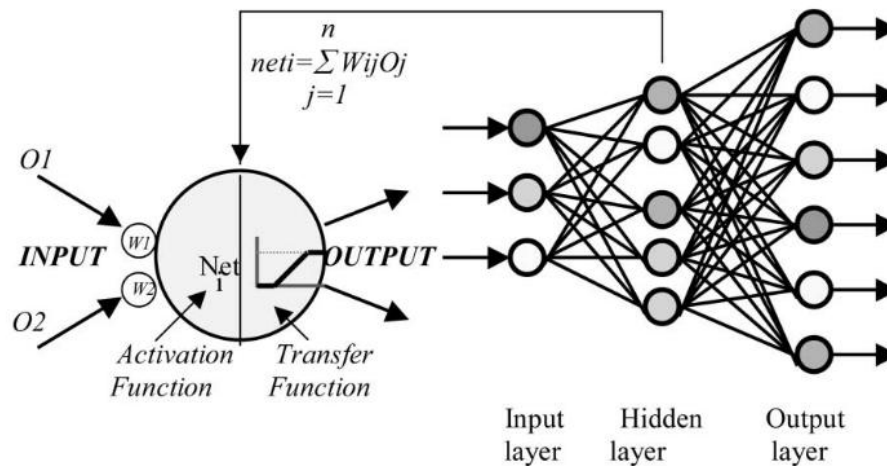
Figure 1 Feed forward Artificial Neural Network Architecture [18]

Each layer processes the data and sends the result to next layer; the output layer shows the predicted output for the inputs given in input layer. A neural network is a parallel system, capable of resolving paradigms that linear computing cannot. As a biological predecessor neural network is adaptive in nature which means during the training of neural network each parameter is changed and is used for solving the problem. During the operation of ANN the dataset is split down into three sets training, validation and testing. Training set is used to train the artificial neural network, i.e. to adjust the artificial neural network weights to maximize the artificial neural network's predictive ability and minimize its forecasting error. Validation set is used to tune the artificial neural network topology or parameters other than weights. Also used for automatic comparison of alternative artificial neural networks. Testing set is used only to test the accuracy of the predictions made by the artificial neural network on new data. Network properties contain network activation and error functions. An activation function controls the amplitude of the output of the neuron. An acceptable range of output is usually between 0 and 1, or -1 and 1. The properties are applied to all networks tested by the architecture search method as well as to a manually selected network.

2. Materials and methods

2.1. Study area

Pakistan is badly plagued with environmental problems due to unlimited population growth and unchecked vehicular emissions. Bad effects of ozone can spread in a wide range and up to very long distances, depending on wind speed and direction and can badly affect the health of inhabitants and agricultural entities in adjacent rural areas. Therefore, there is an urgent need for air pollution impact assessment and prediction studies on crops in the developing areas of Pakistan.

The study area of this research encompasses twin cities of Pakistan, Islamabad and Rawalpindi. Islamabad is capital of Pakistan and Rawalpindi is 15Km apart from it. Twin cities are located at 33°40´N 73°10´E with almost 4.5 million population. The study area is divided into 5 different zones with zero point reference because it is a major gateway between twin cities for many routes. Boundaries of each zone are defined within the 40 km of reference point. 40 km distance is chosen based on previous studies in this domain. Zones are as follows in figure 1.
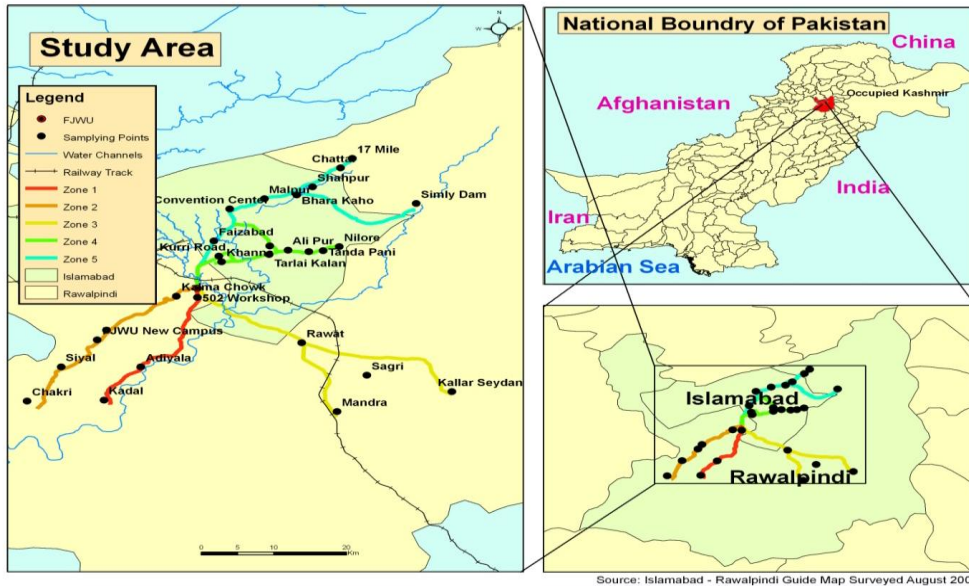
Figure 1 Base Map

Zone 1: 502 workshop, Adyala village, Kadal

Zone 2: Kalma Chowk, Pir Mehr Ali Shah Town, FJWU New Campus, Siyal and Chakri

Zone 3: Rawat, Kallar, Sagri and Mandra

Zone 4: Kuri, Khanna, Tarlahi, Alipur, Jhangi Syedan, Thanda Pani, Nelore and Chakshahzad

Zone 5: Convention Center, Malpur, Bara khau, Shahpur Village, Chattar, 17 Mile and Samli Dam

2.2. Dataset preparation

The ozone concentration was determined by The Model 400E ozone analyzer. The Model 400E ozone analyzer is a microprocessor-controlled analyzer that determines the concentration of Ozone (O_3) in a sample gas drawn through the instrument. The microprocessor uses calibration values, the UV absorption measurements made on the Sample Gas in the absorption tube along with data regarding the current temperature and pressure of the gas to calculate a final O_3 concentration, stores in one of the unit's Internal Data Acquisition System and shows result to the user via front panel.

With the determination of concentration of ozone other environmental factors were also measured and saved along with respective concentration of ozone that includes temperature (˚C), humidity(%) and rainfall(mm) in particular season. The data is collected for 18 consecutive months from november 2009 to march 2011 from 28 different sites of the research.

3.   Results and discussion

3.1. Network Development

The data of database was split into three, mutually exclusive, portions of 70%, 15%, 15% respectively for training, validation and testing datasets. The design of the neural network (architecture) contains 4 hidden layers, layer 1 has 20 neurons, layer 2 contains15 neurons, layer 3 contains 10 neurons and layer 4 contains 5 neurons.

The training pattern for the neural network contains four inputs which are season_id, temperature, humidity and rainfall and the output is concentration of respective area for given inputs. Neural network is trained by using quick propagation algorithm. The Quick propagation algorithm calculates the weight change by using the quadratic function $f(x) = x^2$. Quick propagation coefficient was set to 1.75, learning rate was 0.1 and iterations were 500.

Logistic function is used for input and output activation function which is sigmoid curve and is calculated using the following formula: $F(x) = 1/ (1+e^{-x})$. Its output range is [0.1]. Sum-of-Squares is the most common error function and is used as output error function. The error is the sum of the squared differences between the actual value (target column value) and neural network output.

3.2. Model Results

The data is tested and results are produced for all sets i.e.: training set, validation set, test set. Actual vs. Output graph displays a line graph of the actual and network output values for records displayed in the Actual vs. Output Table. Horizontal axis displays the selected input column values and vertical axis displays the network output. The visualization for actual vs. output is shown in figure 2.
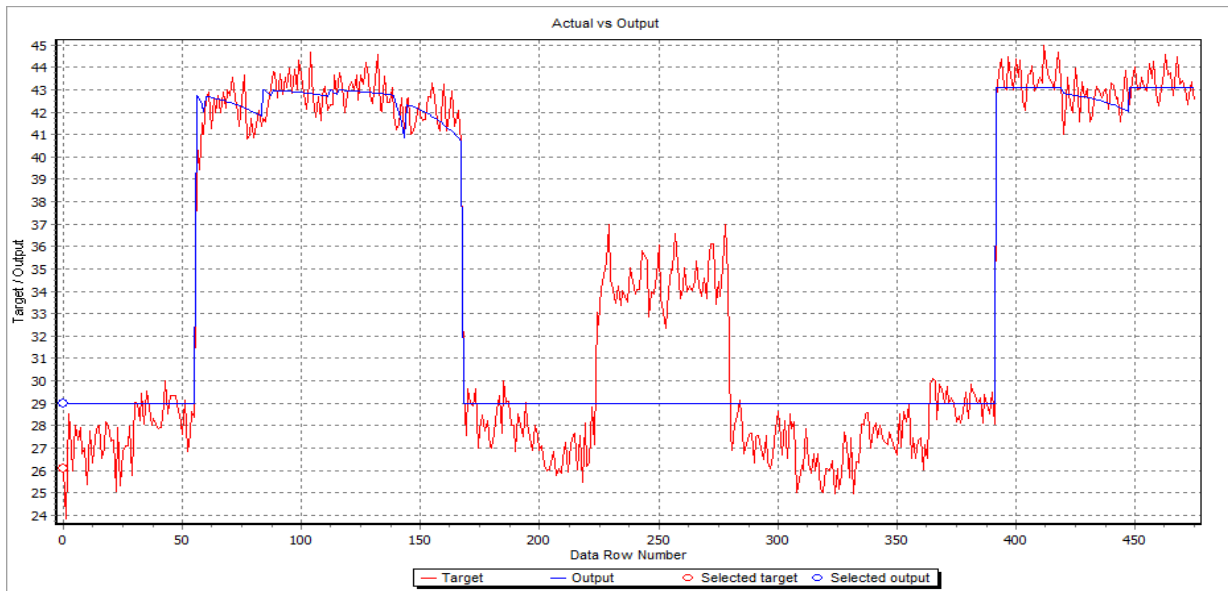

Figure 2 Actual verses Output

The environmental variables which are temperature, humidity and rainfall are very important in prediction of ozone. The information of relationship between climatic variables and ozone concentration is necessary for assembling of database.

ANN along with concentration of ozone also assesses the dependence and importance of input variables which are environmental variables in this case. Figure 3 depicts that the ozone concentration level is negatively related to the relative humidity (RH in %) and rainfall, and positively related to temperature (in C^0). Periods with higher temperature and lower humidity usually lead to the higher level of ozone in the atmosphere and vice versa. Similar changes in ozone concentration levels with respect to the climatic variables have already been described in literature [24] [25]
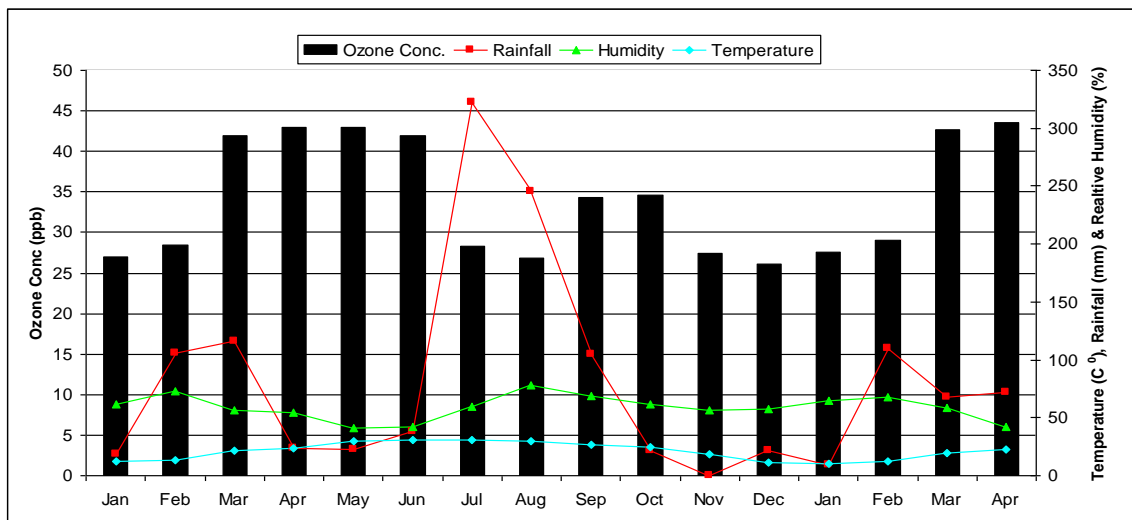
Figure 3 Relationship between O_3 concentration and climatic variables

Fig 4 shows Error dependence graph that displays the network error dependence on values of numerical input columns. The Error Dependence Graph allows analyzing that which ranges of the selected input column tend to produce bigger or smaller network errors.
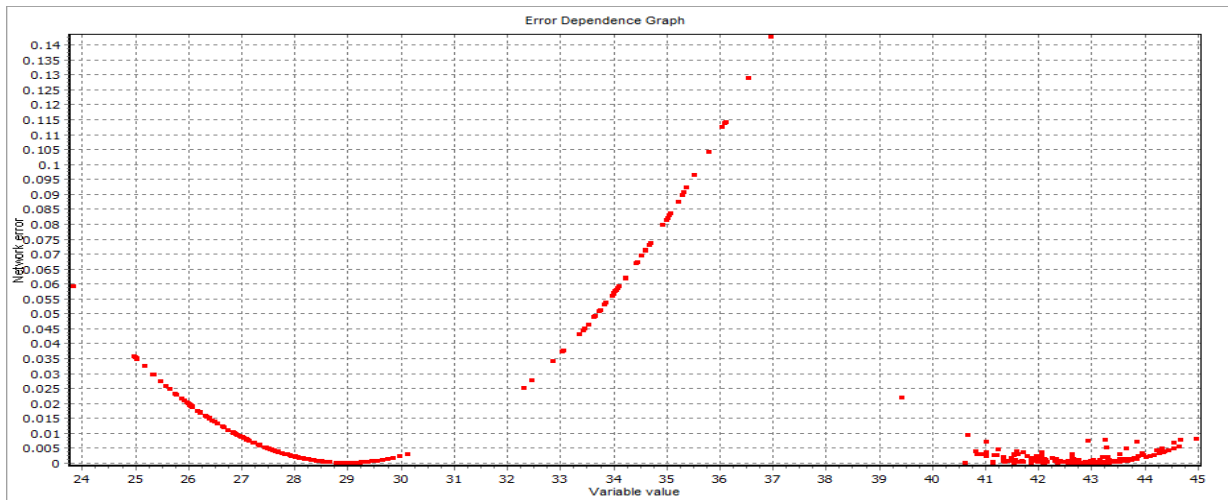

Figure 4 Error Dependence Graph

The neural network is queried after it is trained and tested. The targeted value for the neural network is concentration so querying inputs is season_id, temperature, humidity, rainfall and area_id. The results of the concentrations from neural network are then integrated with GIS.

3.3. Integration of ANN with GIS

GIS is powerful tool that is used to view, understand, question, interpret, and visualize data in many ways that reveal relationships, patterns, and trends in the form of maps, globes, reports, and charts. The results of predicted concentrations of Ozone were mapped on GIS. The results of predicted concentration value of ozone is stored in different excel sheets along with area identifiers. Different excel sheets were used to distinguish between different values of temperature, humidity and rainfall, i.e. the excel sheet contains columns named as area_id, temperature, rainfall, humidity, concentration, longitude and latitude. The values of temperature, rainfall and humidity of same excel sheet are similar with different values of concentration, area_id, longitude and latitude. The excel sheets were imported to ArcMap 9.2 version. The data of excel sheets were mapped by using longitudes and latitudes present in the excel sheet. Inverse distance weighting is the simplest interpolation method and is used for interpolating concentration values on map. Figure 5 and 6 shows two interpolated maps for spring season when temperature is 12 degrees centigrade, humidity is 42 and rainfall is 68 millimeter and for autumn season when temperature is 14 degrees centigrade, humidity is 62 and rainfall is 22 millimeter respectively.
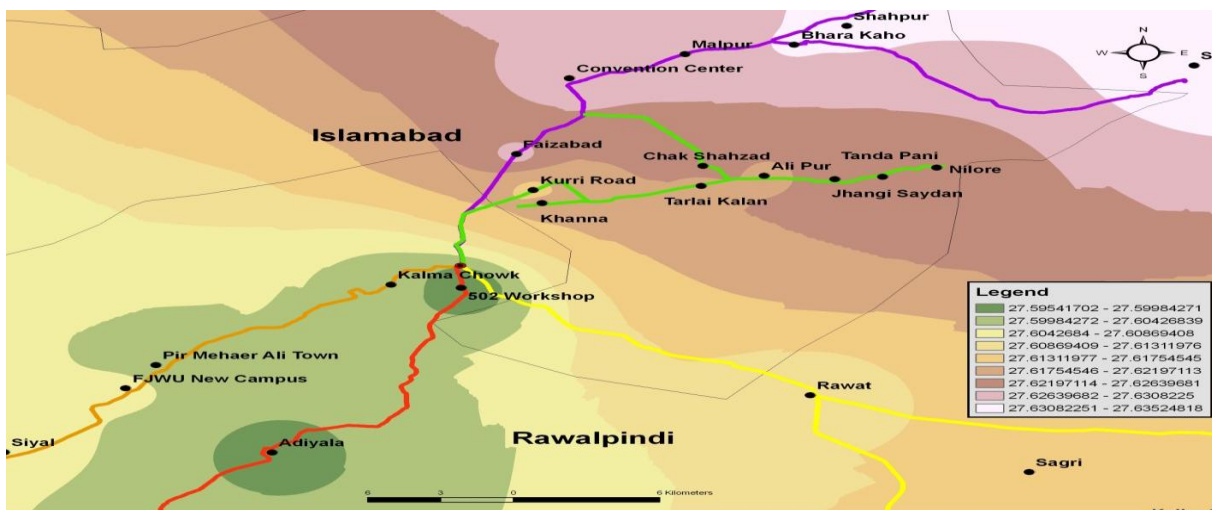

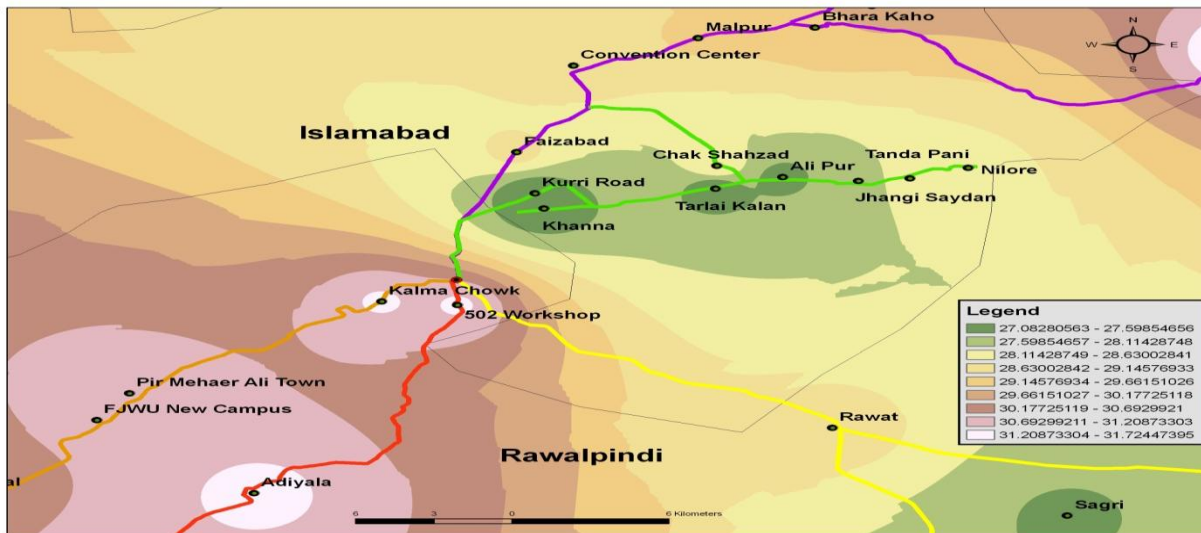**Figure 5** Predicted ozone concentration in spring season

Figure 6 Predicted ozone concentration in autumn season

4. Conclusion

The present research study highlights the importance of air quality management. With the help of artificial neural network it is concluded that O_3 concentration has been increasing day by day due to variable factors. A minor change in temperature, humidity or rainfall directly impacts the concentration of O_3. With the study it is observed that the O_3 concentration was more in Rawalpindi as compared to Islamabad. Spatial interpolation showed variations graphically in O3 concentration at different sampling sites of twin cities in different months. Through present research work hot spots of O3 in twin city have been identified and this work will be helpful in future fort calculation of O_3 in atmosphere and for drawing spatial interpolation of O3. Moreover study highlights the areas of high concentration to control it before it increase above alarming levels.

5. Acknowledgment: Thanks to Higher Education Commission (HEC) of Pakistan for providing the research grant for the study under NRPU Program.

6. References

[1] M. Jerrett, R.T. Burnett, C.A. Pope III, K. Ito, G. Thurston, S. Krewski, Y. Shi, E. Calle, and M. Thun. "Long-Term Ozone Exposure and Mortality", The New England journal o f Medicine, Vol. 360, Issue 11, 2009, pp. 1085–1095.

[2] S.I.V. Sousa, J.C.M. Pires, M.C. Pereira, M.C.M. Alvim-Ferraz, and F.G. Martins. "Potentialities of quantile regression to predict ozone concentrations", Environmetrics, Vol. 20, 2009, pp. 147–158.

[3] J.CM. Pires, and F.G. Martins. "Correction methods for statistical models in tropospheric ozone forecasting", Atmospheric Environment, Vol. 45, 2011, pp. 2413–2417.

[4] M. Gardner and S. Dorling. "Artificial neural network-derived trends in daily maximum surface ozone concentrations". Journal of Air and Waste Management, 51, 2011, pp. 1202–1210.

[5] G. Latini, R.C. Grifoni, and G. Passerini. "The importance of meteorology in determining surface ozone concentrations—a neural network approach", **Coastal Environment: Environmental Problems in Coastal Regions IV**: Ecology and the Environment, Vol. 58, 2002, pp. 405–414

[6] J.R. Kinosian. "Ozone-precursor relationship from EKMA diagrams". Environmental Science and Technology, Vol. 16, Issue 12, 1982, pp. 880-883.

[7] A. Abdul-Wahab, W. Bouhamra, H. Ettouney, B. Sowerby, and B.D. Crittenden. " Predicting ozone levels: a statistical model for predicting ozone levels in the Shuaiba Industrial Area, Kuwait", Environmental Science and Pollution Research, Vol. 3, Issue 4, 1996, pp. 195-204.

[8] U. Utojo, and B.R. Bakshi. "Connection between neural networks and multivariate statistical methods: an overview", In: D.R. Baughman, Y.A. Liu (eds.), Neural Networks in Bioprocessing and Chemical, 1995.

[9]   B. Chelani Asha, C.V. Chalapati rao, K.M. Phadke, and M.Z. Hasan. "Prediction of Sulphur dioxide concentration using artificial neural networks", Environmental Modeling and Software, Vol. 17, 2002, pp. 161-178.

[10]   M.W. Gardner and S.R. Dorling. "Neural network modeling and prediction of hourly NO_x and NO_2 concentrations on urban air in London", Atmospheric Environment, Vol. 33, 1999, pp. 709-719.

[11]   D.R. Baughman, and Y.A. Liu. "Neural Networks in Bioprocessing and Chemical Engineering", Academic Press, New York, 1990, pp. 10-13.

[12]   S. Chen, and S.A. Billings. "Neural network for non linear dynamic system modeling and identification", International Journal of Control, Vol. 56, 1992, pp. 319-346.

[13]   J. Schumuller. "Neural networks and environmental applications", Expert systems for environmental applications, In: H. Hushou (ed.), ACS Symposium Series, 431. ACS, Miami Beach, Florida, 1988, pp. 5-8.

[14]   M. Boznar, M. Lesjak, and P. Mslakar. "A network-based method for short-term predictions of ambient SO2 concentrations in highly polluted industrial areas of complex terrain", Atmospheric Environment, Vol. 27B, 1993, pp. 221-230.

[15]   A. Pasini, and S. Potesta. "Neural Network Modelling: Perspectives of Application for Monitoring and Forecasting Physical-Chemical Variables in the Boundary Layer, in Urban Air Pollution", I. Allegrini and F. De Santis (eds.)), Springer-Verlag, 1996, pp.329-340.

[16]   O. Mayora-Ibarra, L. Motta, and F. Curatelli. "Forecasting of atmospheric pollution levels with neural networks". Neural Networks and their Applications, Marseilles, Vol. 11, 1998, pp. 323-328.

[17]   **C.** Paoli, G. Notton, M.L. Nivet, M. Padovani, and J.L. Savelli. "A Neural Network model forecasting for prediction of hourly ozone concentration in Corsica," 10th International Conference on Environment and Electrical Engineering, , 2011, pp.1-4, 8-11 May 2011, Rome , Italie.

[18]   M. Cai, Y. Yafeng , and X. Min. "Prediction of hourly air pollutant concentrations near urban arterials using artificial neural network approach", Transportation Research Part D: Transport and Environment, Vol. 14, Issue 1, 2009, pp. 32-41.

[19]   J.C. Ruiz-Suarez, O.A. Mayora-Ibarra, and J. Torres-Jimenez. "Short-term ozone forecasting by artificial neural networks", Advance in Engineering Software, Vol. 23, 1995, pp. 143-149.

[20]   J. Yi, and R. Prybutok. "A neural network model forecasting for prediction of daily maximum ozone concentration in an industrialized urban area", Environmental Pollution, Vol. 92, Issue 3, 1996, pp. 349-357.

[21]   A. Elkamel, S. Abdul-Wahab, W. Bouhamra, and E. Alper. "Measurement and prediction of ozone levels around a heavily industrialized area: a neural network approach", Advances in Environmental Research, Vol. 5, 2001, pp. 47-59.

[22]   A. Elkamel. "An artificial neural network for predicting and optimizing immiscible flood performance in heterogeneous reservoirs", Computers and Chemical Engineering, Vol. 22, 1998, pp. 1699-1709.

[23]   H. Mayer. "Air pollution in cities". Atmospheric Environment, Vol. 33, 1999, pp. 3029-4037.

[24]   A.T. Chan, E.S.P. So, and S.C. Samad. "Strategic guidelines for street canyon geometry to achieve sustainable street quality", Atmospheric Environment, Vol. 35, 2001, pp. 5681-5691.

[25]   P. Martin, B. Cabañas, F. Villanueva, M.P. Gallego, I. Colmenar, and S. Salgado. "Ozone and Nitrogen Dioxide Levels Monitored in an Urban Area (Ciudad Real) in Central-southern Spain", Water Air Soil Pollution, Vol. 208, Issue (1-4), 2010, pp. 305-316.

H.264 Based Video Compression

Pranob K Charles[1] Ch.Srinivasu[2] V.Harish[3] M.Swathi[3] Ch.Deepthi[3]

[1](Associate Professor, Dept. of Electronics and Communication Engineering, KLUniversity.)
[2](Professor, Dept. of Electronics and Communication Engineering, KLUniversity.)
[3](Project Students, Dept. of Electronics and Communication Engineering, KLUniversity.)

Abstract

A raw video takes up a lot of space for storage and bandwidth for transmission. Uncompressed video from a video recording device may take up about 20 MB per second of video. Thus, there is a clear necessity for an efficient mechanism which enables the video to be stored and transmitted over limited bandwidths. Compression can be broadly classified into two types, lossy compression and lossless compression. In lossy compression, the video is compressed to very low bit rates which considerably reduce the quality of the video whereas in lossless compression no loss of data is present and it is more visually appealing than lossy compression. This paper discusses about H.264 video compression standard which is a motion-block oriented codec standard developed by ITU-T. The aim of this algorithm is to provide visually better video quality with fewer amount of information transfer. Various motion estimation algorithms are also studied.

Keywords – H.264, lossy compression, motion estimation

I. Introduction

Video compression technology has enabled many services like video calling, video conferencing, internet streaming. The two major parameters of consideration for designing a standard are Bandwidth and storage space. New video compression standard should be compatible and more advanced than the previously developed ones. It is obvious that a new standard should use less bandwidth for transmission and minimum storage space .

Two major groups that are involved in creating the video standards are Video Coding Experts Group (VCEG) from ITU-T and Moving Picture Experts Group (MPEG) from International Organization for Standardization (ISO)/International Electro-technical

Commission (IEC). A previously developed video codec standards, and their released year are mentioned here. The

first video codec standard is H.120 developed in 1984 by ITU-T which is a lossy compression. The newer standard defined in 1990 by ITU-T, is called H.261. It is popular for

video conferencing and telephony. ISO/IEC also released MPEG-1 part 2 in 1993, which is implemented in video CD. In 1995 ITU-T and ISO/IEC jointly released their new video codec known as H.262, popular in Video CD/DVD/Blu-ray, Video broadcasting. In 1995, H.263 and 1999 MPEG-4 part 2 are developed by ITU-T and ISO/IEC respectively.

Finally, H.264 video codec was announced by ITU-T and ISO/IEC, which is popular for all the modern day applications [8].

H.264 is widely accepted video codec standard and is also known as MPEG-4 part-10 AVC (Advanced Video Coding). It took approximately four years to have a Trade off in terms of coding efficiency, complexity on hardware, and cost which are balanced in new proposed standard [1]. Some of its features are high definition resolution, interlaced/progressive scan mode, variable frame rate, high bit rate, supporting I, B, & P-frames, 9 different prediction modes, variable size block matching motion estimation, and motion compensation, quarter pixel accuracy, adaptive length coder, and image enhancement filter. H.264 is compatible with almost all kinds of recent video coding tools which enable it to standout from other video coding standards.

Ii. Basics of video coding

The human visual system works as RGB model. Cones sense the red, green and blue color components and merges them to create a image. Also the human visual system is less sensitive to color component than luminance/brightness of image. Another fact of human eye is that if we pass at-least 15 frame per second in front of human eye, human eye will not differentiate frame boundary and it seem as movie. These limitations of human eye are advantageous to our video compression system.

The raw video is compressed mainly by removing the redundant data present in the video and only transmitting or storing the required amount of data.There are four types of redundancies present in a raw video.

A. Temporal Redundancy

A video is nothing but a group of consecutive pictures called frames. Temporal redundancy is the redundancy present in between two consecutive frames in a video.

B. Spatial Redundancy

The correlation between the neighboring pixels present in the same frame leads to spatial redundancy.

Fig 1. Spatial Redundancy data

It can be clearly seen from the figure 1 that the pixels present inside the box almost have same pixel values.

C. Color Spatial Redundancy

A human eye is insensitive to sudden color variations but is effective in identifying the changes in brightness of a picture. We can save bandwidth if we only send selective samples of chrominance components.

D. Phyco-visual Redundancy

It refers to a high-level limitation of HVS. When HVS visualizes an image, the partial information of image is important. The rest of the information is less important, so we can represent less important data with less number of bits.

Iii. H.264 Video Coding

H.264 video coding consists of Inter frame prediction block, motion compensation block, Discrete Cosine Transform block, Quantizer and Enctropy Encoder . Figure 2 shows the block diagram of H.264 video coding.

algorithm by considering both the computational intensity as well as the PSNR values. The algorithms that are studied are Exhaustive Search, New Three Step Search, Simple and Efficient TSS, Four Step Search, Diamond Search and Adaptive Rood Pattern Search.[17]

The algorithms are tested for the computational intensity and the Peak Signal to Noise Ratio and the best method is chosen by having a tradeoff between the computations and the PSNR values. The best algorithm should have a good PSNR value and at the same time with minimum possible computations.
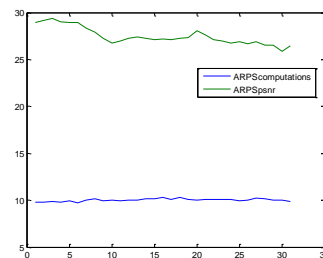

Fig.2. H.264 Video Coding Block Diagram

Motion estimation block is also known as inter frame prediction. The main purpose of the motion compensation block is to remove the temporal redundancy. The prediction of the current frame can be done by using only the previous frame or a group of previous frames.

The residual image which is the output of the entire prediction stage is then sent to DCT block. The DCT of the residual image will convert the image into frequency domain thus differentiating between the high frequency and low frequency components present in the current frame. The main limitation of the human visual system is that it cannot recognize sudden changes in the frames,in other words the human eye is insensitive to high frequency. The quantizer exploits this limitation of the human eye and removes the high frequency components by having a threshold value. Everything that falls below this threshold value will be made zero and the remaining are left intact.

Iv. Prediction and motion estimation

Out of all the blocks present in the coding process, Prediction stage is more computationally intensive. In this paper, we have studied various block matching algorithms and arrived at the best block matching

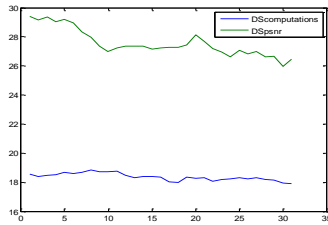**Fig 3.** Computations and PSNR of Adaptive Rood Pattern Search

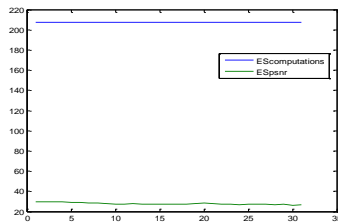**Fig 4.** Computations and PSNR of Diamond search

Fig 5. Computations and PSNR of Exhaustive search
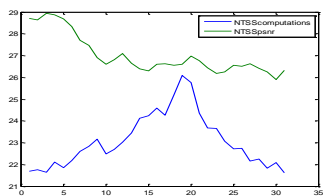

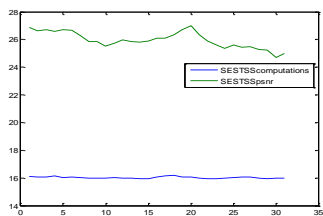**Fig 6.** Computations and PSNR of New Three Step Search

Fig 7. Computations and PSNR of Simple and Efficient TSS
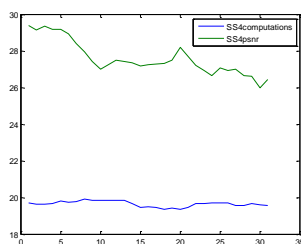

Fig 8. Computations and PSNR of Four Step Search

Four Step Search, Diamond Search and Adaptive Rood Pattern Search prove to be effective with low computations and high PSNR value. When, Computational intensity is critical, Adaptive Rood Pattern Search proves to be effective.

V. Encoding and decoding

The output from the prediction stage is now divided into blocks then a discrete cosine transform is performed on each of the block followed by quantization, zig zag scanning and entropy coding. The block diagram for encoding is given in figure 9.
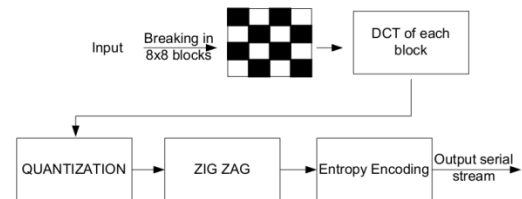

Fig 9. Blocks present in Encoding stage

A. DCT

DCT is performing a math function on the original matrix. It converts a signal into the frequency domain matrix. It represents components in terms of the sum of the cosine function [5]. A typical 8 x 8 DCT matrix element can be represented as shown in figure 10. we can observe that the frequency component is increased from left to right, and top to bottom.
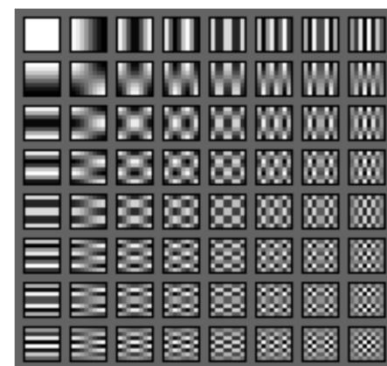

Fig 10. An 8 x 8 DCT matrix in frequency domain

B. Quantization

An 8-by-8 DCT block is ready for the next level of compression, which is known as quantization. It is a process of transformation of continuous set of values to the finite set of small values. When the quantization is performed on the original signal, the part of information is lost from the original signal. It means higher the compression but lower the quality of image, and vice versa.

C. Entropy Coding

The H.264 uses content based adaptive variable length coding, and it is processed in major five steps.

1. Encode the number of coefficient and the trailing ones.

2. Encode the sign of each trailing ones.

3. Encode the level of non-zero coefficient.

4. Encode the total number of zeros before the last coefficient.

5. Encode the location of encoded zeros.

Vi. Results
The PSNR (peak signal to noise ratio) based on MSE (mean square error) is used as a measure of "quality." MSE and PSNR are given by the following relations:

$$MSE = \frac{1}{m*n}\sum_{i=1}^{n}\sum_{j=1}^{m}(x_{i,j} - y_{i,j})^2$$

$$PSNR = 10\log[(255)^2/MSE]$$

Figures 11 and 12 show one of the original and decoded frame. We can observe a little degradation in quality of the decoded frame ,the PSNR values for various resolutions are given in table 2.

Table 1 . Computations and PSNR of various Prediction Methods

Method	Computations	PSNR
Exhaustive search	207.4	27.83
Simple and Efficient Three Step Search	16.02	25.97
New Three Step Search	23.09	27.02
Four Step Search	19.65	27.59
Diamond Search	18.36	27.56
Adaptive Rood Pattern Search	**10.01**	**27.48**

Fig 11. Left : Original frame   Right: decoded frame

Table 2. PSNR values for various video resolutions

Video size	PSNR
176 x 144	31.5865
352 x 288	65.9162

Vii. Conclusions
H.264 is the most advanced and widely used video coding standard available today. H.264 uses more accurate prediction algorithms and motion compensation techniques to achieve better compression and same quality video at the low bit rate without compromising the image quality.

References
[1] G. J. Sullivan, P. Topiwala, and A. Luthra, "The H.264/AVC Advanced Video Coding Standard: Overview and Introduction to the Fidelity Range Extensions", Presented at the SPIE Conference on Applications of Digital Image Processing XXVII Special Session on Advances in the New Emerging Standard: H.264/AVC, August 2004.

[2] http://www.drtonygeorge.com/video_codec.htm

[3] Thomas Wiegand, Gary J. Sullivan, "Overview of the H.264/AVC Video Coding Standard", IEEE Trans. on Circuits and Systems for Video Technology, vol. 13, no. 7, pp. 560–576, July 2003.

[4] H. Jozawa, K. Kamikura, H. Kotera, H.Watanabe, "Two-Stage Motion Compensation Using Adaptive Global MC and Local Affine MC", IEEE Trans. on Circuits and Systems for Video Technology, vol. 7, no. 1, pp. 75–85, February 1997.

[5] N. Ahmed, T. Natarajan, and K. R. Rao, "Discrete Cosine Transform", IEEE Trans. Computers, 90-93, Jan 1974

[6] http://www.cs.uga.edu/~sadiq/pdf/vasim.pdf

[7] Soon-kak Kwon, A. Tamhankar, K.R. Rao, "Special Issue on Emerging H.264/AVC video coding standrad" J. Visual Communication and Image Representation, vol 17.

[8] http://en.wikipedia.org/wiki/Video_compression

[9] K. Peter, "Algorithms,complexity analysis and VLSI architectures for MPEG-4 motion estimation", Kluwer Academic Publishers, Boston, 1999.

[10] Jianhua Lu and Ming L. Liou, "A Simple and Efficient Search Algorithm for Block-Matching Motion Estimation", IEEE Trans. on Circuits and Systems for

Video Technology, vol. 7, no.21, pp. 429-433, April 1997.

[11] R. Li, B. Zeng, and M. L. Liou, "A new three-step search algorithm for block motion estimation" IEEE Transactions on Circuits and Systems Video Technology,vol. 4, pp. 438–443, Aug. 1994.

[12] P. Lai-Man and M. Wing-chung, "A novel four-step search algorithm for fast block motion estimation", IEEE Transactions On Circuits and Systems for Video Technology, vol. 6, pp. 313-317, Jun. 1996.

[13] M.H. Chan,.B. Yu, A.G. Constantinides, "Variable size block matching motion compensation with applications to video coding", IEE Proceeding, Vol. 137, Pt. I , No. 4, pp 205-212, August 1990

[14] Shou-Yi Tseng, Che-How Mak, "A Motion Vector Coding Scheme Based on Bottom-up Merging Procedure", IEEE Transaction on advances in multimedia, pp 125-129, July 2009

[15] L. Kizewski, Student Thesis on "Image Deblocking Using Local Segmentation", School of computer science and software engineering Monash University, November 2004

[16] http://www.vcodex.com/files/H264_intrapred_wp.pdf

[17] http://www.mathworks.com/matlabcentral/fileexchange/8761

Mr. Pranob K Charles, Associate Professor, currently associated with School of Electrical sciences, Department of ECE, K L University, Andhra Pradesh, India. He received B.Tech in Electronics and Communication Engineering from JNTUH and M.E in Applied Electronics from Anna University, Coimbatore. He is a Life Member in IETE. He authored nearly 10 research papers in various International journals and conferences. His research interests include Image Processing, Video Processing, and Artificial Neural Networks.

Motion control - Fault diagnosis in Machines using VHDL

K.M.Krishnan[1] and N.Rajeswaran2

[1]P.G Student/VLSI Design, SNS College of Technology, Coimbatore, Tamilnadu.
[2]Dept.of ECE, SNS College of Technology, Coimbatore, Tamilnadu.

 Abstract- The machines which have become a part of present day life, even in some cases it overcome human working ways. So for there is major concern in functioning of motor drives because a minute faulty function of motor may lead to drastic damage in working environment. Thus before entering into the fault diagnosis of induction motor the speed control is an important aspect. The speed control in induction motor can be done using SVPWM technique. From the past several years, much progress has been made in Artificial Intelligence (AI) technology. Simplified models of neural processing in the brain have been viewed as artificial intelligence in neural networks. It's an inexpensive, reliable and non-invasive Artificial Neural Network (ANN) based fault diagnosis. Multilayer Perceptron (MLP) is to be used in this paper because the input data contain continuous feature. The fault diagnosis in induction motor using AI technology can be done without resuming the function of induction motor an advantage of this approach compared with other techniques for fault diagnosis[1]. This paper presents the new technique relevant to the design method of artificial intelligence based on VHDL hardware description language and FPGA implementation. The simulation results are obtained from XILINX 12.2 software.

Keywords: ai, svpwm, ann, svm, mlp, vhdl, fpga.

I.   Introduction

In the past few years most of the methods are based on knowledge of status equation for fully or partially controlled systems. However status equation can't be easily obtained. Therefore we go for a smart control method with self-learning capability for better control performance. Thus here in this paper induction motor fault diagnosis and its motion control are going to be delt. Our design users Neural Network for its amazing effect which traditional controllers cannot achieve, when the system involved in an uncertain, time varying or non-linear status. The speed control of induction motor is the main process to be undergone before fault diagnosis is performed. The speed of the motor is of major concern in detection of fault. The speed control and fault diagnosis are performed in comparative manner [1]. The speed control of induction motor is performed by space vector pulse width modulation (SVPWM). Thus three level voltage fed PWM inverter, which shows popularity in industrial drive application. The output voltage waveform which is generated by multilevel inverter. It can be generated at low switching frequency with high efficiency and low distortion. This is the reason why large voltage between the series device is easily shared. The space vector PWM technique is very popular which results in higher magnitude of fundamental output voltage available. The SVPWM is an advanced computation-intensive PWM method and it's the best among all other PWM method as it functions at variable frequency drive applications [2].

II Speed Control of motor

A voltage source inverter type Space vector pulse width modulation for controlling the speed of the induction motor is performed. The pulse width modulation in which several pulse are produced in each half cycle but width of each pulse is not same as in case of multiple pulse width modulation however the width of each pulse is varied in accordance with the amplitude of the sine wave reference voltage. The Space Vector Modulation (SVM) is normally implemented using the direct method. The space Vector is an algorithm for the control of PWM. The principle behind SVPWM is that voltage vector which is to be approximated by using three adjacent vectors. To drive a 3phase AC powered motor at varying speed we require alternate current waveform which can be generated using SVM. Thus Fig 1 shows the SVPWM wave model in response to the sinusoidal input wave. The SVPWM is generated mainly based upon the positive and negative cycles of the sinusoidal wave. The space vector diagram which consist 8 vectors these vectors are given as input to the IGBT inverter through which the speed of the induction motor is controlled. Taking into consideration of these 8 vectors among which 6 vectors starting from V001 to V110 is for supplying signal to Switch ON the transistors present in the IGBT inverter.
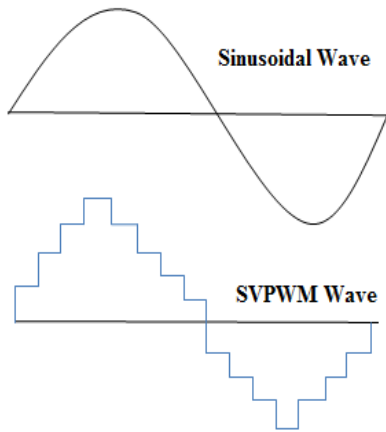
Fig.1 Sinusoidal PWM Modulation

Thus with appropriate SVPWM signals a vector is produced. The vector transit smoothly between the 6 sectors and provide line to line voltages. The line voltages are passed as input to transistors in the inverter. Thus the IGBT inverter makes the induction motor to run. Other than the above said 6 vectors there are two null vectors V000 to V111 which provide 0v (i.e.) IGBT stop generating pulse which in turn stop the motion of induction motor.[3] These null vectors are due to short of transistors. There are two series of transistors in IGBT inverter of these either the upper end or lower end transistor may get shorted which leads to null vector.
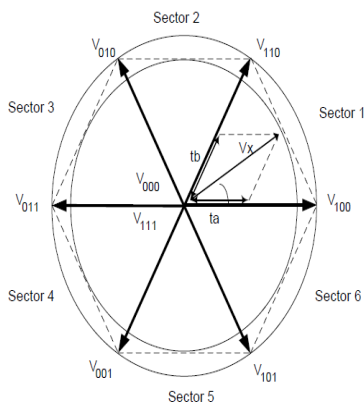

Fig 2 SVPWM Vector Diagram

Upper End Transistors = T1,T3,T5
Lower End Transistors = T2,T4,T6.

Based upon the inverter bridge configuration the six transistor combination has eight permissible switching states as said before which is given in the following table I with vector values of each states are also incorporated. In this there are 8 states and the devices that are in on condition are represented in ON DEVICS and their

corresponding space voltage vectors are represented as V_{000} to V_{111}. In this from state 1 to state 6 the transistors are in ON condition alternatively. Whereas the state0 and state1 in which either the upper end transistors or the lower end transistors are in ON condition. The other end of the transistors are OFF which produces null vectors and the IGBT stop generating pulse thus induction stop functioning particularly in this two vector states.

Table I Inverter Switching States

States	on Devices	Spacevoltagevector
0	T2 T4 T6	V000
1	T1 T4 T6	V100
2	T1 T3 T6	V110
3	T3 T2 T6	V010
4	T2 T3 T5	V011
5	T2 T4 T5	V001
6	T1 T4 T5	V101
7	T1 T3 T5	V111

III Fault Diagnosis

A. Neural Networks

For the past several years there is a progressive development in the field of Neural Networks. Neural network is a network of biological neurons. These neural networks are classified into biological neural networks and artificial neural network [4]. A biological neural network is a population of physical interconnected neurons. An artificial neural network is the mathematical or computational model inspired by the structure & function of biological Neural networks "Adaptive System". Thus the ANN is also termed to be as Artificial intelligence (AI). AI is the intelligence of machine and branch of computer science. Simply to say AI is the science of making computer to do things by its own as like human. We go for AI because without any external learning source it can't make *any intelligent response.*
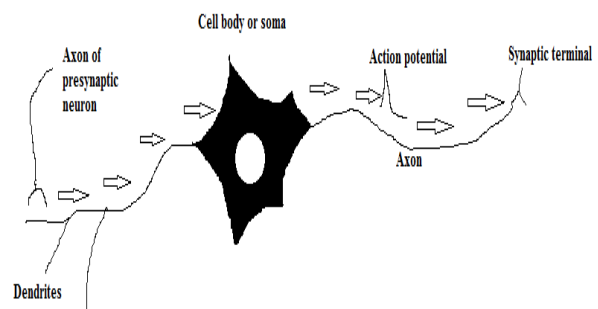

Fig.3 A Neuron

The neurons architecture in which we choose multiply and accumulate structure for neurons. In which single multiplier and accumulators are present [5]. Multiplier in which one input is from previous layer neuron and the other is from the corresponding weighted ROM. The multiplier is 8bit multiplier results in 16 bit product. The weighted ROM whose inputs are address and clock. Neuron has its own individual weight storage ROM. Next to the multiplier is the accumulator where the multiplied values are summed, with the help of clock signals these process are synchronised. The accumulator is of 16 bit wide. The accumulator enable signal which enable accumulator function and out enable signal for 3state outputs. ANN consists of 3 layers input unit connected to hidden unit which is connected to output unit. The activity of input unit represents raw information that is fed into the network. The function of each hidden unit is determined by the activity of input unit and weights on the connection between the inputs and the hidden units. The behaviour of output units depends on the activity of hidden unit and weight between the hidden and output unit. The architecture consists of 20 input nodes with 2 hidden nodes and 1 output node. In the upcoming architecture where the sigmoid activation functions is used. In that the tansig for hidden nodes $f(n)$ and the logsig for output node in $g(a)$. One of the most frequently used activation function is hyperbolic tangent (tanh) sigmoid function referred as tansig in matlab.

B. Multilayer Perceptron Algorithm

The following discussion is about Multilayer Perceptron Algorithm (MLP). MLP which consist of three layers input, hidden and output layer. The input layer which posse's n linear neurons. These neurons receive inputs in vector format from which the MLP starts its operation. Along with these input vector an additional bias neuron are also given as input to the hidden layer which produce signal+1.[6] Thus the hidden layer which posses q sigmoidal neurons to receive input from the input layer and teh output layer which posses p sigmoidal neurons to receive signal from the hidden layer. The network mainly functioning of Data shift and approximate the function. By which the learning problem can be executed.
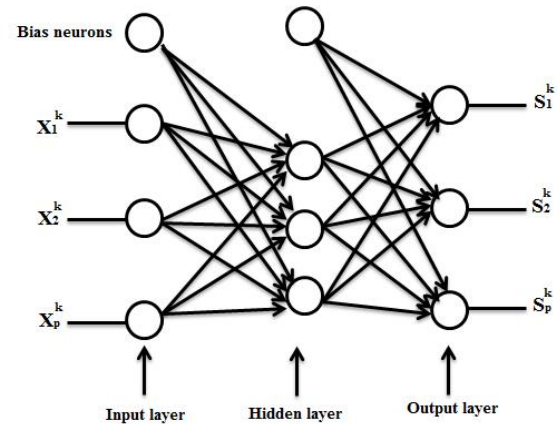

Fig.4 Architecture of Feed forward Neural Network

Once the experiment setup starts it operation each and every input values are passed into the MLP block [7]. The MLP algorithm which compares the input voltage with the reference values and if there is any mismatch in the reference value it will be termed as stator fault occurred in the transcript window in modelsim. Similarly for rotor fault and voltage flow control are exposed in the transcript window.

C. FPGA Implementation

The choice of VHDL is mainly because of its ease of operation, flexibility, and definitive output, to be more precise with one design description many design architecture can be included.[8] The implementation of FPGA in research which reduce the cost of experimentation and increasing the performance. So far concerned the software implementation of neural network into FPGA is discussed but it's not advisable. There are some modifications in the neural network structure and its function mapping has to be done before hardware implementation of the neural network.

IV RESULTS

The simulated outputs are as follows which shows output of sinusoidal wave based on the positive and negative cycles of the sinusoidal output the SVPWM pulses are generated. Thus it shows IGBT switching for functioning of induction motor. Thus following this is the stator fault, rotor fault and voltage flow control of induction motor are given
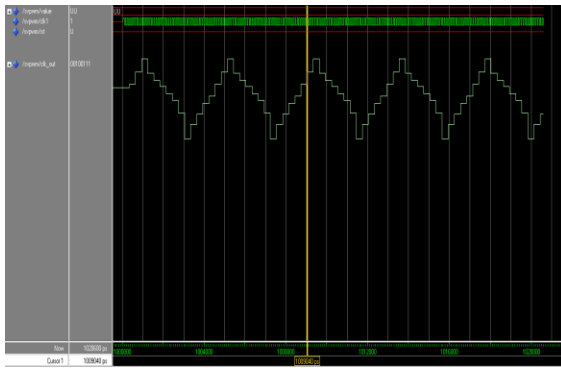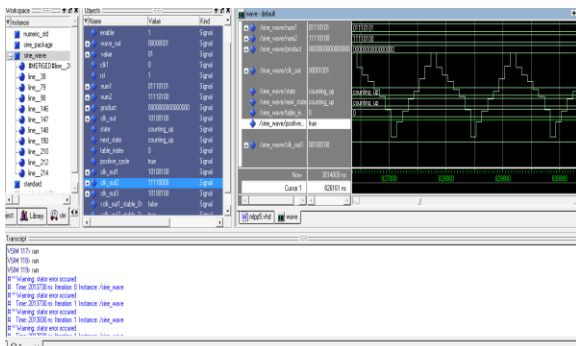
Fig.6 SVPWM Output

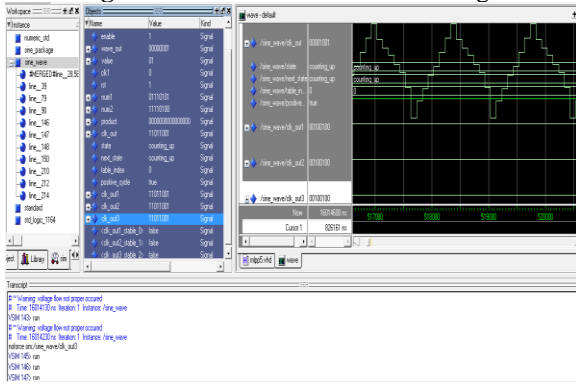**Fig.7** SVPWM with Stator Fault using MLP

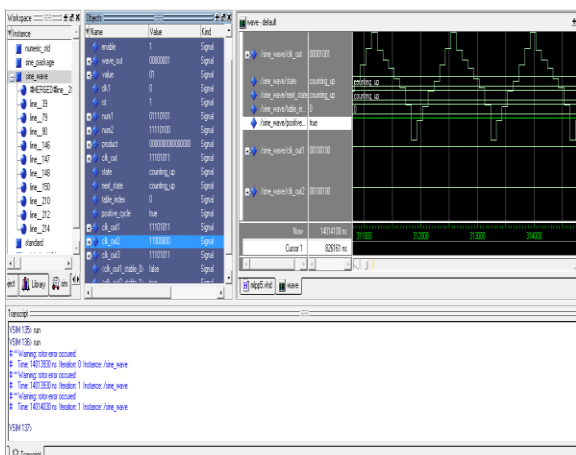**Fig 8.** SVPWM with Voltage Flow problem using MLP

Fig.9 SVPWM with Rotor Fault using MLP

V. Conclusion

Thus the above given techniques for fault diagnosis in induction motor which shows many advantages compared to all other existing method. This is briefly presented over in this paper based on reference works from different authors. The future enhancement is using Back Propagation Network (BPN) fault diagnosis in induction motor is performed and the efficiency between these two algorithms and which one is best suited for fault diagnosis have to be found.

References

[1] SubbaraoTatikonda and PramodAgarwal,"Field Programmable Gate Array (FPGA) Based Neural Network Implementation of Motion Control and Fault Diagnosis of Induction Motor Drive"IEEETrans.Ind.Electronics., 2008 IEEE.

[2] Ayse kocalms, sedat sunter , " simulation of a space vector PWM controller for a three level voltage feed inverter motor drive", FIRAT University, Turkey.

[3] Ing. Pavel GAJDŮŠEK ," Programmable laboratory invertor and space Vector pulse wm", dept. of Electrical Power Engineering, FEEC, VUT.

[4] V. N. Ghate and S. V. Dudul, " Induction Machine Fault Detection Using Generalized Feed Forward Neural Network", Journal of Electrical Engineering and technology, Vol 4, No 3,PP 389-395, 2009.

[5] Aydoğan Savran, and Serkan Ünsal, " Harware implementation of feed Forward neural network using FPGA", Ege University, Department of Electrical and electronics engineering.

[6] Wan Mohd Fahmi Wan Mamat , Nor Ashidi Mat Isa , Kamal Zuhairi Zamali, "HybridVersion of MLP Neural Network of Transformer Fault Diagnosis system", School of Electrical and Electronic Engineering, 978-1-4244-2328, 2008 IEEE.

[7] Hiroomi Hikawa, " Implementation of Simplified Multilayer Neural Networks with On-chip Learning", Oita University, 0-7803-2768-1995 IEEE.

[8] Marco Krips, Thomas Lammert, and Anton Kummert, " FPGA Implementation of a Neural Network for a Real-Time Hand Tracking System" , 0-7695-1453-7, 2002 IEEE.

IMPROVED BRAIN TUMOR DETECTION
WITH ONTOLOGY

*Monika Sinha, Khushboo Mathur

72-S, Sector-7 Jasola Vihar,
B-108, model town, Barielly,
New Delhi-110025
U.P-243001
Department of IT   Amity University Sec-125, NOIDA, Uttar Pradesh

Abstract

Computer aided diagnosis systems for detecting Brain tumour for medical purpose have been   investigated using several techniques. In this paper our concern is to presents an approach which will be useful for improved detection of brain tumour using Post -processing and Pre-processing steps of Digital image processing.

The occurrence of tumour is basically due to mass or cluster formation that will help to classify the type of cancer with the processing method on MRI images for cancer detection. Taking the six variant ways of processing an image is applied on to our MRI images. The result is observed on various types of MRI images with different types of cancer regions.

Keyword: Brain cancer, Ontology, recognition, MRI.

I. Introduction

Brain cancer is one of the most deadly and intractable diseases. Tumors may be embedded in regions of the brain that are critical to provide the body's vital functions, while they shed cells to invade other parts of the brain, forming more tumours that are too small to detect using the normal imaging techniques. Brain cancer's location is sometime hard to identify and that makes it difficult to some people who has to fight with their life.

In Recent years we have seen that the rise in cancer patient have outnumbered than the normal. The tumor in the early stage is certainly hard to identify but once it gets identified the treatment can be done and is curable with techniques like chemotherapy. But certainly late detection of tumour is deadly.

But the cancer is kind of disease in which symptoms are identified late. The use of computer assisted technology have taken a wide step in detection of tumour these days like used in Neuro surgery [1].The availability of 3-D images with the relationships of their critical structures (e.g., functionally significant cortical areas, vascular structures) and disease [2] .

A brain tumor can be defined as a disease in which cells grow uncontrollably in the brain. Brain tumor is basically of two types:
1) Benign tumors
2) Malignant tumors

Benign tumors do not have the ability to spread beyond the brain itself. Benign tumors in the brain have limited self-growth and it do not to be treated. But they can create problem due to their location and has to be treated as early as possible.

Malignant tumor is the actual brain cancer. These tumours can even spread outside of the brain rapidly. Malignant tumors are left almost untreated most of the time as the growth is so fast that it gets too late for the surgeon to control or operate it. Brain malignancies again of two types:

    i)   Primary brain cancer originated in the brain.
    ii) Secondary or metastatic brain cancer spread to the brain from another site in the body.

In general the cell grows in particular speed and in a proper manner but when the rapid growth of cell (here brain cell) is observed, and it keeps on dividing uncontrollably, when the new cells are not required, a mass of tissue forms which seems like a cluster, this is called as tumor.

II. Materials and Methods

The present work implements a system for the improved detection of brain tumor using various steps of processing steps. The implemented work can be useful for biomedical early and improved brain cancer detection. The proposed work will also take input from the output of this application and integrate them with the concept of ontology. [3]

Fig.1 shows a block diagram for the proposed algorithm.

MRI Sample of Brain
↓
Image
↓
RGB to Grey
↓
High pass filter
↓
Enhanced image
↓
Thresholding
↓
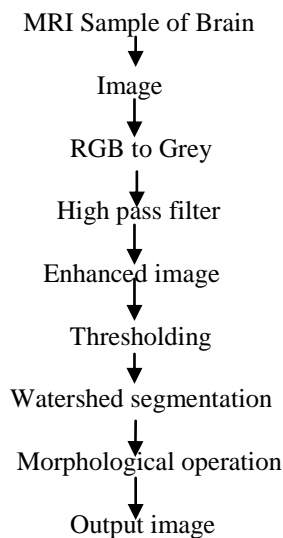Watershed segmentation
↓
Morphological operation
↓
Output image

Image pre-processing including converting RGB image into grey scale then passing that image to the high pass filter in order to remove noise is done and finally the last we get enhanced image for post-processing that will include watershed segmentation and thresholding as well as morphological operation.(erosion and dilation).

1. Data Set
For the implementation of this application we need to have the images of different patients in our database in order to identify their condition. The MRI image is stored along with our main file from various sources. Various class of MRI image is considered.
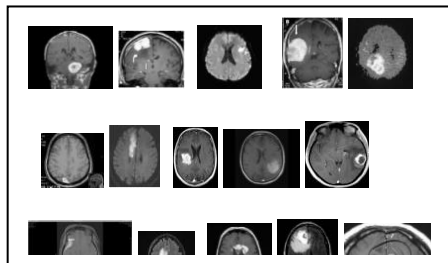
2. Pre-processing
The first step is to get the MRI image and application of pre-processing steps. There are various methods which come under this step; we will be dealing with only grey scale and filters. Basically pre-processing is done to remove noise and blurring as well as ringing effect in order to get the enhanced and much clear image for our purpose. The filter which we have used is median filter but as we are working on image samples that are required for the medical purpose. The median filter has to be passed with mask for better image, to achieve this we are using sobel operator.

3. Image Enhancement
The enhancement is needed in MRI to increase its contrast. Contrast between the brain and the tumour region may be present on a MRI but might be not clearly visible through the eyes of human eyes. Thus, to enhance contrast between the normal brain and tumour region, a high pass filter is applied to the digitized and smoothen the MRI which results in better and enhanced image with fairly visible contrast.

4. Thresholding
Sometimes it is important as well as necessary to separate the region in which we are much more interested from the background. Thresholding provides an easy and the most it is the convenient way to carry out this activity by separating the

foreground and background. We set the certain thresholding value; the pixels which are having intensity value more than the thresholding are set as white as output and rest are assigned as black. Basically it provides binarisation for an image. This is also one of the steps of image segmentation.Thresholding takes filtered image as their input.

5. Morphological operation

For the extraction of text region, we use morphological operator. In text regions, vertical edges, Horizontal edges and diagonal edges are mixed together but they are distributed separately in non-text regions. Since text regions are composed of vertical edges, horizontal edges and diagonal edge. At different orientation these text are connected together differently. We have used Morphological dilation and Erosion operators here, erosion function helps the image to expand and provide better quality picture whereas, the dilation helps to fill the gaps in the image. Opening is said when the erosion is done followed by dilation and closing is done when dilation is done when followed by erosion[4]
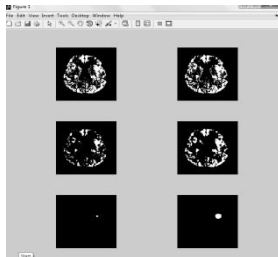

Fig.3 shows the Morphological operated scaled image.

6. Function which is used

i) Pre-processing
img= imread('mala.jpg');
img_gray=rgb2gray('img');
hp_fil=(-1 2 -1,0 0 0,1 -2 1);
ii) To make binary of an image
T=graythresh(c);
bw= im2bw(c ,T+.03);
imshow(bw);

For watershed
bw5= watershed(bw1);
imshow(bw5);
i)   Erode and Dilate functions
bw1= imerode(bw,SE);
imshow(bw);
bw1=imdilate(bw1,SE);
imshow(bw1);

7. Ontology

Various work has been done regarding the detection of brain tumour like Murugavalli1 and Rajamani , A high speed parallel fuzzy c-mean algorithm for brain tumor segmentation[5] Murugavalli1 and Rajamani, An Improved Implementation of Brain Tumor Detection

Using Segmentation Based on Neuro Fuzzy Technique [6], different people have put their different approach in finding of the optimal results for this disease. Some of the technique brain tumor detction using segentation based soft computing [7].

The other work toward this field includes the use of neural network[8] and also Computerized Tumor Boundary Detection Using a Hopfield Neural Netwok",   In recent years the concepts of ontology has taken a wide leap from formal specification to the area of artificial intelligence in the domain of experts system. Ontology has been common on World Wide Web. This concept basically deals with classes, sub-classes and their association from the basic categorisation of product along with their features. The WWW Consortium (W3C) is developing the Resource Description Framework (Brickley and Guha 1999), a language for encoding knowledge on Web pages to make it understandable to electronic agents searching for information. The Defense Advanced Research Projects Agency (DARPA), in conjunction with the W3C, is developing DARPA Agent Markup Language (DAML) by extending RDF with more expressive constructs aimed at facilitating agent interaction on the Web (Hendler and McGuinness 2000)[3]. The Ontology uses the OWL. The software Protégé 4.1 can be downloaded through which we can create

our classes along with their attributes. In the present work our objective is to get the output of our application as its input and perform the data or pattern matching with the data that is stored in our knowledge base. The tool HermiT [9]. is use for analysing the image and is known as a reasoner. HermiT is reasoner for ontologies written using the Web Ontology Language (OWL)[10]. Given an OWL file, HermiT can determine whether or not the ontology is consistent, identify sub assumption relationships between classes, and much more. The user will provide his/her name, then next task is to provide the MRI image of that patient from the database and final its processing, after checking the various symptoms of the patient . The system will check the type of tumor and the reason behind, it might be possible that the cluster formation is due to some other reason, so it is our prime concern to detect the tumour correctly.
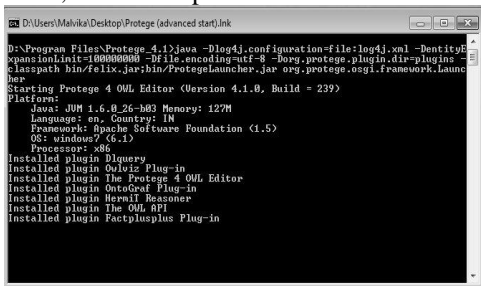

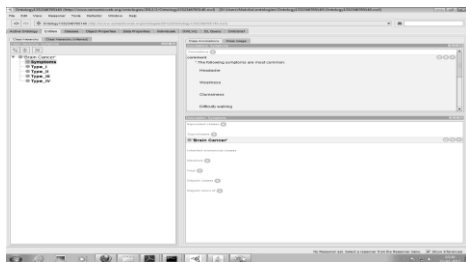**Fig.4** The cmd window before starting of protégé window.

Fig.5 The protégé window with reprsentaion of classes.

III. Result and Discussions

Figure which we get after the application of various fundamental steps of processing on MRI image illustrate the suspicious region of tumour in brain.

The figure 6, figure 7 and figure 8 shows the main GUI of the application, processing steps and the final output with detected tumour respectively.
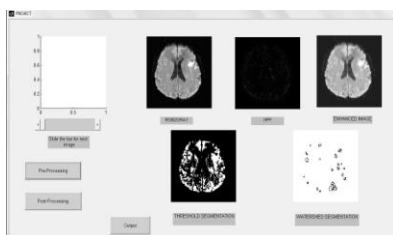

Fig.6 GUI of the Application
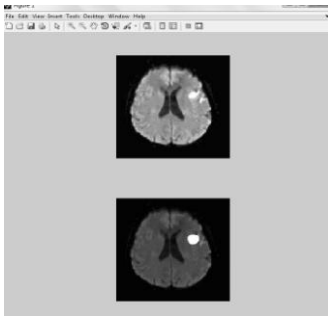

Fig.7 various steps of processing

Fig.8 The original image and the output Image with the suspicious region.

IV. Discussion

This application can be used to detect tumour early and provide us with 50-60% improved result; with the help of processing steps we have. Our application is able to detect the suspicious region on which we would like to work further, its output will be stored in a database so that it can be matched with the some of the sample which will be pre-stored in a database, so that according to the symptoms we would be able to detect tumor in improved manner.

The future work includes the integration with the concept of ontology that can be used for better and accurate results.

V. Acknowledgement

V. References

[1]. Cline HE, Lorensen E, Kikinis R, Jolesz G F.
Three-dimensional segmentation of MR images of
the head using probability and connectivity. J Comput
Assist Tomography 1990;14:1037-1045.

[2]. Velthuizen RP, Clarke LP, Phuphanich S, et at.
Unsupervised measurement of brain tumour volume   on MR images. J Magn Reson Imaging 1995; 5:594-605.

[3]. Article: A Guide to Creating Your First Ontology
Natalya F. Noy and Deborah L. McGuinness Stanford University, Stanford

[4]. Book: Pearson Prentice Hall, Rafael Gonzalez, Richard E.Woods,Digital image processing third edition..

[5]. S. Murugavalli1 , V. Rajamani," A high speed   parallel fuzzy c-mean algorithm for brain tumor segmentation", BIME Journal, Volume (06), Issue (1), Dec., 2006.

[6]. Murugavalli1 , V. Rajamani," An Improved Implementation of Brain Tumor Detection Using Segmentation Based on Neuro Fuzzy Technique" Journal of Computer Science 3 (11): 2007, 841-846

[7]. T.Logeswari and M.Karnan "An Enhanced Implementation of Brain Tumor Detection Using Segmentation Based on Soft Computing", International
Journal of Computer Theory and Engineering, Vol. 2, No. 4, August, 2010, 1793-8201

[8]. Kadam D. B., Gade S. S., M. D. Uplane and R. K. Prasad, "Neural Network Based Brain Tumor Detection
Using MR Images", International Journal of Computer Science and Communication Vol. 2, No. 2, July-December 2011, 325-331.

[9]. Article:HermiT OWL reasoner
Website: http://hermit-reasoner.com/index.html

[10]. Gennari, J.H., Musen, M.A., Fergerson, R.W., Grosso,
W.E.,Crub´ezy, M., Eriksson, H., Noy, N.F., Tu, S.W.:
The evolution of Prot´eg´e: an environment for
knowledge-based systems development. Int. J. Hum.-
Comput. Stud. 58(1), (2003), 89–123

Computationally effecient group re-keying for time sensitive applications

Deepika Rani K[1] & G. Praveen Babu[2]

JNTUH, SIT, Kukatpally, Hyderabad-500028, India.

Abstract—
Key distribution is an important problem for secure group communications. Multicast is an efficient means of distributing data in terms of resources usage. All the designated receivers or members in a multicast group share a session key. Session keys shall change dynamically to ensure both forward secrecy and backward secrecy of multicast sessions. The communication and storage complexity of multicast key distribution problem has been studied extensively. We implement a new multicast key distribution scheme whose computation complexity is significantly reduced. Instead of using conventional encryption algorithms, the scheme employs MDS codes, a class of error control codes, to distribute multicast key dynamically. This scheme drastically reduces the computation load of each group member compared to existing schemes employing traditional encryption algorithms. Easily combined with any key-tree-based schemes, this scheme provides much lower computation complexity while maintaining low and balanced communication complexity and storage complexity for secure dynamic multicast key distribution.

Keywords-distribution, multicast, MDS codes, computation complexity, erasure decoding.

1. Introduction

Key Management is one of the security services required by many Group oriented and distributed applications .In such applications data can be communicated using a secure group key, which helps in key distribution techniques. Multicast is an essential mechanism to achieve scalable information distribution for group-oriented applications. Multicast refers to communication where information is sent from one or more parties to a set of other parties in terms of resource (such as network bandwidth, server computation and I/O load) usage. In this case, information is distributed from one or more senders to a set of receivers, but not to all users of the group. The advantage of multicast is that, it enables the desired applications to service many users without overloading a network and resources in the server.

Security is provided when data is transmitting through an insecure network. Unicast security has several schemes to provide the issues which cannot be extended directly to the multicast environment. As the transmission takes place over multiple network channels, multicasting is more vulnerable than unicasting. In many applications, the multicast group membership changes dynamically, i.e., some new members are authorized to join a new multicast session

while some old members should be excluded.Inorder to ensure both forward secrecy and backward secrecy ,session keys are dynamically changed The forward secrecy is maintained if an old member who has been excluded from the

current session can *not* access the communication of the current session, and the backward secrecy is guaranteed if a new member of the current session can *not* recover the communication of past sessions. This requires each session need a new key that is only known to the current session members, i.e., session keys need to be *dynamically* distributed to authorize session members. Group key management is the major issue in multicast security, which is the fundamental technology to secure group communication by generating and updating secret keys. Access control and data confidentiality can be facilitated using key management by ensuring that the keys used to encrypt group communication are shared only among the legitimate group members and only those members can access the group communication .The shared group key can be used for authentication and also for encrypting the message from a legitimate group member.Inorder to prevent these problems in secure multicast

Communication, the following two security criteria are used. Forward Secrecy: It is maintained if an old member who has been evicted should not be able to access the messages from the current and future sessions. Backward secrecy: It is guaranteed if a new member of the current session cannot recover the communication data of past sessions. The process of changing the session key and communicating the same to only the legitimate group members is called as Re keying.Group key management schemes are of three types. Centralized key management: group members trust a centralized server, referred to as the key distribution center (KDC), which generates and distributes encryption keys. Decentralized scheme: the task of KDC is divided among subgroup managers. Contributory key management schemes: Group members are trusted equally and all participate in key establishment.

In this paper, we study how a multicast group key can efficiently be distributed in computation. In this a centralized key management model is used where session keys are issued and distributed by a central group controller (GC), as it has much less communication complexity, when compared to distributed key exchange protocols. The group controller uses the communication, computation and storage resources for distributing the session key to the group members. The main problem here is how the resources can

be used to distribute the session key, which is referred to as group key distribution problem. There are two approaches that are generally used for distributing the session key to the group of n members. The first approach is that the group controller GC shares an individual key with each group member. That key is used to encrypt a new group session key. In the second approach the group controller shares an individual key with each subset of the group, which can then be used to multicast a session key to a designated. Subset of group members. This approach has less communication, computation and storage complexity when compared to the other approach.

A multicast group with large number of members uses the key-tree-based approach. This approach decomposes a large group into multiple layers of subgroups with smaller sizes. Using this approach communication complexity is reduced, but the storage and computation complexity is increased.

In this paper, the main aim is to reduce the rekeying cost. A new novel approach for computation efficient rekeying for multicast key distribution is introduced, which reduces the rekeying cost by employing a hybrid group key management scheme .It also maintains the same security level without increasing the communication and storage complexity. In this scheme, session keys are encoded using error control codes. In general encoding and decoding using error control code reduces the computation complexity. Thus, the computational complexity of key distribution can be significantly reduced.

2. The basic scheme (dynamic key distribution using maximum distance separable codes)

2.1. Maximum Distance Separable Codes

Block codes that achieve equality in Singleton bound are called **MDS (maximum distance separable) codes**. Examples of such codes include codes that have only one codeword (minimum distance n), codes that use the whole of $(F_q)^n$ (minimum distance 1).

Maximum Distance Separable (MDS) codes are a class of error control codes that meet the Singleton bound Letting GF(q) be a finite field with q elements, an (n, k) (block) error control code is then a mapping from $GF(q)^k$ to $GF(q)^n$: E(m) = c, where m = m1m2 _ _ _mk is the original message block, c = c1c2 _ _ _ cn is its code word block, and E(.) is an encoding function, with k <= n. If a decoding function D (.) exists such that D(ci1ci2 _ _ _ cik; i1; i2; _ _ _ ; ik)= m for 1 <= ij <= n and 1 <= j <= k, then this code is called an (n,k) MDS code. For an (n, k) MDS code, the k original message symbols can be recovered from any k symbols of its code word block. The process of recovering the k message symbols is called erasure decoding. All the symbols are defined over GF(q), and usually, q = 2^m. The well-known Reed-Solomon (RS) codes are a class of widely used MDS codes. The RS codes and other MDS codes can be used to construct secret-sharing and threshold schemes.

2.2 Maximum Distance Separable Codes Algorithm

It mainly consist of three parts, they are as follows:
a) Initializing Group controller.
b) Subscribing new members.
c) Applying the procedure of Re-Keying whenever member leaves the group.

Steps for the Algorithm:

Step I : GC Initialization by constructing codeword C using MDS.
Step II : Applying One-Way Hashfunction
Step III : H(x)=y, propoerty of Hashfunction
Step IV : Subscribing new member
Step V : Ji= +ve integer ji!=jk
Step VI : Select Si
Step VII : Applying the procedure of Re-Keying whenever member leaves the group.
Step VIII: Cj=H(Si+r)
Step IX : Member j every 'n' members in the group

calculates these own codeword C1 C2...........Cn

Fig.1: *MDS Code Algorithm*

3. Proposed system

In our paper we proposed four modules:
a. Group Controller.
b. Client.
c. Group Key Generation.
d. Re-Keying.

A. Group Controller

The group controller is the center of the system. It acts as the server for the system. The GC distributes session key to group members, which can then be used to multicast messages to a designated subset of group members.

Multicasting is a process of sending a message to a selected group. Internet applications, such as online games, newscast, stock quotes, multiparty conferences, and military communications can benefit from secure multicast communications. In most of these applications, users typically receive identical information from a single or multiple senders. Hence, grouping these users into a single multicast group and providing a common session encryption key to all of them will reduce the number of message units to be encrypted by the senders. Various types of data communication are broadcast, Multicast, group communication.
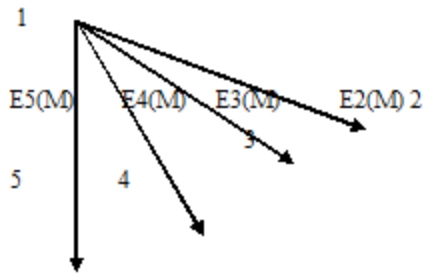
Fig.2: Transmission of the message M through 4 point-to-point connections

Fig.2 shows the transmission of message m to four point to point connections. Here node number 1 is the service provider. Nodes 2,3,4,5 are the receiving nodes. Nodes 2,3,4,5 are receiving the same message.

A. (i) Group communication

For group communications, the server distributes to each member a group key to be shared by all members of the group, distributing the group key securely to all members requires messages encrypted with individual keys (a computation cost proportional to group size). Each such message may be sent separately via unicast. Alternatively, the messages may be sent as a combined message to all group members via multicast. Either way, there is a communication cost proportional to group size (measured in terms of the number of messages or the size of the combined message). Observe that for a point-to-point session, the costs of session establishment and key distribution are incurred just once, at the beginning of the session. A group session, on the other hand, may persist for a relatively long time with members joining and leaving the session. Consequently, the group key should be changed frequently. To achieve a high level of security, the group key should be changed after every join and leave so that a former group member has no access to current communications and a new member has no access to previous communications.

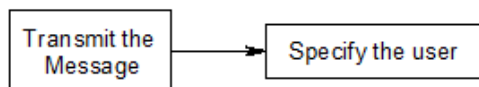**Fig.3:** Multicasting and unicasting in group communication

B. Client

Whenever a new member is authorized to join the multicast group for the first time, the GC sends it (using a secure unicast) a session key. Once a session key is distributed to the group, any member can calculate the secret information that other members in the same group hold.The Login Module is used for the Newly joined users to send a request

to the Group Controller and it is used for to retrieve the Private keys after the Group Controller assign keys to the new users. The user login the group to enter the user Id and Private Key. If the user Id and private key is correct means the user view the inbox and outbox message otherwise to display the message box "Enter the correct Password".
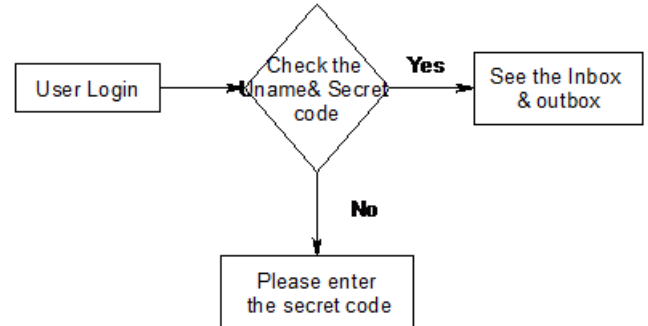

Fig.4: User login

C. Group Key Generation

In cryptography, a group key is a cryptographic key that is shared between groups of users. Typically, group keys are distributed by sending them to individual users, either physically, or encrypted individually for each user.

A common use of group keys is to allow a group of users to decrypt a broadcast message that is intended for that entire group of users, and no-one else. Various group users share their own session key. They can transfer the secret or private information within their groups.The group keys acts as session keys for each groups. It changes whenever a user joins a group or leaves a group.

C. (i) Private Key

The Private Key is generated using MDS code. The GC (Group Controller) sends his number of group members to the KGC (Key Generation Center). The keys are generated by the KGC and submitted to the GC.

C. (ii) Session Key

In session key generation, initially sixteen decimal digits are generated by using random number generation method .Then each decimal digit is splited and compared with pre determined binary format.In DES algorithm the 64 bits session key is considered as a message file and generated user's private key is considered as a key file. DES algorithm encrypts the session key by using user's private key and transmitted to the appropriate users.
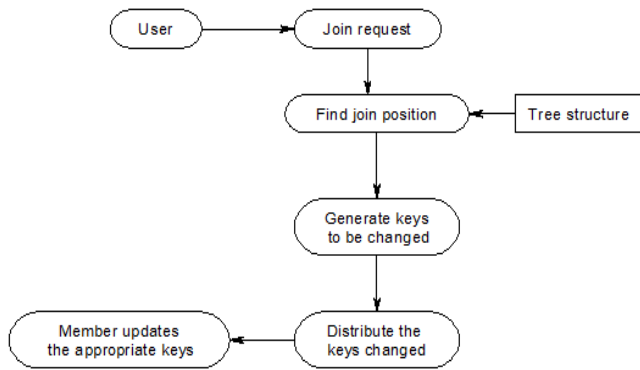
C. (iii) Join operation

Fig.5: *Diagram for Join Operation*

C. (iv) Join Request

A Network node issues a request to GC to join the group. The GC check whether the request is from an authenticated member, if yes the GC accepts the request. The node then communicates its session key through some secure channel.

C. (v) Find join position

The group controller maintains a tree structure. The tree structure is the logical arrangement of members. The GC traverses the tree structure and finds a position for the new member. The GC(Group controller) inserts the member details in this new position, which is a leaf node.

C. (vi) Generate keys

From the new position onwards the GC generates the new key(s) along the path to root. The new keys are used to replace the old keys of the auxiliary nodes.

C. (vii) Update tree structure

Old keys are replaced by their corresponding new keys Henceforth newly generated keys are used for future communication. This operation provides backward secrecy, i.e. it prevents the newly joined member from accessing the previously communicated data.

C. (viii) Distribute keys

A packet is constructed, which consists of newly generated key(s) This packet is encrypted using the old key known by a member or sub-group of members.

C. (ix) User-oriented re-keying

In the user-oriented re keying, the group controller constructs each re keying message, rekey message contains the encrypted form of session key. So that they contain exactly all the messages that some user or a group of users need.

C. (x) Key-oriented re-keying

Key-oriented strategy emphasizes that each new key should be packed into a separate message and distributed to the holders
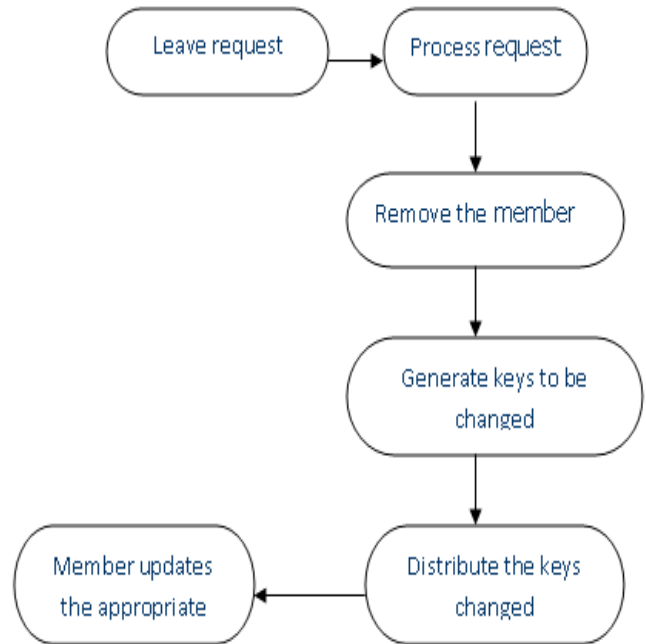
Leave operation

Fig.6: *Diagram for Leave Operation*

C. (xi) Leave Request

The member issues a request to leave the group.

C. (xii) Process Request

The GC checks whether the request is from an existing member, if so the GC accepts the request.

C. (xiii) Find leave position

The GC traverses the tree structure and finds the leaving position of the member. The GC then deletes the member details and removes the node from tree structure.

C. (xiv) Generate keys

From the leaving position onwards the GC generates the new key(s) along the path to root. Old keys are replaced by their corresponding new keys. Henceforth newly generated keys are used for future communication. This operation provides forward secrecy, i.e. it prevents the left member from accessing the data sent in future communication.

C. (xv) Distribute keys

A packet is constructed, which consists of newly generated key(s). This packet is encrypted using the old key known by a member or sub-group of members. These new keys help the members to decrypt the messages sent in future communication.

C. (xvi) Member updates keys

After receiving the message, the member updates the appropriate set of keys.

C. (xvii) User-oriented re-keying

In the user-oriented re keying, the group controller constructs each re keying message, re key message contains

the encrypted form of session key. So that they contain exactly all the messages that some user or a group of users need.

C. (xviii) Key-oriented re-keying

Key-oriented strategy emphasizes that each new key should be packed into a separate message and distributed to the holders.

D. Re-keying

Whenever some new members join or some old members leave a multicast group, the GC needs to distribute a new session key to all the current members. After an old member leaves, the GC needs to distribute a new key to n remaining members to achieve both forward and backward secrecy of the session key.

In the rekeying procedure, the GC needs to multicast a fresh random number r and (n-1) symbols of the new code word m2 …..mn. Each of the codeword symbols has mbits.The random number r is used to guarantee that the new session key is different from all the old keys used.

4. Design & analysis of the system

Design involves identification of classes, their relationships as well as their collaboration. In the Fusion method, some object-oriented approaches like Object Modeling Technique(OMT), Classes, Responsibilities, Collaborators(CRC),etc, are used. Objectory used the term "agents" to represent some of the hardware and software systems .

System Flow Diagram
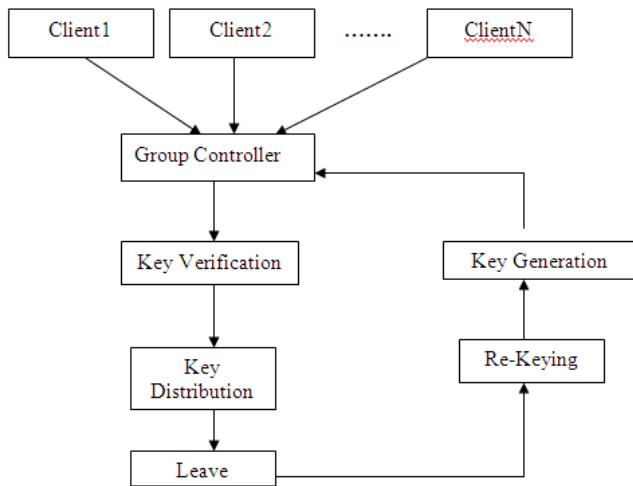
Fig.7: *System flow Diagram*

System Architecture
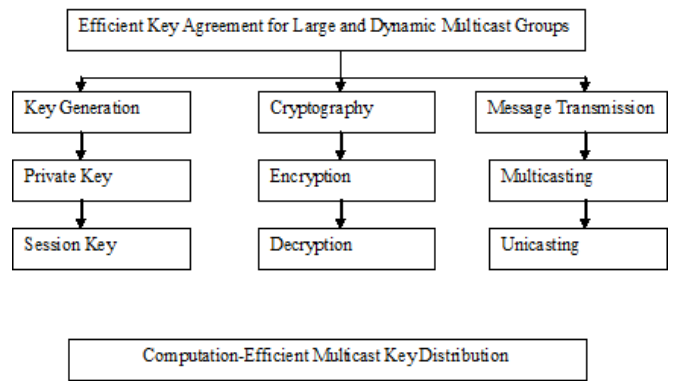
Fig.8: *System Architecture*

Usecase Diagram

Use case diagrams are behavior diagrams used to describe a set of actions (use cases) that some system or systems (subject) should or can perform in collaboration with one or more external users of the system (actors). Each use case should provide some observable and valuable result to the actors or other stakeholders of the system.
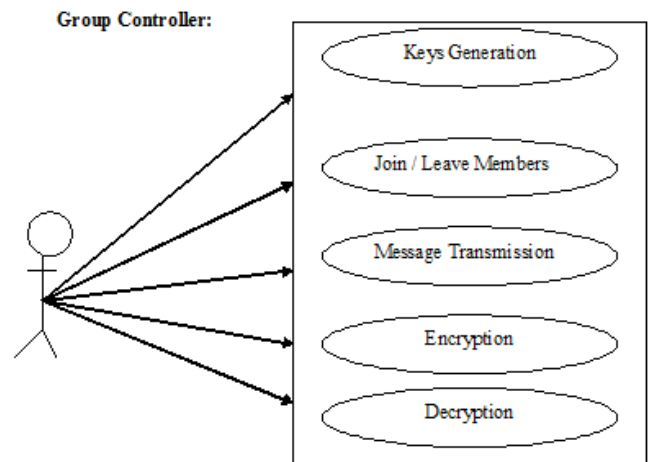
Fig.9: *Interoperability usecase diagram for Group controller*

Sample Code

```
public GrpCtrler(String
id,String sctkey)
{
super();
this.id = id;
g=id;
this.sctkey=sctkey;
initializeComponent();
this.setVisible(true);
setDefaultCloseOperation
(EXIT_ON_CLOSE);
}
```

Fig.10: *Sample code for group controller*

5. Results

The below are the obtained screen shots.

Fig.11: Screen shot for Login
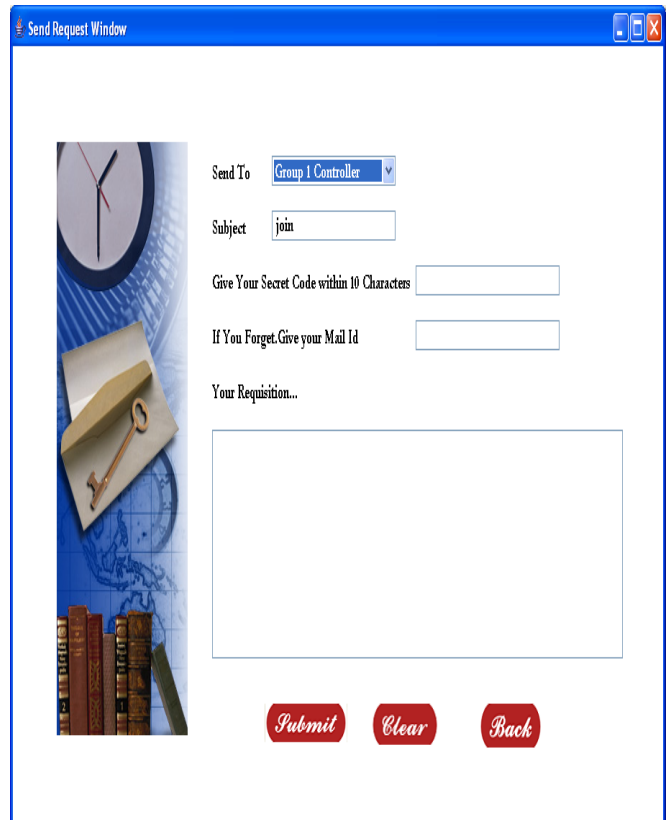
Fig.11: *Screenshot for sending group controller*

Fig.12 : *Screenshot for displaying inbox*

Fig.13: *Screenshot for acknowledging for message which was transmitted*

Conclusion

In this paper we can reduce the complexity of key distribution by using decoding of MDS codes as an alternative for costly encryption and decryption techniques. We concentrate on such a scheme which provides much lower computation complexity while maintaining low and balanced communication complexity and storage complexity for dynamic group key distribution.

Reference

[1] Peter S. Kruus and Joseph P. Macker, "Techniques and issues in multicast security," MILCOM98, 1998.

[2] Paul Judge and Mostafa Ammar, "Security Issues and Solutions in Multicast Content Distribution: A Survey", IEEE Network, February 2003, pp 30 – 36.

[3] M. Moyer, J. Rao and P. Rohatgi, "A Survey of Security Issues in Multicast Communications", IEEE Network Magazine, Vol. 13, No.6, March 1999, pp. 12-23.

[4] Yan Sun, and K.J. Ray Liu, "Securing Dynamic Membership Information in Multicast Communications," *IEEE INFO CONFERENCE 2004*.

[5] T.M. Cover and J.A. Thomas, Elements of Information Theory. John Wiley & Sons, 1991.

[6] S. Rafaeli and D. Hutchison, "A Survey of Key Management for Secure Group Communication," ACM Computing Surveys, vol. 35, no. 3, pp. 309-329, 2003

[7] F.J. MacWilliams and N.J.A. Sloane, The Theory of Error Correcting Codes. North- Holland Math. Library, 1977.

[8] H. Harney and E. Harder, Logical Key Hierarchy Protocol, IETF Internet draft, work in progress, Mar. 1999.

[9] A.J. Menezes, P.C. van Oorschot, and S.A. Vanstone, Handbook of Applied Cryptography, fourth ed. CRC Press, 1999.

[10] M. Waldvogel, G. Caronni, D. Sun, N. Weiler, and B. Plattner,"The VersaKey Framework: Versatile Group Key Management,"IEEE J. Selected Areas in Comm., vol. 7, no. 8, pp. 1614-1631, Aug. 1999

Authors

Deepika Rani Kampally received Bachelor's degree in Computer science and Engineering from JNTUH, Pursuing M.Tech in Computer Science and Engineering from JNTUH. She is a research scholar in field of Information Security.

G. Praveen Babu is presently working as an Associate Professor of Computer Science & Engineering, at School of Information Technology, JNT University.He has a teaching experience of more than 9 years.Presently, pursuing Ph. D. In the area of Computer Networks.Areas of interest are computer Networks, Network Security, Analysis of Algorithms, Artificial Intelligence and Software Engineering Additionally, In-charge of the Placement and Training cell at School of Information Technology, JNTU, Hyderabad.

Simulation and Analysis of Genetic Algorithm Based on FPGA

B.Umamaheswari[1] and N.Rajeswaran[2]

[1]P.G Student/VLSI Design, SNS College of Technology, Coimbatore, Tamilnadu.
[2]Dept.of ECE, SNS College of Technology, Coimbatore, Tamilnadu.

Abstract

In this paper, we propose a technique that utilizes the genetic algorithm for various VLSI circuits. In GA, we proposed the method of automatic test pattern generation (ATPG) is used to generate test vectors. Experiment results showed that the proposed algorithm reduce the complexity of the circuits and also the execution time. The design is realized using VHDL and then fabricated on FPGA.

Keywords: Genetic algorithm (GA), Automatic Test Pattern Generation (ATPG), FPGA.

Introduction

An evolutionary algorithm is a subfield of artificial intelligence. An evolutionary algorithm refers to the evolutionary computational models using randomness and genetic inspired operations. Evolutionary algorithm involves selection, recombination, random variation and competition of the individuals in the population adequately represented potential solutions.

A genetic or evolutionary algorithm applies the principles of evolution found in nature to the problem of finding an optimal solution to a solver problem. In genetic algorithm the problem is encoded in a series of bit strings are manipulated by the algorithm. In a evolutionary algorithm the decision variables and problem functions are used directly.

A drawback of any evolutionary algorithm is that a solution is "better" only in comparisons with others. This algorithm has no concept of an optimal solution or any way to test whether a solution is optimal. This also means that an evolutionary algorithm never knows for certain when to stop or number of iterations or candidate solutions, that you wish to allow it to explore.

Genetic algorithm

Genetic algorithm (GA) is an adaptive heuristic search algorithm based on the mechanism of natural selection and evaluation.GA is a artificial intelligence procedure and robust search method. This technique is efficient for finding combinatorial optimization problem. The objective of GA is to find

optimal solution to a problem. Genetic algorithm belongs to the class of evolutionary algorithm which generates solution to optimization problems using techniques inspired by natural evolution such as inheritance, mutation, selection and crossover [4].

Proposed method

Hardware Architecture of GA

In this paper the evolvable hardware is used. This evolvable hardware can be implemented by combining hardware architecture of GA with evolvable computing logic [10]. This paper describes the implementation of evolvable hardware with the state machine hardware. The hardware architecture of genetic algorithm model based on FPGA consists of two units. They are processing unit and control unit. Figure 2 shows the hardware architecture of genetic algorithm [8].

Processing unit

The function of the processing unit includes initial population generation, fitness evaluation and genetic operation. There are five hardware modules in the processing unit. They are generation modules, selection modules, crossover modules, mutation modules and random number generation module (RNG). RNG generates random number for other modules.

Control unit

The control unit acts as a control state machine. The state machine of the control unit can be used to decide the operating sequence of initial population generation, population storage, fitness evaluation, selection, crossover and mutation. It can automatically send control signal to the processing unit.

Operation

The control signal can assure a correct executing in circles of these modules in the processing unit, depending on the operating rule about the sequence of these operations. The control unit receives the current state signals and generates the next state. These two units work co-ordinately to perform the calculation of GA.
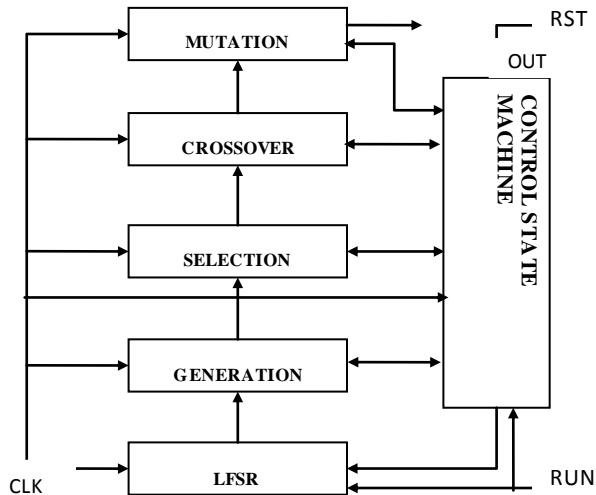
Fig.2 Hardware Architecture of GA

Control state machine

The modules of processing unit are controlled by the control state machine of the control unit and can work on two states. They are active state and sleeping state. The figure 3 shows the binary decision diagram of the control state machine. The state machine consists of four states. They are idle, birth, GA, store.
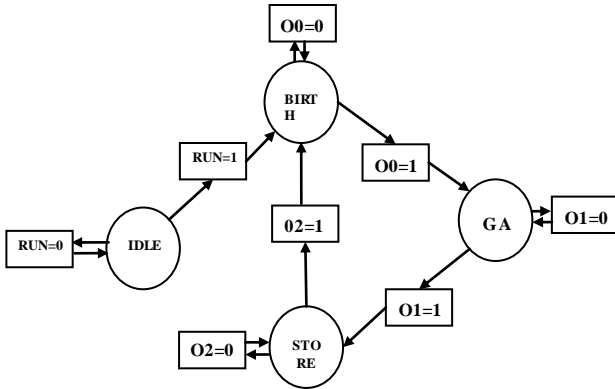
Fig.3 control state machine

Linear feedback shift register

Random number is of great importance to the operation of genetic algorithm. Normally random numbers are made by using linear feedback shift register (LFSR) based random number generators [3]. LFSR is a shift register whose input bit is a linear function of its previous state [6]. The two main parts of the LFSR is the shift register and feedback function.

RESULTS

This experiment is carried on the VLSI circuits. These circuits are simulated and implemented in FPGA. The proposed algorithm is simulated using VHDL language

figure 4, 5 and 6 shows the experimental results for LFSR, control state machine and genetic algorithm.
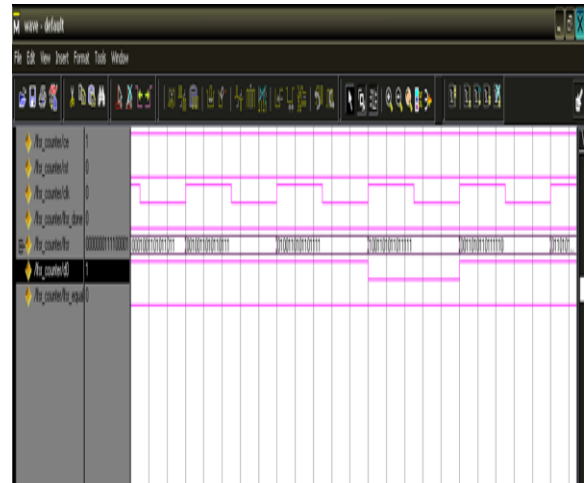
Fig.4 Simulated waveform for LFSR
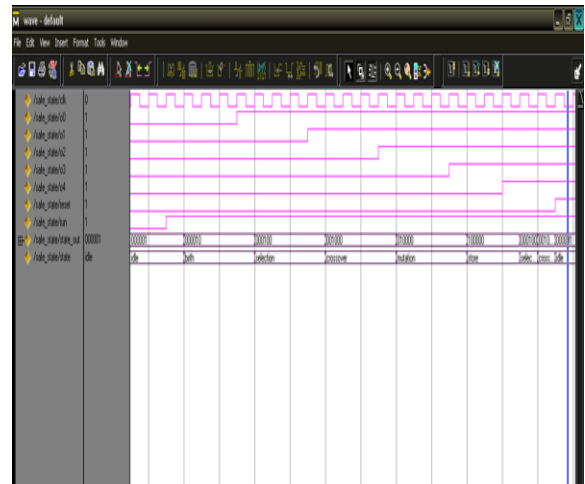
Fig.5 Simulated waveform for control state machine
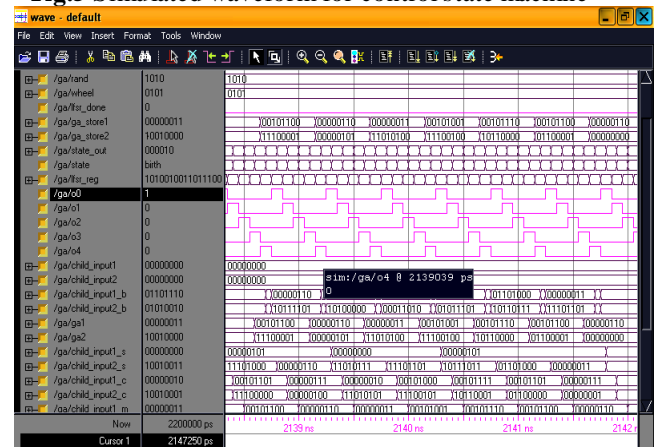
Fig.6 Simulated waveform of Genetic Algorithm

Conclusion

Genetic algorithm is promising methods for solving difficult technological problems. This project proposed a genetic algorithm for automatic test pattern generation in VLSI circuits. This method is used to improve the performance of the system. Here the control state machine and random data generation is used. So the execution time is reduced. GA provides efficient techniques for optimization and machine learning applications.

References

[1] Chatchawit Aporntrwan, Prabhas changstitvatana, 2001,"A Hardware implementation of the compact genetic algorithm".

[2] Iouliia Skliarova, Antonio B. Ferrari, 2001," FPGA- based implementation of genetic algorithm for the travelling salesman problem and its industrial application"

[3] Javad Frounchi, Mohammad Hossein Zarifi, Sanaz Asgari Far, Hamed Taghipour, 2003," design and analysis of random number generator for implementation of genetic algorithm using FPGA"

[4] Manoj Kumar, Mohammad Husain, Naveen Upreti & Deeti Gupta, 2010," Genetic Algorithm: review and application"

[5] Masaya Yoshikawa, Hironori Yamauchi, and Hidekazu Terai, 2008,"Hybrid architecture of Genetic algorithm and simulated annealing"

[6] Rachana singh, Arvind Rajawat, 2010, "Implementation and analysis of immune genetic algorithm for generating test pattern in VLSI circuits".

[7] Shruthi narayanan , Carla purdy, 2005" Hardware implementation of genetic algorithm modules for intelligent systems"

[8] Tatsubiro Tachibana, Yoshibiro Murata, Naoki shibata, kriichi Yasumoto and Minoru Ito, 2000, "General architecture for hardware implementation of genetic algorithm".

[9] Tatsubiro Tachibana, Yoshibiro Murata, Naoki shibata, kriichi Yasumoto and Minoru Ito,"A hardware implementation method of multi-objective genetic algorithms"

[10] Tu Lei and Zhu ming cheng, wang jing_xia, 2002,"The Hardware Implementation of a Genetic Algorithm Model with FPGA".

Application of Fuzzy Logic in Delay Analysis in Construction

Shruti Singh[1] Dr. M.K. Trivedi[2]

[2]Civil department
MITS
Gwalior 474005,
India
[1]Civil Department
MITS
Gwalior, India

Abstract

This paper describes an application of fuzzy logic in analysis of delays in construction projects using Fuzzy toolbox of MATLAB Program Software. Delays in construction projects are inevitable and may result in claims and disputes among different construction parties. Delays in construction projects can be due to a number of causes, which need to be classified and identified. For the success of a construction project, estimation of likelihood of delay resulting from different factors is a must. Fuzzy logic provides a simple way to arrive at a definite conclusion based upon vague, imprecise or missing input information. Fuzzy logic is a form of many-valued logic; it deals with reasoning that is approximate rather than fixed and exact.

Keywords- Construction projects; Fuzzy logic; Delays; Delay cause; MATLAB; Fuzzy Logic Toolbox

I.INTRODUCTION

The major problem occurring in any construction project is the delays occurring during the project, which cause the project to take longer time than planned. A construction project is commonly acknowledged as successful, when it is completed on time, within budget, in accordance with the specifications. A successful project means that the project has accomplished its technical performance, maintained its schedule, and remained within budgetary costs. Projects may differ in size, duration, objectives, uncertainty, complexity, pace, and some other dimensions. It does not matter how different or unique a project is; there is no doubt that every project contains some degree of uncertainty. It is required to be aware of these uncertainties and to develop necessary responses to get the desired level of the project success. Schedule delays are common in various construction projects and cause considerable losses to project parties. It is widely accepted that construction project schedule plays a key role in project management due to its influence on project success. The common results of schedule delays are: Late completion of project, increased cost, disruption of work, loss of productivity, third party claims, disputes and abandonment or termination of contracts. Therefore schedule delays in construction projects give rise to dissatisfaction to all the parties involved.

The aim of this paper is to propose a schedule delay assessment model using Fuzzy Logic Toolbox of MATLAB Program Software. An interview was conducted in which construction project team members were asked questions about the delays taking place in the project. The delay causes were grouped and categorized in different factors. The interview results were used in the assessment model and probability of schedule delay was evaluated. According to the results obtained from the model, the areas of most concern were discussed. The results obtained were accurate and acceptable.

II.CONSTRUCTION PROJECT DELAYS

Construction management focuses on best practices of managing resources such as materials, equipment, and labor. The challenge that the managers face in the construction industry is how to balance time, cost, and quality. Time delays are very clear measurements of project success as a simple comparison between actual and planned time could provide managers with project status.

Schedule delays in a construction project can be defined as the late completion of works as compared to the planned schedule or contract schedule. It could be possibly be interpreted as a loss of time. "Time" refers to the duration for completing the construction project. Time in a construction project is the construction period or in contract administration is the contract period. When the project period is delayed, it means the project cannot be completed within original schedule.

Usually there is no way of predicting how likely it is that a given project will meet its milestones and its predicted completion date. Uncertainty is an inherent aspect of project management. In the planning phase, an estimated project schedule is modeled and a critical path determined where all activities are future events. Uncertainty arises from different aspects such as task duration, resources encountered in execution and the dependency of tasks on the completion of other tasks. But in the execution phase, other non-controllable factors such as weather, resource limitations, and managerial actions can cause

alterations in the planned schedule and result in delays, especially if the task is part of the critical path. Delay in critical activities or near critical activities result in project delay. Some amount of delay on non-critical-path tasks can be tolerated, but any slippage on critical-path tasks directly results in delay of the project as a whole.

III. DELAY CLASSIFICATION

A Several factors can contribute to delays of a project. Analyzing the causes of delays is an essential task for resolving any conflicts or claims. Although many researchers emphasize the high cost and the associated risk related to litigating delay claims, few emphasize the responsibility for project delays. To avoid delays that might result in claims and disputes, the link between the actual tasks undertaken, the time required to complete them, and the ultimate cost estimate of the resources involved all need to be examined.

According to an earlier work by the author related to project schedule and project delay classification Al-Humaidi (2002) , classification of delay causes can follow different logic and can be classified according to their origin, timing, and compensability.

Classification of delays according to origin is when the delay is analyzed based on the party responsible for the delay. The party responsible for the delay can be the owner, the designer, or the contractor. The second classification of delay is based on compensability of delay. Compensable delays are classified further into excusable delays or non-excusable delays. The third classification of delay is based on timing of delay. If two or more delays occur simultaneously, then a concurrent delay takes place. If a single delay takes place at a time, then a non-concurrent delay occurs.

Delays can be classified as:

1. ORIGIN
   • Those over which neither party has control
   • Those over which the owner has control
   • Those over which the designer has control
   • Those over which the contractor has control

2. COMPENSABILITY
   • Excusable delays
   • Non-excusable delays
3. TIMING
   • Concurrent delays
   • Non-concurrent

IV. DELAY FACTORS

The project team members from different construction projects were interviewed about the delays occurring in their projects. They were asked to fill in the questionnaire and give values to the delay causes ranging from 0 to 100. These values were converted into percentage values and used as fuzzy weights to be used in the Fuzzy Logic Toolbox of Matlab as rule weights to be given to the delay causes. They were also asked to give scores to the factors as 'Least causable'; 'Medium Causable' and 'Highly Causable'. The delay factors are shown below in the form of table:

Factors	Causes	Values
Labor Related Factors	a)Labor strike	0.34
	b)Conflicts among labor	0.37
	c)Inexperienced Labor	0.70
	d)Labor shortage	0.79
	e)Absent labors	0.49
Project Related Factors	a)Short original contract duration	0.69
	b)Delay penalties	0.54
	c)Project complexity	0.36
	d)Disputes among project parties	0.60

Consultant Related Factors	a)Improper project management assistance	0.56
	b)Inexperienced consultants	0.72
	c)Inspecting and testing delays	0.80
	d)Conflicts between consultants and design engineer	0.47
	e)Poor communication and coordination with other parties	0.74
	f)Delay in approval of design documents	0.61
Contractor Related Factors	a)Poor site management and supervision	0.79
	b)Poor planning and scheduling of project	0.83
	c)Shuffling of subcontractors	0.34
	d)Poor communication and coordination with other parties	0.74
	e)Rework due to errors	0.50
	f)Inexperienced contractors	0.81
External Related Factors	a)Inclement weather conditions	0.81
	b)Variations in price	0.61
	c)Global financial crisis	0.87
	d)Changes in government regulations and laws	0.42
	e)Unexpected surface and subsurface conditions	0.79

	f)Delay in providing services from utilities	0.52
	g)Delay in transportation	0.35
Owner Related Factors	a)Slow decision making	0.76
	b)Delay in approving design documents	0.46
	c)Late site delivery	0.71
	d)Change in orders by owners	0.89
	e)Improper study of designs	0.55
	f)Progress payments delays	0.62
	g)Poor communication and coordination with other parties	0.81
	h)Inexperienced owners	0.72
Material Related Factors	a)Material manufacturing delay	0.35
	b)Damage of material	0.42
	c)Material shortage	0.77
	d)Delay in delivery	0.73
	e)Rising prices of materials	0.43
Design Related Factors	a)Inadequate experience of design team	0.64
	b)Complexity in project design	0.38
	c)Errors made by designers	0.62
	d)Delays in making design documents	0.65
	e)Unclear details in drawing	0.56
	f)Insufficient data collection	0.50
Equipment Related Factors	a)Damaged equipment	0.46
	b)Equipment shortage	0.45
	c)Breakdown of equipment	0.54
	d)Low efficiency	0.71
	e)Problem in allocation	0.65

V. CASE STUDY

A real case study was undertaken and an interview was conducted in a housing project in Gwalior, to assess the causes of scheduled delays in the project, thereby causing delay in the planned duration of the project. The project manager was requested to form a group of decision makers to perform the following tasks:

1. To check the delay factors cited in the questionnaire.
2. To cite additional factors if necessary.
3. To assign values to the factors ranging from 1 to 100 as probability of schedule delay (1 being probability very low and 100 being probability very high).Following results were obtained after the interview.

Factors	Causes	Probability
Labor Related Factors	a)Labor strike	20
	b)Conflicts among labor	60
	c)Inexperienced Labor	65
	d)Labor shortage	60
	e)Absent labors	30
	a)Short original contract	65

Project Related Factors	duration	
	b)Delay penalties	20
	c)Project complexity	50
	d)Disputes among project parties	40
Consultant Related Factors	a)Improper project management assistance	50
	b)Inexperienced consultants	60
	c)Inspecting and testing delays	30
	d)Conflicts between consultants and design engineer	75
	e)Poor communication and coordination with other parties	40
	f)Delay in approval of design documents	60
Contractor Related Factors	a)Poor site management and supervision	60
	b)Poor planning and scheduling of project	55
	c)Shuffling of subcontractors	35
	d)Poor communication and coordination with other parties	60
	e)Rework due to errors	65
	f)Inexperienced contractors	25
External Related Factors	a)Inclement weather conditions	25
	b)Variations in price	70
	c)Global financial crisis	95
	d)Changes in government regulations and laws	85
	e)Unexpected surface and subsurface conditions	20

	f)Delay in providing services from utilities	65
	g)Delay in transportation	35
Owner Related Factors	a)Slow decision making	55
	b)Delay in approving design documents	55
	c)Late site delivery	40
	d)Change in orders by owners	85
	e)Improper study of designs	45
	f)Progress payments delays	60
	g)Poor communication and coordination with other parties	50
	h)Inexperienced owners	20
	a)Material manufacturing	30

Material Related Factors	delay	
	b)Damage of material	30
	c)Material shortage	60
	d)Delay in delivery	85
	e)Rising prices of materials	65
Design Related Factors	a)Inadequate experience of design team	60
	b)Complexity in project design	75
	c)Errors made by designers	60
	d)Delays in making design documents	70
	e)Unclear details in drawing	50
	f)Insufficient data collection	40
Equipment Related Factors	a)Damaged equipment	50
	b)Equipment shortage	20
	c)Breakdown of equipment	30
	d)Low efficiency	40
	e)Problem in allocation	50

The project members also estimated a range from 40-60 showing a medium probablity schedule delay of the project.

The results obtained from Table1 in the form of 'Rule viewer' of Matlab Program Software, were then used to obtain graphs for probability schedule delay factors obtained from the interview, using Matlab Program Software. Fuzzy Logic Toolbox of Matlab Program Software did the calculations easily and saved time, thereby giving suitable results. Following schedule delay probability outputs of the case study was obtained using Fuzzy Logic Toolbox of Matlab Program Software:

Group of Factors	Probability output
Labor Related Factors	44.8
Project Related Factors	41
Consultant Related Factors	49.1
Contractor Related Factors	40.1
External Related Factors	42.2
Owner Related Factors	49.6
Material Related Factors	57.5
Design Related Factors	61.9
Equipment Related Factors	36.8
Schedule Delay	47.7

VI. DISCUSSION OF RESULTS

1. **Labor Related Factors**
   Probability output was calculated as 44.8 showing low-medium probability delay level. The most contributing factors for this delay are:

Very high probability	Very low probability
Inexperienced labor (65)	Labor strike (20)

2. **Project Related Factors**
   Probability output was calculated as 41 showing low-medium probability delay level. The most contributing factors for this delay are:

Very high probability	Very low probability
Short original contractor duration (65)	Delay penalties (20)

3. **Consultant Related Factors**
   Probability output was calculated as 49.1 showing low-medium probability delay level. The most contributing factors for this delay are:

Very high probability	Very low probability
Conflicts between consultant and design engineer(75)	Inspecting and testing delays(30)

4. Contractor Related Factors
Probability output was calculated as 40.1 showing very low-medium probability delay level. The most contributing factors for this delay are:

Very high probability	Very low probability
Rework due to error(65)	Inexperienced contractors(25)

5. External Related Factors
Probability output was calculated as 42.2 showing very low-medium probability delay level. The most contributing factors for this delay are:

Very high probability	Very low probability
Global financial crisis(95)	Inclement weather condition(25)

6. Owner Related Factors
Probability output was calculated as 49.6 showing very low-medium probability delay level. The most contributing factors for this delay are:

Very high probability	Very low probability
Change in orders by owner(85)	Inexperienced owner(20)

7. Material Related Factors
Probability output was calculated as 57.5 showing high-medium probability delay level. The most contributing factors for this delay are:

Very high probability	Very low probability
Delay in delivery(85)	Material manufacturing; and damage of materials(30)

8. Design Related Factors
Probability output was calculated as 61.9 showing very high-medium probability delay level. The most contributing factors for this delay are:

Very high probability	Very low probability
Complexity in project design(75)	Insufficient data collection(40)

9. Equipment Related Factors
Probability output was calculated as 36.8 showing very low-medium probability delay level. The most contributing factors for this delay are:

Very high probability	Very low probability
Damaged equipment, and problem in allocation(50)	Equipment shortage(20)

Schedule Delay
Schedule delay probability output was calculated as 47.7, showing a range of medium-low probability level for this project.

VII.REFRENCES

[1]   Hanouf M. AL-Humadi (2007): A fuzzy Logic approach to model delays in construction projects

[2] Al-Humaidi 2002 After the Fact Delay Analysis Techniques, Masters Thesis, Texas A&M University, 2002.

[3] Al-Ghafly, M.A. (1995) Delays in the construction of public utility projects in Saudi Arabia. Master thesis, CEM Dept., KFUPM, Dhahran, Saudi Arabia.

[4] Baldwin, J. and Manthei, J. (1971) Causes of delay in the construction industry. Journal of the Construction Division ASCE, 97(2):
177- 87.

[5] Fuzzy Logic Toolbox™ 2 User's Guide (2008), MATLAB, The MathWorks, Inc.